VIBRATION-BASED DAMAGE DETECTION ON A MULTI-GIRDER BRIDGE SUPERSTRUCTURE

A Thesis

Submitted to the College of Graduate Studies and Research

in Partial Fulfillment of the Requirements

for the

Degree of Doctor of Philosophy

in the

Department of Civil and Geological Engineering

University of Saskatchewan

Saskatoon

By

Yufeng Wang

2011

PERMISSION TO USE

In presenting the thesis in partial fulfillment of the requirements for a postgraduate degree from the University of Saskatchewan, I agree that the libraries of this University may make it freely available for inspection. I further agree that permission for copying of this thesis in any manner, in whole or in part, for scholarly purposes may be granted by the professor who supervised my thesis work or, in his absence, by the Head of the Department or the Dean of the College in which my thesis work was done. It is understood that any copying or publication or use of this thesis or parts thereof for financial gain shall not be allowed without my written permission. It is also understood that due recognition shall be given to me and to the University of Saskatchewan in any scholarly use which may be made of any material in my thesis.

Requests for permission to copy or to make other use of material in this thesis in whole or part shall be addressed to:

Head of the Department of Civil and Geological Engineering

University of Saskatchewan

Saskatoon, Saskatchewan, S7N 5A9, Canada

ABSTRACT

Vibration-based damage detection (VBDD) techniques have been proposed as a potential form of structural health monitoring with which an entire structure can be evaluated simultaneously using relatively few sensors. Since these methods rely on the identification of small changes in dynamic properties (notably natural frequencies and mode shapes) to infer the existence and the location of damage, reliable estimates of these properties are essential for the successful implementation of VBDD schemes.

The research described in this thesis was primarily focused on an experimental investigation of the application of VBDD on a multi-girder bridge superstructure, with the objectives of identifying the most reliable test procedures, developing VBDD techniques that could be used for identifying the presence of damage, and evaluating the performance of VBDD techniques for such structures. The experimental investigation was supplemented by theoretical analyses and numerical verifications. The structure used for this investigation was a one-third scale model of a slab-on-girder composite bridge superstructure featuring four steel girders supporting a steel-free concrete deck, based on the North Perimeter Red River Bridge in Winnipeg, Manitoba.

The experimental tests were conducted in a well-controlled laboratory environment. Forced dynamic excitation was supplied by means of a feedback-controlled hydraulic shaker. Instrumentation used to measure the dynamic response included a closely-spaced grid of accelerometers mounted on the surface of the deck along the girder lines, as well as electrical-resistance foil strain gauges bonded to the girder webs. Damage cases investigated included damage to the steel girders, to the diaphragm members, to the lateral steel straps, and to the concrete deck.

A damage detection indicator was developed based on mode shapes that had been normalized to enclose an area of unity. The resulting area under the plot of the difference between two independently measured mode shapes was then used as the damage indicator. To demonstrate the features and verify the capability of the newly developed damage indicator in the absence of experimental uncertainties, a finite

element model of the bridge superstructure was developed and used to generate theoretical data for the modal properties.

A database of pairs of independently measured mode shapes, in which both mode shapes in the pair were obtained with the structure in an identical condition, was used to ascertain the variability of the area of mode shape change indicator when different test procedures were followed. This allowed the definition of threshold values of the damage indicator for each set of test procedures, corresponding to the 90th or 95th percentile of the probability distribution of the damage indicator. When the damage indicator exceeds this value, the presence of damage can be inferred with a high level of confidence. A total of 28 different test protocols were investigated, which included two different excitation methods (resonant harmonic and white noise random), four different instrumentation schemes (accelerometers and strain gauges at various locations), and five different vibration modes (the lowest five).

Five commonly available VBDD indicators were also selected to identify the location of damage after its presence had been detected. The performance of the VBDD indicators were examined and evaluated while two different normalization schemes were adopted.

The newly developed damage indicator, the area of mode shape change, was shown to be capable of successfully identifying the presence of damage with a high confidence level using both numerical and experimental data.

Of the 28 test protocols investigated, those that used forced harmonic excitation in combination with the fundamental vibration mode consistently resulted in the lowest threshold values for the area of mode shape change, and therefore resulted in the highest sensitivity to the presence of damage.

The presence of most single damage scenarios could be identified with a relatively high confidence level (at least 90%) when harmonic excitation was used, regardless of the instrumentation scheme used to measure the mode shape (except for the scheme that used data from strain gauges near the top flanges of the girders), since the area changes in the fundamental mode shape due to damage exceeded the corresponding threshold

values. Among the instrumentation schemes investigated, both acceleration measurements and measurements of flexural strains near the bottom flanges of the girders were able to identify the presence of damage with a high level of confidence.

In general, all VBDD methods selected could localize the damage investigated with varying degrees of accuracy when the fundamental mode was used, as long as the presence of damage had previously been detected with a high confidence level.

ACKNOWLEDGEMENTS

I wish to express sincerely my appreciation to my supervisors, Dr. Bruce Sparling and Dr. Leon Wegner for their invaluable guidance, suggestions, encouragement, and continuous assistance throughout the present study.

I also want to appreciate the advice from other members of my advisory committee: Dr. Moh Boulfiza, Dr. Lisa Feldman, Dr. Allan Dolovich, and Dr. Amin Elshorbagy.

The help from the laboratory technicians in the Structures and Materials Laboratory, Mr. Dale Pavier and Mr. Brennan Pokoyoway, is deeply appreciated. I also would like to extend my gratitude to those staff in the university and friends who helped me during this research.

Also, I would like to express my deepest and sincerest gratitude to my family, especially my parents and my wife, Ying Chen, for their support and encouragement throughout my life. This thesis is dedicated to our lovely little boy Luke to compensate a little bit for the time spent on this thesis rather than him.

TABLE OF CONTENTS

LIST OF TABLES

LIST OF FIGURES

LIST OF SYMBOLS

a	Lower limit of the segment of the beam over which damage is being evaluated
A	State matrix which represents the dynamic properties of the system
$Area\ (\phi_o)$	Area enclosed by the plot of the absolute value of the mode shape
b	Upper limits of the segment of the beam over which damage is being evaluated
C	Output matrix which refers to how system states are transformed to the output (response) of the system
C_2	Damping matrix
$\boldsymbol{f}^{"}$	Uniform flexibility curvature vectors before damage
$\boldsymbol{f}^{"*}$	Uniform flexibility curvature vectors after damage
$\boldsymbol{F}$	Flexibility matrix before damage
$\boldsymbol{F}^*$	Flexibility matrix after damage
$F(t)$	Excitation force vector
h	Distance between measurement points
$H(\omega)$	Complex dynamic amplification factor of the system
$[\boldsymbol{I}]$	Identity matrix
$icdf(p, \mu, \sigma)$	Inverse cumulative distribution function which returns a threshold value in the population of ΔA for the given value of p, defined as pth percentile
k	Number of measurement points
$\boldsymbol{K}$	Stiffness matrix
L	Length of the beam
$\boldsymbol{M}$	Mass matrix
$[\boldsymbol{M}]$	Mass matrix of the system
m_c	Constant scalar
n	Number of locations where modal curvature is calculated along the beam

p	Statistical probability or confidence limit
$P(\omega)$	Fourier transform (ft) of the excitation force
t	Continuous time
$Threshold(p, \Delta A)$	Threshold value for δA
$U(t)$	Displacement vector
$\dot{U}(t)$	First derivative of the displacement with respect to continuous time
$\ddot{U}(t)$	Second derivative of the displacement with respect to continuous time
v_k	Measurement noise due to the inaccuracy of the data acquisition system
w_k	Process noise due to disturbances of input data
x	Distance along the beam; the relative flexural stiffness change
x_k	State vector with elements that independently describe the state of the system
$X(\omega)$	Displacement response spectrum of the system
y	Area of mode shape change due to damage
y_k	Output vector at discrete time interval k
Z_j	Normalized damage indicator
β_{ij}	Damage index for the ith mode at location j
$\overline{\delta_j}$	Absolute maximum value of elements in column j of the matrix $\Delta\boldsymbol{F}$
ΔA	Normalized area of the mode shape change
$\boldsymbol{\Delta f}^{"}$	Absolute value of the change in uniform flexibility curvature
$\Delta\boldsymbol{F}$	Change in flexibility of the structure considered
ΔF_{ij}	Elements of the matrix $\Delta\boldsymbol{F}$
$\Delta\boldsymbol{\phi}$	Change in mode shape vector
$\Delta\boldsymbol{\phi}^{"}$	Absolute difference between the mode shape curvature before and after damage
$\boldsymbol{\Delta\phi_{mn}}$	Change in mode shape from two independently obtained unit-area normalized mode shapes

ζ	Damping ratio of system
μ	Mean of damage indices; the mean of the population of ΔA for a normal distribution; the mean of the natural logarithm of ΔA for a log-normal distribution
σ	Standard deviation of damage indices; the standard deviation of the population of ΔA for a normal distribution; the standard deviation of the natural logarithm of ΔA for a log-normal distribution
$\boldsymbol{\phi}$	Normalized (or scaled) mode shape vector before damage
$\boldsymbol{\phi}^*$	Normalized mode shape vector after damage
$\boldsymbol{\phi}^{"}$	Mode shape curvature vector before damage
$\boldsymbol{\phi}^{"*}$	Mode shape curvature vector after damage
ϕ_i	ith element of normalized mode shape vector $\boldsymbol{\phi}$
$\{\phi_i\}$	ith normalized mode shape vector for undamaged states
$\{\phi_i{}^*\}$	ith normalized mode shape vector for damaged states
$\phi_i^{"}(x)$	Mode shape curvature function of the ith mode for the undamaged states as a function of distance x along the beam
$\phi_i^{"*}(x)$	Mode shape curvature function of the ith mode for the damaged states as a function of distance x along the beam
ϕ_j	Mode shape amplitude at measurement point *j*
$\boldsymbol{\phi_m}$	Mode shape vector; the unit-mass normalized mode shape vector
$\boldsymbol{\phi_n}$	Mode shape vector
$\boldsymbol{\phi_o}$	Original mode shape vector $\boldsymbol{\phi_o}$ before normalization
$\phi_{o\,i}$	ith element of $\boldsymbol{\phi_o}$
$\phi_o(x)$	Interpolated mode shape function where x corresponds to the distance along the measurement line
ω_0	Natural frequency of the system
ω_i	ith angular natural frequency for undamaged states
ω_i^*	ith angular natural frequency for damaged states

LIST OF ABBREVIATIONS

2D	Two Dimensional
3D	Three Dimensional
ADC	Analogue-to-Digital Converter
ANPSD	Averaged Normalized Power Spectral Densities
ASTM	American Standards for Testing and Materials
Avg.	Average
C.O.V.	Coefficient of Variation
CFRP	Carbon Fibre Reinforced Polymer
CMIF	Complex Mode Identification Function
COMAC	Coordinate Modal Assurance Criterion
CPS	Cross Power Spectrum
DAQ	Data Acquisition
DC	Direct Current
DFT	Discrete Fourier Transform
DOF	Degree of Freedom
ERA	Eigen Realisation Algorithm
FE	Finite Element
FFT	Fast Fourier Transform
FRF	Frequency Response Function
FRFs	Frequency Response Functions
FT	Fourier Transform
LabView	Laboratory Virtual Instrumentation Engineering Workbench
LDT	Linear Displacement Transducers
MAC	Modal Assurance Criterion
MACEC	A Matlab Toolbox for Experimental and Operational Modal Analysis
NDE	Non-Destructive Evaluation

NExT	Natural Excitation Technique
NI	National Instruments
PCMCIA	Peripheral Component Micro-Channel Interconnect Architecture
PP	Peak Picking Method
R.R.S.D.	Regular Residual Standard Deviation
S.S.R.	Sum of Square of the Residuals
SHM	Structural Health Monitoring
SPICE	A Matlab Toolbox for Experimental and Operational Modal Analysis
SSH	Simultaneous Sample and Hold
SSI	Stochastic Subspace Identification
STDEV	Standard Deviation
VBDD	Vibration-Based Damage Detection
VBDI	Vibration-Based Damage Identification
W.R.S.D.	Weighted Residual Standard Deviation

CHAPTER 1. **INTRODUCTION**

1.1 Background

Due to the aging of materials, environment-related corrosion, overuse, overloading, and an absence of sufficient maintenance, the existing inventory of bridges world-wide continues to experience structural degradation. There are numerous reports about the rapid deterioration of bridges. The majority of highway bridges in Japan are close to the end of their design lives since most were built directly after World War II (Shrive 2005, based on the work of Rahman 2000). Around 40% of all bridges in the United States urgently need to be strengthened, rehabilitated, or replaced to remain in service, and this number increases by about 5000 bridges a year (Shrive 2005, based on the work of Aktan and Farhey 1996). More than 40% of the bridges in service in Canada were built over 30 years ago. Many of these bridges need extensive works of maintenance, rehabilitation or reconstruction to remain in good condition (or health) (Mufti 2001, ISIS Canada 2001). To manage the resulting requirements for maintenance, rehabilitation or reconstruction in a rational manner, there is an increasing need for effective structural health monitoring (SHM) of bridges.

However, bridges are generally inspected at intervals of two or more years, mainly relying on visual inspection (Biswas et al. 1990). Thus, there is the possibility that the bridges may deteriorate to unsafe conditions as a result of experiencing damage between inspection intervals. Also, visual inspections alone have been proven to be highly unreliable due to the fact that the inspections rely heavily on the inspector's experience and knowledge (FHWA 2001). As a result, additional health monitoring, or condition assessment, techniques need to be investigated for further application.

A large number of local non-destructive evaluation (NDE) methods have been developed and successfully applied to some simple and small structures (Kobayashi 1993, Uomoto 2000, Chong et al. 2001, Raj et al. 2002). The local NDE methods include X-ray, gamma-ray, ultrasonics, acoustic emissions, magnetic particles, half-cell potential readings, liquid penetrants, and eddy currents. The NDE methods are generally capable of interrogating only small areas at a time but with relatively high levels of accuracy. In addition, the components under inspection have to be accessible. As a result, the inspection of a large structure (like a complicated bridge) using the local NDE methods alone could be costly and time consuming (Wegner et al. 2004).

Vibration-based damage detection (VBDD) techniques, sometimes referred to as vibration-based damage identification (VBDI) techniques, have been proposed as a potential form of SHM with which the entire structure can be evaluated simultaneously using relatively few sensors. The basis for this approach is that damage to a structure will modify its global dynamic characteristics (notably natural frequencies and mode shapes). In theory, since these dynamic characteristics are readily quantifiable and can be related directly to specific physical properties of the structure, any measurable changes over time may be used to detect, locate and possibly quantify damage at an early stage before visible signs of distress are apparent (Wolf and Richardson 1989).

From a review of the literature, some successful applications of VBDD methods have been conducted on rotating machinery, well-defined mechanical systems, and simple structures such as beams and trusses (e.g., Roth and Pandit 1999, Rizos et al. 1990, Stubbs and Osegueda 1990a and 1990b, Fox 1992, Fritzen et al. 1995, Stubbs et al. 1990, Doebling et al. 1993a and 1993b). Also, VBDD methods have been successfully applied to some real bridge structures for relatively severe damage scenarios (e.g. Biswas et al. 1990, Stubbs et al. 1995, Farrar and Jauregui 1998a and 1998b). However, it is still challenging to successfully apply the VBDD methods to complicated bridge systems for small scale damage scenarios, since the existing inherent uncertainties in the systems and monitoring processes make the measured modal properties less repeatable. As a result, global-based methods (like VBDD) may not be sensitive enough to the small scale damage (Wegner et al. 2004).

Despite the challenges, it is still believed that the application of VBDD methods to bridge superstructures has not been investigated fully. As a result, a comprehensive research program investigating issues relating to the practical application of VBDD methods to bridges has been undertaken at the University of Saskatchewan (Wegner et al. 2004).

As part of this program, the research described in this thesis focuses on the application of VBDD methods to a multi-girder bridge superstructure. Some successful applications of VBDD methods were achieved on simple bridge superstructure components in laboratory environments (Zhou et al. 2007, 2010). However, numerical studies carried out on a multi-girder overpass structure suggest more complex response patterns for multi-girder bridges, which may complicate the identification and localization of damage (Siddique et al. 2007). No experimental verification was performed on multi-girder bridge systems in previous studies. In addition, it is necessary to develop reliable methods that are capable of identifying damage for this more complex type of bridge superstructure.

Since VBDD methods rely on the identification of small changes in dynamic properties to infer the nature of the damage, reliable estimates of these properties are essential for a successful implementation of VBDD schemes (Wegner et al. 2004). However, all experimental procedures result in a certain degree of uncertainty, which induces variability in the measured dynamic properties. As a result, it is necessary to identify specific test procedures or protocols that would produce the lowest levels of uncertainty, and therefore produce the greatest likelihood of detecting damage using VBDD methods. More specifically, in the present study, extensive well controlled dynamic tests and damage detection trials were carried out on a multi-girder bridge superstructure.

1.2 Objectives

The primary objective of this thesis was to investigate the application of VBDD methods to multi-girder bridge superstructures. The detailed objectives of the current research were as follows:

- to investigate the influence of various test parameters on the reliability and repeatability of the measured dynamic properties (i.e., frequencies and mode shapes) of a multi-girder bridge superstructure. Specifically, the issues investigated included:
  - the influence of sensor types and locations, excitation types, sampling rates, recording periods, and modal analysis methods on mode shape definition;
  - the influence of normalization methods on mode shape definition and changes in mode shapes due to damage;
- to develop appropriate damage detection techniques to identify the presence of damage;
- to define the damage detection resolutions of different test protocols based on the statistical variability of the resulting damage indicator, and to use these to identify the most appropriate test protocols;
- to investigate the performance of the newly developed VBDD method on the multi-girder bridge superstructure; and
- to investigate patterns of damage induced changes across a spatially distributed complex system (like a multi-girder bridge superstructure) using commonly available VBDD indicators.

1.3 Contributions to Original Knowledge

A new Level 1 VBDD damage indicator was developed in this study. The resolutions of different test protocols were defined based on the statistical characteristics of the new damage indicator, as calculated both when there was no change in the condition of the structure and when damage was present. The VBDD method, in combination with the protocols identified as being most sensitive to damage, can be used effectively as the initial component of a comprehensive SHM package for bridges by permitting a relatively quick identification of the presence or absence of damage on the structure with a high level of confidence.

It should be acknowledged that a VBDD damage indicator, called mode shape area index, very similar to the one developed as part of this thesis work was found in the literature during the later stages of preparation of this thesis (Huth et al. 2005). However, the work presented in this thesis was developed independently and was defined and applied in a different manner on a different application. In addition, the application of the VBDD technique using a statistical approach is believed to be original. A detailed comparison between two indicators is presented in Section 5.2.3.

The performance of the newly developed damage indictor was investigated on a multi-girder bridge superstructure under well-controlled testing environments.

Also, five commonly used VBDD methods were applied on the complex, spatially distributed multi-girder bridge superstructure system using well-controlled experimental data.

1.4 Scope and Methodology

The current research focused primarily on the experimental application of vibration-based damage detection on a multi-girder bridge superstructure. The structure used for this investigation was a one-third scale model of a slab-on-girder composite bridge superstructure featuring four steel girders supporting a steel-free concrete deck. Constructed in the Structural Laboratory, University of Saskatchewan, the model was based on a prototype superstructure forming part of the North Perimeter Red River Bridge located in Winnipeg, Manitoba.

To facilitate the design and construction of the scaled bridge model, a preliminary field test was conducted on the prototype bridge. Dimensions were measured and compared with the as-built drawings. The dynamic properties (primarily the natural frequencies) were measured using four accelerometers as the bridge was subjected to traffic excitation forces.

Prior to carrying out the laboratory-based experimental test, a preliminary numerical study was conducted to investigate the influence of several factors on the performance

of VBDD methods when applied to bridge decks, which were simulated using commercial finite element (FE) software, ANSYS (2005).

The experimental tests were conducted within a well-controlled laboratory environment. Forced dynamic excitation was supplied by means of a feedback-controlled hydraulic shaker. The shaker was securely attached to the surface of the bridge deck at locations chosen to excite the vibration modes of interest. Since it is often difficult, costly, and sometimes impossible to measure the excitation (input) information of a real civil structure (like a bridge), most modal analysis methods used in civil structural health monitoring are "output-only" methods (James et al. 1995, Peeters and De Roeck 2001). As a result, the current research focused solely on "output-only" identification methods to extract dynamic properties, for which it was assumed that the input forces were unknown, even though the input force from the hydraulic shaker was monitored indirectly using readings from LDT's attached to the moving mass.

Instrumentation used to measure the dynamic response included a closely-spaced grid of accelerometers mounted on the surface of the deck along the girder lines, as well as electrical-resistance foil strain gauges bonded to the girder webs.

Measurement of the dynamics properties of the multi-girder bridge superstructure was carried out in two phases (see Table 3.1). In Phase I, the influence of various test parameters on the repeatability and reliability of modal property extraction was investigated using the intact bridge model (i.e., Health State 1, see Section 3.4). More specifically, the test parameters that were considered in the intact bridge model tests included sampling rates, the length of the recording period, excitation methods, sensor type, and sensor locations (i.e., the vertical locations of strain gauges on the steel web).

In Phase II of the measurements, extensive dynamic tests were conducted on 17 Health States (see Section 3.4) of the bridge superstructure when various specific test protocols (see Section 3.5) were followed. Explanation of measurement results collected in this phase was carried out in two stages. Initially, the data were used to establish the resolution of each test protocol, defined as the threshold value of the damage indicator above which a change could be considered statistically significant, given the level of

uncertainty. Subsequently, the performance of selected VBDD indicators was investigated on the bridge superstructure under the 17 Health States.

1.5 Layout of the Thesis

The thesis is organized in seven chapters, with additional information provided in the appendices. An overview of each chapter is described below.

Chapter 1 presents an overview of the research background, showing the need for structural health monitoring and VBDD. The objectives, scope, and methodology are also presented in the chapter. In addition, contributions to original knowledge are identified.

In Chapter 2, a literature review, including an overview of the theoretical background of SHM and VBDD, dynamic testing methods, and signal processing methods, is presented.

The experimental program is described in Chapter 3, including descriptions of the bridge model, the measurement of dynamic properties, data processing, and damage cases considered.

Chapter 4 focuses on the evaluation of extracted dynamic properties and the influence of test parameters on dynamic properties.

In Chapter 5, a new Level 1 VBDD indicator is presented. The development of the damage indicator is described, and verification of the indicator using data from a FE model is presented.

Chapter 6 presents the application of the newly developed damage indicator to the model bridge superstructure. Specifically, a procedure used to define the resolution of a specific test protocol is described. The results of threshold values for different test procedures are presented. Detailed results of the application of the damage indicator to the bridge are presented for the various damage cases considered. Also discussed in this chapter is the performance of five commonly used VBDD methods when applied to the multi-girder bridge for the damage cases considered.

Chapter 7 presents a summary and conclusions, as well as recommendations for future research.

CHAPTER 2. **LITERATURE REVIEW**

2.1 Overview

There are numerous reports worldwide about the rapid deterioration of civil infrastructure in general, and bridges in particular. Around 40% of all bridges in the United States urgently need to be strengthened, rehabilitated, or replaced to remain in service (Aktan and Farhey. 1996). In Canada, over 40% of the bridges currently in use were built more than 30 years ago (Mufti 2001). The majority of highway bridges in Japan are close to the end of their design lives since most of them were built directly after World War II (Rahman 2000). Many of these bridges are deficient due to the aging of materials, environment-related corrosion, overuse, overloading, and an absence of sufficient maintenance. The extremely cold weather and extensive use of de-icing salts in some parts of Canada in the winter has accelerated the process of deterioration. In addition, some of these bridges need to be strengthened, widened, or replaced due to the increasing demands of traffic loads and changed design standards (Mufti 2001). To monitor the behaviour of the structures accurately and efficiently and to manage the resulting requirements for maintenance, rehabilitation or reconstruction in a rational manner, there is an increasing need for effective structural health monitoring (SHM) of bridges.

As long as the techniques used in SHM are able to provide reliable and quantifiable information regarding the condition of the structures monitored, the owner of the infrastructure could use the information for risk analysis and then select the most suitable option for risk mitigation (Wong 2001). In addition, the information supplied by SHM could be useful for designing a similar structure in the future. From a long-

term point of view, it could reduce the life cycle costs of the infrastructure by providing either a continuous or periodic indication of structural health (Mufti et al. 2005).

There are a large number of SHM techniques available, which include visual inspections, local non-destructive evaluation (NDE) techniques such as X-ray, gamma-ray, ultrasonics, acoustic emissions, magnetic particles, half-cell potential readings, liquid penetrants, and eddy currents (e.g., Kobayashi 1993, Uomoto 2000, Chong et al. 2001, Raj et al. 2002), and global-based methods which use changes in the global response of a structure to evaluate the health or condition of the structure (e.g., Pandey et al. 1991, Fox 1992, Srinivasan and Kot 1992, Salawu and Williams 1994, and Zhang and Aktan 1995). Although the local NDE methods are generally capable of characterizing damage on a structure with relatively higher accuracy compared with other methods, the inspection of a large structure (like a complicated bridge) using NDE methods alone could be costly and time consuming (Wegner et al. 2004). This observation has led to further investigation of effective global-based SHM methods.

Vibration-based damage detection (VBDD) techniques, a set of global SHM techniques, have the potential to evaluate an entire structure simultaneously using relatively few sensors. The basis for this approach is that damage to a structure will modify its global dynamic characteristics (notably natural frequencies and mode shapes). In theory, since these dynamic characteristics are readily quantifiable and can be related directly to specific physical properties of the structure, any measurable changes over time may be used to detect, locate and possibly quantify damage at an early stage before visible signs of distress are apparent (Wolf and Richardson 1989). Although it is simple in concept, extensive research is still required before VBDD methods can be applied reliably to complex structures like bridges with multiple girders and spans. While quite a large number of VBDD methods have been developed and successfully applied on some simple structures, it is still a significant challenge to successfully apply VBDD methods to real, large civil engineering structures (Wegner et al. 2004).

As a result, the primary objective of the current research is to investigate the application of VBDD methods to multi-girder bridge superstructures. Specifically, in this chapter,

several of the main aspects of VBDD-related issues are reviewed and discussed. Firstly, a broad overview of damage detection related issues are provided. To effectively evaluate the condition of a structure based on its dynamic properties, it is important to estimate or measure the modal properties of the structure with a high level of reliability and confidence. It is therefore necessary to find a set of dynamic test procedures and data processing methods which are suitable for the purpose of VBDD. As a result, dynamic testing related issues and modal analysis methods are reviewed and discussed based on the literature. Some commonly used VBDD methods are also reviewed in this chapter, followed by a review of the application of VBDD methods to bridges. In the final section of this chapter, a brief review of the VBDD related research conducted at the University of Saskatchewan is provided.

2.2 Damage Detection

Damage (or fault) detection refers to the identification of a change in the performance of a system compared with a previous, desired level of performance of the system using a structural health monitoring process (Doebling et al. 1996). The previously existing, desired level of performance serves as a reference point to define the state of health (or damage) at some future time. Damage to a structure could include any of the following, acting either individually or in combination: deteriorated material properties, changes in physical and boundary conditions, lack of integrity in connections, and large deformations in geometry. The damage can occur due to the aging of materials, environment-related corrosion, overuse, overload, and an absence of sufficient maintenance. Also, damage can occur suddenly due to unusual natural forces (like an earthquake) and unexpected activities (like an impact force from a collision) (Farrar and Doebling 1997).

Current damage detection methods applied to large civil engineering structures, like bridges, are either visual or local non-destructive evaluation (NDE) methods (Biswas et al. 1990). Visual inspections rely heavily on the inspector's experience and knowledge, which have been shown to be highly unreliable (FHWA 2001). The local NDE methods can be applied to only small areas at a time. In practice, for assessing a larger system,

the local techniques require that the vicinity of the possible damage is known ahead of time and that the components under inspection are accessible. Subjected to these limitations, use of the local methods alone usually can only detect damage on or near the surface of a large structure and the inspection could be costly and time consuming (Wegner et al. 2004). Although the local NDE methods are generally capable of detecting damage with higher accuracy compared with other methods, and are capable of quantifying the extent of damage, no detailed review and discussion will be provided here due to the limitations of the methods stated above. This research focused on the global damage detection approach, specifically vibration-based damage detection (VBDD) methods.

VBDD methods have received considerable attention in the literature. The basic idea for these methods is that damage to a structure will modify its global dynamic characteristics (notably natural frequencies and mode shapes). In theory, since these dynamic characteristics are readily quantifiable and can be related directly to specific physical properties of the structure, any measurable changes over time may be used to detect, locate and possibly quantify damage at an early stage before visible signs of distress are apparent. There are numerous VBDD methods proposed in the literature which will be reviewed in detail in Section 2.5.

Rytter (1993) classified the damage detection methods into the following four categories:

- Level 1: Determination of the presence of damage in a structure;
- Level 2: Determination of the location of damage in the structure, in addition to Level 1;
- Level 3: Quantification of the severity of the damage, in addition to Level 1 and 2; and
- Level 4: Prediction of the remaining service life of the structure, in addition to Level 1, 2, and 3.

The ultimate goal of structural health monitoring is that a set of damage detection procedures is developed that is able to detect the presence of damage at a very early stage, locate the damage within acceptable resolution, estimate the severity of the damage, and predict the remaining useful life of the structure (Doebling et al. 1996). However, only Level 1 and Level 2 methods (i.e., determination of the presence and location of damage) will be investigated in this research.

The application of VBDD methods is very broad and has experienced a degree of success in some areas, such as when applied to simple structural members (e.g Rizos et al. 1990, Stubbs and Osegueda 1990b, Fox 1992, Fritzen et al. 1995, Stubbs et al. 1990, Doebling et al. 1993a and 1993b), to shells and frames (e.g. Friswell et al. 1994, Nwosu et al. 1995, Saitoh and Takei 1996), to aerospace structures (e.g., Hunt et al. 1990, Grygier 1994, Doebling 1995), to offshore platforms (e.g., Yang, et al. 1984, Swamidas and Chen 1992), to rotating machinery (e.g., Roth and Pandit 1999), to bridges (e.g. Biswas et al. 1990, Stubbs et al. 1995, Farrar and Jauregui 1998a and 1998b), and to other civil engineering structures (e.g. Salawu 1994, Skjaerbaek et al. 1996). However, this research only focused on the application VBDD methods to bridges. A summary of the literature on this application is provided in Section 2.6.

2.3 Dynamic Tests

2.3.1 Overview

One of the major topics of this research is vibration-based damage detection. The success of the application of VBDD methods depends strongly on the quality of the measured dynamic properties of the structure investigated. A set of proper dynamic testing procedures is essential for the reliable estimation of the properties of the system. To make a system vibrate with a certain energy level, and to keep it vibrating, the system must be excited using external forces, which may include random environmental excitation and forced excitation. To effectively collect and record the vibration response in order to infer the modal properties of the system, a set of sensors is necessary for the dynamic tests. In addition, uncertainties inherent in the test procedures lead to

variability, to some extent, in the measured modal properties between different test trials. As a result, issues related to dynamic testing are addressed in this section.

2.3.2 Dynamic excitation

Excitation methods include the two general categories of ambient excitation (such as traffic loading and wind loading) and forced excitation. Forced excitation may be achieved by using a shaker (Biswas et al. 1990, Peeters and de Roeck 2000), impact hammer (Samman and Biswas 1994), and drop weights (Peeters and de Roeck 2000).

From the literature review, it was found that random excitation appeared to be less reliable for VBDD than harmonic loading (Zhou et al. 2005). Also, one advantage of the forced vibration test is that the input force is typically strong enough to dominate other noise disturbances, resulting in a strong signal to noise ratio, so that more reliable measurements can be expected (Sohn et al. 2003). However, for online, real-time SHM, the use of ambient excitation provides an attractive means of exciting field bridges since the ambient traffic excitation is the most readily available source in field bridge vibration tests. As a result, ambient excitation must be explored fully, as well as forced excitation. Furthermore, it was found that the ambient vibration data provided adequate estimates of the modal frequencies and modal damping ratios (Farrar and Cone 1995). Similar conclusions were presented by Peeters and de Roeck (2000), who also found that ambient excitation gave comparable results with much less cost. As a result, both white noise random excitation and forced harmonic excitation were adopted and investigated in this research.

2.3.3 Sensors

Accelerometers, strain gauges, anemometers, temperature sensors, and displacement transducers were among the types of instrumentation cited in the literature. Anemometers and temperature sensors were used to quantify the environmental conditions, which is important for distinguishing the environmental influence on structural dynamic properties. Strain gauges were employed in cable-supported bridges

to monitor the vertical bending, horizontal bending, torsion, vertical shear force, and longitudinal compression forces (Ko et al. 1999).

In the laboratory, both accelerometers and strain gauges have been found to be capable of generating data that can be used for VBDD purposes, although higher amplitude forced vibrations are required to generate strain signals with sufficient magnitudes. In addition, the bending curvature, which can be used for damage identification, can be directly collected by bonding strain gauges to girder webs in vertically aligned groups (Zhou et al. 2003). As a result, the more economically attractive strain gauges should be investigated fully, as well as accelerometers (Wegner et al. 2004). Also, it has been found that the number and configuration of sensors significantly influence the accuracy of damage detection (Siddique et al. 2005).

2.3.4 Noise and uncertainty in dynamic tests

Ideally, two independent measurements of modal properties for a structure in the same health state (or condition) would result in identical measured results. However, practically, the measured modal properties obtained from different data sets in the same health state always experienced variability due to the uncertainties inherent in the test procedures. The uncertainties may be due to random noise, errors in sensor readings, and disturbances of the input data during the data processing. Therefore, it is necessary to investigate the influence of uncertainties on the performance of VBDD methods and to evaluate the reliability of the measured modal properties in a statistical manner. There were some investigations and statements related to the uncertainty issue available in the literature.

Kim and Stubbs (1995) investigated the influence of uncertainties in measured modal properties on the performance of vibration-based damage detection applied to a plate girder model. The uncertainties considered in this research included different FE models used to approximate the response of the plate girder, different estimation methods used to calculate the stiffness parameters, and different methods used in the definition of mode shapes. It was concluded that the uncertainties in measured modal

properties, especially the uncertainty in mode shape definition, had a great influence on the accuracy of damage detection.

Alampalli et al. (1997) investigated the feasibility of using measured modal properties to detect damage on a one-sixth scale steel-girder bridge model, as well as on a field bridge. This research evaluated the influence of the uncertainty in the measured modal properties on damage detection based on the calculated statistical parameters of the modal properties. The damage detection methods used in this research included change in natural frequencies, change in modal amplitudes, and change in Modal Assurance Criterion (MAC) and Coordinate Modal Assurance Criterion (COMAC) values. It was concluded that the damage indicators were not sensitive enough to detect the damage when uncertainties (or random variation) were considered in the process.

Farrar and Doebling (1997), and Kirkegaard and Andersen (1998), stated in their literature reviews that using statistical information of the measured modal properties is a key issue for successful application of VBDD methods to civil engineering structures; however, at that time, there was very little research investigating the application of VBDD methods in a statistical manner.

Doebling et al. (1997) investigated the influence of the uncertainty of measured modal properties on the performance of damage detection on a bridge structure excited by impact forces. Monte Carlo simulations applied to the Frequency Response Function (FRF) were used to calculate the uncertainties of the measured natural frequencies, modes shapes and mode shape curvatures. It was concluded that, to detect the damage using the VBDD methods, the measured modal properties had to experience some changes, and the changes had to be statistically significant.

Doebling and Farrar (1998) investigated the application of VBDD methods on the I-40 Bridge, located in New Mexico, in a statistical manner. The researchers assumed that the calculated modal properties of the FRF data followed a normal probability distribution. In this manner, the statistical significance of changes in damage detection indicators was evaluated. It was concluded that the changes in both modal properties

and damage indicators were statistically significant, which means that the damage could be detected with a certain statistical confidence level.

2.4 Signal Processing and Modal Analysis

2.4.1 Overview

The performance of VBDD methods directly depends on the accuracy of measured modal properties of structures investigated. It is essential to obtain reliable modal properties since small-scale damage has been found to cause very small changes to mode shapes and natural frequencies (Zhou et al. 2005, 2007). There are two general steps required to reach this goal. The first step is to accurately acquire the dynamic response through suitable vibration test protocols, as discussed in Section 2.3. The second step is to process the collected vibration data to extract reliable modal properties through suitable signal pre-processing techniques and post-processing modal analysis methods.

Due to the imperfections inherent in practical dynamic testing systems, there are unavoidable linear trends and/or noise combined into the actual response data. Also, it is impossible to record data with absolute continuity in an infinitely long sampling period, no matter how advanced the system is. To minimize the influence of these factors on the measured modal properties, it is necessary to perform pre-processing on the recorded data. Pre-processing techniques include functions to remove the initial average baseline and linear trends, low-pass filters to reduce random noise, and window functions to minimize the "leakage" of signals (Maia and Silva 1997).

Modal analysis is a post-processing method that extracts the modal properties of a structure (i.e., natural frequencies, mode shapes, and damping ratios) through processing of the recorded dynamic response of the structure (Ewins 2000). Traditional modal analysis methods require both input (excitation forces) and output (vibration response) information to estimate the modal properties of a structure; however, it is often difficult, costly, and sometimes impossible to measure the excitation (input) information of a real structure (like a bridge). As a result, most modal analysis methods used in civil

structural health monitoring are "output-only" methods, which assume the excitation force to be white noise with a uniform spectrum in the frequency range of interest (James et al. 1995, Peeters and De Roeck 2001). Generally, modal analysis methods can be classified as frequency domain methods and time domain methods, depending on whether frequency transform functions are used for the analysis (Maia and Silva 1997).

2.4.2 Frequency domain modal analysis methods

Frequency domain methods are modal analysis methods which extract the modal properties based on the frequency response spectra obtained by transforming the signals measured in the time domain. The most commonly used transform function is the Fast Fourier Transform (FFT), which is an algorithm for computing the Discrete Fourier Transform (DFT), a special Fourier Transform (FT) for discrete signals recorded through a data acquisition system. The FFT is able to quickly transform data from the time domain to the frequency domain using the periodicities of sinusoidal functions. In this way, the FFT can analyze large amounts of waveform samples in much less time, compared with the traditional Fourier transform process (Ramirez 1985).

Some commonly cited frequency domain methods in the literature included the Peak Picking (PP) Method (Bendat and Piersol 1993), the Cross-Power Spectrum (CPS) (James et al. 1995, Herman and Van Der Auweraer 1999, Farrar et al. 2000), Averaged Normalized Power Spectral Densities (ANPSD) (Felber 1993), and Complex Mode Indication Function (CMIF) methods (Shih et al. 1988, Brickner et al. 2000). Among the methods, the Pick Picking (PP) method is the most widely used modal analysis method in civil engineering, due mainly to the fact that it is the most simple and straightforward method in both concept and practice. The PP method can be used to identify the natural frequencies of a structure by picking the peaks in the response spectra of the structure investigated. A detailed discussion of this method is presented in the following paragraphs.

The dynamic response of a structure to an excitation force depends on both the characteristics of the excitation force (mainly its amplitudes and frequency content) and the inherent properties of the structure (mainly the distribution of its mass and stiffness).

For a single degree of freedom system, the displacement response spectrum of the system, $X(\omega)$, can be defined as (Clough and Penzien 1975, 2003)

$$X(\omega) = H(\omega) \cdot P(\omega) \qquad [2.1]$$

where ω is the frequency of the excitation force, $H(\omega)$ is the complex dynamic amplification factor of the system, and $P(\omega)$ is the Fourier transform (FT) of the excitation force. The well-known magnitude of the amplification factor is defined as

$$|H(\omega)| = \frac{1}{\sqrt{\left[1-\left(\frac{\omega}{\omega_0}\right)^2\right]^2+\left[2\zeta\left(\frac{\omega}{\omega_0}\right)\right]^2}} \qquad [2.2]$$

where ω, ω_0, and ζ are the frequency of the excitation force, the natural frequency of the system, and the damping ratio of system (i.e., the ratio of damping coefficient to the critical damping of the system; a dimensionless measure describing how oscillations in a system decay after a disturbance), respectively. The dynamic amplification factor $H(\omega)$ for different damping ratios is plotted in the Figure 2.1. It can be seen from this figure that the amplification factor reaches a peak when the frequency of the excitation force is close to the natural frequency of the system, which is referred to as resonance; the amplification factor becomes especially large for lower damping cases. For structures in civil engineering, damping ratios usually vary from 0.5% to 2%, depending on the material and connection types used in the system. As a result, at the peak in the magnification function, the difference between the natural frequency and the excitation frequency is less than 1%. In this manner, the frequency at the peak location in the plot of the displacement response spectrum of the system, $X(\omega)$, can be referred to as the damped natural frequency (very close to the un-damped natural frequency for civil engineering structures), as long as the excitation force approximates white noise with a flat spectrum (i.e., a force with equal energy content at all frequencies in the frequency range of interest).

A similar situation exists for multiple degree of freedom systems, for which there are multiple peaks in the Frequency Response Function (FRF) (one peak for each degree of freedom (DOF); i.e., there is one possible mode for each DOF). As a result, the PP

method can be used to identify the natural frequencies by picking the peaks in the FRF diagram. Once the natural frequencies are identified, the relative modal amplitudes at various measurement locations can be determined to calculate the mode shapes of the system (Bendat and Piersol 1993).

In practice, however, the excitation forces are difficult to quantify, especially for random excitation from traffic and wind. This means that the excitation forces are unknown and have to be assumed to be random white noise input to use the PP method. In this way, the PP method would experience difficulties in distinguishing peaks that represent natural frequencies from those due to persistent harmonics in the excitation and noise (Paultre et al. 1995, Farrar and James 1997). In addition, it is difficult to identify modes with frequencies that are too close, which may be the case for complicated systems with both flexural and torsional modes. There are unavoidable uncertainties involved which will produce potential variations in measured modal properties when excitation forces are not pure white noise signals in this case.

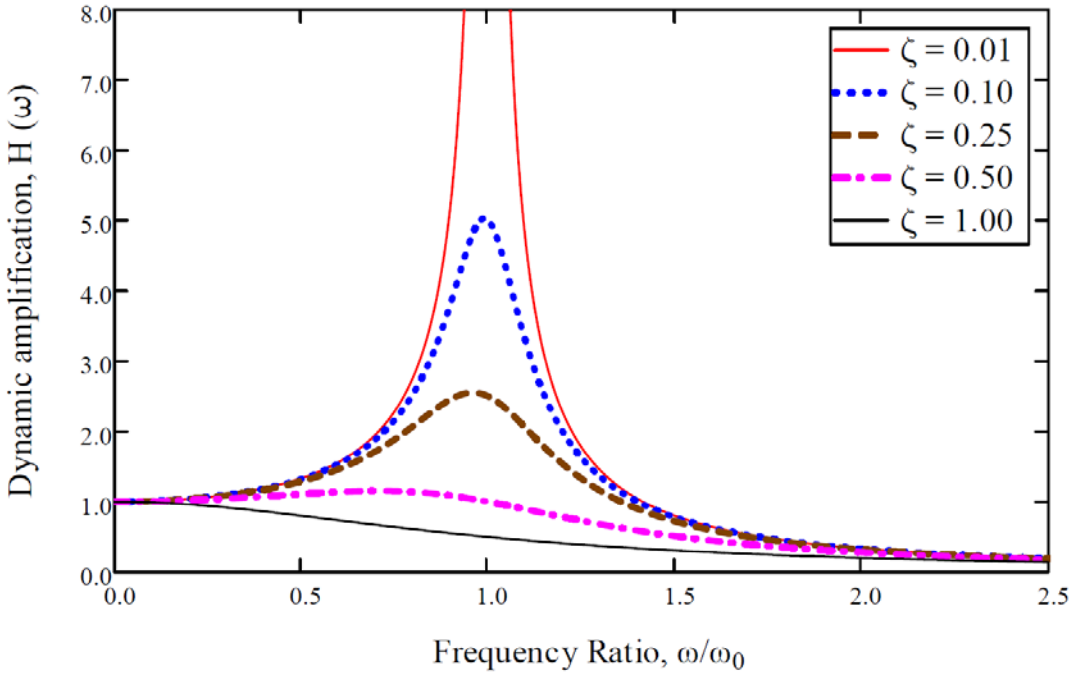

Figure 2.1. Variation of the dynamic amplification factor with the frequency ratio (ω/ω_0).

2.4.3 Time domain modal analysis methods

Time domain methods are modal analysis methods which can extract the modal properties directly from the recorded data in the time domain (i.e., no Fourier transform is required). Less commonly, time domain methods may use time history data which have been transformed from the measured (or recorded) frequency spectra using inverse Fourier transforms (Maia and Silva 1997).

Some commonly cited time domain methods in the literature include the Eigen Realisation Algorithm (ERA) method (Juang and Papa 1985), the Natural Excitation Technique (NExT) (James et al. 1992, 1995), the Stochastic Subspace Identification (SSI) method (Van Overschee and De Moor 1996, Peeters and De Roeck 2001), and some other methods based on the SSI method.

The Eigen Realisation Algorithm (ERA) method can be used to identify the modal properties of a structure through realizing the state-space system which is built based on the recorded vibration data. The state-space system is the representation of a physical system through a set of first-order differential equations with variables including input (measured or assumed excitation forces) and output (recorded displacement or acceleration response) information. The modal properties (eigenvalues and eigenvectors) are extracted from the realized state-space matrices by processing the equations in the time domain.

Stochastic Subspace Identification (SSI) is a time domain method which can extract the modal properties of a system by identifying a stochastic state-space model from a system with unknown ambient input excitation forces, and only available output measurements. The state model deals with linear vibration systems excited by a stochastic process (white noise), which makes the SSI method much faster and more robust than some nonlinear system-based methods like the Prediction Error Method (Ljung 1987), even though it is somewhat slower than the frequency domain-based PP method (Peeters and De Roeck 2001).

The dynamic behaviour of a structure with discrete masses connected through springs and dampers can be defined by the following second-order differential matrix equation:

$$M\ddot{U}(t) + C_2\dot{U}(t) + KU(t) = F(t) \quad [2.3]$$

where M, C_2, and K are the mass, damping and stiffness matrices, respectively; $U(t)$ is the displacement vector; $F(t)$ is the excitation force vector; and $\ddot{U}(t)$ and $\dot{U}(t)$ are the second and first derivatives, respectively, of the displacement with respect to continuous time. For a system with distributed or continuous mass, finite element methods can be used to discretize the system first, so that the same equation applies. Practically, to describe structures in civil engineering (like bridges), Equation 2.3 needs to be converted to a more suitable form to represent the discrete-time stochastic state model, which is based on the practical situation that only a few measurement points are usually selected (instead of measurements of all degrees of freedom), that the data are sampled at discrete time intervals, that no excitation forces are usually measured, and that there are measurement and process noise involved in the data.

Peeters and De Roeck (1998) converted Equation 2.3 into the following simplified forms:

$$x_{k+1} = Ax_k + w_k \quad [2.4a]$$

$$y_k = Cx_k + v_k \quad [2.4b]$$

where A is the state matrix which represents the dynamic properties of the system; C is the output matrix which refers to how system states are transformed to the output (response) of the system; x_k is the state vector with elements that independently describe the state of the system; y_k is the output vector at discrete time interval k; w_k and v_k are the process noise due to disturbances of input data and the measurement noise due to the inaccuracy of the data acquisition system, respectively. After the state-space model of the structure is established, the model properties of the system can be identified through an eigenvalue analysis.

2.5 VBDD Methods

2.5.1 Overview

Structural health monitoring (SHM) or condition assessments on structures (like bridges) are generally carried out by visual inspection at intervals of two or more years (Biswas et al. 1990). The visual inspections are highly subjective and rely heavily on the inspector's experience and knowledge, which makes the method unreliable if no other methods are used in combination at the same time (FHWA 2001). As a result, a large number of local non-destructive evaluation (NDE) methods have been developed and applied successfully to some simple and small structures (Kobayashi 1993, Uomoto 2000, Chong et al. 2001, Raj et al. 2002). The NDE methods are generally capable of assessing the condition of structures with relatively higher accuracy. However, the local NDE methods can only examine a small area at a time. In addition, the components to be inspected have to be accessible. As a result, the inspection of a large structure (like a complicated bridge) using the NDE methods alone could be costly and time consuming (Wegner et al. 2004). It is still important to look for other potential methods, like global methods.

Numerous VBDD methods, a set of global methods, have been proposed as potential forms of SHM, all related in some manner to changes in modal parameters (notably natural frequencies, damping, and mode shapes). The methods are able to evaluate the entire structure simultaneously using relatively few sensors. The basis for this approach is that damage to a structure will modify its global dynamic characteristics. In theory, since these dynamic characteristics are readily quantifiable and can be related directly to specific physical properties of the structure, any measurable changes over time may be used to detect, locate and possibly quantify damage at an early stage before visible signs of distress are apparent (Wolf and Richardson 1989). Detailed literature reviews of VBDD methods had been provided by Doebling et al. (1996, 1998) and Sohn et al. (2003). A summary of the reviews is presented in the following paragraphs.

Changes in natural frequency have been investigated and cited by many researchers (Loland and Dodds 1976, Cawley and Adams 1979, Doebling et at. 1996, Salawu 1997).

This method uses the changes in natural frequencies between two health states (or conditions) of a structure to infer the presence of possible damage on the structure. Theoretically, the stiffness of a structure decreases after damage occurs, which will induce some decrease in the measured natural frequencies. In this manner, the changes in the natural frequencies can be used to infer the presence of damage. Practically, however, changes in frequency have been proven not to be sensitive enough to detect small scale damage when considering the influence of temperature changes and other environmental conditions (Doebling et al. 1996).

There is some research reported in the literature related to the use of damping for damage assessment (Adams et al. 1975, Casas and Aparicio 1994, Salawu and Williams 1995, Kong et al. 1996, and Farrar and Jauregui 1998a), even though the amount of damping-related literature is much more limited than that related to frequencies and mode shapes. In general, it was found that the damage detection methods based on damping are unreliable and not sensitive to small-scale damage due to the fact that the accuracy of the measured damping from vibration tests is usually poor and there has not been a consistent relationship observed between the measured damping and the damage induced.

On the other hand, the VBDD methods based on mode shapes and their derivatives has received considerable attention. Some of these methods have been successfully applied to simple structures in the field, as well as some complex structures in simulation (Pandey et al. 1991, Fox 1992, Srinivasan and Kot 1992, Salawu and Williams 1994, and Zhang and Aktan 1995). There are several commonly cited VBDD methods based on mode shapes and their derivatives, including changes in mode shape, changes in mode shape curvature, changes in flexibility, changes in uniform flexibility curvature, and the damage index method. These five VBDD methods will be discussed in detail in the following sections. Also, the performance of the five VBDD methods on the multi-girder bridge superstructure addressed in this research was investigated in Chapter 6.

2.5.2 Change in mode shape method

The change in mode shape method, as an indicator of damage, simply uses the difference between the undamaged and damaged mode shapes. Due to its simplicity, the change in mode shape method has received a large amount attention and has been cited by many researchers (e.g., Mazurek and DeWolf 1990, Srinivasan and Kot 1992).

The method is defined as:

$$\Delta\boldsymbol{\phi} = \boldsymbol{\phi}^* - \boldsymbol{\phi} \qquad [2.5]$$

in which, for each individual vibration mode, $\boldsymbol{\phi}$ represents a normalized (or scaled) mode shape vector before damage; $\boldsymbol{\phi}^*$ is a normalized mode shape vector after damage; therefore, $\Delta\boldsymbol{\phi}$ represents the calculated change in mode shape vector.

The mode shapes, $\boldsymbol{\phi}^*$ and $\boldsymbol{\phi}$, must be normalized (or scaled) to a common basis to allow for meaningful comparisons due to the fact that the scale of mode shape amplitudes is arbitrary. Siddique et al. (2007) found that near optimal normalization for VBDD was achieved when mode shape vectors were scaled to have a unit norm, i.e., $\boldsymbol{\phi}^T\boldsymbol{\phi} = 1$. Various mode shape normalization schemes, and their effect on calculated mode shape changes, are discussed in Chapter 4.

Since damage to a structure is expected to cause a localized decrease in stiffness, the greatest change in the mode shape amplitude is expected to occur at the location of damage. It should be mentioned that the change in mode shape method is able to detect and localize the damage on the structure. Practically, however, the method alone has difficulty in determining quantitatively whether or not damage is present. As a result, a new Level 1 damage indicator (i.e., one capable of identifying the presence, but not location, of damage) was developed based on the change in mode shape method. The detailed information about this is presented in Chapter 5.

2.5.3 Damage index method

Stubbs et al. (1995) derived the damage index method to detect damage on a structure. It is based on the change in the strain energy stored in a beam-like structure when it deforms in one of its mode shapes. The damage index β_{ij} for the ith mode at location j on the beam can be defined in continuous form as

$$\beta_{ij} = \frac{\left(\int_a^b \left[\phi_i^{"*}(x)\right]^2 dx + \int_0^L \left[\phi_i^{"*}(x)\right]^2 dx\right)}{\left(\int_a^b \left[\phi_i^{"}(x)\right]^2 dx + \int_0^L \left[\phi_i^{"}(x)\right]^2 dx\right)} \times \frac{\int_0^L \left[\phi_i^{"}(x)\right]^2 dx}{\int_0^L \left[\phi_i^{"*}(x)\right]^2 dx} \quad [2.6]$$

in which $\phi_i^{"}(x)$ and $\phi_i^{"*}(x)$ are the mode shape curvature functions of the ith mode for the undamaged and damaged states, respectively, as a function of distance x along the beam; L represents the length of the beam; and a and b represent the limits of the segment of the beam over which damage is being evaluated.

In discrete form, assuming that the spacing between measurement points in the mode shape vectors is uniform, the damage index can be rewritten as:

$$\beta_{ij} = \frac{\left(\phi_{ij}^{"*}\right)^2 + \sum_{k=1}^{n}\left(\phi_{ik}^{"*}\right)^2}{\left(\phi_{ij}^{"}\right)^2 + \sum_{k=1}^{n}\left(\phi_{ik}^{"}\right)^2} \times \frac{\sum_{k=1}^{n}\left(\phi_{ik}^{"}\right)^2}{\sum_{k=1}^{n}\left(\phi_{ik}^{"*}\right)^2} \quad [2.7]$$

in which n is the number of locations where modal curvature is calculated along the beam. Assuming that the set of damage indices for the beam forms a sample of a normally distributed population, a normalized damage indicator then can be defined as:

$$Z_j = (\beta_j - \mu)/\sigma \geq 2.0 \quad [2.8]$$

in which Z_j represents the normalized damage indicator; μ and σ represent the mean and standard deviation of damage indices, respectively, for all locations considered. Normalized damage indices falling two or more standard deviations from the mean are expected to be indicative of the presence of damage and a possible damage location.

2.5.4 Change in flexibility method

As developed by Pandey and Biswas (1994), the flexibility matrices for a structure in both undamaged and damaged states, for use in the change in flexibility method, can be estimated from several normalized vibration modes using the following definition:

$$\boldsymbol{F} = \sum_{i=1}^{n} \frac{1}{\omega_i{}^2} \{\phi_i\}\{\phi_i\}^T \quad [2.9a]$$

$$\boldsymbol{F}^* = \sum_{i=1}^{n} \frac{1}{\omega_i^{*2}} \{\phi_i{}^*\}\{\phi_i{}^*\}^T \quad [2.9b]$$

in which $\{\phi_i\}$ and $\{\phi_i{}^*\}$ are the ith normalized mode shape vectors for undamaged and damaged states, respectively, and ω_i and ω_i^* are the ith angular natural frequencies for undamaged and damaged states, respectively. The flexibility matrices, $\boldsymbol{F}$ and $\boldsymbol{F}^*$, are calculated approximately because only some of the lower vibration modes are used in the equation (in many cases, only the fundamental vibration mode is considered for this calculation). The change in flexibility is then defined as the difference between the flexibility matrices:

$$\Delta\boldsymbol{F} = \boldsymbol{F}^* - \boldsymbol{F} \quad [2.10]$$

in which $\Delta\boldsymbol{F}$ represents the change in flexibility of the structure considered. To identify the possible location of damage, the absolute maximum value of elements in column j of the matrix, $\Delta\boldsymbol{F}$, can be defined as:

$$\overline{\delta_j} = max\left(\left|\Delta F_{ij}\right|\right) \quad i = 1, \cdots, n \quad [2.11]$$

in which ΔF_{ij} represents the elements of the matrix $\Delta\boldsymbol{F}$; n represents the number of points where the mode shape is defined. The position corresponding to the largest value of $\overline{\delta_j}$ is considered to be the possible location of damage.

2.5.5 Change in uniform flexibility curvature method

The jth column of the flexibility matrix $\boldsymbol{F}$, calculated by Equation 2.9, corresponds to the deflected shape of the structure when an assumed unit load is applied at the jth

degree of freedom. As a result, the sum of all columns of the flexibility matrix represents the deflected shape, if an unit load is applied at each degree of freedom simultaneously, which is referred to as the uniform load flexibility. The change in uniform flexibility curvature was defined to detect the location of damage by Zhang and Aktan (1998) as follows:

$$\boldsymbol{\Delta f}'' = \left| \boldsymbol{f}''^{*} - \boldsymbol{f}'' \right| \qquad [2.12]$$

where $\boldsymbol{f}''$ and $\boldsymbol{f}''^{*}$ are the uniform flexibility curvature vectors before and after damage, respectively; $\boldsymbol{\Delta f}''$ is a vector containing the absolute value of elements (or components) of the change in uniform flexibility curvature (notes: all absolute signs used in this thesis denote the absolute value of elements instead of the norm of the vector). The elements of the uniform flexibility curvature vector $\boldsymbol{f}''$ can be calculated from the uniform load flexibility vector $\boldsymbol{f}$ using the central difference approximation as follows:

$$f_j'' = \frac{f_{j+1} - 2f_j + f_{j-1}}{h^2} \qquad [2.13]$$

in which h represents the distance between measurement points.

The following variation of Equation 2.12 was made in this study for a better separation of peaks in the plots of the change in uniform flexibility curvature:

$$\boldsymbol{\Delta f}'' = \left| \boldsymbol{f}''^{*} \right| - \left| \boldsymbol{f}'' \right| \qquad [2.14]$$

2.5.6 Change in mode shape curvature method

Damage to a beam-like structure will decrease the local flexural rigidity of that section as well as the global flexural stiffness of the beam. Since the curvature of a beam is proportional to the inverse of its flexural rigidity, theoretically, a localized reduction in rigidity caused by damage should produce an increase in curvature at that location. As a result, change in mode shape curvature (i.e., the second derivative of the mode shape with respect to position) could be a good indicator for damage detection, and especially

for damage localization if the presence of damage has been assumed or proven. Pandey et al. (1991) defined the change in mode shape curvature as:

$$\Delta\boldsymbol{\phi}^{"} = \left|\boldsymbol{\phi}^{"*} - \boldsymbol{\phi}^{"}\right| \quad [2.15]$$

in which $\boldsymbol{\phi}^{"}$ and $\boldsymbol{\phi}^{"*}$ are the mode shape curvature vectors before and after damage, respectively, for each specific vibration mode; $\Delta\boldsymbol{\phi}^{"}$ represents the absolute difference between the mode shape curvature before and after damage.

Alternatively, the following equation is used in this research for a better separation of peaks in the plot of change in mode shape curvature:

$$\Delta\boldsymbol{\phi}^{"} = \left|\boldsymbol{\phi}^{"*}\right| - \left|\boldsymbol{\phi}^{"}\right| \quad [2.16]$$

The mode shape curvature can be directly measured using a set of strain gauges (at least two) on the beam in a vertically aligned installation. In this study, 57 strain gauges (19 sets of 3 gauges each) were bonded to the girder webs in vertically aligned sets of three gauges to facilitate the determination of girder curvatures. Alternatively, the curvature of a mode shape can be calculated from the second derivative of the mode shape with respect to position. In discrete form, the curvature of the mode shape can be estimated numerically using a central difference approximation as:

$$\phi_j^{"} = \frac{\phi_{j+1} - 2\phi_j + \phi_{j-1}}{h^2} \quad [2.17]$$

in which ϕ_j is the mode shape amplitude at measurement point j (i.e., the jth element in the mode shape vector $\boldsymbol{\phi}$); h represents the distance between measurement points.

2.6 Application of VBDD Methods to Bridges

A large amount of research related to the application of VBDD methods to bridges has been presented since the 1980s. Doebling et al. (1996) provided a detailed literature review about the application. The following paragraphs in this section list a brief summary of the applications of the VBDD methods to bridges, which vary in the type of

bridge tested, excitation forces used, damage considered, and the VBDD methods implemented.

Salane et al. (1981) investigated vibration-based damage detection on a three-span highway bridge. The stiffness (directly related to the dynamic properties) of the bridge was extracted from the experimental test data collected during a fatigue test. Excitation forces were provided by an electro-hydraulic actuator. It was found that changes in bridge stiffness and mechanical impedance plots could be used as a good indicator of damage resulting from fatigue cracks.

Biswas et al. (1990) performed an investigation of VBDD on a two-span composite highway bridge. Excitation forces were supplied by a shaker. Damage was simulated by unfastening a set of bolts at a steel girder splice connection. Changes in frequency response functions (FRFs) were found to be detectable and quantifiable. The natural frequencies decreased consistently due to the incremental increase in damage, even though the reduction was small.

Mazurek and DeWolf (1990) performed laboratory vibration tests on a two-span aluminum plate-girder bridge model. Excitation was provided by a small scale vehicle model. Damage was simulated by support failure and progressive cracking of the bridge girder at mid-span. It was found that major structural deterioration can cause significant changes to both natural frequencies and mode shapes. It was also shown that changes in mode shapes can be used to locate the damage as long as the presence of the damage had been identified.

Farrar et al. (1994) conducted vibration tests on the I-40 bridge over the Rio Grande, located in Albuquerque, NM, to investigate the performance of several VBDD methods. The bridge consisted of a concrete deck supported by two steel plate girders (a so-called "fracture critical" design based on the fact that failure of either of the main girders is assumed to produce catastrophic failure of the bridge). Damage was introduced to the bridge by incrementally cutting through one of the main girders. The bridge was excited using both ambient excitation (automobile traffic on the adjacent bridge) and a hydraulic shaker. Accelerometers were used to measure the vibration response. In general, the

results indicated that natural frequency was not a sensitive indicator of damage. However, the mode shape-related damage indicators, including the damage index, the mode shape curvature, and change in flexibility, change in uniform flexibility curvature, were shown to be more sensitive to the damage induced.

Farrar and Cone (1995) presented further analysis of the I-40 bridge damage detection data described by Farrar et al. (1994). It was concluded that ambient excitation provided a good estimate for the extracted natural frequencies for SHM while the measured changes due to the damage in both natural frequencies and mode shapes were not large enough to detect the damage at an early stage.

Stubbs et al. (1995) applied the damage index method to the I-40 bridge data (the same bridge that was studied by Farrar and Cone 1995). The data was interpolated at 160 locations using a spline function before the application of the damage index method. It was concluded that the method could locate the damage with an error (or the difference between the actual and predicted damage location) of 2.5% of the span.

Wang et al. (1997) conducted an investigation of the damage index method on a scaled simple span bridge model supported by plate girders. Excitation for the dynamic tests was provided by an impact hammer applied at a fixed point. Damage was induced on the girder flanges. The lowest six mode shapes were extracted from the measured acceleration data. The normalized damage index was found to be sensitive to damage for severe damage cases.

Farrar and Jauregui (1998a, 1998b) investigated the performance of five damage detection methods on a three-span bridge, which consisted of a concrete deck supported by two steel plate girders, using both experimental and numerical data. The VBDD methods considered in this study included the damage index method, mode shape curvature method, change in flexibility method, change in uniform load surface curvature method, and change in stiffness method. Different severity levels of damage were introduced to the bridge to investigate the performance of the selected VBDD indicators. It was concluded that all methods could locate severe damage cases while

the performance of the methods varied for small scale damage cases. In general, the damage index method performed best in most cases.

Using dynamic tests, Stubbs et al. (1999) investigated the performance of the damage index method on a four lane highway bridge that crossed I-40. Both the natural frequencies and mode shapes for the five lowest modes were extracted through the data collected from the bridge in an already damaged state. A finite element (FE) model was developed, which was based on the information from as-built drawings of the bridge, to serve as a baseline (or pristine condition) reference. It was concluded that damage can be detected by comparing the mode shapes of the real structure and the FE model. The estimated damage locations using the damage index method showed a good correlation with the observed cracking patterns.

Pearson et al. (2001) conducted experimental dynamic tests on a quarter-scale simply supported concrete bridge deck supported by Tee beams. Accelerometers were used to collect the vibration data while excitation was provided by an instrumented hammer. Different severity levels of damage were considered on the bridge once the baseline dynamic properties of the model had been established in the intact condition. Cracks were induced by applying four point bending loads. It was found that changes in dynamic properties for higher modes (mode 3 and above) were more sensitive to damage than those for lower modes. It was also found that induced damage either produced an entirely new vibration mode or changed the order of vibration modes.

Huth et al. (2005) performed large scale dynamic tests on a prestressed concrete highway bridge to investigate the sensitivity of several damage detection methods using measured modal properties. Output-only modal identification methods were used in this research to extract modal properties. From the results of this research, it was found that a change in natural frequencies may not be a sensitive indicator since the changes of natural frequencies were minor even when severe cracks were introduced. A novel damage indictor, called the mode shape area index was developed and found to be a sensitive damage detection approach (it should be acknowledged that a similar VBDD damage indicator, called the area of mode shape change, has been developed in this

thesis prior to finding this reference. However, the work presented in this thesis was developed independently and was defined and applied in a different manner on a different application. A detailed comparison between two indicators is presented in Section 5.2.3).

Galvín and Domínguez (2007) conducted dynamic tests on the Barqueta Bridge, a cable stayed bridge deck over the Guadalquivir River in Seville, Spain. The bridge was excited using ambient traffic, and dynamic measurements were collected by accelerometers. There was no significant change observed for damage indices between two tests separated by an interval of one year; therefore, it was claimed that the structure had no damage induced during the period. Vibration tests on a simpler laboratory model showed that the damage index method could locate damage with an error of less than 3% of the span.

2.7 VBDD Research Conducted at the University of Saskatchewan

The research described in this thesis is part of a comprehensive program undertaken at the University of Saskatchewan to investigate issues relating to the practical application of VBDD methods to bridges. This comprehensive research program includes both well-controlled experimental studies and field tests with various environmental conditions, while both actual testing methods and numerical simulations were considered (Wegner et al. 2004). The topics investigated in this comprehensive program include the influence of sensor type and configuration on the performance of VBDD, the influence of excitation sources on the structural health monitoring, a comparison between different VBDD methods based on both experimental and simulated vibration data, the influence of temperature on the measured modal properties, and the influence of data processing (including normalization methods and interpolation methods) on the performance of VBDD on the specific structures investigated (Wegner et al. 2004). The following paragraphs list detailed descriptions and findings for the specific topics.

Zhou et al. (2004 and 2010) investigated the performance of five VBDD techniques on the damage detection of a full-scale pre-stressed concrete girder. The tests were

conducted under well-controlled laboratory environments. Damage cases considered included the removal of small blocks of concrete from the surface of the concrete girder. Both accelerometers and strain gauges were used to collect vibration response data. It was found that as few as six accelerometers located along the span of the girder were sufficient to detect and locate the damage, while only the fundamental mode shape was used for this purpose. The accuracy of the damage detection depended on the spacing of the sensors, the distance between sensors and the induced damage, and the location of the damage relative to the supports. It was also found that the change in mode shape method was the most reliable method to detect the damage.

Zhou et al. (2007) performed both numerical and experimental investigations on VBDD of a scaled bridge deck model featuring two steel girders supporting a steel-free concrete bridge deck, while the structure was simply supported. The performance of five selected VBDD methods was investigated to detect and localize small-scale damage on the deck. A small number of sensors including both accelerometers and strain gauges were adopted in the well controlled experimental tests. The fundamental mode shape alone was found to be sufficient to detect and locate the damage in this case, while higher modes tended to be less reliable. It was found that damage could be detected and localized using as few as five measurement points in the longitudinal direction of the bridge with reasonable accuracy. The paper also stated that it was difficult to detect the damage located near the supports.

Siddique et al. (2005, 2006, and 2007) performed both field tests and numerical studies on the application of VBDD methods to a two-span, multi-girder, integral abutment bridge in Saskatoon, Canada. From the field tests, it was found that the ambient temperature significantly influenced the measured natural frequencies. A calibrated FE model was used to evaluate the effect of sensor spacing, mode shape normalization, and uncertainty on the performance of several selected VBDD methods. It was stated that small-scale damage on the bridge deck could be detected and/or located if measurement points were located close enough to the location of the damage. It was also concluded that the reliability of the measured mode shapes could be improved by averaging the repeated trials.

Pham et al. (2007) performed both field vibration tests and numerical studies on a two-span integral abutment overpass, which was the same bridge investigated by Siddique et al. (2007), located in Saskatoon, Canada. This study focused on the influence of temperature variation on the dynamic properties of the overpass and the ability of VBDD methods to detect and localize simulated damage. It was concluded that the variation of ambient temperature affected the stiffness of the structure and therefore changed the measured natural frequencies and mode shapes significantly. It was shown that the natural frequencies for the three lowest modes increased when the temperature decreased. It was also found that the patterns of mode shape changes caused by small-scale damage were different from those due to temperature effects when a sufficient number of measurement points was used and the measurement points were located close to the simulated damage.

Alwash et al. (2005, 2006, and 2009) investigated several issues related to application of VBDD in the structural health monitoring of bridges, but primarily focused on the influence of the excitation sources on the performance of VBDD methods through both experimental and numerical studies. The research was conducted on a three span reinforced concrete bridge strengthened by the addition of external steel reinforcement in regions of high positive moment. It was found that the characteristics of the excitation sources had significant effects on the quality of modal properties extracted from the dynamic response of the bridge. From the calibrated numerical model, it was concluded that harmonic excitation, impact excitation, and free vibration after random excitation was discontinued were consistent enough to be used to detect the simulated damage. In the field tests, free vibration after the vehicle left the bridge generated the most reliable modal properties. It was also stated that noise had a significant influence on the performance of VBDD on bridges.

2.8 Summary

Numerous VBDD methods, a set of global methods, have been proposed as a potential form of SHM, all related in some manner to changes in modal parameters (notably natural frequencies, damping, and mode shapes). The methods are able to evaluate the

entire structure simultaneously using relatively few sensors. Although there were some successful applications of the proposed VBDD methods, great challenges are still apparent in the practical application of the methods to complicated structural systems like bridges. As a result, the primary objective of the current research was to investigate the application of VBDD methods to multi-girder bridge superstructures.

The performance of VBDD methods directly depends on the accuracy of measured modal properties of structures investigated. It is essential to obtain reliable modal properties since small-scale damage has been found to cause very small changes to mode shapes and natural frequencies. As a result, a part of this research was designed to investigate and quantify the influence of various test procedures on the reliability and repeatability of the measured dynamic properties of the multi-girder bridge superstructure through extensive dynamic tests.

From the literature review, it was found that the changes in natural frequencies have proven not to be sensitive enough to detect small scale damage practically, especially considering the experimental uncertainties like the influence of temperature changes and other environmental conditions. In general, the damage detection methods based on change in damping were found to be unreliable and not sensitive to small-scale damage due to the fact that the accuracy of the measured damping from vibration tests is usually poor and there is no consistent relationship between the measured damping and the damage induced. The methods based on mode shapes and their derivatives, on the other hand, appear to be a good source to seek a sensitive and effective damage indicator. However, most of the proposed methods based on mode shapes have not really answered the questions related to determining the presence of damage with a specific, statistically-based level of confidence, which is generally acknowledged to be the most effective approach for practical problems involving great uncertainties. This limitation may be partially due to the fact that the definition of the mode shape, as it is commonly performed, is not unique, making investigation of mode shapes in a statistical manner more difficult. As a result, a new Level 1 VBDD indicator (i.e., one capable of identifying the presence, but not location, of damage) was proposed in this research to fill this gap.

Ideally, two independent measurements of modal properties for a structure in the same health state (or condition) would result in identical measured results. However, uncertainties inherent in the test procedures lead to variability, to some extent, in the measured modal properties obtained from different data sets. The uncertainties may be due to random noise, errors in sensor readings, and disturbances of the input data during the data processing. Thus, a change in dynamic properties will be obtained even when the condition of the structure has not changed. As a result, for the practical application of the VBDD methods, it is necessary to define the resolution of the test procedures adopted. The target of this investigation was to find a test protocol which had the best resolution, thereby leading to the greatest likelihood of detecting the damage.

In addition, the performance of the newly developed VBDD method and the VBDD techniques commonly cited in the literature were investigated in this research on the multi-girder bridge superstructure.

CHAPTER 3. **EXPERIMENTAL PROGRAM**

3.1 Description of Bridge Model

The structure used for this investigation was a one-third scale model of a slab-on-girder composite bridge superstructure featuring four steel girders supporting a steel-free concrete deck (Fig. 3.1). Constructed in the Structural Laboratory, University of Saskatchewan, the model was based on a prototype bridge superstructure forming part of the North Perimeter Red River Bridge located in Winnipeg, Manitoba. Additional information for the prototype bridge is available in Appendix A. Information related to scaling factors utilized for the scaled model may be found in Appendix B, while information related to the fabrication process of the bridge model is available in Appendix C. The bridge model was constructed using the steel-free design techniques developed by Mufti et al. (1993). However, it should be acknowledged that the steel-free design concept was not investigated in this research.

Figure 3.1. Slab on girder bridge superstructure built at 1/3rd scale (with inset showing the girder splice).

Figure 3.2 shows the plan and cross-section view of the composite bridge model showing the structural components and general layout. The W410X39 girders (fabricated from CSA G40.21-350W with yielding strength of 350 MPa) had a simple span of 8 m and were spaced at 900 mm on centre, while the deck had a total length of 8.16 m (edge to edge), a width of 3.6 m, and a thickness of 75 mm at midspan that tapered to 100 mm over the girders. To provide the necessary lateral restraint for the steel-free concrete deck (fabricated with a design concrete strength of 30MPa; measured concrete strengths are provided in Appendix C) to develop internal arching forces, the top flanges of the girders were connected by steel straps spaced at 800 mm, located as shown in Fig. 3.3. Shear studs were also used to make the system composite, although no detailed design was conducted on the composite beams, and they were considered to

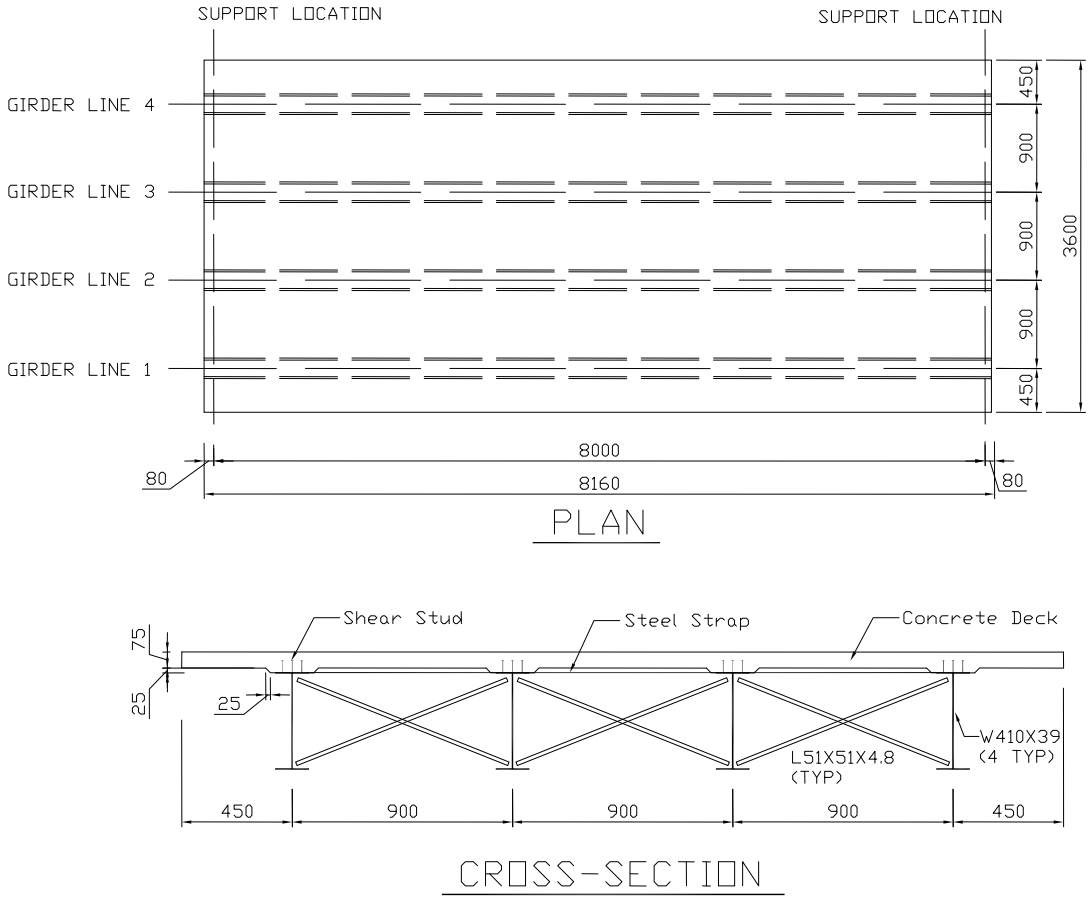

Figure 3.2. Plan and cross-section view of the composite bridge deck showing the structural components and general layout (dimensions in mm).

be partially rather than fully composite. Diaphragms composed of cross-braced structural angles were placed at 12 locations to enhance load sharing between girders and provide lateral stability (denoted as D-Xx.xYy.y on Fig. 3.3, where x.x and y.y refer to their longitudinal and transverse locations, in meters, relative to the origin shown).

To facilitate the subsequent introduction of well-defined and controlled damage states, a number of bolted member splices and end connections were incorporated into the model. First, a splice joint was introduced at the mid-span of Girder 4 (see the inset in Fig. 3.1) at the location shown in Fig. 3.3 (denoted as SP-X4.0Y2.7). Splice joints were also included at five locations on the steel straps (denoted as ST-Xx.xYy.y on Fig. 3.3, where x.x and y.y refer to their longitudinal and transverse locations, in meters, relative to the origin shown). Finally, all diaphragm angle members featured bolted end connections so that any one or combination of these members could be easily disconnected.

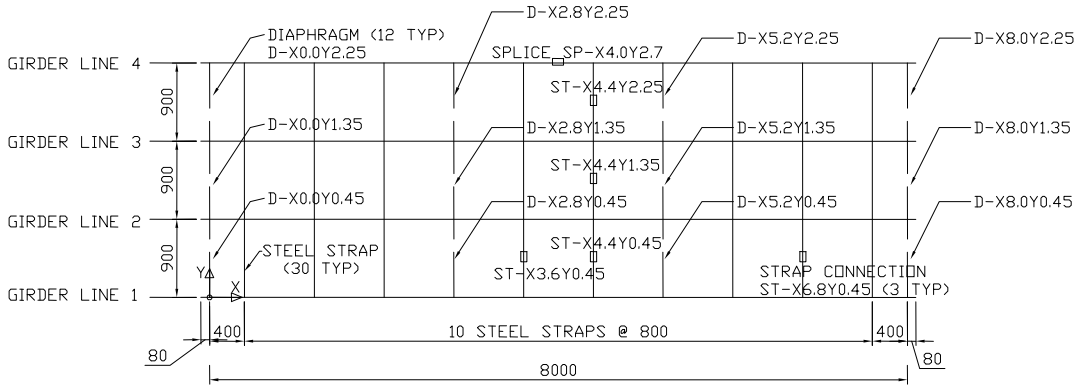

Figure 3.3. Plan view of the structural steel superstructure of the model showing splice, steel strap, and diaphragm locations (dimension in mm).

3.2 Measurement of Dynamic Properties

3.2.1 Overview

The basic principle of VBDD methods is that changes in dynamic properties over time allow one to infer the nature of damage in a structure. However, the changes tend to be

relatively small when the damage is minor. Furthermore, the inherent uncertainties associated with the testing system reduce the repeatability of measured modal properties. As a result, reliable estimates of these dynamic properties are essential for a successful implementation of VBDD schemes.

Measurement of the modal properties of the multi-girder bridge superstructure was carried out in two phases (see Table 3.1). In Phase I, the influence of various test parameters on the repeatability and reliability of modal property extraction was investigated using the intact bridge model (i.e., Health State 1, see Section 3.4). More specifically, the test parameters that were considered in the intact bridge model tests included sampling rates, the length of the recording period, excitation methods, sensor type, and sensor locations (i.e., the vertical locations of strain gauges on the steel web). Four different sampling rates were used in this investigation: 200, 500, 800, and 1000 Hz (or samples per second). To study the benefits of averaging on the reliability of the extracted modal parameters, data recording periods of 10, 20, 40, 80, and 160 seconds were considered. Two different forms of excitation, provided by a hydraulic shaker, were employed: harmonic and random (white noise) forcing. For the tests conducted in this phase, only seven accelerometer and 15 strain gauges locations (5 sets of 3 gauges each) along Girder Line 1 were monitored to measure vertical vibration. A detailed discussion of the results of this study is presented in Chapter 4.

In Phase II of the measurement, extensive dynamic tests were conducted on 17 Health States (see Section 3.4) of the bridge superstructure when various specific test protocols (see Section 3.5) were followed. The purposes of the tests were to define the damage detection resolution of 28 different test protocols and to investigate the application of VBDD techniques on the multi-girder bridge superstructure under various health conditions. For the tests conducted in this phase, 28 accelerometer locations and 57 strain gauges (19 sets of 3 gauges each) over the four girder lines were used to record the vibration signals (see Section 3.2.2). Analyses of measurement results collected in this phase were carried out in two stages. Initially, the data were used to establish the resolution of each test protocol, defined as the threshold value of the damage indicator above which a change could be considered statistically significant, given the level of

Table 3.1. The summary of the test program.

Phase	Description
Phase I	Purpose: • To investigate the influence of various test parameters on the measurement reliability of the dynamic properties. Test parameters investigated: • Sampling rate; • Length of the recording period; • Excitation method; • Sensor type; • Vertical location of strain gauge on the steel web. Instrumentation and measurement points used: • Seven accelerometer locations using one setup along Girder line 1; • 15 strain gauges (5 sets of 3 gauges each) installed on Girder 1. Excitation: • A set of preliminary vibration tests was excited by a hydraulic frame shaker; • Both white noise random and harmonic excitation were applied by another hydraulic shaker. Health condition investigated: • Only the intact bridge model (Health State 1, see Section 3.4).
Phase II	Purpose: • To define the damage detection resolutions of different test protocols; • To investigate the application of VBDD techniques on the multi-girder bridge superstructure. Test protocols investigated (28 in total, see Section 3.5): • Four instrumentation schemes; • Two forced excitation methods; and • Five different modes. Instrumentation and measurement points used: • 28 accelerometer locations using 5 setups • 57 strain gauges (19 sets of 3 gauges each) Excitation: • Both white noise random and harmonic excitation were applied by the hydraulic shaker. Health condition investigated: • 17 Health States (see Section 3.4).

uncertainty associated with that protocol. Subsequently, the performance of selected VBDD indicators was investigated on the bridge superstructure under the 17 Health States. A detailed discussion of the results for this phase is presented in Chapter 6.

3.2.2 Instrumentation

3.2.2.1 Overview

Instrumentation used to measure the dynamic response included a closely-spaced grid of accelerometers mounted on the surface of the deck along the girder lines, as well as electrical-resistance foil strain gauges bonded to the girder webs.

3.2.2.2 Accelerometers

In this study, seven accelerometers (EpiSensor FBA ES-U, manufactured by Kinemetrics Inc., California, USA) were used. With a maximum measurement range of 0-4 g and response bandwidth from DC to 200 Hz, the low-noise force-balance uniaxial accelerometers are ideal for civil engineering applications, where the structural response is generally of small magnitude and whose natural frequencies are usually below 50 Hz (Ward 1984, Levi 1997). For the vibration tests of this research, the accelerometers were configured for a maximum range of ±0.5g with a precision of 0.00025g. A typical accelerometer is shown in Fig. 3.4.

Different accelerometers may exhibit different levels of vibration response for a given input excitation. As a result, a set of preliminary tests was carried out to quantify the differences between the seven accelerometers and to find their corresponding calibration factors relative to each other. This was done by stacking the seven accelerometers one on top of the other into a channel-like device, and then attaching the device onto the bridge deck (see Fig. 3.5 for the setup).

To have efficient calibration measurements, the bridge system and the attached accelerometers were excited by the hydraulic shaker using harmonic loads with different frequencies. For example, the input frequencies of 12.70 and 34.56 Hz (the 1st and 3rd natural frequencies of the system, respectively, see Section 4.2.2 for the natural

Figure 3.4. EpiSensor FBA ES-U accelerometer.

Figure 3.5. Calibration of the EpiSensor FBA ES-U accelerometers for mode shape measurement.

frequencies of the system) were selected to excite the bridge to produce a resonant response. The measured mode shape amplitudes and resulting calibration factors for Mode 1 and Mode 3 are listed in Table 3.2, in which the values were averaged from results of 20 trials after the mode shape amplitudes were normalized to the reference channel (or Ch 2).

From the results shown in Table 3.2, it can seen that the mode shape amplitudes varied from 0.9955 to 1.0046 for Mode 1, and from 0.9998 to 1.0127 for Mode 3. Thus, the maximum relative differences in mode shape amplitude measurement between the seven channels were 0.93% and 1.27% for Mode 1 and Mode 3, respectively; these relatively small differences suggest that measurements from each accelerometer were close to identical.

To improve the repeatability of mode shape measurements, it may be useful to apply the corresponding calibration factors shown in Table 3.2 to the measurements of each channel. However, the calibration factors are different for different mode shapes, as shown in Table 3.2. For example, the calibration factors of Channel 7 were 1.0018 for Mode 1 and 0.9875 for Mode 3, which means that the readings of this channel need to be increased by 1.0018 for Mode 1, while needing to be decreased by 0.9875 for Mode 3. As result, not only the values, but also the trends for the calibration are different for different modes.

Table 3.2. The summary of accelerometer calibration factors from 20 trials.

	Mode 1		Mode 3	
Channels	Averaged mode	Calibration factor	Averaged mode	Calibration factor
Ch 1	0.9955	1.0046	1.0017	0.9983
Ch 2*	1.0000	1.0000	1.0000	1.0000
Ch 3	1.0048	0.9952	1.0028	0.9972
Ch 4	1.0020	0.9980	1.0034	0.9967
Ch 5	0.9976	1.0024	0.9998	1.0002
Ch 6	0.9984	1.0016	1.0034	0.9967
Ch 7	0.9982	1.0018	1.0127	0.9875

*: Reference channel.

Considering that the differences were small but unequal for each channel, and to simplify the process of measurement and data processing, no calibration factor was used in the subsequent studies. Alternatively, to reduce the uncertainties in the measurements conducted later, exactly the same layout of accelerometers was arranged for all tests in all 17 Health States (see Section 3.4) (i.e., each measurement location had the same accelerometer connected to the same data acquisition channel for all tests).

The plan locations of the accelerometers are indicated in Fig. 3.6. The vertical displacements (or accelerations) along the two support lines were assumed to be zero (i.e., no vertical movement occurred during the vibration tests) since the system was designed to be simply supported on two sides, although there may have been some small movement at those locations. As a result, no accelerometers were placed along support lines. Altogether, 31 accelerometer locations were used to record the vertical vibration of the bridge system. Due to the limited number of accelerometers available for the tests, five separate setups, each featuring seven accelerometers, were used to capture the response at all 31 locations, as described in Table 3.3. To permit normalization of all readings to a common basis (i.e., to glue the readings from different setups together), one stationary reference accelerometer (Ch2 or location N30) was included in all setups.

However, only 28 accelerometer locations (7 equally spaced locations along each of four girder lines) were actually used to extract the dynamic properties of the bridge

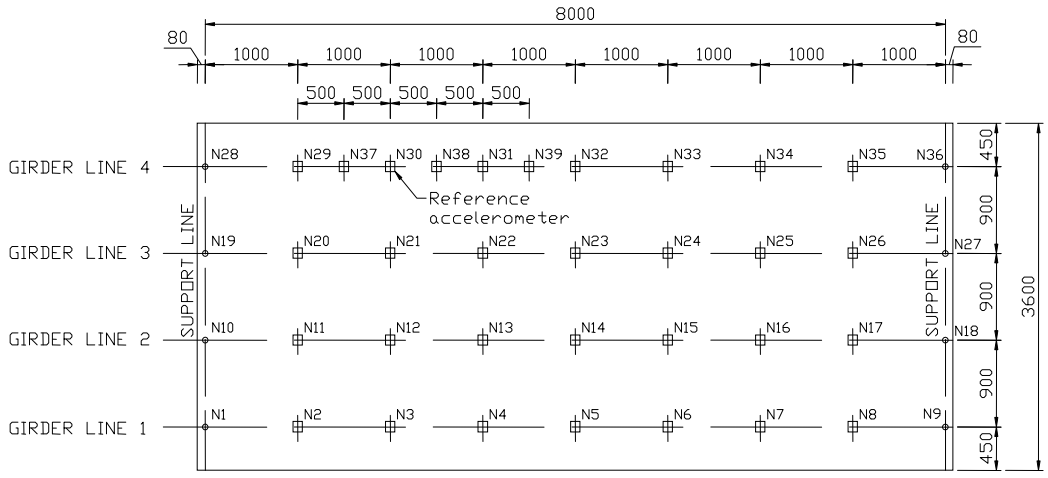

Figure 3.6. The locations of acceleration measurement points (dimensions in mm).

Table 3.3. The summary of setups of accelerometers with a common reference channel.

Channels	Set 1	Set 2	Set 3	Set 4	Set 5
Ch 1	N29	N20	N11	N2	N37†
Ch 2*	N30	N30	N30	N30	N30
Ch 3	N31	N22	N13	N4	N38†
Ch 4	N32	N23	N14	N5	N39†
Ch 5	N33	N24	N15	N6	N21
Ch 6	N34	N25	N16	N7	N12
Ch 7	N35	N26	N17	N8	N3

*: Reference channel.
†: These are extra measurement points which were not used in this thesis. However, the readings may be useful for future research.

system in this research. As shown in Table 3.3, three extra accelerometer measurement points were included along Girder Line 4 but not evaluated: N37, N38, and N39. These data may be useful for future research.

3.2.2.3 Strain gauges

The electrical-resistance foil strain gauges used in this study were 6 mm long with a resistance of 120 Ω. They were designed for strain measurement of common carbon steel, with a model number of KYOWA KFG-6-120-C1-11L3M3R (manufactured by KYOWA Electronic Instruments Co., LTD., Japan). Since the tests were conducted at room temperature (around 20 °C), it was not necessary to consider temperature drift (including gain drift and offset) in the strain gauge configuration. The original 3-wire lead-wire cable was 3 m long and vinyl-coated. The extension cables used were twisted-pair shielded cables of gauge AWG 18, which is heavier than usual wire gauge so that the lead-wire resistance was reduced, thus improving the strain gauge sensitivity. A quarter-bridge configuration was used to connect the strain gauge into the data acquisition system. When signal conditioning modules SCXI-1520 and SCXI-1121 were used to measure the strain (see Section 3.2.4), the system noise (or strain error) was ±40 με (or 0.1% of reading) for a single point value, or ±4 με for a 100-point averaged value. Since only the changes of strain readings were of interest for this

research, the small initial offset and drift of the strain readings were compensated for during the digital data processing (see Section 3.3).

In total, 57 strain gauges (19 sets of 3 gauges each) were bonded to the girder webs in vertically aligned sets of three gauges to facilitate the determination of girder curvatures. The plan locations of the groups of strain gauges are indicated in Fig. 3.7. There were no strain gauges installed at the mid-span of Girder 4 due to the fact that a splice was present at that location. Figure 3.8 shows a typical installation. In subsequent discussions, the three strain gauges at each instrumented girder web location are designated as the bottom, middle, and top strain gauges, which were located, respectively, at 65, 170, and 275 mm above the bottom of the bottom flange of the girders. This corresponds to distances of 313, 208, and 103 mm, respectively, below the estimated neutral axis, where the averaged neutral axis location was calculated from the strain gauge sets at all 19 locations, and extracted from dynamic test data. Figure 3.9 shows the typical setup of the strain gauges on the girder web (see Section 3.2.4 for data acquisition and Section 3.3 for data processing of strain data in detail).

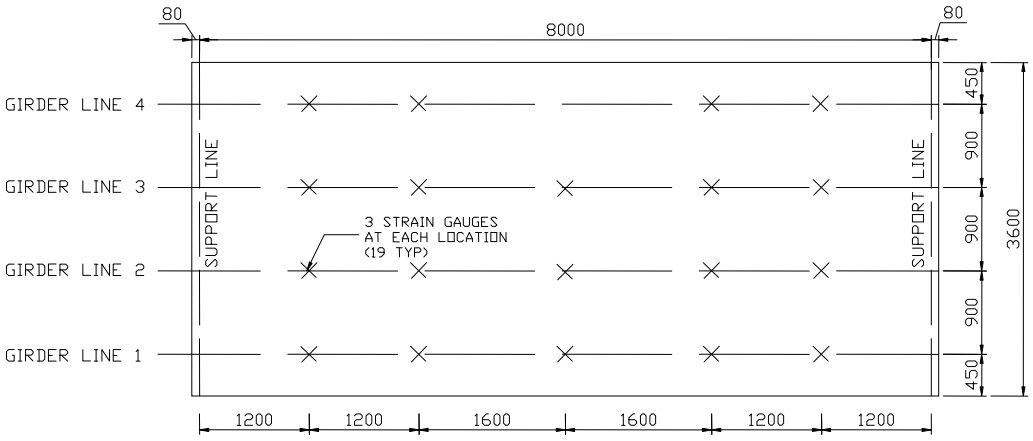

Figure 3.7. Plan view of bridge deck, showing the locations of strain gauge clusters (dimensions in mm).

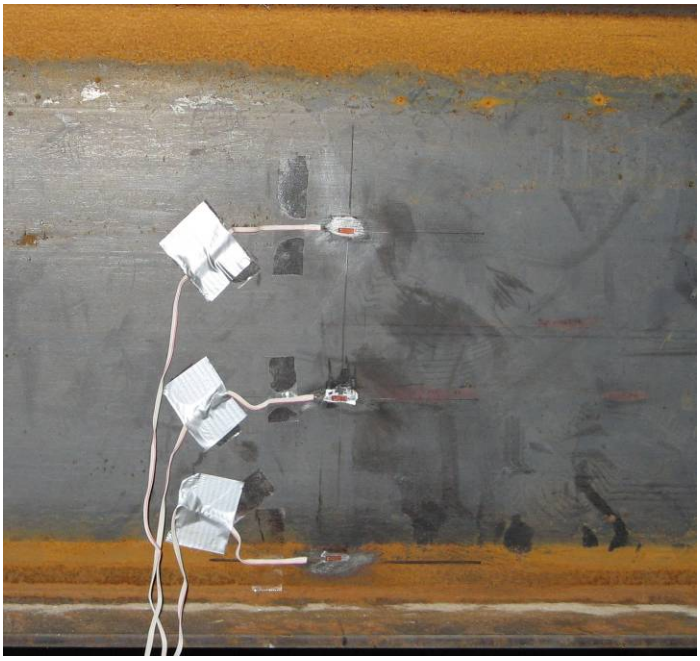

Figure 3.8. KYOWA KFG-6-120-C1-11L3M3R electronic strain gauges bonded on the girder web of the bridge deck.

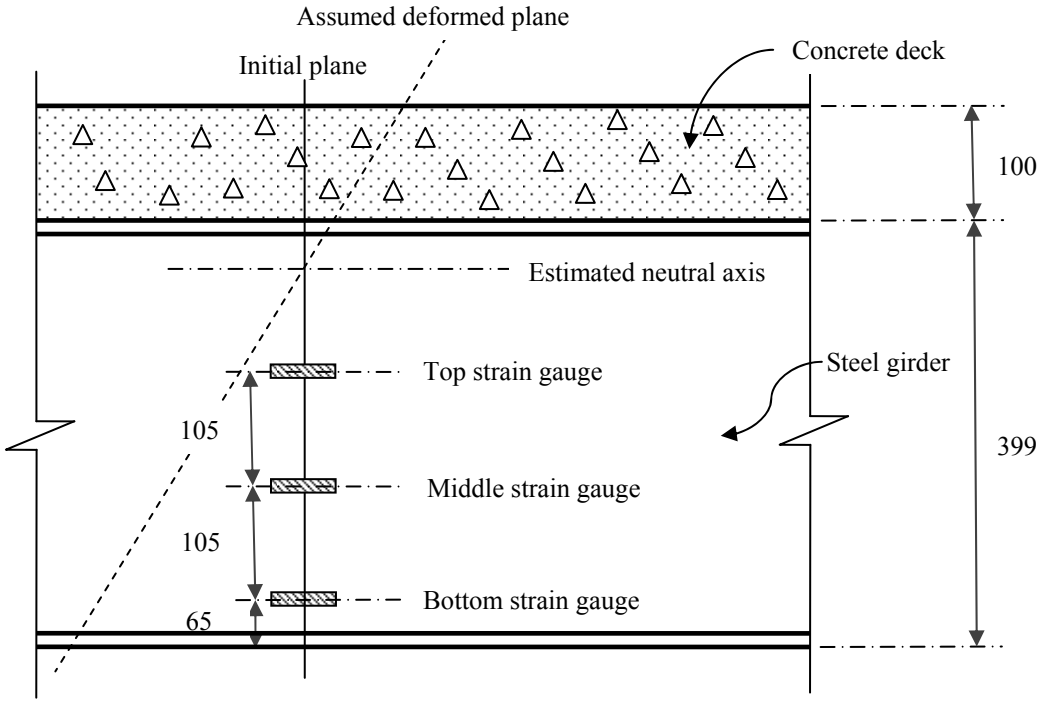

Figure 3.9. Setup of the strain gauge sets on the girder web (19 typical, dimensions in mm).

3.2.3 Excitation force

To accurately measure the dynamic properties of a bridge, the structure has to be excited to a certain level (depending on the sensitivity of sensors used). Although readily accessible for field vibration tests, traffic and other ambient loads, which are random in nature and difficult to quantify, introduce considerable uncertainty into the extracted modal properties of a bridge. Ambient environmental excitations in a laboratory have also proven to be unreliable sources for dynamic tests. Controlled excitations, on the other hand, appear to be more reliable for the extraction of modal properties, especially for VBDD applications (Wegner et al. 2004). As a result, controlled excitation forces were used in this research to excite the bridge model for dynamic tests.

Initially, a set of preliminary test was performed. For the preliminary tests, a hydraulic frame-mounted shaker was applied on the surface of the concrete deck to excite the bridge (see Fig. 3.10). The shaker consisted of a hydraulic cylinder mounted vertically on the frame, which was bolted down to the laboratory strong floor. The shaker was capable of exciting the bridge model to measure the dynamic properties with relatively high level of repeatability. However, the measured mode shapes were somewhat different from the expected results, which may have been due to the extra restraints applied at the contact points on the deck surface from the fixed frame. To accurately measure the modal properties of the system, the frame-mounted hydraulic shaker was abandoned for subsequent tests.

To fit the purpose of the dynamic tests, another hydraulic shaker was built based on a shaker available in the Mechanical Laboratory, University of Saskatchewan. The new shaker consisted of a hydraulic cylinder mounted vertically in the centre of a steel frame, with a steel plate of a selected mass (75 lb or 34.02 kg) supported at the bottom end of the cylinder (Fig. 3.11). The shaker was securely attached to the surface of the bridge deck using a bracket that was bolted to threaded inserts embedded in the concrete deck. The location of the shaker, along Girder Line 2 at a distance of 2.5 m from the left support, was chosen to permit excitation of the vibration modes of interest (the lowest five modes) after several preliminary tests were conducted at other locations.

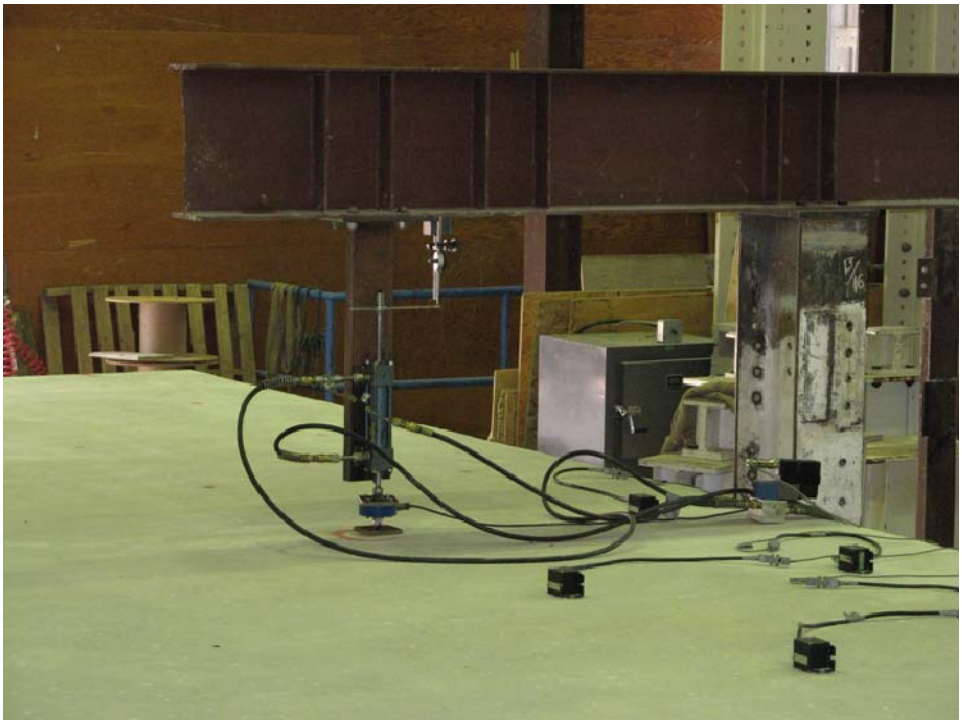

Figure 3.10. The hydraulic frame-mounted shaker used for preliminary tests.

Excitation forces applied in the experimental tests included both harmonic and white noise random vibration loads applied by the hydraulic shaker.

A hardware feedback-controlled signal for the shaker plate motion was generated using LabView™ 8.0 software installed on a laptop computer and monitored using a linear displacement transducer (LDT). The input signal for the shaker plate was controlled by a separate data acquisition system (or, more specifically for this application, a system controller), and consisting of a data acquisition PCMCIA card (model NI DAQ Card-6036E), SCXI-1000 data acquisition chassis, and several other modules from National Instruments™. This system was independent of the data acquisition system used for recording the accelerometer, strain gauge, and LDT readings (see details in Section 3.2.4). The reason for using two separate data acquisition systems (or, rather, a system controller and a data acquisition system) was that when only one system was used, the software feedback controller failed to control the shaker effectively and record the data simultaneously. As a result, a hardware feedback controller was developed to control

Figure 3.11. The hydraulic shaker used to excite both resonant harmonic and white noise noise random vibration in the experiments.

the fluid flow in a proportional directional valve, with a model number of KBSDG4V-5, (manufactured by Vickers, Incorporated, USA); the user's manual for the developed hardware controller is available in Appendix L. Thus, two separate data acquisition systems, one for input and another for output, were adopted in the tests.

To identify the natural frequencies of the system for each condition tested, white noise random signals were initially used to excite the bridge deck. In fact, the corresponding mode shapes were also extracted in this manner, but with relatively lower accuracy than the procedure described below. White noise random forces, a special random process, were adopted to excite the bridge partially due to their characteristic feature of having an approximately constant amplitude for all frequencies in the power spectrum density function. Based on random vibration theory, the displacement response power spectrum of a linear system is defined as the product of the power spectrum density function of the input and the frequency response function. Since the power spectrum density function of a white noise random signal is theoretically constant, the shape of the

displacement or acceleration response spectrum is the same as that of the system's frequency response function, with only the amplitude being different. In this manner, the natural frequencies of the system can be identified with a high degree of accuracy through measuring the displacement (or acceleration) response spectrum, with less influence of the excitation forces on the measured modal properties. This is especially important for the output-only identification method adopted in this research, for which it was assumed that the input forces were unknown, even though the input signals were recorded through the LDT readings. The LDT readings may be useful for future research.

After the natural frequencies had been identified, further testing using harmonic (or purely sinusoidal) excitation applied at each individual natural frequency was undertaken to accurately measure the corresponding mode shapes. Higher measurement accuracy was possible using this method because a resonant response, with a large constant amplitude vibration, occurred when the frequency of the harmonic excitation force coincided with one of the natural frequencies of the system.

3.2.4 Data acquisition

Data were acquired using a data acquisition system consisting of a 12-bit NI PCI-6024E data acquisition card and a model SCXI-1001 data acquisition chassis from National Instruments™, along with 12 signal conditioning modules (one SCXI-1120, four SCXI-1520, and seven SCXI-1121) used to acquire and modulate the sensor signals from both accelerometers and strain gauges (see Fig. 3.12 for the setup of the data acquisition system).

The 12-bit resolution means that the range of the measured signal could be divided into 2^{12} segments, for a resolution of 1 in 4096. The data acquisition card had built-in 16 channels (in a single-ended configuration) or 8 channels (in the differential configuration). However, actually, no built-in internal channels of the card were used to collect any data. The NI PCI-6024E card was only treated as an analog-to-digital converter (ADC), which converted the analog signals from the twelve signal conditioning modules installed in the Chassis SCXI-1001. The ADC still had 12-bit

resolution and 200 kS/s sampling rates (i.e., a maximum sampling rate of 200,000 samples per second were guaranteed, although the actual sampling rate may be higher), which is sufficiently efficient to convert all samples with the rate of 65 kS/s (65 channels with the sampling rate 1000 Hz) from the twelve modules, so that no delay and cutoff happened.

The 12 signal conditioning modules consisted of one SCXI-1120 (featuring 8-channels with 333 kS/s maximum sampling rate and simultaneous scanning) for seven accelerometers and one LDT sensor, four SCXI-1520 (featuring 8-channels, 333 kS/s sampling rate and simultaneous scanning) for 32 strain gauges, and seven SCXI-1121 (featuring 4-channels, 333 kS/s, and simultaneous scanning) for 25 strain gauges (there were 3 channels left empty). Since all modules were built with the capability of sampling data simultaneously, with sampling architecture of Simultaneous Sample and Hold (SSH), they should not have experienced significant phase delay during data acquisition. For example, scanning the 8-channel module (using the maximum sampling rate of 333 kS/s) takes 24 microseconds, so that the maximum phase delay is 0.024 milliseconds, or 0.11 degrees for the first mode with a natural frequency of 12.7 Hz (scanning the 4-channel module produced less phase delay).

The 12-bit DAQ card, even though inferior to a 16-bit card, was capable of a relative accuracy (or theoretical resolution) of 2.441 millivolts for the nominal range of 10 (or ±5) volts, and still gave a sufficient resolution, capable of distinguishing small changes in the measured signal (for example, due to damage, if any was present).

Data processing theory required that the data sampling rate for data acquisition be at least twice the maximum frequency of interest. However, a higher sampling rate is required to better represent the dynamic signal with good resolution. To better understand the influence of the sampling rate on the reliability of measured modal properties (mainly mode shapes), four different sampling rates were investigated: 200, 500, 800, and 1000 Hz (or samples per second) in Phase I of the modal property measurement of the bridge superstructure. The results of this investigation are presented in Chapter 4.

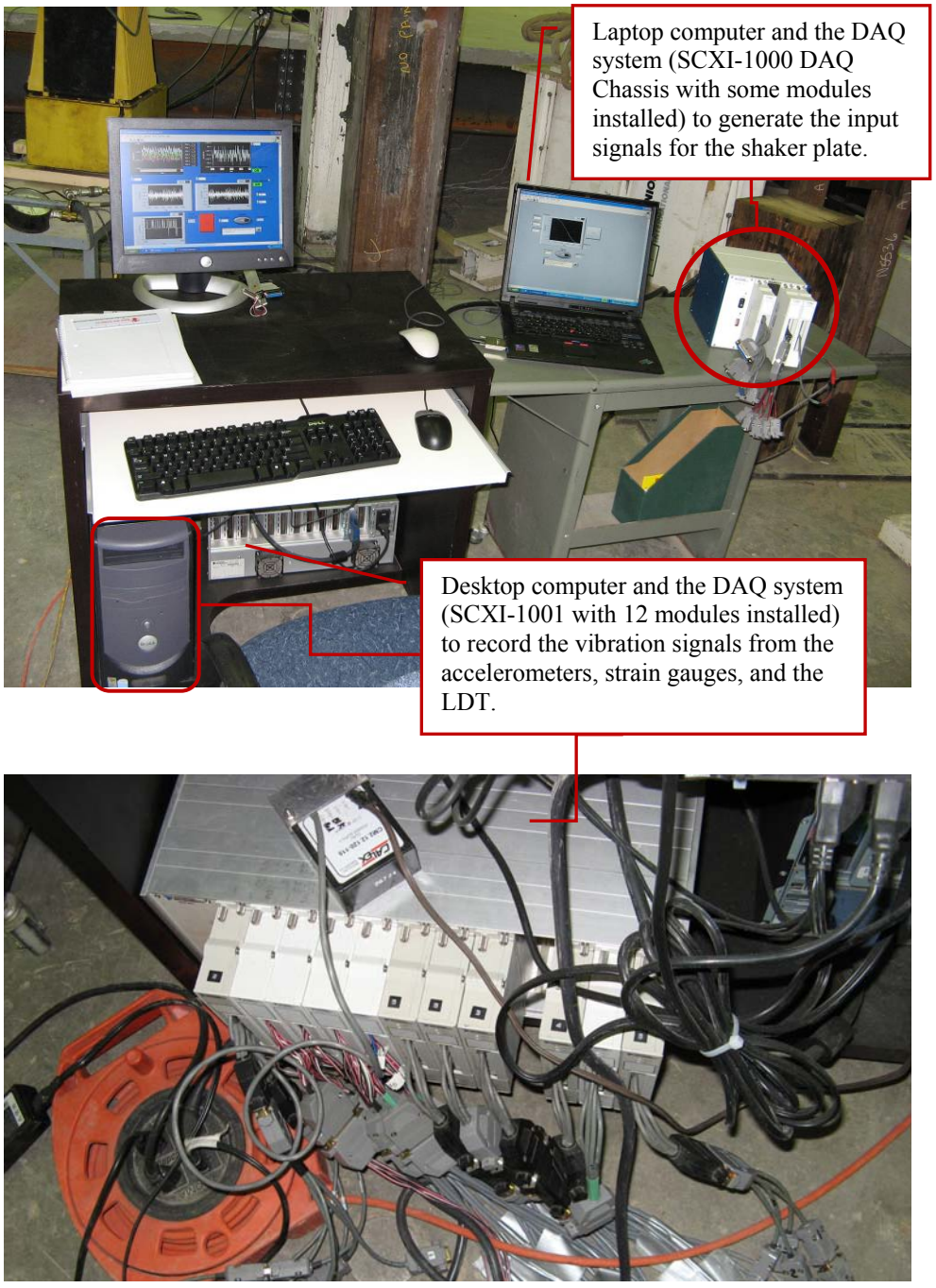

Figure 3.12. Data acquisition system.

The data acquisition system was controlled by LabView™ software installed on a personal computer. To identify the natural frequencies of the system for each condition tested, white noise random signals were initially used to excite the bridge deck, while data were acquired at 1000 samples per second. In this manner, the natural frequencies for the first five vibration modes of the undamaged model were found to be 12.70, 13.89, 34.56, 35.89, and 38.83 Hz. After the natural frequencies had been identified, further testing using harmonic excitation applied at each individual natural frequency was undertaken to accurately measure the corresponding mode shapes. For these tests, data were acquired at 500 samples per second. The lower sampling rate was used due to the lower uncertainty associated with harmonic excitation compared with white noise random excitation. A detailed explanation is available in Chapter 4.

For each health state investigated (as described in Section 3.4), the data for all 65 channels were continuously recorded in one file and instantaneously saved on the hard drive of the personal computer. A sampling period of 800 seconds of data was saved for each white noise excitation input, while 400 seconds of data were saved for each harmonic excitation input. In this manner, for each health state, five files were generated when white noise excitation was used, one file for each of the five separate setups for the accelerometers, as described in Section 3.2. Each file contained data for all vibration modes and was 580 Mega-bytes in size. Ten files were generated for each health state when harmonic excitation was used, five for the first mode (one per accelerometer setup), and five for the second mode. Each of these files was 145 Mega-bytes in size.

3.3 Data Processing

Data processing consisted of two steps, referred to here as data pre-processing and post-processing. Figure 3.13 shows a flow chart for data processing. Data were preprocessed by applying filtering, averaging, and windowing before the post processing to obtain modal properties.

In the first step, the data were separated into individual files for each sensor type (i.e., accelerometers, strain gauges, and LDT) and each 80 s segment of data. In this manner,

for each health state, twenty-five files for each of the three different sensor types were generated when harmonic excitation was used (five segments of 80 seconds for each of five accelerometer setups), while fifty files were generated when white noise excitation was used (ten segments of 80 seconds for each of five setups). Any combination of five files (one from each one of the five accelerometer setups) for acceleration was able to define one vibration mode (for harmonic excitation) or one set of multiple vibration modes (i.e., the 1st to the 5th mode, for white noise excitation). As a result, this process could produce 3125 (or 5^5) possible trials for vibration modes with harmonic excitation; while 10^5 possible trials were available for vibration modes with white noise excitation (these trials are only partially independent from each other). However, only five trials (i.e., the combinations of T_{11111}, T_{22222}, T_{33333}, T_{44444}, and T_{55555}, where s in T_{sssss} denotes the sequence of segments), which are totally independent from each other, were generated and used in the subsequent sections of this thesis for both harmonic (the 1st and 2nd mode) and white noise excitations (the 1st to the 5th mode). On the other hand, each file for strain gauges was able to define the vibration mode (or modes) of the whole bridge model by itself. Therefore, twenty-five trials were available for definition of mode shapes when harmonic inputs were used, while fifty trials were available to define the mode shapes when white noise excitation was used. It should be noted that the process of file separation experienced some challenges due to the extremely large size files (up to 580 Mega-bytes per file). A LabView subroutine was finally developed to perform the separation process by dynamically reading the original files, processing, and writing to separate files. This is similar to the way that LabView records data to files.

After the data were separated into individual files according to sensor types, a "detrend" subroutine available in Matlab (2004) was used to remove any average baseline offset (DC components) and linear trends from the recorded data by means of a linear regression process. A moving average low-pass filter, decimating the data by an order of 5, was adopted to filter the signals, resulting in a smoothed signal at a lower sampling rate. In this way, the inherent random noise was reduced through the moving average technique, which could increase the accuracy of the measured dynamic properties. The resulting effective sampling rates were 100 Hz for harmonic excitation and 200 Hz for random white noise excitation.

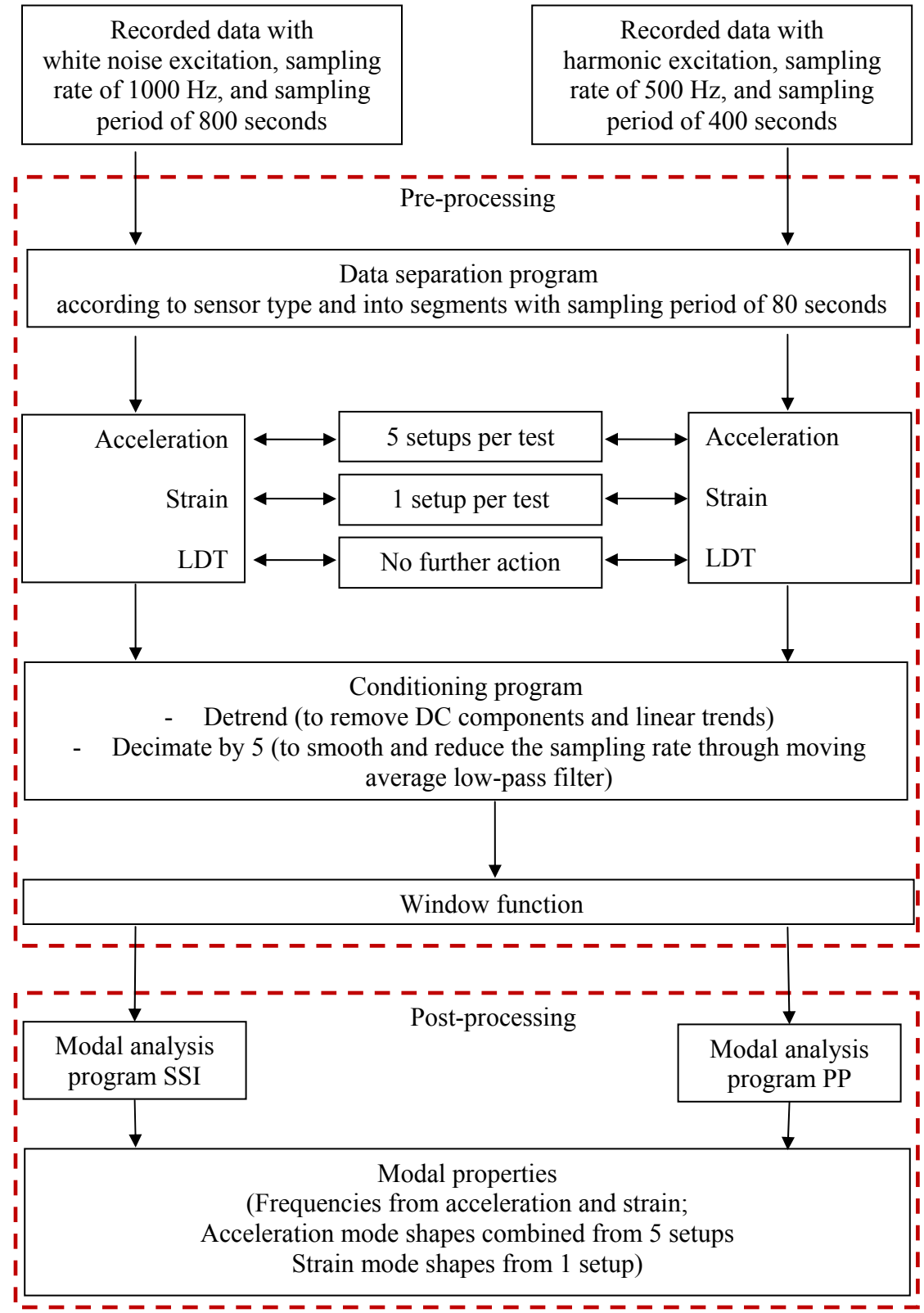

Figure 3.13. The flow chart of data processing.

A Hanning window (Mathworks 2006, Ramirez 1985) was used to reduce "leakage" in the resulting spectrum. Leakage occurs when signals are truncated at either their beginning or end, so that the spectral energy appears to spread to neighboring frequencies (Maia and Silva 1997). However, it was found in the current tests that the window function had little influence on the accuracy of measured modal properties. In fact, there was no noticeable difference between measured modal properties no matter which window function was used or whether or not a window function was used at all. This may be partially due to the fact that a relatively long sampling period of 80 seconds was used, compared with the fundamental period of 0.079 seconds (i.e., the sampling period was 1016 times the fundamental period), and that well-controlled excitation forces were adopted to excite the bridge model. Controlled excitation appears to produce more periodic data than environmental or traffic excitations. As a result, no further study was conducted on the performance of window functions, even though window functions are usually considered to be important for processing dynamic test data.

In the post-processing phase, the modal properties of the bridge model were extracted from the pre-processed sensor data, using both the Pick Picking method (PP) (Section 2.4.2), and the Stochastic Subspace Identification method (SSI) (Section 2.4.3), as implemented in the commercially available software package SPICE (or MACEC) (Van den Branden et al. 1999, Van Overschee and De Moor 1996). For the purposes of modal parameter estimation, it was assumed that the exciting force was not known or measured, so that "output-only" modal extraction techniques were required. A comparison between the PP and SSI methods is presented in Chapter 4 in terms of their influence on the reliability of extracted modal properties. The results in Chapter 4 show that the SSI method provided more reliable modal properties than the PP method when white noise excitation was used. For subsequent investigations, therefore, the SSI method was used for modal analysis of the data with white noise excitation, while the PP method was adopted for the processing of data with harmonic excitation to take advantage of faster processing, the more straightforward procedure, and comparable reliability of measured modal properties.

It should be acknowledged that no conversion from voltage readings to actual accelerations was performed in Phase I of the vibration tests. Instead, accelerometer readings were recorded as relative voltages while strain gauge readings were saved as strain values. All data processing was performed on the original recorded data in this phase of tests, although the relationships for conversion were recorded for other purposes. However, the voltage readings from accelerometers were converted to actual accelerations according to the configuration of accelerometers (i.e., a range of ±0.5g) in Phase II of the vibration tests, before performing further data processing. As before, strain gauge readings were also saved as strain values directly in this phase.

3.4 Description of Damage Cases

Once the baseline dynamic properties of the model had been established, four categories of damage were introduced into the bridge model, including damage to the steel girders, to the diaphragm members, to the lateral steel straps, and to the concrete deck. Combinations of these were also investigated (Fig. 3.14).

In damage category 1, the bottom plate was removed from the splice at midspan of Girder 4 (SP-X4.0Y2.7 in Fig. 3.3; see also the inset in Fig. 3.1 and Fig. 3.14 a), thereby producing a reduction in the flexural rigidity of approximately 32% at that location. Damage category 2 featured the removal of bolt connections from the cross-braced diaphragm members at some of locations labeled D-Xx.xYx.x in Fig. 3.3 (see Fig. 3.14b). Similarly, damage category 3 featured the disconnection of spice joists on the steel straps at some of locations labeled ST-Xx.xYx.x in Fig. 3.3 (see Fig. 3.14c). In damage category 4, small square blocks of concrete, 100 x 100 mm in plan and 25 mm deep, were physically removed from the top surface of the deck at various locations referred to as C-Xx.xYx.x, in which the coordinates Xx.x and Yx.x (measured to the centre of the damage) are defined relative to the origin as shown in Fig. 3.15 (see Fig. 3.14d). In addition, a different size of concrete block, 200 x 200 x 25 mm, was also considered in this category at the location C2-X4.5Y2.25, for which the previous damage (C-X4.5Y2.25) at the same location was enlarged.

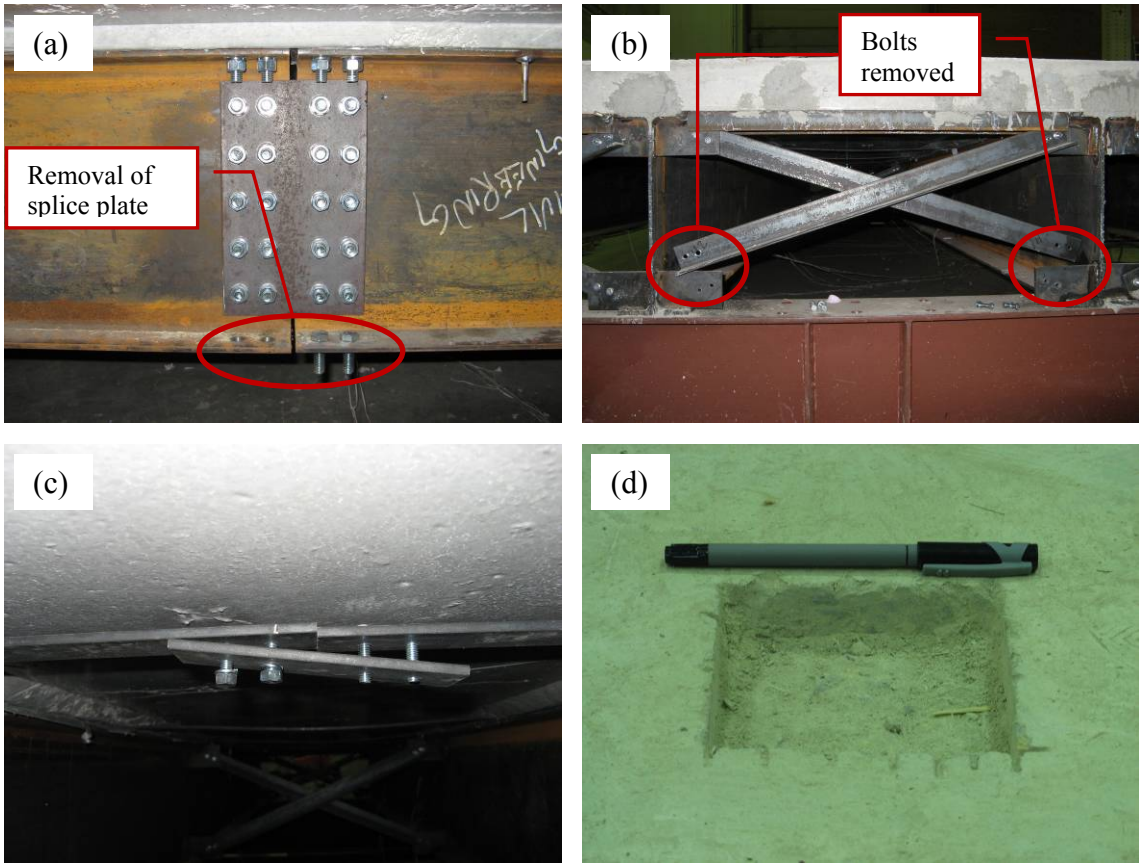

Figure 3.14. Damage states introduced to (a) the steel girders, (b) the diaphragm members, (c) the lateral steel straps, and (d) the concrete deck of the bridge model.

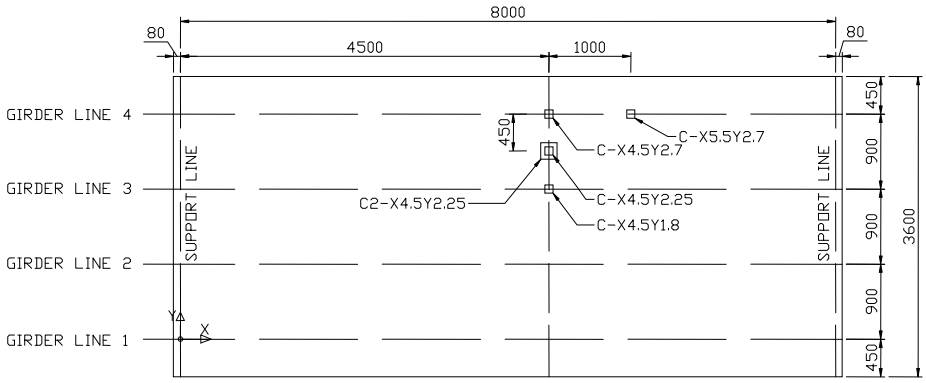

Figure 3.15. Plan view of bridge deck, showing the locations of damage to the concrete deck (dimensions in mm).

Vibration tests were conducted on the bridge model in seventeen different health states (or physical conditions), while the other test parameters, including excitation forces, sensors, and data processing methods, remained the same. Table 3.4 lists the 17 health states, as well as the descriptions for each health state. Health State 1 was the intact condition, which means that no physical damage had been introduced since the bridge model was constructed. Extensive dynamic tests were performed with the model in this health state. Some initial tests were conducted first to establish consistent and reliable test procedures through checking and calibrating various factors, including the connection of cables, sensors, data acquisition system, LabView programs, suitable excitation forces and locations, and efficient data processing procedures. Then, Phase I tests were conducted to investigate the influence of several testing parameters on the variability of measured modal properties, as described in Section 3.2.1. In this phase, only the data from Girder Line 1 were used for this purpose, and results are presented in Chapter 4.

After the testing parameters were quantified in Phase I, the vibration tests carried out in Phase II were conducted with selected values of some testing parameters to measure both the natural frequencies and mode shapes of the whole superstructure bridge model over all girder lines. For example, a combination of sampling rate of 1000 Hz and sampling period of 800 seconds was used to record the vibration data for white noise excitation cases. The measured modal properties are evaluated in Chapter 4. The modal properties in Health State 1 were also used as a baseline for some of the other health states for damage detection. A detailed discussion of damage detection is available in Chapter 6.

For Health States 2 to 5, a new state of damage was incrementally introduced in the model without repairing previous damage. The individual damage states and combinations of these states included damage to the steel girder splice and the cross bracing diaphragms at different locations (SP-X4.0Y2.7, D-X5.2Y2.25, D-X8.0Y1.35, and D-X0.0Y2.25).

For Health States 6 to 10, a new state of damage was introduced into the model after all previous damage had been repaired, except for the damage to the steel girder splice (SP-X4.0Y2.7). The new damage states considered included damage to the diaphragms and the steel straps at various locations. The purpose of these damage states was an attempt to investigate the influence of damage location on the performance of VBDD methods

Table 3.4. The health states investigated on the bridge model.

Health States	Description of Health States
State 1	Intact condition
State 2	SP-X4.0Y2.7
State 3	SP-X4.0Y2.7 and D-X5.2Y2.25
State 4	SP-X4.0Y2.7, D-X5.2Y2.25, and D-X8.0Y1.35
State 5	SP-X4.0Y2.7, D-X5.2Y2.25, D-X8.0Y1.35, and D-X0.0Y2.25
State 6	SP-X4.0Y2.7 and D-X8.0Y1.35
State 7	SP-X4.0Y2.7 and D-X0.0Y0.45
State 8	SP-X4.0Y2.7 and D-X2.8Y1.35
State 9	SP-X4.0Y2.7 and ST-X6.8Y0.45
State 10	SP-X4.0Y2.7 and ST-X4.4Y0.45
State 11	SP-X4.0Y2.7, ST-X4.4Y0.45, and ST-X4.4Y1.35
State 12	SP-X4.0Y2.7, ST-X4.4Y0.45, ST-X4.4Y1.35, and ST-X4.4Y2.25
State 13	C-X4.5Y2.7
State 14	C-X4.5Y2.7 and C-X4.5Y1.8
State 15	C-X4.5Y2.7, C-X4.5Y1.8, and C-X5.5Y2.7
State 16	C-X4.5Y2.7, C-X4.5Y1.8, C-X5.5Y2.7, and C-X4.5Y2.25
State 17	C-X4.5Y2.7, C-X4.5Y1.8, C-X5.5Y2.7, C-X4.5Y2.25, and C2-X4.5Y2.25

X4.0Y2.7 indicates that the damage was located at x and y coordinates of 4.0 m and 2.7 m, respectively, as defined in Fig. 3.3;
SP = The splice joint in Girder 4 was disconnected at location Xx.xYy.y;
D = Diaphragms were disconnected at location Xx.xYy.y;
ST = Splice joints on the steel straps were disconnected at location Xx.xYy.y;
C = Concrete block with dimension of 100*100*25 mm was removed from the surface of the concrete deck at location Xx.xYy.y;
C2 = Concrete block with dimension of 200*200*25 mm, on the base of the previous case C-X4.5Y2.25 at the same location, was removed from the surface of the concrete deck at location X4.5Y2.25.

while the severity of damage remained the same. Health States 11 and 12 considered incremental damage to the steel straps.

Before inducing Health State 13, all previous damage was repaired by reconnecting the members using bolts. It should be noted that the repairs could not restore the bridge system to the original condition exactly, due to the fact that the repairs were conducted after the model had been loaded multiple times, even though the differences may not have been significant. A detailed discussion based on testing results is available in Chapter 6.

For Health States 13 to 16, a new state of damage was introduced incrementally by physically removing small square blocks of concrete (100 x 100 x 25 mm) from the top surface of the deck at various locations. In Health State 17, a larger size of concrete block, 200 x 200 x 25 mm, was removed, enlarging the previous damage at the same location (i.e., the effective change in physical condition from Health State 16 to Health State 17 was 200 x 200 x 25 mm minus 100 x 100 x 25 mm).

Damage states (to be distinguished from health states) were defined as the change in physical properties between two health states (or conditions): the initial (or undamaged) state and the new (or damaged) state. In this manner, a health state previously defined as "damaged" could be reconsidered to be an "undamaged" state for subsequent health states investigated later on. By comparing two health states listed in Table 3.4, and treating the earlier state as the "undamaged state" and the later state as the "damaged state", 26 damage cases were generated and investigated in this research. For example, to generate Damage Case 1, Health State 1 was considered as "undamaged" and Health State 2 was considered as "damaged". Table 3.5 lists all 26 damage cases considered, defining the corresponding "undamaged" and "damaged" states, and describing the damage for each damage case. The results for the application of VBDD methods to the damage cases are discussed in Chapter 6.

3.5 Test Protocols Investigated

For each health state considered, 28 different test protocols were investigated, as listed in Table 3.6, which included combinations of four different instrumentation schemes (use of accelerometer data, use of data from only the bottom strain gauge in each cluster, use of data from only the middle strain gauge in each cluster, and use of data from only the top strain gauge in each cluster), two different forced excitation methods (resonant harmonic and random white noise), and five different modes. It should be acknowledged that the modes are not really a "test protocol". They were simply a result of post-processing. However, the use of different modes was actually treated as a component of a test protocol, since there were different uncertainties involved in the measurement of different vibration modes (see Chapter 4 and 6 for details). The lowest five vibration modes were extracted when using random excitation, while only the lowest two modes were investigated when using harmonic excitation. The resulting detailed mode shape definitions and comparisons are available in Chapter 4. The resolutions of different test protocols and the results for application of VBDD methods under specific test protocols are presented in Chapter 6.

Table 3.5. The summary of damage cases considered for the bridge model.

Damage Case	Undamaged State	Damaged State	Description of damage
Case 1	State 1	State 2	SP-X4.0Y2.7
Case 2	State 2	State 3	D-X5.2Y2.25
Case 3	State 3	State 4	D-X8.0Y1.35
Case 4	State 4	State 5	D-X0.0Y2.25
Case 5	State 2	State 6	D-X8.0Y1.35
Case 6	State 2	State 7	D-X0.0Y0.45
Case 7	State 2	State 8	D-X2.8Y1.35
Case 8	State 2	State 9	ST-X6.8Y0.45
Case 9	State 2	State 10	ST-X4.4Y0.45
Case 10	State 10	State 11	ST-X4.4Y1.35
Case 11	State 11	State 12	ST-X4.4Y2.25
Case 12	State 1	State 13	C-X4.5Y2.7
Case 13	State 13	State 14	C-X4.5Y1.8
Case 14	State 14	State 15	C-X5.5Y2.7
Case 15	State 15	State 16	C-X4.5Y2.25
Case 16	State 16	State 17	C2-X4.5Y2.25
Case 17	State 1	State 3	SP-X4.0Y2.7 and D-X5.2Y2.25
Case 18	State 1	State 4	SP-X4.0Y2.7, D-X5.2Y2.25, and D-8.0Y1.35
Case 19	State 1	State 5	SP-X4.0Y2.7, D-X5.2Y2.25, D-X8.0Y1.35, and D-X0.0Y2.25
Case 20	State 1	State 10	SP-X4.0Y2.7 and ST-X4.4Y0.45
Case 21	State 1	State 11	SP-X4.0Y2.7, ST-X4.4Y0.45, and ST-X4.4Y1.35
Case 22	State 1	State 12	SP-X4.0Y2.7, ST-X4.4Y0.45, ST-X4.4Y1.35, and ST-X4.4Y2.25
Case 23	State 1	State 14	C-X4.5Y2.7 and C-X4.5Y1.8
Case 24	State 1	State 15	C-X4.5Y2.7, C-X4.5Y1.8, and C-X5.5Y2.7
Case 25	State 1	State 16	C-X4.5Y2.7, C-X4.5Y1.8, C-X5.5Y2.7, and C-X4.5Y2.25
Case 26	State 1	State 17	C-X4.5Y2.7, C-X4.5Y1.8, C-X5.5Y2.7, C-X4.5Y2.25, and C2-X4.5Y2.25

Table 3.6. The summary of test protocols investigated.

Test Protocol	Vibration Mode	Excitation	Instrumentation
1	Mode 1	Harmonic	Accelerometer
2	Mode 1	Harmonic	Bottom strain gauge
3	Mode 1	Harmonic	Middle strain gauge
4	Mode 1	Harmonic	Top strain gauge
5	Mode 1	White noise random	Accelerometer
6	Mode 1	White noise random	Bottom strain gauge
7	Mode 1	White noise random	Middle strain gauge
8	Mode 1	White noise random	Top strain gauge
9	Mode 2	Harmonic	Accelerometer
10	Mode 2	Harmonic	Bottom strain gauge
11	Mode 2	Harmonic	Middle strain gauge
12	Mode 2	Harmonic	Top strain gauge
13	Mode 2	White noise random	Accelerometer
14	Mode 2	White noise random	Bottom strain gauge
15	Mode 2	White noise random	Middle strain gauge
16	Mode 2	White noise random	Top strain gauge
17	Mode 3	White noise random	Accelerometer
18	Mode 3	White noise random	Bottom strain gauge
19	Mode 3	White noise random	Middle strain gauge
20	Mode 3	White noise random	Top strain gauge
21	Mode 4	White noise random	Accelerometer
22	Mode 4	White noise random	Bottom strain gauge
23	Mode 4	White noise random	Middle strain gauge
24	Mode 4	White noise random	Top strain gauge
25	Mode 5	White noise random	Accelerometer
26	Mode 5	White noise random	Bottom strain gauge
27	Mode 5	White noise random	Middle strain gauge
28	Mode 5	White noise random	Top strain gauge

CHAPTER 4. **EXPERIMENTAL RESULTS**

4.1 Overview

As explained in Chapter 3, the vibration tests were conducted in two phases, with Phase I undertaken to investigate the influence of various testing parameters on the repeatability and reliability of modal property extraction, and Phase II focussing on damage detection and the sensitivity of various approaches to damage. To give a general idea of the testing results for better understanding the whole process of testing, some of the results for the Phase II tests are presented in this chapter first. The results of the Phase II vibration tests presented here include the recorded vibration time history data, the filtered time history series accompanied by the corresponding spectra, the extracted natural frequencies using both accelerometers and strain gauges in various health states, the lowest five mode shapes defined using both accelerometer and strain gauge data, and a general comparison of mode shapes in various health states.

Following this, the results of the Phase I tests are presented. In particular, the influence of sensor type and location, data sampling rate, data sampling period, and excitation method on the repeatability and reliability of modal property extraction are presented.

Since the amplitude of mode shapes is indeterminate in most cases, it is necessary to normalize (or scale) the mode shapes to a common base in order to identify the changes in mode shapes caused by damage. An investigation of the influence of normalization methods and schemes on the definition of mode shapes and changes in mode shapes was conducted, with results presented in this chapter. To clarify, the term "normalization method" is used to refer to the method used to scale the mode shape, while "normalization scheme" refers to whether the entire structure is considered as a unit during the normalization process, or different subsets of the structure are normalized

separately. A new normalization method was developed as part of this work. Comparisons among various normalization methods and two different schemes were preformed. The results of the comparison are presented in this chapter.

4.2 Dynamic Properties of the Bridge Model

4.2.1 Recorded vibration data and the corresponding modal identification

Figure 4.1 (a) shows a typical acceleration time history of the original recorded data

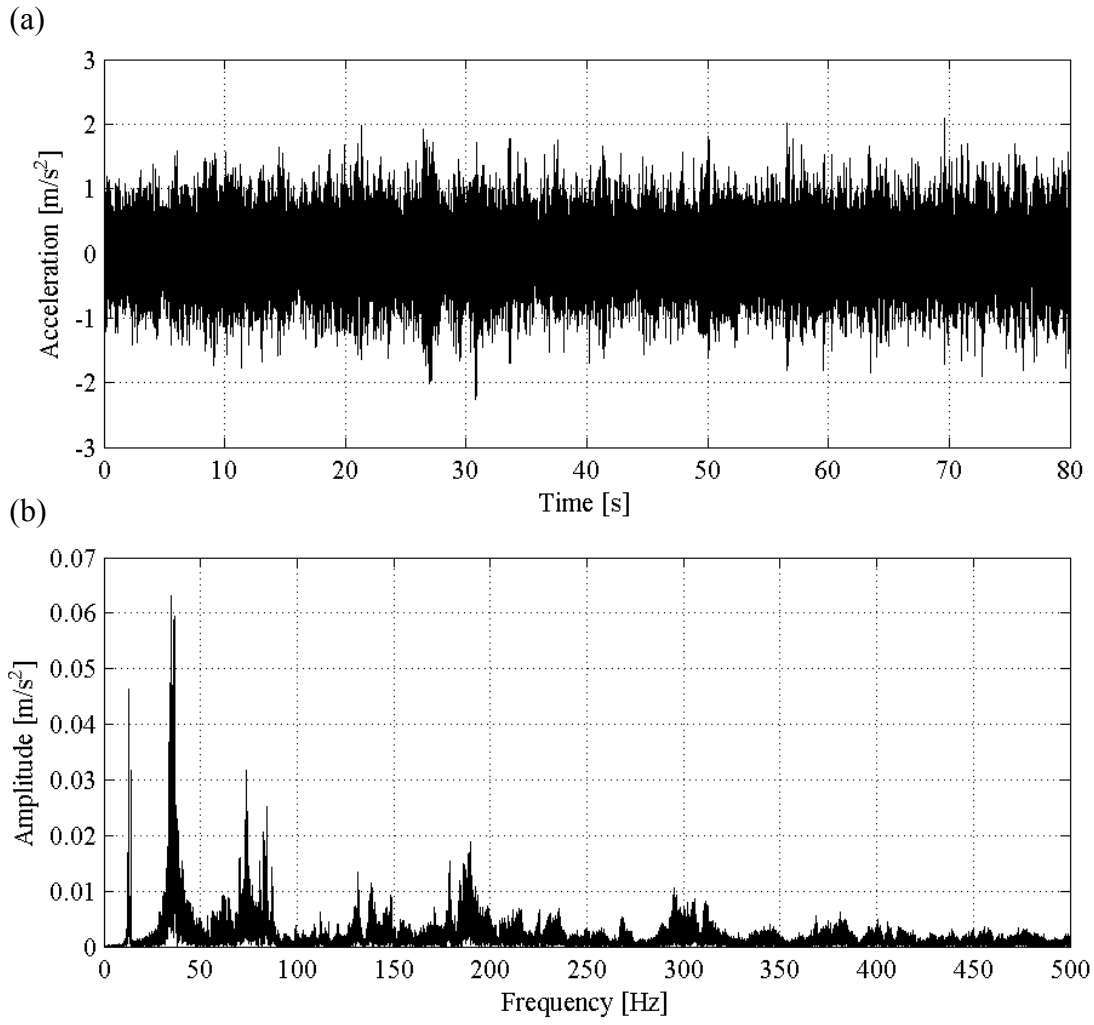

Figure 4.1. Vibration response to random white noise excitation for the original recorded reference accelerometer data: (a) acceleration time history; (b) acceleration spectrum.

induced by the random white noise excitation, while Figure 4.1 (b) presents the corresponding acceleration frequency spectrum of the same signal. The signal shown in Fig. 4.1 was recorded by the reference accelerometer (see Table 3.3) for the Health State 1 (i.e., the intact condition). The signals for other channels in other health states were similar to those shown in Fig. 4.1, except that they exhibited different amplitudes and small shifts in frequencies. From Fig. 4.1 (b), it can be seen that the maximum frequency (usually called the Nyquist frequency) in the frequency spectrum plot is 500 Hz, which is one-half of the sampling rate of 1000 Hz, based on Nyquist–Shannon sampling theorem (Marks 1991). This sampling theorem supplied a sufficient condition, under which bandlimited signals (i.e., signals which have a maximum frequency) can be reconstructed perfectly from their sampled data, if the sampling rate is more than twice the maximum frequency. As a result, the frequency equal to one-half of the sampling rate is the highest frequency that can be unambiguously represented by the sampled signal. The relatively high sampling rate was adopted to take advantage of the benefit of oversampling and then, using low-pass digital filter techniques, to allow for the decimation of the digitized data. In this manner, the inherent random noise could be reduced, potentially increasing the accuracy of measured dynamic properties.

The frequencies of interest for civil engineering structures are usually below 50 Hz. Specifically, in this case, the signals were decimated to a lower sampling rate of 200 Hz, which resulted in a maximum frequency of 100 Hz in the frequency spectrum. Figure 4.2 (a) shows the decimated results for the same signal, while Fig. 4.2 (b) presents the corresponding spectrum of the decimated signal from the 80 second record (16000 sampling points), in which the maximum frequency is 100 Hz. Figure 4.2 (c) presents the averaged spectrum from ten equal length segments of the record, which did not feature any overlap but were modified by a Hanning window (see Section 3.3). To clarify, the 80 second record was divided into ten segments of equal length, with 1600 sampling points each. As a result, the spectrum shown in Fig. 4.2 (c) features much less noise. To more clearly show the decimated signal and the corresponding frequency spectrum, Fig. 4.3 presents a two second segment of the signal and frequency spectra up to 45 Hz (a closer view of Fig. 4.2).

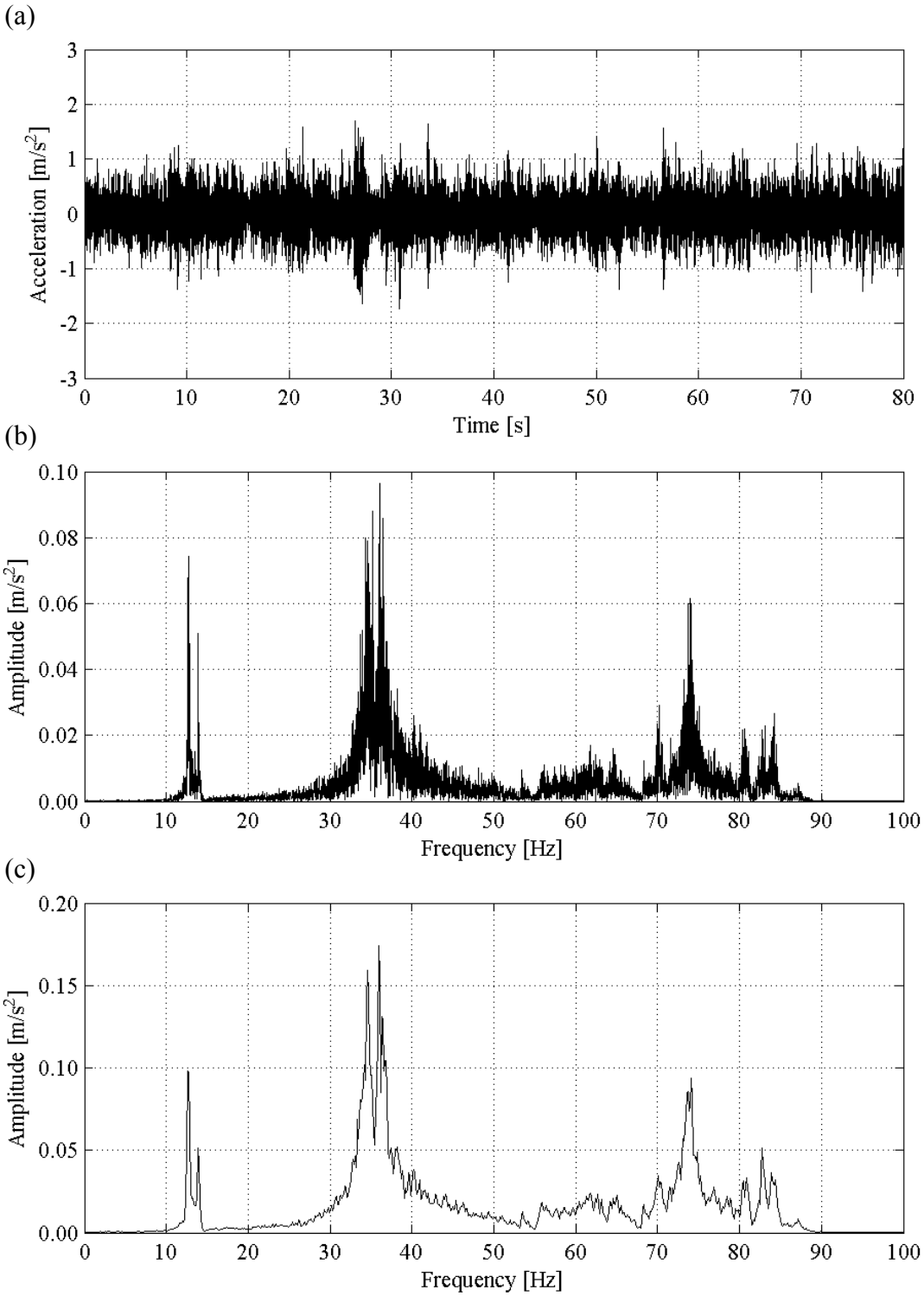

Figure 4.2. Vibration response to random white noise excitation for the decimated accelerometer data: (a) acceleration time history; (b) spectrum from one record; (c) averaged spectrum from ten equal length segments without overlap using a Hanning window.

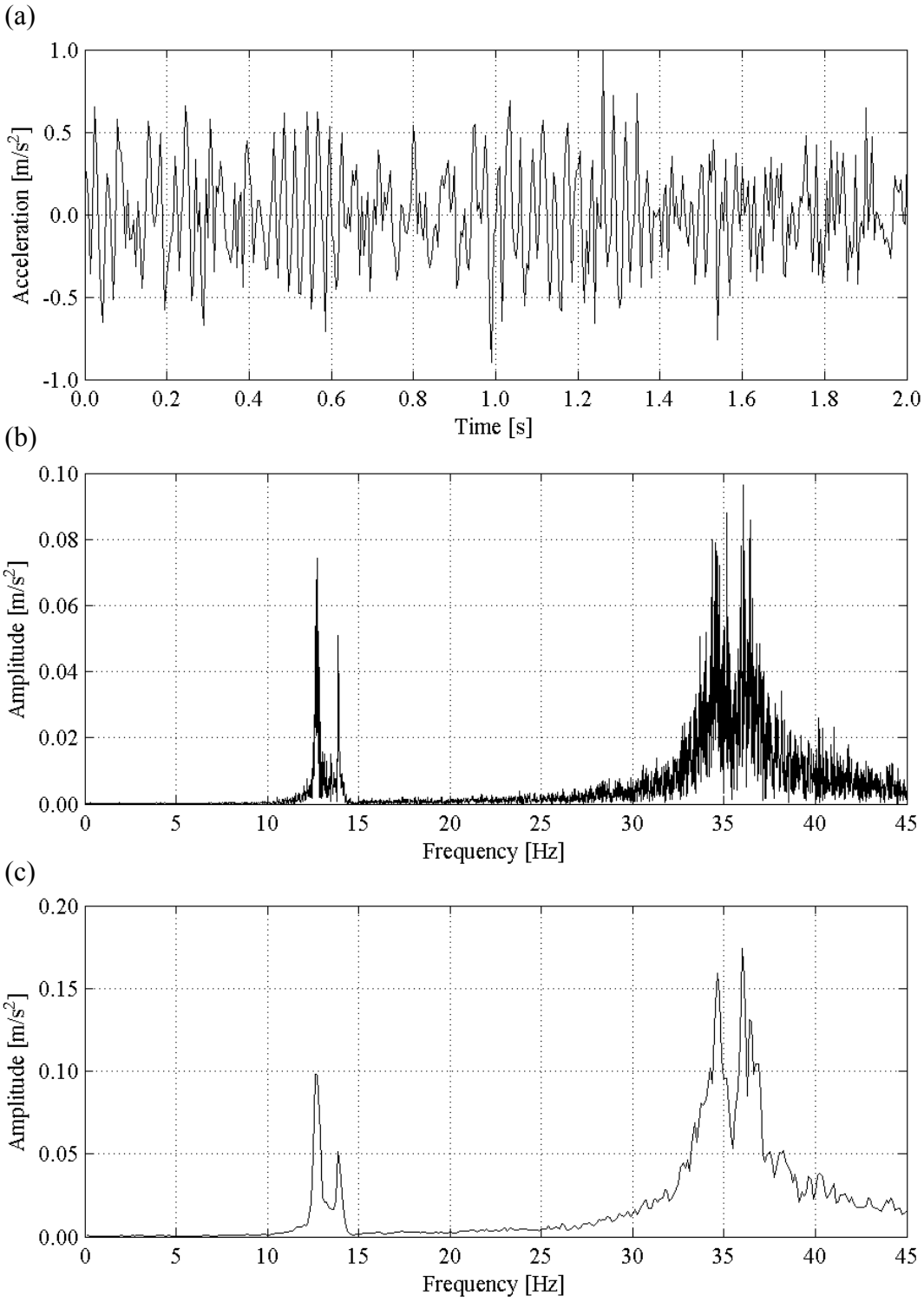

Figure 4.3. Closer view of vibration response to random white noise excitation for the decimated accelerometer data: (a) acceleration time history (a two second segment of the signal); (b) spectrum from one record (up to 45 Hz); (c) averaged spectrum from ten equal length segments without overlap using a Hanning window (up to 45 Hz).

In the same manner, Fig. 4.4 presents a closer view of a typical strain response to random white noise excitation, in this case for a bottom strain gauge. The signal shown in Fig. 4.4 (a) came from a bottom strain gauge channel located at the mid-span of Girder 1 during the same test that produced the signal shown in Fig. 4.3 (a). The amplitude of the frequency spectrum in the region of 35 Hz was much smaller in Fig. 4.4 (b) and (c) than that present in Fig. 4.3 (b) and (c), which may due to the fact that the strain gauges used in the tests are generally not as sensitive to higher frequency vibration as the accelerometers that were used. This means that the accelerometers may generate more accurate higher frequency data than the strain gauges.

The many peaks observed in both Fig. 4.3 (b) and Fig. 4.4 (b) demonstrate that it was difficult to reliably identify the natural frequencies of the system using the PP method, especially in the vicinity of 35 Hz. As a result, the SSI method, a time domain modal analysis method, as implemented in the commercially available software SPICE (or MACEC) (Van den Branden et al. 1999, Van Overschee and De Moor 1996) was adopted to identify the natural frequencies and the corresponding mode shapes of the system. Figure 4.5 shows the stabilization plots (implemented in the software SPICE) to identify the modal properties of the bridge superstructure, where Fig. 4.5 (a) corresponds to the accelerometer signal shown in Fig. 4.3 (a) and Fig. 4.5 (b) corresponds to the bottom strain gauge signal shown in Fig. 4.4 (a). Stabilization plots show the stability of the poles (using symbols of "+" in the plots) as a function of increasing model order (plotted in the vertical axis, and denoting the order of the sub-space) under certain pre-set stabilization criteria (here this was set at 0.5% for frequencies, 5% for damping ratios, and 1% for mode shape vectors). The stricter these criteria are, the better the quality of the resulting data (i.e., the more stable the estimation). The averaged power spectrum density (APSD) plot of all channels in the current file is also plotted in the background. Stabilized eigenfrequencies calculated using the SSI method often coincide with the peaks in the APSD spectrum shown in the background (Peeters et al. 1998). From these plots, it can be seen that the second mode, around 13.9 Hz, was the least stable mode, especially for strain gauge data (Fig. 4.5b). This implies that the second mode extracted in this manner could be the least reliable

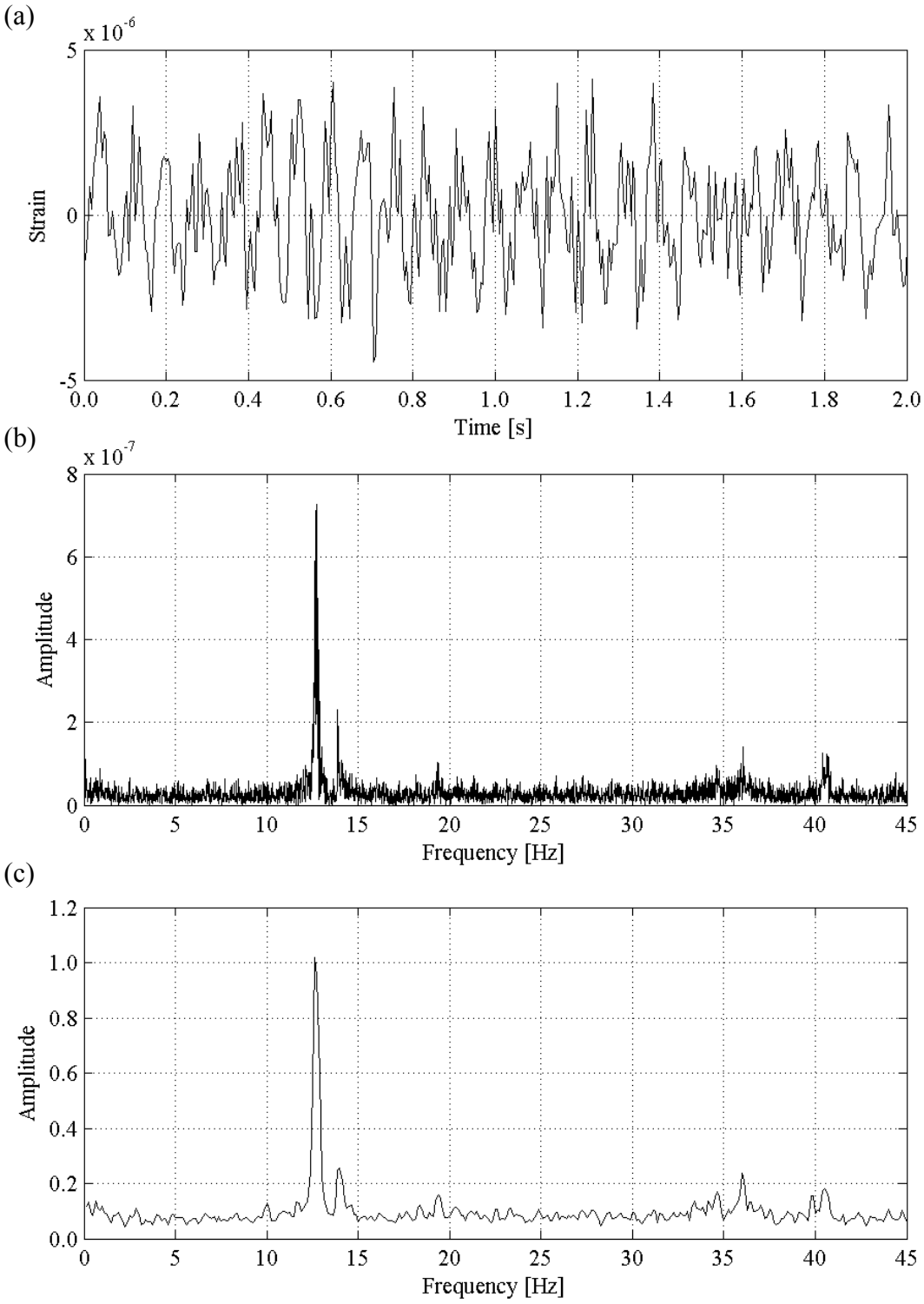

Figure 4.4. Closer view of vibration response to random white noise excitation for the decimated bottom strain gauge data: (a) strain time history (a two second segment of the signal); (b) spectrum from one record (up to 45 Hz); (c) averaged spectrum from ten equal length segments without overlap using a Hanning window (up to 45 Hz).

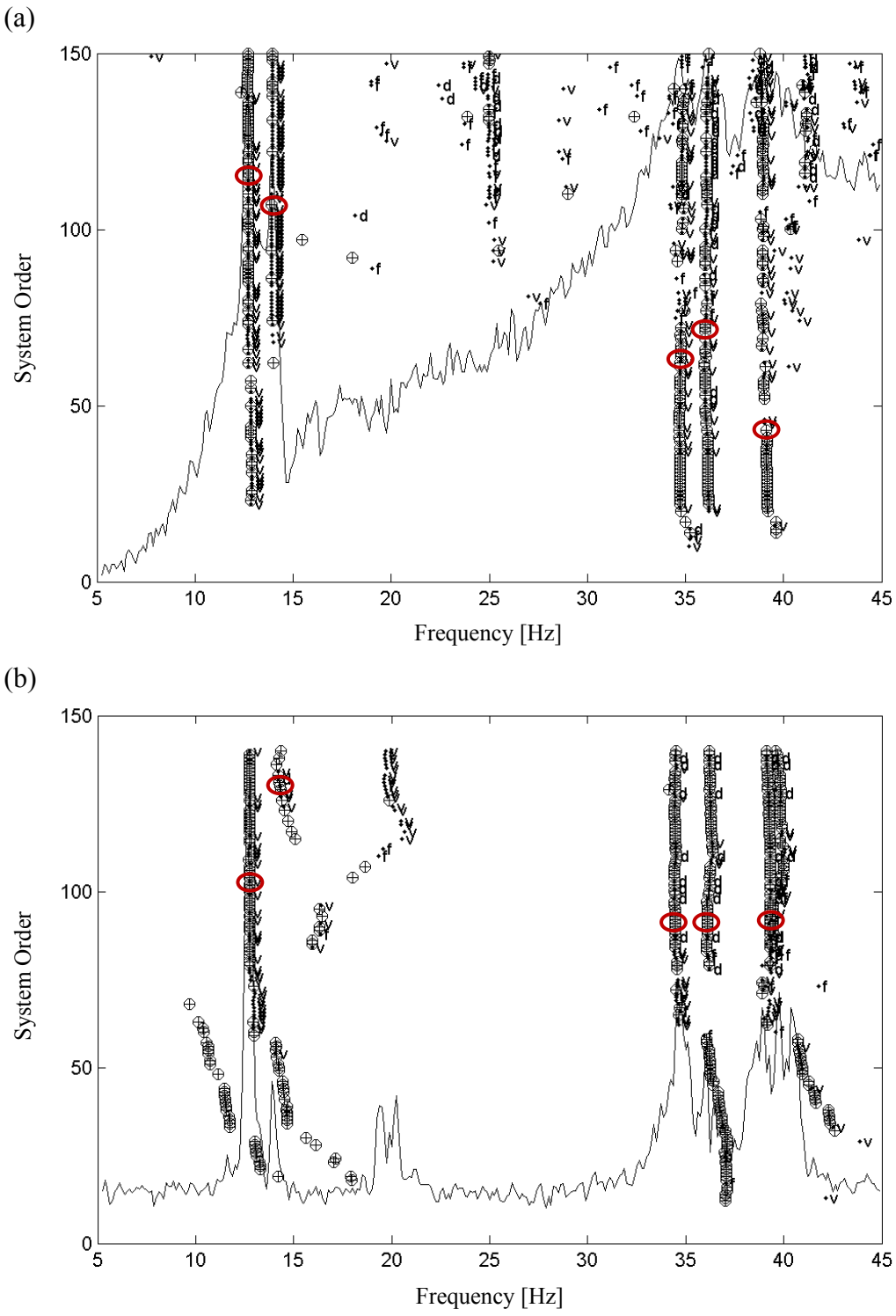

Figure 4.5. Modal property identification using the Stochastic Subspace Identification (SSI) method for: (a) accelerometer data; (b) strain gauge data (the red circles mean the selected stabilized poles for modal property identification).

vibration mode. Detailed comparisons of extracted mode shapes are presented in Section 4.2.3.

By using the SSI method on the vibration response data from the white noise random excitation tests, the lowest five vibration modes were extracted. The measured natural frequencies of the system for various health states are presented and compared in Section 4.2.3, while the corresponding mode shapes are described in Section 4.2.4.

After the natural frequencies had been identified, harmonic excitation was applied at each individual natural frequency to permit accurate measurement of the corresponding mode shapes. Figure 4.6 shows a typical vibration response to harmonic excitation for the data from the reference accelerometer, where Fig. 4.6 (a) shows the acceleration time history and Fig. 4.6 (b) presents the corresponding frequency spectrum. The signal shown in Fig. 4.6 (a) came from the reference accelerometer channel during the tests for Health State 1 (i.e., the intact condition) when the model was excited by harmonic loading at the first natural frequency, as identified during the white noise random excitation tests. Figure 4.7 presents a typical vibration response to harmonic excitation for the data from a bottom strain gauge under identical testing conditions. Both Fig. 4.6 (b) and Fig. 4.7 (b) show only one apparent and dominant peak, which implies that using the simple PP method can produce a highly repeatable mode shape definition. As a result, the PP method was adopted to process the data with harmonic excitation. The measured first and second mode shapes using harmonic excitation for various health states are presented and compared in Section 4.2.4.

4.2.2 Measured natural frequencies

The lowest five natural frequencies of the bridge model in Health State 1, extracted from both the accelerometer and strain gauge data in five trials, as obtained using the white noise random excitation, are listed in Table 4.1 and Table 4.2, respectively. To define one vibration mode, each trial requires five setups for accelerometer data while only one setup was required for strain gauge data. One set of data could generate one natural frequency value for each mode using the SSI modal analysis method (i.e., for each individual vibration mode, one common natural frequency could be generated from each

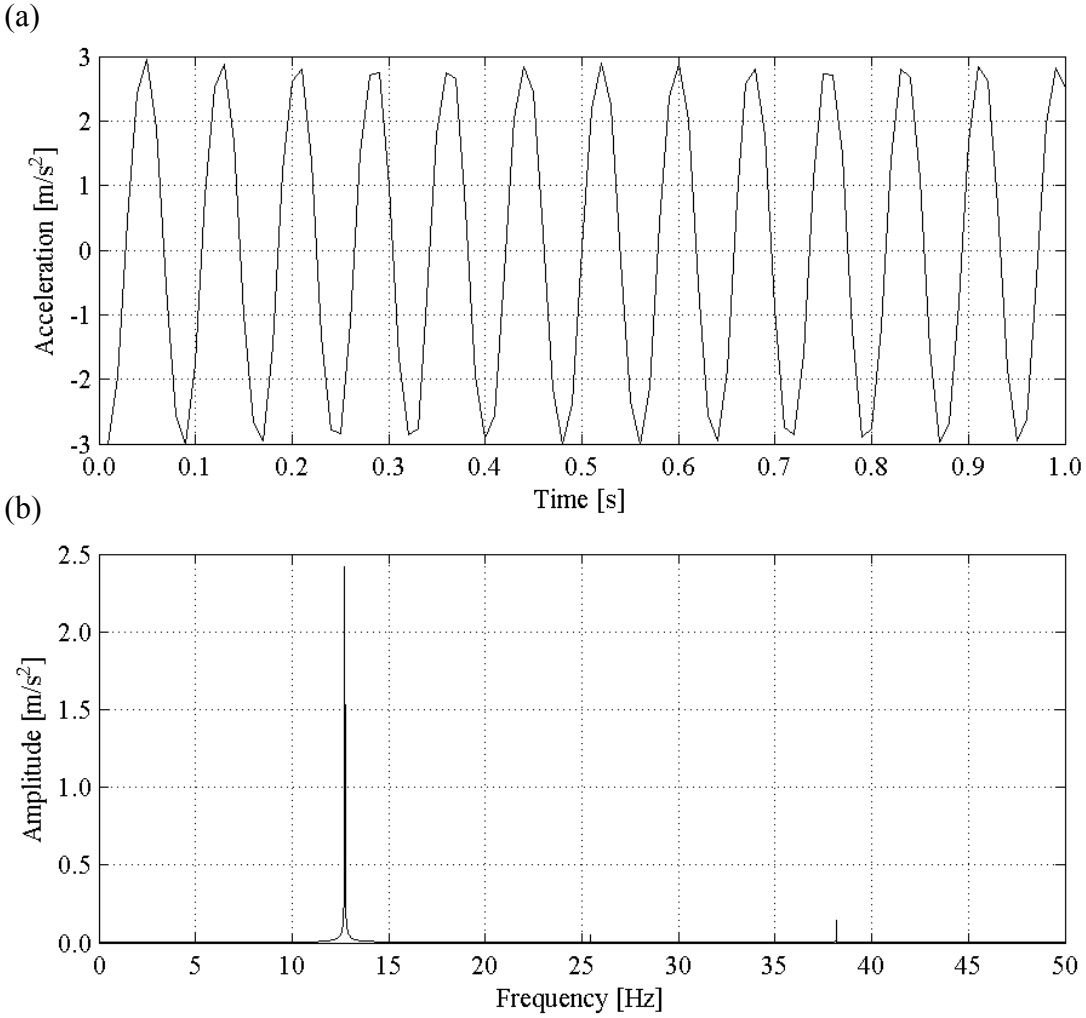

Figure 4.6. Closer view of acceleration response to harmonic excitation at the 1st mode for the reference accelerometer in Health State 1: (a) acceleration time history (a one second segment of the signal); (b) acceleration spectrum (frequency range showing up to 50 Hz).

set of data recorded by either seven accelerometers or 57 strain gauges). As a result, Table 4.1 shows 25 different natural frequencies for each vibration mode from 25 sets of data (five trials of five setups). The averaged frequencies from the five different setups are also listed in Table 4.1 for each individual trial and each individual mode. The averaged frequency, the standard deviation, and the corresponding coefficient of variation, of all measured frequencies from the 25 sets of data, are also presented in Table 4.1 for each individual mode. In a similar manner, Table 4.2 lists the results of

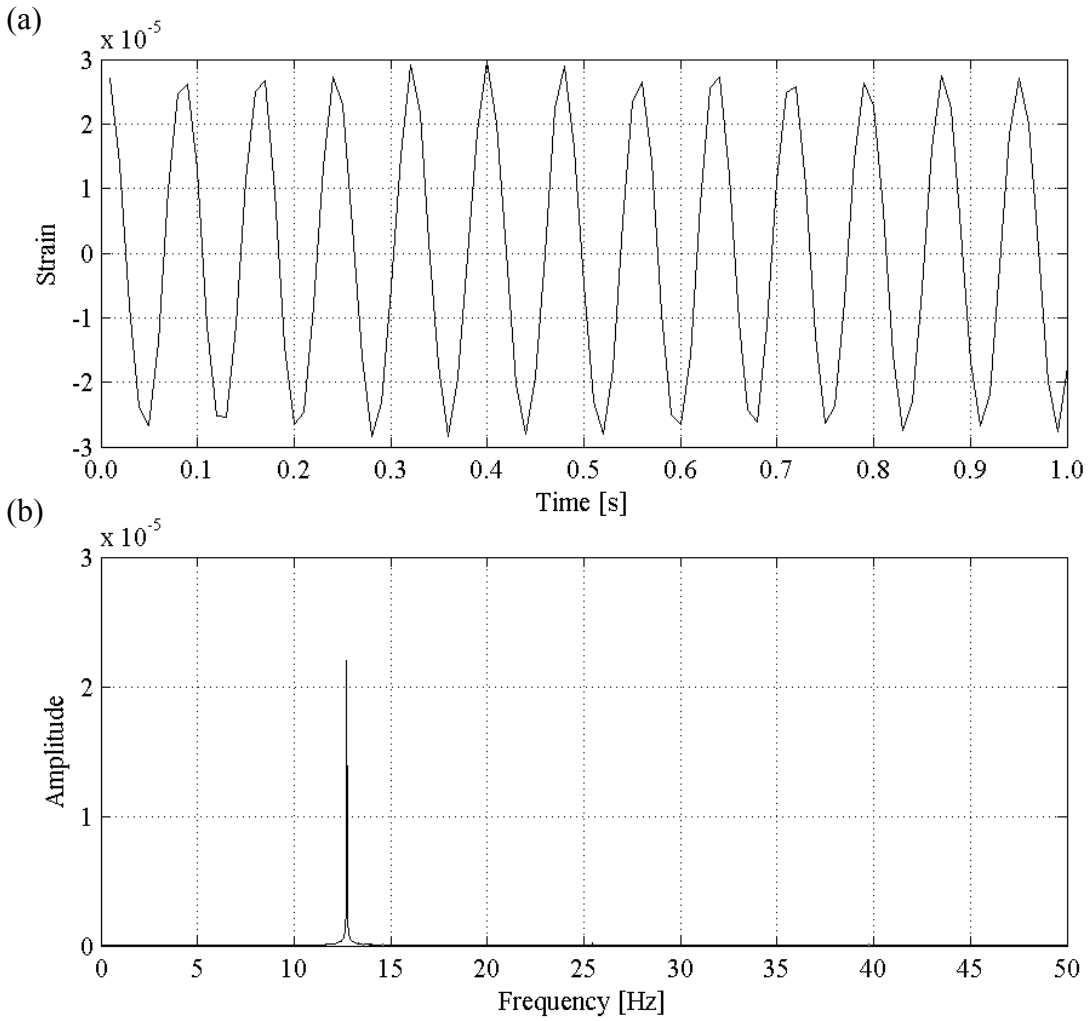

Figure 4.7. Closer view of vibration response to harmonic excitation at the 1st mode for a bottom strain gauge near mid-span for Health State 1: (a) strain time history (a one second segment of the signal); (b) strain spectrum (frequency range showing up to 50 Hz).

the natural frequencies from strain gauge data, where only five values (five trials of one setup, producing five sets of data) are available for each individual mode.

As expected, the first natural frequency was measured with the lowest variability, giving coefficients of variation of 0.09% for both the accelerometer and strain gauge data. The second natural frequency extracted from strain gauge data was measured with the highest variability, with a coefficient of variation of 1.41%, although the variation is still

Table 4.1. Measured natural frequencies using accelerometers for Health State 1.

Trials	Setups	Measured natural frequency (Hz)				
		Mode 1	Mode 2	Mode 3	Mode 4	Mode 5
Trial 1	Set 1_1	12.700	13.871	34.656	36.043	39.133
	Set 2_1	12.689	13.884	34.557	35.973	38.841
	Set 3_1	12.693	13.901	34.445	35.879	38.829
	Set 4_1	12.693	13.892	34.537	35.845	38.719
	Set 5_1	12.680	13.858	34.580	35.804	38.830
	Average (Hz)	12.691	13.881	34.555	35.909	38.871
Trial 2	Set 1_2	12.719	13.876	34.679	35.945	39.147
	Set 2_2	12.708	13.891	34.582	35.881	38.799
	Set 3_2	12.696	13.914	34.486	35.908	38.722
	Set 4_2	12.705	13.885	34.555	35.874	38.717
	Set 5_2	12.679	13.871	34.523	35.815	38.730
	Average (Hz)	12.701	13.888	34.565	35.885	38.823
Trial 3	Set 1_3	12.711	13.876	34.664	35.958	39.051
	Set 2_3	12.706	13.895	34.588	36.035	38.798
	Set 3_3	12.701	13.893	34.485	35.788	38.625
	Set 4_3	12.697	13.867	34.503	35.805	38.787
	Set 5_3	12.682	13.861	34.539	35.822	38.735
	Average (Hz)	12.699	13.878	34.556	35.882	38.799
Trial 4	Set 1_4	12.712	13.918	34.701	35.957	39.122
	Set 2_4	12.697	13.892	34.548	35.926	38.798
	Set 3_4	12.706	13.906	34.534	35.790	38.771
	Set 4_4	12.699	13.903	34.561	35.884	38.763
	Set 5_4	12.688	13.858	34.486	35.795	38.742
	Average (Hz)	12.700	13.896	34.566	35.870	38.839
Trial 5	Set 1_5	12.701	13.879	34.636	35.990	39.157
	Set 2_5	12.694	13.895	34.554	35.926	38.737
	Set 3_5	12.718	13.915	34.464	35.940	38.825
	Set 4_5	12.686	13.889	34.530	35.886	38.709
	Set 5_5	12.683	13.864	34.509	35.819	38.688
	Average (Hz)	12.696	13.888	34.539	35.912	38.823
All Data	Average (Hz)	12.698	13.886	34.556	35.892	38.831
	STDEV (Hz)	0.011	0.018	0.068	0.077	0.157
	C.O.V.	0.09%	0.13%	0.20%	0.21%	0.41%

STDEV = Standard deviation;
C.O.V. = Coefficient of variation.

Table 4.2. Measured natural frequencies using strain gauges for Health State 1.

	Measured natural frequency (Hz)				
Trials	Mode 1	Mode 2	Mode 3	Mode 4	Mode 5
Trial 1	12.755	14.074	34.469	36.285	39.262
Trial 2	12.771	13.948	34.381	36.300	39.261
Trial 3	12.780	14.378	34.456	36.194	39.350
Trial 4	12.771	14.408	34.480	36.162	39.414
Trial 5	12.786	14.286	34.325	36.280	39.470
Average (Hz)	12.773	14.219	34.422	36.244	39.352
STDEV (Hz)	0.012	0.200	0.067	0.062	0.092
C.O.V.	0.09%	1.41%	0.19%	0.17%	0.23%

STDEV = Standard deviation;
C.O.V. = Coefficient of variation.

considered to be quite small for this kind of dynamic test. Therefore, the tests provided a good estimation of the natural frequencies of the system. A comparison of the lowest five natural frequencies (i.e., the averaged frequencies from 25 values for acceleration data, but from five values for strain data) extracted from the accelerometer and strain gauge data shows that the agreement between the two types of sensors is excellent, with corresponding frequencies differing by less than 1.3% for all modes. Although the differences were small, the natural frequencies extracted from the strain gauge data were generally higher than those from the accelerometer data.

Once the baseline (Health State 1) dynamic properties of the bridge model had been established, four categories of damage states were introduced into the model. Altogether, seventeen different health states were investigated. In a similar manner to the results presented in Table 4.1 and Table 4.2, a comparison of the measured natural frequencies in various health states is presented in Table 4.3, based on both accelerometer and strain gauge data. The frequencies shown in Table 4.3 are the averaged values from 25 sets of data (five trials of five setups) for accelerometers, and from five sets of data (five trials of one setup) for strain gauges.

As was the case in Health State 1, the natural frequencies extracted from the strain gauge data were generally higher than those from the accelerometer data for all modes

Table 4.3. Comparison of measured frequencies in different health states based on accelerometer and strain gauge data.

Sensor type	Health state	Natural frequency (Hz)				
		Mode 1	Mode 2	Mode 3	Mode 4	Mode 5
Accelerometer	State 1	12.70	13.89	34.56	35.89	38.83
	State 2	12.63	13.71	34.52	35.69	38.65
	State 3	12.61	13.70	30.08	34.15	38.62
	State 4	12.60	13.70	30.00	33.90	38.60
	State 5	12.60	13.75	29.95	34.28	38.60
	State 6	12.60	13.75	34.08	35.79	38.90
	State 7	12.58	13.73	33.75	35.84	38.92
	State 8	12.58	13.75	31.07	34.69	38.85
	State 9	12.60	13.73	34.58	35.81	39.07
	State 10	12.59	13.72	34.52	35.80	39.04
	State 11	12.58	13.71	34.40	35.79	38.88
	State 12	12.57	13.70	34.39	35.80	38.84
	State 13	12.63	13.88	34.30	36.08	38.63
	State 14	12.63	13.90	34.50	36.09	38.89
	State 15	12.62	13.90	34.49	36.10	38.93
	State 16	12.62	13.91	34.49	36.11	38.84
	State 17	12.61	13.90	34.50	36.08	38.88
Strain gauge	State 1	12.77	14.22	34.42	36.24	39.35
	State 2	12.68	13.92	34.71	36.28	38.69
	State 3	12.69	13.84	34.15	37.60	38.81
	State 4	12.69	13.83	34.01	36.86	38.62
	State 5	12.64	13.96	34.06	35.58	39.28
	State 6	12.63	13.91	33.69	35.84	38.77
	State 7	12.67	13.97	33.23	35.99	39.19
	State 8	12.66	13.98	31.22	34.68	38.92
	State 9	12.70	13.97	34.78	36.22	38.67
	State 10	12.67	14.00	34.54	36.60	39.02
	State 11	12.66	13.92	34.22	36.06	39.16
	State 12	12.68	14.00	34.34	36.16	39.24
	State 13	12.74	14.57	33.86	36.14	38.70
	State 14	12.79	14.31	34.12	36.20	38.76
	State 15	12.77	14.52	34.19	36.22	38.67
	State 16	12.72	14.78	34.31	36.45	39.00
	State 17	12.73	14.33	34.26	36.26	38.79

in all health states. The maximum change in the fundamental natural frequency among various health states was relatively small, 0.98% and 1.26% for the frequencies extracted from accelerometer and strain gauge data, respectively. The small changes imply that the change in fundamental natural frequency may not be a sensitive damage indicator, particularly when considering environmental effects experienced by a real structure. The maximum change in the frequency of Mode 5 (the second flexural mode shape, as seen in the next section) among various health states was also relatively small, at 1.20% and 1.86% for the frequency extracted from accelerometer and strain gauge data, respectively.

On the other hand, the maximum change in the frequency of Mode 3 among various health states was relatively large, at 13.37% and 10.23% for the frequency extracted from accelerometer and strain gauge data, respectively. In fact, for accelerometer data, the frequency of Mode 3 (around 30 Hz) in several health states, including Health States 3, 4, 5, and 8, was significantly different from the corresponding frequency in other health states (around 34 Hz). The common feature of the Health States 3, 4, 5, and 8 (see Table 3.4) was that one cross-bracing diaphragm located around the mid-span of the bridge (i.e., D-X5.2Y2.25 or D-X2.8Y1.35, see Fig. 3.3) was disconnected, which could reduce the lateral and torsional stiffness of the structure significantly.

The largest changes in frequency were found to result from shifts in modes (i.e., the mode shifts to another different mode due to the presence of damage, which means that the two modes compared may be treated as two different modes) instead of changes in the same mode. In other words, a completely different new mode shape (i.e., Mode 3 with a frequency around 30 Hz) was introduced for the Health States 3, 4, 5, and 8, due to the disconnection of the cross-bracing diaphragms around mid-span of the bridge. Mode 4 in these health states is most likely similar to Mode 3 in other health states, while the vibration mode around 35.8 Hz (similar to Mode 4 in other health states) either disappeared or was inadvertently not extracted since the modes were so close to each other and five other modes had already been detected. For strain gauge data, there are similar results for Health State 8 (with frequency of 31.22 Hz). However, the lower frequency mode (around 30 Hz) in Health States 3, 4, and 5 was not extracted, which

may be due to the fact that the strain gauges were not sensitive to the higher frequency signals; also, the vibration mode around 30 Hz did not appear to be as dominant in these health states.

Although comparison of two different modes may be meaningless in one sense, from another perspective, it could be very useful because the large shifting in modes could be a good indicator for global damage. For example, in the current study, the disconnection of cross-bracing diaphragms changed the load sharing between different girders, hence the global stiffness, and ultimately the resulting torsional modes.

4.2.3 Measured mode shapes

Mode shapes for the lowest five vibration modes of the intact (i.e., Health State 1) bridge model, as derived from accelerometer and strain gauge data, are presented in Figures 4.8 and 4.9, respectively. In both cases, the mode shapes were averaged from five unit-area normalized mode shapes (see Section 4.4.3), which were extracted from data recorded in five repeated tests, each with a recorded period of 80 seconds, using white noise random excitation. The strain-based mode shapes represent the relative magnitudes of modal strain responses measured at the lowest of the three strain gauges at each instrumented location.

It should be acknowledged that the strain-based mode shapes are somewhat different from the traditional definition of mode shape using deflection. Actually, the strain-based mode shape is directly related to the curvature of the deflection mode shape, based on the assumption that the location of the neutral axis remains constant both in tension and compression under small deflections and that the structure remains in a linear elastic state. However, the change in strain-based mode shapes can still be used in structural health monitoring, whether or not this assumption is correct. This is because the strain gauges were permanently installed, and therefore the locations and conditions of sensors were consistent between various tests. As a result, any change in the physical condition of the structure (reflecting its stiffness and load capacity) should be reflected in the strain gauge measurements.

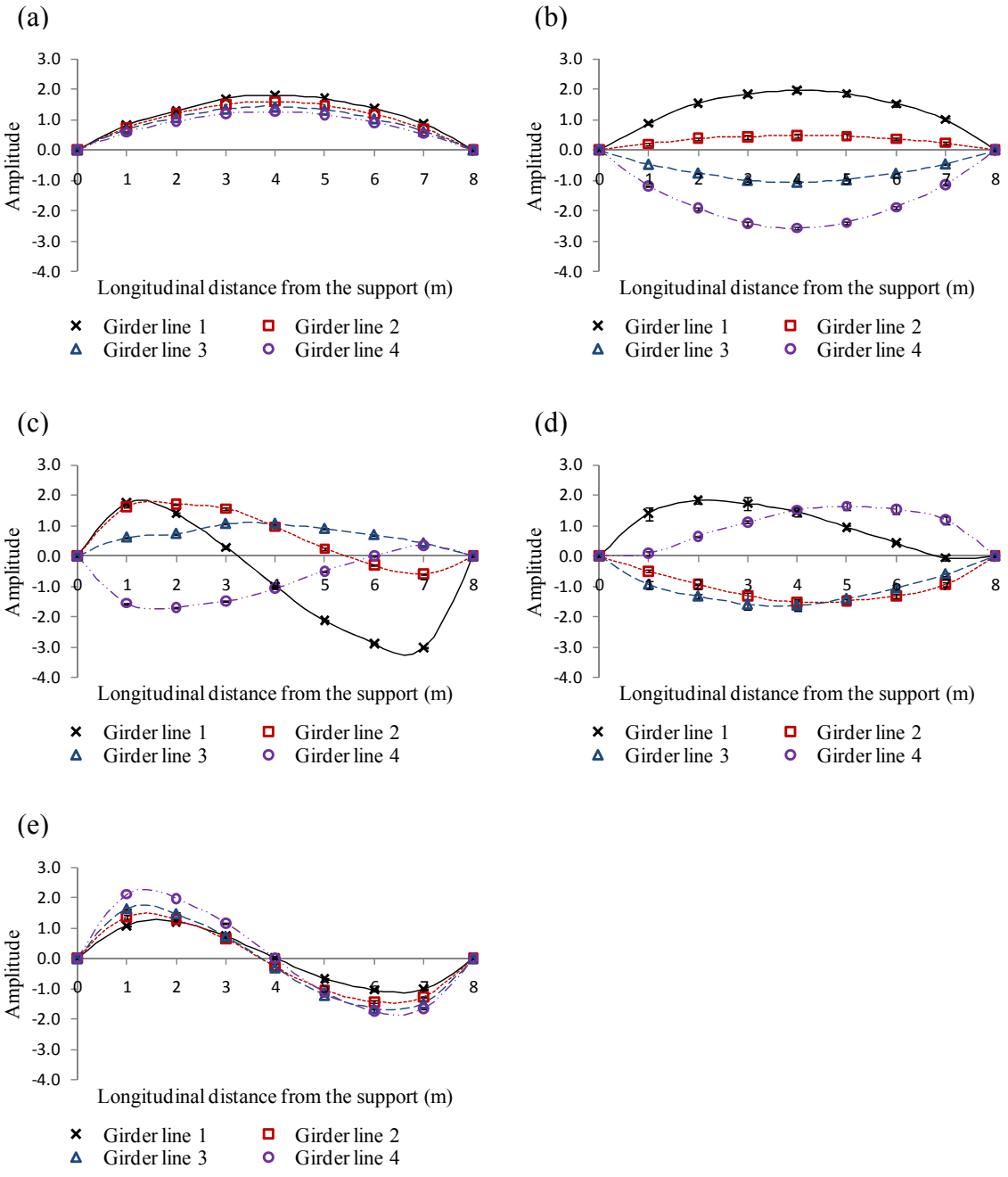

Figure 4.8. The lowest five vibration mode shapes for Health State 1 based on accelerometer data: (a) Mode 1, (b) Mode 2, (c) Mode 3, (d) Mode 4, and (e) Mode 5.

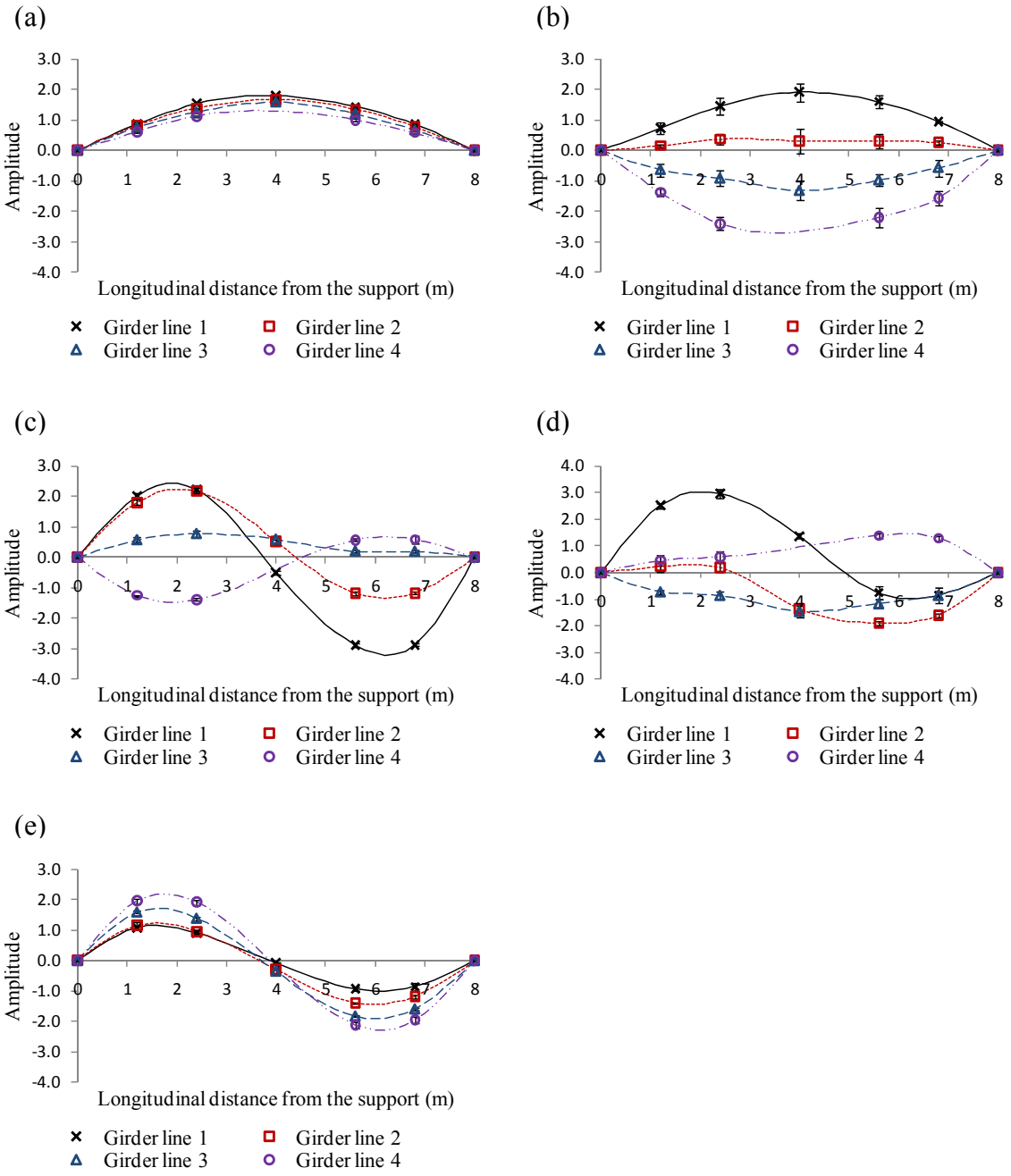

Figure 4.9. The lowest five vibration mode shapes for Health State 1 based on bottom strain gauge data: (a) Mode 1, (b) Mode 2, (c) Mode 3, (d) Mode 4, and (e) Mode 5.

From the shapes shown in Figs. 4.8 and 4.9, it is apparent that Mode 1 was an unsymmetrical flexural mode shape, with the asymmetry likely due to the presence of the over-designed splice connection on Girder 4 (approximately 10% over-designed in terms of the cross-sectional rigidity). Mode 2 was a torsional mode shape, while Mode 3 and Mode 4 exhibited combined flexural and torsional behaviour. Mode 5 was the second flexural mode shape.

The acceleration-based mode shapes (Fig. 4.8) were defined by 28 measurement points (seven points for each girder). The strain-based mode shapes (Fig. 4.9) were defined by 19 bottom strain gauges (five strain gauges for Girders 1, 2, and 3, and only four strain gauges for Girder 4 due to the presence of the splice connection on the girder). In both cases, to better represent the vibration mode shapes, the mode shape lines were interpolated using a natural cubic spline interpolation function, creating a piecewise cubic polynomial that passed through all the measured amplitudes. The spline function featured continuous first and second derivatives at measurement points, and zero curvature at supports.

The values shown in Figs. 4.8 and 4.9 were averaged from the normalized mode shapes from five tests (a detailed discussion of mode shape normalization is presented in Section 4.4). The standard deviations of the modal amplitudes are also plotted in Figs. 4.8 and 4.9 using error bars. However, the error bars are not noticeable except in Fig. 4.8 (d) and Fig. 4.9 (b) and (d), where small scale error bars can be observed. Lower variability in the measured mode shape amplitudes means a higher repeatability and reliability of the measured mode shapes.

A visual examination of Figs. 4.8 and 4.9 suggests that the two sensor types resulted in consistent mode shape definitions. In fact, some of the apparent differences are due to the absence of one strain gauge at the mid-span of Girder 4. To better visualize the vibration modes, three-dimensional plots of mode shapes are presented in Fig. 4.10, where the lowest five vibration mode shapes in Health State 1 were extracted based on accelerometer data using white noise random excitation.

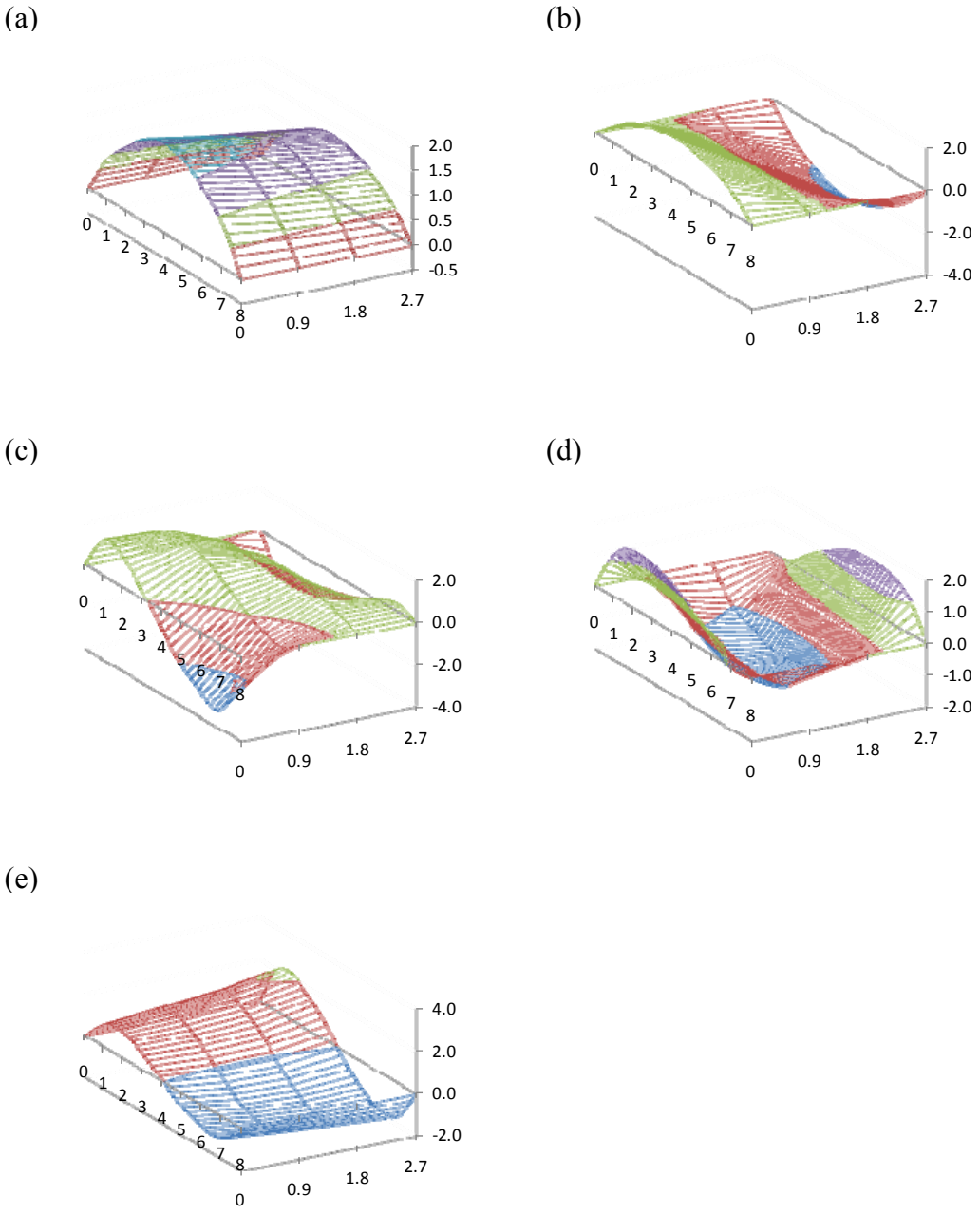

Figure 4.10. The lowest five vibration mode shapes for Health State 1 based on accelerometer data with white noise random excitation: (a) Mode 1, (b) Mode 2, (c) Mode 3, (d) Mode 4, and (e) Mode 5.

4.2.4 Comparison of the measured mode shapes in different health states

A comparison of the first and second mode shapes measured for different health states is presented in Figs. 4.11 and 4.12. In all cases, the vibration mode shapes shown were averaged from the normalized modal amplitudes using a unit-area normalization method (see Section 4.4.3), extracted from the accelerometer data of five repeated tests, using harmonic excitation. These are slightly different from the mode shapes defined in Fig. 4.8, where white noise excitation was used. To better compare the results, the mode shapes corresponding to different health states have been divided into four groups and presented in four plots, with the mode shape for Health State 1 appearing in each plot as a common reference. Also, to improve the clarity in each plot, the mode shapes along individual girder lines have been separated and strung end to end.

A visual examination of Figs. 4.11 and 4.12 demonstrates that the mode shapes in different health states were very similar, although some differences in mode shape amplitudes are noticeable for some health states. The major noticeable differences were due to the disconnection (Health State 2) or re-connection (Health State 13) of the splice on Girder 4. Quantitative comparisons of mode shapes are available in Chapter 6. Additional information about the definition of other mode shapes is available in Appendix E.

4.3 Influence of Test Parameters on Dynamic Properties

4.3.1 Overview

Since VBDD methods rely on the identification of small changes in dynamic properties to infer the nature of the damage, reliable estimates of these properties are essential for a successful implementation of VBDD schemes. As a result, the influence of various testing parameters on the repeatability and reliability of modal property extraction was investigated on the intact bridge model (i.e., Health State 1, see Section 3.4) in Phase I of the dynamic tests (see Table 3.1). To simplify the process, only the sensors located on Girder 1 were used for this investigation. More specifically, the testing parameters investigated in this study included sensor type and vertical location of strain gauges,

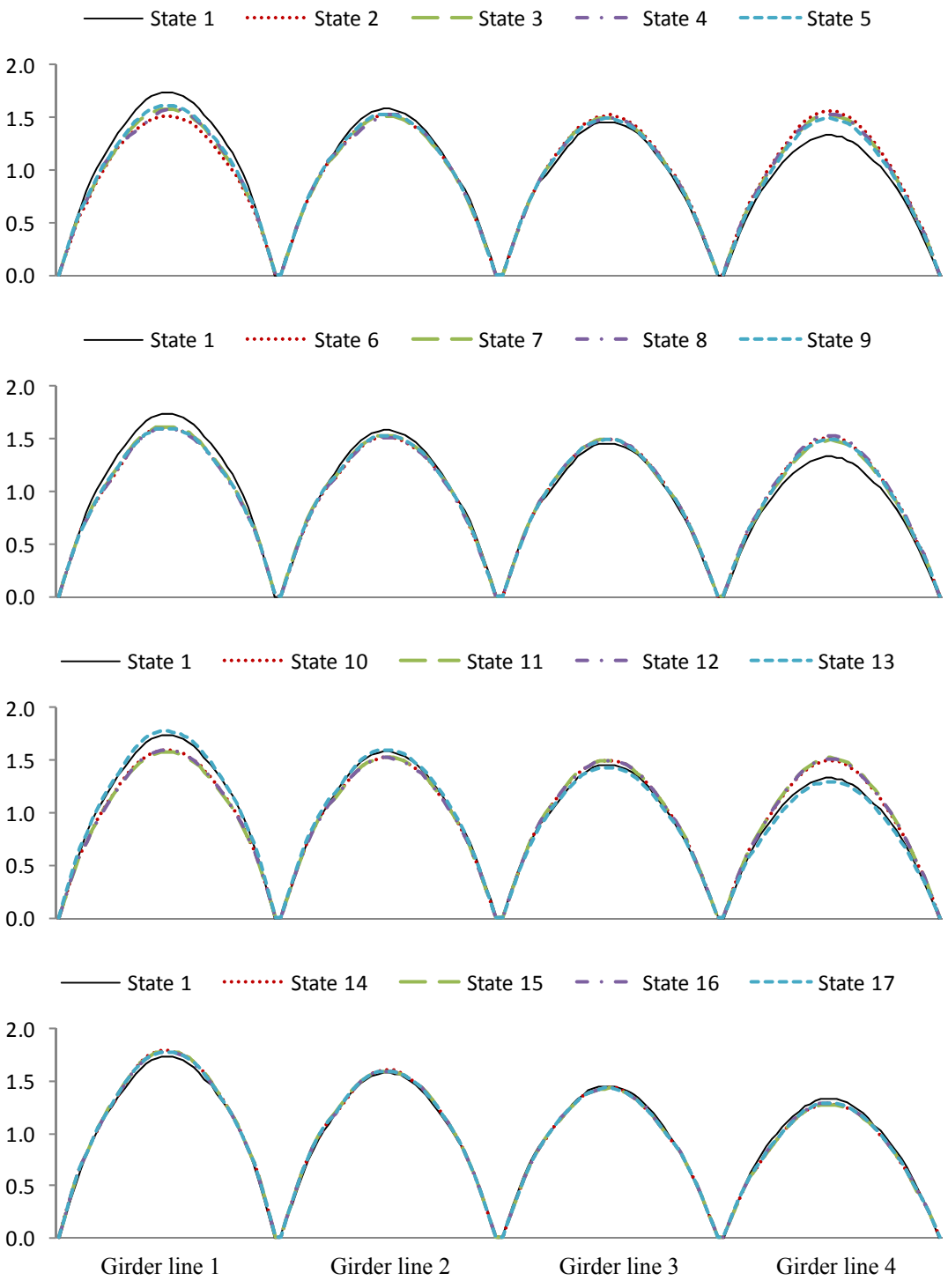

Figure 4.11. Comparison of the first mode shape for different health states using accelerometer data with harmonic excitation.

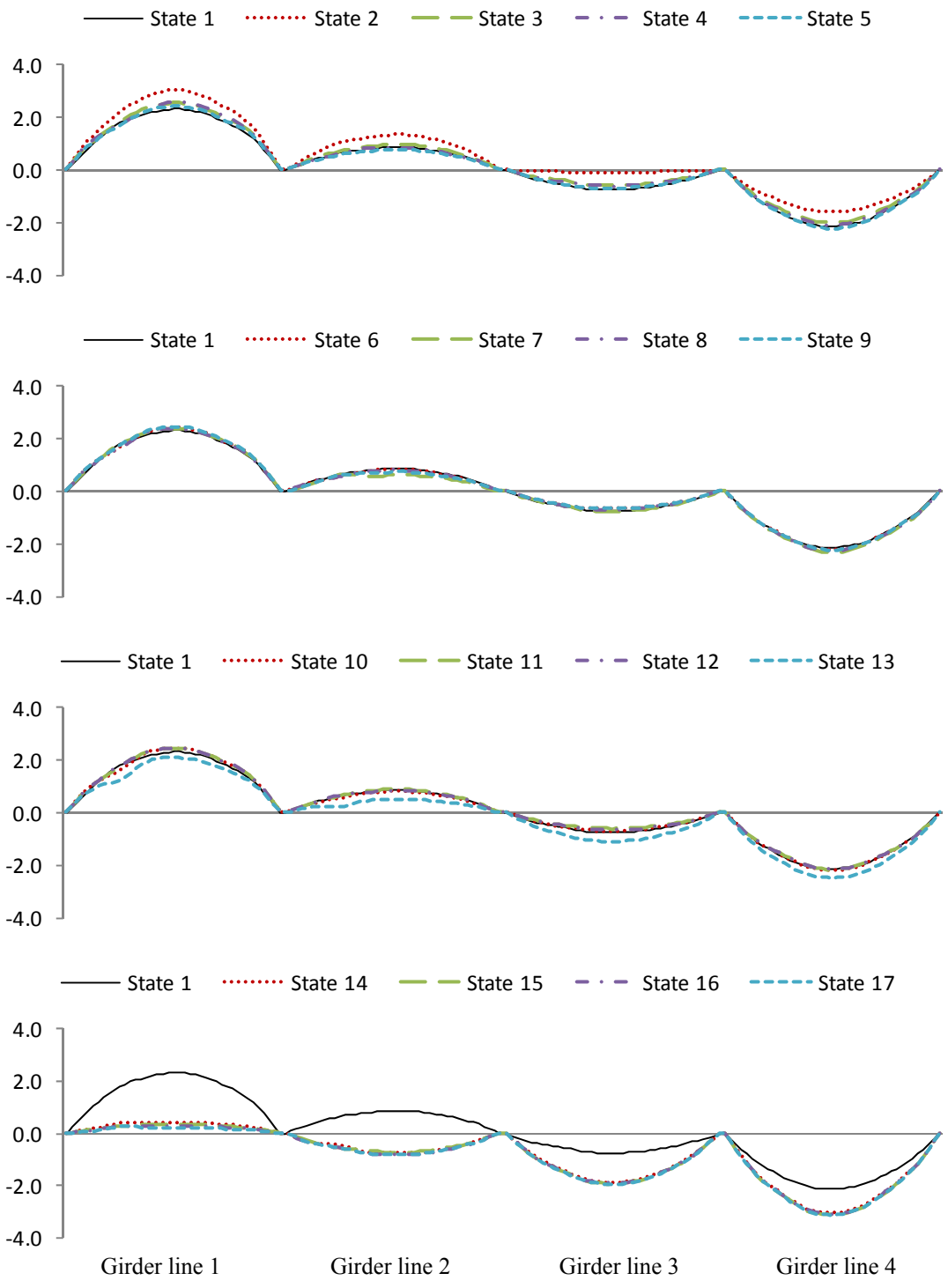

Figure 4.12. Comparison of the second mode shape for different health states using accelerometer data with harmonic excitation.

excitation methods, data sampling period (the length in time of recorded signal), modal analysis method, and data sampling rates.

4.3.2 Influence of sensor type and vertical location of strain gauges

The lowest five vibration mode shapes along Girder 1 of the intact bridge model were extracted using the SSI method from accelerometer and strain gauge data, where data from three separate groups of strain gauges were considered as individual cases, corresponding to data from only the bottom, middle, or top strain gauges at all locations. The data were recorded for a period of 80 seconds with a sampling rate of 1000 Hz, under white noise random excitation. Before using the SSI method to identify the modal properties, the recorded signals were decimated to a lower sampling rate of 200 Hz using low-pass digital filter techniques. A quantitative comparison of the mode shapes is summarized in Table 4.4 according to the four groups of sensors used to define the mode shapes. Here, the mode shapes are compared based on the Modal Assurance Criteria (MAC) (Ewins 2000), defined as:

$$MAC = \frac{\left[\sum_{i=1}^{k}(\boldsymbol{\phi_m})_i \cdot (\boldsymbol{\phi_n})_i\right]^2}{[\sum_{i=1}^{k}(\boldsymbol{\phi_m})_i{}^2]\cdot[\sum_{i=1}^{k}(\boldsymbol{\phi_n})_i{}^2]} \quad [4.1]$$

where $\boldsymbol{\phi_m}$ and $\boldsymbol{\phi_n}$ are two mode shape vectors being compared, the subscript i indicates an element in the vectors (corresponding to a particular sensor location), and k represents the number of measurement points. The MAC value represents the degree of correlation between two mode shapes and varies from zero to unity. A MAC value of unity denotes perfectly correlated mode shapes, while a MAC value of zero would suggest a complete lack of correlation (i.e., orthogonal shapes).

As suggested above, in addition to mode shapes based on accelerometer readings, results in Table 4.4 are also provided for mode shapes defined by the three groups of strain gauges considered (the bottom, middle and top strain gauges at each instrumented location). For all of these, MAC values provided in Table 4.4 represent averaged comparisons between unit-norm normalized mode shapes (see Section 4.4.2), extracted from individual trials and the averaged normalized mode shape generated from all five

Table 4.4. Influence of sensor group on mode shape reliability based on averaged MAC values from five repeated trials with white noise random excitation.

Instrumentation		Mode 1	Mode 2	Mode 3	Mode 4	Mode 5
Acceleration	Avg.	0.9999968	0.9995244	0.9998721	0.9958494	0.9997260
	C.O.V.	*0.00032%*	*0.04091%*	*0.01181%*	*0.46720%*	*0.02529%*
Bottom Strain	Avg.	0.9998726	0.9977945	0.9991574	0.9940285	0.9982590
	C.O.V.	*0.00662%*	*0.13401%*	*0.03676%*	*0.32077%*	*0.13412%*
Middle Strain	Avg.	0.9994881	0.9939806	0.9991072	0.9936696	0.9977089
	C.O.V.	*0.04697%*	*0.50404%*	*0.04621%*	*0.34150%*	*0.15767%*
Top Strain	Avg.	0.9992558	0.9850748	0.9987266	0.9899599	0.9956863
	C.O.V.	*0.04638%*	*1.11304%*	*0.07789%*	*0.65779%*	*0.18205%*

Avg. = Average;
C.O.V. = Coefficient of variation.

trials for a given group of sensors. To clarify, first, the individual mode shapes were extracted from the sensor data for five repeated trials. Then, the averaged mode shape was calculated from the five extracted, individually unit-norm normalized mode shapes. Next, the averaged mode shape was normalized again using unit-norm normalization. Next, MAC values were calculated for each individual mode shape by comparing the individual normalized mode shape and the averaged normalized mode shape using Eq. 4.1. Finally, the averaged MAC values were calculated from the five individual MAC values for each sensor group and each vibration mode.

Overall, the accelerometer data produced the most reliable mode shape estimates, with averaged MAC values exceeding 0.995 for all of the lowest five modes, and an averaged MAC value exceeding 0.99999 for the fundamental mode, together with the lowest coefficient of variation of 0.00032%. As expected, the bottom gauges provided the most reliable results among the strain gauge groups, with averaged MAC values (exceeding 0.9998 for the fundamental mode with coefficient of variation of 0.00662%) only slightly lower than those based on accelerometer readings. The consistent trend of deteriorating reliability as the gauges moved up toward the neutral axis illustrates the role of the signal-to-noise ratio in the resulting uncertainty in measured mode shapes. The comparable quality of the bottom strain gauge and accelerometer results, though, suggests that the less expensive strain gauges may be a viable option for dynamic

system identification as long as the reliability of the measured signal can be maintained at a sufficiently high level. However, mode shapes discussed in subsequent sub-sections in Section 4.3 were based exclusively on accelerometer data.

4.3.3 Influence of excitation type

As described previously, both resonant harmonic and white noise random inputs were used to excite the bridge model. A comparison of the mode shape reliability for the two types of excitation is provided in Table 4.5. As described in the previous sub-section, MAC results presented here represent averaged comparisons between unit-norm normalized mode shapes extracted from individual trials and the averaged normalized mode shape generated from all five trials using accelerometer data. Results using strain gauge data are presented in Appendix E. The data were recorded for a period of 80 seconds for both white noise random and harmonic excitations. The data sampling rate was 1000 Hz for white noise random excitation, then decimated to a lower sampling rate of 200 Hz before using the SSI method to identify the modal properties. However, a lower sampling rate of 500 Hz was used to record the data for harmonic excitation (due to less uncertainty), which was then decimated to 100 Hz for modal identification using the SSI method. For the harmonic loading trials, preliminary tests using random excitation were required to identify system natural frequencies; for the random loading trials, on the other hand, all modal parameters were extracted simultaneously from the same data sets.

Table 4.5. Influence of excitation type on mode shape reliability based on averaged MAC values using accelerometer data from five replicate trials.

Excitation		Mode 1	Mode 2	Mode 3	Mode 4	Mode 5
White Noise	Avg.	0.9999968	0.9995244	0.9998721	0.9958494	0.9997260
	C.O.V.	*0.00032%*	*0.04091%*	*0.01181%*	*0.46720%*	*0.02529%*
Harmonic	Avg.	1.0000000	0.9999997	0.9999861	0.9999935	0.9999588
	C.O.V.	*0.00000%*	*0.00004%*	*0.00110%*	*0.00049%*	*0.00488%*

Avg. = Average;
C.O.V. = Coefficient of variation.

As demonstrated in Table 4.5, resonant harmonic loading produced mode shapes with exceptionally high repeatability (i.e., a MAC value greater than 0.99999999 for the fundamental mode and greater than 0.9999 for all of the lowest five modes, with a coefficient of variation less than 0.005% for all of the five modes). Results using white noise random excitation were decidedly more uncertain, with MAC values as low as 0.995 for some modes, and a coefficient of variation as high as 0.467%.

4.3.4 Influence of recording period and modal analysis method

Based on random process theory, it may be expected that the detrimental effects of random measurement and signal processing errors may be attenuated by making use of longer measurement records in the estimation of modal properties. To help quantify the extent of such benefits, a series of trials was carried out featuring five different sampling periods ranging from 10 s to 160 s in length (i.e., from 128 to 2044 times the fundamental period). First, five trials were carried out for each sampling period, using a sampling frequency of 200 Hz when both harmonic and white noise random excitations were used. Then, the same process was carried out using a sampling rate of 1000 Hz for white noise random excitation only.

For resonant harmonic excitation using a sampling rate of 200 Hz (then decimated to 100 Hz in data pre-processing), the measured fundamental mode shapes for various sampling periods (from 10 s to 160 s) are presented in Figure 4.13, where both the SSI and PP methods were used to extract modal properties. As before, the mode shapes presented in Fig. 4.13 were averaged from five unit-norm normalized mode shapes. The standard deviations of the amplitudes of mode shapes from five trials are also plotted in the figure using error bars. However, the error bars are not noticeable visually for any of the sampling periods no matter which modal analysis method was adopted (i.e., SSI or PP method), which suggests that the measured mode shapes are highly repeatable with little variation even for a recording period as short as ten seconds. Also, it can be seen from the results that the PP method resulted in a comparable accuracy of mode shape definition compared with the SSI method. As a result, it was considered suitable to use the simple and time-saving PP modal analysis method to extract modal properties

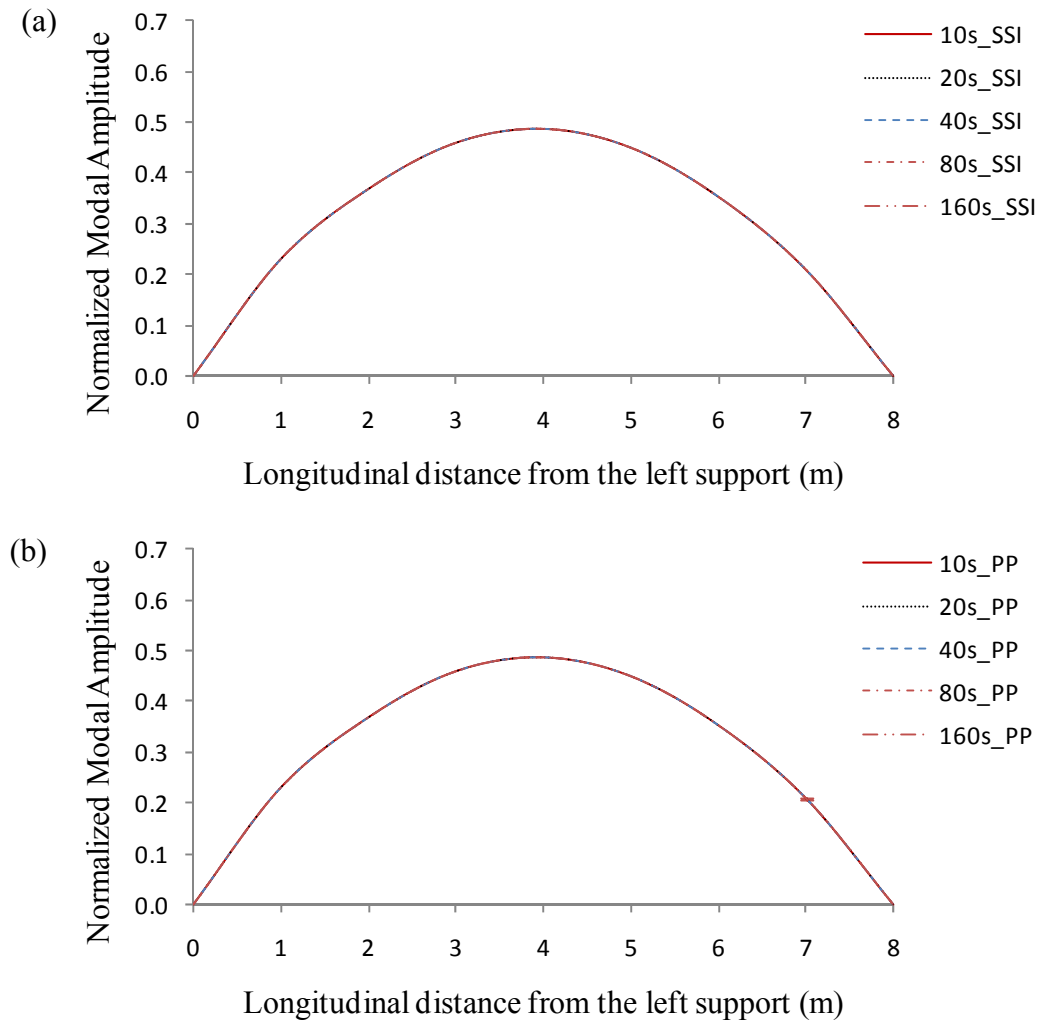

Figure 4.13. Influence of recording period on mode shape definition for resonant harmonic excitation when both (a) SSI and (b) PP methods were used to extract modal properties.

for Phase II vibration tests conducted later on (see Table 3.1) when using resonant harmonic excitation.

A quantitative comparison of the fundamental mode shape repeatability for various sampling periods, using the same mode shapes shown in Fig. 4.13, is presented in Table 4.6. As before, the averaged MAC values in Table 4.6 were calculated from five individual MAC values that represent a comparison between the normalized mode shape extracted from a single trial under a specific set of conditions (i.e., excitation type and sampling period) and the averaged normalized mode shape computed for all five trials

Table 4.6. Influence of recording period on the repeatability of the fundamental mode shape based on averaged MAC values from five repeated trials with harmonic excitation and sampling rate of 200 Hz.

Recording Time (s)		Averaged MAC value				
		10	20	40	80	160
SSI	Avg.	0.99999993	0.99999998	0.99999999	0.99999996	0.99999997
	C.O.V.	*0.000007%*	*0.000001%*	*0.000000%*	*0.000006%*	*0.000003%*
PP	Avg.	0.99999713	0.99999998	0.99999999	0.99999999	0.99999998
	C.O.V.	*0.000259%*	*0.000001%*	*0.000001%*	*0.000001%*	*0.000002%*

Avg. = Average;
C.O.V. = Coefficient of variation.

conducted under those conditions. From the table, it can be seen that a high level of reliability with very little variation was attained for the harmonic excitation (a MAC of 0.9999999 for the SSI method with a coefficient of variation of 0.000007%, and a MAC of 0.9999964 for PP method with a coefficient of variation of 0.000259%) using sampling periods as short as 10 s, beyond which there was little improvement.

For white noise random excitation using a sampling rate of 200 Hz (then decimated to 100 Hz in data pre-processing), the extracted fundamental mode shapes with error bars for various sampling periods are plotted in Figs. 4.14 and 4.15, using the SSI and PP modal analysis methods, respectively. As before, the mode shapes presented in the figures were averaged from five unit-norm normalized mode shapes. A visual examination of Figs. 4.14 and 4.15 demonstrates that the mode shape reliability increased consistently with an increase in the recording period, no matter which modal analysis method was used, and that the shorter recording periods of 10 s and 20 s produced great variation in the measured mode shape, while a longer recording period of 160 s generated relatively low variation in the extracted mode shape.

The mode shape shown in Fig. 4.15 (c) (extracted using the PP method) is far from the expected true mode shape (see Fig. 4.8 (a) for Girder line 1) even with a recording period as long as 160 seconds, and is not a reliable estimation. This may due to the fact that more than one mode contributed to the operational deflection mode shape identified using the PP method. In fact, the PP method assumes that the dynamic response at

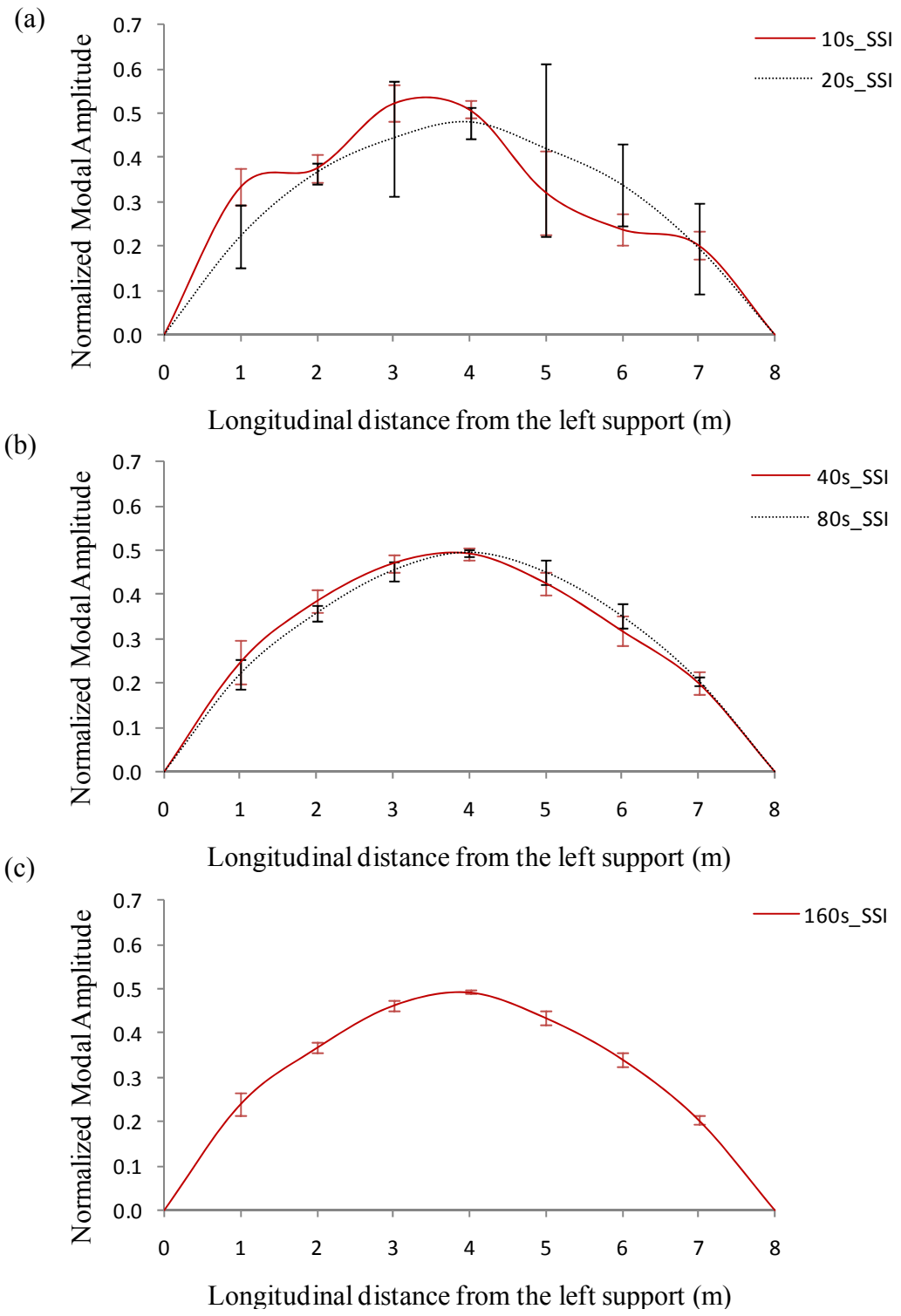

Figure 4.14. Influence of recording period on mode shape definition for white noise random excitation with sampling rate of 200 Hz when the SSI method was used to extract modal properties.

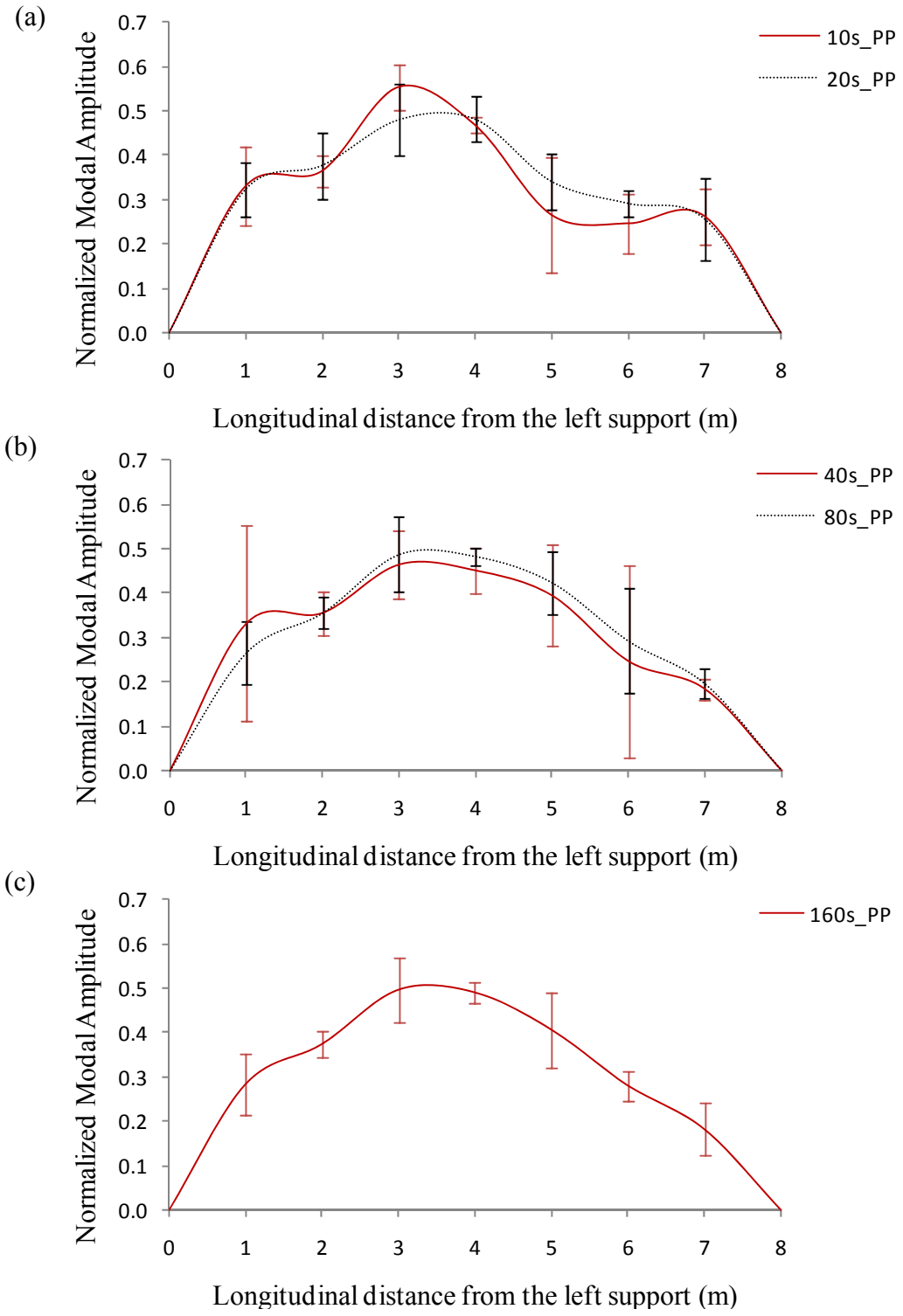

Figure 4.15. Influence of recording period on mode shape definition for white noise random excitation with sampling rate of 200 Hz when the PP method was used to extract modal properties.

resonance is only influenced by one mode. The validity of this assumption decreases when the modes are not well separated (Peeters et al. 1998). In this case, the second mode, with a natural frequency of 13.8 Hz, was not well separated from the first mode with natural frequency of 12.7 Hz. This can be partially proven from the results shown in Table 4.9 and Fig. 4.18, produced using a sampling rate of 200 Hz, as discussed in next sub-section, where the second mode was difficult to identify (it had a very high variability) even using the SSI method. Simply adding the shapes together using appropriate scaling factors in Figs. 4.18 (a) (Mode 1) and 4.18 (b) (Mode 2) for 200 Hz could give a shape close to the one shown in Fig. 4.15 (c).

On the other hand, the mode shape shown in Fig. 4.14 (c) (extracted using the SSI method for a recording period of 160 s) presents a much more accurate shape than that shown in Fig. 4.15 (c), even though the shape still experiences some variation. As a result, the SSI method was adopted to extract modal properties for Phase II vibration tests (see Table 3.1), when using white noise random excitation.

A quantitative comparison of the mode shapes shown in Figs. 4.14 and 4.15 is presented in Table 4.7. As before, the averaged MAC values shown in Table 4.7 represent averaged comparisons from five trials conducted under same conditions. From the results shown in Table 4.7 for white noise excitation, the mode shape repeatability generally increased with an increase in recording period for both modal analysis methods, achieving a MAC value of 0.999 with a coefficient of variation of 0.09%, and

Table 4.7. Influence of recording period on the repeatability of the fundamental mode shape based on averaged MAC values from five repeated trials with white noise random excitation and sampling rate of 200 Hz.

Recording Time (s)		Averaged MAC value				
		10	20	40	80	160
SSI	Avg.	0.987	0.936	0.995	0.997	0.999
	C.O.V.	*1.15%*	*6.23%*	*0.36%*	*0.27%*	*0.09%*
PP	Avg.	0.970	0.975	0.906	0.973	0.982
	C.O.V.	*1.67%*	*2.50%*	*11.30%*	*1.83%*	*1.15%*

Avg. = Average;
C.O.V. = Coefficient of variation.

a MAC value of 0.982 with a coefficient of variation of 1.15%, for a recording period of 160 s when SSI and PP methods were used, respectively.

The error (or inaccuracy) shown in Fig. 4.15 (c) may also be partially due to the relatively low sampling rate, 200 Hz, that was selected for these specific tests, since a higher sampling rate of 1000 Hz conducted later on produced a much better mode shape definition (see Figs. 4.16 and 4.17). The results shown in Figs. 4.16 and 4.17 for the SSI and PP methods, respectively, were extracted from data using the same sensors, data acquisition system, and data processing techniques as the data used for Figs. 4.14 and 4.15, except that a sampling rate of 1000 Hz (then decimated to 100 Hz in data pre-processing) was used instead of 200 Hz (then decimated to 100 Hz in data pre-processing). The shapes shown in these figures are much closer to the expected true mode shape, even for the mode shapes shown in Fig. 4.17 (a) using the PP method with a recording period as short as 10 seconds. As a result, they represent a more reliable mode shape estimation.

A quantitative comparison of the mode shapes shown in Figs. 4.16 and 4.17 was also conducted and is presented in Table 4.8. As before, the averaged MAC values shown in Table 4.8 represent averaged comparisons from five trials conducted under same conditions. The results shown in Table 4.8 feature similar trends to those shown in Table 4.7. The mode shape repeatability increased consistently with an increase in recording period for both modal analysis methods. However, the MAC values are much

Table 4.8. Influence of recording period on the repeatability of the fundamental mode shape based on averaged MAC values from five repeated trials with white noise random excitation and sampling rate of 1000 Hz.

Recording Time (s)		Averaged MAC value				
		10	20	40	80	160
SSI	Avg.	0.99999759	0.99999914	0.99999885	0.99999975	0.99999980
	C.O.V.	*0.000069%*	*0.000039%*	*0.000080%*	*0.000008%*	*0.000013%*
PP	Avg.	0.99945579	0.99991662	0.99991400	0.99999365	0.99990645
	C.O.V.	*0.046451%*	*0.011674%*	*0.006862%*	*0.000236%*	*0.008279%*

Avg. = Average;
C.O.V. = Coefficient of variation.

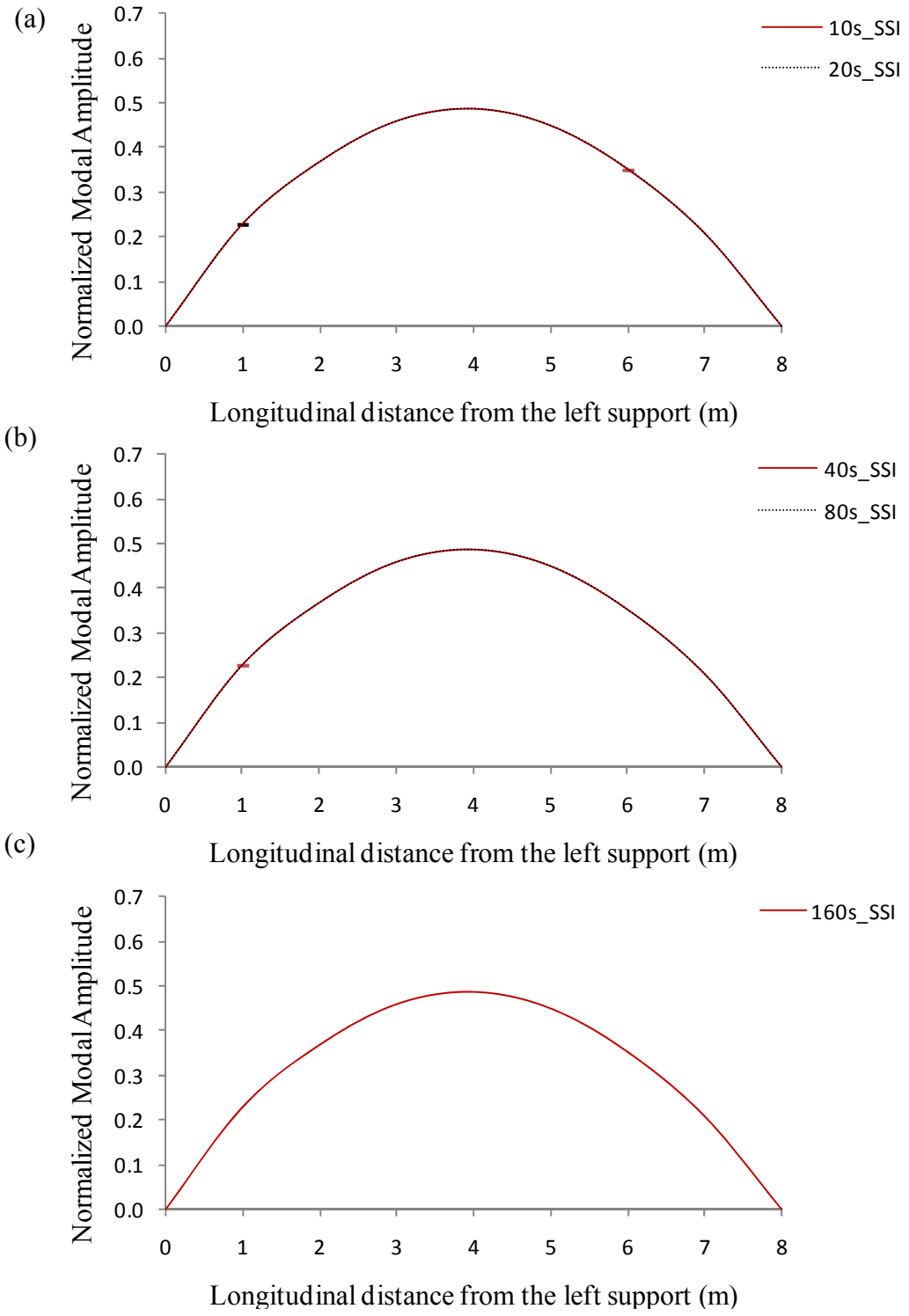

Figure 4.16. Influence of recording period on mode shape definition for white noise random excitation with sampling rate of 1000 Hz when SSI method was used to extract modal properties.

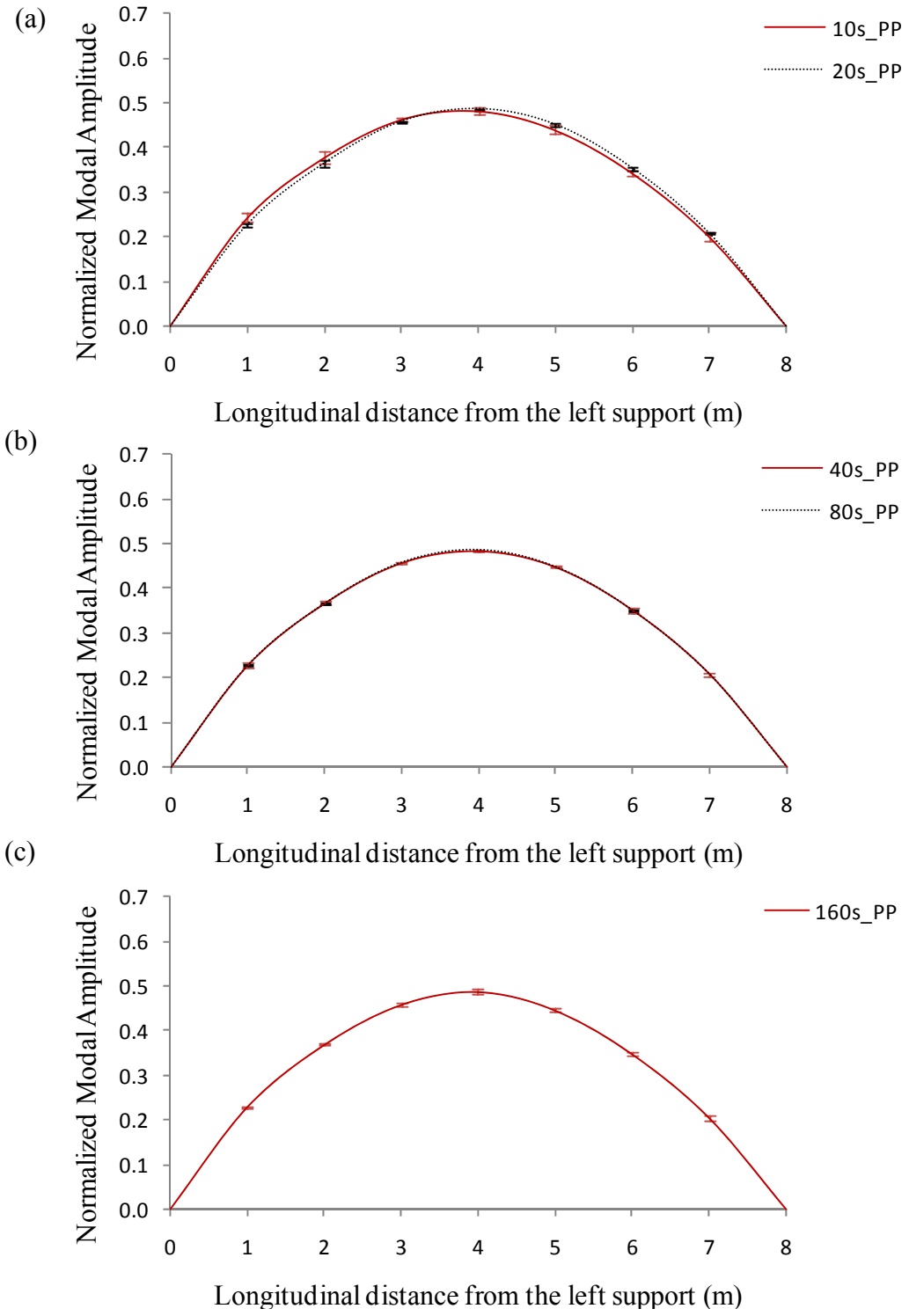

Figure 4.17. Influence of recording period on mode shape definition for white noise random excitation with sampling rate of 1000 Hz when PP method was used to extract modal properties.

higher than those in Table 4.7, together with much less variation for both modal analysis methods, achieving a MAC value of 0.999997 with a coefficient of variation of 0.000069%, and a MAC value of 0.9994 with a coefficient of variation of 0.046%, for a recording period as short as ten seconds, when SSI and PP methods were used, respectively. As a result, the sampling rate was shown to play an important role in the reliability of the measured mode shapes. A detailed discussion about the influence of sampling rate on the reliability of measured mode shapes is presented in the next sub-section.

4.3.5 Influence of sampling rate and data smoothing

Another method of reducing the effects of random noise is through averaging achieved in the time domain using digital filters. To study the potential benefits of time domain averaging on mode shape reliability, random excitation trials were carried out using four different sampling rates: 200, 500, 800, and 1000 Hz. Prior to modal property extraction, however, all acceleration time histories were decimated using a low-pass filter, creating modified (smoothed) data sets with an effective sampling rate of 100 Hz. For all sampling rates, five trials were conducted, each with a period of 80 seconds (or 1,022 times the fundamental natural period).

The extracted mode shapes using the SSI method for the various sampling rates are presented in Figs. 4.18 (for Modes 1 and 2) and 4.19 (for Modes 3, 4, and 5). As before, the mode shapes presented in Figs. 4.18 and 4.19 were averaged from five unit-norm normalized mode shapes. The standard deviations of the amplitudes of mode shapes from five trials are also plotted in the figure using error bars. From the results shown in figures, it can be seen that the estimation of Modes 2 and 4 produced the greatest variability when a sampling rate of 200 Hz was used. Also, the variation in mode shape definition generally decreased with increasing sampling rates.

Comparisons of mode shape reliability achieved using different sampling rates are also presented in Table 4.9 using MAC values. For these tests, results for Mode 2 with a sampling rate of 200 Hz were significantly different from others, with an averaged MAC value of 0.4776 and coefficient of variation of 71.86 %, which means that the

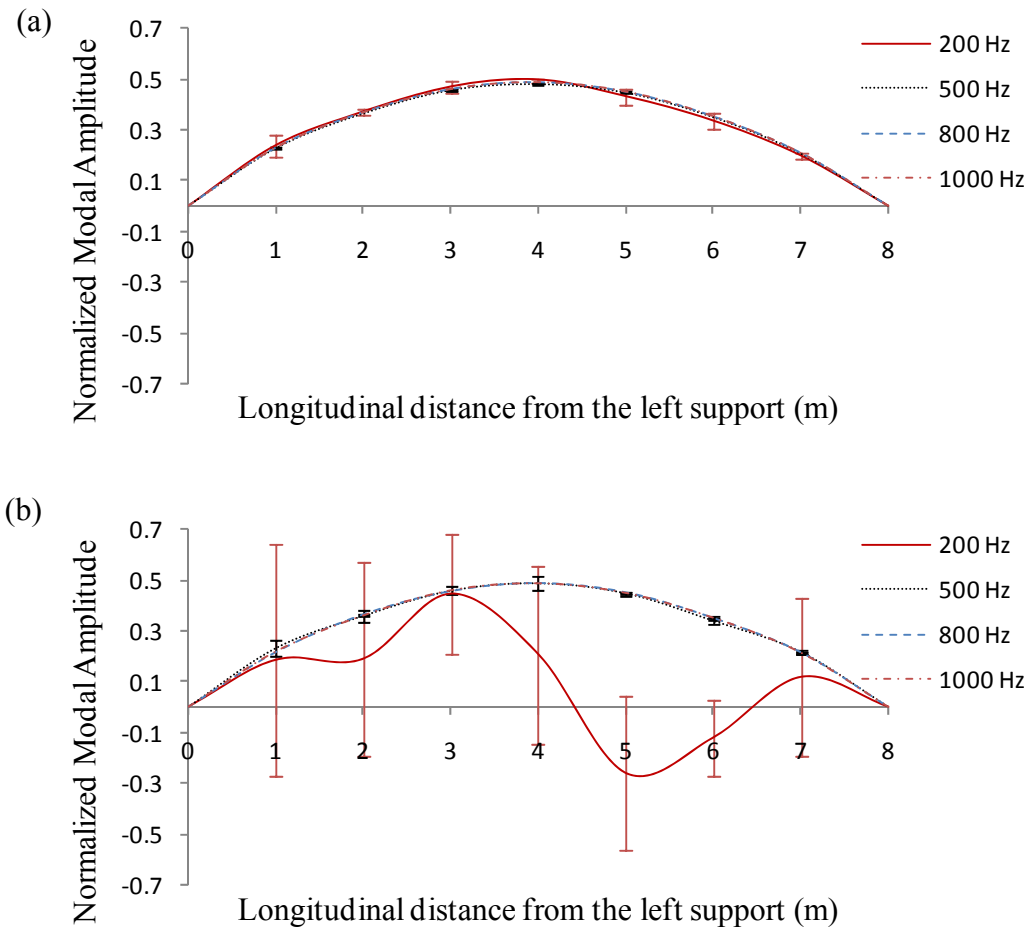

Figure 4.18. Influence of sampling rate on mode shape definition of: (a) Mode 1; (b) Mode 2 for white noise random excitation with recording period of 80 seconds, when the SSI method was used to extract modal properties.

mode shape estimation was highly unreliable. Actually, there were no stable poles available for this mode in the stabilization plots using the SSI modal identification method; in fact, this mode was inadvertently overlooked in previously published results (Wang et al. 2008). From the results listed in Table 4.7, it can be seen that the reliability of the fundamental mode shape continued to improve with increasing sampling rates up to 1000 Hz. As the mode number increased, however, the benefits of the time domain averaging made possible by higher sampling rates appeared to diminish until, for Mode 5, there is no apparent improvement in mode shape reliability associated with increased sampling rates.

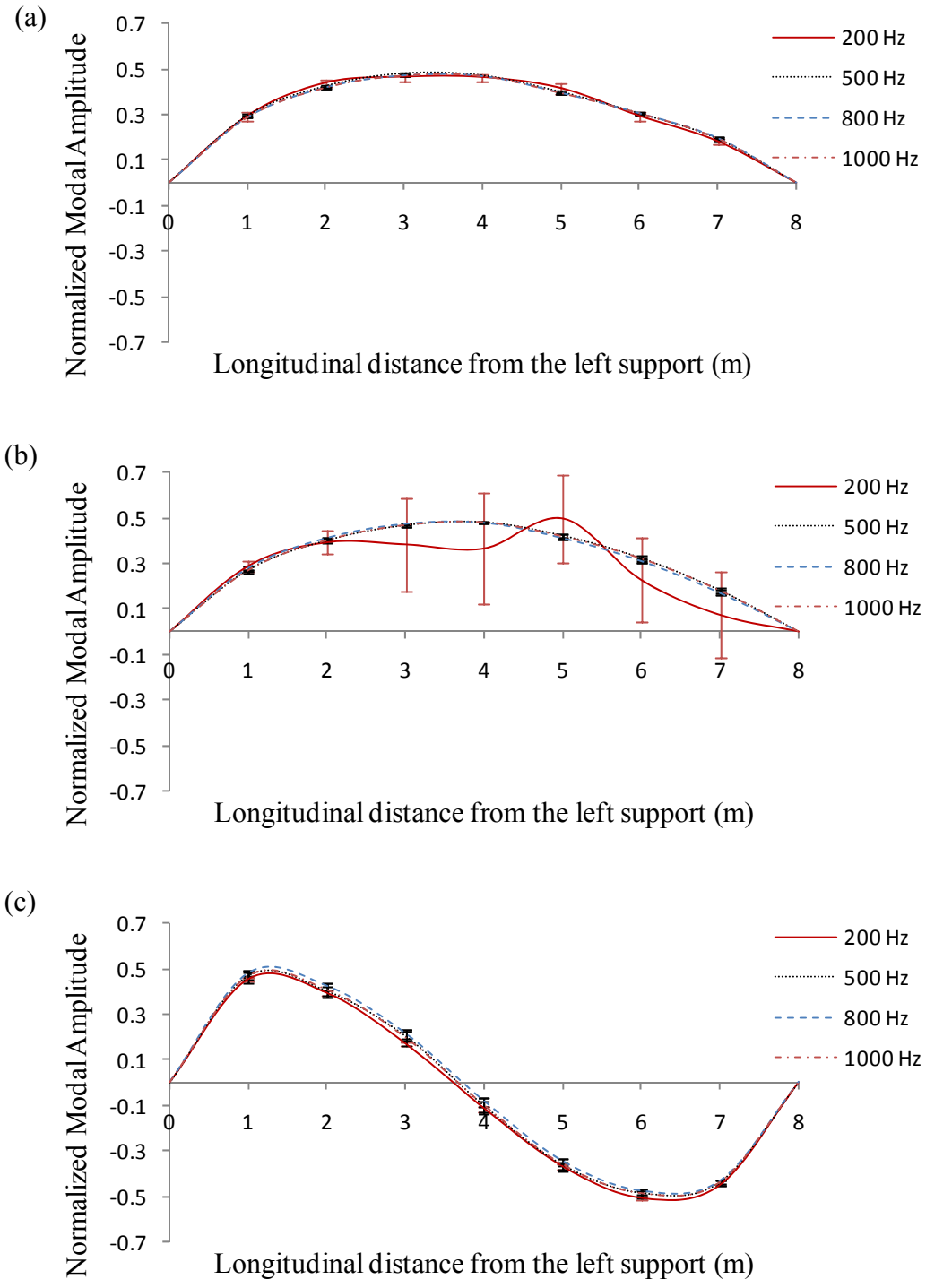

Figure 4.19. Influence of sampling rate on mode shape definition of: (a) Mode 3; (b) Mode 4; (c) Mode 5 for white noise random excitation with recording period of 80 seconds, when the SSI method was used to extract modal properties.

Table 4.9. Influence of sampling rates and time domain averaging on mode shape reliability based on averaged MAC values from five repeated trials with white noise random excitation.

Sampling rate (Hz)		Averaged MAC value			
		200	500	800	1000
Mode 1	Avg.	0.99640644	0.99996793	0.99999927	0.99999975
	C.O.V.	*0.42458%*	*0.00371%*	*0.00003%*	*0.00001%*
Mode 2	Avg.	0.47760945	0.99773264	0.99995200	0.99998641
	C.O.V.	*71.85969%*	*0.26686%*	*0.00573%*	*0.00116%*
Mode 3	Avg.	0.99816765	0.99976419	0.99995609	0.99993072
	C.O.V.	*0.13198%*	*0.01505%*	*0.00592%*	*0.00823%*
Mode 4	Avg.	0.84915608	0.99981073	0.99992883	0.99903376
	C.O.V.	*29.69770%*	*0.01003%*	*0.01152%*	*0.11394%*
Mode 5	Avg.	0.99945380	0.99842765	0.99864071	0.99547048
	C.O.V.	*0.03571%*	*0.11925%*	*0.08802%*	*0.72215%*

Avg. = Average;
C.O.V. = Coefficient of variation.

4.4 Influence of Normalization on Mode Shape Definition and Change in Mode Shape Due to Damage

4.4.1 Overview

Although the shape of vibration modes (i.e., the ratio of modal amplitudes at different measurement points) is determinate, the amplitude of mode shapes is indeterminate in most cases, especially for dynamic tests of civil engineering structures, where the input excitation forces are typically not quantified. As a result, it is necessary to normalize (or scale) the mode shapes with respect to a common base in order to investigate the relative changes in mode shapes caused by damage. There are many different ways to normalize the mode shapes.

One normalization method commonly used in eigenvector analysis is to select one element as a benchmark point (usually the element with maximum relative amplitude) and scale it to a constant value (for example, unity); the remaining elements are then

scaled using the same scaling factor. This method is straightforward and easy to use. However, the method is a localized method (i.e., the scaling factor is based on only one element). Thus, the disadvantage of this method is that the change in mode shape at the damage location will be zero if the location of the selected benchmark point coincides with the location of the damage.

A global-based mode shape normalization method (i.e., one in which all elements are involved in determining the scaling factor) may be more suitable for identifying changes in mode shapes. In this section, a unit-norm normalization method and its influence on mode shape definition were investigated. For the purpose of comparing different normalization methods, a new normalization method, namely unit-area normalization, was developed and is described in this section. Also, different normalization schemes (i.e., different sets of measurement points selected for the normalization) and their effects were investigated.

4.4.2 Unit-norm normalization

4.4.2.1 Definition of unit-norm normalization

A widely used mode shape normalization method is unit-norm normalization, which is a global-based normalization method. In this method, a mode shape is scaled as follows:

$$\phi_i = \frac{\phi_{oi}}{\left[\sum_{i=1}^{n} \phi_{oi}^{2}\right]^{1/2}} \qquad [4.2]$$

where ϕ_i is the ith element of the normalized mode shape vector $\boldsymbol{\phi}$ with n elements; and ϕ_{o_i} is the ith element of the original mode shape vector $\boldsymbol{\phi_o}$ before normalization. This method is derived from unit-mass normalization, defined as:

$$\boldsymbol{\phi_m^T}[\boldsymbol{M}]\boldsymbol{\phi_m} = 1 \qquad [4.3]$$

where $[\boldsymbol{M}]$ is the mass matrix of the system and $\boldsymbol{\phi_m}$ is the unit-mass normalized mode shape vector. By assuming that the mass distribution of the system is uniform (which is roughly correct for prismatic beam-like structures), Eq. 4.3 can be simplified to be

$$m_c \cdot \boldsymbol{\phi}_{\boldsymbol{m}}^{\boldsymbol{T}}[\boldsymbol{I}]\boldsymbol{\phi}_{\boldsymbol{m}} = 1 \quad [4.4]$$

where $[\boldsymbol{I}]$ is the identity matrix and m_c is a constant scalar. Scaling Eq. 4.4 results in the unit-norm normalization equation, expressed as:

$$\boldsymbol{\phi}^{\boldsymbol{T}}\boldsymbol{\phi} = 1 \quad [4.5]$$

Equation 4.5 simply states that the norm of the mode shape vector is one. The unit-norm normalized mode shape calculated using Eq. 4.2 is based on Eq. 4.5.

4.4.2.2 Application of the unit-norm normalization

To investigate the influence of normalization method on the definition of mode shapes and changes in mode shapes due to damage, the unit-norm normalization method was selected to compare with a newly developed normalization method. Different numbers of measurement points and different measurement locations were used in these comparisons; the results are presented in the following paragraphs. Results of a similar exercise using the new normalization method are then presented in the following section.

Figures 4.20 (a) and (b) show the unit-norm normalized fundamental mode shape along Girder 4 for Health States 1 and 2 (see Table 3.4), respectively, when 9 and 41 measurement points (or points interpolated using a natural cubic spline interpolation function, as described in Section 4.2.3) were used to define the mode shape. These figures show that the amplitude of the normalized mode shape decreases with an increase in the number of measurement points, although the shape itself remains consistent. Figure 4.20 (c) shows the change in the fundamental mode shape from Health State 1 to Health State 2 (i.e., Damage Case 1, Table 3.5). This figure illustrates that the amplitude of the change in mode shape is not consistent for different numbers of measurement points.

Figures 4.21 (a) and (b) show the effects of using different measurement (or interpolated) locations on the definition of the fundamental mode shape along Girder 4 for Health States 1 and 2, respectively, when the unit-norm normalization method is used.

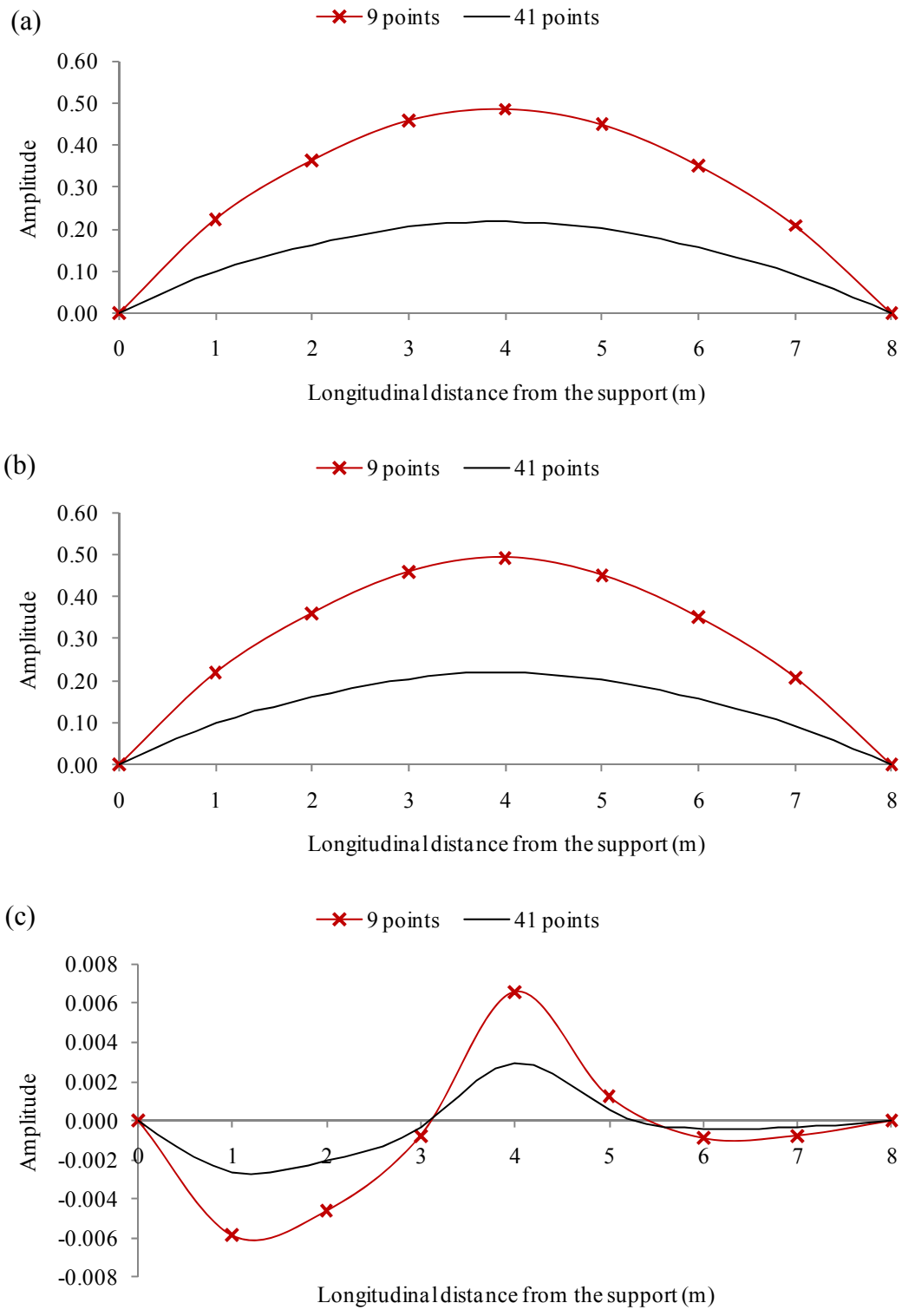

Figure 4.20. Influence of unit-norm normalization on: (a) Mode 1 in Health State 1, (b) Mode 1 in Health State 2, and (c) Change in mode shape for Damage Case 1, when a different number of measurement points was used.

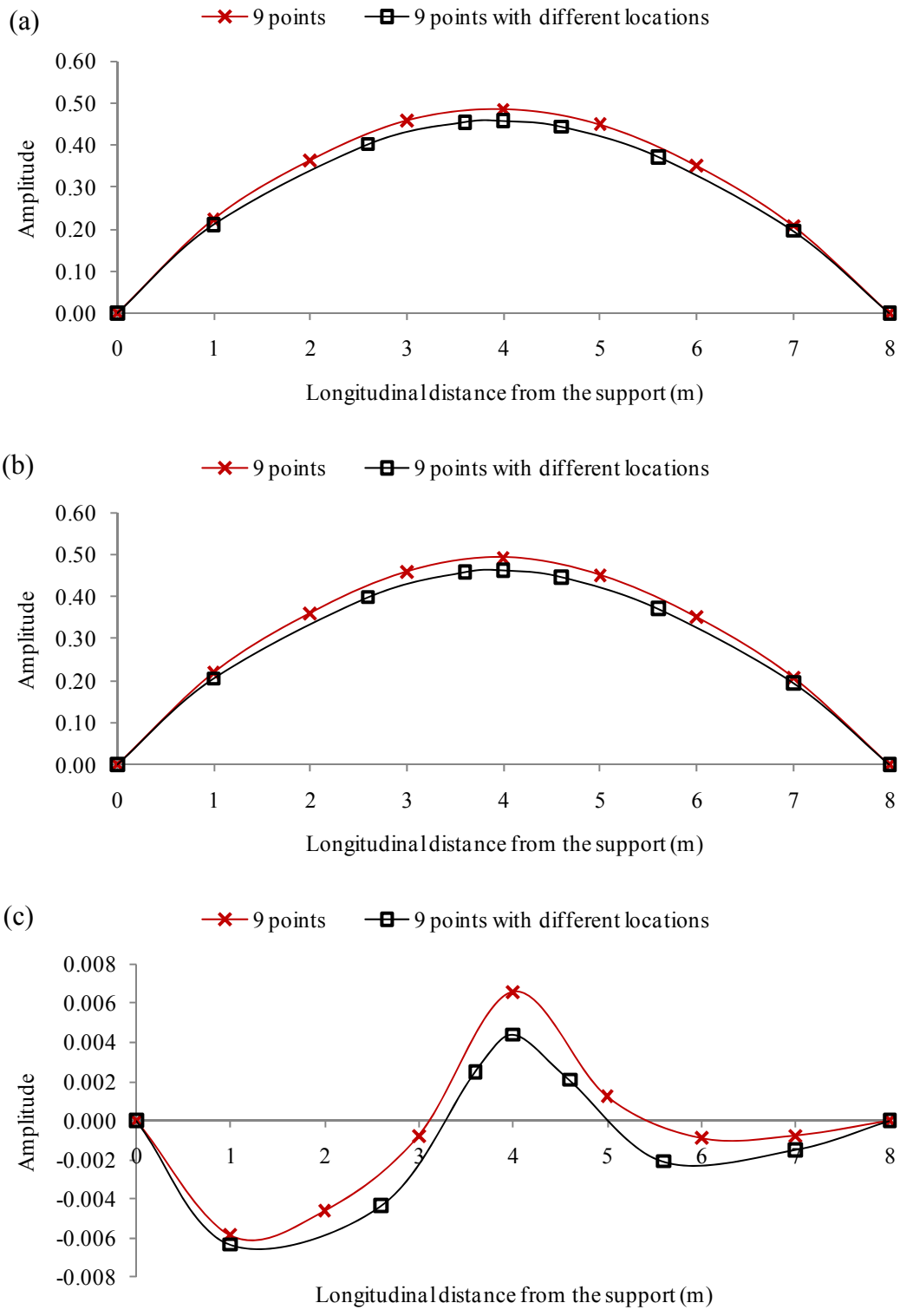

Figure 4.21. Influence of unit-norm normalization on: (a) Mode 1 in Health State 1, (b) Mode 1 in Health State 2, and (c) Change in mode shape in Damage Case 1, when different measurement locations were used.

Figure 4.21 (c) shows the influence of using different measurement locations on the change in the fundamental mode shape due to Damage Case 1 when unit-norm normalization was used. From these figures, it can be seen that both the amplitude of the mode shape and the amplitude of the change in mode shape due to damage vary when different measurement locations are used.

In summary, it can be concluded that both the amplitude of mode shapes and the amplitude of changes in mode shapes due to damage depend on the number and locations of measurement points selected, when the unit-norm normalization method is adopted to normalize the mode shapes. Thus, the mode shape definition and change in mode shape are not unique, which makes it inconvenient to analyze the results in a statistical manner, since the statistical values depends on the number and locations of measurement points selected. It is still possible to use unit-norm normalization to calculate changes in mode shapes, and characterize the results in terms of statistical distributions. However, statistical evaluations of unit-norm mode shapes are usually based on the statistical values (for example, standard deviation and coefficient of variation) of components of mode shapes (i.e., the statistical values of mode shape amplitudes at certain measurement points) or their combinations (i.e., using the mode shape amplitudes at multiple measurement points together), instead of the mode shapes themselves, which usually have no clear physical meaning.

More importantly, it is not easy to determine whether or not damage is present only from examining peaks in the plots of change in mode shape, even though peaks often coincide with locations of damage and may also indicate the presence of damage. This is because the peaks may be due to either damage or random variability in the measurements, while the amplitude of mode shapes, as well as the changes in mode shapes, decrease with an increasing number of measurement points. In other words, it is not easy to claim the presence of damage by only checking the amplitude of changes in mode shapes, no matter how big or small they are. The amplitudes of the changes in mode shapes using unit-norm normalization are usually very small, with numbers of the order of 10^{-5}, 10^{-6}, or 10^{-7}, depending on the number of measurement (or interpolation) points used and the severity of damage experienced. For example, the different numbers

of measurement (or interpolation) points used in this research included 19 strain gauge points (five gauges along the first three girders, four gauges along the fourth girder), 28 accelerometer points (seven points along each girder line), 41 interpolated points for both strain gauges and accelerometers, and an infinite number points expressed as a continuous function for both sensors.

However, uncertainties inherent in the practical dynamic tests led to variability in the measured mode shapes from separate data sets. Thus, there are some peaks present in the plots of changes in mode shapes resulting from the comparison of those separate data sets even when the condition of the structure has not changed during the tests. If the mode shapes are normalized using unit-norm normalization, it is not easy to determine whether these peaks are caused by random variability or other uncertainties by observing the amplitude of changes, no matter how small the amplitudes are, because amplitudes caused by some severe damage case could be small if the number of measurement (or interpolation) points is large enough. On the other hand, it is not easy to claim that there is damage present no matter how big the amplitude of change in mode shape is.

As a result, it is necessary to identify a normalization method by which the normalized mode shapes would be uniquely defined no matter how many measurement points are used and where the sensors are located. Furthermore, it is necessary to look for a statistically-based Level 1 damage indicator for the practical application of VBDD.

4.4.3 Unit-area normalization

4.4.3.1 Definition of the unit-area normalization

A global-based normalization method, referred to as the unit-area method, was developed in this research, providing a unique definition of mode shape, in part, so that the normalization process would depend to a lesser extent on the number and location of measurement points used. This method was also well-suited for use as a Level 1 damage identification method. It should be acknowledged that a very similar

normalization method was found in the literature, but only after it had been independently developed as part of this thesis work (Huth et al. 2005).

The method is defined as follows:

$$\phi_i = \frac{\phi_{o_i}}{Area\ (\phi_o)} \qquad [4.6]$$

where ϕ_i is the ith element of the normalized mode shape vector $\boldsymbol{\phi}$ with n elements; and ϕ_{o_i} represents the ith element of the original mode shape vector $\boldsymbol{\phi_o}$ before normalization. In addition, $Area\ (\phi_o)$ represents the area enclosed by the plot of the absolute value of the mode shape, defined as:

$$Area(\phi_o) = \int_0^1 |\phi_o(x)| dx \qquad [4.7]$$

where $\phi_o(x)$ represents the interpolated mode shape function and x corresponds to the distance along the measurement line (in this case, the girder lines). The mode shape function $\phi_o(x)$ was found by first fitting a natural cubic spline interpolation function to the modal amplitudes at sensor locations along each girder, creating a piecewise cubic polynomial that passed through all the measured amplitudes. The spline function featured continuous first and second derivatives at measurement points, and zero curvature at supports. The range of integration is expressed here from 0 to 1 because the length of the measurement line is first scaled to be equal to one. For the case of multiple measurement lines, the individual mode shapes for all measurement lines are strung end to end to create a single mode shape vector for the entire structure, with the resulting length adjusted to be equal to one (see Fig. 4.22). It should be acknowledged that other schemes, including different interpolation and numerical integration methods, are also acceptable to calculate the area enclosed by the mode shapes.

4.4.3.2 Application of unit-area normalization

To compare the different effects of the unit-norm and unit-area normalization methods on the definition of mode shapes and changes in mode shapes due to damage, the unit-area normalization method, given in Eq. 4.6, was adopted to normalize the same mode

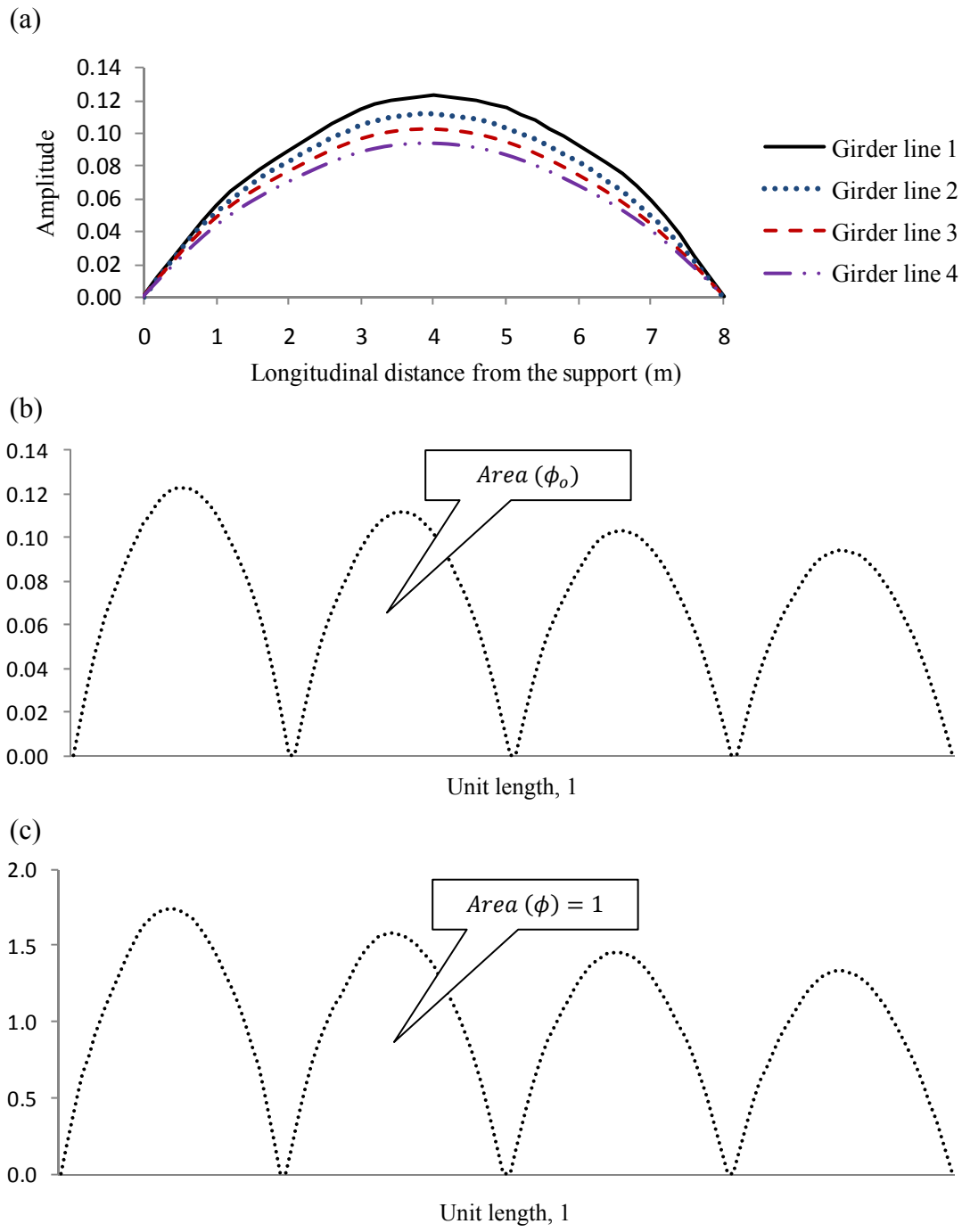

Figure 4.22. Definition of unit-area normalization method: (a) the original unit-norm normalized mode shape; (b) the individual mode shapes in (a) are strung end to end to create a single mode shape vector, with the resulting length adjusted to be equal to one; and (c) the mode shape in (b) is scaled to make the enclosed area equal to unity.

shapes used in Figs. 4.20 and 4.21, where different numbers of measurement points and different measurement locations were considered. The resulting normalized mode shapes and changes in mode shapes are presented in Figs. 4.23 and 4.24.

Figure 4.23 shows the influence of using different numbers of measurement (or interpolation) points (9 and 41 points) on the mode shape definitions and the change in mode shape for Damage Case 1, when unit-area normalization is used. It is evident that unit-area normalization generated the same mode shape definition (Figs. 4.23 (a) and (b)) and the same definition of the corresponding change in mode shape (Fig. 4.23 (c)), when different numbers of measurement points were used.

Figures 4.24 (a) and (b) show the influence of using different measurement (or interpolation) locations on the definition of the fundamental mode shape along Girder 4 for Health States 1 and 2, respectively, while Figure 4.24 (c) presents the effects on the change in the fundamental mode shape due to Damage Case 1, when the unit-area method was adopted to normalize the mode shapes. It can be seen that the mode shape definition and the corresponding changes in mode shapes were consistent and coincided with each other no matter where the sensors were located.

In summary, it can be concluded that the unit-area normalization process produced a more consistent mode shape definition and corresponding change in mode shape than the widely used unit-norm method, when considering different numbers and locations of measurement points. As a result, the unit-area normalization method was adopted in this research, in part, so that the normalization process would be less sensitive to the number and location of sensors used. More importantly, the feature of a unique mode shape definition makes it convenient to analyze the change in mode shape for damage detection in a statistical manner. Based on the unit-area method, a scalar damage indicator was developed in Chapter 5 and the sensitivities of the various test procedures were investigated in Chapter 6.

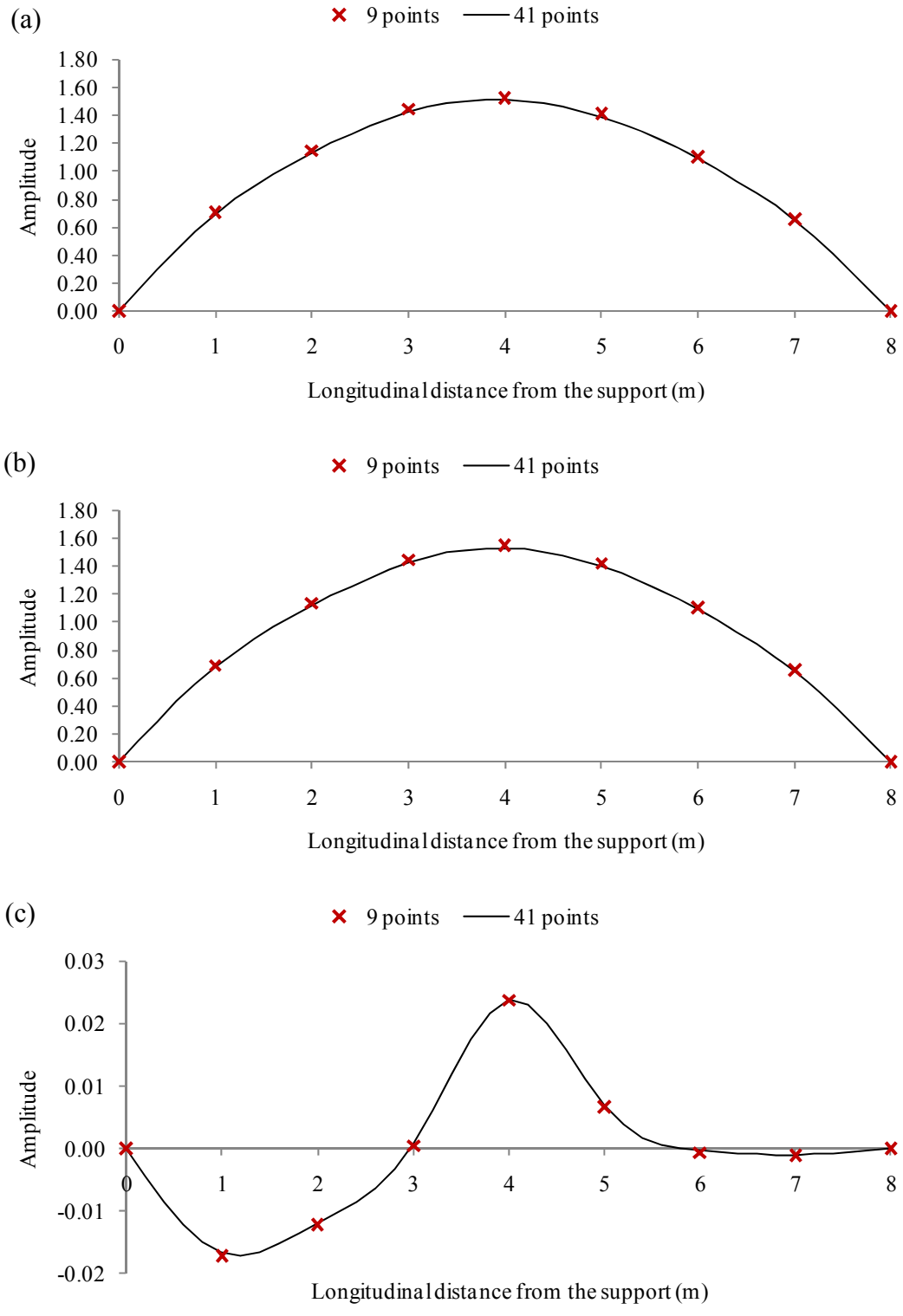

Figure 4.23. Influence of unit-area normalization on: (a) Mode 1 in Health State 1, (b) Mode 1 in Health State 2, and (c) Change in mode shape for Damage Case 1, when different numbers of measurement points were used.

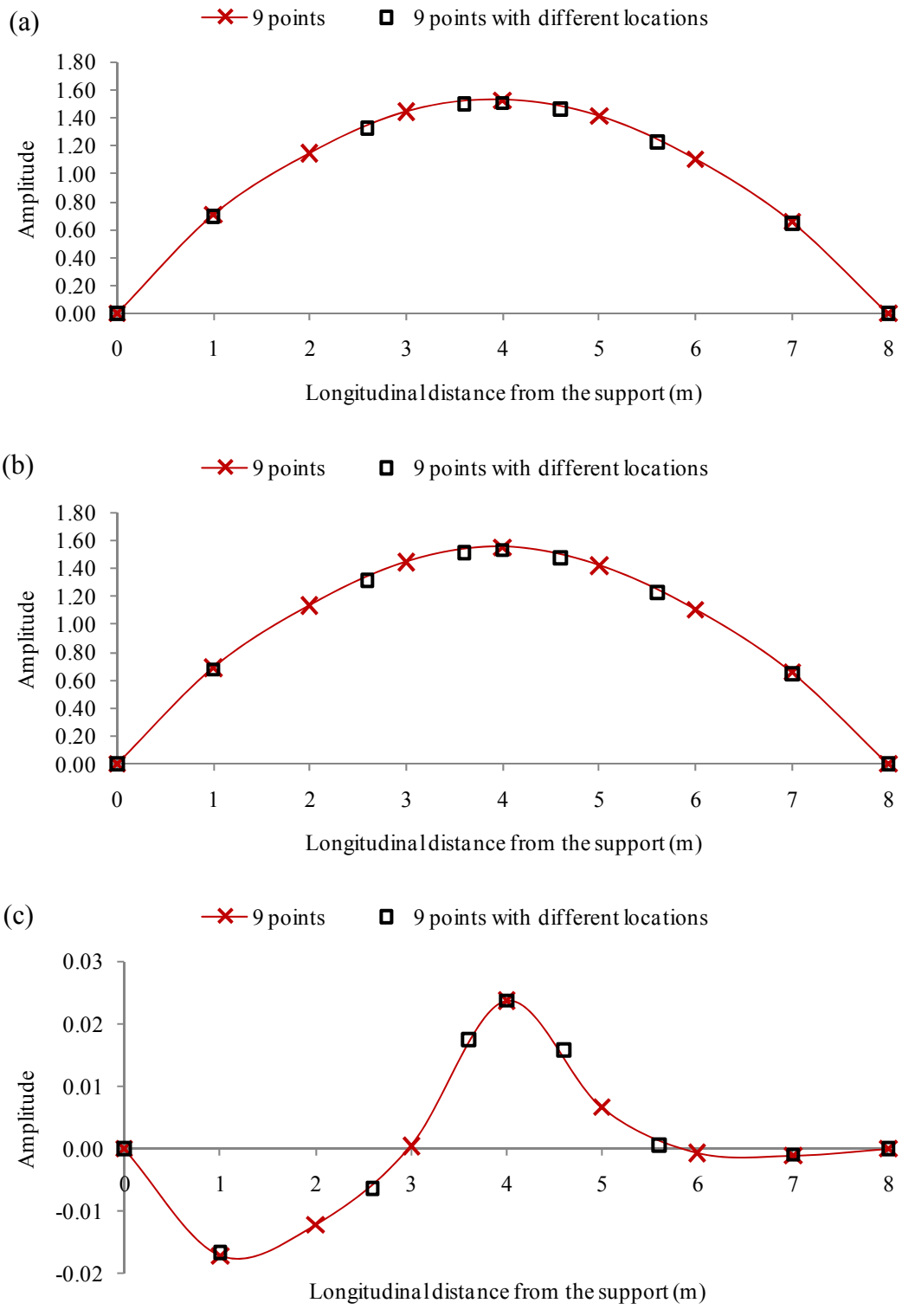

Figure 4.24. Influence of unit-area normalization on: (a) Mode 1 in Health State 1, (b) Mode 1 in Health State 2, and (c) Change in mode shape for Damage Case 1, when different measurement locations were used.

4.4.4 Different normalization schemes

As described previously, the amplitudes of mode shapes are indeterminate. Therefore, it is necessary to scale the mode shapes to be compared (for example, undamaged and damaged cases) to a common base. As presented before, the unit-area method was developed for this purpose. However, even when the same general normalization method is used, different normalized mode shapes can be produced, depending on whether the entire structure is considered as a unit during the normalization process, or different subsets of the structure are normalized separately. Two normalization schemes were selected in this research: normalization over all measurement points (i.e., only one scaling factor is used for normalizing the amplitude of all measurement points from the four girder lines, denoted as Scheme I) and normalization along individual girder lines (i.e., mode shapes are normalized independently along individual girder lines, resulting in four different scaling factors for four individual girder lines, denoted as Scheme II). Conceptually, the mode shapes normalized using all measurement points should better present the global features of mode shapes and changes in mode shape, while the mode shapes normalized along individual girder lines should emphasize the localized features of damage information.

Figure 4.25 shows the effects of the two normalization schemes using unit-area normalization on the definition of mode shapes and change in mode shapes due to Damage Case 1 (see Table 3.5). Figure 4.25 (a) presents the averaged unit-area normalized fundamental mode shape from five trials for both Health States 1 and 2 using the normalization scheme considering all measurements points. Using this approach, the area under the entire length (scaled to be equal to one) of four girders is unity; and the entire collection of four bumps is treated as one mode shape. From results shown in Fig. 4.25 (a), the differences between mode shapes in Health States 1 and 2 can be noticed visually. On the other hand, Fig. 4.25 (b) shows the same vibration modes as presented in Fig. 4.25 (a), but using normalization along individual girder lines. By doing this, the area under the each individual bump (scaled to have unit-base) is unity, and each individual bump effectively represents one individual mode shape. It can be seen that the difference in unit-area normalized mode shapes using normalization

Scheme II shown in Fig. 4.25(b) between Health States 1 and 2 is not noticeable visually, although the difference may still be significant.

Figures 4.25 (c) and (d) represent the changes in fundamental mode shape due to Damage Case 1 (a comparison of Health States 1 and 2) using the unit-area normalization over all measurements points and along individual girder lines, respectively. It can be concluded that the normalization over all measurement points reflects the global changes in mode shape, which may locate the possible damage in both the longitudinal and transverse directions. For example, in Fig. 4.25 (c), the maximum change in mode shape is located at the mid-span of Girder 4, coinciding with the damage location for Damage Case 1. It can be also concluded that normalization along individual girder lines can magnify the changes locally, narrowing the range of possible damage locations and thereby benefitting the damage localization in another way. As a result, in practice, the two different normalization schemes should be used simultaneously to reflect both global and magnified local information regarding changes in mode shapes. The application of the two normalization schemes is presented in Chapter 6.

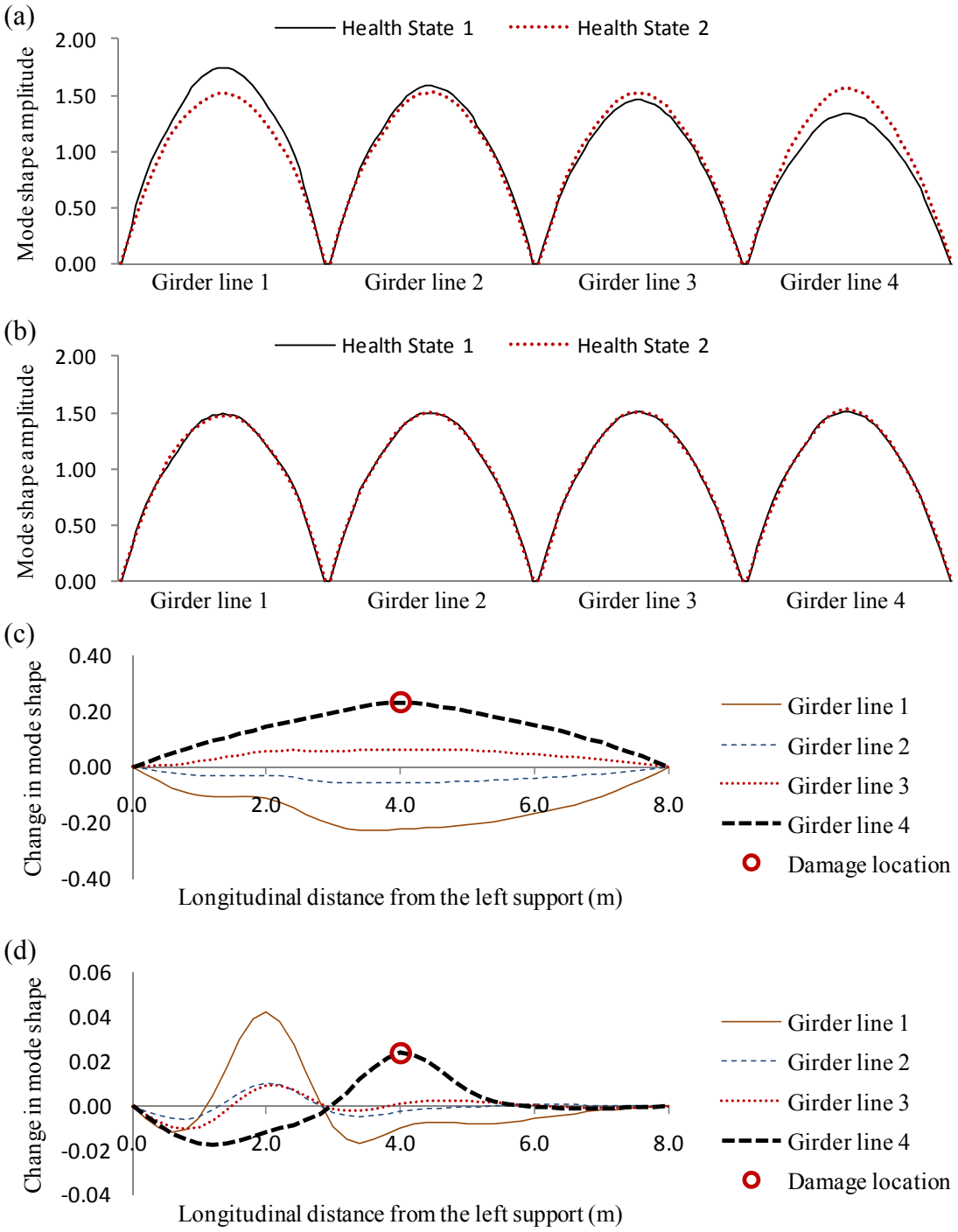

Figure 4.25. Influence of the different normalization schemes on the definition of mode shapes and changes in mode shapes due to Damage Case 1 for the fundamental mode shape using the unit-area normalization: (a) over all measurement points; and (b) along individual girder lines; (c) the change in fundamental mode shape due to Damage Case 1 using the unit-area normalization over all measurement points; and (d) along individual girder lines.

CHAPTER 5. **LEVEL 1 VBDD INDICATOR DEVELOPED: THE AREA OF MODE SHAPE CHANGE**

5.1 Overview

Numerous VBDD methods which are related in some manner to changes in modal parameters (notably natural frequencies, damping, and mode shapes) have been proposed as a potential techniques for structural health monitoring (Wolf and Richardson 1989, Wegner et al. 2004). Although there have been some successful applications of the proposed VBDD methods, there are still great challenges associated with practically applying the methods to complicated structural systems like bridges. Changes in natural frequencies have proven not to be sensitive enough to detect small scale damage in practical situations, especially considering the experimental uncertainties associated with temperature and other environmental conditions (Doebling et at. 1996). The damage detection methods based on changes in damping have been found to be unreliable and also not sensitive to small scale damage (Casas and Aparicio 1994, Salawu and Williams 1995, and Farrar and Jauregui 1998a). On the other hand, methods based on mode shapes and their derivatives have been found to be effective damage indicators (Pandey et al. 1991, Fox 1992, Srinivasan and Kot 1992, Salawu and Williams 1994, and Zhang and Aktan 1995 and 1998). However, most of the proposed methods based on mode shapes have not really addressed the problem of identifying the presence of damage considering statistically reliable levels of confidence, which is considered to be the most appropriate approach for practical problems with high levels of uncertainty. This limitation may be partially due to the fact that the definition of a mode shape is not unique, which makes the investigation of mode shapes in a statistical manner difficult.

As a result, a new Level 1 VBDD indicator (i.e., one capable of identifying the presence of damage, but not necessarily its location), the area of mode shape change, is proposed in this chapter to fill the gap. The new VBDD indicator was developed based on the widely used change in mode shape method using the unit-area normalization method described in Section 4.4.3. To demonstrate the features and verify the capability of the new damage indicator in the absence of experimental uncertainties, a finite element model was developed and used to generate theoretical data for the modal properties of the bridge superstructure model. Then, the simulated data were used to test the proposed damage indicator.

5.2 Development of the Damage Indicator

5.2.1 Description of the damage indicator

A new Level 1 VBDD damage indicator was developed for this study, based on the widely used change in mode shape VBDD parameter. Its calculation requires that mode shapes first be scaled using a unit-area normalization procedure. This was achieved by first fitting a natural cubic spline interpolation function to the modal amplitudes at sensor locations along each girder, creating a piecewise cubic polynomial that passed through all the measured amplitudes. The spline function featured continuous first and second derivatives at measurement points, and zero curvature at supports. The mode shapes along all girders were then strung end to end. Finally, modal amplitudes were scaled to ensure that the total area under the absolute value of the resulting mode shape function was equal to one. The unit-area normalization scheme was adopted, in part, so that the normalization process would be less sensitive to the number and location of sensors used.

After mode shapes were normalized using Eq. 4.6, the change in mode shape, $\boldsymbol{\Delta\phi_{mn}}$, was calculated using Eq. 2.5 and expressed as:

$$\boldsymbol{\Delta\phi_{mn}} = \boldsymbol{\phi_m} - \boldsymbol{\phi_n} \qquad [5.1]$$

in which $\boldsymbol{\phi}$ represents a unit-area normalized mode shape vector, and the subscripts m and n indicate two independently obtained mode shapes. A scalar damage indicator was

derived from the change in mode shape vector by calculating the absolute value of the area under $\boldsymbol{\Delta\phi_{mn}}$:

$$\Delta A = \int_0^1 |\Delta\phi_{mn}(x)| dx \qquad [5.2]$$

where x corresponds to the distance along girders (with all four girders included). While the areas under the two mode shape vectors, $\boldsymbol{\phi_m}$ and $\boldsymbol{\phi_n}$, are identical by virtue of the unit-area normalization procedure, the distribution of the area over the length of the structure will differ, producing a non-zero area under the difference function. The area of the mode shape change, ΔA, can therefore be used as an indicator of the presence of damage. The ΔA parameter can be expected to increase as damage becomes more severe, leading to an increase in the likelihood of detecting the damage.

5.2.2 Features of the new damage indicator

One of the primary features of the new area of mode shape change damage indicator is that its variability can be defined in terms of statistical parameters such that the presence of damage can be established by comparison with certain levels of confidence. Specific features of the indicator are as follows:

- It was developed based on the widely used change in mode shape method;
- The mode shapes used for a comparison must first be scaled to a common basis using unit-area normalization;
- The values calculated by the indicator are well-suited to statistical analysis; and
- It is relatively insensitive to the number and location of measurement points used.

5.2.3 Differences between the area of mode shape change and "mode shape area index"

It should be acknowledged that a VBDD damage indicator, called mode shape area index, very similar to the one developed as part of this thesis work was found in the literature during the later stages of preparation of this thesis (Huth et al. 2005). However, the work presented in this thesis was developed independently and was

defined and applied in a different manner on a different application. Some differences between two damage indicators are as follows:

- They are somewhat different at the normalization stage. For the area of mode shape indicator developed in this study, the length of the measurement line is first scaled to be equal to one before calculating the area enclosed by mode shapes. For the case of multiple measurement lines, the individual mode shapes for all measurement lines are strung end to end to create a single mode shape vector for the entire structure, with the resulting length adjusted to be equal to one (see Section 4.4.3). This normalization method results in a unique mode shape definition no matter how many measurement lines are used and what the span of a particular bridge is; this makes the method convenient to apply the change in mode shape for damage detection in statistical manner. There is no such process for the "mode shape area index" indicator.
- The "mode shape area index" indicator was evaluated by calculating ratios of the area of one health state to that of the reference state. Since the longitudinal axis of the tested bridge was divided into several parts, different ratios were calculated for different parts of the bridge. These ratios are either larger or smaller than one if the condition of the bridge changed. However, in the area of mode shape indicator, the resulting area under the plot of the difference between two independently measured mode shapes was calculated to evaluate the changes of health conditions. In this way, only one value (from 0 to 1) was generated for the mode shapes compared (see Section 5.2.1).
- The application of the area of mode shape change indicator using a statistical approach is believed to be original, and was not found in Huth et al. (2005).

5.3 Verification of the Damage Indicator Using Numerical Data

5.3.1 Description of the finite element model

Figure 5.1 shows the finite element model used for this verification, which was created using the commercial finite element analysis software ANSYS (2005) based on the experimental bridge model. The model featured four steel girders supporting a

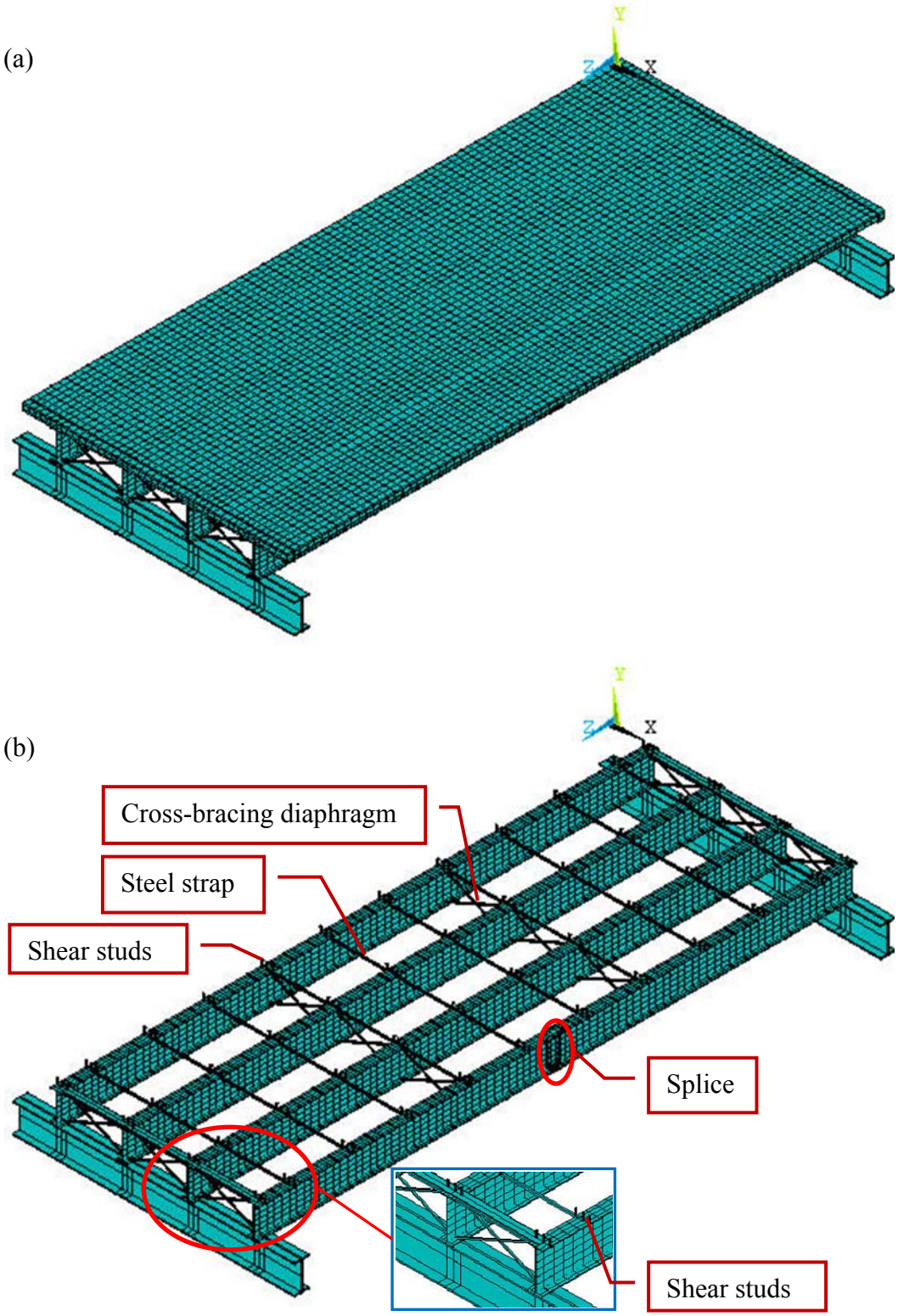

Figure 5.1. The finite element model of the experimental bridge model showing: (a) the whole finished model; and (b) the structural steel superstructure including the splice, steel straps, diaphragms, and shear studs.

steel-free concrete deck. The concrete deck was simulated using 8-node 3-dimensional isoparametric brick elements, while the steel girders were modelled using 4-node 3-dimensional plate elements. To provide the necessary lateral restraint for the steel-free concrete deck, the top flanges of the girders were connected by transverse steel straps modelled by 2-node linear truss elements. Shear studs were simulated using 2-node 3-dimensional linear beam elements to build the connection between the concrete deck and the steel girders. The top flange of the beams and the concrete deck shared common nodes only at the locations with shear studs, producing a partially composite beam connection. In other words, there were no common nodes between the top flange of the beams and the concrete deck except the nodes at the bottom end of shear studs, even though some of the nodes share common coordinates. By adopting this approach, the stiffness of the partially composite beams may have been underestimated, since the contact restraint between the top flange of the beams and the concrete deck was ignored. However, this under-estimation in stiffness was compensated for by adjusting the stiffness of the shear studs. The cross-braced structural angle diaphragms were modelled using 2-node truss elements to provide lateral stability for the system and enhance load sharing between girders. The material properties used in the finite element model are shown in Table 5.1. All materials were modelled as linear elastic.

The boundary conditions consisted of pin supports for all girders at one end and roller supports for all girders at the other end of the bridge model. The FE model was roughly calibrated to the first two natural frequencies and mode shapes of the undamaged physical laboratory bridge system by adjusting the density of the concrete and the flexural stiffness of the shear studs. The maximum relative difference between the first two natural frequencies of the calibrated FE model and the physical bridge (using strain

Table 5.1. Material properties of the multi-girder bridge model used in FE simulation

Material	Density (kg/m^3)	Young's modulus (GPa)	Poisson's ratio
Concrete	2450	28.6	0.15
Steel	7800	200	0.3

gauge data) was 2.73%. It should be acknowledged that the FE model could have been calibrated to a better representation of the physical system if more parameters and adjustments had been made. However, the calibrated model described was considered to be sufficiently accurate to fulfill the purpose of this verification. The FE model was treated as an independent model to generate some theoretical data of modal properties in the absence of experimental uncertainties. No comparison between the FE model and the physical model were made.

5.3.2 Description of simulated health states and damage cases

Once the FE model had been calibrated and the baseline dynamic properties of the model had been established, two categories of damage states were introduced into the simulated model, consisting of damage to the steel girders and damage to the concrete deck. Altogether, twelve different health states were investigated in this simulation, as described in the following paragraphs.

For damage category 1 (Fig. 5.2), simulated damage states were incrementally introduced into the steel Girder 4 at mid-span. Figure 5.2 (a) shows the intact condition of the splice at mid-span of Girder 4 before any damage was introduced; this was considered as simulated Health State 1. Figure 5.2 (b) represents the damage case in which the bottom plate was removed from the splice. This was similar to Damage Case 1 for the physical model, as shown in Table 3.5; it is referred to here as simulated Health State 2 or simulated Damage Case 1 since Health State 1 was treated as the baseline condition. Figure 5.2 (c) and d show the incrementally increasing level of damage induced at the splice by eliminating some plate elements in the web splice connection; these are described as simulated Damage Cases 10 and 11, respectively. The incrementally increasing damage conditions shown in Figs. 5.2 (b), (c), and (d) produced reductions in the vertical flexural stiffness at that location of 7.76%, 9.17%, and 19.02%, respectively (see Table 5.2). The flexural stiffness for each health state was calculated by applying a concentrated vertical force at the splice location and observing the corresponding displacement at the same location. For example, a localized flexural stiffness of 88 kN/mm was calculated for Health State 1 by applying a

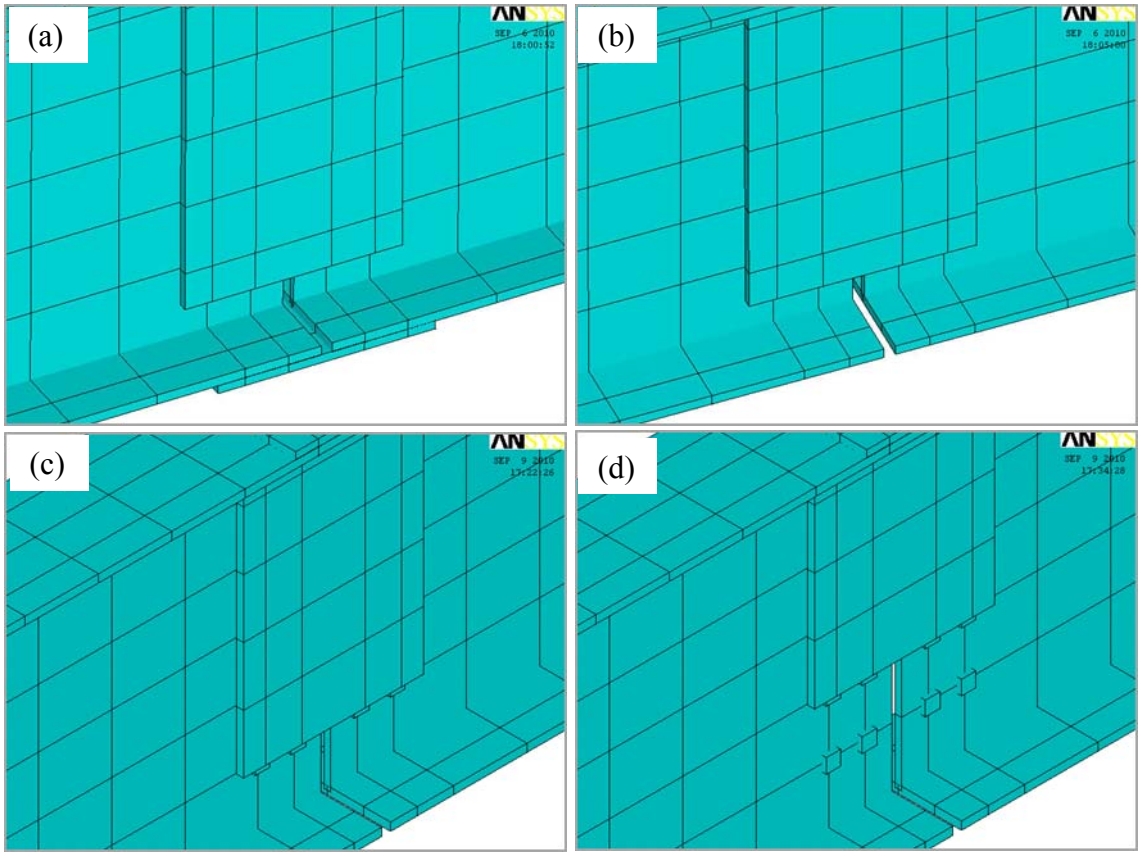

Figure 5.2. The simulated damage states incrementally introduced to steel Girder 4 at the splice connection: (a) Health State 1 (the intact condition), (b) Health State 2 (or Damage Case 1), (c) Health State 11 (or Damage Case 10), and (d) Health State 12 (or Damage Case 11).

vertical load of 1 kN and using the corresponding vertical displacement of 0.0114 mm at that location.

For damage category 2 (Fig. 5.3), small square blocks of concrete, 100 X 100 mm in plan and 25 mm deep, were incrementally removed from the top surface of the concrete deck by eliminating one element at a time at a location near mid-span of Girders 3 and 4. Figure 5.3 shows Health States 3 to 10, with one to eight elements removed from the surface of the simulated concrete deck, while Fig. 5.4 shows the general locations of the removed elements. It should be noted that the previous damage (i.e., the damage case in Health State 2, for which the bottom plate was removed from the splice) was not repaired for the Health States 3 to 10. Thus Health State 2, instead of Health State 1, was treated as the baseline condition for Damage Cases 2 to 9, as shown in Table 5.2.

These damage states produced reductions in the vertical flexural stiffness at the mid-span of Girder 4 of 0.05% to 0.30 %, following a roughly linear relationship (see Table 5.2).

5.3.3 Results and discussion

5.3.3.1 Simulated model properties

The lowest five vibration modes of the FE model for various health states were extracted using a modal analysis method, the Block Lanczos eigenvalue extraction method, available in the finite element software ANSYS. This method is suitable for large symmetric eigenvalue problems. Typically, the Block Lanczos method is applicable to the type of problems solved using the Subspace eigenvalue method, however, at a faster convergence rate. A comparison of the extracted natural frequencies in various health states is presented in Table 5.3. Generally, the first two natural frequencies decreased with increasing damage conditions. For damage category 1, the first natural frequency decreased by a maximum of 2.44 %, while the second natural frequency decreased by 4.82 % (Health State 12). However, in Damage Category 2, including Health States 3 through 10, the changes in natural frequencies

Table 5.2. Comparison of the flexural stiffness of the FE model for different health states extracted from the finite element model

Damage Case	Undamaged State	Damaged State	Type of damage	Relative change in vertical flexural stiffness
Case 1	State 1	State 2	To steel girder splice	7.76%
Case 2	State 2	State 3	To concrete deck	0.05%
Case 3	State 2	State 4	To concrete deck	0.09%
Case 4	State 2	State 5	To concrete deck	0.12%
Case 5	State 2	State 6	To concrete deck	0.15%
Case 6	State 2	State 7	To concrete deck	0.21%
Case 7	State 2	State 8	To concrete deck	0.24%
Case 8	State 2	State 9	To concrete deck	0.26%
Case 9	State 2	State 10	To concrete deck	0.30%
Case 10	State 1	State 11	To steel girder splice	9.17%
Case 11	State 1	State 12	To steel girder splice	19.02%

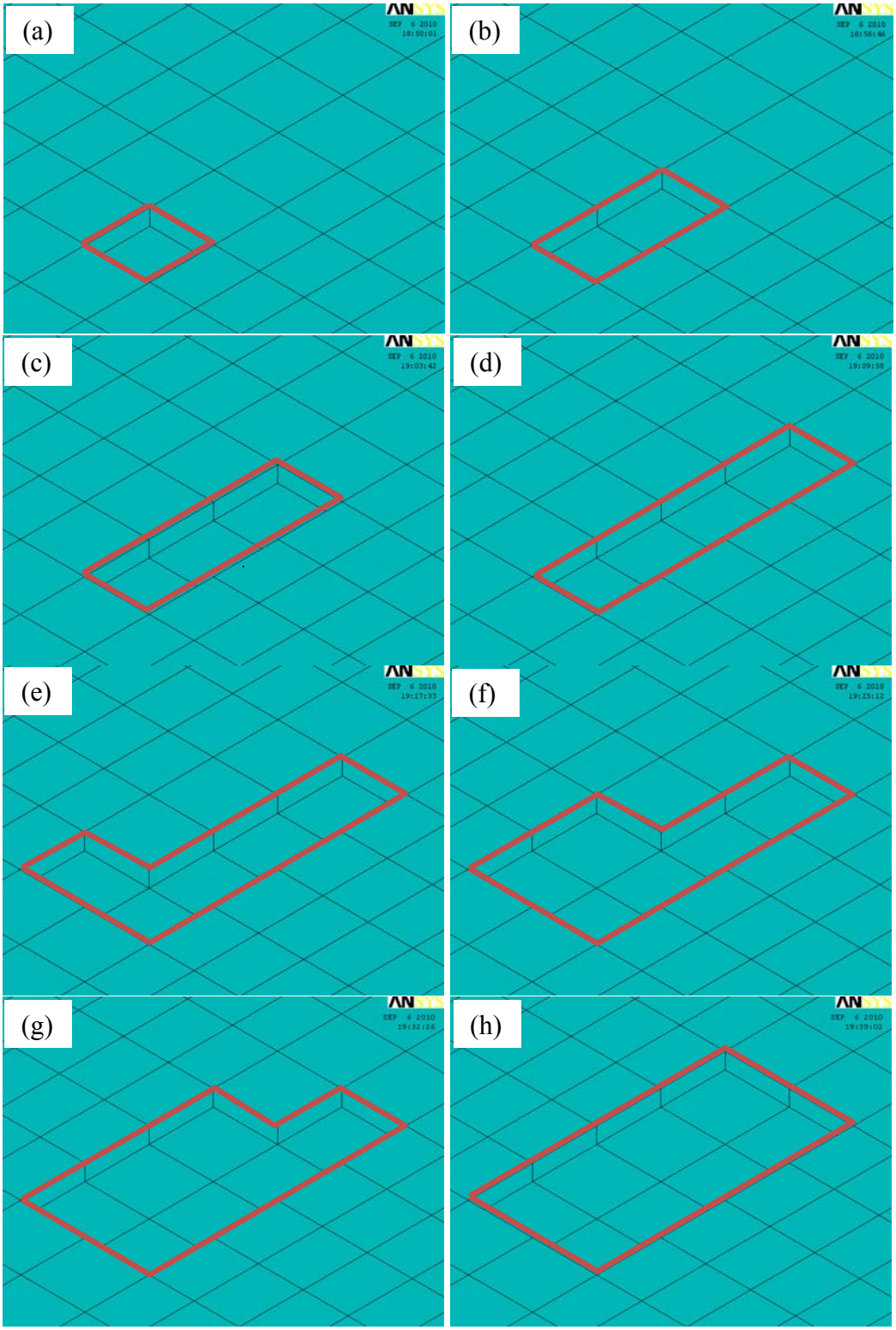

Figure 5.3. The simulated damage states incrementally introduced to the concrete deck at a location near mid-span of Girders 3 and 4 for Health States 3 to 10, respectively, with: (a) one, (b) two, (c) three, (d) four, (e) five, (f) six, (g) seven, and (f) eight elements (100 X 100 X 25 mm) removed from the surface of the simulated concrete deck.

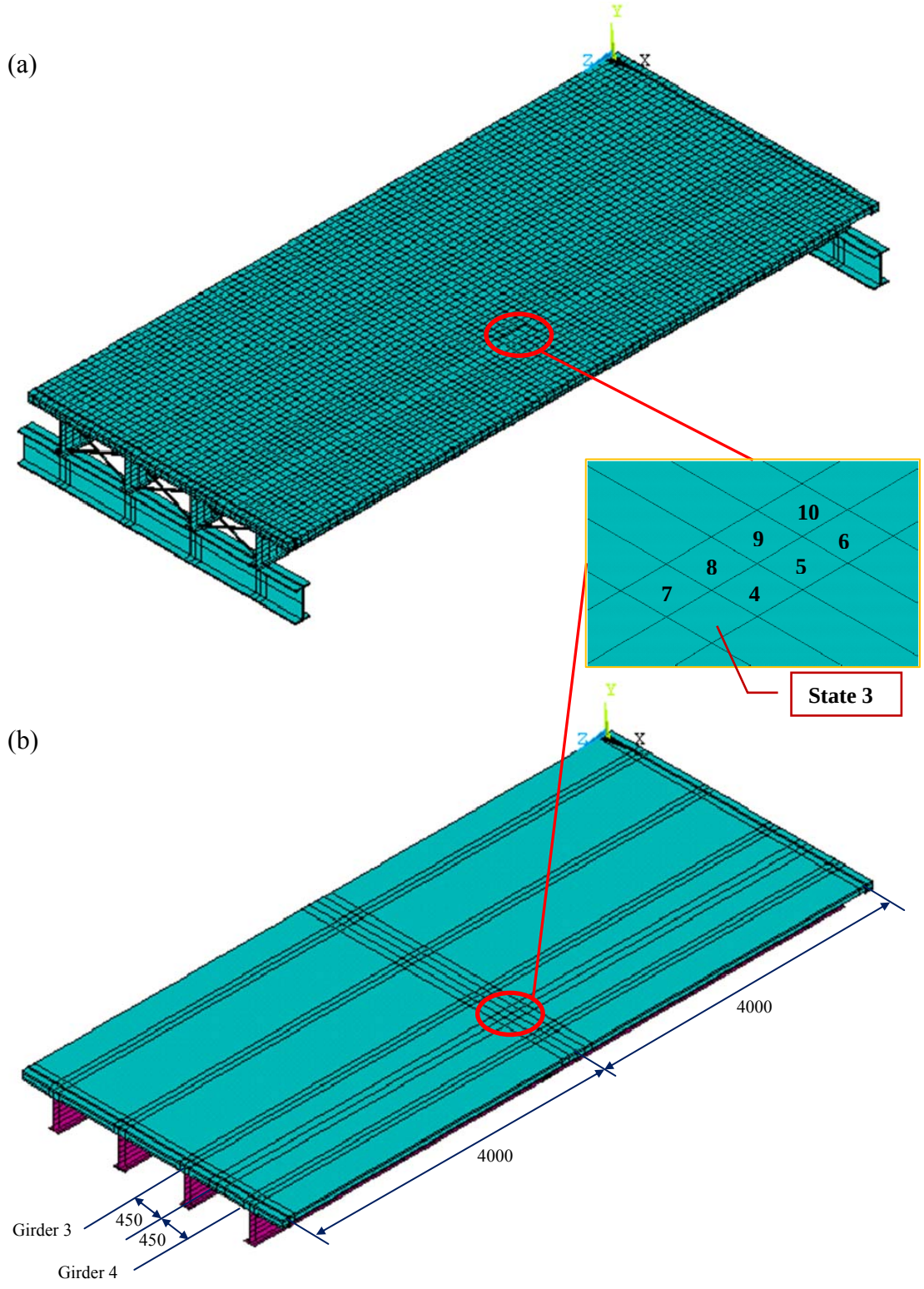

Figure 5.4. The finite element model of the experimental bridge model: (a) the whole meshed model; and (b) the physical model (before meshing), showing dimensions in mm; with an inset showing the order of the removed elements in Health States 3 to 10.

were very small for all cases and were unnoticeable in some cases, with maximum changes of 0.02%, considering all modes and all damage cases. This implies that change in natural frequencies may not be a sensitive damage indicator for such small scale damage cases.

The lowest five vibration mode shapes extracted for Health State 1 are presented in Fig. 5.5. The mode shapes are similar to those of the physical model (see Figs. 4.8, 4.9, and 4.10) except for Mode 5. Mode 1 is an unsymmetrical flexural mode shape; the asymmetry is likely due to the presence of the over-designed splice connection on Girder 4. Mode 2 is a torsional mode shape, while Mode 3 and Mode 4 exhibit combined flexural and torsional behaviour. Mode 5 also presents a combination of flexural and torsional behaviour, which is different from the physical model case, where Mode 5 was the second flexural mode shape. No further calibration or investigation was conducted regarding this difference.

Table 5.3. Comparison of simulated natural frequencies in different health states extracted from the finite element model

Mode	The simulated natural frequencies (Hz)					
	State 1	State 2	State 3	State 4	State 5	State 6
1	13.119	13.049	13.049	13.050	13.050	13.051
2	14.298	13.977	13.978	13.979	13.979	13.980
3	29.408	29.294	29.294	29.295	29.295	29.295
4	32.242	32.175	32.176	32.176	32.177	32.177
5	36.148	32.999	32.999	32.999	32.998	32.998
Mode	The simulated natural frequencies (Hz)					
	State 7	State 8	State 9	State 10	State 11	State 12
1	13.050	13.051	13.051	13.051	13.031	12.799
2	13.980	13.981	13.981	13.982	13.926	13.609
3	29.295	29.296	29.296	29.296	29.318	29.332
4	32.178	32.179	32.179	32.180	32.176	32.111
5	32.998	32.997	32.997	32.997	33.426	33.684

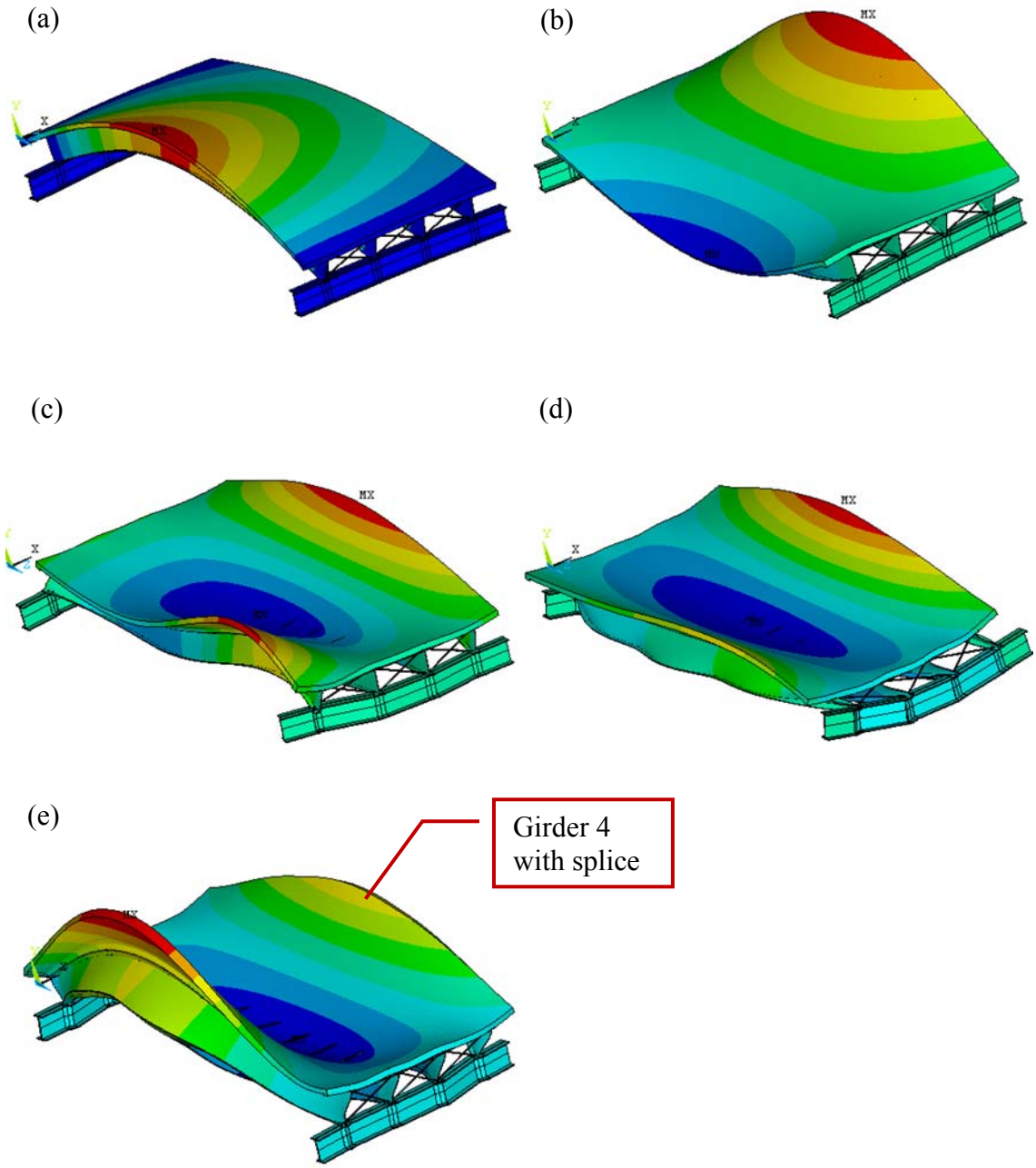

Figure 5.5. The lowest five vibration mode shapes for Health State 1 (the undamaged condition) extracted from the finite element model: (a) Mode 1, (b) Mode 2, (c) Mode 3, (d) Mode 4, and (e) Mode 5.

5.3.3.2 Change in modal properties due to damage

To calculate the area of mode shape change described in Eq. 5.2, the mode shapes to be compared had to be normalized to a common basis using the unit-area normalization method. Figures 5.6 and 5.7 give examples of the normalized mode shapes of the FE model using the two different normalization schemes described in Section 4.4.4. Figure 5.6 presents the unit-area normalized first mode shape using the normalization scheme

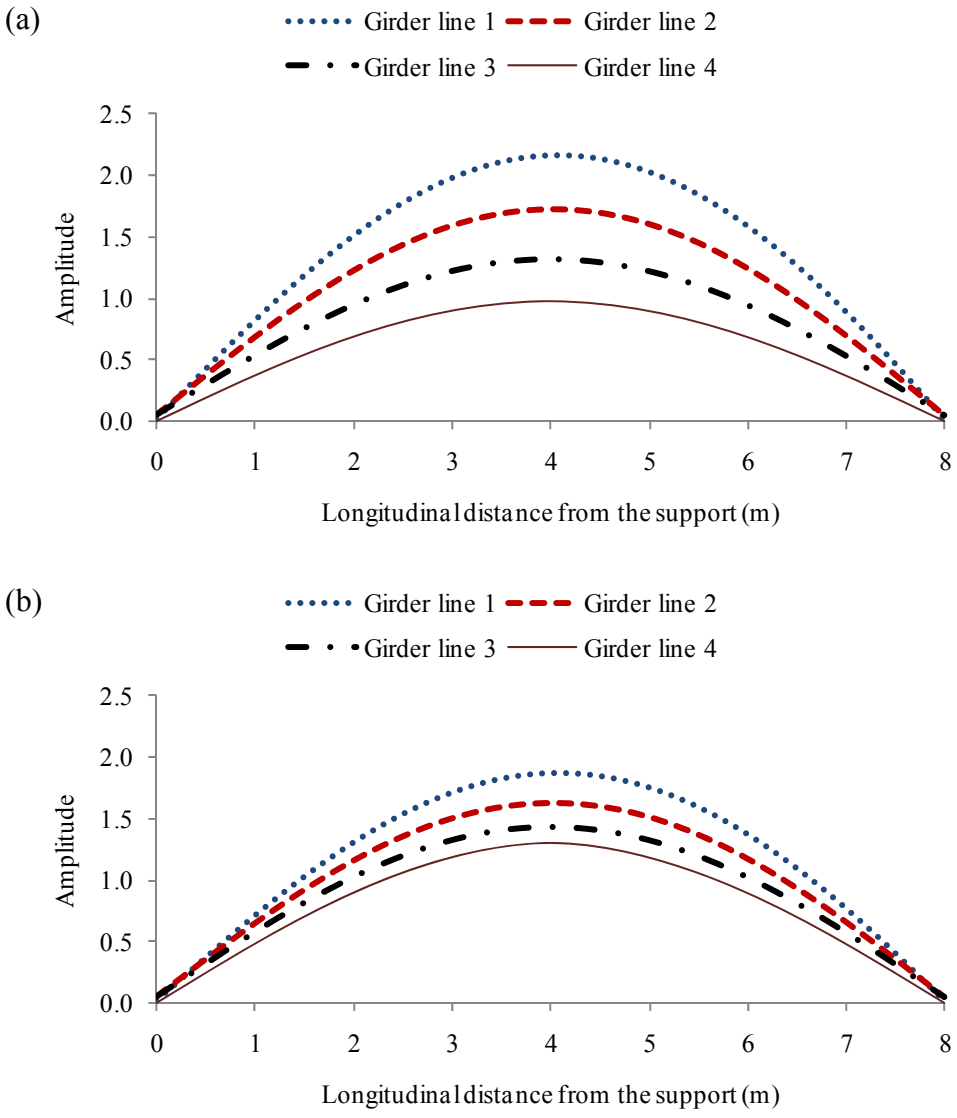

Figure 5.6. The normalized mode shape of Mode 1 using the normalization scheme over all measurement points for: (a) simulated Health State 1 and (b) simulated Health State 2.

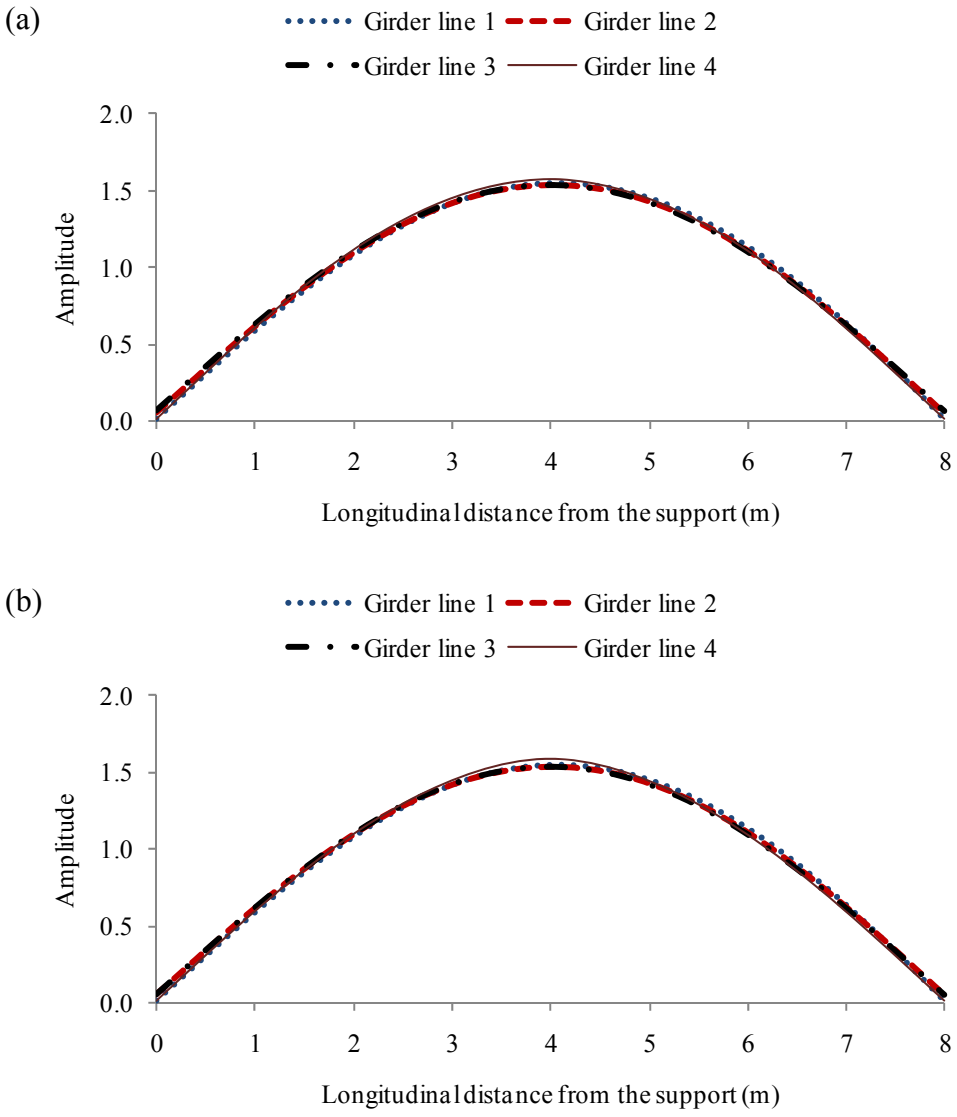

Figure 5.7. The normalized mode shape of Mode 1 using the normalization scheme along individual girder lines for: (a) simulated Health State 1 and (b) simulated Health State 2.

over all measurement points (or selected nodes) for Health States 1 and 2, where the global features of the mode shape can be noticed; in other words, the different girders had different vibration amplitudes while the scaling ratio between girders remained constant. Comparing Figs. 5.6(a) and (b), the difference in the distribution of modal amplitudes due to damage can be visually noticed. Figures 5.7(a) and (b) show the unit-area normalized first mode shape using the normalization scheme along individual girder lines for simulated Health States 1 and 2, respectively. In this case, no

pronounced differences can be noticed between mode shapes along different girder lines.

After the mode shapes were normalized using unit-area normalization, Eq. 5.2 was used to calculate the change in the mode shapes investigated. Using the same mode shapes presented in Figs. 5.6 and 5.7, the change in mode shape due to the simulated damage (Damage Case 1) is presented in Fig. 5.8, where Fig. 5.8(a) corresponds to normalization over all measurement points and Fig. 5.8(b) corresponds to normalization along the individual girder lines. Figure 5.8(a) shows global changes in mode shapes due to the simulated Damage Case 1, featuring relatively large changes in modal amplitudes for all girders. The maximum modal amplitude change (or increase due to the presence of the simulated damage) occurred at the mid-span of Girder 4, with a value of 0.324, which was 33.2 % of the mode shape amplitude at that location (0.977), for this normalization scheme at the same location (see Fig. 5.6(a)). On the other hand, Fig. 5.8(b) shows maximized local changes in mode shapes due to the same simulated damage case, featuring relatively small, but localized, mode shape changes for all girders. The maximum amplitude increase shown in Fig. 5.8(b) also occurred at the mid-span of Girder 4, but with a much smaller value of 0.022, or 1.4 % of the mode shape amplitude at the same location (see Fig. 5.7(a)). However, the shapes in Fig. 5.8(b) feature a much more prominent peak along Girder Line 4 than those shown in Fig. 5.8(a). The ranges with positive amplitudes (i.e., indicating mode shape amplitude increases due to damage) shown in Fig. 5.8(b) are much narrower (or more localized) than those shown in Fig. 5.8(a); for example, for Girder Line 4, the range with positive amplitudes in plots is from 2.8 to 5.2 m (longitudinal distance from the left support) in Fig. 5.8(b), while in Fig. 5.8(a) the range is from 0 to 8.0 m.

Both normalization schemes were selected for further application to take advantage of the combination of their benefits, reflecting both global changes (with relatively larger amplitudes and perhaps less sensitivity to potential noise), which may be good for determining the presence of damage globally, and maximized local changes in mode shapes due to the damage, which may be useful to narrow the localized position of damage. In this manner, the changes in mode shape for various simulated damage cases

were calculated, which was required for the calculation of the area of mode shape change described in the next section.

5.3.3.3 The area of mode shape change due to simulated damage cases

To demonstrate the features and to verify the capabilities of the new damage indicator to detect the presence of damage, the FE model described above was used to generate the

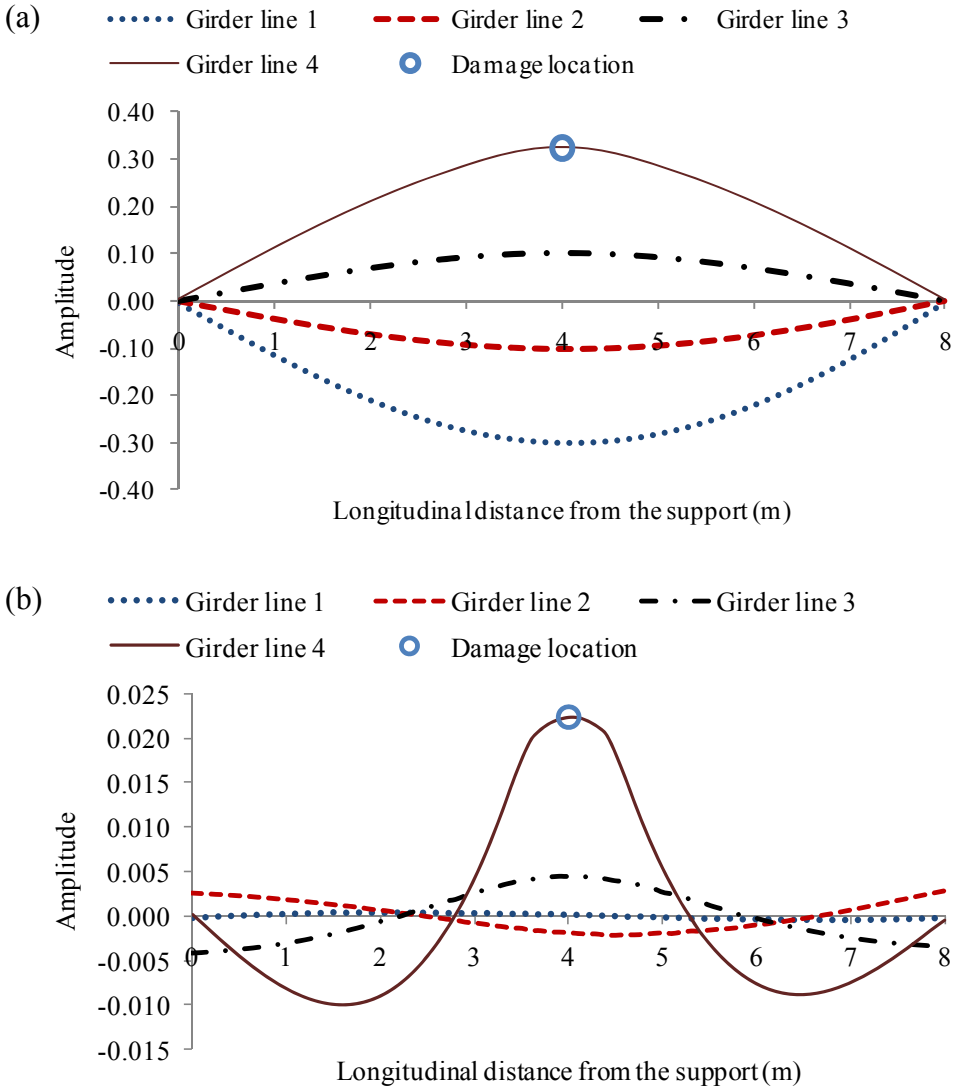

Figure 5.8. Change in mode shape due to the simulated Damage Case 1 using the normalization schemes: (a) over all measurement points and (b) along the individual girder lines.

modal properties in the absence of experimental uncertainties. Since Mode 3, Mode 4, and Mode 5 were all flexural and torsional combined mode shapes, only Mode 3 together with Mode 1 and Mode 2 were selected for this verification. Firstly, the changes in mode shapes for the lowest three modes in various damage conditions were calculated using Eq. 5.1. Then, Eq. 5.2 was used to calculate the area of mode shape change for all simulated damage cases for the lowest three vibration modes.

Table 5.4 lists the resulting area of mode shape changes for the lowest three modes due to various simulated damage cases when mode shapes were normalized over all measurement points. From Table 5.4, it can be concluded that the damage indicator was able to detect the presence of damage theoretically in the absence of uncertainties since the area of mode shape change values were non-zero for all cases. It can also be concluded that the area of mode shape change generally increases as damage becomes more severe. For example, the area of mode shape change for Mode 1 increased from 12.89% to 15.87% to 43.32% for the three damage cases in Damage Category 1 (Case 1, 10, and 11) as the damage became more severe. The area of mode shape change for Mode 1 increased from 0.02% for Damage Case 2 to 0.19% for Damage Case 10 in Damage Category 2.

Table 5.4. The area of mode shape change due to various simulated damage cases when mode shapes were normalized over all measurement points.

	The area of mode shape change		
Damage Case	Mode 1	Mode 2	Mode 3
Case 1	12.89%	17.74%	2.89%
Case 2	0.02%	0.04%	0.03%
Case 3	0.05%	0.11%	0.07%
Case 4	0.09%	0.17%	0.12%
Case 5	0.13%	0.25%	0.17%
Case 6	0.11%	0.23%	0.20%
Case 7	0.14%	0.29%	0.23%
Case 8	0.17%	0.34%	0.28%
Case 9	0.19%	0.39%	0.33%
Case 10	15.87%	21.88%	2.53%
Case 11	43.32%	60.95%	3.08%

To investigate the influence of different normalization schemes on the performance of the new damage indicator, Tables 5.5, 5.6, and 5.7 present the resulting area of mode shape changes for vibration Mode 1, Mode 2, and Mode 3, respectively, due to various simulated damage cases when mode shapes were normalized along individual girder lines. The results in Tables 5.5, 5.6, and 5.7 show the same trends as those in Table 5.4,

Table 5.5. The area of mode shape change due to various simulated damage cases for vibration Mode 1 when mode shapes were normalized along individual girder lines.

	The area of mode shape change			
Damage Case	Girder 1	Girder 2	Girder 3	Girder 4
Case 1	0.02882%	0.14373%	0.25328%	0.84113%
Case 2	0.00162%	0.00209%	0.00237%	0.00499%
Case 3	0.00163%	0.00249%	0.00409%	0.00683%
Case 4	0.00199%	0.00280%	0.00513%	0.01008%
Case 5	0.00197%	0.00351%	0.00548%	0.01223%
Case 6	0.00182%	0.00383%	0.00972%	0.01665%
Case 7	0.00191%	0.00467%	0.01116%	0.01911%
Case 8	0.00200%	0.00540%	0.01199%	0.02166%
Case 9	0.00172%	0.00511%	0.01294%	0.02429%
Case 10	0.03659%	0.17976%	0.30784%	0.99906%
Case 11	0.13495%	0.56361%	0.77905%	2.14263%

Table 5.6. The area of mode shape change due to various simulated damage cases for vibration Mode 2 when mode shapes were normalized along individual girder lines.

	The area of mode shape change			
Damage Case	Girder 1	Girder 2	Girder 3	Girder 4
Case 1	0.13946%	13.97484%	0.50314%	0.85583%
Case 2	0.00189%	0.00722%	0.00330%	0.00273%
Case 3	0.00154%	0.02139%	0.00518%	0.00465%
Case 4	0.00222%	0.03724%	0.00717%	0.00699%
Case 5	0.00185%	0.05425%	0.00908%	0.00801%
Case 6	0.00153%	0.04690%	0.01514%	0.01167%
Case 7	0.00192%	0.05726%	0.01735%	0.01297%
Case 8	0.00216%	0.06897%	0.01992%	0.01499%
Case 9	0.00230%	0.08129%	0.02284%	0.01632%
Case 10	0.16223%	14.55567%	0.63649%	1.01500%
Case 11	0.29479%	16.52069%	3.09104%	2.16526%

in which the area of mode shape change increases as damage becomes more severe. However, the magnitudes of the values in Tables 5.5, 5.6, and 5.7 are much smaller than those in Table 5.4, especially for Mode 1 and Mode 2. This implies that the measurement noise and errors due to truncation may have larger influences on the damage indicator when normalization schemes over individual girder lines are used. However, no further investigation was conducted regarding this observation.

To better understand the relationship between the area of mode shape change and the severity of damage, the results listed in the Tables 5.4, 5.5, 5.6, and 5.7 are plotted in Figs. 5.9, 5.10(a), 5.10(b), and 5.10(c), respectively, against the relative vertical flexural stiffness change due to the damage (presented in Table 5.2). From these figures, it can be clearly noticed that the area of mode shape change increases with the increase of damage severity.

Figure 5.9 presents the relationships between the area of mode shape change and the relative flexural stiffness change due to damage when mode shapes were normalized over all measurement points. A power function trend line was selected to fit each data set for Mode 1, Mode 2, and Mode 3. From a visual inspection of the figure, it can be

Table 5.7. The area of mode shape change due to various simulated damage cases for vibration Mode 3 when mode shapes were normalized along individual girder lines.

	The area of mode shape change			
Damage Case	Girder 1	Girder 2	Girder 3	Girder 4
Case 1	5.65878%	0.52388%	0.20551%	0.96381%
Case 2	0.05245%	0.00606%	0.00425%	0.00582%
Case 3	0.12679%	0.01632%	0.00857%	0.01232%
Case 4	0.20993%	0.02709%	0.01376%	0.01721%
Case 5	0.30026%	0.04025%	0.01994%	0.01992%
Case 6	0.35266%	0.04776%	0.02098%	0.03190%
Case 7	0.41926%	0.05728%	0.02476%	0.04095%
Case 8	0.49124%	0.06785%	0.03058%	0.04548%
Case 9	0.56343%	0.08062%	0.04102%	0.04168%
Case 10	4.79213%	0.46981%	0.13956%	1.02406%
Case 11	5.17256%	0.60540%	0.16365%	1.85992%

noticed that the power function tread-lines fit the data very well, at least for Mode 1 and Mode 2. The trend-lines show consistent relationships between the area of mode shape change and the severity of damage (i.e., the relative vertical flexural stiffness change in this case) over several orders of magnitude. For example, in Mode 1, a power function trend-line is expressed as

$$y = 3.3 \cdot x^{1.26} \quad [5.3]$$

where x denotes the relative flexural stiffness change and y is the area of mode shape change due to damage. This consistent relationship between the area of mode shape change and the severity of damage could be used to quantify the damage by measuring the area of mode change. It should be acknowledged, though, that the values of the constants in Eq. 5.3 may depend on many factors, such as the type of structure, the distribution of stiffness, the location of damages, etc. A much larger number of damage cases, covering a wider range of damage severity, would be required to understand the influence of these factors. However, the idea shown in this investigation could be a potential way to quantify the severity of damage (i.e., Level 3 of damage detection). As this was not the focus of this thesis, no further investigation concerning damage severity quantification was conducted as part of this research.

Figure 5.10 presents the relationship between the new damage indicator and the severity of damage when mode shapes were normalized along individual girder lines. Power functions were selected to fit the data points for each individual girder line for Mode 1, Mode 2, and Mode 3. Generally, the functions appear to fit the data points very well by a vision inspection. By inspecting Fig. 5.10(a), it is seen that the relative amplitudes of the trend-lines representing the fundamental mode occurred in order: Girder 4, Girder 3, Girder 2, and Girder 1, from top to bottom. This may imply that the damage was located around Girder 4, since the maximum area of mode shape change always happened on Girder 4 for each specific damage case. This means that the damage indicator (the area of mode shape change) may also be able to locate the damage in a general sense if multiple normalization paths are chosen to scale the mode shapes. However, this trend is not apparent for the higher modes (Figs. 5.10(b) and (c)). The

main contribution of this new damage indicator is to detect the presence of damage, especially for cases where large experimental uncertainties are involved. This is discussed in the next chapter, where the resolutions of the various test procedures are defined in a statistical manner.

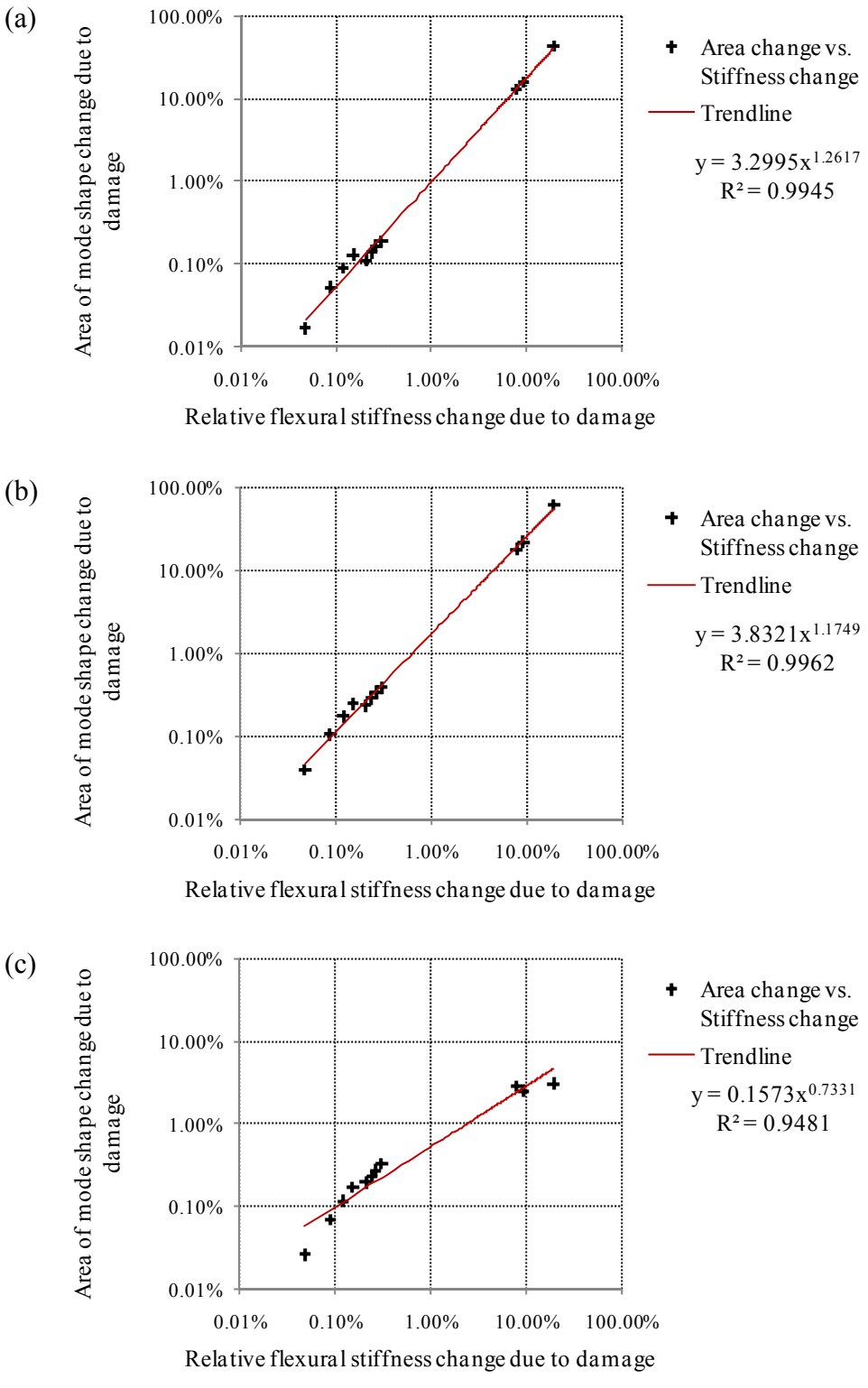

Figure 5.9. Relationship between the area of mode shape change and the relative flexural stiffness change due to damage for: (a) Mode 1, (b) Mode 2, and (c) Mode 3 when mode shapes were normalized over all measurement points.

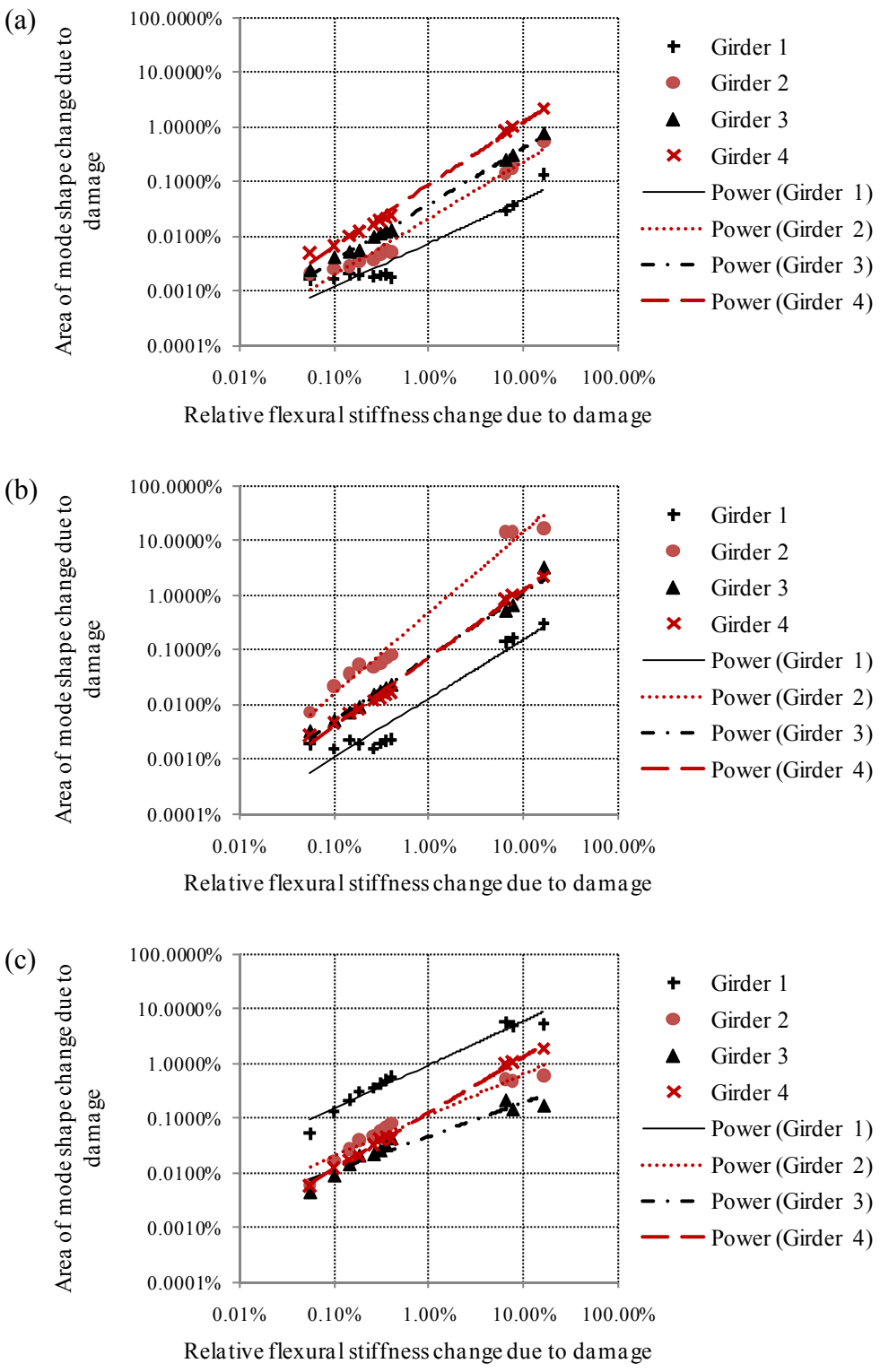

Figure 5.10. Relationship between the area of mode shape change and the relative flexural stiffness change due to damage for: (a) Mode 1, (b) Mode 2, and (c) Mode 3 when mode shapes were normalized along individual girder lines.

CHAPTER 6. APPLICATION OF VBDD METHODS TO THE MULTI-GIRDER BRIDGE SUPERSTRUCTURE

6.1 Overview

This chapter presents the application of various VBDD methods to the multi-girder bridge model using the experimental data collected from both accelerometers and strain gauges with both harmonic and white noise random excitation.

First, the distribution of the area of mode shape change is investigated when there is no change in condition. Next, the resolution of various test protocols is defined and calculated based on the statistical distribution of the area change in mode shape damage indicator, expressed as threshold values which correspond to certain statistical confidence levels. Then, detection of the presence of damage using the area of mode shape change method is investigated in a statistical manner, based on the calculated probability that there is no change in condition. Next, the detection of the presence of damage using the area of mode shape change damage indicator is investigated based on an alternative and simplified procedure by comparing the mean of the measurements with the corresponding threshold values of the test protocols.

In the last part of this chapter, five commonly available VBDD indicators are used to identify the location of damage after the presence of damage had been detected. The performance of the VBDD indicators was investigated and compared while two different normalization schemes were adopted.

6.2 Detection of the Presence of Damage Using the Area of Mode Shape Change Damage Indicator

6.2.1 Overview

Ideally, two independent measurements of a particular mode shape for a structure in the same condition would result in identical unit-area normalized mode shapes. However, uncertainties inherent in the test procedures lead to variability in the measured mode shapes obtained from separate data sets. Thus, a non-zero area of mode shape change will be obtained even when the condition of the structure has not changed. As a result, for the practical application of the VBDD methods, it is necessary to define the resolutions of test procedures adopted. In other words, how large does the value of the area of mode shape change have to be before one can say with confidence that damage has occurred? The target of this investigation was to find a test protocol which has the best resolution, therefore leading to the greatest likelihood of detecting the damage.

6.2.2 Distribution of the area of mode shape change when there is no change in condition

Uncertainties inherent in the test protocols lead to a non-zero area of mode shape change even when there is no change in the bridge's physical condition. Also, the value of the area of mode shape change, ΔA, varies between different test samples. To quantify the level of variation, it is necessary to investigate the statistical distribution of the area of mode shape change.

For the current study, a total of 170 independent pairs of mode shapes from 85 independent mode shape measurements (i.e., five independent measurement sets for each of 17 health states), were used to obtain the statistical variation of ΔA, in which each mode shape in the pair was obtained from the structure in an identical condition. For each pair of mode shapes, $\boldsymbol{\phi_n}$ and $\boldsymbol{\phi_m}$, the change in mode shape was first obtained using Eq. 5.1, and the area of mode shape change, ΔA, was then calculated using Eq. 5.2. In this manner, a total of 170 values of ΔA were obtained to generate the mean and the standard deviation of the area of mode shape change for an assumed normal

distribution, as well as to calculate the mean and standard deviation of the natural logarithm of ΔA for an assumed Log-Normal distribution.

To better understand the statistical characteristics of the population represented by the tested sample group, Figs. 6.1 and 6.2 present comparisons of the actual cumulative probability distributions and the assumed Normal and Log-Normal distributions of ΔA for the first mode with harmonic (Test Protocols 1 to 4, see Table 3.6) and white noise excitation (Test Protocols 5 to 8), respectively. The actual cumulative distributions were defined using the 170 calculated values, assuming that each value had an identical probability of occurring. From a visual inspection of Figs. 6.1 and 6.2, it can be noticed that both the Normal and Log-Normal distributions fit the actual distributions very well for Test Protocols 2, 3, and 5 to 8. However, for Test Protocol 1 (Fig. 6.1(a)), the Normal distribution fits the actual distribution better than the Log-Normal distribution, where the Log-Normal distribution underestimated the cumulative probability for specific ΔA values in the higher probability region above 0.8. For Test Protocol 4 (Fig. 6.1(d)), the Log-Normal distribution looks somewhat better than the Normal distribution to fit the actual distribution, where the Normal distribution underestimated the cumulative probability for specific ΔA in the middle probability region from 0.5 to 0.9. More information about comparisons of the actual cumulative probability distribution and assumed Normal and Log-Normal distributions is available in Appendix G for other test protocols.

A quantitative comparison of the actual cumulative probability distributions and the assumed Normal and Log-Normal distributions are listed in Table 6.1. In this table, the sum of squares of the residuals (S.S.R.), regular residual standard deviation (or standard error of estimate), and weighted residual standard deviation were used to quantify how well the assumed Normal and Log-Normal distributions fit the actual cumulative probability distributions. The best-fit curve is often assumed to be that which minimizes the sum of squares of the residuals (i.e., the difference between observed and predicted values). To reach a better physical understanding that is straightforward to compare to the reading in the plots, the regular residual standard deviation (i.e., non-weighted) was also used to compare the assumed and actual distributions. However, in cases where the

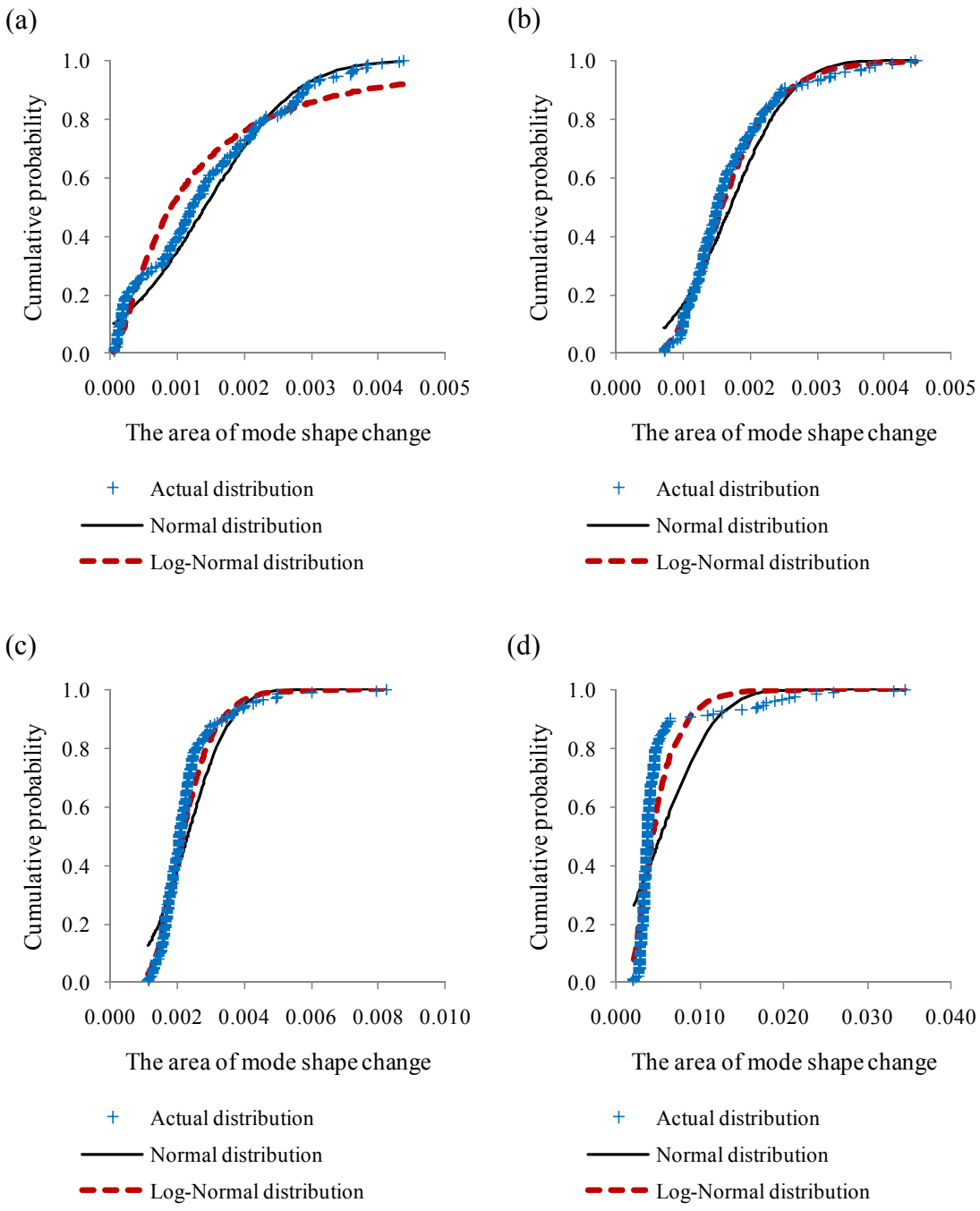

Figure 6.1. Comparison of the actual cumulative probability distributions and the assumed Normal and Log-Normal distributions of ΔA, for Test Protocols: (a) 1, (b) 2, (c) 3, and (d) 4.

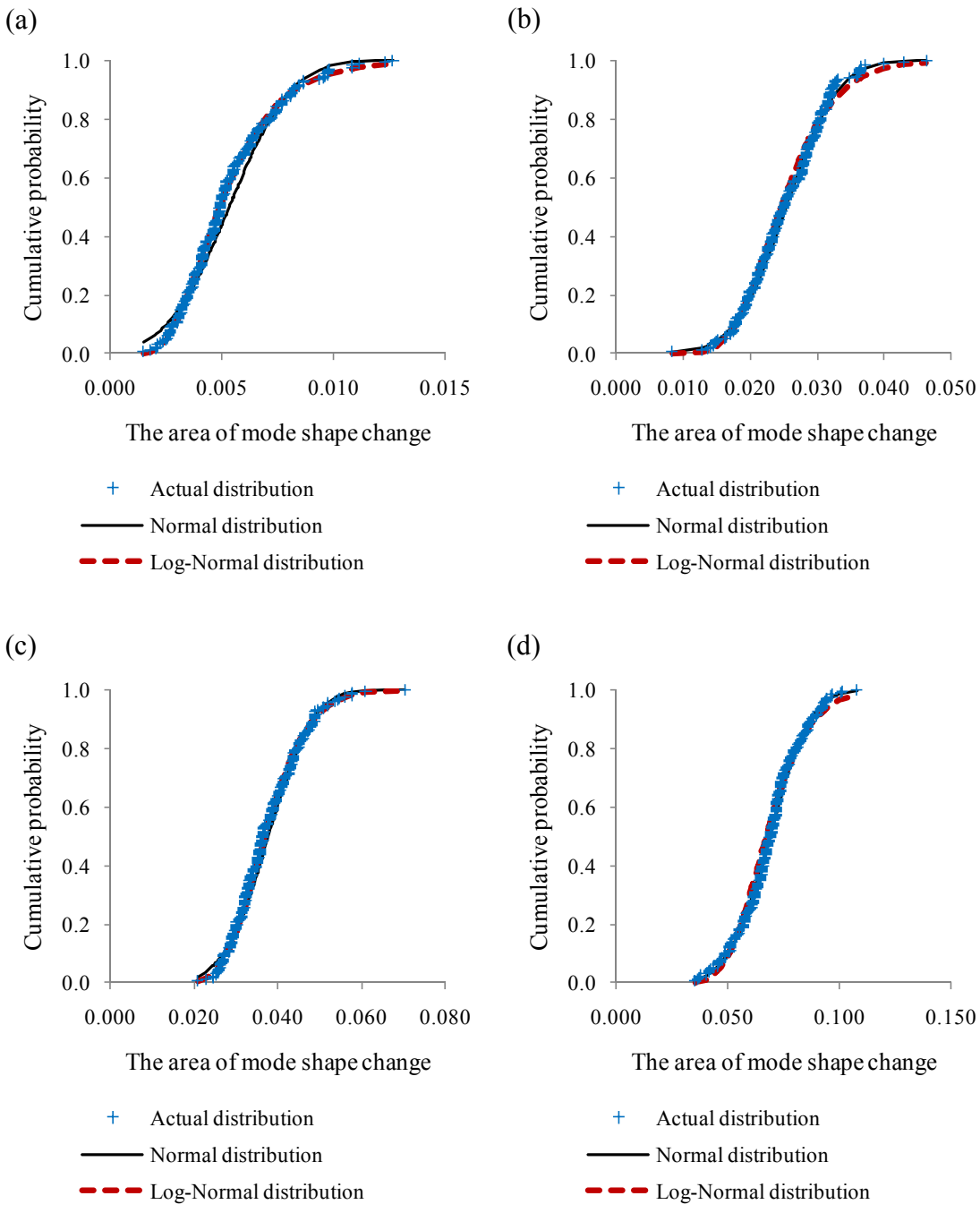

Figure 6.2. Comparison of the actual cumulative probability distributions and the assumed Normal and Log-Normal distributions of ΔA, for Test Protocols: (a) 5, (b) 6, (c) 7, and (d) 8.

Table 6.1. Comparison of the actual cumulative probability distributions and the assumed Normal and Log-Normal distributions.

Test protocol	Normal distribution			Log-Normal distribution		
	S.S.R.	R.R.S.D.	W.R.S.D	S.S.R.	R.R.S.D.	W.R.S.D
1	0.415	0.050	1.508	1.048	0.079	0.277
2	2.856	0.130	4.168	10.739	0.253	6.878
3	11.837	0.265	6.566	19.715	0.343	9.568
4	48.016	0.535	12.365	37.324	0.471	12.787
5	48.700	0.538	9.896	39.729	0.486	11.559
6	56.168	0.578	16.474	55.684	0.576	16.187
7	56.168	0.578	16.474	56.040	0.578	16.438
8	56.168	0.578	16.474	56.148	0.578	16.466
9	29.938	0.422	3.097	30.839	0.428	4.114
10	48.657	0.538	12.049	40.455	0.491	12.660
11	55.522	0.575	15.537	47.740	0.533	14.260
12	56.167	0.578	16.473	53.401	0.564	15.654
13	56.167	0.578	16.473	55.520	0.575	15.737
14	56.168	0.578	16.474	56.165	0.578	16.472
15	56.168	0.578	16.474	56.167	0.578	16.474
16	56.168	0.578	16.474	56.168	0.578	16.474
17	56.168	0.578	16.474	55.288	0.574	16.086
18	56.168	0.578	16.474	56.141	0.578	16.463
19	56.168	0.578	16.474	56.158	0.578	16.470
20	56.168	0.578	16.474	56.166	0.578	16.473
21	56.141	0.578	16.332	55.662	0.576	15.341
22	56.168	0.578	16.474	56.163	0.578	16.469
23	56.168	0.578	16.474	56.166	0.578	16.474
24	56.168	0.578	16.474	56.167	0.578	16.474
25	56.168	0.578	16.474	55.866	0.577	16.340
26	56.168	0.578	16.474	56.130	0.578	16.455
27	56.168	0.578	16.474	56.158	0.578	16.469
28	56.168	0.578	16.474	56.166	0.578	16.474

S.S.R. = Sum of square of the residuals;
Residuals = differences between observed and predicted values;
R.R.S.D. = Regular residual standard deviation (or standard error of estimate);
W.R.S.D. = Weighted residual standard deviation (or weighted standard error of estimate).

dependent variable does not have constant variance, a sum of weighted squared residuals may be minimized. As a result, the weighted residual standard deviation was also included in this comparison. The Mathcad (Mathcad 14.0) routines for calculating the results listed in Table 6.1 are presented in Appendix M.

From the results listed in Table 6.1, it can be seen that the assumed Normal and Log-Normal distributions provided a very similar estimation of actual distribution for all test protocols based on R.R.S.D. values, except that the Normal distribution was slightly better than Log-normal distribution for Test Protocols 1, 2, and 3, while the Log-Normal distribution was slightly better than Normal distribution for Test Protocols 4, 5, 10, and 11.

To better understand the variation of the area of mode shape change from independent measurements when there is no change in physical condition, Tables 6.2 and 6.3 list the actual probability distribution density of the measured ΔA for Test Protocols 1 and 2, respectively. To calculate the distribution density of ΔA, the range of ΔA (from 0.0 to 1.0) was subdivided into six sub-regions consisting of a beginning tail, four equally spaced intervals (equal to the value of the difference between the maximum and

Table 6.2. Actual probability distribution density of the measured area of mode shape change for Test Protocol 1 when there is no change in physical condition.

Range of ΔA	Mean of ΔA in the range	Frequency	Normalized density
0.0000 — 0.0005	0.0002	45	345.82
0.0005 — 0.0013	0.0010	47	361.19
0.0013 — 0.0022	0.0017	40	307.40
0.0022 — 0.0031	0.0027	25	192.12
0.0031 — 0.0039	0.0035	10	76.85
0.0039 — 1.0000	0.0042	3	23.05

Frequency = the number of ΔA values occurring in the corresponding range from the total of 170 ΔA values; the sum of counted numbers in all ranges should be 170.
Normalized density: the normalized density was calculated by scaling the counted number using a scaling factor that equals the area enclosed by an interpolation line of the counted numbers and assumed end conditions; by doing this, the area covered by the density line equals unity.

Table 6.3. Actual probability distribution density of the measured area of mode shape change for Test Protocol 2 when there is no change in physical condition.

Range of ΔA	Mean of ΔA in the range	Frequency	Normalized density
0.0000 — 0.0011	0.0009	29	240.77
0.0011 — 0.0018	0.0014	87	722.30
0.0018 — 0.0026	0.0022	38	315.49
0.0026 — 0.0033	0.0030	8	66.42
0.0033 — 0.0041	0.0037	5	41.51
0.0041 — 1.0000	0.0043	3	24.91

Frequency = the number of ΔA values occurring in the corresponding range from the total of 170 ΔA values; the sum of counted numbers in all ranges should be 170.
Normalized density: the normalized density was calculated by scaling the counted number using a scaling factor that equals the area enclosed by an interpolation line of the counted numbers and assumed end conditions; by doing this, the area covered by the density line equals unity.

minimum values of readings, divided by five), and an ending tail. The six sub-ranges were selected in this case to balance the variation requirements for both ΔA and probability density of each specific ΔA. For example, at one extreme, if no subdivision and only one range is used, only one averaged ΔA value (with a counted number of 170) can be produced to generate the density function, which has no variation in ΔA, and is therefore meaningless. At the other extreme, if too many sub-ranges are used (at least 170 sub-ranges), only one sample may be available in each sub-range, which then has no variation in the probability density (i.e., each sub-range has only one ΔA included and frequency is one for this sub-range). The number of ΔA values in each range was counted, a value which was defined as the frequency of ΔA, and recorded together with the mean value of ΔA that occurred in the corresponding range. The sum of frequency in all ranges should equal to the total number of ΔA values of 170. To define the probability density function, the counted number (or frequency) had to be normalized in order that the area covered by the probability density function was equal to unity. As a result, the counted numbers (or frequency) were scaled using a scaling factor equal to the area covered by a line interpolated from the data points and based on assumed end conditions. In this case, to simplify the process, the frequency was assumed to be zero

at the ΔA value of zero, which means that the probability of producing two mode shapes that are exactly the same from two independent measurements under practical testing conditions is negligible. Another boundary condition that was assumed was that the probability of producing a large value of ΔA (i.e., significantly large changes in condition) is exceedingly small. In this case, the frequency was assumed to be 0.1 (i.e., one tenth of one count) for a ΔA value equal to twice the maximum of the 170 ΔA values. The detailed Mathcad (Mathcad 14.0) calculations are presented in Appendix M.

The probability density results listed in Tables 6.2 and 6.3 are also plotted in Fig. 6.3, together with the assumed Normal and Log-Normal distributions, where the mean and standard deviation of the assumed distributions were calculated from the 170 ΔA values, as described in previous paragraphs for Figs. 6.1 and 6.2. Also, the 95th percentile of the assumed Normal and Log-Normal distribution are plotted in Figs. 6.3. In a similar way, Figs. 6.4, 6.5, and 6.6 present comparisons of the probability density between the actual distribution and the assumed Normal and Log-Normal distributions of ΔA for Test Protocols 3 to 8. The comparisons of probability density for all other test protocols are presented in Appendix G.

From a visual inspection of the results shown in Figs. 6.3 to 6.6, it can be seen that Normal distribution fits the actual distribution slightly better than Log-Normal distribution for Test Protocols 1 and 6, while the Log-Normal distribution fits slightly better than Normal distribution for Test Protocols 2, 4, and 5. Generally, the actual distributions were located between the assumed Normal and Log-Normal distributions. Considering the 95th percentile values, the values for Log-Normal distribution were generally larger than those for Normal distribution, except for Test Protocols 3 and 4. This suggests that using the 95th percentile from Log-Normal distribution as the threshold value, as described in the next section, may be more suitable for damage detection from a conservative point of view. Detailed discussion on this is available in Section 6.2.3 and 6.2.4.

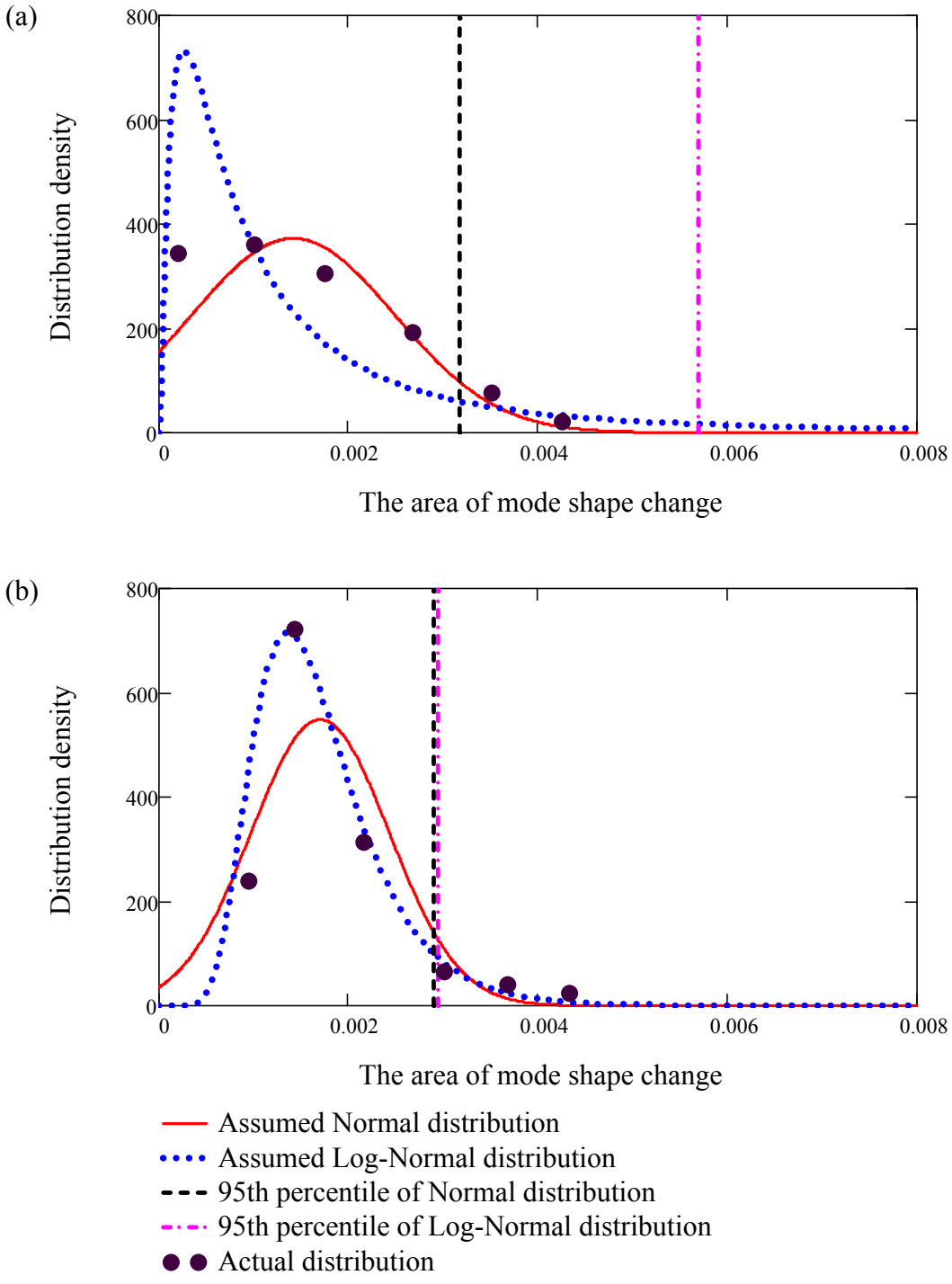

Figure 6.3. Comparison of the probability density between the actual distribution and the assumed Normal and Log-Normal distributions of ΔA, for Test Protocols: (a) 1 and (b) 2.

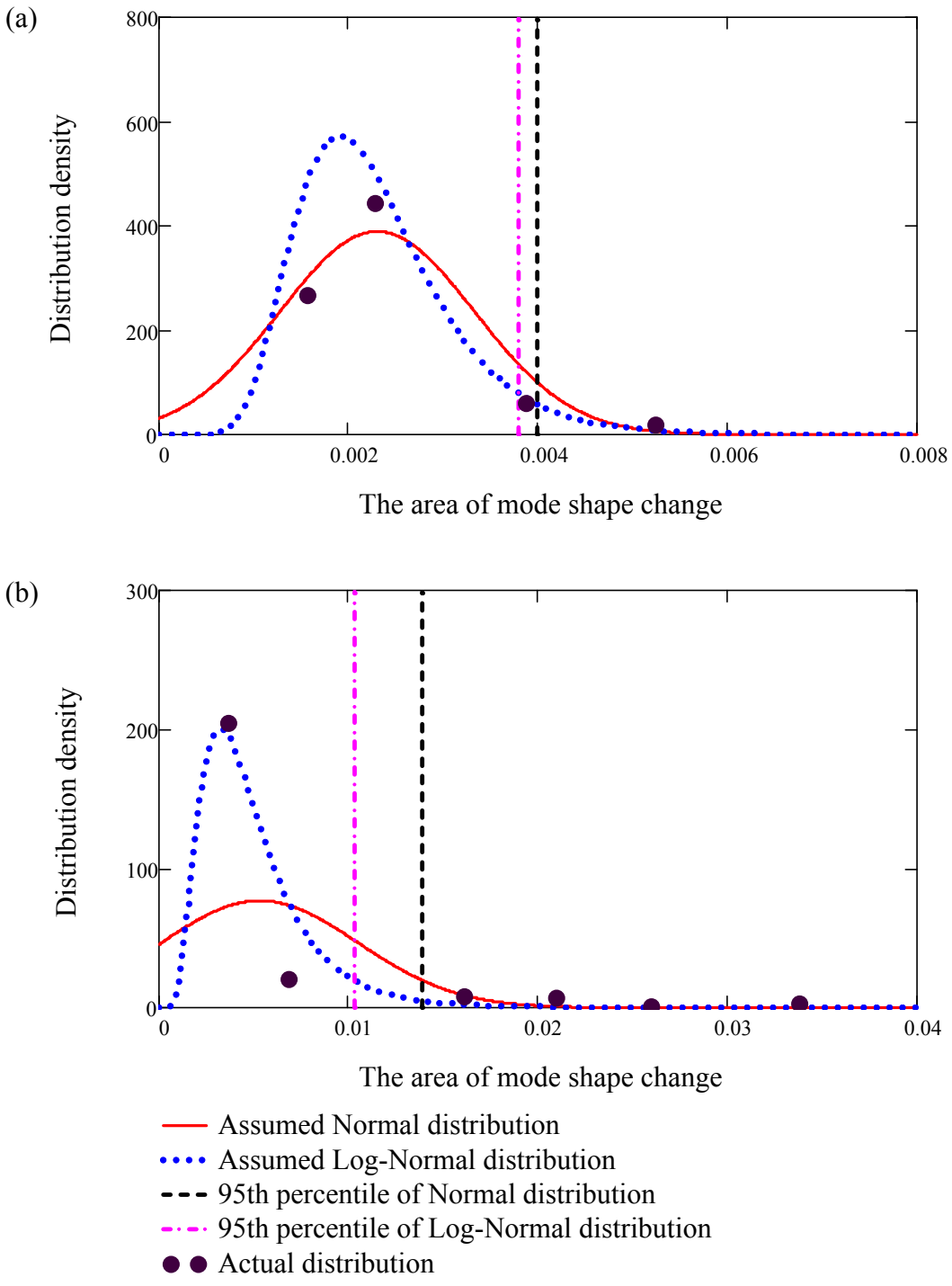

Figure 6.4. Comparison of the probability density between the actual distribution and the assumed Normal and Log-Normal distributions of ΔA, for Test Protocols: (a) 3 and (b) 4.

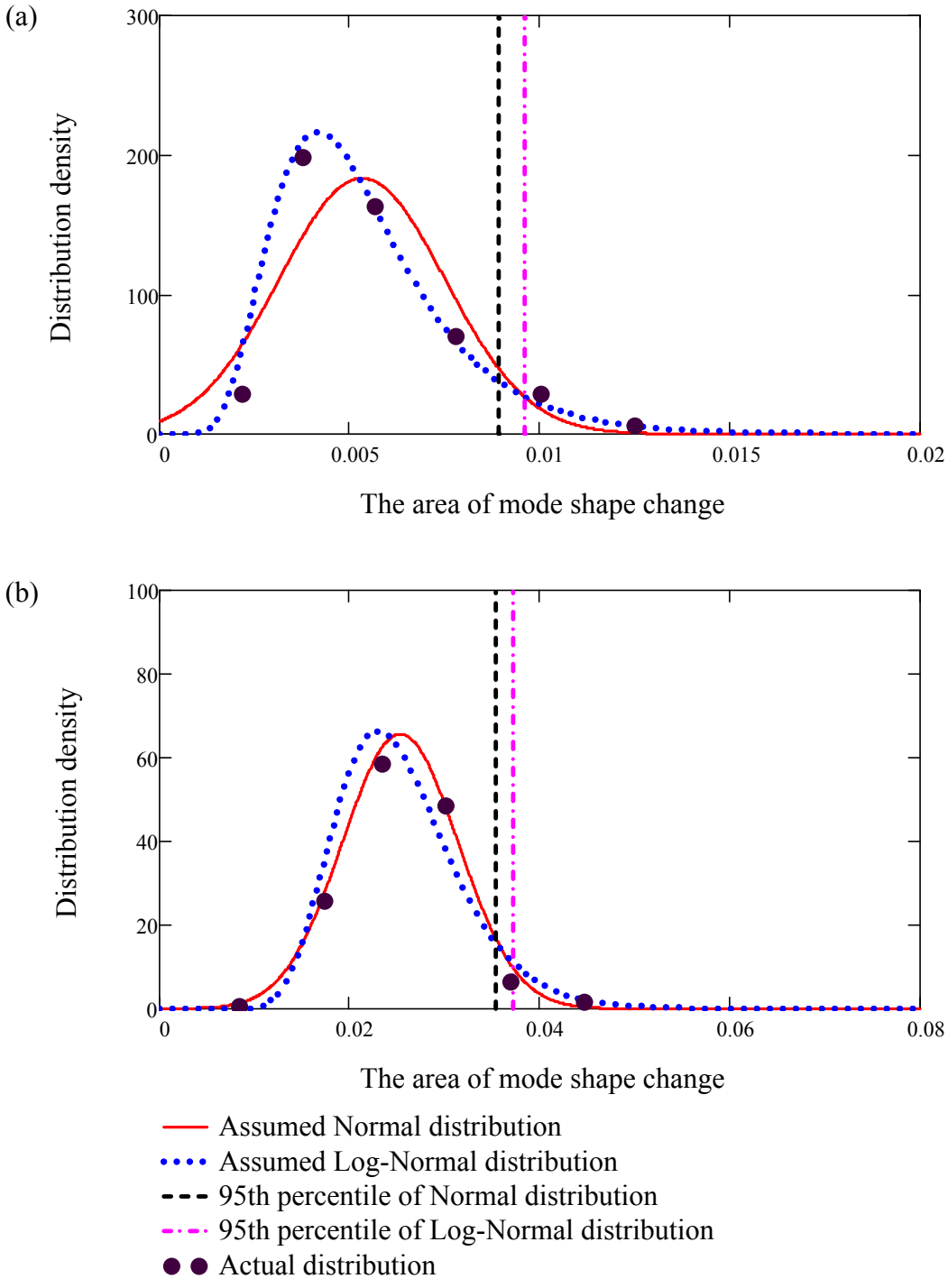

Figure 6.5. Comparison of the probability density between the actual distribution and the assumed Normal and Log-Normal distributions of ΔA, for Test Protocols: (a) 5 and (b) 6.

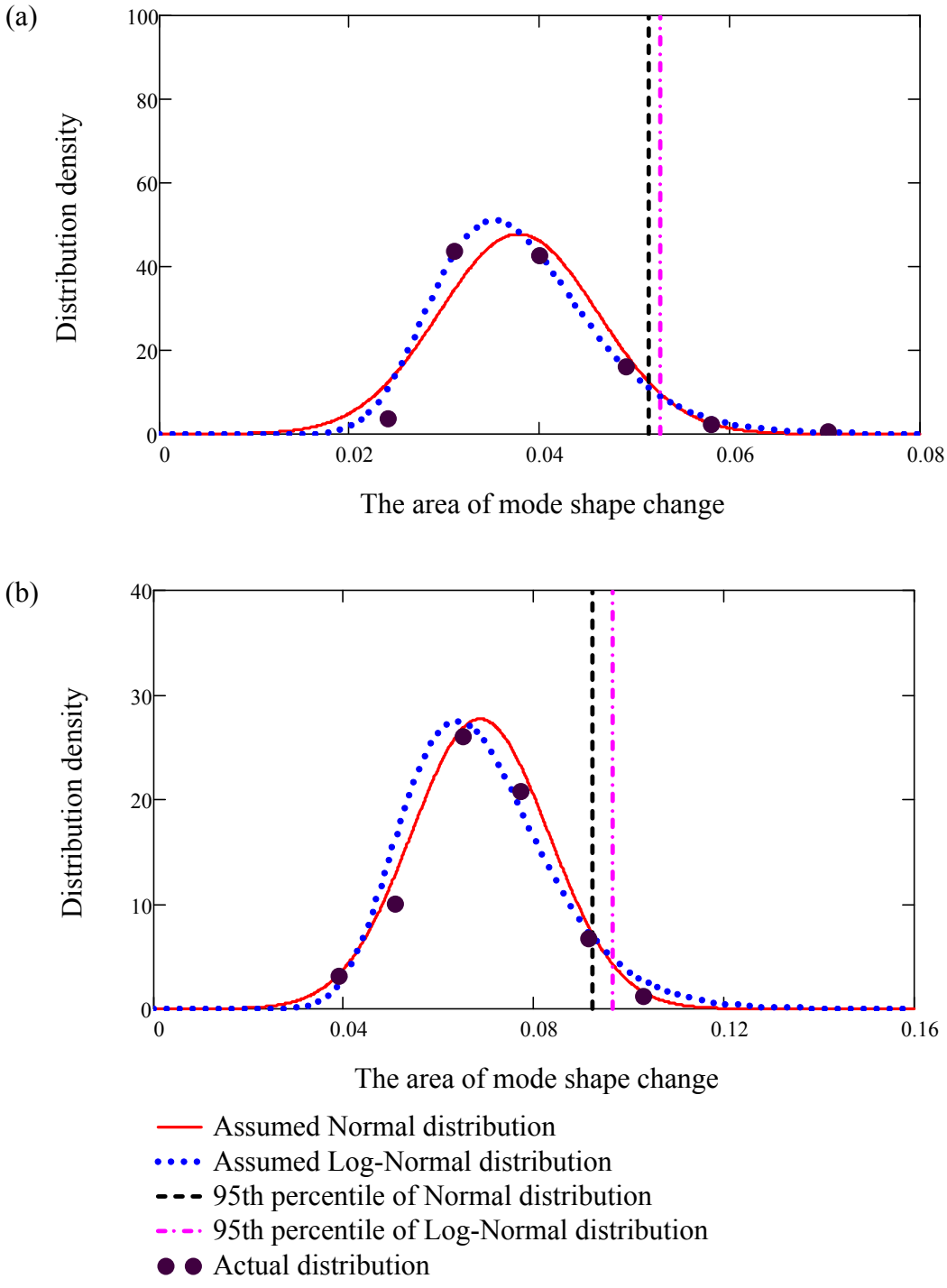

Figure 6.6. Comparison of the probability density between the actual distribution and the assumed Normal and Log-Normal distributions of ΔA, for Test Protocols: (a) 7 and (b) 8.

6.2.3 Definition of the resolution of a specific test protocol

The resolution of a particular test protocol can be defined as a threshold value of the area of mode shape change, ΔA, below which that test protocol is incapable of identifying damage because the observed changes are not statistically significant. These resolutions were obtained by observing the statistical variation of ΔA produced using pairs of mode shapes measured when there was no change in the health condition.

The threshold value for ΔA can be defined as follows,

$$Threshold(p, \Delta A) = icdf(p, \mu, \sigma) \quad [6.1]$$

where p is a statistical probability or confidence limit; μ and σ are the mean and the standard deviation, respectively, of the population of ΔA for a Normal distribution, or of the natural logarithm of ΔA for a Log-Normal distribution, estimated from measured samples. In addition, $icdf(p, \mu, \sigma)$ is an inverse cumulative distribution function which returns a threshold value in the population of ΔA for the given value of p, defined as pth percentile. For example, in the case of an expected statistical probability p of 95%, the threshold value for ΔA was defined as the 95th percentile of the distribution—that is, the value that would be exceeded by only 5% of the population. In other words, the threshold value of ΔA corresponded to the limiting value above which a calculated change in area would have a less than 5% probability of occurring when there is, in fact, no change in the condition of the structure (i.e., the probability of a false positive indicator). Thus, if a change in area above the threshold is observed, the chance that the condition of the structure is unchanged is sufficiently small (not greater than 5%) if only one measurement is conducted, so as to conclude that a change in condition (i.e., damage) has indeed occurred. The actual probability of a false positive indicator is usually much less than 5% if the mean of multiple measurements of ΔA is observed above the threshold, defined as the 95^{th} percentile. More discussions on the actual probability of a false positive indicator are available in Section 6.2.5.

6.2.4 Threshold values for different test procedures

Table 6.4 presents the threshold values, defined as the 95th percentile of the "actual" and assumed Normal and Log-Normal distributions, for the area of mode shape change observed for all 28 test protocols investigated. Here, the 95th percentile value for the actual distribution was defined as a ΔA value which was not smaller than 95% of the ΔA values but was smaller than 5% of the ΔA values from the recorded samples (170 values in current study). The Mathcad (Mathcad 14.0) routines for calculating the threshold values are presented in Appendix M (Section M.5). A smaller threshold value is indicative of a higher resolution for that protocol and a more repeatable estimate of mode shapes, which makes the protocol more sensitive to changes in structural condition.

From the results shown in Table 6.4, there are no specific trends and relationships available between the threshold values of the actual and the assumed Normal and Log-Normal distributions. The relative difference in threshold values can be as high as 48.75% for the Normal distribution, or 67.17% for the Log-Normal distribution, with respect to the actual distribution. Also, the threshold values of the assumed distributions could either be overestimated or underestimated. However, for the most commonly used test protocols, including the combinations of the fundamental vibration mode and sensors with relatively high signal to noise ratio (like Test Protocols 1 to 3, and 5 to 7 in this case), the estimation of threshold values was relatively good no matter which distribution was assumed, except for Test Protocol 1 using the Log-Normal distribution, where the threshold value was overestimated by 58.39%. Using the threshold values from the actual distributions is acceptable and workable in this case, since there was a large number of test samples (170 values) available in current study. Practically, however, using assumed distributions may be more suitable since the number of measured samples is usually limited. Furthermore, there are always unavoidable cut-off errors on both sides of the distributions (i.e., in the two tails beyond the minimum and maximum values of ΔA), when actual distributions are used to produce the threshold values.

Table 6.4. Threshold values of the area of mode shape change for different test protocols, defined as the 95th percentile of the actual and assumed distributions.

Test protocol	Actual	Normal	Relative Difference	Log-Normal	Relative Difference
1	0.0036	0.0032	-11.51%	0.0057	58.39%
2	0.0033	0.0029	-11.04%	0.0029	-9.46%
3	0.0043	0.0040	-6.81%	0.0038	-11.48%
4	0.0179	0.0139	-22.69%	0.0104	-42.21%
5	0.0097	0.0089	-8.21%	0.0096	-0.88%
6	0.0362	0.0353	-2.30%	0.0372	2.99%
7	0.0518	0.0515	-0.51%	0.0527	1.85%
8	0.0930	0.0924	-0.67%	0.0966	3.86%
9	0.0509	0.0451	-11.52%	0.0852	67.17%
10	0.0203	0.0195	-3.72%	0.0210	3.32%
11	0.0291	0.0251	-13.63%	0.0264	-9.21%
12	0.0484	0.0448	-7.39%	0.0485	0.30%
13	0.1074	0.1597	48.75%	0.1130	5.23%
14	0.5867	0.4777	-18.58%	0.5290	-9.83%
15	0.5113	0.4757	-6.96%	0.5221	2.11%
16	0.6775	0.6542	-3.43%	0.7149	5.52%
17	0.0462	0.0455	-1.63%	0.0478	3.47%
18	0.1370	0.1317	-3.89%	0.1323	-3.41%
19	0.1857	0.1728	-6.96%	0.1801	-3.01%
20	0.2700	0.2595	-3.86%	0.2694	-0.21%
21	0.2480	0.2300	-7.25%	0.3212	29.53%
22	0.5039	0.4096	-18.71%	0.4024	-20.13%
23	0.6035	0.4369	-27.61%	0.4160	-31.07%
24	0.5865	0.5150	-12.19%	0.5335	-9.05%
25	0.0516	0.0501	-2.89%	0.0531	2.94%
26	0.1967	0.1824	-7.27%	0.1893	-3.77%
27	0.2536	0.2182	-13.96%	0.2228	-12.14%
28	0.3601	0.3325	-7.67%	0.3485	-3.22%

Relative Difference = Relative difference in the threshold values between the assumed distribution and actual distribution, calculated using (assumed-actual)/actual;

To better understand the trends of threshold values and the influence of the level of confidence on the threshold values, the 90th percentile of the actual and assumed Normal and Log-Normal distributions for the area of mode shape change observed for all 28 test protocols were calculated and are listed in Table 6.5. As expected, all values in Table 6.5 are smaller than the corresponding ones in Table 6.4 since the confidence level was decreased from 95% to 90%. However, the general trends for different sensor schemes and excitation types remained similar to those found in Table 6.4.

To simplify the concepts involved, only the threshold values from the assumed Log-Normal distribution are discussed in detail in the following paragraphs in this sub-section. To clarify the influence of excitation and sensor types on the threshold values, the threshold values listed in Table 6.4 for the Log-Normal distribution are reorganized and presented in Table 6.6 along with an explicit name of components for the various test protocols.

The results presented in Table 6.6 show that when white noise excitation was used, the use of the fundamental vibration mode obtained by acceleration measurements (or Test Protocol 5) was clearly superior to all other protocols (or Test Protocols 6 to 8). Measurement of the fundamental mode using the bottom strain gauges (or Test Protocol 6) resulted in the next most reliable results, although the threshold value was around four times that obtained using acceleration measurements. The use of acceleration measurements to obtain higher modes, also produced better resolutions than those obtained by strain measurements, with bottom strain measurements producing the next best results. However, with the possible exception of measurements of modes 3 and 5 using accelerometers, threshold values achieved for higher modes were high enough that the protocols would likely be insensitive to all but the most severe of damage cases.

The use of harmonic excitation to measure the fundamental vibration mode resulted in the lowest threshold values of all protocols considered, with all four instrumentation schemes producing similar results (the threshold value was only slightly higher for the top strain gauges, which were found to produce much lower signal-to-noise ratios than other sensor schemes). These protocols can therefore be considered to be the most

Table 6.5. Threshold values of the area of mode shape change for different test protocols, defined as the 90th percentile of the actual and assumed distributions.

Test protocol	Actual	Normal	Relative Difference	Log-Normal	Relative Difference
1	0.0029	0.0028	-3.24%	0.0038	31.61%
2	0.0025	0.0026	6.41%	0.0026	3.77%
3	0.0035	0.0036	4.22%	0.0033	-3.63%
4	0.0065	0.0120	85.34%	0.0085	32.23%
5	0.0082	0.0081	-0.88%	0.0083	1.26%
6	0.0321	0.0331	3.16%	0.0340	5.82%
7	0.0488	0.0485	-0.74%	0.0487	-0.22%
8	0.0876	0.0871	-0.51%	0.0891	1.75%
9	0.0390	0.0390	0.03%	0.0518	32.78%
10	0.0175	0.0171	-2.28%	0.0162	-7.59%
11	0.0229	0.0221	-3.45%	0.0209	-8.77%
12	0.0462	0.0394	-14.65%	0.0381	-17.48%
13	0.0744	0.1354	82.06%	0.0878	18.04%
14	0.4559	0.4232	-7.18%	0.4221	-7.42%
15	0.4308	0.4257	-1.18%	0.4296	-0.28%
16	0.6020	0.5931	-1.48%	0.6073	0.89%
17	0.0371	0.0411	10.88%	0.0409	10.26%
18	0.1141	0.1194	4.64%	0.1151	0.88%
19	0.1600	0.1574	-1.67%	0.1565	-2.19%
20	0.2305	0.2379	3.22%	0.2374	3.00%
21	0.2082	0.2022	-2.89%	0.2338	12.29%
22	0.3419	0.3593	5.09%	0.3230	-5.53%
23	0.3599	0.3853	7.05%	0.3424	-4.86%
24	0.4612	0.4604	-0.18%	0.4452	-3.48%
25	0.0464	0.0463	-0.16%	0.0472	1.84%
26	0.1737	0.1618	-6.83%	0.1546	-11.00%
27	0.2018	0.1956	-3.07%	0.1879	-6.88%
28	0.3037	0.3013	-0.79%	0.2993	-1.46%

Relative Difference = Relative difference in the threshold values between the assumed distribution and actual distribution, calculated using (assumed-actual)/actual;

Table 6.6. Threshold values of area of mode shape change for different test protocols, defined as the 95th percentile of the Log-Normal distribution, expressed as percentage of total area under the original unit-area normalized mode shape.

	White noise excitation					Harmonic excitation	
Instrumentation	Mode 1	Mode 2	Mode 3	Mode 4	Mode 5	Mode 1	Mode 2
Acceleration	0.96%	11.30%	4.78%	32.12%	5.31%	0.57%	8.52%
Bottom strain	3.72%	52.90%	13.23%	40.24%	18.93%	0.29%	2.10%
Middle strain	5.27%	52.21%	18.01%	41.60%	22.28%	0.38%	2.64%
Top strain	9.66%	71.49%	26.94%	53.35%	34.85%	1.04%	4.85%

sensitive to changes in structural condition, and therefore the most likely to identify the presence of damage. Interestingly, the protocols making use of strain gauge measurements (especially from the bottom and middle gauges) typically resulted in lower threshold values than those using accelerometer measurements when harmonic excitation was used, despite the fact that mode shapes generated from accelerometer data have previously been shown to be more repeatable than those produced using the strain gauge data (see the results in Chapter 4). This might be explained in part by the fact that multiple independent setups were required for acceleration measurements due to the limited number of accelerometers available, whereas the permanently installed strain gauges required only a single setup.

6.2.5 Detection of the presence of damage using the area of mode shape change method based on the calculated probability values

As described in Section 3.4, sixteen single damage cases were induced in the bridge model after the undamaged dynamic properties had been established (see Table 3.5). For each damage case, the area of mode shape change was calculated for all five vibration modes using Eqs. 5.1 and 5.2, in which five separate tests were conducted to measure each of the damaged and undamaged unit-area normalized mode shape vectors, $\boldsymbol{\phi_m}$ and $\boldsymbol{\phi_n}$, respectively. As a result, a total of 25 values of area of mode shape change were generated by the 25 independent pairs of damaged and undamaged mode shape vectors for each vibration mode and each damage case. Table 6.7 presents a sample of

Table 6.7. The summary of area of change in the first mode shape due to Damage Cases 1 to 3 for different test trials when Test Protocol 1 was used.

	Area of mode shape change		
Trials	Case 1	Case 2	Case 3
set11	8.77%	2.10%	0.84%
set12	8.78%	1.98%	0.90%
set13	8.80%	1.99%	0.83%
set14	8.88%	1.95%	1.01%
set15	8.87%	1.87%	0.84%
set21	8.76%	2.07%	0.80%
set22	8.76%	1.97%	0.91%
set23	8.78%	1.96%	0.78%
set24	8.87%	1.93%	0.97%
set25	8.86%	1.85%	0.78%
set31	8.77%	2.12%	0.84%
set32	8.77%	2.00%	0.88%
set33	8.79%	2.01%	0.79%
set34	8.88%	1.97%	0.96%
set35	8.87%	1.89%	0.79%
set41	8.77%	2.24%	0.86%
set42	8.78%	2.11%	0.87%
set43	8.80%	2.13%	0.79%
set44	8.89%	2.09%	0.96%
set45	8.87%	2.00%	0.80%
set51	8.78%	2.21%	0.79%
set52	8.79%	2.08%	0.88%
set53	8.81%	2.10%	0.75%
set54	8.89%	2.06%	0.94%
set55	8.88%	1.97%	0.76%
Min	8.76%	1.85%	0.75%
Mean	8.82%	2.03%	0.85%
STDEV	0.05%	0.10%	0.07%
C.O.V	0.57%	4.90%	8.58%

Min = Minimum value of the area of mode shape change in all trials;
Mean = The average value of the area of mode shape change in all trials;
STDEV = Standard deviation of the samples;
C.O.V = Coefficient of variation of the samples.

the calculated results for Damage Case 1, Case 2, and Case 3, in which only accelerometer data with harmonic excitation were used to generate the results (i.e., Test Protocol 1). The statistical values, including the minimum, mean, standard deviation, and coefficient of variation of the ΔA values are also listed in Table 6.7. It can be seen that all values listed in Table 6.7 exceed the 95th percentile value shown in Table 6.6 (0.57%) for this test protocol, meaning that all three damage cases could be detected at least a confidence level of 95%. The results for all damage cases and Test Protocols 1 to 8 are included in Appendix H.

It was assumed that the set of 25 values of ΔA also formed a sample from a population with a Normal or Log-Normal distribution, in a similar manner to that defined for the set of 170 values of ΔA when there was no change in physical condition, as described previously. Now, two distributions were defined. One distribution was estimated using 170 values of ΔA when there was no change in condition, and the other was estimated using 25 values of ΔA when there was (or may have been) a change in condition. Figures 6.7 and 6.8 present the two distributions with the assumed Normal and Log-Normal distributions, respectively, for Damage Cases 1 to 3, when Test Protocol 1 was used. Both figures show similar results. The two groups shown in the two figures (one for the undamaged group and the other for the damaged group) are well separated from each other for Damage Cases 1 and 2; in addition, the distance between the mean values of two groups is relatively large for Damage Cases 1 and 2. For Damage Case 3, there is only a small region of intersection between the distribution density lines of the two groups. As a result, one can confidently say that the two groups are from different populations. This means that there has been a change in condition with a relatively high confidence. Similar figures for other damage cases are presented in Appendix H.

Using the two distributions, it is possible to calculate the probability that the second value (from damaged group) exceeds the first one (from undamaged group) (i.e., the probability that there has been a change in condition). Conversely, one could calculate the probability that the second value does not exceed the first (i.e., the probability that there is no change in condition). The Mathcad (Mathcad 14.0) routines for calculating the probabilities are presented in Appendix M (Section M.5).

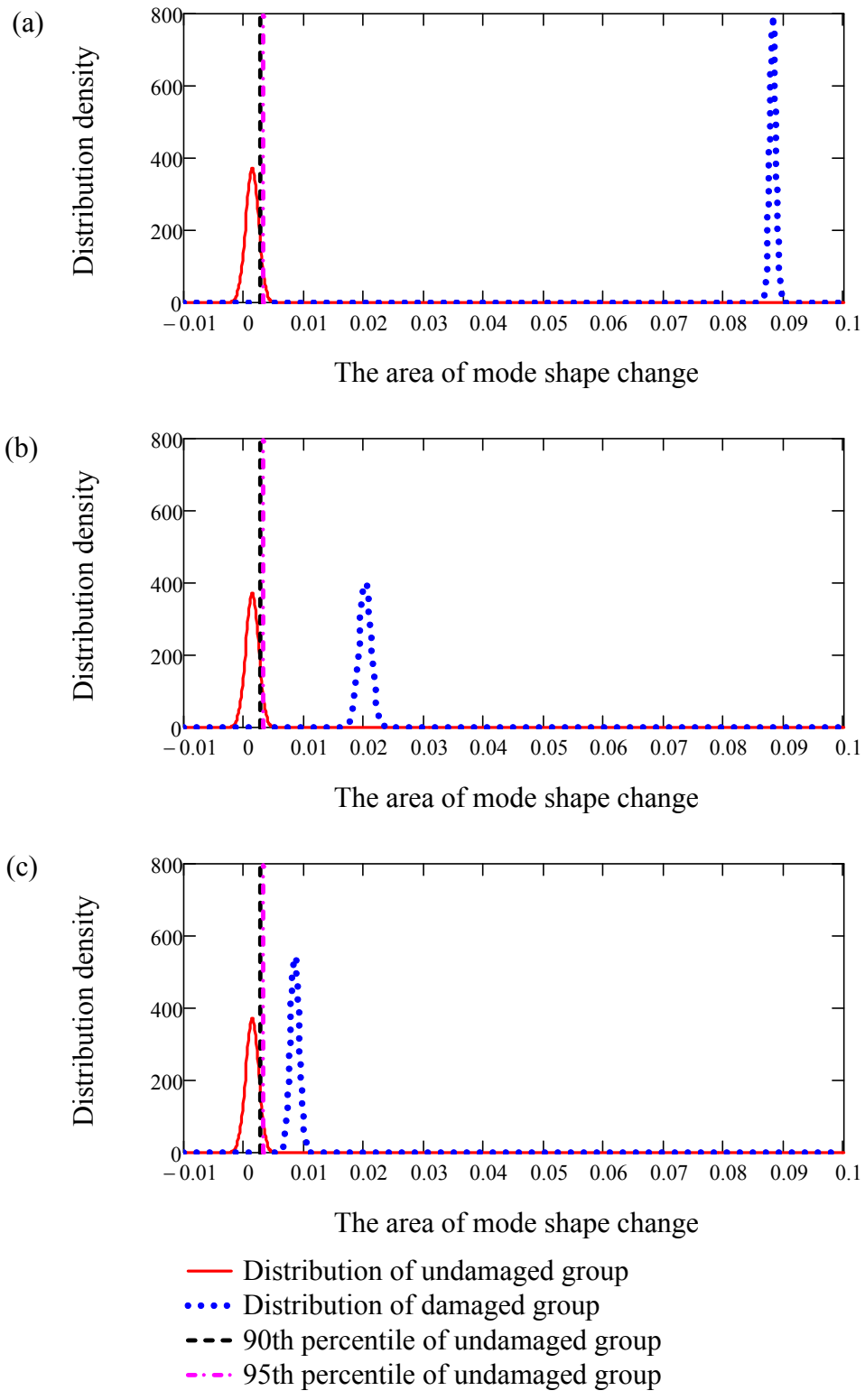

Figure 6.7. Comparison of Normal distributions of the area of mode shape change for the undamaged group of 170 pairs and the damaged group of 25 data pairs for Damage Case: (a) 1, (b) 2, and (c) 3, when the Test Protocol 1 was used.

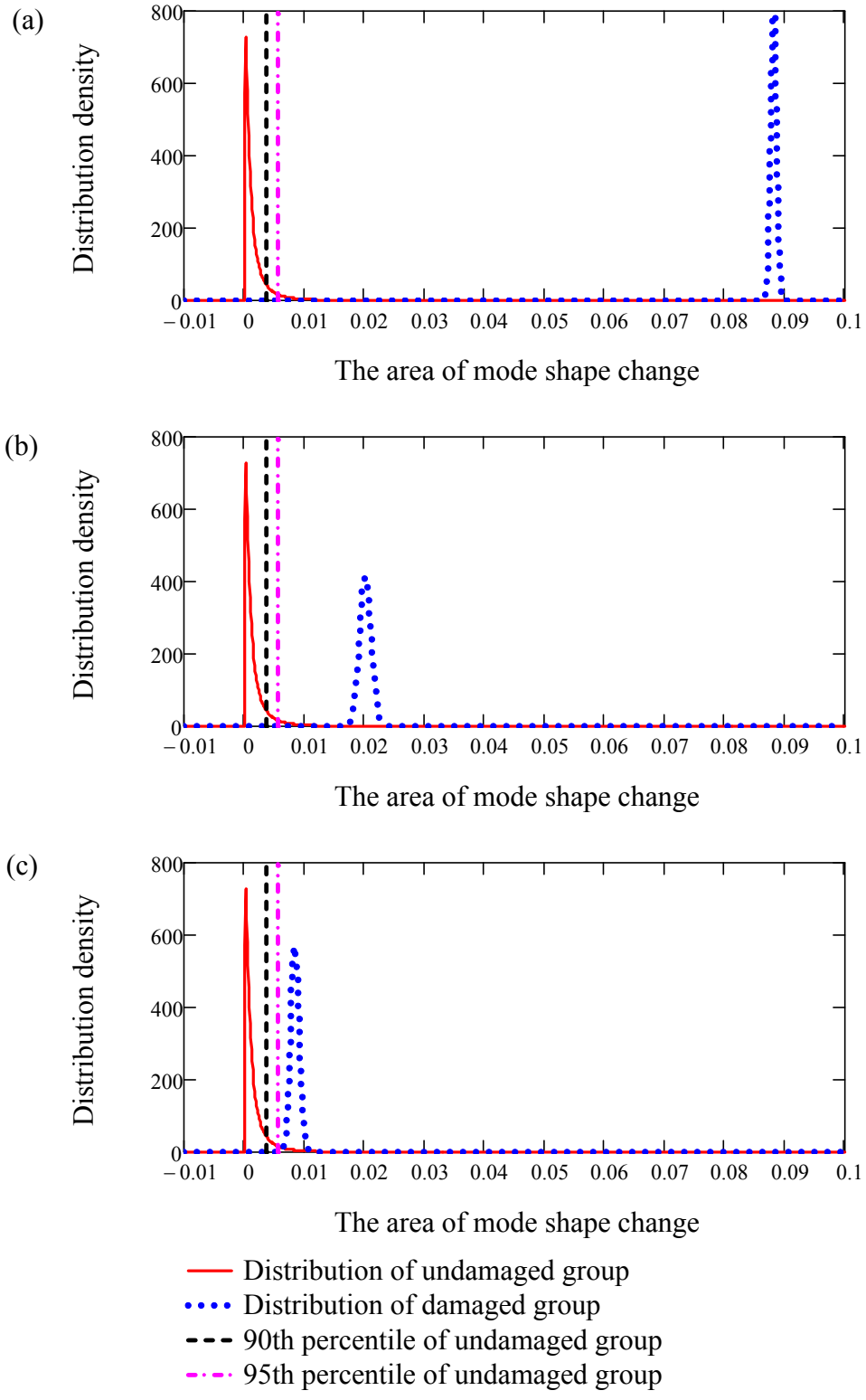

Figure 6.8. Comparison of Log-Normal distributions of the area of mode shape change for the undamaged group of 170 pairs and the damaged group of 25 data pairs for Damage Case: (a) 1, (b) 2, and (c) 3, when the Test Protocol 1 was used.

Tables 6.8 and 6.9 present the calculated probabilities that there was no change in condition for Damage Cases 1 to 3 using all 28 test protocols, where the probability values in the first row of the tables correspond to Figs. 6.7 and 6.8, respectively, for Test Protocol 1. The values for other damage cases are listed in Appendix H. From the results shown in these tables, it can be seen that the presence of Damage Cases 1 to 3 can be detected with an extremely high level of confidence of almost 100% for most cases when Test Protocols 1, 2, and 3 (i.e., the combination of the fundamental mode, harmonic excitation, and the accelerometers, bottom and middle strain gauges, respectively, as described in Table 3.6) were used, except for Test Protocol 1 using a Log-Normal distribution, where the confidence level was at least 97.3% (the probability that there was no change in condition was 2.279).

When harmonic excitation and top strain gauges were used for Mode 1 (i.e., Test Protocol 4), the presence of Damage Case 1 could still be detected with a confidence level of 100%, while the presence of Damage Case 3 could only be detected with a confidence level of 86.7% when a Log-Normal distribution was assumed. Using the combination of the fundamental mode, white noise random excitation, and accelerometer data (i.e. Test Protocol 5), the presence of all three damage cases could be detected with a very high confidence level of at least 98.45%. However, using the combination of the fundamental mode, white noise random excitation, and strain gauge data (for example, Test Protocols 6, 7, and 8) produced relatively low confidence levels, less than 65%, to detect the presence of Damage Cases 2 and 3, no matter which distribution was assumed: Normal or Log-Normal.

Using the combination of higher vibration modes and white noise generally produced lower levels of confidence to detect the presence of damage (at least for localized damage, like Damage Case 1). However, the combination of vibration Modes 3 and 4 (torsional modes) with white noise excitation could actually detect the presence of Damage Cases 2 and 3 (global stiffness related damage cases) with much higher confidence levels than the combination of the fundamental mode and white noise excitation (i.e., Test Protocols 5 to 8); for example, the confidence levels were 100% using Test Protocol 18 versus 64% using Test Protocol 6 for Damage Case 2. As a

Table 6.8. The probability that there was no change in condition using the assumed Normal distributions (i.e., the probability that the ΔA value obtained when there was a change in the condition did not exceed those that obtained when there was no change in condition), for Damage Cases 1 to 3 using all 28 Test Protocols.

Test Protocol	Damage Case		
	Case 1	Case 2	Case 3
1	0.000%	0.000%	0.000%
2	0.000%	0.000%	0.000%
3	0.000%	0.000%	0.000%
4	0.000%	4.412%	0.001%
5	0.000%	1.269%	0.292%
6	0.012%	35.924%	45.264%
7	4.616%	57.933%	48.554%
8	20.766%	49.092%	61.447%
9	0.000%	0.000%	4.084%
10	0.000%	0.000%	2.612%
11	0.000%	0.000%	4.303%
12	0.000%	0.000%	18.636%
13	25.462%	64.898%	62.606%
14	49.884%	75.615%	76.095%
15	47.427%	77.188%	77.093%
16	62.880%	85.769%	82.425%
17	0.001%	0.000%	1.556%
18	2.437%	0.000%	0.005%
19	11.748%	0.000%	0.320%
20	29.171%	0.000%	23.045%
21	14.696%	0.000%	3.534%
22	13.143%	0.170%	1.826%
23	14.823%	0.206%	3.209%
24	18.462%	0.544%	8.157%
25	16.268%	3.276%	0.007%
26	45.442%	49.606%	28.135%
27	42.437%	47.934%	35.181%
28	52.922%	52.050%	61.713%

Table 6.9. The probability that there was no change in condition using the assumed Log-Normal distributions (i.e., the probability that the ΔA value obtained when there was a change in the condition did not exceed those that obtained when there was no change in condition), for Damage Cases 1 to 3 using all 28 Test Protocols.

Test Protocol	Damage Case		
	Case 1	Case 2	Case 3
1	0.002%	0.272%	2.279%
2	0.000%	0.000%	0.000%
3	0.000%	0.000%	0.000%
4	0.000%	0.844%	13.286%
5	0.000%	1.551%	0.423%
6	0.012%	34.887%	45.912%
7	4.398%	57.789%	49.105%
8	20.808%	48.806%	60.087%
9	0.285%	0.580%	9.498%
10	0.000%	0.000%	3.632%
11	0.000%	0.000%	5.022%
12	0.000%	0.000%	13.901%
13	9.981%	73.389%	65.342%
14	43.082%	75.660%	77.649%
15	40.025%	77.658%	79.352%
16	58.256%	88.621%	83.858%
17	0.053%	0.000%	2.823%
18	2.112%	0.000%	0.178%
19	10.475%	0.001%	1.421%
20	25.520%	0.029%	19.687%
21	15.433%	0.806%	9.266%
22	8.900%	0.579%	2.219%
23	9.617%	0.543%	3.095%
24	14.373%	1.465%	7.932%
25	15.564%	2.301%	0.013%
26	38.148%	51.069%	19.882%
27	35.276%	44.935%	26.534%
28	48.676%	49.615%	59.400%

result, higher vibration modes, especially torsional-related modes, should also be fully investigated in vibration-based damage detection, especially for damage cases which may change the global stiffness.

Practically, it may be necessary to assume more than one distribution to estimate the properties of a population, since the assumed Normal and Log-Normal distributions don't always produce consistent results. Also, it is difficult to say which distribution is always the most representative of the actual situation. As a result, the use of both the Normal and Log-Normal distributions may be a good choice to determine the presence of damage with a certain confidence level based on the current research.

6.2.6 Detection of the presence of damage using the area of mode shape change method based on the threshold values of test protocols

An alternative simplified and conservative damage detection procedure is defined by simply comparing the mean of ΔA from multiple measurements with the threshold values of the corresponding test protocols. Thus, if a mean value above the threshold is observed, the chance that the condition of the structure is unchanged is sufficiently small (less than 5%), so as to conclude that a change in condition (i.e., damage) has indeed occurred. This comparison is somewhat inconsistent from a statistical point of view, since the mean of a group is compared with an individual percentile value of a distribution. However, this procedure is still acceptable logically by comparing the average value with a preset standard (or threshold). Furthermore, the concepts of this procedure are straightforward and easy to use since there is no integration involved to calculate the corresponding probability. As a result, in subsequent discussions on damage detection using the area of mode shape change, only the mean values were selected to compare with the threshold values of the corresponding test protocols to evaluate the performance of the damage indicator under the selected test protocols.

For demonstration purposes, only Damage Case 1, Case 2, and Case 3 were selected to show the detailed damage detection results using the area of mode shape change for the various test protocols. Results for other damage cases and other test protocols are included in Appendix H (see Tables H.48 to H.51, where only the ratios of the area of

the mode shape changes to the corresponding threshold values are listed). The probabilities that there is no change in condition for other damage cases and other test protocols are listed separately in Tables H.44 to H.47. The mean values of the area changes in mode shape from the 25 trials were compared to the threshold values, defined as the 95th percentile of the distribution, as presented in Table 6.6. Tables 6.10 and 6.11 present the area of mode shape change values obtained for the three damage cases when harmonic and random excitation were used, respectively, for Test Protocols 1 to 8. The tables also show the ratio of the mean value to the corresponding threshold value. The probability that there was a change in the condition (i.e., damage) for each damage case and test protocol is also presented in the table, where the probability values were calculated as one minus the probability that there is no change in condition, as listed in Table 6.9. When the ratio is larger than one, the threshold value has been exceeded, and one can confidently conclude that damage is present, since the observed changes are statistically very significant. For example, ratios of 15.50, 3.35, and 1.50 gave probability values of 99.998%, 99.718%, and 97.721% for Damage Cases 1, 2, and 3, respectively, when Test Protocol 1 was used. On the other hand, the chance of detecting damage using a specific test protocol would be considered low when the

Table 6.10. Comparison of the area of the mode shape changes due to Damage Cases 1 to 3 with the corresponding threshold values, defined as the 95th percentile of assumed Log-Normal distributions, when Test Protocols 1 to 4 (harmonic excitation) were used.

Test	95%	Area of mode shape change					
Protocol	Threshold	Case 1	Ratio	Case 2	Ratio	Case 3	Ratio
1	0.57%	8.82%	15.50	2.03%	3.56	0.85%	1.50
		Prob.	99.998%	Prob.	99.728%	Prob.	97.721%
2	0.29%	7.99%	27.08	1.05%	3.56	0.68%	2.30
		Prob.	100.000%	Prob.	100.000%	Prob.	100.000%
3	0.38%	7.45%	19.68	1.24%	3.27	0.72%	1.89
		Prob.	100.000%	Prob.	100.000%	Prob.	100.000%
4	1.04%	7.92%	7.65	2.22%	2.15	0.79%	0.76
		Prob.	100.000%	Prob.	99.156%	Prob.	86.714%

Prob. = probability that there is a change in condition, equal to one minus the probability that there is no change in condition as listed in Table 6.9.

Table 6.11. Comparison of the area of the mode shape changes due to Damage Cases 1 to 3 with the corresponding threshold values, defined as the 95th percentile of assumed Log-Normal distributions, when Test Protocols 5 to 8 (white noise excitation) were used.

Test Protocol	95% Threshold	Area of mode shape change					
		Case 1	Ratio	Case 2	Ratio	Case 3	Ratio
5	0.96%	6.60%	6.87	1.49%	1.55	1.67%	1.74
		Prob.	100.000%	Prob.	98.449%	Prob.	99.577%
6	3.72%	6.82%	1.83	2.82%	0.76	2.65%	0.71
		Prob.	99.988%	Prob.	65.113%	Prob.	54.088%
7	5.27%	6.22%	1.18	3.55%	0.67	3.82%	0.72
		Prob.	95.602%	Prob.	42.211%	Prob.	50.895%
8	9.66%	8.64%	0.89	6.91%	0.72	6.34%	0.66
		Prob.	79.192%	Prob.	51.194%	Prob.	39.913%

Prob. = probability that there is a change in condition, equal to one minus the probability that there is no change in condition as listed in Table 6.9.

corresponding ratio is less than one. For example, ratios of 0.89, 0.72, and 0.66 gave probability values of 79.192%, 51.194%, and 39.913% for Damage Cases 1, 2, and 3, respectively, when Test Protocol 8 was used.

Overall, accelerometers (Protocols 1 and 5) consistently performed better than strain gauges (Protocols 2 to 4 and 6 to 8), particularly when random excitation was used. The presence of all three damage cases could be confidently detected using either random or harmonic excitation when accelerometer data were used. On the other hand, the ability to detect damage using a combination of strain gauge data and white noise excitation was relatively low, except when bottom strains (Protocol 6) were used to detect Damage Case 1. In terms of the preferred excitation method, the data show that, for all instrumentation schemes, harmonic excitation produced consistently higher ratios of actual to threshold values than random excitation (at least 2.3 times higher, except for Case 3 using acceleration and top strain gauge data).

To understand the influence of confidence level and different damage types on damage detection, Figure 6.9 presents the area changes in the first mode shape for all 16 single damage cases, together with the corresponding threshold values for both the 90% and

95% confidence levels, when a combination of harmonic excitation and accelerometer data was used. The threshold values correspond to those listed in Tables 6.4 and 6.5. As expected, the line for the 90% threshold is lower than the one for the 95% threshold. From Fig. 6.9, it can be noticed that the detection of Damage Case 1 is relatively easier than other damage cases, since the area of mode shape change is much higher than the corresponding threshold value, with ratios of actual to threshold values of 15.50 and 23.21, for the 95% and 90% confidence levels, respectively. On the other hand, the detection of Damage Case 10, Case 11, Case 13, and Case 15 is marginal. The resulting area changes in the first mode shape due to Damage Case 10 and Case 13 are located above the 95% threshold; however, they could be located below a line with a higher confidence level. For Damage Case 11 and Case 15, the resulting area changes are located between the 90% and 95% threshold lines, which means that the conclusion that damage is present would be accepted when the 90% threshold was used, but rejected

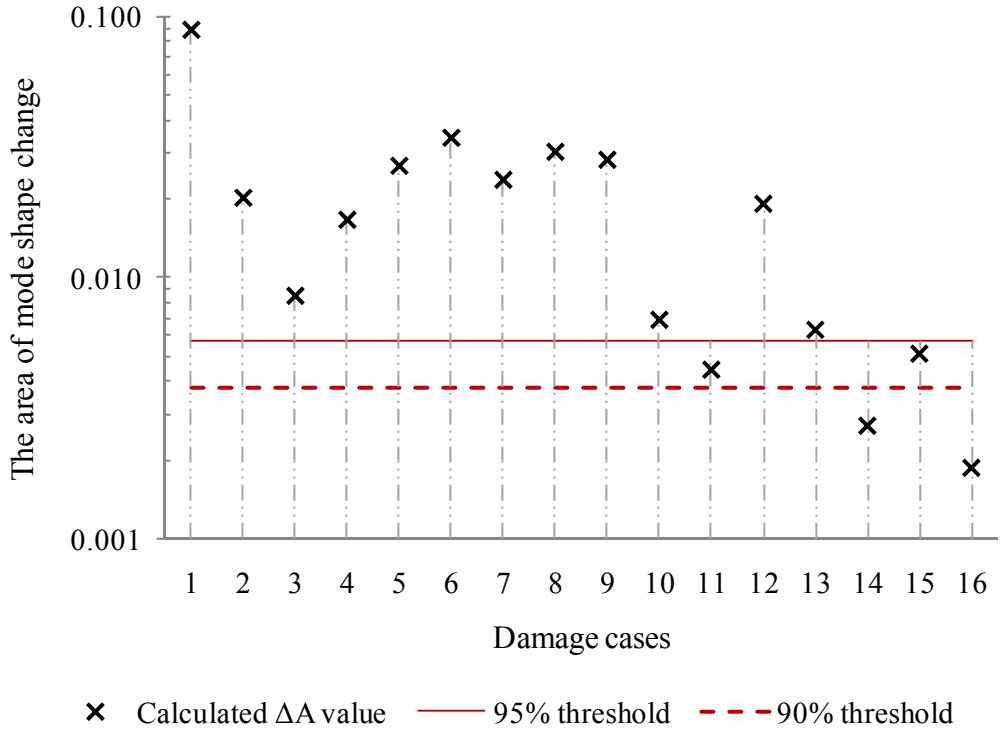

Figure 6.9. Comparison of mean ΔA values from 25 data pairs for all single damage cases to the 90% and 95% threshold values, when the first mode, harmonic excitation, and accelerometer data were used (Test Protocol 1).

when the 95% threshold was used. For Damage Case 14 and Case 16, there would be little chance of detecting damage since the resulting area changes are located considerably below both threshold lines. Results for other sensor schemes and excitation types are available in Appendix H.

6.2.7 Influence of sensor scheme on the performance of the damage indicator

To ascertain the influence of the sensor scheme on the performance of the area of mode shape change damage indicator, the ratios of ΔA values (using the average values of 25 trials) to the 95% threshold values were calculated for all damage cases and all sensor schemes. The resulting ratios were then plotted, with all sensor schemes and damage cases shown on a single plot. Since ratios are used, the threshold values (or relative threshold value) are equal to one for all test protocols.

Figure 6.10 presents the results for the first mode when harmonic excitation was used (Test Protocols 1 to 4). As previously described, the likelihood that the condition of the bridge has not changed is considered too high to conclude the presence of the damage when the values of area change fall below the threshold line. On the other hand, if a change in area above the threshold line is observed, the chance that the condition of the structure is unchanged is sufficiently small (less than 5%) so as to conclude that a change in health condition (i.e., damage) has indeed occurred, since the area change is statistically significant. From Fig. 6.10, it can be clearly noticed that all sensor schemes, except for the one that used the top strain gauges, showed similar performance for damage detection when the fundamental mode shape and harmonic excitation were used. This means that the low cost strain gauges are capable of generating mode shapes of sufficient quality for damage detection, as long as they are properly positioned and the excitation forces are strong enough to produce strain readings with high signal to noise ratios. Generally, the presence of damage for damage cases involving the steel girder (Case 1), the diaphragms (Cases 2 through 7), and the steel straps (Cases 8 through 11) could be detected using all sensor schemes, except for several cases when the top strain gauges were used in conjunction with Damage Case 11. The chance of detecting the presence of the damage to the concrete deck (Cases 12-16) was relatively

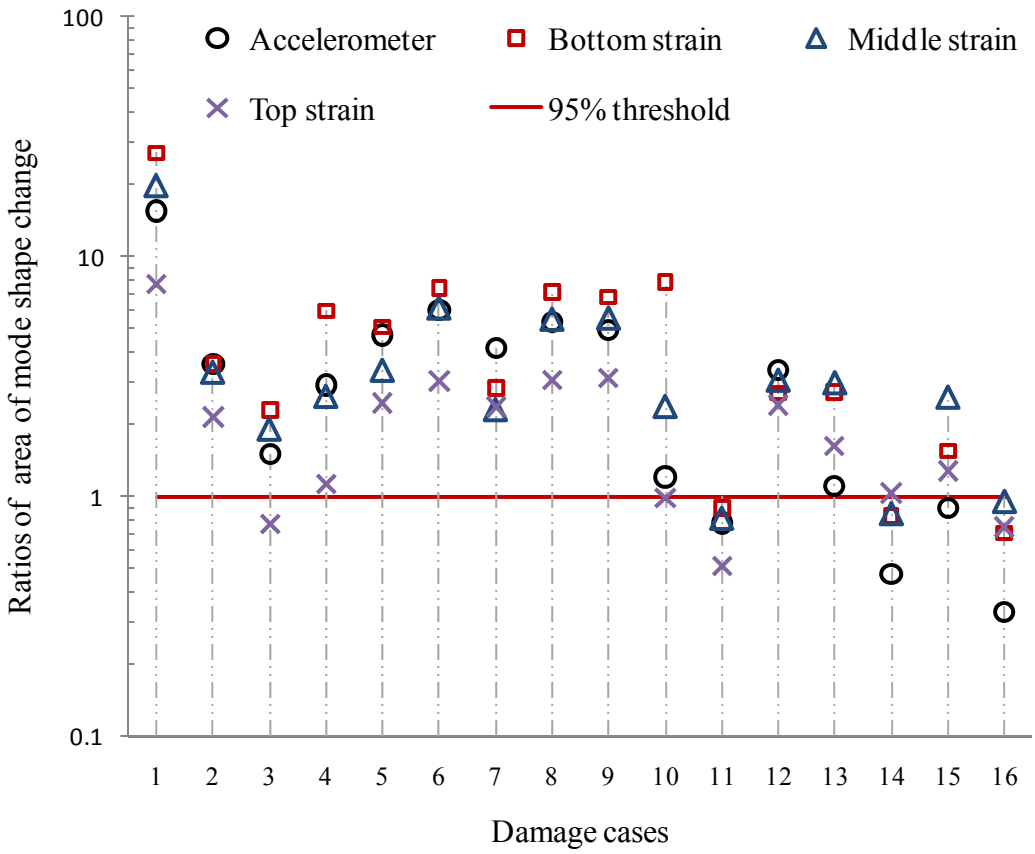

Figure 6.10. Ratios of area of mode shape change (the average of 25 values) to the 95% threshold values for all sensor schemes and damage cases, when the first mode and harmonic excitation were used (Test Protocols 1 to 4).

small no matter which sensor scheme was selected, which is similar to the results found for simulated damage to the concrete deck, as described in Chapter 5.

When white noise excitation was used in combination with the first mode, as presented in Fig. 6.11, the use of accelerometers was clearly superior to all other sensor schemes. The use of accelerometer data allowed the detection of all damage cases to the steel girder, diaphragms, and steel straps except for Damage Case 7 (D-X2.8Y1.35) and Case 10 (ST-X4.4Y1.35). None of the strain gauge schemes were capable of detecting the presence of any of the damage cases, except for Damage Case 1, since the area changes were not statistically significant. For damage category 4 (i.e., damage to the concrete

deck, Cases 12 through 16), none of the sensor schemes could detect the presence of the damage when the fundamental vibration mode and white noise excitation were used.

Figure 6.12 presents the results of damage detection using the area change in the second mode shape when harmonic excitation was used (Test Protocols 9 to 12). The results for strain gauges are similar to those presented in Fig. 6.11 using the fundamental mode shape. The strain gauges were capable of detecting the presence of damage for most damage cases. Interestingly, however, the performance of the accelerometers was not always better than that of the strain gauges, especially when compared to bottom strain gauge data. This may be partially due to the multiple setups of accelerometers required, compared to only one single setup of strain gauges for each test.

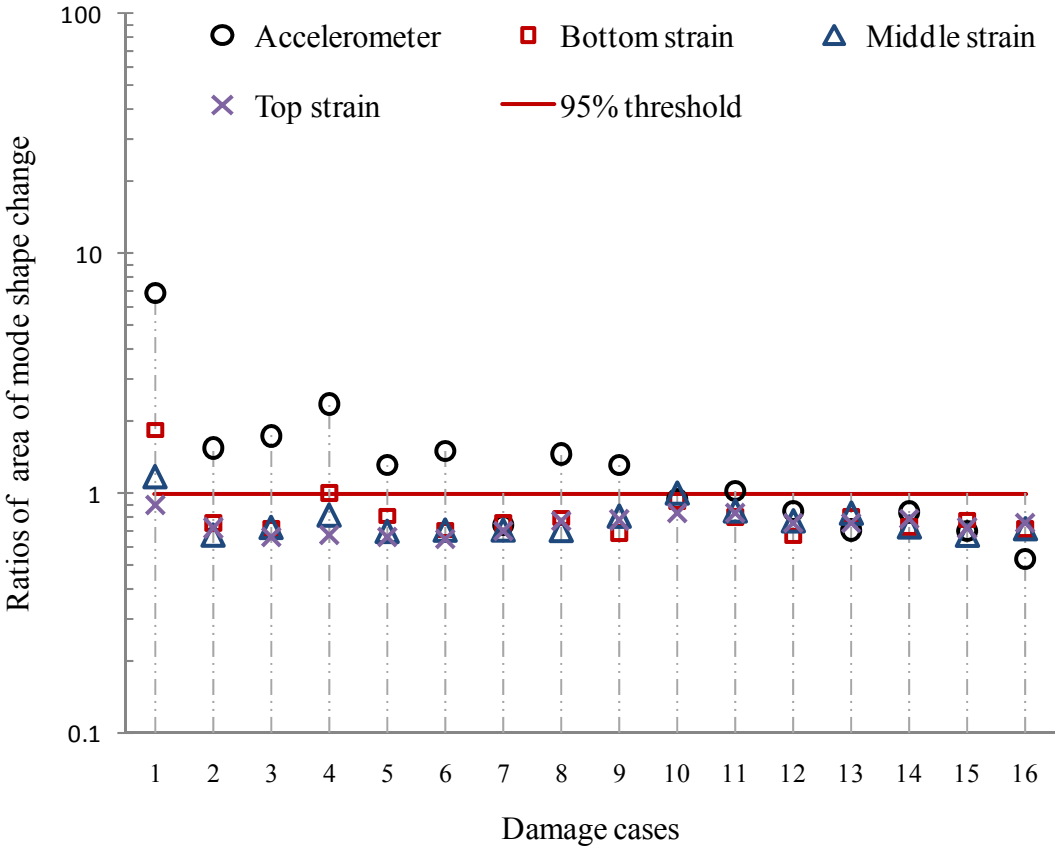

Figure 6.11. Ratios of area of mode shape change (the average of 25 values) to the 95% threshold values for all sensor schemes and damage cases, when the first mode and white noise random excitation were used (Test Protocols 5 to 8).

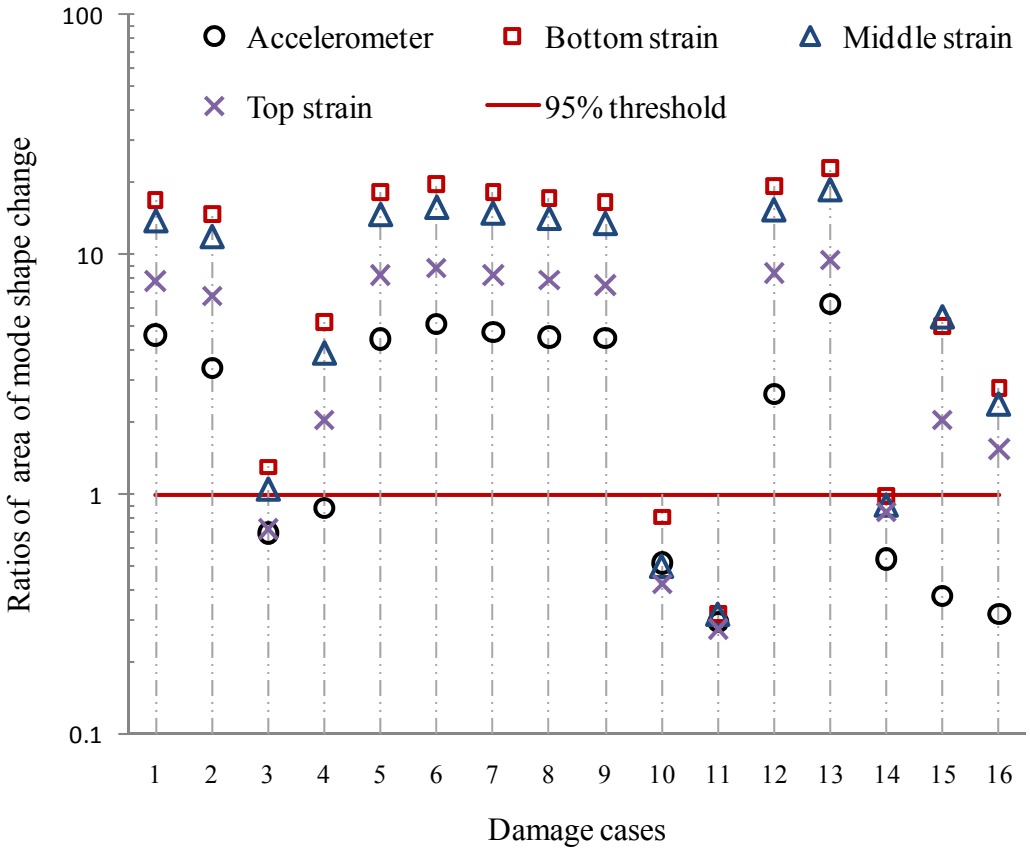

Figure 6.12. Ratios of area of mode shape change (the average of 25 values) to the 95% threshold values for all sensor schemes and damage cases, when the second mode and harmonic excitation were used (Test Protocols 9 to 12).

Figure 6.13 shows the resulting area changes in the second mode shape when white noise excitation was used (Test Protocols 13 to 16). From the figure, it can be seen that the test protocols included here were not sensitive to any of the damage cases investigated, no matter which sensor scheme was used, since the area changes using the test protocols were not statistically significant. The results in Figs. 6.12 and 6.13 using the second mode shape were similar to or generally worse than those in Figs. 6.10 and 6.11 using the fundamental mode shape; in some cases, though, the resulting ratios were higher for the second mode than for the first mode (Fig. 6.10), when bottom and middle strain gauges were used with harmonic excitation (Fig. 6.12). Based on this, it may be beneficial to acquire data for the second mode in some cases.

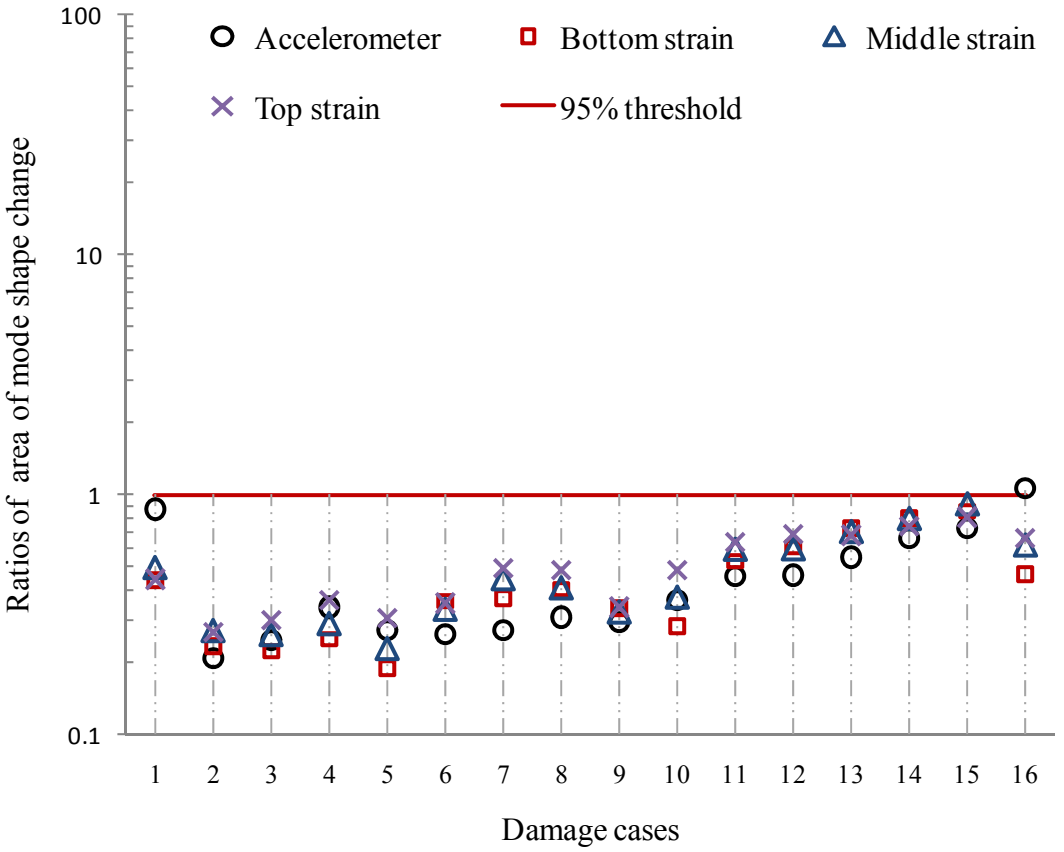

Figure 6.13. Ratios of area of mode shape change (the average of 25 values) to the 95% threshold values for all sensor schemes and damage cases, when the second mode and white noise random excitation were used (Test Protocols 13 to 16).

Figures 6.14, 6.15, and 6.16 present the damage detection results for all 16 single damage cases using the area of mode shape change method when white noise excitation was used to acquire the 3rd, 4th, and 5th vibration modes, respectively (Test Protocols 17 through 28). The results in Figs. 6.15 and 6.16 using the 4th and 5th mode shapes do not provide much additional insight, except that some damage cases could be detected using the accelerometer data, although the ratios were typically not very high. However, interestingly, the damage detection results using the 3rd mode shape with white noise excitation (Fig. 6.14) were, in many cases, better than those using the fundamental mode shape with white noise random excitation (Fig. 6.11). This was especially true for the

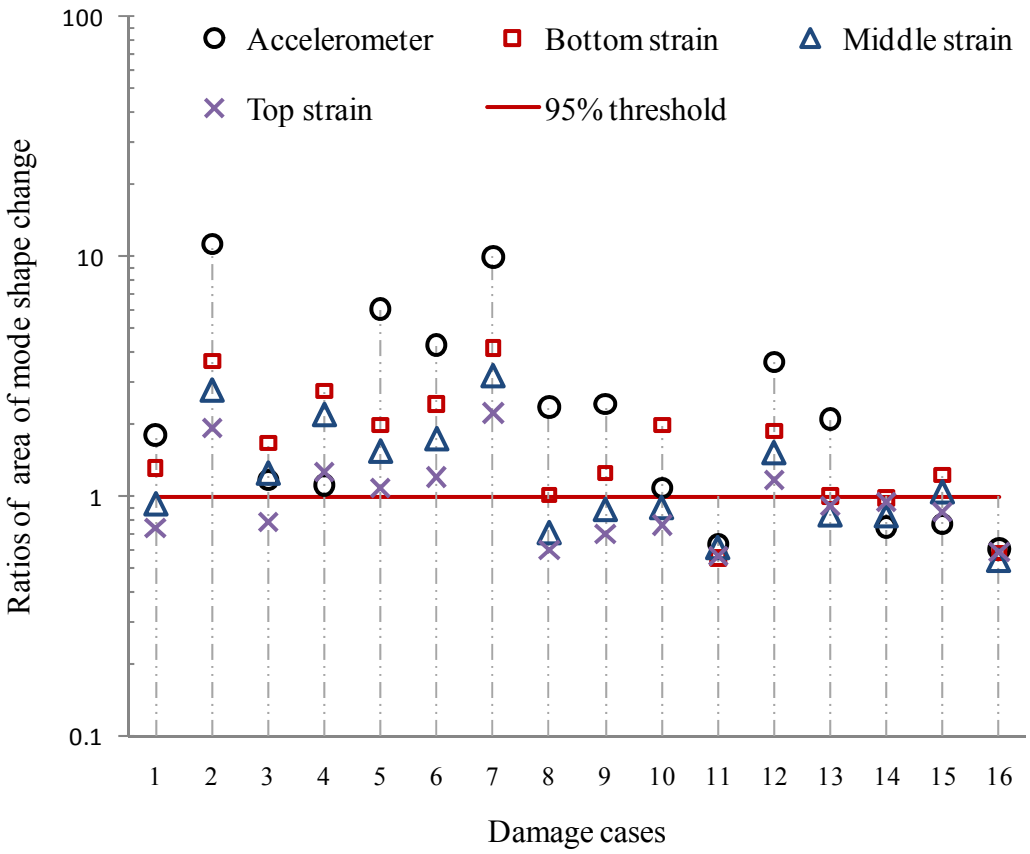

Figure 6.14. Ratios of area of mode shape change (the average of 25 values) to the 95% threshold values for all sensor schemes and damage cases, when the third mode and white noise random excitation were used (Test Protocols 17 to 20).

damage cases which could produce the greatest changes in global load sharing (i.e., the damage to diaphragms and steel straps, which included Cases 2 through 11), even though the threshold values for all sensor schemes using the 3rd mode were much higher than those using the fundamental mode. In fact, the threshold values for the 3rd mode were at least 2.79 times higher, which means that the test protocols using the 3rd mode should be much less sensitive to damage than those using the fundamental mode. The reason for this may be explained by the fact that the combined flexural and torsional 3rd mode shape transformed to a new mode (or a mode which was very different from the one before the damage was introduced) due to the introduction of damage that changed the global stiffness distribution of the structure (for example, see Fig. E.4 in Appendix E, for a comparison of the third mode shape before and after Damage Case 2 or Health

State 3). Usually, accurate measurement of higher mode shapes is more difficult in practice. However, one should not abandon the investigation of higher vibration modes (at a reasonable level) for the purpose of damage detection, especially in cases where a potential mode transformation could be caused by damage.

6.2.8 Conclusions

Several conclusions may be drawn from the results presented in this section. First, the area of mode shape change indicator has been shown to be capable of successfully identifying the presence of several forms of damage at a relatively high confidence level.

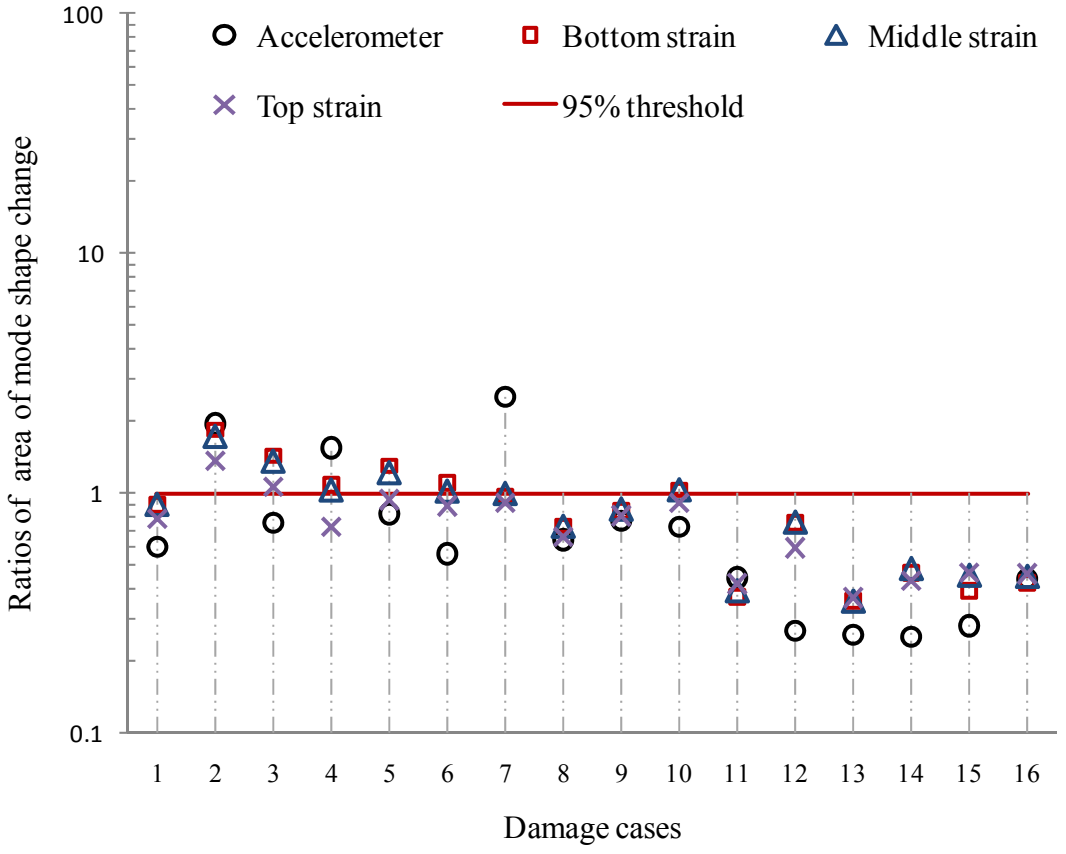

Figure 6.15. Ratios of area of mode shape change (the average of 25 values) to the 95% threshold values for all sensor schemes and damage cases, when the fourth mode and white noise random excitation were used (Test Protocols 21 to 24).

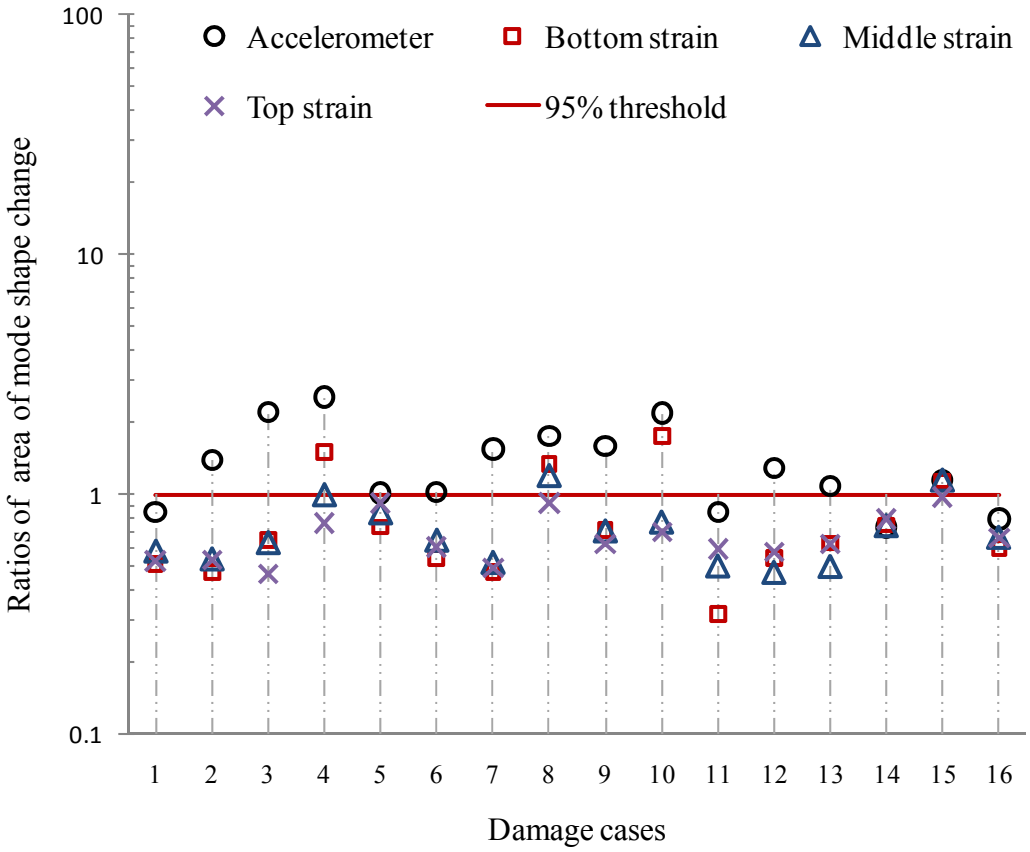

Figure 6.16. Ratios of area of mode shape change (the average of 25 values) to the 95% threshold values for all sensor schemes and damage cases, when the fifth mode and white noise random excitation were used (Test Protocols 25 to 28).

Secondly, of the 28 test protocols investigated, those that used forced harmonic excitation in combination with the fundamental vibration mode consistently resulted in the lowest threshold values for the area changes in mode shape. This held true regardless of whether acceleration or strain measurements were used to represent mode shapes. These protocols are therefore the most sensitive to changes in the structural condition. Random (white noise) excitation produced much higher threshold values (meaning that they should be less sensitive to damage), with only acceleration measurements for the fundamental mode resulting in a comparable threshold value of area changes.

Thirdly, the presence of all single damage cases (i.e. Damage Cases 1 to 16), except for the cases involving damage to the concrete deck (i.e. Damage Cases 12 to 16), could be identified with a relatively high confidence level (at least 90% based on the percentile threshold value, or at least 91.9% based on the probability calculated using assumed Log-Normal distribution) when harmonic excitation was used, except when strain gauges near the top flanges of the girders were used, since the area changes in the fundamental mode shape due to damage exceeded the corresponding threshold values. This was true regardless of the type of instrumentation scheme used to measure mode shape. Among the instrumentation schemes investigated, both acceleration measurements and strain measurements near the bottom flanges of the girders were able to identify the presence of damage with a high level of confidence. When random excitation was used, the use of acceleration measurements greatly increased the ability to identify the presence of damage, since the protocols using strain measurements produced values of area change in mode shape that fell close to, or below, the corresponding threshold values for damage detection.

Fourthly, in general, the higher modes were less sensitive to damage than the fundamental mode. However, one should not abandon the use of higher vibration modes, especially modes featuring torsional behaviour, for the purpose of damage detection, especially for damage cases which may produce a potential mode transformation or produce a change in global stiffness characteristics.

6.3 Damage Localization Using Commonly Available VBDD Indicators

6.3.1 Overview

After the presence of the damage was identified with a certain level of confidence using the method described in the previous section, damage localization was investigated next, and is presented in this section. The performance of several widely used VBDD indicators was investigated using the experimental data from the multi-girder bridge superstructure model. The VBDD indicators used in this investigation included the change in mode shape method, damage index method, change in uniform flexibility

curvature method, change in flexibility method, and change in mode shape curvature method. These methods are described in Section 2.5.

To ensure that mode shapes were scaled to a common basis, the mode shapes used in this investigation were first normalized by the unit-area normalization method as described in Section 4.4.3. Prior to normalization, modal amplitudes between the measurement points were interpolated using the natural cubic spline interpolation method (see Section 4.4.3) to produce mode shapes that were defined at 49 points along each girder line. For each individual health (or damage) condition, five repeated trials were conducted for each vibration mode. Then, the average mode shapes calculated from the five trials for both undamaged and damaged conditions were used to apply the damage detection equations described in Section 2.5.

Of the 28 test protocols included in this research, only the most sensitive one -- the fundamental mode shape extracted using the accelerometer data with the harmonic excitation -- was selected and investigated in this section. To demonstrate the method, only Damage Case 1, for which the bottom plate was removed from the splice at mid-span of Girder 4 (see Table 3.5), was investigated in detail. Results related to damage localization for other damage cases using other test protocols are available in Appendix I, Appendix J, and Appendix K.

Figure 6.17 to Figure 6.21 show the distributions of the selected VBDD indicators for this damage case. The circle in the figures indicates the actual location of damage. In these distributions, the highest peak(s) in the graph corresponds to the likely longitudinal location(s) of damage. It can be seen from the figures that, in general, all methods produced a peak at the damage location, although in most cases it was the second highest peak. Therefore, as long as one was able to establish the presence of damage with a certain level of confidence, these results would limit the possible locations of damage to a relatively small number. A detailed discussion of the results for each VBDD indictor is available in the following sections.

6.3.2 Change in mode shape method

Changes in the fundamental mode shape due to Damage Case 1 are illustrated in Fig. 6.17, both in 2D form showing plots along individual girder lines and in 3D form showing the entire deck surface. In parts (a) and (b) of this figure, the mode shapes have been normalized using all measurement and interpolated points; thus, a total of 196 points were used for the normalization, 49 points for each girder. These figures therefore show the global shape of the change in mode. In part (c), on the other hand, the mode shapes have been normalized separately along each individual girder line (see Section 4.4.4), resulting in a different mode shape scaling factor for each girder line; this approach shows the localized shape of the changes along each girder.

Considering the normalization scheme over all measurement points (Figs. 6.17(a) and (b)), mode shape changes were found to be broadly distributed, producing smooth mode shape change plots along all girder lines. Also, the mode shape change patterns for this damage case are nearly symmetric about the longitudinal centreline of the deck. Since the largest positive peak in the change in mode shape plots coincides with the actual location of damage at mid-span of Girder 4, damage localization may be deemed to be successful in this case, in both the longitudinal and transverse directions. However, further investigations need to be conducted to draw concrete conclusions about the damage localization ability in the transverse direction. Furthermore, the presence of damage could be detected using measurements at any location on the deck due to the wide dispersion of the mode shape change.

When the mode shapes were normalized separately along individual girder lines (Fig. 6.17(c)), the change in mode shape patterns was altered significantly. In this case, the positive peak at the damage location along Girder Line 4 is more clearly defined, making damage localization more precise. However, a larger positive peak also exists along Girder Line 1, introducing the possibility of a spurious diagnosis of damage at that location. This spurious diagnosis is common for multiple girder systems, even in numerical studies (Siddique 2008). In addition, the amplitudes of mode shape changes along Girder lines 2 and 3 were relatively small, suggesting that damage detection using

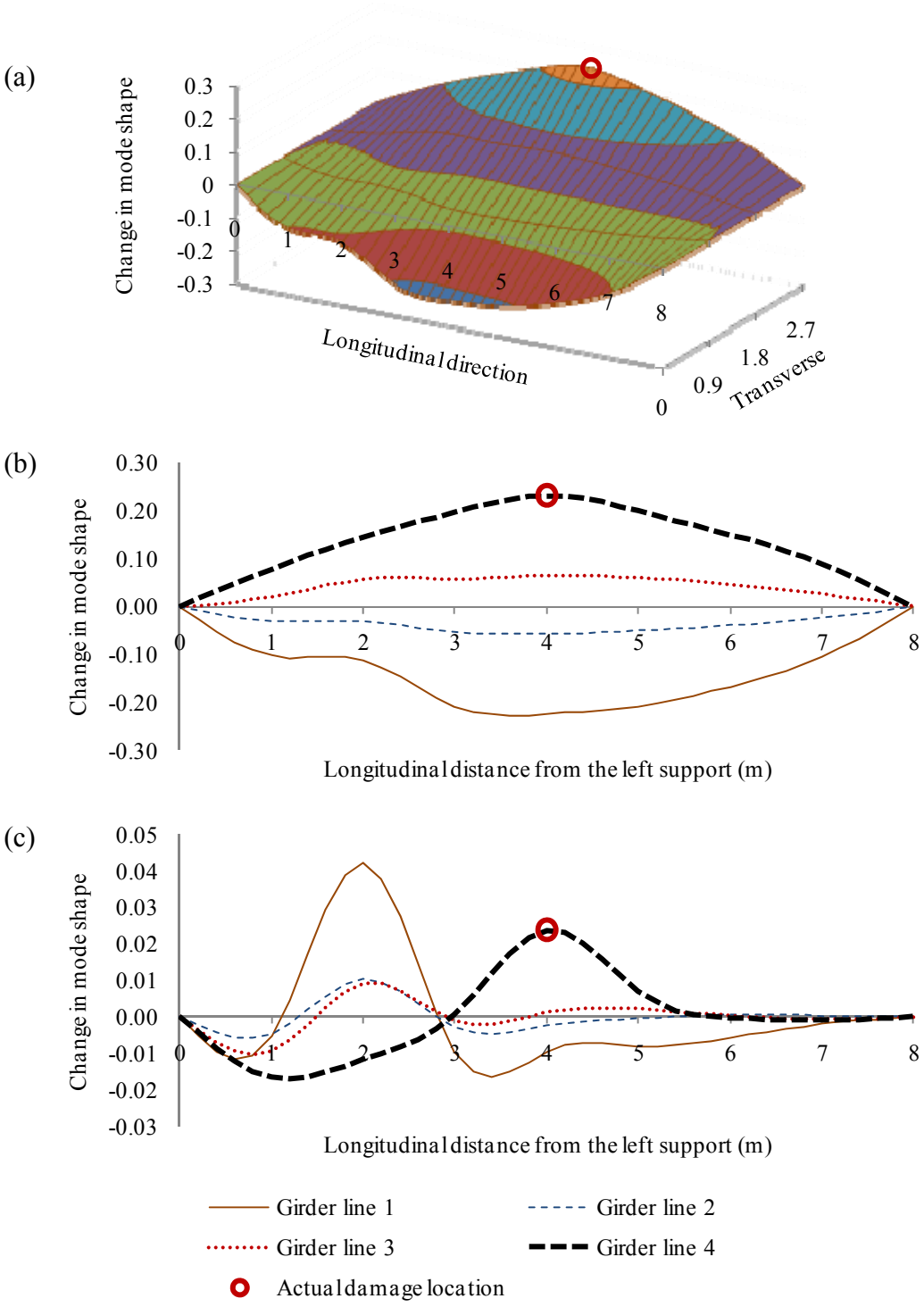

Figure 6.17. Distribution of the change in the first mode shape due to Damage Case 1 using accelerometer data with harmonic excitation: (a) 3D figure with unit area normalization over all measurement points; (b) 2D figure with unit area normalization over all measurement points; and (c) 2D figure with unit area normalization along individual girder lines.

this normalization scheme may require sensors placed in close proximity to the damage, unlike the normalization scheme over all measurement points discussed above. Similar comparison using strain gauges may be found in Appendix I.

In summary, changes in the fundamental mode shape are capable of identifying the location of Damage Case 1 in the longitudinal and transverse directions. However, the mode shape normalization scheme was found to have a significant influence on resulting mode shape change patterns. Provided that a sufficient number and distribution of sensors are used, the simultaneous use of both normalization schemes may be an effective approach to localize damage using the change in mode shape method.

6.3.3 Damage index method

Similar to the case for change in mode shape, Figure 6.18 also shows 2D and 3D forms of the damage indicator calculated using mode shapes normalized using the two different normalization schemes. However, the two different normalization schemes produced exactly the same distributions of the damage index, which means that the mode shape normalization scheme has no influence on the resulting distribution of the damage index, unlike the case discussed above for the change in mode shape method. This may be explained based on the following facts. One fact is that the normalization schemes, as described in this thesis, are performed on mode shapes rather than curvatures. As a result, the different normalization schemes should have less influence on relative curvature change than relative mode shape change (see a sample calculation using the data for Health States 1 and 2, when Test Protocol 1 was used, in Section M.6 of Appendix M). Actually, a calculation of curvatures of Figs. 6.17 (b) and (c) should produce a very similar curvature profile (see Section 6.3.6), even though the changes in mode shapes shown in Figs. 6.17 (b) and (c) are very different. It should be acknowledged that calculating the curvature of mode shape changes is not the same as calculating the changes in mode shape curvatures. However, the two calculations should produce similar results in this case. A sample calculation is available in Section M.6, where the two procedures produced exactly the same results except that the signs are different (see pg. 496 vs. pg. 499 for unit-area normalization over all measurement

points and pg. 497 vs. pg. 500 for unit-area normalization along individual girder lines). The sign difference is due to the fact that the changes in mode shape curvatures were calculated using absolute values, as described in Section 2.5.6. Since the damage index is a function of mode shape curvature, the normalization schemes should have less influence on the values of damage index. Furthermore, the damage index used in this calculation was normalized (or scaled) to a standard normal distribution (see Eq. 2.8), which produced exactly the same amplitudes and shape of the damage index for the two different normalization schemes. As a result, the two different mode shape normalization schemes produced exactly the same damage index profile. Similar results were found in numerical studies on a multiple girder system (see Fig. 7.6 in Siddique 2008).

Since the largest positive peak in the damage index plots coincides with the actual location of damage at mid-span of Girder 4, one can conclude that the damage location could be successfully located. In addition, the narrow range of the positive peak at the damage location gives a clear indication of the location of damage, which makes damage localization relatively precise. However, the relatively large peak in the damage index at the quarter span of the other three girders may lead to some ambiguity regarding where the damage might actually be located.

6.3.4 Change in uniform flexibility curvature method

Figure 6.19 presents the distribution of change in uniform flexibility curvature for the first mode shape due to Damage Case 1 using accelerometer data with harmonic excitation. Once again, parts (a) and (b) of this figure show the results when the mode shapes were normalized using all measurement points, while part (c) represents the results when mode shapes were normalized separately along individual girder lines. Comparing parts (b) and (c), it can seen that the two normalization schemes produced similar results, except that normalization along individual girder lines (part c) generated relatively flatter curves near the supports. As described above, since the normalization is performed on mode shapes rather than curvatures, the relative curvature relationship

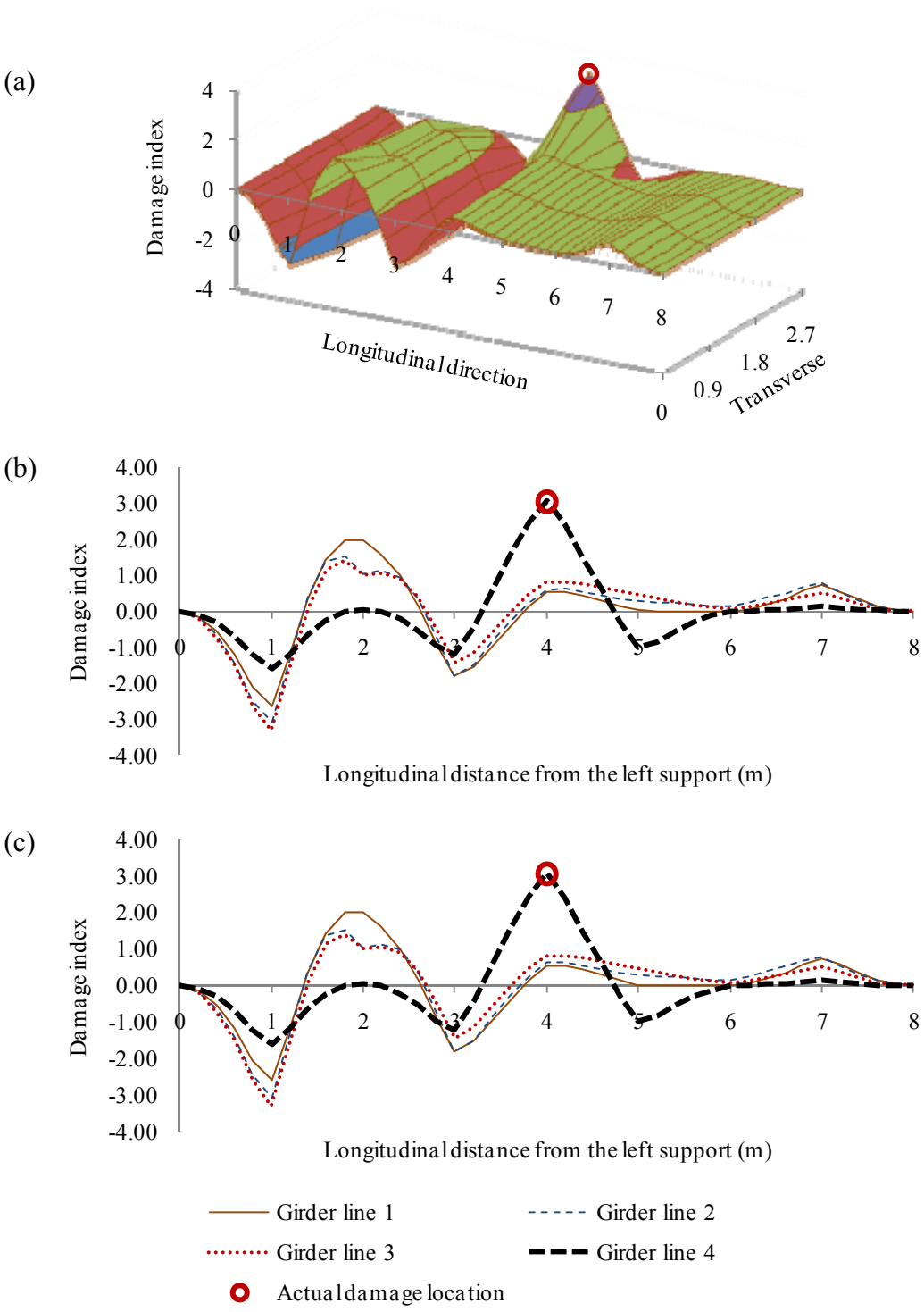

Figure 6.18. Distribution of the damage index for the first mode due to Damage Case 1 using accelerometer data with harmonic excitation: (a) 3D figure with unit area normalization over all measurement points; (b) 2D figure with unit area normalization over all measurement points; and (c) 2D figure with unit area normalization along individual girder lines.

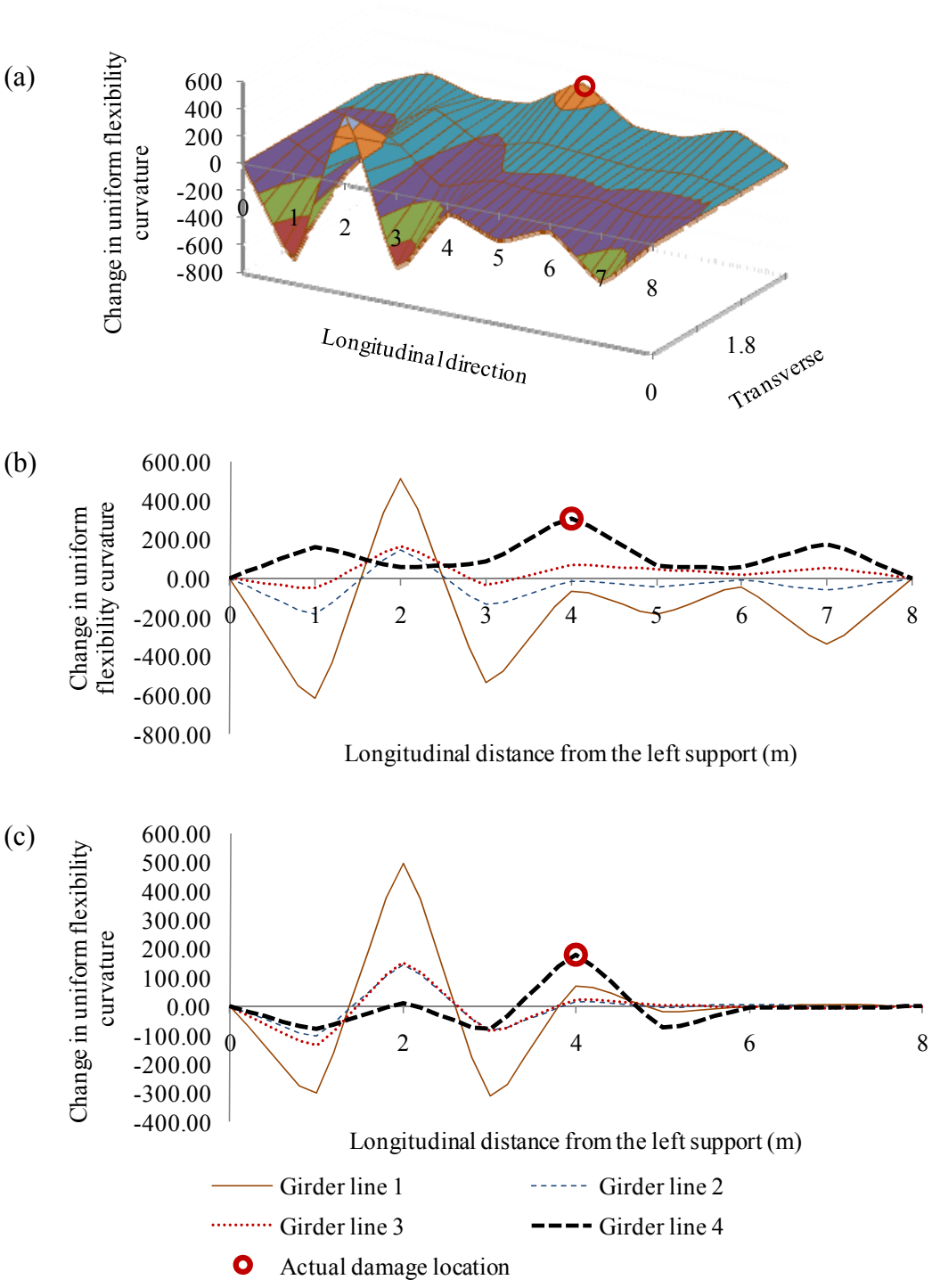

Figure 6.19. Distribution of the change in uniform flexibility curvature for the first mode due to Damage Case 1 using accelerometer data with harmonic excitation: (a) 3D figure with unit area normalization over all measurement points; (b) 2D figure with unit area normalization over all measurement points; and (c) 2D figure with unit area normalization along individual girder lines.

between compared pairs is not changed significantly. As a result, the normalization schemes should have less influence on relative curvature change.

For both normalization schemes, the second largest peak coincided with the actual damage location, implying that this method is capable of locating the damage, or at least limiting the possible location of damage to two locations. The largest peak corresponds to a false indicator, as stated above.

6.3.5 Change in flexibility method

Figure 6.20 presents the results using the change in flexibility method, which is similar to those of the change in mode shape method (Fig. 6.17).

When normalization over all measurement points was used (Figs. 6.20(a) and (b)), the change in flexibility was found to be broadly distributed, producing smooth plots along all girder lines. Similar to the previous description for change in mode shape, the change in flexibility patterns for this damage case are nearly symmetric about the longitudinal centreline of the deck. Unlike the case for the change in mode shape method, the largest positive peak in the change in flexibility plots occurred close to the mid-span of Girder 1, which would be a false positive indicator. However, the second highest peak coincided with the actual location of the damage; this can be deemed to be a successful damage localization in the sense that the possible location of damage was limited to two locations.

For the case using normalization along individual girder lines, as shown in Fig. 6.20(c), the results were very similar to those of the change in mode shape method. The second highest positive peak coincided with the actual damage location, while the highest positive peak may correspond to a false indicator. As a result, one can claim that the damage indicator is capable of identifying the location of damage although not without some possible ambiguity.

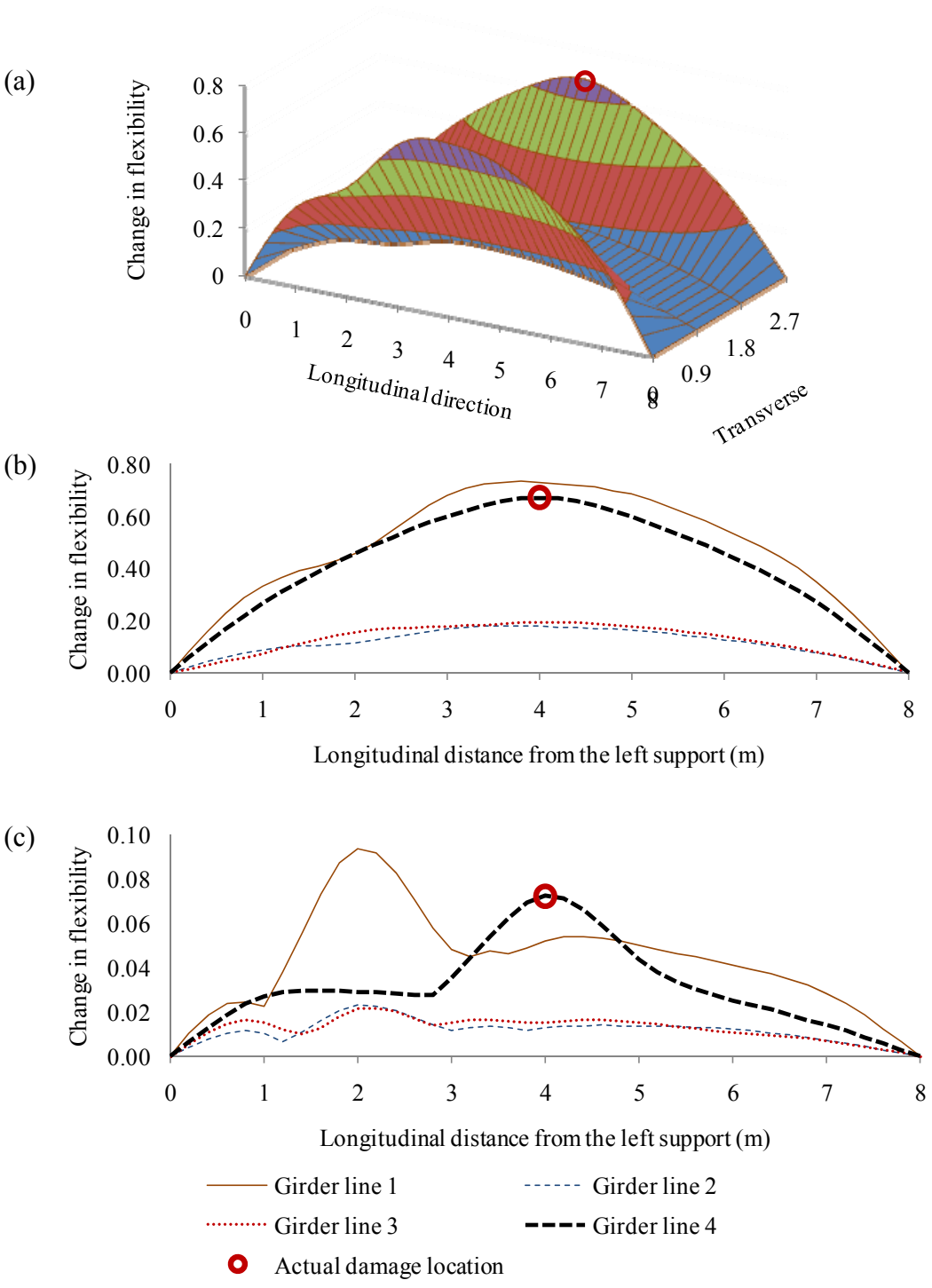

Figure 6.20. Distribution of the change in flexibility for the first mode due to Damage Case 1 using accelerometer data with harmonic excitation: (a) 3D figure with unit area normalization over all measurement points; (b) 2D figure with unit area normalization over all measurement points; and (c) 2D figure with unit area normalization along individual girder lines.

6.3.6 Change in mode shape curvature method

The damage localization results for Damage Case 1 using the change in mode shape curvature method are presented in Fig. 6.21. The results shown in this figure are very similar to those in Fig. 6.19, except for the differences in the amplitude of changes. As a result, the description and conclusions for change in uniform flexibility curvature method (Section 6.3.4) also apply to the change in mode shape curvature.

The change in mode shape curvature method investigated is capable of identifying the location of damage after the presence of damage has been established, as described in Section 6.2. In addition, the normalization schemes appear to have little influence on the damage localization results when this VBDD method is used, as described in Section 6.3.3.

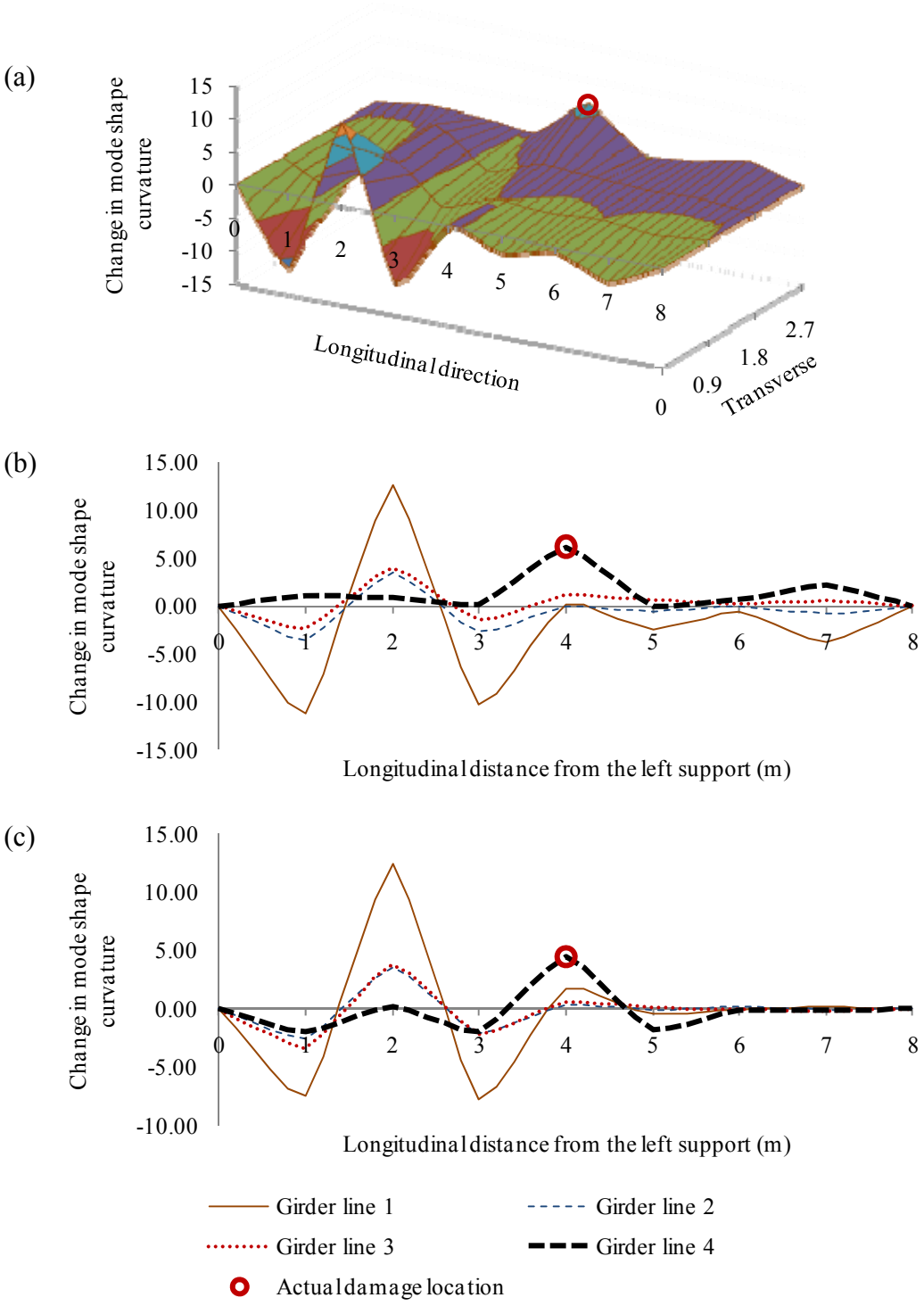

Figure 6.21. Distribution of the change in mode shape curvature for the first mode due to Damage Case 1 using accelerometer data with harmonic excitation: (a) 3D figure with unit area normalization over all measurement points; (b) 2D figure with unit area normalization over all measurement points; and (c) 2D figure with unit area normalization along individual girder lines.

CHAPTER 7. **SUMMARY AND CONCLUSIONS**

7.1 Summary

This thesis investigated a number of issues related to the potential use of vibration-based damage detection (VBDD) methods for the structural health monitoring (SHM) of bridge superstructures using both experimental and numerical studies. The primary objective of this research was to investigate the application of VBDD methods to multi-girder bridge superstructures.

The research focused primarily on an experimental investigation of VBDD on a multi-girder bridge superstructure, while theoretical analyses and numerical verifications were also included. The structure used for this investigation was a one-third scale model of a slab-on-girder composite bridge superstructure featuring four steel girders supporting a steel-free concrete deck.

The experimental tests were conducted under well-controlled environments. Forced dynamic excitation was supplied by means of a feedback-controlled hydraulic shaker. Instrumentation used to measure the dynamic response included a closely-spaced grid of accelerometers mounted on the surface of the deck along the girder lines, as well as electrical-resistance foil strain gauges bonded to the girder webs.

Measurement of the modal properties of the multi-girder bridge superstructure was carried out in two phases. In Phase I, the influence of various test parameters on the repeatability and reliability of modal property extraction was investigated using the intact bridge model. More specifically, the test parameters that were considered in the intact bridge model tests included sampling rates, the length of the recording period, excitation methods, sensor type, and sensor locations (i.e., the vertical locations of strain

gauges on the steel web). For the tests conducted in this phase, only seven accelerometer and 15 strain gauges locations (5 sets of 3 gauges each) along one girder line were monitored to measure vertical vibration.

In Phase II of the measurements, extensive dynamic tests were conducted on 17 health states (i.e., states with varying levels and types of damage) of the bridge superstructure when various specific test protocols were followed. The purposes of the tests were to define the damage detection resolution of 28 different test protocols and to investigate the application of VBDD techniques on the multi-girder bridge superstructure under various health conditions. For the tests conducted in this phase, 28 accelerometer locations and 57 strain gauges (19 sets of 3 gauges each) over the four girder lines were used to record the vibration signals. Analyses of measurement results collected in this phase were carried out in two stages. Initially, the data were used to establish the resolution of each test protocol, defined as the threshold value of the damage indicator above which a change could be considered statistically significant, given the level of uncertainty. These threshold values corresponded to the 95^{th} percentile upper exclusion confidence limits for each test protocol. Subsequently, the performance of selected VBDD indicators was investigated on the bridge superstructure under the 17 health states.

An investigation of the influence of normalization methods and schemes on the definition of mode shape and changes in mode shapes was conducted in this research. A new normalization method, unit-area normalization, was developed. A comparison between two normalization methods and two different normalization schemes (i.e., whether one or more scaling factors were applied to different portions of the bridge) was performed.

A Level 1 VBDD indicator (i.e., one capable of identifying the presence, but not necessarily the location, of damage), the area of mode shape change, was proposed in this research. The VBDD indicator was developed based on the widely used change in mode shape method using the unit-area normalization method. To demonstrate the features and verify the capability of the damage indicator in the absence of experimental

uncertainties, a finite element (FE) model was developed to generate theoretical data for the modal properties. The simulated data were used to test the damage detection performance of the proposed damage indicator.

The resolutions of various test protocols were defined and calculated based on the probability distributions of the area changes in mode shape, estimated using experimental data gathered during a large number of repeated tests when the bridge condition had not changed. The resolutions were expressed as the threshold values at a certain statistical confidence level. For selected damage cases, detection of the presence of damage was investigated in statistical manner by comparing mean values of the area of mode shape change with the threshold values of the test protocols. In addition, the probability of successful damage identification was calculated based on the distributions of area changes in mode shape obtained when there was no change in condition and when there was a change in the condition of the bridge superstructure.

Finally, five commonly available VBDD indicators were selected to identify the location of damage after the presence of damage had been established. The performance of the VBDD indicators was examined and evaluated while two different normalization schemes were adopted.

7.2 Conclusions

Several conclusions may be drawn from this research. A summary of main experimental, analytical, and numerical results and conclusions are presented in the following paragraphs.

A comparison of the lowest five natural frequencies extracted from the accelerometer and strain gauge experimental data showed that the agreement between the two types of sensors was excellent, with corresponding frequencies differing by less than 1.3% for all modes. Although the differences were small, the natural frequencies extracted from the strain gauge data were generally higher than those from the accelerometer data.

While natural frequencies derived from accelerometer and strain gauge experimental data were nearly identical, mode shapes generated from the accelerometer data were

slightly more reliable (i.e., they had higher Modal Assurance Criteria (MAC) values, higher resolutions, or lower threshold values, as defined in this thesis). Also, the uncertainty in the strain gauge-based mode shapes increased as the signal-to noise ratio decreased, which occurred as the location of the strain gauges used to define the mode shapes moved closer to the estimated neutral axis of the composite girder.

Considering the influence of the type of excitation force on the repeatability of mode shape definition, harmonic excitation applied at the system's natural frequencies produced mode shapes with excellent repeatability using as few as five replicate trials. A similar number of trials using white noise random excitation resulted in significantly more mode shape uncertainty, particularly for higher modes.

In general, mode shape repeatability was found to increase with an increasing sampling period (i.e., data recording length), along with an increasing sampling rate, particularly where white noise excitation was used.

Natural frequencies of the system decreased steadily as damage states were introduced incrementally to various structural elements. However, the changes in the fundamental natural frequencies were very small. The maximum relative changes of the fundamental natural frequency in all 17 health states, including one damage case that decreased the flexural rigidity of one of the girders by approximately 34% (producing reductions in the vertical flexural stiffness at that location of 7.76% based on FE results), were only 0.09% and 1.27% for the frequency extracted from accelerometer and strain gauge data, respectively. The small changes implied that the change in fundamental natural frequency may not be a sensitive damage indicator, considering that potential changes due to environmental effects are known to be larger.

On the other hand, the maximum change in the frequency of Mode 3 (a torsional mode) among various health states was relatively large, at 13.37% and 10.23% for the frequency extracted from accelerometer and strain gauge data, respectively. In fact, for accelerometer data, the frequency of Mode 3 (around 30 Hz) in several health states, was significantly different from the corresponding frequency in other health states (around 34 Hz). The largest change in frequency was found to result from shifts in

modes instead of changes in the same mode. In this case, the mode changed to a completely different mode due to the presence of damage, which means that the two modes compared may be treated as two different modes. In other words, a completely different new mode shape (i.e., Mode 3 with the frequency around 30 Hz) was introduced for these health states, due to the disconnection of a cross-bracing diaphragms around the mid-span of the bridge. Mode 4 in these health states was most likely similar to Mode 3 in other health states, while the vibration mode around 35.8 Hz (similar to Mode 4 in other health states) either disappeared or was inadvertently not extracted since the modes were so close to each other, and five other modes had already been detected.

Although comparison of two different modes may be meaningless in one sense, from another perspective, it could be very useful because the large shifting in modes could be a good indicator for global damage. For example, in the current study, the disconnection of cross-bracing diaphragms changed the load sharing between different girders, hence the global stiffness, and ultimately the resulting torsional modes.

The newly developed damage indicator, the area of mode shape change, was found to be capable of successfully identifying the presence of damage with a relatively high confidence level using both numerical and experimental data.

From the numerical analysis using the FE model, a constant relationship was found between the area of mode shape change and the severity of damage (i.e., the extent of the relative flexural stiffness change due to damage) for given specific conditions. The relationship was found to be a power function with two constants. For example, in Mode 1, the function was expressed as $y = 3.3 \cdot x^{1.26}$, where x denotes the relative flexural stiffness change and y is the area of mode shape change due to damage. The constant relationship could be used to quantify the severity of damage (i.e., Level 3 damage detection) by measuring the area of mode shape change due to damage. It should be acknowledged, though, that the constants in the power function may depend on many factors, such as the type of structure, the distribution of stiffness, and the location of damage, which were not investigated as part of this research. However, the

concept demonstrated by this investigation could be a potential way to quantify the severity of damage in the practical implementation of VBDD methods.

Of the 28 test protocols investigated, those that used forced harmonic excitation in combination with the fundamental vibration mode consistently resulted in the lowest threshold values, and therefore the lowest levels of uncertainty for the area changes in mode shape. This held true regardless of whether acceleration or strain measurements were used to represent mode shapes. These protocols are therefore the most sensitive to changes in the structural condition. Random excitations produced much higher threshold values, and were therefore less sensitive to damage, with only acceleration measurements for the fundamental mode resulting in a comparable threshold value of area changes.

The presence of all single damage scenarios, except for damage cases affecting the surface of the concrete deck, could be identified with a relatively high confidence level (at least 90% based on percentile threshold value, or at least 91.9% based on the probability calculated using an assumed Log-Normal distribution) when harmonic excitation was used, since the area changes in the fundamental mode shape due to damage exceeded the corresponding threshold values; therefore, the changes were considered statistically significant. This was true for all instrumentation schemes except when the strain gauges near the top flanges of the girders nearest the estimated neutral axis were used to measure mode shapes. Among the instrumentation schemes investigated, both acceleration measurements and strain measurements near the bottom flanges of the girders were able to identify the presence of damage with a high level of confidence. When random excitation was used, the use of acceleration measurements greatly increased the ability to identify the presence of damage, since the protocols using strain measurements produced values of area change in mode shape that fell close to, or below, the corresponding threshold values for damage detection.

In general, higher modes produced less sensitive mode shapes for damage detection as compared to the fundamental mode. However, it is believed that there is still merit in investigating the use of higher vibration modes for the purpose of damage detection,

especially for cases which may involve mode switching (i.e., when mode shapes change to an entirely new mode, or to a mode with a large difference compared to the one before the damage was introduced). More specifically, this is probably true for modes featuring torsional behaviour and damage that affects the torsional stiffness.

Regarding the performance of the VBDD methods examined and evaluated for damage localization in this research, in general, all methods could localize the damage to within two or three possible locations when the fundamental mode was used, as long as the presence of damage could be established with a certain confidence level. However, it should be acknowledged that there were several false positive indicators (i.e., a damage location was indicated where there was no damage). As a result, it is recommended that more than one VBDD technique be applied simultaneously in the practical implementation of damage detection, as different methods showed different features in damage localization. In general, the change in mode shape method and the damage index method performed slightly better than other methods for the specific damage cases and test protocols investigated in this research. It was also found that the manner in which the measured mode shapes were normalized had a significant influence on the precision of the damage characterization, as well as on the sensitivity of a given sensor, depending on the location of that sensor relative to the damage. In practice, it is recommended that more than one normalization scheme be used to reflect both global and localized features of mode shapes and changes due to damage.

It is believed that the VBDD method developed as part of this research, the area of mode shape change, in combination with the protocols identified as being most sensitive to damage, can be used effectively as the initial component of a comprehensive SHM package for bridges by permitting a relatively quick identification of the presence of damage on the structure. An initial assessment using the proposed procedures could then be followed up with a more extensive investigation to locate and quantify the damage, if required.

7.3 Recommendations for Future Research

The experimental results and conclusions presented in this research were based on laboratory tests conducted under well-controlled environments. As a result, it is recommended that this research be extended to field bridge vibration tests. The resolutions of various test protocols in field conditions should be quantified and evaluated both with and without temperature effects (i.e., based on the assumption that the temperature effects may be separated through further research). It is expected that ambient traffic excitation could generate poorer resolutions (i.e., higher threshold values) of area change in mode shape, which may make the method insensitive to small-scale damage. However, one should not abandon the use of the test protocols, in combination with the more sensitive sensor schemes (e.g., accelerometers and low-noise strain gauges installed in higher strain regions) and traffic excitation, since traffic excitation is readily available and well-suited for continuous monitoring of bridges.

It is recommended that damage localization methods, like those described in this research, should also be applied using a statistical approach, in order that the location of damage may be identified with a certain confidence level.

The constant relationship between the area of mode shape change and the severity of damage found in the numerical study in this research should be extended to and evaluated in more general cases, so that the conclusions for this research can be generalized. This approach could be useful for Level 3 damage detection in the practical application of VBDD methods.

REFERENCES

Adams, R.D., Walton, D., Flitcroft, J.E., and Short, D. 1975. Vibration testing as a nondestructive test tool for composite materials. Composite Reliability, ASTM STP 580, pp.159-175 (American Society For Testing and Materials).

Aktan, A.E. and Farhey, D. 1996. Condition and Reliability Assessment of Constructed Facilities. ACI SP, 162, pp: 73-92, August, 1996.

Alampalli, S., Fu, G., and Dillon, W. 1997. Signal versus noise in damage detection by experimental modal analysis. ASCE Journal of Structural Engineering, 123(2): 237-245.

Alwash, M., Sparling, B.F., and Wegner, L.D. 2005. Excitation sources for vibration-based damage detection on the Red Deer River Bridge. Proceedings of 1st Canadian Society of Civil Engineering (CSCE) Specialty Conference on Infrastructure Technologies, Management and Policy. Toronto, Ontario, paper FR-124.

Alwash, M., Sparling, B.F., and Wegner, L.D. 2006. Influence of the excitation source on modal parameter estimation for the Red Deer River Bridge. Proceedings of the 1st Canadian Society of Civil Engineering (CSCE) International Structural Specialty Conference, Calgary, Alberta, Paper No. ST-028.

Alwash, M., Sparling, B.F., and Wegner, L.D. 2009. Influence of Excitation Dynamic System Identification for a Multi-span Reinforced Concrete Bridge. Advances in Civil Engineering, Volume 2009, Article ID 859217, 18 pages.

ANSYS user's manual (Version 8.1), ANSYS Inc., Canonsburg, PA.

Bendat, J.S. and Piersol, A.G. 1993. Engineering Applications of Correlation and Spectral Analysis. 2nd edition, John Wiley & Sons, New York, NY.

Biswas, M., Pandey, A.K., and Samman, M.M. 1990. Diagnostic Experimental Spectral/ Modal Analysis of a Highway Bridge. Modal Analysis: The International Journal of Analytical and Experimental Modal Analysis, 5: 33–42.

Cawley, P. and Adams, R.D. 1979. The location of defects in structures from measurements of natural frequencies. Journal of Strain Analysis, 14(2): 49-57.

Casas, J.R. and Aparicio, A.C. 1994. Structural damage identification from dynamic-test data. Journal of Structural Engineering, ASCE, 120(8): 2437-2450.

Chong, K.P., Carino, N.J., and Washer, G. 2001. Health monitoring of civil infrastructures. Health Monitoring and Management of Civil Infrastructure Systems,Proceedings of SPIE's International Symposium on NDE and Health Monitoring Diagnostics, Vol. 4337, S.B. Chase and A.E. Aktan, eds., SPIE, Bellingham, WA, pp. 1-16.

Clough, R.W. and Penzien, J. 1975. Dynamics of Structures. 2nd Edition, McGraw-Hill.

Clough, R.W., and Penzien, J. 2003. Dynamics of Structures, 3rd Edition. Computers and Structures Inc., Berkeley, CA, USA.

Doebling, S.W., 1995. Measurement of Structural Flexibility Matrices for Experiments with Incomplete Reciprocity. Ph. D. Dissertation, University of Colorado, Boulder, CO, Department of Aerospace Engineering Sciences, CU-CAS-95-10.

Doebling, S.W. and Farrar, C.R. 1998. Statistical damage identification techniques applied to the I-40 Bridge over the Rio Grande River. Proceedings of the 16th International Modal Analysis Conference (IMAC), Santa Barbara, Calif. pp. 1717-1724.

Doebling, S.W., Farrar, C.R., and Cornwell, P.J. 1997. A Computer Toolbox for Damage Identification Based on Changes in Vibration Characteristics. Structural Health Monitoring, Current Status and Perspectives, Stanford University, Palo Alto, California, pp. 241–254.

Doebling, S.W., Farrar, C.R., and Prime, M.B. 1998. A summary review of vibration-based damage identification methods. Shock Vibration Digest, 30(2): 91-105.

Doebling, S.W., Farrar, C.R., Prime, M.B., and Shevitz, D.W. 1996. Damage identification and health monitoring of structural and mechanical systems from changes

in their vibration characteristics: A literature review. Report No. LA-13070-MS, Los Alamos National Laboratory.

Doebling, S.W., Hemez, F.M., Barlow, M.S., Peterson, L.D., and Farhat, C. 1993a. Damage Detection in a Suspended Scale Model Truss Via Model Update. Proceedings of the 11th International Modal Analysis Conf., 1083–1094.

Doebling, S.W., Hemez, F.M., Barlow, M.S., Peterson, L.D., and Farhat, C. 1993b. Selection of Experimental Modal Data Sets for Damage Detection Via Model Update. Proceedings of 34th AIAA/ASME/ASCE/AHS/ASC Structures, Structural Dynamics, and Materials Conference, 1506–1517, AIAA-93-1481-CP.

Ewins, D.J. 2000. Modal testing: theory, practice and application. 2nd Ed. Research Studies Press Ltd., Baldock, Hertfordshire, England.

Farrar, C.R., Baker, W.E., Bell, T.M., Cone, K.M., Darling, T.W., Duffey, T.A., Eklund, A., and Migliori, A. 1994. Dynamic Characterization and Damage Detection in the I-40 Bridge Over the Rio Grande. Los Alamos National Laboratory report LA-12767-MS.

Farrar, C.R. and Cone, K.M. 1995. Vibration Testing of the I-40 Bridge Before and After the Introduction of Damage. Proceedings of 13th International Modal Analysis Conference, pp. 203–209.

Farrar, C. R., Cornwell, P. J., Doebling, S.W. and Prime, M. B. 2000. Structural health monitoring studies of the Alamosa Canyon and I-40 Bridge. Los Alamos National Laboratory Report LA-13635-MS, New Mexico, U.S.A.

Farrar, C.R. and Doebling, S.W. 1997. An overview of modal-based damage identification methods. EUROMECH 365 International Workshop: DAMAS 97, Structural Damage Assessment Using Advanced Signal Processing Procedures, Sheffield, UK.

Farrar, C.R. and James, G.H. 1997. System identification from ambient vibration measurements on a bridge. Journal of Sound and Vibration, 205(1): 1-18.

Farrar, C.R. and Jauregui, D.A. 1998a. Comparative study of damage identification algorithms applied to a bridge: I. Experiment. Smart Materials and Structures, 7: 704-719.

Farrar, C.R. and Jauregui, D.A. 1998b. Comparative study of damage identification algorithms applied to a bridge: II. Numerical study. Smart Materials and Structures, 7: 720-731.

Felber, A. J. 1993. Development of a hybrid bridge evaluation system. Ph. D. Thesis, Department of Civil Engineering, University of British Columbia, B.C., Canada.

FHWA 2001. Reliability of visual inspection. Federal Highway Administration, Report. Nos. FHWA-RD-01-020 and FHWA-RD-01-021, Washington, DC.

Fox, C.H.J. 1992. The location of defects in structures: a comparison of the use of natural frequency and mode shape data. Proceedings of the10th International Modal Analysis Conference, San Diego, California, pp. 522-528.

Friswell, M.I., Penny, J.E.T., and Wilson, D.A.L. 1994. Using Vibration data and Statistical Measures to Locate Damage in Structures. Modal Analysis: The International Journal of Analytical and Experimental Modal Analysis, 9(4), 239–254.

Fritzen, C.P., Seibold, S., and Buchen, D. 1995. Application of Filter Techniques for Damage Identification in Linear and Nonlinear Mechanical Structures. Proceedings of the 13th International Modal Analysis Conference, 1874–1881.

Galvín, P., and Domínguez, J. 2007. Dynamic analysis of a cable-stayed deck steel arch bridge. Journal of Constructional Steel Research, 63:1024-1035.

Grygier, M.S. 1994. Modal Test Technology as Non-Destructive Evaluation of Space Shuttle Structures. NASA Conference Publication 3263.

Hunt, D.L., Weiss, S.P., West, W.M., Dunlap, T.A., and Freesmeyer, S.R. 1990. Development and Implementation of a Shuttle Modal Inspection System. Sound and Vibration, 24(9), 34–42.

Huth, O., Maeck, J., Kilic, N., and Motavalli, M. 2005. Damage identification using modal data: Experiences on a prestressed concrete bridge. Journal of Structural Engineering, 131 (12): 1898-1910.

ISIS Canada. 2001. Reinforcing Concrete Structures with Fibre Reinforced Polymers. Design Manual No. 3, ISIS Canada, Winnipeg, Canada.

James, G.H., Crane, T.G., Lauffer, J.P., and Nord, A.R. 1992. Modal testing using natural excitation. Proceedings of the 10th International Modal Analysis Conference (IMAC), San Diego, USA, pp. 1209-1216.

James, G.H., Carne, T.G., and Lauffer, J.P. 1995. The natural excitation technique (NExT) for modal parameter extraction from operating structures. The International Journal of Analytical and Experimental Modal Analysis 10(4): 260-277.

Juang, J.N., Papa, R.S. 1985. An eigensystem realization algorithm for modal parameter identification and model reduction. Journal of Guidance, Control and Dynamics, 8(5): 620-627.

Kim, J.T. and Stubbs, N. 1995. Model-uncertainty impact and damage-detection accuracy in plate girder. ASCE, Journals of Structural Engineering, 121(10): 1409-1417.

Kirkegaard, P.H. and Andersen, P. 1998. Use of statistical information for damage assessment of civil engineering structures. Proceedings of the 16th International Modal Analysis Conference (IMAC) Santa Barbara, CA. pp. 363-368.

Ko, J., Ni, Y., and Chan, T. 1999. Dynamic Monitoring of Structural Health in Cable-Supported Bridges. Smart Structures and Materials 1999: Smart Systems for Bridges, Structures, and Highways, Proceedings of SPIE, Vol. 3,671, pp. 161–172.

Kobayashi, A. S. 1993. Non-destructive evaluation. Hand book on Experimental Mechanics, VCH, New York, N.Y., and SEM, Bethel, CT, USA.

Kong, F., Liang, Z., and Lee, G.C. 1996. Bridge Damage Identification Through Ambient Vibration Signature. Proceedings of 14th International Modal Analysis Conference, pp. 717–724.

LabVIEW 7.1 (2003), National Instruments Corporation, Austin, Texas.

LabVIEW 8.0 (2008), National Instruments Corporation, Austin, Texas.

Levi, A. 1997. Instrumented monitoring and diagnostic load testing for condition assessment and evaluation of bridges. Ph.D. Dissertation, College of Engineering, University of Cincinnati, Cincinnati, Ohio, USA.

Loland, O. and Dodds, J.C. 1976. Experience in developing and operating integrity monitoring system in North Sea. Proceedings of the 8th Annual Offshore Technology Conference, pp. 313-319.

Ljung, L. 1987. System identification: theory for the user, Prentice Hall, Englewood Cliffs, New Jersey, USA.

MACEC / SPICE (v 2.0), Departement Burgerlijke Bouwkunde, Katholieke Universiteit Leuven.

Maia, N. and Silva, J. Eds. 1997. Theoretical and experimental modal analysis. Research Studies Press Ltd., Somerset, England.

Marks, R.J. II. 1991. Introduction to Shannon Sampling and Interpolation Theory. Springer-Verlag, New York.

Matlab (v7.0). 2004. The Mathworks, Inc.

Mathcad 14.0 User's Guide. Parametric Technology Corporation, Needham, MA, USA

Mathworks, Inc. 2006. MATLAB users manual. Massachusetts, USA.

Mazurek, D.F. and DeWolf, J.T. 1990. Experimental Study of Bridge Monitoring Technique. ASCE Journal of Structural Engineering, 116, 2532–2549.

Mufti, A.A. 2001. Guidelines for structural health monitoring. ISIS Canada (The Canadian Network of Centres on Intelligent Sensing for Innovative Structures), Design Manual No.2, Winnipeg, Manitoba.

Mufti A.A., Bakht, B., Tadros, G., Horosko, A.T. and Sparks, G. 2005. Are civil structural engineers "risk averse"? Can civionics help? Sensing issues in civil structural health monitoring. F. Ansari, ed. Springer, Netherlands, pp. 3-12.

Mufti, A.A., Jaeger, L.G., Bakht, B., and Wegner, L.D. 1993. Experimental investigation of FRC deck slabs without internal steel reinforcement. Canadian Journal of Civil Engineering, 20(3): 398-406.

Nwosu, D.I., Swamidas, A.S.J., Guigne, J.Y., and Olowokere, D.O. 1995. Studies on Influence of Cracks on the Dynamic Response of Tubular T-Joints for Nondestructive Evaluation. Proceeding of the 13th International Modal Analysis Conference, 1122–1128.

Pandey, A.K. and Biswas, M. 1994. Damage detection in structures using changes in flexibility. Journal of Sound Vibration, 169(1): 3-17.

Pandey, A.K., Biswas, M., and Samman, M.M. 1991. Damage detection from changes in curvature mode shapes. Journal of Sound Vibration, 145(2): 321-332.

Paultre, P., Proulx, J. and Talbot, M. 1995. Dynamic testing procedures for highway bridges using traffic loads. ASCE, Journals of Structural Engineering, 121(2): 362-376.

Pearson, S.R., Owen, J.S., and Choo, B.S. 2001. The use of vibration signatures to detect flexural cracking in reinforced concrete bridge decks. Key Engineering Materials, 204-205, pp. 17-26.

Peeters, B., D Roeck, G., Hermans, L., Wauters, T., Kramer, C., and De Smet, C. 1998. Comparison of system identification methods using operational data of a bridge test. Proceedings of ISMA 23, K. U. Leuven, Belgium, pp. 923-930.

Peeters, B. and De Roeck, G. 1998. Stochastic subspace system identification of a steel transmitter mast. Proceedings of IMAC 16, Santa Barbara, USA, pp. 130-136.

Peeters, B. and De Roeck, G. 2000. Damage Identification on the Z24-Bridge Using Vibration Monitoring. European COST F3 Conference on System Identification and Structural Health Monitoring, Madrid, Spain, pp. 233–242.

Peeters, B. and De Roeck, G. 2001. Stochastic system identification for operational modal analysis: a review. ASME Journal of Dynamics Systems, Measurement and Control, 123(4): 659-667.

Pham, A.T., Sparling, B.F., and Wegner, L.D. 2007. Temperature effects on structural health monitoring of an integral abutment bridge. 2nd International Operational Modal Analysis Conference. Copenhagen, Denmark, Paper No. 63.

Rahman, M.S. 2000. Damage Diagnosis by NNE and Development of Smart Monitoring System for Aging Bridges. Ph.D. Dissertation, Faculty of Civil Engineering, Kitami Institute of Technology, Japan.

Raj, B., Jayakumar, T., and Thavasimuthu, M. 2002. Practical non-destructive testing. 2nd ed., Narosa Publishing House, New Delhi, India.

Ramirez, R.W. 1985. The FFT: Fundamentals and Concepts. Prentice-Hall, Englewood Cliffs, New Jersey, USA.

Rizos, P.F., Aspragathos, N., and Dimarogonas, A.D. 1990. Identification of Crack Location and Magnitude in a Cantilever Beam from the Vibration Modes. Journal of Sound and Vibration, 138(3): 381–388.

Roth, J.T. and Pandit, S.M. 1999. Condition monitoring and failure prediction for various rotating equipment components. Proceedings of the 17th International Modal Analysis Conference, Kissimee, Florida, pp. 1674-1680.

Rytter, A. 1993. Vibration based inspection of civil engineering structures. Ph.D. Dissertation, Department of Building Technology and Structural Engineering, Aalborg University, Denmark.

Saitoh, M. and Takei, B.T. 1996. Damage Estimation and Identification of Structural Faults Using Modal Parameters. Proceeding of the 14th International Modal Analysis Conference, 1159–1164.

Salane, H.J., Baldwin, J.W., and Duffield, R.C. 1981. Dynamics Approach for Monitoring Bridge Deterioration. Transportation Research Record, 832: 21–28.

Salawu, O.S. 1994. Nondestructive Evaluation of Constructed Facilities Using Vibration Testing. Insight, 36(8): 611–615.

Salawu, O.S. 1997. Detection of structural damage through changes in frequency: a review. Engineering Structures, 19(9): 718-723.

Salawu, O.S. and Williams, C. 1994. Damage location using vibration mode shapes. Proceedings of the 12th International Modal Analysis Conference, Honolulu, HI, pp. 933-939.

Salawu, O.S. and Williams, C. 1995. Bridge assessment using forced-vibration testing. Journal of structural engineering, 121(2): 161-173.

Samman, M.M. and Biswas, M. 1994. Vibration Testing for Nondestructive Evaluation of Bridges. Journal of Structural Engineering, 120(1): 290–306.

Shih, C.Y., Tsuei, Y.G., Allemang, R.J., and Brown, D.L. 1988. Complex mode indication function and its application to spatial domain parameter estimation. Mechanical Systems and Signal Processing, 2(4): 367-377.

Shrive, P.L. 2005. Evaluating GFRP and SHM in the Centre Street Bridge Project. Ph.D. Thesis, University of Calgary, Calgary, Canada.

Siddique, A.B. 2008. Structural health monitoring of attridge drive overpass. M.Sc. Thesis, Department of Civil and Geological Engineering, University of Saskatchewan, Saskatoon.

Siddique, A B., Sparling, B.F., and Wegner, L.D. 2007. Assessment of vibration-based damage detection for an integral abutment bridge. Canadian Journal of Civil Engineering, 34(3): 438-452.

Siddique, A.B., Wegner, L.D., Sparling, B.F. 2005. Application of vibration-based damage detection to an integral abutment bridge. Proceedings of SPIE - The International Society for Optical Engineering, v 5767, pp 225-235, San Diego, CA

Siddique, A.B., Wegner, L.D., Sparling, B.F. 2006. Identifying damage on a bridge deck using vibration-based damage indices derived from limited measurement. Proceedings of SPIE, V 6176, Nondestructive Evaluation and Health Monitoring of Aerospace Materials, Composites, and Civil Infrastructure V

Skjaerbaek, P.S., Nielsen, S.R.K., and Cakmak, A.S. 1996. Assessment of Damage in Seismically Excited RC-Structures from a Single Measured Response. Proceeding of the 14th International Modal Analysis Conference, 133–139.

Sohn, H., Farrar, C.R., Hemez, F.M., Shunk, D.D., Stinemates, D.W., and Nadler, B.R. 2003. A Review of Structural Health Monitoring Literature: 1996–2001. Los Alamos National Laboratory Report, LA-13976-MS

Srinivasan, M.G. and Kot, C.A. 1992. Effects of damage on the modal parameters of a cylindrical shell. Proceedings of the 10th International Modal Analysis Conference, San Diego, Calif., pp. 529-535.

Stubbs, N., Kim, J.T., and Farrar, C.R. 1995. Field Verification of a Nondestructive Damage Localization and Severity Estimation Algorithm. Proceedings of 13th International Modal Analysis Conference, pp. 210–218.

Stubbs, N. and Osegueda, R. 1990a. Global Non-Destructive Damage Evaluation in Solids. Modal Analysis: The International Journal of Analytical and Experimental Modal Analysis, 5(2): 67–79.

Stubbs, N. and Osegueda, R. 1990b. Global Damage Detection in Solids–Experimental Verification. Modal Analysis: The International Journal of Analytical and Experimental Modal Analysis, 5(2): 81–97.

Stubbs, N., Sikorsky, C., Park, S.C., and Bolton, R. 1999. Verification of a Methodology to Nondestructively Evaluate the Structural Properties of Bridges. Structural Health Monitoring 2000, Stanford University, Palo Alto, California, pp. 440–449.

Stubbs, N., Broome, T.H., and Osegueda, R. 1990. Nondestructive Construction Error Detection in Large Space Structures. AIAA Journal, 28(1): 146–152.

Swamidas, A.S.J. and Chen, Y. 1995. Monitoring crack Growth Through Change of Modal Parameters. Journal of Sound and Vibration, 186(2): 325–343.

Uomoto, T.ed. 2000. Non-destructive testing in civil engineering 2000. Elsevier Science Ltd., Amsterdam.

Van den, B., Peeters, B., and De Roeck, G. 1999. Introduction to MACEC 2, modal analysis of civil engineering constructions, Dept. Civil Engineering, K. U. Leuvwen.

Van Overschee, P., and De Moor, B. 1996. Subspace identification for linear systems: theory, implementation, applications. Kluwer Academic Publishers. Dordrecht, the Netherlands.

Wang, M.L., Satpathi, D., and Heo, G. 1997. Damage Detection of a Model Bridge Using Modal Testing. Structural Health Monitoring, Current Status and Perspectives, Stanford University, Palo Alto, California, pp. 589–600.

Wang, Y., Sparling, B.F., and Wegner, L.D. 2008. Vibration-based damage detection on a multi-girder bridge deck. Proceedings of the 37th Annual Conference of the Canadian Society for Civil Engineering, Quebec City, Canada.

Ward, H.S. 1984. Traffic generated vibrations and bridge integrity. ASCE Journal of Structural Engineering, 110(10): 2487-2498.

Wegner, L.D., Zhou, Z., Alwash, M., Siddique, A.B., and Sparling, B.F. 2004. Vibration-based damage detection on bridge superstructures. Proceedings of the 2nd International Workshop on Structural Health Monitoring of Innovative Civil Engineering Structures, pp. 429-439;

Wolf, T. and Richardson, M. 1989. Fault detection in structures from changes in their modal parameters. Proceedings of the 7th International Modal Analysis Conference, Las Vegas, USA, pp. 87-94.

Wong, F.S. 2001. Health monitoring and structural reliability as a value chain. Computer-Aided Civil and Structural Engineering, 16: 71-78.

Yang, J.C.S., Chen, J., and Dagalakis, N.G. 1984. Damage Detection in Offshore Platforms by the Random Decrement Technique. ASME Journal of Energy Resources Technology, 106: 38–42.

Zhang, Z. and Aktan, A.E. 1995. The damage indices for constructed facilities. Proceedings of the 13th International Modal Analysis Conference, Nashville, TN, pp. 1520-1529.

Zhang, Z. and Aktan, A.E. 1998. Application of modal flexibility and its derivatives in structural identification. Research of Non-destructive Evaluation, 10(1): 43-61.

Zhou, Z., Sparling, B.F., and Wegner, L.D. 2005. Damage detection on a steel-free bridge deck using random vibration. Proceedings of SPIE - The International Society for Optical Engineering, v 5767, Nondestructive Evaluation and Health Monitoring of Aerospace Materials, Composites, and Civil Infrastructure IV, 2005, pp. 108-119.

Zhou, Z., Wegner, L.D., and Sparling, B.F. 2003. Vibration-based damage detection on a steel-free bridge deck. Proceedings of the International Workshop on Structural Health Monitoring, Kitami, Japan, September 2003 (Japan Society of Civil Engineers, Tokyo, 2003), pp.109-116.

Zhou, Z., Wegner, L.D., Sparling, B.F. 2004. Vibration-based damage detection on a prestressed concrete girder. Proceedings of the 5th Structural Specialty Conference of the Canadian Society for Civil Engineering, Saskatoon, Saskatchewan, Canada.

Zhou, Z., Wegner, L.D., Sparling, B.F. 2007. Vibration-based detection of small-scale damage on a bridge deck. ASCE Journal of Structural Engineering 133(9): 1275-1267.

Zhou, Z., Wegner, L.D., Sparling, B.F. 2010. Structural Health Monitoring of Precast Concrete Box Girders Using Selected Vibration-Based Damage Detection Methods. Advances in Civil Engineering, Volume 2010 (2010), Article ID 280685.

APPENDIX A. **A PRELIMINARY FIELD TEST ON THE PROTOTYPE BRIDGE**

A.1 Overview

The current research primarily focused on the experimental application of vibration-based damage detection on a multi-girder bridge superstructure. The structure used for this investigation was a one-third scale model of a slab-on-girder composite bridge superstructure featuring four steel girders supporting a steel-free concrete deck. Constructed in the Structural Laboratory, University of Saskatchewan, the model was based on a prototype superstructure forming part of the North Perimeter Red River Bridge located in Winnipeg, Manitoba.

To facilitate the design and construction of the scaled bridge model, a preliminary field test was conducted on the prototype bridge on Oct. 19, 2005 (see Fig. A.1). Dimensions

(a) (b)

Figure A.1. The North Perimeter Red River Bridge (a) the whole bridge view and (b) the the west end span (steel-free concrete deck).

were measured and compared with the as-built drawings. The dynamic properties (primarily the natural frequencies) were measured using four accelerometers (Fig. A. 2) as the bridge was subjected to traffic excitation forces (Fig. A.3).

A.2 Measurement of Dynamic Properties

Automobile traffic loads were used as a source of ambient excitation (see Fig. A.3). The data acquisition system consisted of a SCXI-1000 chassis and a modular of SCXI-1120, which was controlled by LabView 7.1 (2003) software. Data was acquired at 256 samples per second when big trucks were passing the bridge. Thirty-five sets of vibration data were collected by LabView 7.1.

Figure A.2. Installation of accelerometers.

Figure A.3. Ambient excitation by automobile traffic loads.

Figure A.4 gives a sample of one data series. Fast Fourier Transform (FFT) analyses were used to transfer the signal from the time domain to the frequency domain (see Fig. A.5).

Since there was measurement noise and electrical interference in the signals, two filters supplied within LabView 7.1 were used to process the signals. First, a Low-pass filter (with a cutoff 50 Hz) was used to eliminate high frequency (primarily electrical) noise.

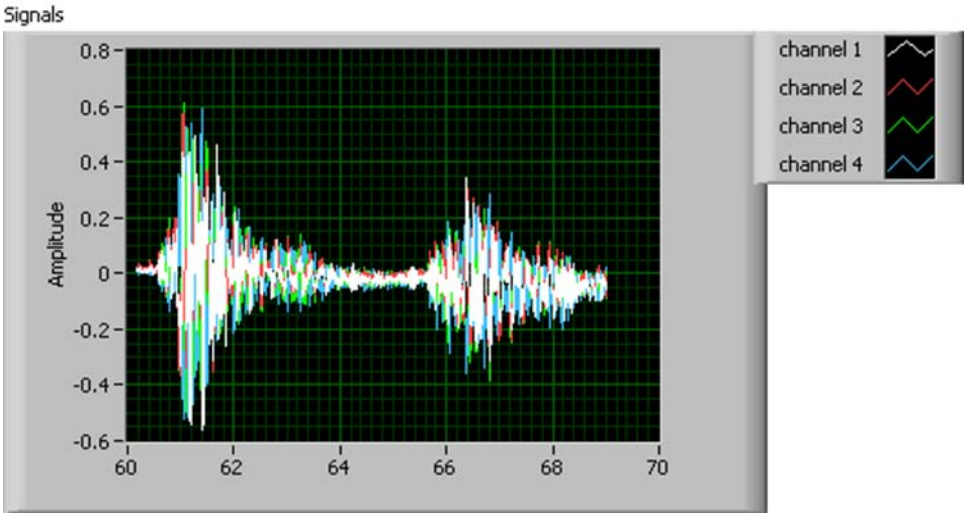

Figure A.4. Vibration response to ambient traffic excitation for the original recorded accelerometion time history using four accelerometers.

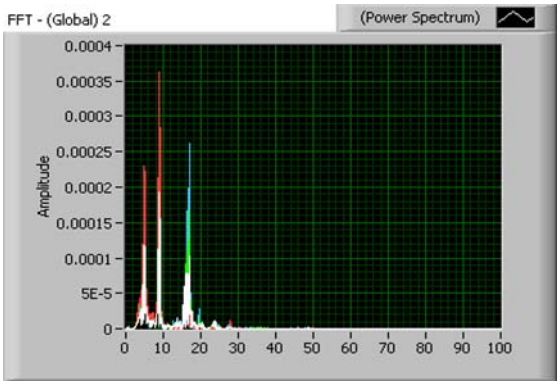

Figure A.5. The acceleration spectrum for the recorded time history data using four accelerometers.

Secondly, a high-pass filter (with a cutoff 0.5 Hz) was used to attenuate low frequency signal drift. From Figure A.5, three resonant frequencies (or natural frequencies) could be picked out: 4.6, 8.9, and 16.9 Hz.

To check these values, the measured data were also analyzed using the commercial software SPICE (or MACEC), which utilizes Peak-picking (PP) and Stochastic Sub-space Identification (SSI) techniques to extract dynamic properties from vibration data. Figs. A.6 and A.7 show the results obtained using the PP and SSI methods, respectively. The results are also listed in Table A.1. It can be seen from this table that the natural frequencies are consistent with the results obtained directly from the LabView built-in program.

The temperature was recorded as 11°C when the field test was conducted. In addition, the dimensions of the bridge and components were verified against the design drawings. These as-built dimensions provide original information for inputs into the numerical and experimental studies conducted later on.

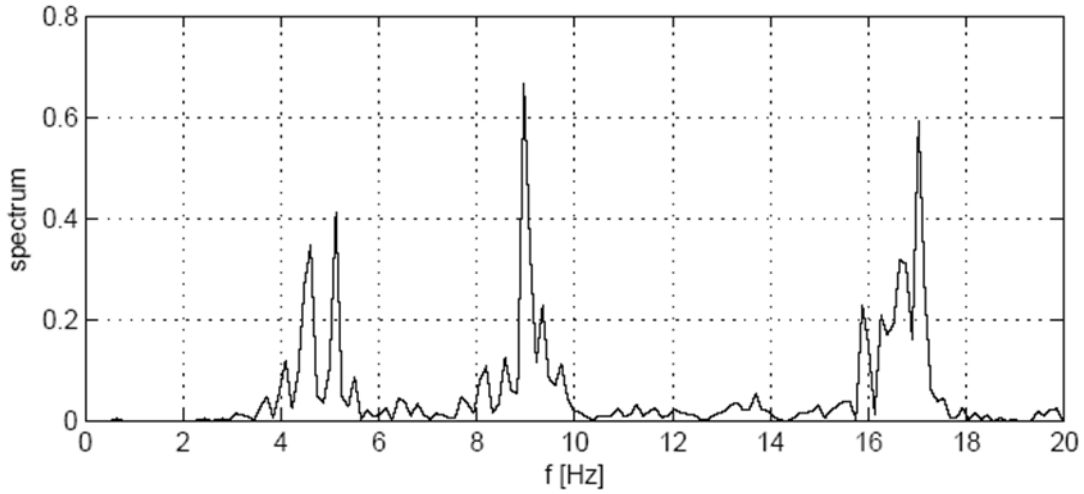

Figure A.6. Modal property extraction using Peak Picking (PP) method.

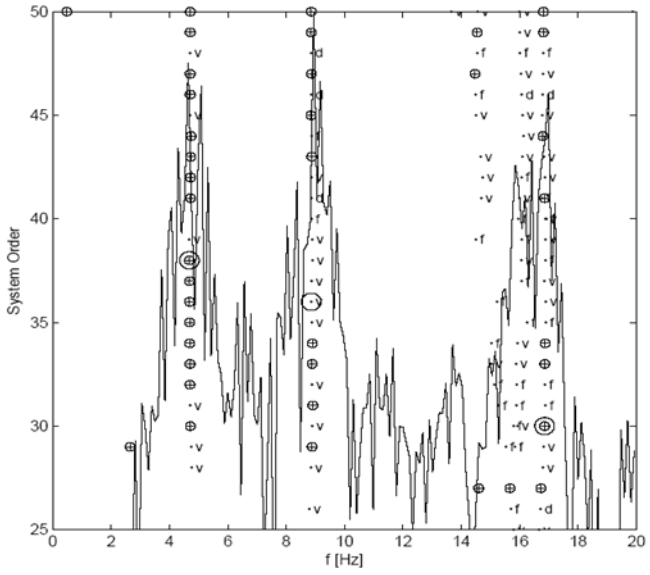

Figure A.7. Modal property extraction using Stochastic Subspace Identification (SSI) method.

Table A.1. The measured natural frequencies of the prototype bridge using ambient excitation.

	Measured natural frequency (Hz)		
Modal Extraction Methods	Mode 1	Mode 2	Mode 3
LabView built-in program	4.6	8.9	16.9
Peak Picking	4.66	8.96	16.99
SSI	4.68	9.03	16.93

APPENDIX B. **PRELIMINARY NUMERICAL STUDIES**

B.1 Introduction

The structure used for this investigation was a one-third scale model of a slab-on-girder composite bridge superstructure featuring four steel girders supporting a steel-free concrete deck. The model was based on a prototype superstructure forming part of the North Perimeter Red River Bridge located in Winnipeg, Manitoba.

Prior to constructing the laboratory model, a preliminary numerical study was carried out to investigate the appropriate scaling model method to ensure that the dynamic behaviour of the laboratory mode could reproduce that of the prototype. Therefore, it was necessary to investigate a scaling model method to properly scale the laboratory model from the prototype. Specifically, in this preliminary study, half scale and quarter scale models were initially selected to verify the scaling model method, even though a one-third scale model was built finally based on the available space in the structural laboratory of the University of Saskatchewan.

B.2 Scaling Model with Gravitational Force Neglected

The dimensional homogeneity among the physical parameters of the length L, modulus of elasticity E, gravitational acceleration g, and mass density ρ cannot be satisfied simultaneously when the bridge deck is scaled, because there are only three independent basic quantities (fundamental dimensions) which can be chosen arbitrarily. In the VBDD method, the primary variables are natural frequencies and mode shapes. Gravitational force has little influence on the values of natural frequencies and mode shapes, suggesting that the influence of the gravitational force can be neglected in the scaling process. The length L, modulus of elasticity E, and mass density ρ can then be

chosen as the independent basic quantities. In that case, there are the following equations:

$$L_p = S_l L_m$$

$$E_p = S_E E_m$$

$$\rho_p = S_\rho \rho_m$$

where subscripts *p* and *m* refer to prototype and model, respectively, and *S* denotes the relevant scaling factor. For example, S_E denotes the scaling factor for the modulus of elasticity, relating the prototype and model values. The scaling factors for all other quantities associated with the model can be calculated from S_E, S_l and S_ρ. Some scaling relationships for important physical parameters are listed in Table B.1.

Table B.1. Similitude requirements for the scale bridge model.

Scaling Parameters	Dimension	Scaling Factors
Length	L	S_l
Displacement	L	S_l
Force	F	S_l^2
Time	T	S_l
Frequency	T^{-1}	S_l^{-1}
Velocity	LT^{-1}	1
Gravitational acceleration	LT^{-2}	Neglected
Acceleration	LT^{-2}	S_l^{-1}
Mass density	$FL^{-4}T^{2}$	1
Strain	--	1
Stress	FL^{-2}	1
Modulus of Elasticity	FL^{-2}	1
Poisson's ratio	--	1

Modeling with gravitational force neglected is convenient because the same density and strength values for concrete and structural steel could be used for the scaling model as that of the prototype bridge. However, a full investigation was needed to determine whether or not the gravitational force will seriously influence the values of natural frequencies and mode shapes after the damage is introduced into the bridge deck.

B.3 Finite Element Verification for the Feasibility of the Scaling Model Method

Three sets of scaled 4-girder steel-free bridge deck models were generated using ANSYS, a commercial finite element (FE) software, including a full scale model, a half scale model, and a quarter scale model. Undamaged cases, single damage cases, and multiple damage cases were studied to verify the feasibility of the scaling model method with gravitational force neglected.

According to the theory of scaling with gravitational force neglected, the length L, modulus of elasticity E, and mass density ρ were chosen as the independent basic quantities as discussed previously. For convenience, therefore, scaling factors of $S_E = 1$, and $S_\rho = 1$ were selected. That is, the same elastic modulus and density were used for the model and prototype. The only parameter which varied between models and prototype was length, L, which was scaled according to the relationship $L_p = S_l L_m$. In this study, $S_l = 1$, $S_l = 2$, and $S_l = 4$ were selected for the full scale, half scale, and quarter scale models, respectively.

For the undamaged cases, the values of the frequencies of the full scale, half scale, and quarter scale models are listed in Table B.2. For single damage cases, the values of the frequencies of the full scale, half scale, and quarter scale models are listed in Table B.3.

These results demonstrate that the natural frequencies scaled as expected in all cases (i.e. properly scaled natural frequencies of the scale models matched full scale values). Therefore, it was concluded that scaling by ignoring gravitational forces was valid for dynamic testing.

Table B.2. The natural frequencies (Hz) of the undamaged 4-girder steel free bridge deck.

Mode No.	Full Scale (Frequency *f*)	Half Scale ($S_l = 2$)		Quarter Scale ($S_l = 4$)	
		f	$f \bullet S_l^{-1}$	f	$f \bullet S_l^{-1}$
1	3.3772	6.7545	3.37725	13.507	3.37675
2	4.8881	9.7762	4.8881	19.551	4.88775
3	9.3131	18.626	9.313	37.260	9.315
4	12.733	25.465	12.7325	50.926	12.7315
5	14.878	29.757	14.8785	59.511	14.87775

Table B.3. The natural frequencies (Hz) for a single-damage case on the 4-girder steel free bridge deck.

Mode No.	Full Scale (Frequency *f*)	Half Scale ($S_l = 2$)		Quarter Scale ($S_l = 4$)	
		f	$f \bullet S_l^{-1}$	f	$f \bullet S_l^{-1}$
1	3.3745	6.7491	3.37455	13.497	3.37425
2	4.8814	9.7628	4.8814	19.525	4.88125
3	9.2705	18.541	9.2705	37.090	9.2725
4	12.714	25.428	12.714	50.852	12.713
5	14.861	29.723	14.8615	59.443	14.86075

B.4 Conclusions

For scaling model properties from prototype values, it was found that using the approach in which gravitational forces were neglected produced the similitude relation for natural frequency of $S_f = S_l^{-1}$ which was found to be satisfied very well before and after damage introduced. Therefore, the scaling model with gravitational force neglected was demonstrated to be an appropriate scaling method for the VBDD study.

APPENDIX C. **FABRICATION OF EXPERIMENTAL MODEL**

In this appendix, some information related to the fabrication of the experimental model, including the measured compressive strength of concrete samples used for the bridge deck, the fabrication of the steel superstructure of the bridge model, and the construction process of the concrete deck, is presented.

Table C.1. The measured compressive strength of concrete samples used for the bridge deck.

Sample No.	Beaking force (kN)	Compressive strength (MPa)
A1	266.88	34.00
A2	306.91	39.10
A3	244.64	31.16
B1	271.33	34.56
B2	275.78	35.13
B3	235.74	30.03
C1	266.88	34.00
C2	269.10	34.28
C3	240.19	30.60
Avg.	264.16	33.65
STDEV	21.84	2.78
C.O.V.	8.27%	8.27%

Avg. = Average;
STDEV = Standard deviation;
C.O.V. = Coefficient of variation.
Notes:

a. The design strength of concrete is 30 MPa;
b. Nine concrete cylinders, with a diameter of 100 mm and a height of 200 mm, were cast on December 20, 2006;
c. The samples were moist-cured for 28 days;
d. The cylinders were tested on January 17, 2007.

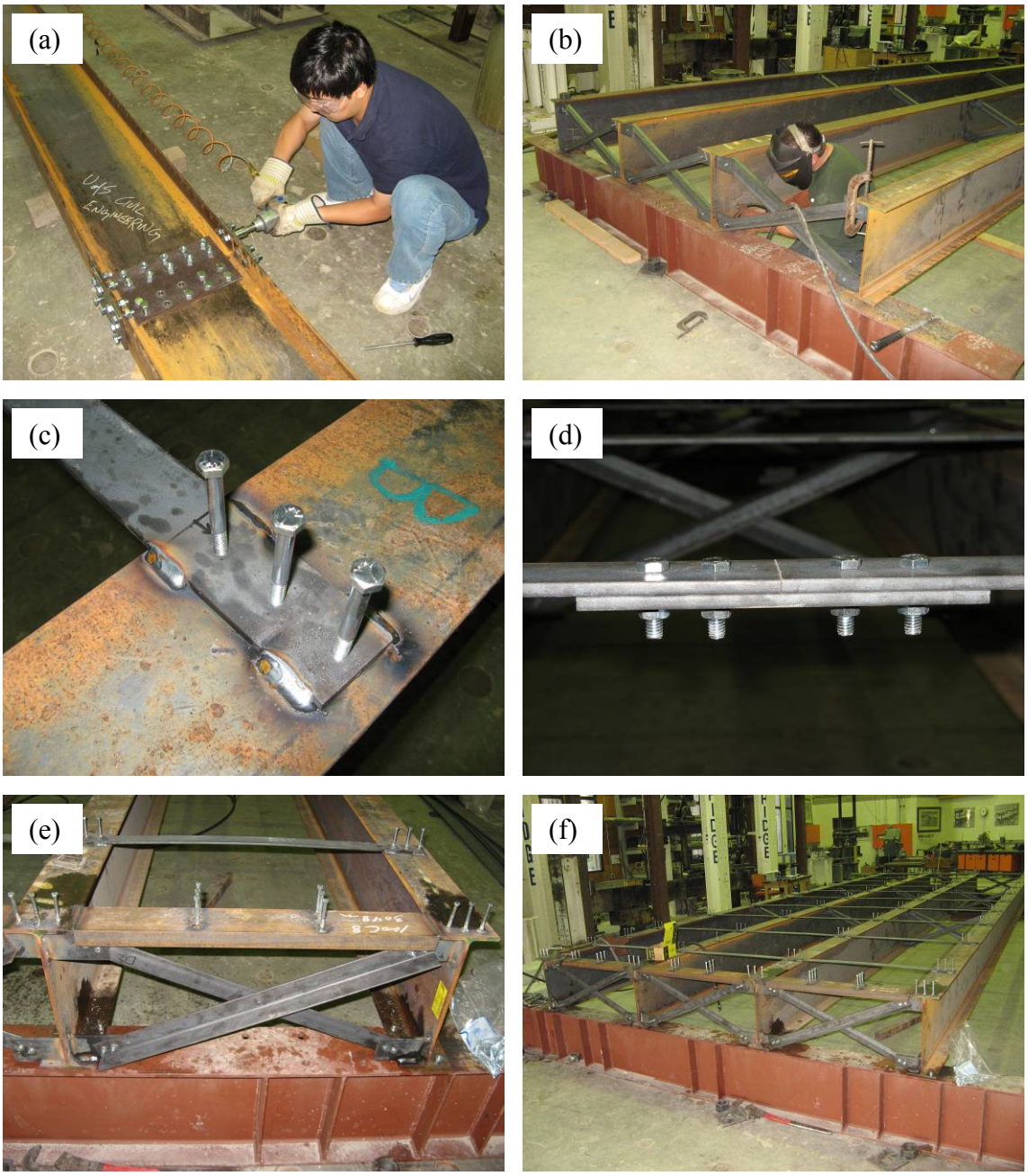

Figure C.1. Fabrication of steel superstructure of the bridge model: (a) bolt connected girder splice, (b) cross bracing diaphragm, (c) shear studs, (d) bolt connected steel strap splice, (e) extra channel member with shear studs at the end of the girders, and (f) the fabricated whole steel superstructure.

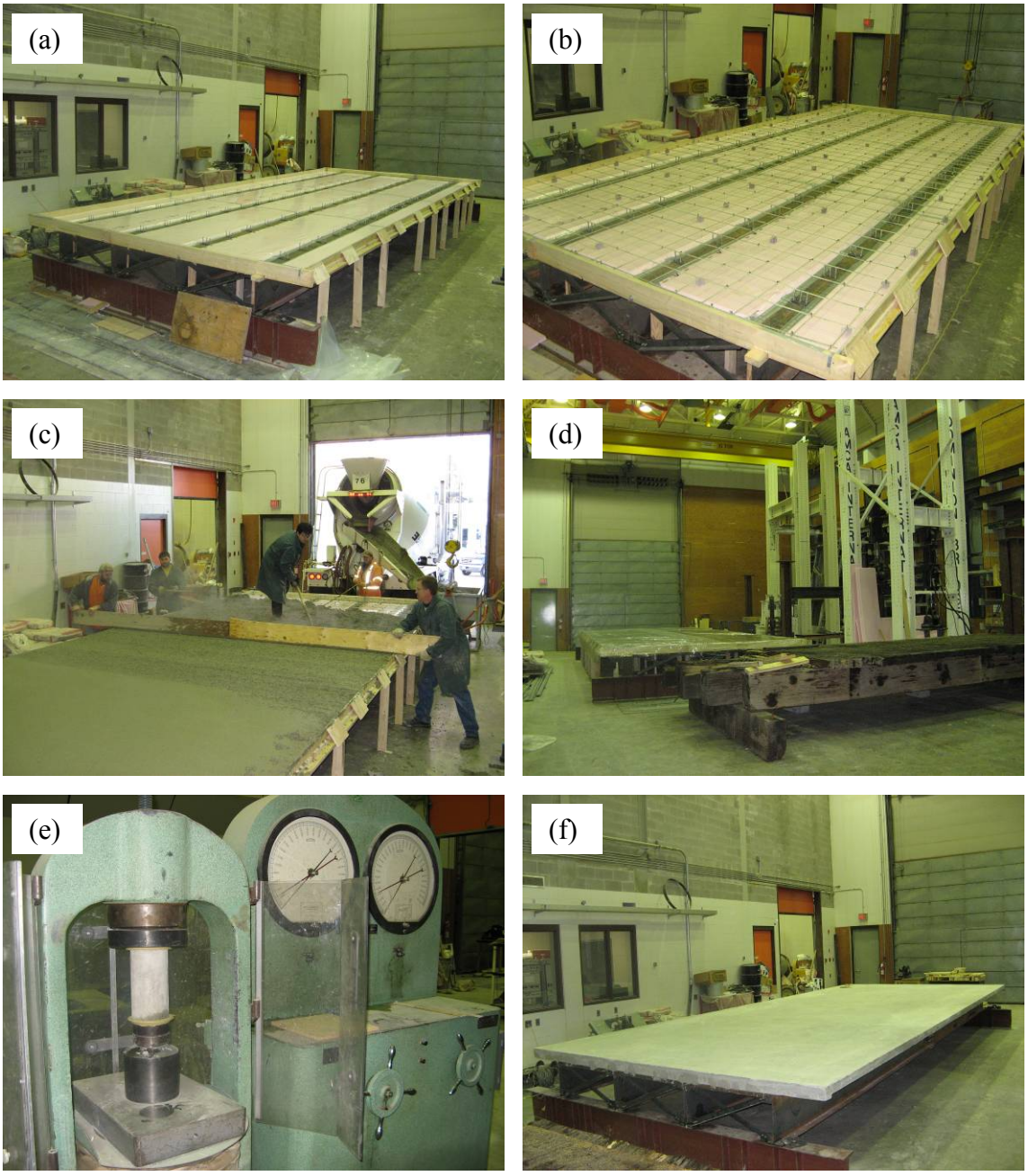

Figure C.2. Construction of the concrete deck of the bridge model: (a) formwork, (b) FRP rebars, (c) pouring concrete, (d) curing concrete, (e) testing a concrete cylinder, and (f) the finished composite bridge model.

APPENDIX D. **ADDITIONAL INFORMATION FOR INFLUENCE OF TEST PARAMETERS ON DYNAMIC PROPERTIES**

This appendix presents additional information for the influence of test parameters on dynamic properties. Specifically, results for the influence of excitation type on mode shape reliability and repeatability are presented based on averaged MAC values using bottom, middle, and top strain gauge data from five replicate trials, which supplies additional information for Section 4.3.3.

Table D.1. Influence of excitation type on mode shape reliability based on averaged MAC values using bottom strain gauge data from five replicate trials.

Excitation		Mode 1	Mode 2	Mode 3	Mode 4	Mode 5
White Noise	Avg.	0.9998726	0.9977945	0.9991574	0.9940285	0.9982590
	C.O.V.	0.00662%	0.13401%	0.03676%	0.32077%	0.13412%
Harmonic	Avg.	0.9999996	0.9999970	0.9997925	0.9995726	0.9995963
	C.O.V.	0.00003%	0.00023%	0.01783%	0.02842%	0.02049%

Avg. = Average;
C.O.V. = Coefficient of variation.

Table D.2. Influence of excitation type on mode shape reliability based on averaged MAC values using middle strain gauge data from five replicate trials.

Excitation		Mode 1	Mode 2	Mode 3	Mode 4	Mode 5
White Noise	Avg.	0.9994881	0.9939806	0.9991072	0.9936696	0.9977089
	C.O.V.	0.04697%	0.50404%	0.04621%	0.34150%	0.15767%
Harmonic	Avg.	0.9999989	0.9999921	0.9998106	0.9970549	0.9990439
	C.O.V.	0.00004%	0.00038%	0.01404%	0.19892%	0.08378%

Avg. = Average;
C.O.V. = Coefficient of variation.

Table D.3. Influence of excitation type on mode shape reliability based on averaged MAC values using top strain gauge data from five replicate trials.

Excitation		Mode 1	Mode 2	Mode 3	Mode 4	Mode 5
White Noise	Avg.	0.9992558	0.9850748	0.9987266	0.9899599	0.9956863
	C.O.V.	0.04638%	1.11304%	0.07789%	0.65779%	0.18205%
Harmonic	Avg.	0.9999984	0.9999757	0.9984081	0.9333263	0.9900844
	C.O.V.	0.00010%	0.00087%	0.06939%	3.19241%	0.70144%

Avg. = Average;
C.O.V. = Coefficient of variation.

APPENDIX E. **EVALUATION OF EXTRACTED DYNAMIC PROPERTIES**

This appendix presents additional information for Chapter 4. Specifically, Tables E.1 to E.16 present the lowest five natural frequencies of the bridge model in Health States 2 to 17, extracted from the accelerometer data in five trials, as obtained using the white noise random excitation, which supplies additional information for Table 4.1.

Tables E.17 to E.32 present the lowest five natural frequencies of the bridge model in Health States 2 to 17, extracted from the strain gauge data in five trials, as obtained using the white noise random excitation, which supplies additional information for Table 4.2.

Figure E.1 presents exactly the same mode shapes as presented in Fig. 4.10. However, a different figure style was used for this figure to understand the mode shapes better.

Figures E.2 to E.13 present additional information for Section 4.2.4, including comparisons of the measured mode shapes in different health states using white noise random excitation, strain gauge data, and higher modes.

Table E.1. Measured natural frequencies using accelerometers for Health State 2.

Trials	Setups	Measured natural frequency (Hz)				
		Mode 1	Mode 2	Mode 3	Mode 4	Mode 5
Trial 1	Set 1_1	12.628	13.718	34.450	35.677	38.701
	Set 2_1	12.650	13.720	34.505	35.734	38.600
	Set 3_1	12.634	13.699	34.470	35.616	38.598
	Set 4_1	12.622	13.713	34.499	35.663	38.652
	Set 5_1	12.630	13.708	34.603	35.793	38.681
	Average (Hz)	12.633	13.712	34.506	35.697	38.646
Trial 2	Set 1_2	12.631	13.720	34.465	35.650	38.614
	Set 2_2	12.628	13.712	34.543	35.616	38.672
	Set 3_2	12.624	13.707	34.450	35.602	38.575
	Set 4_2	12.623	13.709	34.491	35.621	38.727
	Set 5_2	12.620	13.715	34.624	35.759	38.728
	Average (Hz)	12.625	13.713	34.515	35.650	38.663
Trial 3	Set 1_3	12.629	13.720	34.522	35.750	38.656
	Set 2_3	12.623	13.719	34.537	35.693	38.638
	Set 3_3	12.633	13.696	34.482	35.610	38.577
	Set 4_3	12.626	13.708	34.500	35.653	38.662
	Set 5_3	12.625	13.709	34.581	35.769	38.663
	Average (Hz)	12.627	13.710	34.524	35.695	38.639
Trial 4	Set 1_4	12.608	13.704	34.501	35.664	38.592
	Set 2_4	12.629	13.710	34.506	35.705	38.620
	Set 3_4	12.615	13.692	34.472	35.674	38.644
	Set 4_4	12.616	13.692	34.518	35.653	38.615
	Set 5_4	12.634	13.718	34.601	35.744	38.675
	Average (Hz)	12.620	13.703	34.520	35.688	38.629
Trial 5	Set 1_5	12.629	13.710	34.504	35.708	38.700
	Set 2_5	12.621	13.700	34.498	35.720	38.677
	Set 3_5	12.626	13.694	34.507	35.690	38.654
	Set 4_5	12.630	13.707	34.501	35.661	38.683
	Set 5_5	12.623	13.712	34.594	35.700	38.603
	Average (Hz)	12.626	13.704	34.521	35.696	38.664
All Data	Average (Hz)	12.626	13.708	34.517	35.685	38.648
	STDEV (Hz)	0.008	0.009	0.049	0.053	0.044
	C.O.V.	0.06%	0.06%	0.14%	0.15%	0.11%

STDEV = Standard deviation;
C.O.V. = Coefficient of variation.

Table E.2. Measured natural frequencies using accelerometers for Health State 3.

Trials	Setups	Measured natural frequency (Hz)				
		Mode 1	Mode 2	Mode 3	Mode 4	Mode 5
Trial 1	Set 1_1	12.602	13.700	30.027	34.176	38.681
	Set 2_1	12.628	13.712	30.100	34.159	38.622
	Set 3_1	12.605	13.687	30.082	34.102	38.569
	Set 4_1	12.631	13.744	30.097	34.210	38.753
	Set 5_1	12.612	13.677	30.067	34.080	38.581
	Average (Hz)	12.615	13.704	30.075	34.146	38.641
Trial 2	Set 1_2	12.590	13.709	30.094	34.109	38.676
	Set 2_2	12.607	13.696	30.096	34.143	38.690
	Set 3_2	12.623	13.694	30.088	34.098	38.324
	Set 4_2	12.624	13.730	30.152	34.222	38.711
	Set 5_2	12.612	13.676	30.082	34.094	38.624
	Average (Hz)	12.611	13.701	30.102	34.133	38.605
Trial 3	Set 1_3	12.624	13.705	30.064	34.168	38.732
	Set 2_3	12.607	13.688	30.047	34.116	38.788
	Set 3_3	12.608	13.690	30.066	34.125	38.606
	Set 4_3	12.597	13.740	30.159	34.249	38.692
	Set 5_3	12.595	13.683	30.055	34.133	38.553
	Average (Hz)	12.606	13.701	30.078	34.158	38.674
Trial 4	Set 1_4	12.606	13.728	30.089	34.138	38.748
	Set 2_4	12.603	13.697	30.085	34.156	38.631
	Set 3_4	12.596	13.707	30.064	34.131	38.504
	Set 4_4	12.625	13.737	30.135	34.199	38.636
	Set 5_4	12.607	13.682	30.053	34.169	38.555
	Average (Hz)	12.607	13.711	30.085	34.159	38.615
Trial 5	Set 1_5	12.615	13.702	30.104	34.165	38.514
	Set 2_5	12.607	13.694	30.085	34.122	38.676
	Set 3_5	12.600	13.695	30.042	34.137	38.512
	Set 4_5	12.617	13.729	30.133	34.250	38.573
	Set 5_5	12.601	13.680	30.036	34.141	38.592
	Average (Hz)	12.608	13.700	30.080	34.163	38.573
All Data	Average (Hz)	12.610	13.703	30.084	34.152	38.622
	STDEV (Hz)	0.011	0.021	0.034	0.046	0.101
	C.O.V.	0.09%	0.15%	0.11%	0.13%	0.26%

STDEV = Standard deviation;
C.O.V. = Coefficient of variation.

Table E.3. Measured natural frequencies using accelerometers for Health State 4.

Trials	Setups	Measured natural frequency (Hz)				
		Mode 1	Mode 2	Mode 3	Mode 4	Mode 5
Trial 1	Set 1_1	12.604	13.699	29.977	33.863	34.717
	Set 2_1	12.613	13.705	29.996	33.891	35.093
	Set 3_1	12.587	13.686	30.025	33.853	34.951
	Set 4_1	12.603	13.697	29.907	33.881	34.764
	Set 5_1	12.616	13.697	30.013	33.889	34.808
	Average (Hz)	12.605	13.697	29.983	33.875	34.867
Trial 2	Set 1_2	12.619	13.695	29.958	33.889	34.644
	Set 2_2	12.612	13.682	30.019	33.888	35.139
	Set 3_2	12.602	13.697	30.022	33.886	34.838
	Set 4_2	12.585	13.711	29.994	33.863	34.766
	Set 5_2	12.600	13.700	29.900	33.900	34.700
	Average (Hz)	12.603	13.697	29.979	33.885	34.817
Trial 3	Set 1_3	12.605	13.711	29.911	33.838	34.899
	Set 2_3	12.597	13.709	30.000	33.918	35.386
	Set 3_3	12.604	13.695	29.997	33.867	34.861
	Set 4_3	12.621	13.685	29.986	33.889	34.722
	Set 5_3	12.600	13.700	30.100	33.800	34.800
	Average (Hz)	12.605	13.700	29.999	33.863	34.934
Trial 4	Set 1_4	12.598	13.720	30.059	33.858	34.751
	Set 2_4	12.613	13.686	30.007	33.789	35.149
	Set 3_4	12.596	13.724	29.995	33.862	34.801
	Set 4_4	12.610	13.683	30.015	33.798	34.757
	Set 5_4	12.600	13.700	30.000	33.900	34.800
	Average (Hz)	12.604	13.703	30.015	33.842	34.852
Trial 5	Set 1_5	12.606	13.688	30.013	33.954	34.997
	Set 2_5	12.608	13.710	29.971	33.845	35.413
	Set 3_5	12.594	13.699	30.023	33.829	34.933
	Set 4_5	12.623	13.692	30.029	33.888	34.753
	Set 5_5	12.600	13.700	30.000	33.800	34.800
	Average (Hz)	12.606	13.698	30.007	33.863	34.979
All Data	Average (Hz)	12.605	13.699	29.997	33.866	34.890
	STDEV (Hz)	0.010	0.011	0.044	0.040	0.203
	C.O.V.	0.08%	0.08%	0.15%	0.12%	0.58%

STDEV = Standard deviation;
C.O.V. = Coefficient of variation.

Table E.4. Measured natural frequencies using accelerometers for Health State 5.

Trials	Setups	Measured natural frequency (Hz)				
		Mode 1	Mode 2	Mode 3	Mode 4	Mode 5
Trial 1	Set 1_1	12.584	13.713	29.953	34.267	38.611
	Set 2_1	12.595	13.745	29.945	34.357	38.639
	Set 3_1	12.598	13.754	29.931	34.227	38.498
	Set 4_1	12.624	13.815	30.014	34.436	38.877
	Set 5_1	12.604	13.715	29.885	34.224	38.250
	Average (Hz)	12.601	13.749	29.946	34.302	38.575
Trial 2	Set 1_2	12.594	13.742	29.947	34.162	38.504
	Set 2_2	12.607	13.731	29.950	34.321	38.759
	Set 3_2	12.577	13.752	29.926	34.228	38.464
	Set 4_2	12.628	13.802	29.987	34.430	38.934
	Set 5_2	12.581	13.718	29.939	34.222	38.386
	Average (Hz)	12.597	13.749	29.950	34.272	38.609
Trial 3	Set 1_3	12.576	13.747	29.975	34.174	38.597
	Set 2_3	12.591	13.745	29.940	34.294	38.656
	Set 3_3	12.586	13.750	30.009	34.338	38.464
	Set 4_3	12.629	13.798	30.087	34.109	38.944
	Set 5_3	12.582	13.730	29.931	34.145	38.498
	Average (Hz)	12.593	13.754	29.988	34.212	38.632
Trial 4	Set 1_4	12.593	13.735	29.944	34.204	38.455
	Set 2_4	12.605	13.748	29.964	34.244	38.660
	Set 3_4	12.588	13.752	29.984	34.410	38.620
	Set 4_4	12.636	13.798	29.954	34.359	38.735
	Set 5_4	12.597	13.734	29.911	34.195	38.592
	Average (Hz)	12.604	13.753	29.951	34.282	38.612
Trial 5	Set 1_5	12.610	13.747	29.926	34.167	38.534
	Set 2_5	12.596	13.748	29.936	34.288	38.558
	Set 3_5	12.585	13.745	29.950	34.417	38.488
	Set 4_5	12.633	13.799	29.933	34.454	38.814
	Set 5_5	12.573	13.736	29.945	34.217	38.586
	Average (Hz)	12.599	13.755	29.938	34.309	38.596
All Data	Average (Hz)	12.599	13.752	29.955	34.276	38.605
	STDEV (Hz)	0.019	0.028	0.040	0.101	0.168
	C.O.V.	0.15%	0.21%	0.13%	0.29%	0.44%

STDEV = Standard deviation;
C.O.V. = Coefficient of variation.

Table E.5. Measured natural frequencies using accelerometers for Health State 6.

Trials	Setups	Measured natural frequency (Hz)				
		Mode 1	Mode 2	Mode 3	Mode 4	Mode 5
Trial 1	Set 1_1	12.568	13.733	34.022	35.677	38.824
	Set 2_1	12.617	13.762	34.025	35.814	38.928
	Set 3_1	12.590	13.725	34.042	35.711	38.891
	Set 4_1	12.608	13.746	34.043	35.715	38.844
	Set 5_1	12.608	13.789	34.239	35.926	39.074
	Average (Hz)	12.598	13.751	34.074	35.768	38.912
Trial 2	Set 1_2	12.582	13.761	34.090	35.889	38.832
	Set 2_2	12.609	13.749	33.984	35.755	38.941
	Set 3_2	12.595	13.746	33.976	35.667	38.840
	Set 4_2	12.582	13.745	34.097	35.807	38.970
	Set 5_2	12.604	13.799	34.175	35.922	39.103
	Average (Hz)	12.594	13.760	34.064	35.808	38.937
Trial 3	Set 1_3	12.594	13.752	33.959	35.809	38.885
	Set 2_3	12.605	13.750	33.994	35.822	38.869
	Set 3_3	12.600	13.743	33.986	35.782	38.770
	Set 4_3	12.611	13.748	34.190	35.751	38.891
	Set 5_3	12.596	13.779	34.282	35.983	39.030
	Average (Hz)	12.601	13.754	34.082	35.829	38.889
Trial 4	Set 1_4	12.580	13.715	34.078	35.798	38.821
	Set 2_4	12.592	13.741	33.974	35.809	38.869
	Set 3_4	12.603	13.729	34.074	35.743	38.764
	Set 4_4	12.607	13.745	34.119	35.696	38.967
	Set 5_4	12.585	13.806	34.277	35.910	39.145
	Average (Hz)	12.593	13.747	34.104	35.791	38.913
Trial 5	Set 1_5	12.590	13.754	34.016	35.835	38.785
	Set 2_5	12.590	13.768	33.987	35.787	38.783
	Set 3_5	12.588	13.736	34.057	35.750	38.816
	Set 4_5	12.591	13.739	34.106	35.682	38.925
	Set 5_5	12.602	13.794	34.174	35.781	38.966
	Average (Hz)	12.592	13.758	34.068	35.767	38.855
All Data	Average (Hz)	12.596	13.754	34.079	35.793	38.901
	STDEV (Hz)	0.012	0.023	0.096	0.084	0.104
	C.O.V.	0.09%	0.17%	0.28%	0.23%	0.27%

STDEV = Standard deviation;
C.O.V. = Coefficient of variation.

Table E.6. Measured natural frequencies using accelerometers for Health State 7.

Trials	Setups	Measured natural frequency (Hz)				
		Mode 1	Mode 2	Mode 3	Mode 4	Mode 5
Trial 1	Set 1_1	12.555	13.718	33.572	35.749	38.863
	Set 2_1	12.584	13.719	33.696	35.953	38.814
	Set 3_1	12.580	13.729	33.767	35.870	38.812
	Set 4_1	12.598	13.739	33.925	35.951	39.011
	Set 5_1	12.605	13.746	33.662	35.777	38.885
	Average (Hz)	12.584	13.730	33.724	35.860	38.877
Trial 2	Set 1_2	12.592	13.728	33.653	35.742	38.816
	Set 2_2	12.585	13.737	33.773	35.951	38.943
	Set 3_2	12.569	13.715	33.803	35.869	38.904
	Set 4_2	12.593	13.746	33.994	35.880	39.059
	Set 5_2	12.576	13.747	33.619	35.670	38.842
	Average (Hz)	12.583	13.735	33.768	35.822	38.913
Trial 3	Set 1_3	12.600	13.723	33.633	35.709	38.888
	Set 2_3	12.573	13.730	33.803	35.861	38.830
	Set 3_3	12.553	13.726	33.803	35.896	38.920
	Set 4_3	12.587	13.762	33.942	35.940	39.020
	Set 5_3	12.587	13.744	33.664	35.802	38.983
	Average (Hz)	12.580	13.737	33.769	35.841	38.928
Trial 4	Set 1_4	12.575	13.709	33.600	35.696	38.864
	Set 2_4	12.584	13.740	33.757	35.860	38.848
	Set 3_4	12.583	13.722	33.768	35.893	38.882
	Set 4_4	12.582	13.742	33.957	35.933	39.105
	Set 5_4	12.584	13.735	33.645	35.733	38.899
	Average (Hz)	12.582	13.729	33.745	35.823	38.919
Trial 5	Set 1_5	12.590	13.718	33.615	35.697	38.899
	Set 2_5	12.574	13.733	33.808	35.960	38.969
	Set 3_5	12.588	13.723	33.734	35.892	38.905
	Set 4_5	12.591	13.748	33.988	35.917	39.030
	Set 5_5	12.586	13.732	33.694	35.866	38.990
	Average (Hz)	12.586	13.731	33.768	35.866	38.958
All Data	Average (Hz)	12.583	13.732	33.755	35.843	38.919
	STDEV (Hz)	0.012	0.013	0.127	0.094	0.082
	C.O.V.	0.10%	0.09%	0.37%	0.26%	0.21%

STDEV = Standard deviation;
C.O.V. = Coefficient of variation.

Table E.7. Measured natural frequencies using accelerometers for Health State 8.

Trials	Setups	Measured natural frequency (Hz)				
		Mode 1	Mode 2	Mode 3	Mode 4	Mode 5
Trial 1	Set 1_1	12.565	13.738	31.071	34.496	38.916
	Set 2_1	12.602	13.764	31.036	34.492	38.715
	Set 3_1	12.573	13.752	31.117	34.666	38.762
	Set 4_1	12.588	13.749	31.061	34.810	38.900
	Set 5_1	12.608	13.761	31.095	34.694	38.899
	Average (Hz)	12.587	13.752	31.076	34.632	38.838
Trial 2	Set 1_2	12.582	13.765	31.068	34.611	38.889
	Set 2_2	12.591	13.755	31.010	34.698	38.765
	Set 3_2	12.574	13.730	31.053	34.672	38.797
	Set 4_2	12.591	13.758	31.064	34.868	38.990
	Set 5_2	12.581	13.735	31.107	34.760	38.919
	Average (Hz)	12.584	13.749	31.061	34.722	38.872
Trial 3	Set 1_3	12.574	13.718	31.108	34.666	38.817
	Set 2_3	12.594	13.752	31.052	34.573	38.694
	Set 3_3	12.597	13.762	30.992	34.759	38.729
	Set 4_3	12.590	13.774	31.142	34.821	39.130
	Set 5_3	12.593	13.767	31.051	34.656	38.881
	Average (Hz)	12.590	13.754	31.069	34.695	38.850
Trial 4	Set 1_4	12.566	13.756	31.056	34.710	38.890
	Set 2_4	12.585	13.751	31.093	34.695	38.707
	Set 3_4	12.573	13.756	31.070	34.735	38.679
	Set 4_4	12.567	13.773	31.014	34.837	38.992
	Set 5_4	12.612	13.756	31.113	34.631	38.928
	Average (Hz)	12.581	13.758	31.069	34.722	38.839
Trial 5	Set 1_5	12.585	13.737	31.095	34.606	38.855
	Set 2_5	12.558	13.734	31.062	34.615	38.603
	Set 3_5	12.571	13.753	31.059	34.655	38.692
	Set 4_5	12.573	13.774	31.081	34.827	39.067
	Set 5_5	12.581	13.746	31.090	34.708	38.951
	Average (Hz)	12.574	13.749	31.077	34.682	38.834
All Data	Average (Hz)	12.583	13.753	31.070	34.690	38.847
	STDEV (Hz)	0.014	0.014	0.035	0.098	0.131
	C.O.V.	0.11%	0.10%	0.11%	0.28%	0.34%

STDEV = Standard deviation;
C.O.V. = Coefficient of variation.

Table E.8. Measured natural frequencies using accelerometers for Health State 9.

Trials	Setups	Measured natural frequency (Hz)				
		Mode 1	Mode 2	Mode 3	Mode 4	Mode 5
Trial 1	Set 1_1	12.580	13.703	34.511	35.805	39.006
	Set 2_1	12.592	13.721	34.568	35.981	39.126
	Set 3_1	12.569	13.723	34.620	35.903	39.028
	Set 4_1	12.625	13.763	34.730	35.812	39.183
	Set 5_1	12.585	13.737	34.602	35.845	39.044
	Average (Hz)	12.590	13.729	34.606	35.869	39.077
Trial 2	Set 1_2	12.603	13.700	34.567	35.807	39.056
	Set 2_2	12.604	13.736	34.563	35.795	39.010
	Set 3_2	12.581	13.731	34.539	35.799	39.008
	Set 4_2	12.621	13.754	34.632	35.857	39.218
	Set 5_2	12.582	13.719	34.603	35.772	39.133
	Average (Hz)	12.598	13.728	34.581	35.806	39.085
Trial 3	Set 1_3	12.577	13.702	34.541	35.756	39.057
	Set 2_3	12.591	13.727	34.532	35.867	38.990
	Set 3_3	12.609	13.732	34.527	35.824	38.917
	Set 4_3	12.608	13.770	34.664	35.807	39.279
	Set 5_3	12.616	13.725	34.617	35.686	39.040
	Average (Hz)	12.600	13.731	34.576	35.788	39.057
Trial 4	Set 1_4	12.594	13.716	34.527	35.741	39.070
	Set 2_4	12.582	13.747	34.536	35.896	39.077
	Set 3_4	12.589	13.727	34.542	35.775	38.906
	Set 4_4	12.612	13.735	34.625	35.742	39.281
	Set 5_4	12.597	13.722	34.703	35.785	38.942
	Average (Hz)	12.595	13.730	34.586	35.788	39.055
Trial 5	Set 1_5	12.579	13.711	34.478	35.829	38.984
	Set 2_5	12.603	13.757	34.510	35.905	39.101
	Set 3_5	12.567	13.735	34.494	35.830	39.022
	Set 4_5	12.626	13.763	34.639	35.770	39.175
	Set 5_5	12.589	13.747	34.544	35.756	39.077
	Average (Hz)	12.593	13.743	34.533	35.818	39.072
All Data	Average (Hz)	12.595	13.732	34.577	35.814	39.069
	STDEV (Hz)	0.017	0.019	0.065	0.064	0.100
	C.O.V.	0.13%	0.14%	0.19%	0.18%	0.26%

STDEV = Standard deviation;
C.O.V. = Coefficient of variation.

Table E.9. Measured natural frequencies using accelerometers for Health State 10.

Trials	Setups	Measured natural frequency (Hz)				
		Mode 1	Mode 2	Mode 3	Mode 4	Mode 5
Trial 1	Set 1_1	12.594	13.715	34.538	35.792	39.074
	Set 2_1	12.584	13.710	34.531	35.892	39.071
	Set 3_1	12.583	13.735	34.528	35.834	39.097
	Set 4_1	12.583	13.704	34.487	35.690	39.019
	Set 5_1	12.593	13.720	34.539	35.767	39.019
	Average (Hz)	12.587	13.717	34.525	35.795	39.056
Trial 2	Set 1_2	12.599	13.728	34.478	35.768	39.099
	Set 2_2	12.579	13.712	34.483	35.804	39.051
	Set 3_2	12.581	13.728	34.537	35.842	39.061
	Set 4_2	12.595	13.733	34.554	35.804	39.101
	Set 5_2	12.605	13.722	34.560	35.821	39.089
	Average (Hz)	12.592	13.725	34.523	35.808	39.080
Trial 3	Set 1_3	12.597	13.714	34.504	35.794	38.964
	Set 2_3	12.596	13.700	34.568	35.910	39.011
	Set 3_3	12.594	13.742	34.583	35.974	39.088
	Set 4_3	12.592	13.734	34.446	35.740	39.076
	Set 5_3	12.587	13.726	34.562	35.804	38.993
	Average (Hz)	12.593	13.723	34.532	35.844	39.027
Trial 4	Set 1_4	12.590	13.735	34.513	35.780	39.144
	Set 2_4	12.609	13.725	34.487	35.881	39.086
	Set 3_4	12.590	13.732	34.530	35.806	39.016
	Set 4_4	12.575	13.734	34.462	35.811	39.046
	Set 5_4	12.599	13.734	34.483	35.768	38.962
	Average (Hz)	12.593	13.732	34.495	35.809	39.051
Trial 5	Set 1_5	12.593	13.700	34.559	35.770	39.051
	Set 2_5	12.581	13.725	34.471	35.824	38.908
	Set 3_5	12.583	13.729	34.471	35.780	38.967
	Set 4_5	12.595	13.725	34.554	35.754	39.037
	Set 5_5	12.587	13.736	34.532	35.686	39.016
	Average (Hz)	12.588	13.723	34.517	35.763	38.996
All Data	Average (Hz)	12.591	13.724	34.518	35.804	39.042
	STDEV (Hz)	0.008	0.012	0.038	0.064	0.055
	C.O.V.	0.07%	0.09%	0.11%	0.18%	0.14%

STDEV = Standard deviation;
C.O.V. = Coefficient of variation.

Table E.10. Measured natural frequencies using accelerometers for Health State 11.

Trials	Setups	Measured natural frequency (Hz)				
		Mode 1	Mode 2	Mode 3	Mode 4	Mode 5
Trial 1	Set 1_1	12.580	13.696	34.426	35.788	38.997
	Set 2_1	12.575	13.691	34.442	35.856	38.816
	Set 3_1	12.608	13.730	34.392	35.864	38.763
	Set 4_1	12.577	13.699	34.461	35.789	38.748
	Set 5_1	12.572	13.710	34.433	35.815	38.743
	Average (Hz)	12.582	13.705	34.431	35.822	38.813
Trial 2	Set 1_2	12.570	13.704	34.409	35.773	39.001
	Set 2_2	12.586	13.713	34.320	35.799	38.751
	Set 3_2	12.575	13.723	34.385	35.781	38.807
	Set 4_2	12.584	13.729	34.500	35.860	38.919
	Set 5_2	12.592	13.716	34.405	35.852	38.891
	Average (Hz)	12.581	13.717	34.404	35.813	38.874
Trial 3	Set 1_3	12.583	13.684	34.344	35.699	38.960
	Set 2_3	12.567	13.709	34.409	35.819	38.866
	Set 3_3	12.593	13.718	34.404	35.870	38.850
	Set 4_3	12.572	13.716	34.421	35.755	38.859
	Set 5_3	12.598	13.695	34.422	35.785	38.842
	Average (Hz)	12.583	13.705	34.400	35.786	38.875
Trial 4	Set 1_4	12.593	13.740	34.352	35.765	39.086
	Set 2_4	12.582	13.716	34.367	35.702	38.712
	Set 3_4	12.567	13.694	34.370	35.758	38.704
	Set 4_4	12.574	13.701	34.420	35.743	39.095
	Set 5_4	12.594	13.720	34.341	35.731	38.820
	Average (Hz)	12.582	13.714	34.370	35.740	38.883
Trial 5	Set 1_5	12.572	13.707	34.429	35.804	38.945
	Set 2_5	12.574	13.706	34.315	35.788	38.845
	Set 3_5	12.567	13.720	34.395	35.874	38.806
	Set 4_5	12.579	13.741	34.422	35.767	39.319
	Set 5_5	12.581	13.701	34.417	35.796	38.852
	Average (Hz)	12.575	13.715	34.396	35.806	38.953
All Data	Average (Hz)	12.581	13.711	34.400	35.793	38.880
	STDEV (Hz)	0.011	0.015	0.043	0.050	0.140
	C.O.V.	0.09%	0.11%	0.13%	0.14%	0.36%

STDEV = Standard deviation;
C.O.V. = Coefficient of variation.

Table E.11. Measured natural frequencies using accelerometers for Health State 12.

Trials	Setups	Measured natural frequency (Hz)				
		Mode 1	Mode 2	Mode 3	Mode 4	Mode 5
Trial 1	Set 1_1	12.547	13.694	34.372	35.802	39.041
	Set 2_1	12.577	13.689	34.375	35.869	38.812
	Set 3_1	12.589	13.698	34.388	35.793	38.745
	Set 4_1	12.553	13.667	34.368	35.716	38.887
	Set 5_1	12.580	13.708	34.363	35.773	38.814
	Average (Hz)	12.569	13.691	34.373	35.790	38.860
Trial 2	Set 1_2	12.580	13.698	34.445	35.825	39.063
	Set 2_2	12.585	13.718	34.364	35.803	38.770
	Set 3_2	12.580	13.686	34.385	35.766	38.869
	Set 4_2	12.558	13.693	34.381	35.732	38.835
	Set 5_2	12.570	13.709	34.422	35.731	38.765
	Average (Hz)	12.575	13.700	34.399	35.771	38.860
Trial 3	Set 1_3	12.573	13.699	34.448	35.842	38.870
	Set 2_3	12.569	13.703	34.360	35.841	38.907
	Set 3_3	12.573	13.697	34.429	35.811	38.838
	Set 4_3	12.567	13.679	34.376	35.794	38.830
	Set 5_3	12.574	13.697	34.383	35.852	38.926
	Average (Hz)	12.571	13.695	34.399	35.828	38.874
Trial 4	Set 1_4	12.591	13.705	34.355	35.808	38.859
	Set 2_4	12.557	13.700	34.384	35.826	38.785
	Set 3_4	12.576	13.701	34.357	35.853	38.732
	Set 4_4	12.574	13.692	34.374	35.785	38.843
	Set 5_4	12.599	13.707	34.429	35.810	38.866
	Average (Hz)	12.579	13.701	34.380	35.817	38.817
Trial 5	Set 1_5	12.578	13.699	34.344	35.769	38.810
	Set 2_5	12.586	13.726	34.359	35.818	38.831
	Set 3_5	12.580	13.699	34.366	35.811	38.801
	Set 4_5	12.549	13.708	34.435	35.869	38.748
	Set 5_5	12.579	13.704	34.380	35.779	38.748
	Average (Hz)	12.574	13.707	34.377	35.809	38.788
All Data	Average (Hz)	12.574	13.699	34.386	35.803	38.840
	STDEV (Hz)	0.013	0.012	0.030	0.041	0.082
	C.O.V.	0.10%	0.09%	0.09%	0.11%	0.21%

STDEV = Standard deviation;
C.O.V. = Coefficient of variation.

Table E.12. Measured natural frequencies using accelerometers for Health State 13.

Trials	Setups	Measured natural frequency (Hz)				
		Mode 1	Mode 2	Mode 3	Mode 4	Mode 5
Trial 1	Set 1_1	12.631	13.890	34.252	36.056	38.679
	Set 2_1	12.627	13.903	34.193	36.095	38.571
	Set 3_1	12.628	13.892	34.334	36.131	38.586
	Set 4_1	12.639	13.883	34.359	36.132	38.647
	Set 5_1	12.616	13.863	34.273	36.064	38.547
	Average (Hz)	12.628	13.886	34.282	36.096	38.606
Trial 2	Set 1_2	12.635	13.880	34.345	36.075	38.677
	Set 2_2	12.625	13.880	34.321	36.042	38.563
	Set 3_2	12.632	13.900	34.335	36.090	38.669
	Set 4_2	12.630	13.882	34.312	36.107	38.625
	Set 5_2	12.618	13.887	34.226	36.069	38.509
	Average (Hz)	12.628	13.886	34.308	36.076	38.609
Trial 3	Set 1_3	12.620	13.854	34.342	36.025	38.609
	Set 2_3	12.633	13.894	34.290	36.081	38.563
	Set 3_3	12.628	13.882	34.335	36.111	38.676
	Set 4_3	12.634	13.901	34.285	36.079	38.667
	Set 5_3	12.637	13.872	34.281	36.087	38.640
	Average (Hz)	12.630	13.880	34.307	36.077	38.631
Trial 4	Set 1_4	12.656	13.879	34.315	36.046	38.506
	Set 2_4	12.630	13.896	34.285	36.085	38.604
	Set 3_4	12.636	13.882	34.339	36.095	38.702
	Set 4_4	12.633	13.890	34.331	36.115	38.696
	Set 5_4	12.614	13.877	34.313	36.054	38.609
	Average (Hz)	12.634	13.885	34.317	36.079	38.623
Trial 5	Set 1_5	12.629	13.876	34.291	36.068	38.514
	Set 2_5	12.620	13.886	34.308	36.103	38.620
	Set 3_5	12.651	13.888	34.346	36.103	38.678
	Set 4_5	12.622	13.896	34.305	36.046	38.855
	Set 5_5	12.622	13.885	34.284	36.041	38.600
	Average (Hz)	12.629	13.886	34.307	36.072	38.653
All Data	Average (Hz)	12.630	13.885	34.304	36.080	38.624
	STDEV (Hz)	0.010	0.011	0.039	0.029	0.076
	C.O.V.	0.08%	0.08%	0.12%	0.08%	0.20%

STDEV = Standard deviation;
C.O.V. = Coefficient of variation.

Table E.13. Measured natural frequencies using accelerometers for Health State 14.

Trials	Setups	Measured natural frequency (Hz)				
		Mode 1	Mode 2	Mode 3	Mode 4	Mode 5
Trial 1	Set 1_1	12.633	13.896	34.549	36.018	38.897
	Set 2_1	12.646	13.907	34.508	36.135	38.934
	Set 3_1	12.629	13.917	34.512	36.113	38.837
	Set 4_1	12.623	13.893	34.549	36.115	38.941
	Set 5_1	12.639	13.901	34.491	36.122	38.892
	Average (Hz)	12.634	13.903	34.522	36.101	38.900
Trial 2	Set 1_2	12.641	13.916	34.487	36.084	38.908
	Set 2_2	12.629	13.928	34.486	36.141	38.997
	Set 3_2	12.639	13.925	34.470	36.133	38.865
	Set 4_2	12.632	13.894	34.533	36.095	38.939
	Set 5_2	12.619	13.891	34.508	36.128	38.899
	Average (Hz)	12.632	13.911	34.497	36.116	38.922
Trial 3	Set 1_3	12.640	13.890	34.529	36.090	38.971
	Set 2_3	12.633	13.892	34.536	36.075	38.926
	Set 3_3	12.623	13.901	34.507	36.090	38.849
	Set 4_3	12.637	13.910	34.496	36.021	38.803
	Set 5_3	12.624	13.896	34.447	36.053	38.830
	Average (Hz)	12.631	13.898	34.503	36.066	38.876
Trial 4	Set 1_4	12.637	13.873	34.423	36.064	38.889
	Set 2_4	12.637	13.914	34.476	36.081	38.832
	Set 3_4	12.626	13.916	34.509	36.071	38.733
	Set 4_4	12.625	13.914	34.542	36.101	38.919
	Set 5_4	12.609	13.904	34.492	36.012	38.819
	Average (Hz)	12.627	13.904	34.489	36.066	38.838
Trial 5	Set 1_5	12.652	13.887	34.457	36.127	38.858
	Set 2_5	12.641	13.905	34.540	36.054	38.931
	Set 3_5	12.627	13.884	34.486	36.146	38.980
	Set 4_5	12.633	13.890	34.529	36.062	38.959
	Set 5_5	12.635	13.889	34.511	36.109	38.910
	Average (Hz)	12.638	13.891	34.505	36.100	38.928
All Data	Average (Hz)	12.632	13.901	34.503	36.090	38.893
	STDEV (Hz)	0.009	0.014	0.032	0.039	0.062
	C.O.V.	0.07%	0.10%	0.09%	0.11%	0.16%

STDEV = Standard deviation;
C.O.V. = Coefficient of variation.

Table E.14. Measured natural frequencies using accelerometers for Health State 15.

Trials	Setups	Measured natural frequency (Hz)				
		Mode 1	Mode 2	Mode 3	Mode 4	Mode 5
Trial 1	Set 1_1	12.632	13.910	34.561	36.059	38.994
	Set 2_1	12.624	13.926	34.473	36.072	38.883
	Set 3_1	12.636	13.903	34.478	36.060	38.880
	Set 4_1	12.633	13.903	34.472	36.044	38.820
	Set 5_1	12.613	13.909	34.450	36.104	38.893
	Average (Hz)	12.628	13.910	34.487	36.068	38.894
Trial 2	Set 1_2	12.620	13.872	34.480	36.090	39.044
	Set 2_2	12.625	13.914	34.479	36.073	38.850
	Set 3_2	12.632	13.935	34.528	36.147	38.894
	Set 4_2	12.614	13.880	34.498	36.115	39.018
	Set 5_2	12.639	13.890	34.519	36.126	38.924
	Average (Hz)	12.626	13.898	34.501	36.110	38.946
Trial 3	Set 1_3	12.624	13.946	34.452	36.093	38.959
	Set 2_3	12.631	13.893	34.418	36.050	38.907
	Set 3_3	12.632	13.935	34.528	36.147	38.894
	Set 4_3	12.630	13.871	34.583	36.113	38.931
	Set 5_3	12.616	13.897	34.534	36.132	38.922
	Average (Hz)	12.627	13.908	34.503	36.107	38.923
Trial 4	Set 1_4	12.635	13.902	34.490	36.101	39.013
	Set 2_4	12.635	13.910	34.450	36.080	38.892
	Set 3_4	12.605	13.884	34.490	36.107	38.977
	Set 4_4	12.628	13.896	34.485	36.080	38.891
	Set 5_4	12.617	13.916	34.468	36.084	38.966
	Average (Hz)	12.624	13.902	34.477	36.090	38.948
Trial 5	Set 1_5	12.618	13.864	34.472	36.106	38.981
	Set 2_5	12.614	13.911	34.487	36.127	38.921
	Set 3_5	12.620	13.901	34.437	36.119	38.983
	Set 4_5	12.617	13.860	34.521	36.093	38.811
	Set 5_5	12.618	13.905	34.451	36.129	38.945
	Average (Hz)	12.617	13.888	34.474	36.115	38.928
All Data	Average (Hz)	12.624	13.901	34.488	36.098	38.928
	STDEV (Hz)	0.009	0.022	0.039	0.029	0.060
	C.O.V.	0.07%	0.16%	0.11%	0.08%	0.15%

STDEV = Standard deviation;
C.O.V. = Coefficient of variation.

Table E.15. Measured natural frequencies using accelerometers for Health State 16.

Trials	Setups	Measured natural frequency (Hz)				
		Mode 1	Mode 2	Mode 3	Mode 4	Mode 5
Trial 1	Set 1_1	12.620	13.878	34.543	36.193	38.862
	Set 2_1	12.641	13.909	34.557	36.126	38.872
	Set 3_1	12.601	13.924	34.377	36.106	38.701
	Set 4_1	12.612	13.924	34.526	36.062	38.962
	Set 5_1	12.607	13.898	34.357	36.028	38.635
	Average (Hz)	12.616	13.907	34.472	36.103	38.806
Trial 2	Set 1_2	12.595	13.883	34.435	36.072	38.719
	Set 2_2	12.610	13.928	34.495	36.167	38.912
	Set 3_2	12.618	13.895	34.577	36.110	38.777
	Set 4_2	12.617	13.918	34.484	36.068	38.885
	Set 5_2	12.633	13.918	34.370	36.022	38.727
	Average (Hz)	12.615	13.908	34.472	36.088	38.804
Trial 3	Set 1_3	12.608	13.920	34.580	36.096	39.021
	Set 2_3	12.625	13.932	34.491	36.284	38.923
	Set 3_3	12.610	13.905	34.424	36.121	38.766
	Set 4_3	12.607	13.909	34.505	36.053	38.962
	Set 5_3	12.623	13.900	34.448	36.122	38.696
	Average (Hz)	12.615	13.913	34.490	36.135	38.874
Trial 4	Set 1_4	12.609	13.880	34.570	36.076	38.954
	Set 2_4	12.626	13.898	34.504	36.183	38.963
	Set 3_4	12.605	13.901	34.561	36.124	38.729
	Set 4_4	12.623	13.914	34.435	36.053	38.943
	Set 5_4	12.598	13.894	34.486	36.056	38.741
	Average (Hz)	12.612	13.898	34.511	36.098	38.866
Trial 5	Set 1_5	12.635	13.902	34.556	36.188	39.019
	Set 2_5	12.645	13.917	34.502	36.256	38.909
	Set 3_5	12.607	13.916	34.460	36.155	38.747
	Set 4_5	12.615	13.913	34.474	36.065	38.829
	Set 5_5	12.623	13.905	34.417	36.080	38.662
	Average (Hz)	12.625	13.911	34.482	36.149	38.833
All Data	Average (Hz)	12.616	13.907	34.485	36.115	38.837
	STDEV (Hz)	0.013	0.014	0.066	0.067	0.118
	C.O.V.	0.10%	0.10%	0.19%	0.19%	0.30%

STDEV = Standard deviation;
C.O.V. = Coefficient of variation.

Table E.16. Measured natural frequencies using accelerometers for Health State 17.

Trials	Setups	Measured natural frequency (Hz)				
		Mode 1	Mode 2	Mode 3	Mode 4	Mode 5
Trial 1	Set 1_1	12.602	13.924	34.457	36.055	38.968
	Set 2_1	12.631	13.900	34.491	36.084	38.805
	Set 3_1	12.594	13.895	34.555	36.093	38.896
	Set 4_1	12.604	13.905	34.490	36.070	38.876
	Set 5_1	12.605	13.897	34.498	36.102	38.980
	Average (Hz)	12.607	13.904	34.498	36.081	38.905
Trial 2	Set 1_2	12.597	13.915	34.458	36.059	38.924
	Set 2_2	12.620	13.911	34.486	36.032	38.825
	Set 3_2	12.607	13.907	34.490	36.066	38.798
	Set 4_2	12.602	13.901	34.496	36.058	38.953
	Set 5_2	12.600	13.900	34.600	36.200	38.800
	Average (Hz)	12.605	13.907	34.506	36.083	38.860
Trial 3	Set 1_3	12.632	13.921	34.554	35.974	39.001
	Set 2_3	12.598	13.904	34.509	36.078	38.842
	Set 3_3	12.614	13.906	34.491	36.099	38.866
	Set 4_3	12.617	13.885	34.462	36.017	38.813
	Set 5_3	12.613	13.917	34.495	36.068	38.909
	Average (Hz)	12.615	13.907	34.502	36.047	38.886
Trial 4	Set 1_4	12.621	13.898	34.537	36.045	38.975
	Set 2_4	12.620	13.896	34.433	36.134	38.853
	Set 3_4	12.643	13.909	34.424	36.053	38.833
	Set 4_4	12.607	13.899	34.485	36.137	38.845
	Set 5_4	12.617	13.897	34.565	36.179	38.947
	Average (Hz)	12.622	13.900	34.489	36.110	38.891
Trial 5	Set 1_5	12.617	13.868	34.565	35.967	39.031
	Set 2_5	12.601	13.883	34.473	36.151	38.857
	Set 3_5	12.628	13.911	34.498	36.095	38.757
	Set 4_5	12.614	13.899	34.410	36.038	38.813
	Set 5_5	12.622	13.896	34.534	36.127	38.862
	Average (Hz)	12.617	13.891	34.496	36.076	38.864
All Data	Average (Hz)	12.613	13.902	34.498	36.079	38.881
	STDEV (Hz)	0.012	0.012	0.047	0.056	0.073
	C.O.V.	0.10%	0.09%	0.13%	0.15%	0.19%

STDEV = Standard deviation;
C.O.V. = Coefficient of variation.

Table E.17. Measured natural frequencies using strain gauges for Health State 2.

	Measured natural frequency (Hz)				
Trials	Mode 1	Mode 2	Mode 3	Mode 4	Mode 5
Trial 1	12.657	13.910	34.627	36.250	38.644
Trial 2	12.712	13.807	34.770	36.043	38.745
Trial 3	12.670	13.910	34.725	36.971	38.861
Trial 4	12.691	13.921	34.683	35.820	38.739
Trial 5	12.651	14.039	34.724	36.306	38.462
Average (Hz)	12.676	13.917	34.706	36.278	38.690
STDEV (Hz)	0.025	0.082	0.054	0.432	0.149
C.O.V.	0.20%	0.59%	0.15%	1.19%	0.38%

STDEV = Standard deviation;
C.O.V. = Coefficient of variation.

Table E.18. Measured natural frequencies using strain gauges for Health State 3.

	Measured natural frequency (Hz)				
Trials	Mode 1	Mode 2	Mode 3	Mode 4	Mode 5
Trial 1	12.659	13.909	34.149	37.967	38.820
Trial 2	12.687	13.664	34.171	35.507	38.785
Trial 3	12.708	13.890	34.154	38.805	38.840
Trial 4	12.672	13.871	34.154	38.829	38.869
Trial 5	12.716	13.884	34.138	36.884	38.721
Average (Hz)	12.688	13.844	34.153	37.598	38.807
STDEV (Hz)	0.024	0.102	0.012	1.413	0.057
C.O.V.	0.19%	0.73%	0.04%	3.76%	0.15%

STDEV = Standard deviation;
C.O.V. = Coefficient of variation.

Table E.19. Measured natural frequencies using strain gauges for Health State 4.

	Measured natural frequency (Hz)				
Trials	Mode 1	Mode 2	Mode 3	Mode 4	Mode 5
Trial 1	12.684	13.814	34.043	36.633	38.634
Trial 2	12.695	13.880	33.977	37.380	38.599
Trial 3	12.692	13.811	34.007	36.887	38.596
Trial 4	12.710	13.863	33.997	36.434	38.624
Trial 5	12.672	13.782	34.003	36.982	38.647
Average (Hz)	12.691	13.830	34.005	36.863	38.620
STDEV (Hz)	0.014	0.040	0.024	0.360	0.022
C.O.V.	0.11%	0.29%	0.07%	0.98%	0.06%

STDEV = Standard deviation;
C.O.V. = Coefficient of variation.

Table E.20. Measured natural frequencies using strain gauges for Health State 5.

	Measured natural frequency (Hz)				
Trials	Mode 1	Mode 2	Mode 3	Mode 4	Mode 5
Trial 1	12.646	13.917	34.148	35.686	39.440
Trial 2	12.659	13.963	34.081	35.155	39.510
Trial 3	12.623	13.894	34.047	35.139	39.490
Trial 4	12.651	14.024	34.075	35.943	39.535
Trial 5	12.645	13.966	34.044	35.956	38.485
Average (Hz)	12.645	13.953	34.079	35.576	39.292
STDEV (Hz)	0.013	0.050	0.042	0.406	0.453
C.O.V.	0.11%	0.36%	0.12%	1.14%	1.15%

STDEV = Standard deviation;
C.O.V. = Coefficient of variation.

Table E.21. Measured natural frequencies using strain gauges for Health State 6.

	Measured natural frequency (Hz)				
Trials	Mode 1	Mode 2	Mode 3	Mode 4	Mode 5
Trial 1	12.637	13.866	33.667	35.807	38.820
Trial 2	12.636	13.855	33.704	35.970	38.826
Trial 3	12.642	13.997	33.571	35.814	38.859
Trial 4	12.615	13.811	33.784	35.760	38.677
Trial 5	12.625	14.021	33.726	35.843	38.669
Average (Hz)	12.631	13.910	33.690	35.839	38.770
STDEV (Hz)	0.011	0.093	0.079	0.079	0.090
C.O.V.	0.09%	0.67%	0.23%	0.22%	0.23%

STDEV = Standard deviation;
C.O.V. = Coefficient of variation.

Table E.22. Measured natural frequencies using strain gauges for Health State 7.

	Measured natural frequency (Hz)				
Trials	Mode 1	Mode 2	Mode 3	Mode 4	Mode 5
Trial 1	12.624	14.108	33.178	36.095	39.154
Trial 2	12.754	13.970	33.097	35.941	39.246
Trial 3	12.704	13.966	33.381	35.903	39.134
Trial 4	12.623	13.920	33.399	35.969	39.227
Trial 5	12.664	13.864	33.117	36.020	39.183
Average (Hz)	12.674	13.966	33.235	35.985	39.189
STDEV (Hz)	0.056	0.090	0.145	0.075	0.047
C.O.V.	0.44%	0.65%	0.44%	0.21%	0.12%

STDEV = Standard deviation;
C.O.V. = Coefficient of variation.

Table E.23. Measured natural frequencies using strain gauges for Health State 8.

	Measured natural frequency (Hz)				
Trials	Mode 1	Mode 2	Mode 3	Mode 4	Mode 5
Trial 1	12.652	14.164	31.203	34.060	38.938
Trial 2	12.674	13.952	31.235	34.722	38.922
Trial 3	12.639	13.998	31.228	35.801	38.844
Trial 4	12.647	13.764	31.216	34.416	38.971
Trial 5	12.681	14.012	31.230	34.394	38.938
Average (Hz)	12.658	13.978	31.222	34.679	38.922
STDEV (Hz)	0.018	0.144	0.013	0.670	0.047
C.O.V.	0.14%	1.03%	0.04%	1.93%	0.12%

STDEV = Standard deviation;
C.O.V. = Coefficient of variation.

Table E.24. Measured natural frequencies using strain gauges for Health State 9.

	Measured natural frequency (Hz)				
Trials	Mode 1	Mode 2	Mode 3	Mode 4	Mode 5
Trial 1	12.735	13.900	34.853	36.265	38.560
Trial 2	12.728	14.068	34.863	36.067	38.772
Trial 3	12.702	13.918	34.707	36.214	38.618
Trial 4	12.689	14.053	34.815	36.269	38.695
Trial 5	12.651	13.912	34.658	36.286	38.711
Average (Hz)	12.701	13.970	34.779	36.220	38.671
STDEV (Hz)	0.034	0.083	0.092	0.090	0.083
C.O.V.	0.26%	0.59%	0.26%	0.25%	0.21%

STDEV = Standard deviation;
C.O.V. = Coefficient of variation.

Table E.25. Measured natural frequencies using strain gauges for Health State 10.

	Measured natural frequency (Hz)				
Trials	Mode 1	Mode 2	Mode 3	Mode 4	Mode 5
Trial 1	12.698	14.154	34.443	36.410	38.656
Trial 2	12.642	13.809	34.418	36.717	38.870
Trial 3	12.695	14.044	34.619	37.271	39.281
Trial 4	12.690	13.822	34.587	36.574	39.161
Trial 5	12.645	14.190	34.608	36.027	39.127
Average (Hz)	12.674	14.004	34.535	36.600	39.019
STDEV (Hz)	0.028	0.180	0.096	0.455	0.253
C.O.V.	0.22%	1.29%	0.28%	1.24%	0.65%

STDEV = Standard deviation;
C.O.V. = Coefficient of variation.

Table E.26. Measured natural frequencies using strain gauges for Health State 11.

	Measured natural frequency (Hz)				
Trials	Mode 1	Mode 2	Mode 3	Mode 4	Mode 5
Trial 1	12.628	13.863	34.269	35.974	39.103
Trial 2	12.671	14.089	34.177	36.041	39.173
Trial 3	12.645	13.846	34.266	36.074	39.215
Trial 4	12.659	13.805	34.123	35.996	39.207
Trial 5	12.731	13.985	34.248	36.206	39.122
Average (Hz)	12.667	13.917	34.216	36.058	39.164
STDEV (Hz)	0.040	0.117	0.064	0.091	0.050
C.O.V.	0.31%	0.84%	0.19%	0.25%	0.13%

STDEV = Standard deviation;
C.O.V. = Coefficient of variation.

Table E.27. Measured natural frequencies using strain gauges for Health State 12.

	Measured natural frequency (Hz)				
Trials	Mode 1	Mode 2	Mode 3	Mode 4	Mode 5
Trial 1	12.717	14.003	34.361	36.266	39.197
Trial 2	12.679	14.001	34.253	36.031	39.224
Trial 3	12.681	14.022	34.391	36.121	39.247
Trial 4	12.717	14.129	34.361	36.192	39.372
Trial 5	12.646	13.923	34.200	36.249	39.217
Average (Hz)	12.688	14.016	34.313	36.172	39.251
STDEV (Hz)	0.030	0.074	0.082	0.097	0.070
C.O.V.	0.24%	0.53%	0.24%	0.27%	0.18%

STDEV = Standard deviation;
C.O.V. = Coefficient of variation.

Table E.28. Measured natural frequencies using strain gauges for Health State 13.

	Measured natural frequency (Hz)				
Trials	Mode 1	Mode 2	Mode 3	Mode 4	Mode 5
Trial 1	12.722	14.749	33.983	36.053	38.711
Trial 2	12.725	14.569	33.845	36.203	38.905
Trial 3	12.757	14.302	33.805	36.114	38.635
Trial 4	12.773	14.919	34.032	36.192	38.685
Trial 5	12.721	14.334	33.644	36.163	38.541
Average (Hz)	12.740	14.575	33.862	36.145	38.695
STDEV (Hz)	0.024	0.265	0.154	0.062	0.134
C.O.V.	0.19%	1.82%	0.45%	0.17%	0.35%

STDEV = Standard deviation;
C.O.V. = Coefficient of variation.

Table E.29. Measured natural frequencies using strain gauges for Health State 14.

	Measured natural frequency (Hz)				
Trials	Mode 1	Mode 2	Mode 3	Mode 4	Mode 5
Trial 1	12.739	14.320	34.317	36.200	38.876
Trial 2	12.811	14.495	34.206	36.225	38.758
Trial 3	12.840	13.998	33.879	36.212	38.778
Trial 4	12.750	14.092	34.154	36.165	38.741
Trial 5	12.818	14.655	34.059	36.199	38.629
Average (Hz)	12.792	14.312	34.123	36.200	38.757
STDEV (Hz)	0.045	0.273	0.165	0.022	0.088
C.O.V.	0.35%	1.91%	0.48%	0.06%	0.23%

STDEV = Standard deviation;
C.O.V. = Coefficient of variation.

Table E.30. Measured natural frequencies using strain gauges for Health State 15.

	Measured natural frequency (Hz)				
Trials	Mode 1	Mode 2	Mode 3	Mode 4	Mode 5
Trial 1	12.815	13.970	34.220	36.229	38.705
Trial 2	12.756	15.158	34.327	36.199	38.730
Trial 3	12.756	14.426	34.202	36.147	38.545
Trial 4	12.762	14.739	34.232	36.419	38.639
Trial 5	12.761	14.292	33.976	36.098	38.720
Average (Hz)	12.770	14.517	34.191	36.218	38.668
STDEV (Hz)	0.025	0.452	0.130	0.123	0.077
C.O.V.	0.20%	3.11%	0.38%	0.34%	0.20%

STDEV = Standard deviation;
C.O.V. = Coefficient of variation.

Table E.31. Measured natural frequencies using strain gauges for Health State 16.

	Measured natural frequency (Hz)				
Trials	Mode 1	Mode 2	Mode 3	Mode 4	Mode 5
Trial 1	12.717	14.484	34.423	36.576	39.077
Trial 2	12.690	14.612	34.246	36.375	38.860
Trial 3	12.751	14.582	34.393	36.537	39.052
Trial 4	12.713	15.027	34.169	36.404	38.992
Trial 5	12.729	15.174	34.309	36.381	39.038
Average (Hz)	12.720	14.776	34.308	36.455	39.004
STDEV (Hz)	0.022	0.305	0.104	0.095	0.086
C.O.V.	0.18%	2.06%	0.30%	0.26%	0.22%

STDEV = Standard deviation;
C.O.V. = Coefficient of variation.

Table E.32. Measured natural frequencies using strain gauges for Health State 17.

	Measured natural frequency (Hz)				
Trials	Mode 1	Mode 2	Mode 3	Mode 4	Mode 5
Trial 1	12.731	14.353	34.463	36.267	38.881
Trial 2	12.719	14.044	34.091	36.180	38.567
Trial 3	12.710	14.229	34.072	36.179	38.827
Trial 4	12.734	14.470	34.505	36.336	38.755
Trial 5	12.769	14.578	34.174	36.336	38.937
Average (Hz)	12.733	14.335	34.261	36.260	38.793
STDEV (Hz)	0.022	0.208	0.208	0.079	0.143
C.O.V.	0.17%	1.45%	0.61%	0.22%	0.37%

STDEV = Standard deviation;
C.O.V. = Coefficient of variation.

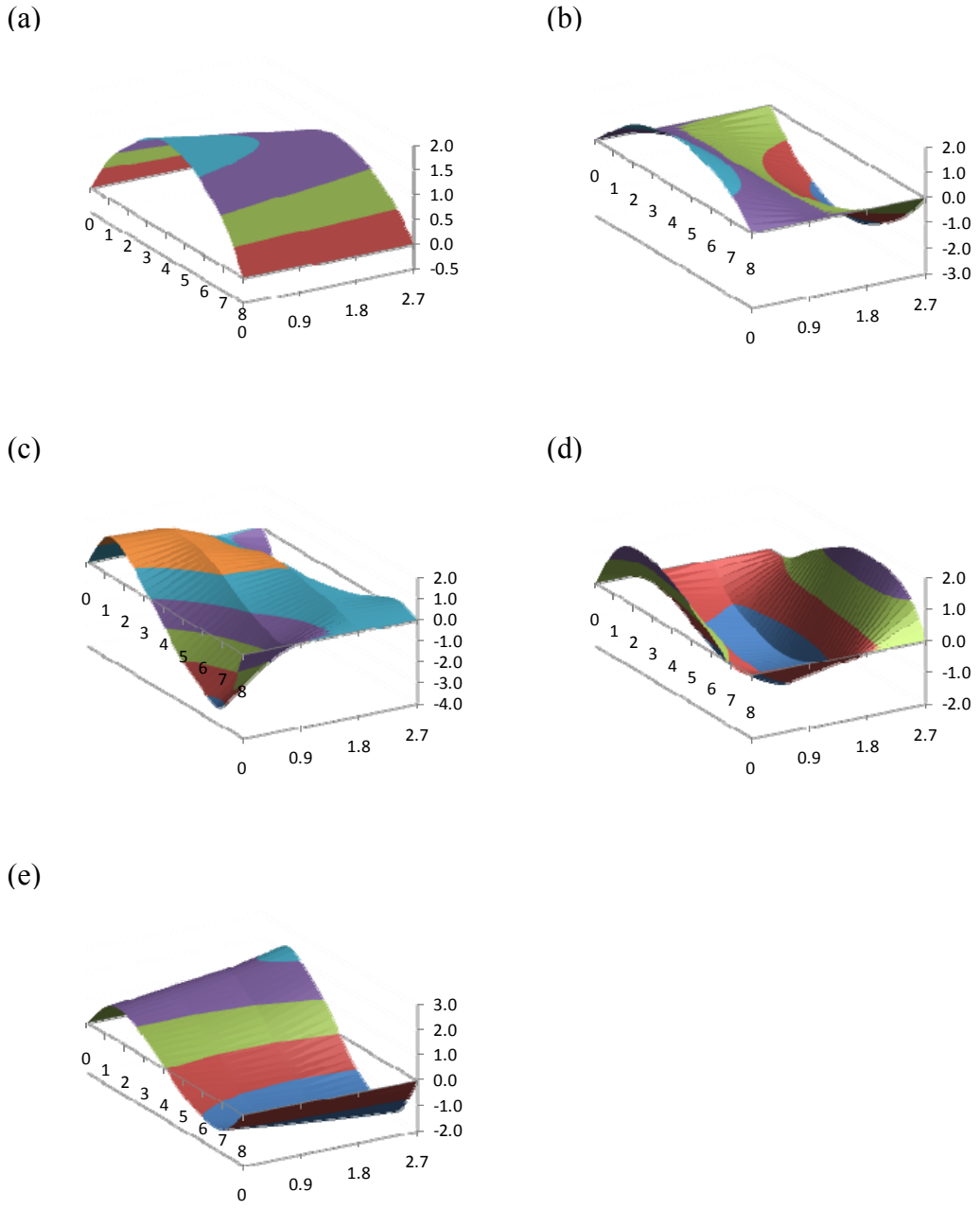

Figure E.1. The lowest five vibration mode shapes for Health State 1 based on accelerometer data with white noise random excitation: (a) Mode 1, (b) Mode 2, (c) Mode 3, (d) Mode 4, and (e) Mode 5.

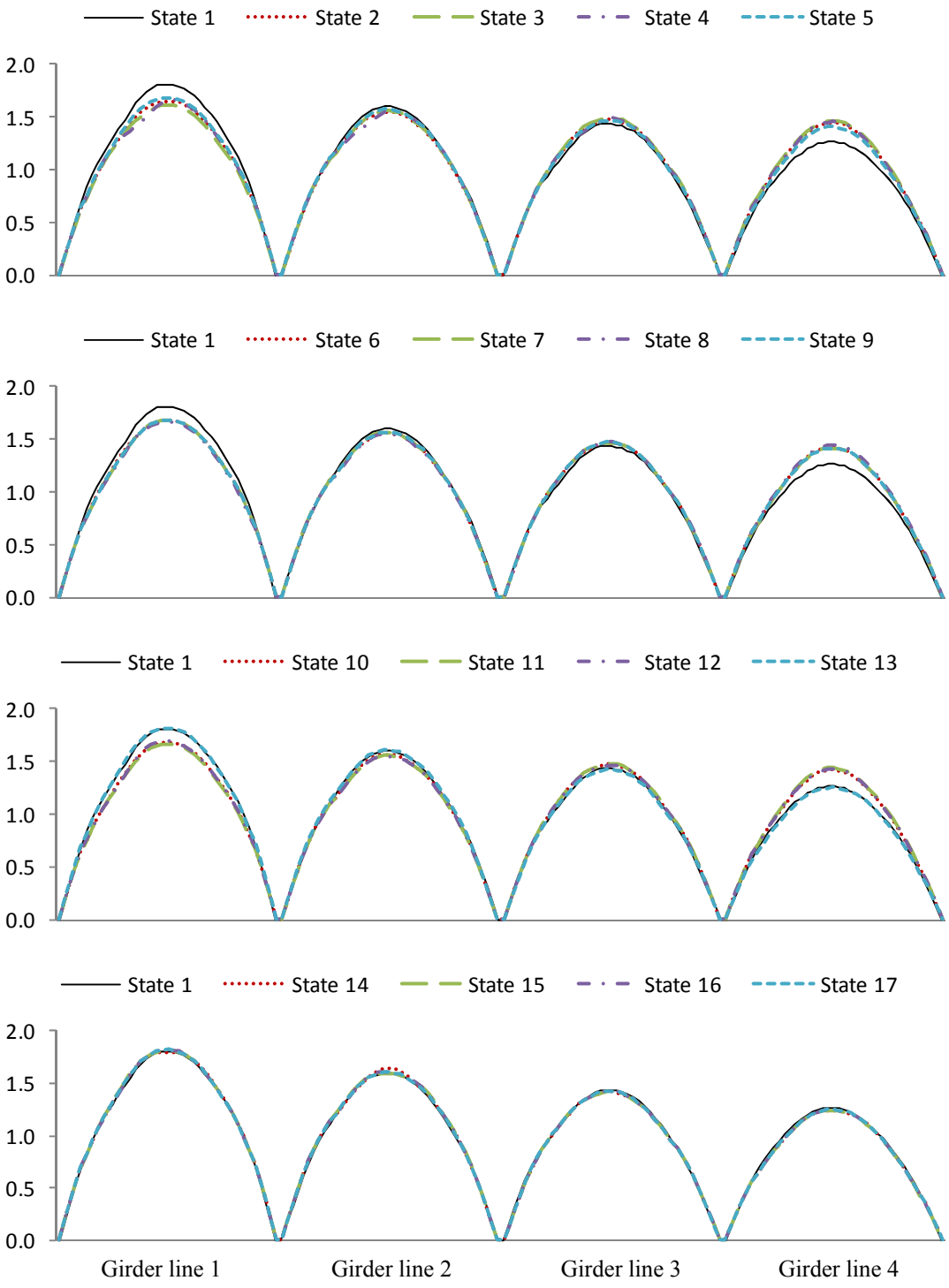

Figure E.2. Comparison of the first mode shape averaged from five repeated tests for different health states using accelerometer data with white noise random excitation.

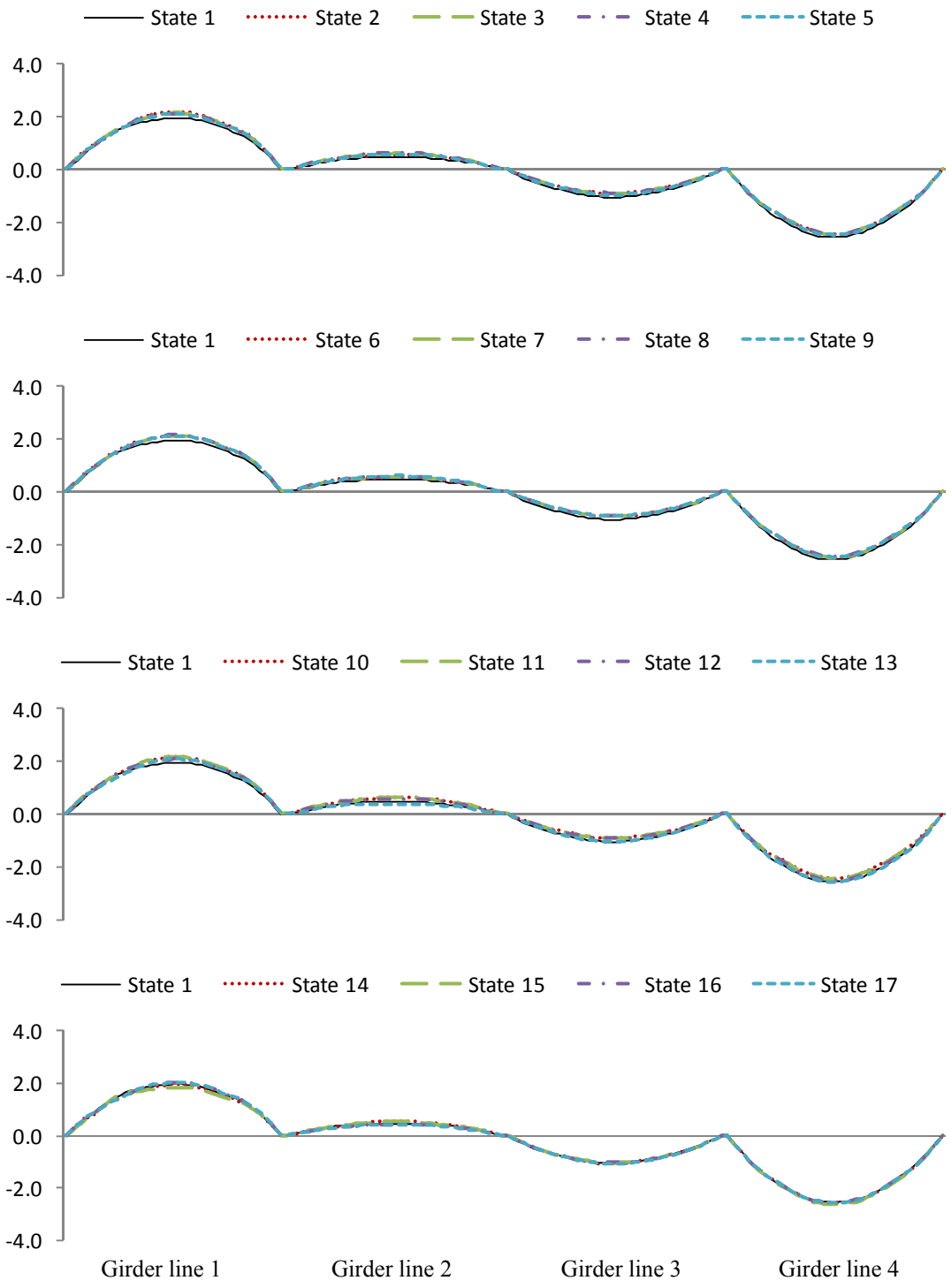

Figure E.3. Comparison of the second mode shape averaged from five repeated tests for different health states using accelerometer data with white noise random excitation.

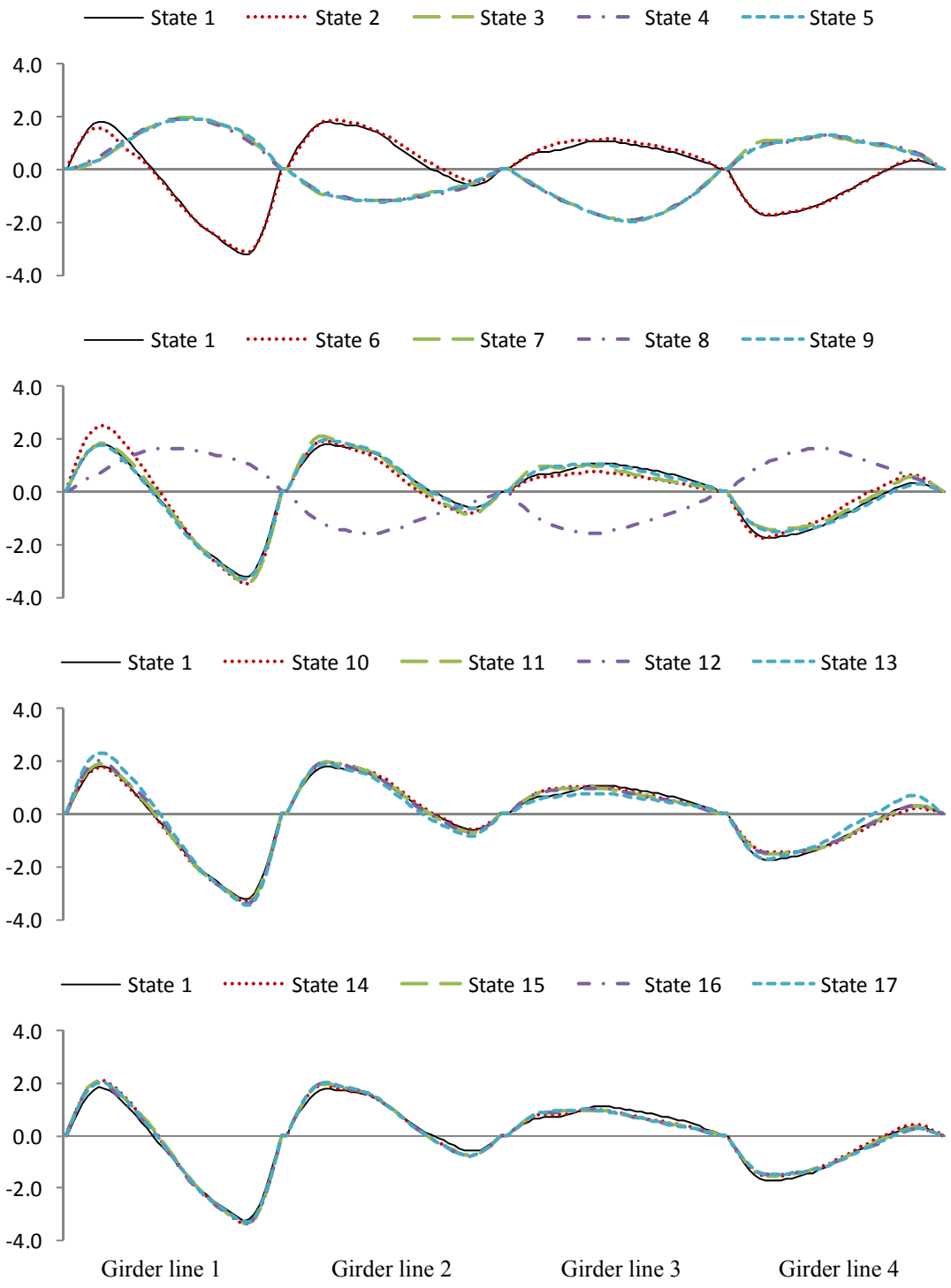

Figure E.4. Comparison of the third mode shape averaged from five repeated tests for different health states using accelerometer data with white noise random excitation.

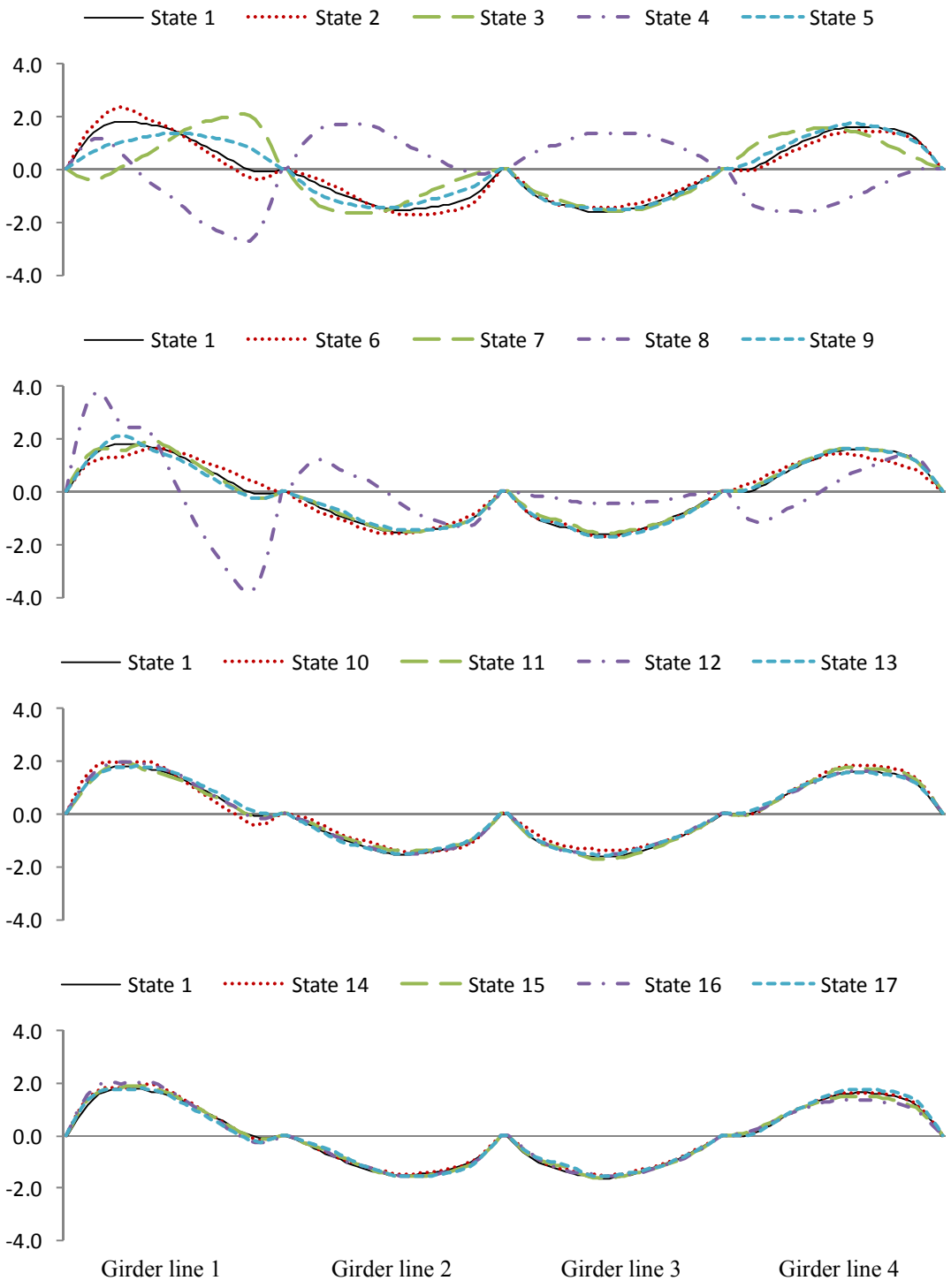

Figure E.5. Comparison of the fourth mode shape averaged from five repeated tests for different health states using accelerometer data with white noise random excitation.

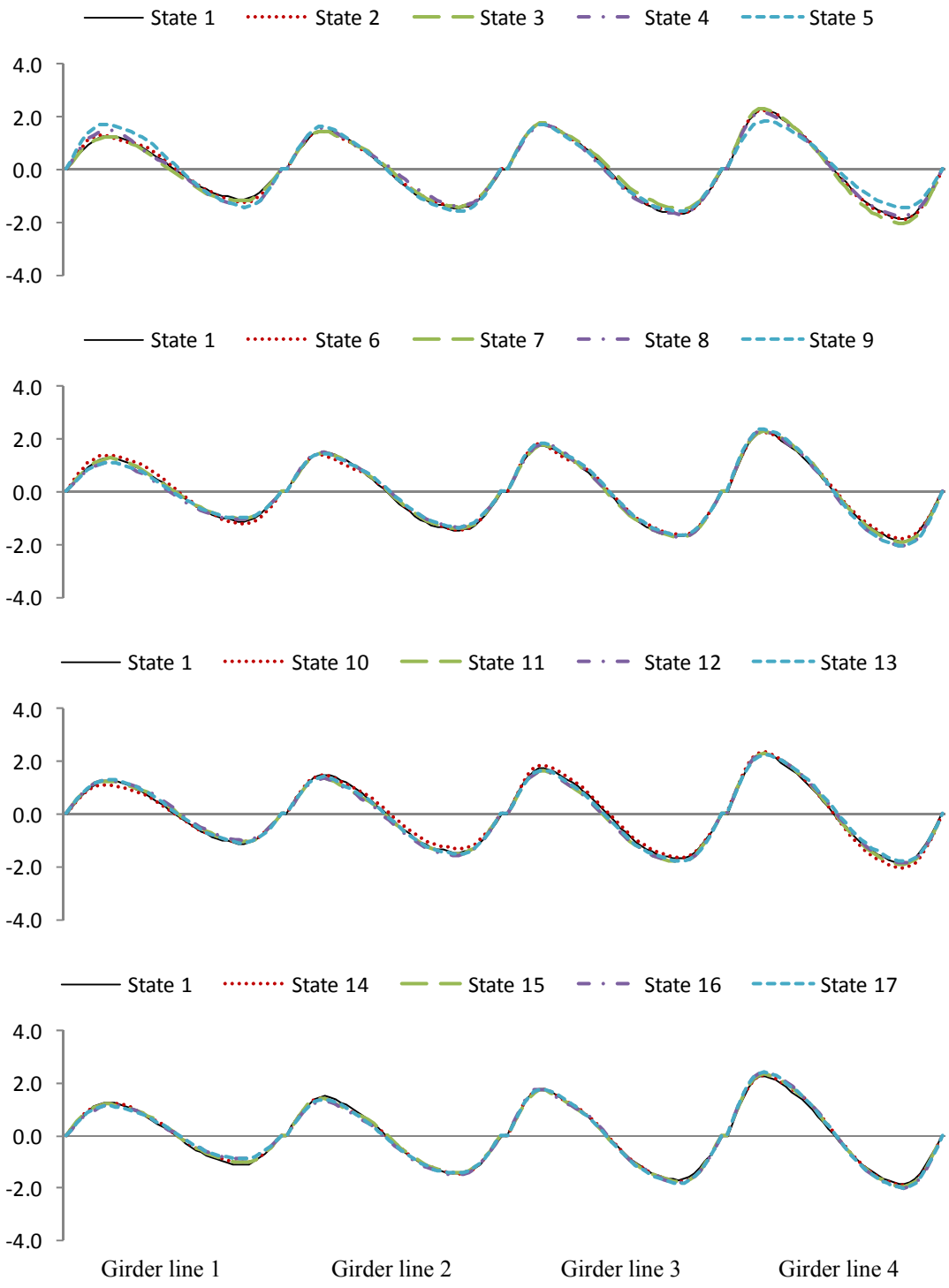

Figure E.6. Comparison of the fifth mode shape averaged from five repeated tests for different health states using accelerometer data with white noise random excitation.

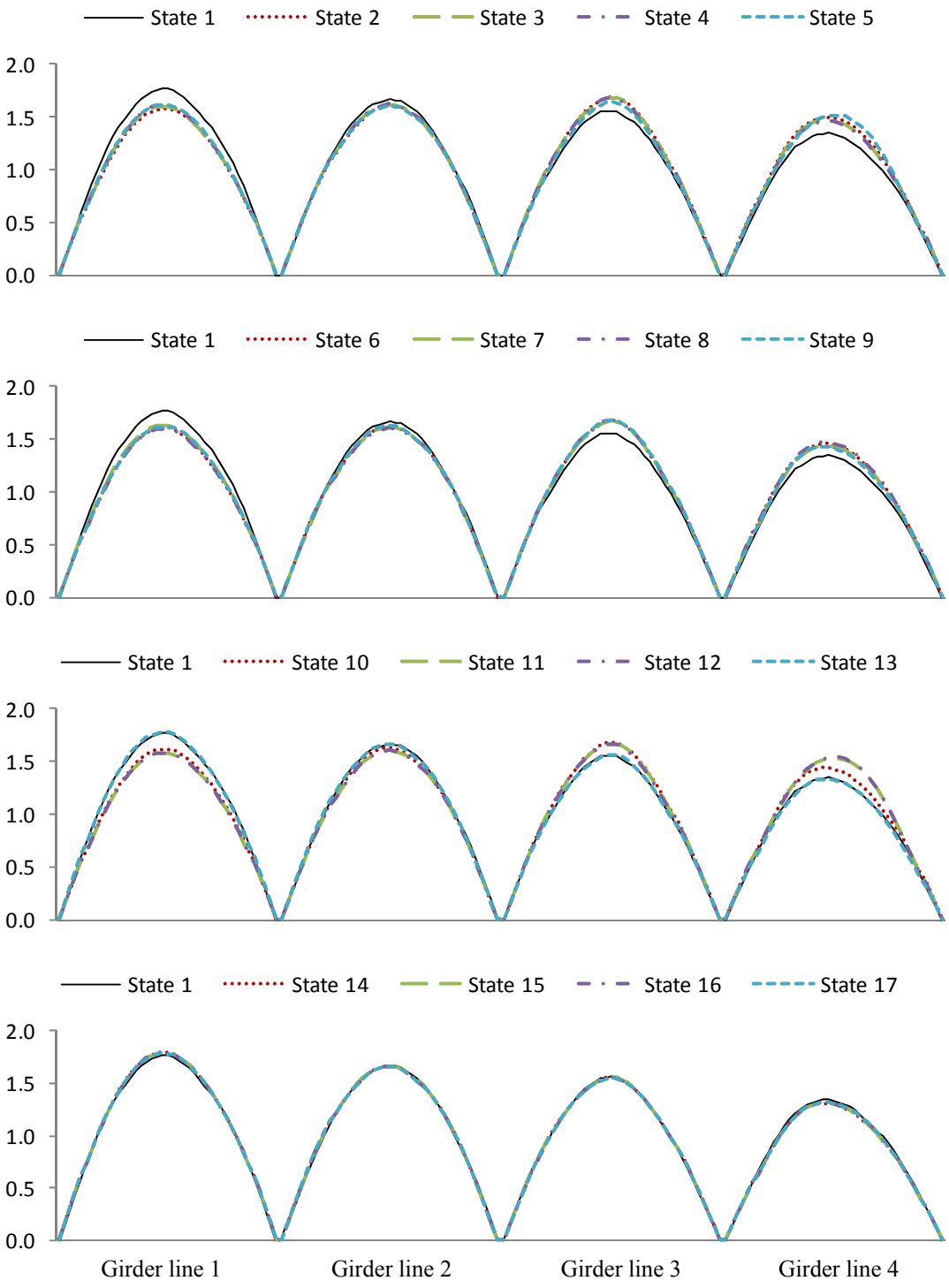

Figure E.7. Comparison of the first mode shape averaged from five repeated tests for different health states using bottom strain gauge data with harmonic excitation.

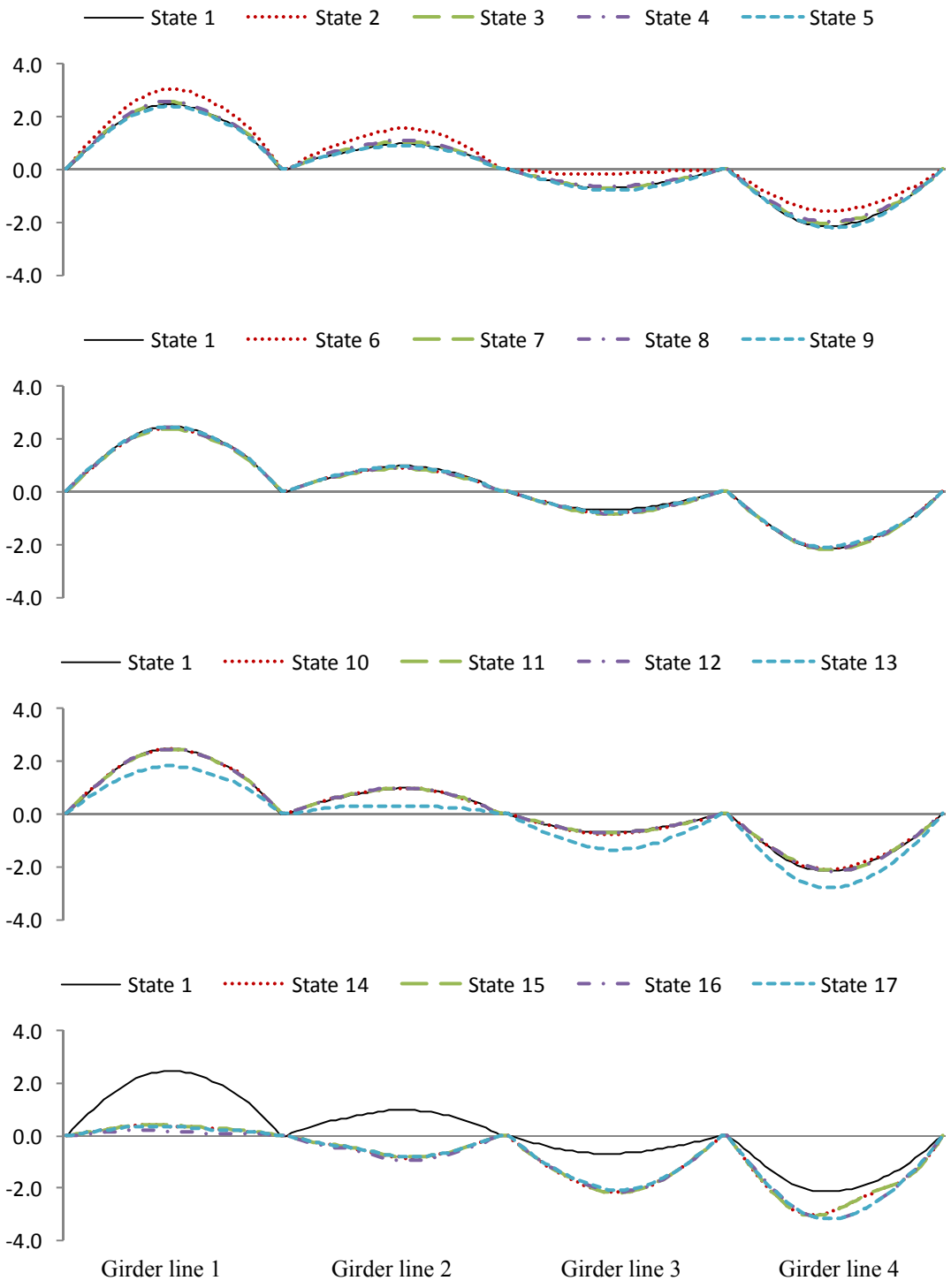

Figure E.8. Comparison of the second mode shape averaged from five repeated tests for different health states using bottom strain gauge data with harmonic excitation.

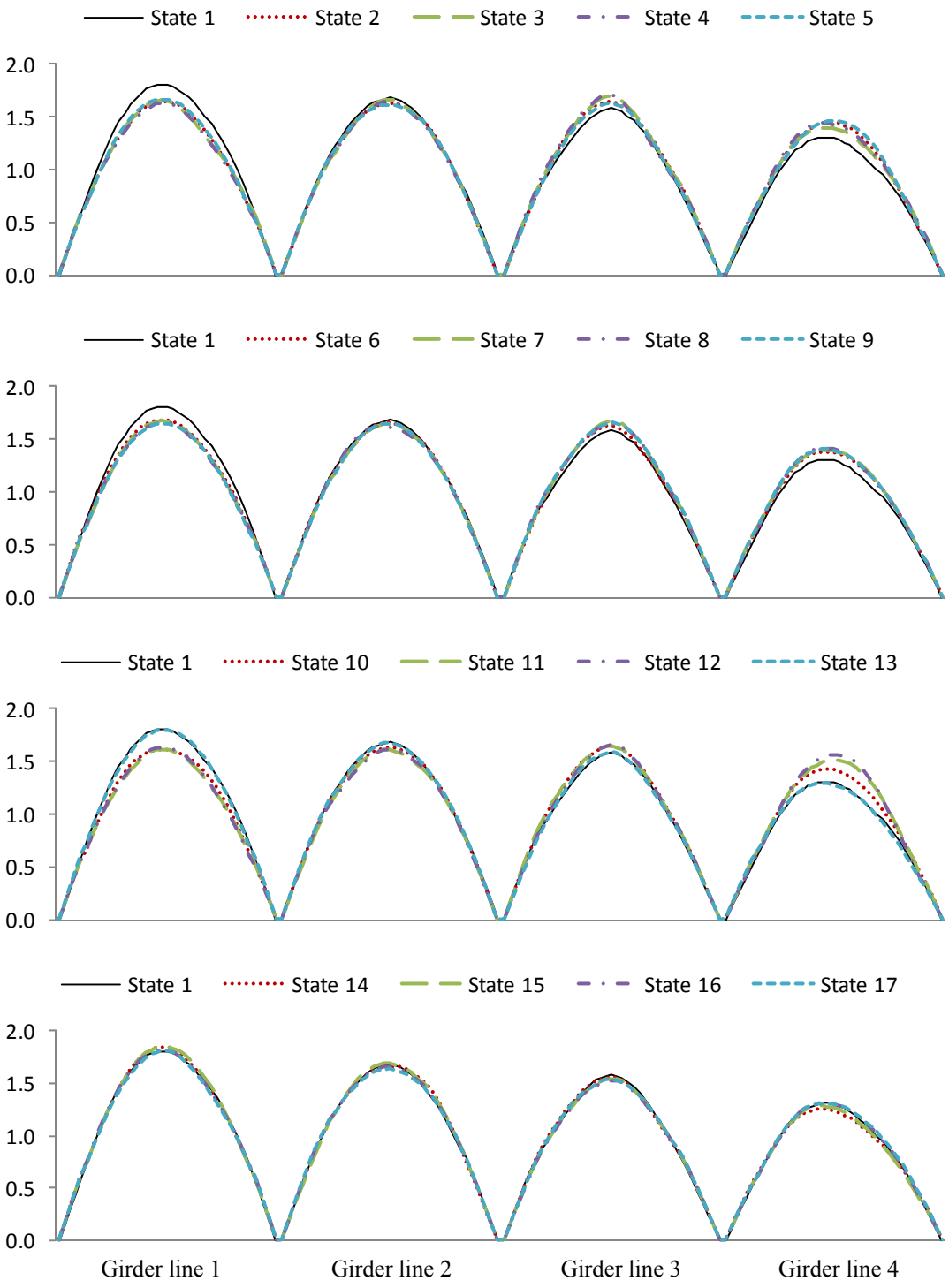

Figure E.9. Comparison of the first mode shape averaged from five repeated tests for different health states using bottom strain gauge data with white noise random excitation.

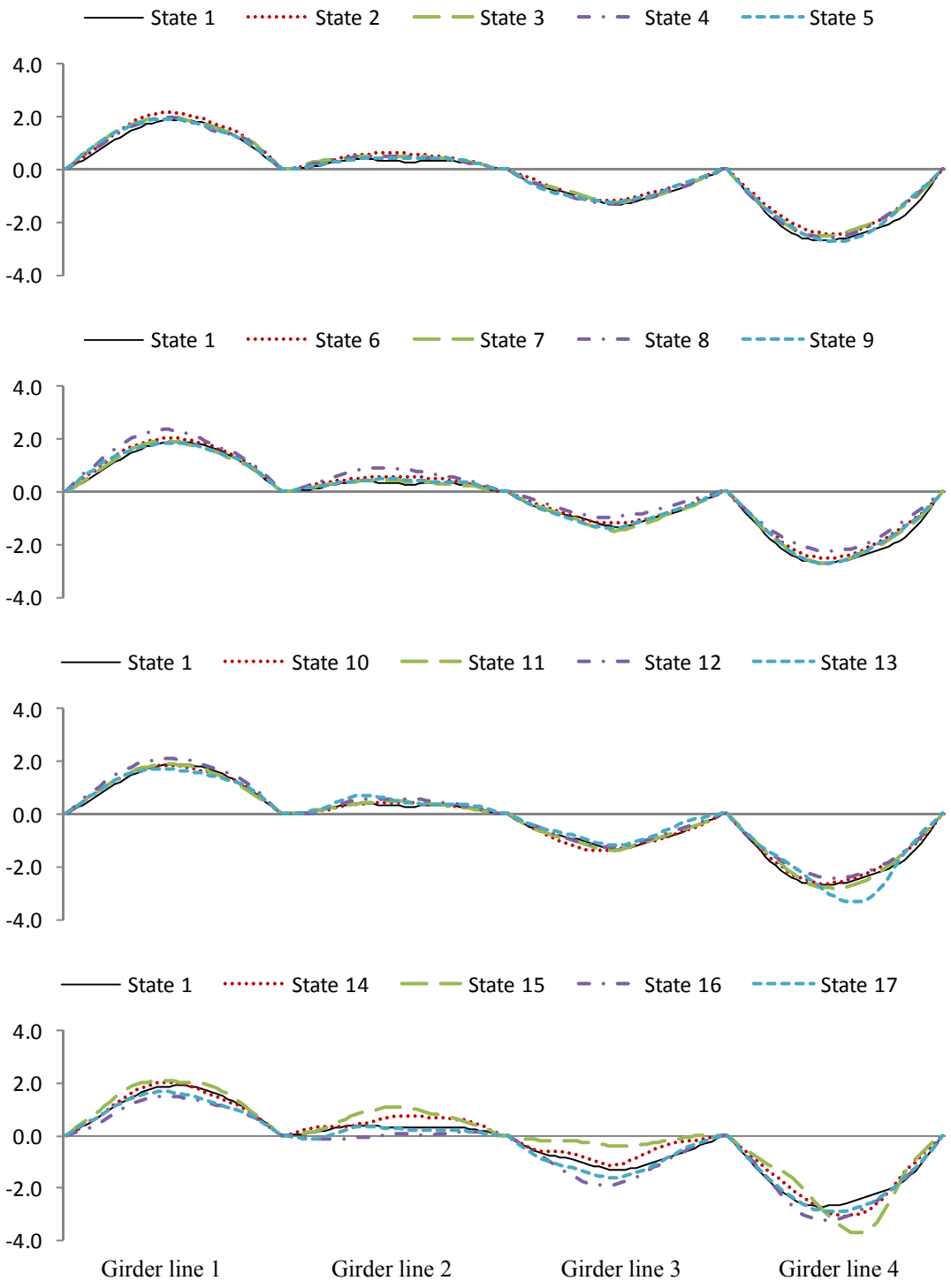

Figure E.10. Comparison of the second mode shape averaged from five repeated tests for different health states using bottom strain gauge data with white noise random excitation.

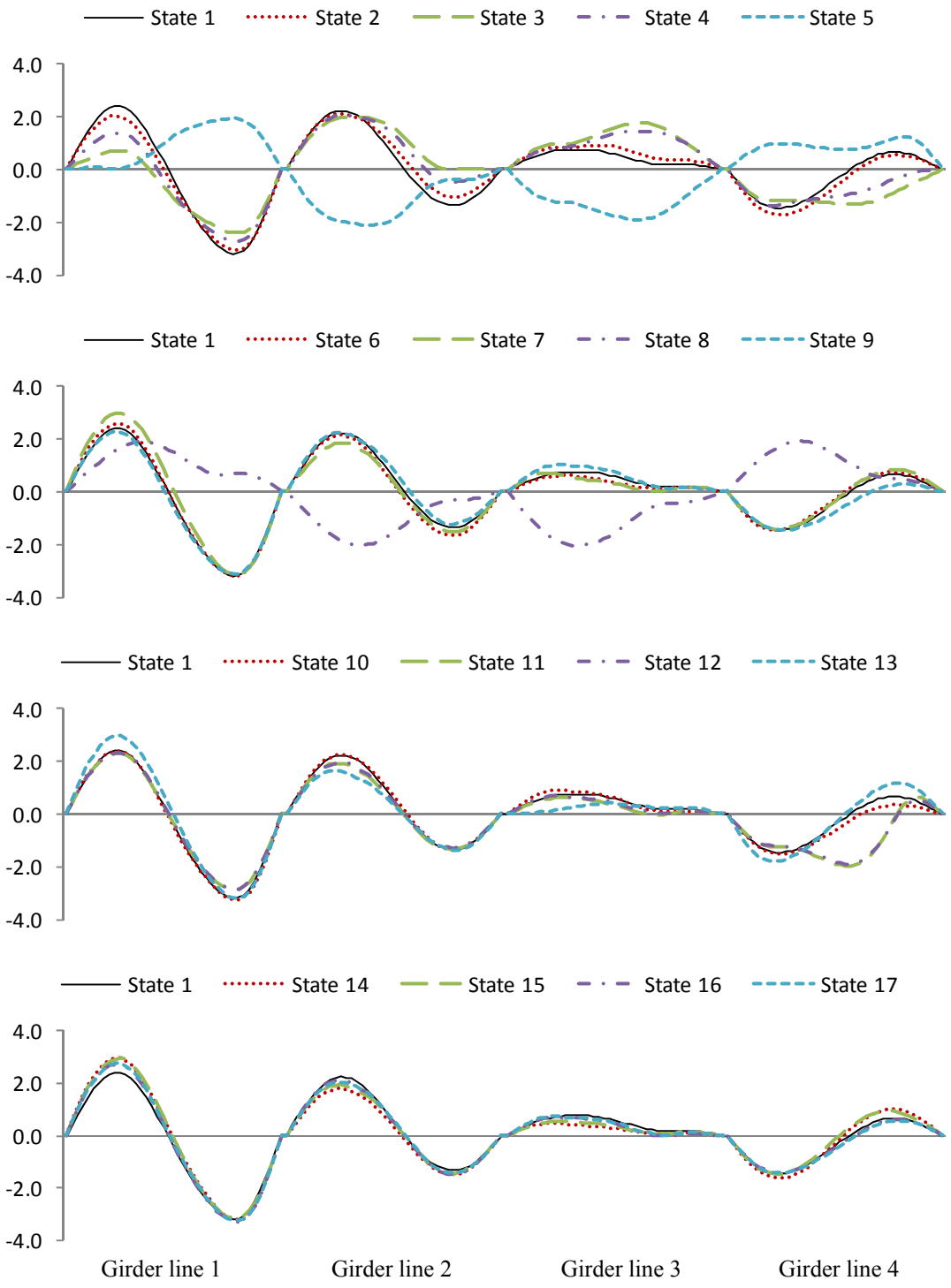

Figure E.11. Comparison of the third mode shape averaged from five repeated tests for different health states using bottom strain gauge data with white noise random excitation.

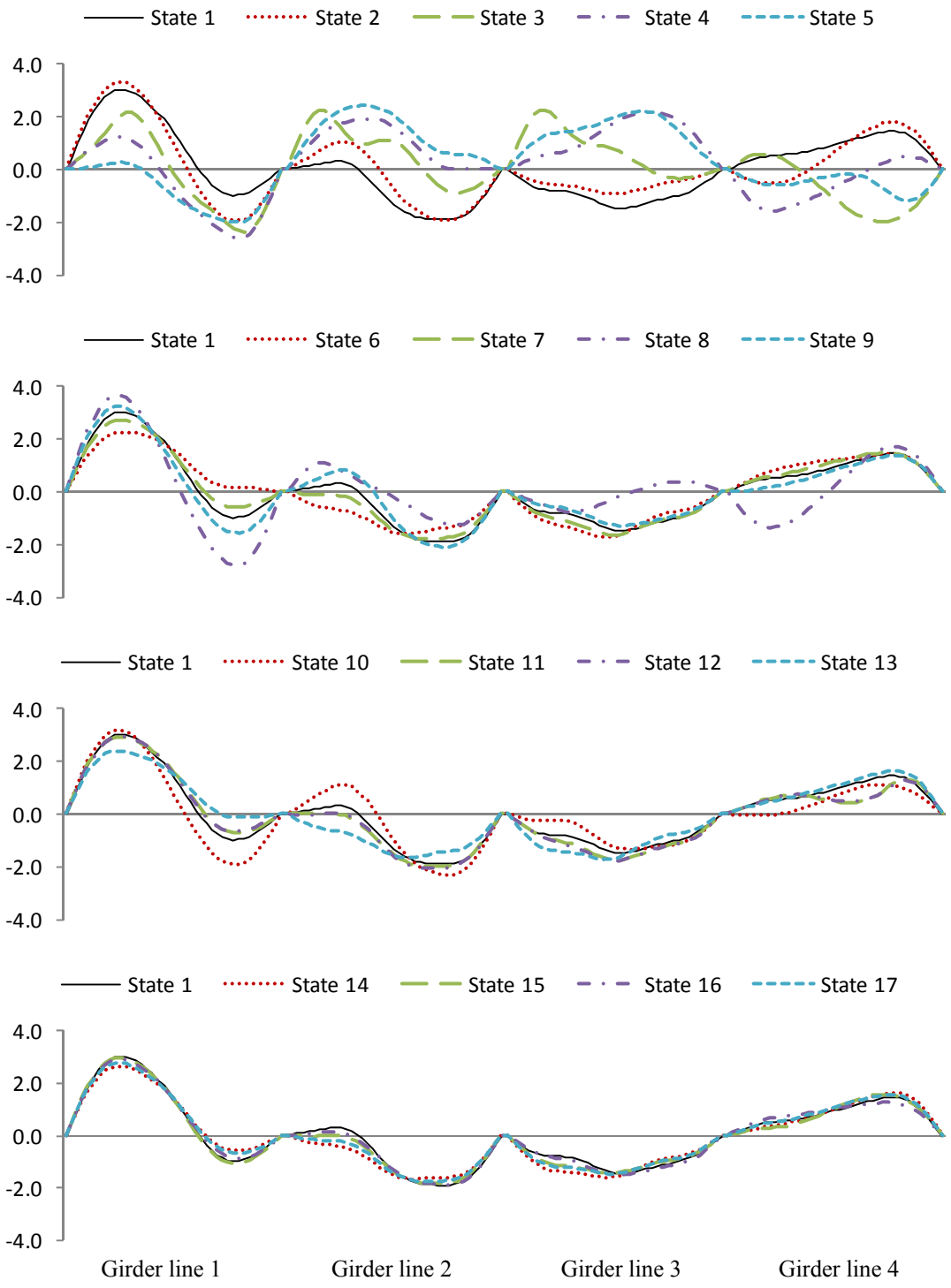

Figure E.12. Comparison of the fourth mode shape averaged from five repeated tests for different health states using bottom strain gauge data with white noise random excitation.

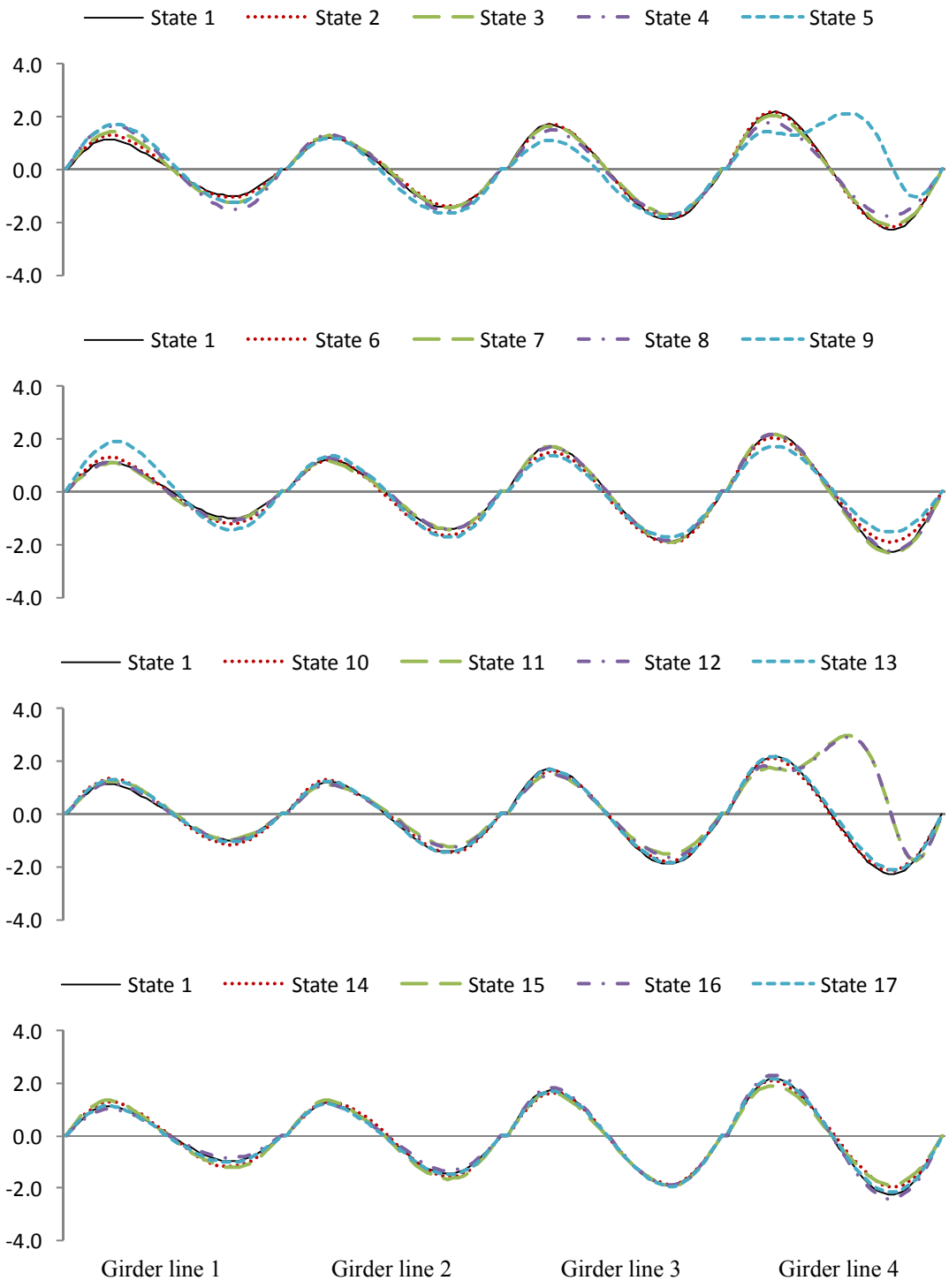

Figure E.13. Comparison of the fifth mode shape averaged from five repeated tests for different health states using bottom strain gauge data with white noise random excitation.

APPENDIX F. **ADDITIONAL INFORMATION FOR THE FE MODEL**

This Appendix presents additional explanation of results generated using the FE model, as described in Chapter 5. Specifically, Figure F.1 presents exactly the same results as shown in Fig. 5.10. To better understand the relationship between the area of mode shape change and the relative flexural stiffness, however, a linear scale was used in this figure while a logarithmic scale was used in Fig. 5.10.

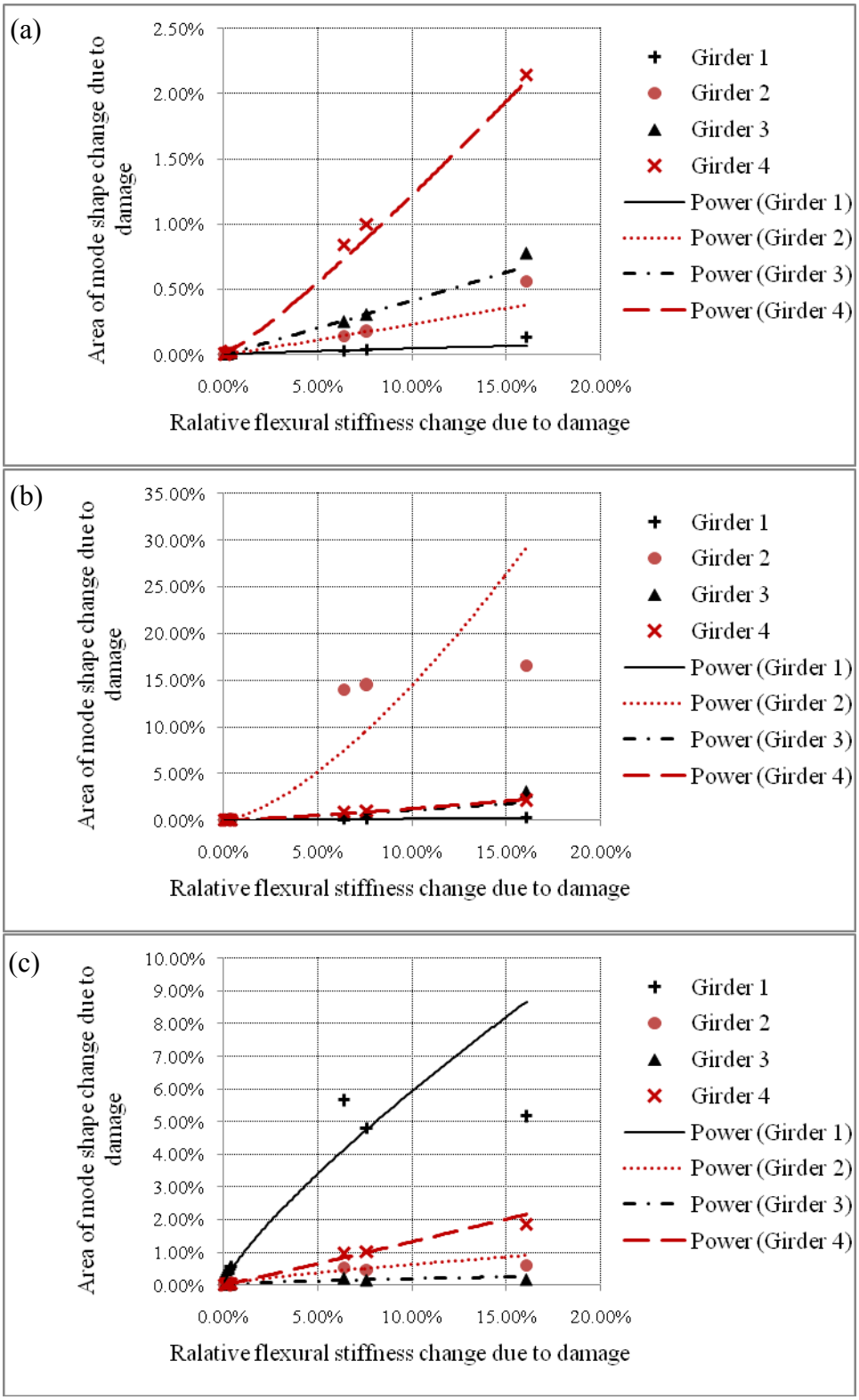

Figure F.1. Relationship between the area of mode shape change and the relative flexural stiffness change due to damages for: (a) Mode 1, (b) Mode 2, and (c) Mode 3 when mode shapes were normalized along individual girder lines.

APPENDIX G. **ADDITIONAL INFORMATION FOR DISTRIBUTION OF THE AREA OF MODE SHAPE CHANGE**

This appendix presents additional information for the distribution of the area of mode shape change when there is no change in condition, as described in Section 6.2.2.

Figures G.1 to G.5 present comparisons of the actual cumulative probability distributions and the assumed Normal and Log-Normal distributions of ΔA for Test Protocols 9 to 28, which are similar to results presented in Figs. 6.1 and 6.2.

Figures G.6 to G.15 present comparison of the probability density between the actual distribution and the assumed Normal and Log-Normal distributions of ΔA, for Test Protocols 9 to 28, which supply additional information for Figs. 6.3 to 6.6.

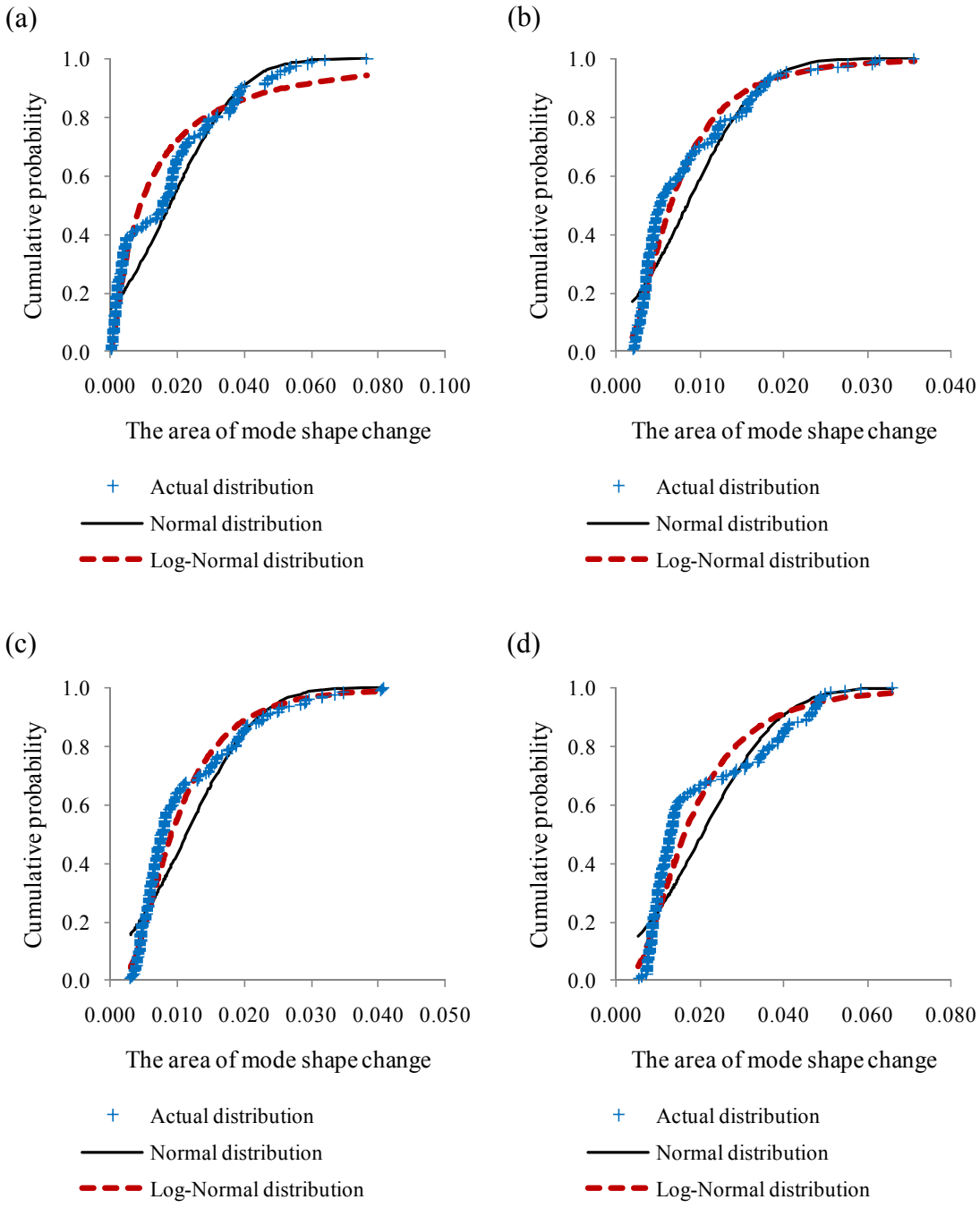

Figure G.1. Comparison of the actual cumulative probability distributions and the assumed Normal and Log-Normal distributions of ΔA, for Test Protocols: (a) 9, (b) 10, (c) 11, and (d) 12.

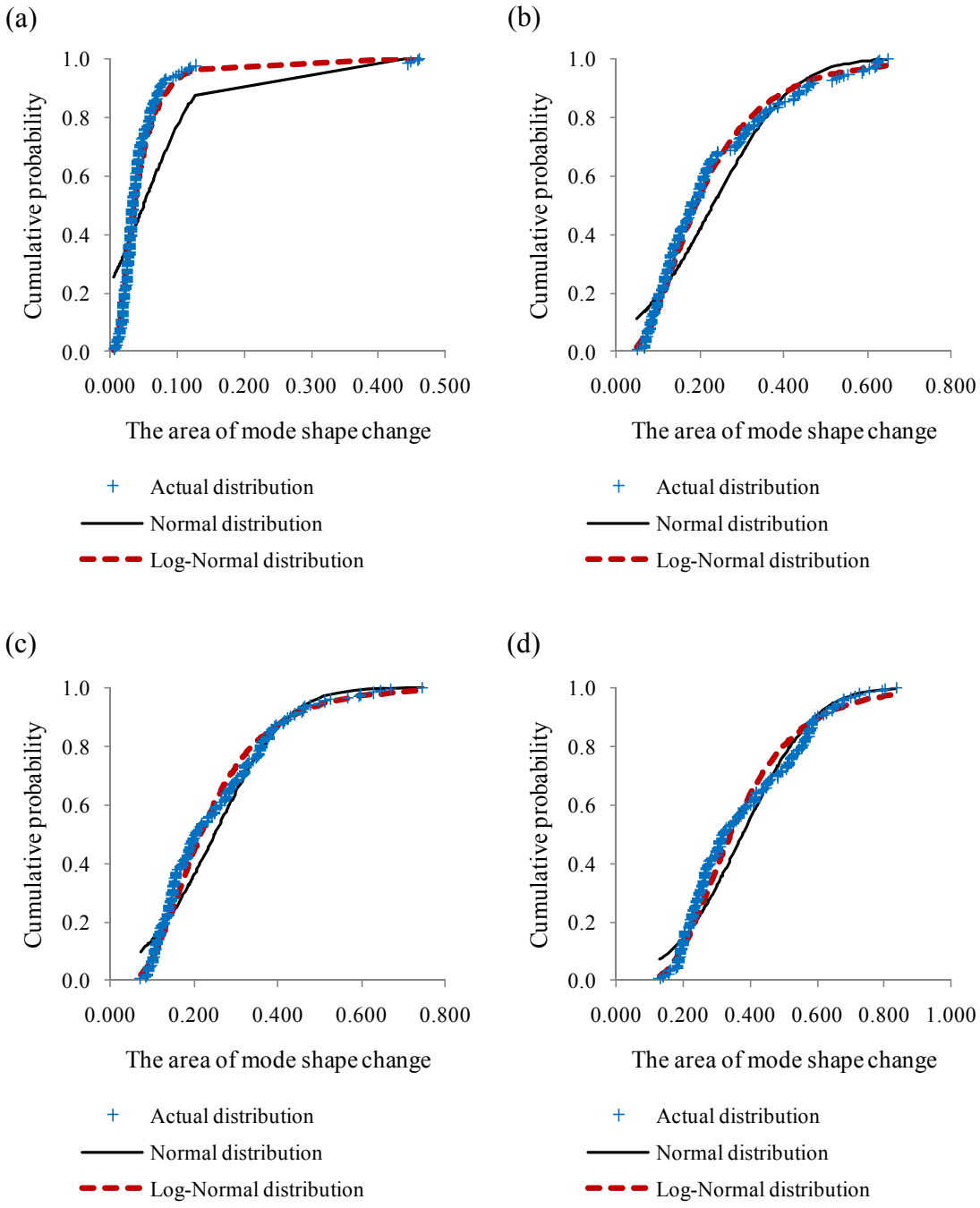

Figure G.2. Comparison of the actual cumulative probability distributions and the assumed Normal and Log-Normal distributions of ΔA, for Test Protocols: (a) 13, (b) 14, (c) 15, and (d) 16.

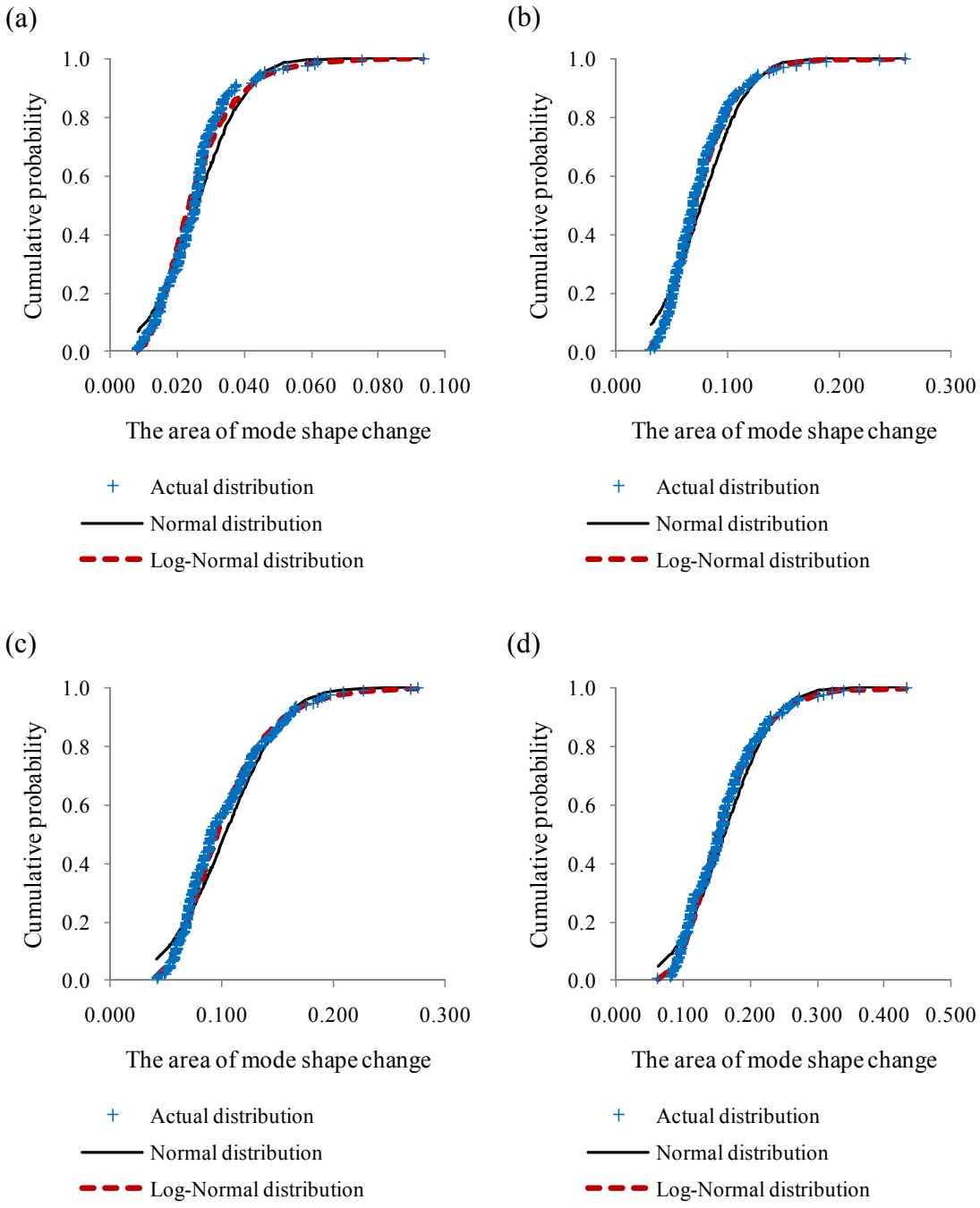

Figure G.3. Comparison of the actual cumulative probability distributions and the assumed Normal and Log-Normal distributions of ΔA, for Test Protocols: (a) 17, (b) 18, (c) 19, and (d) 20.

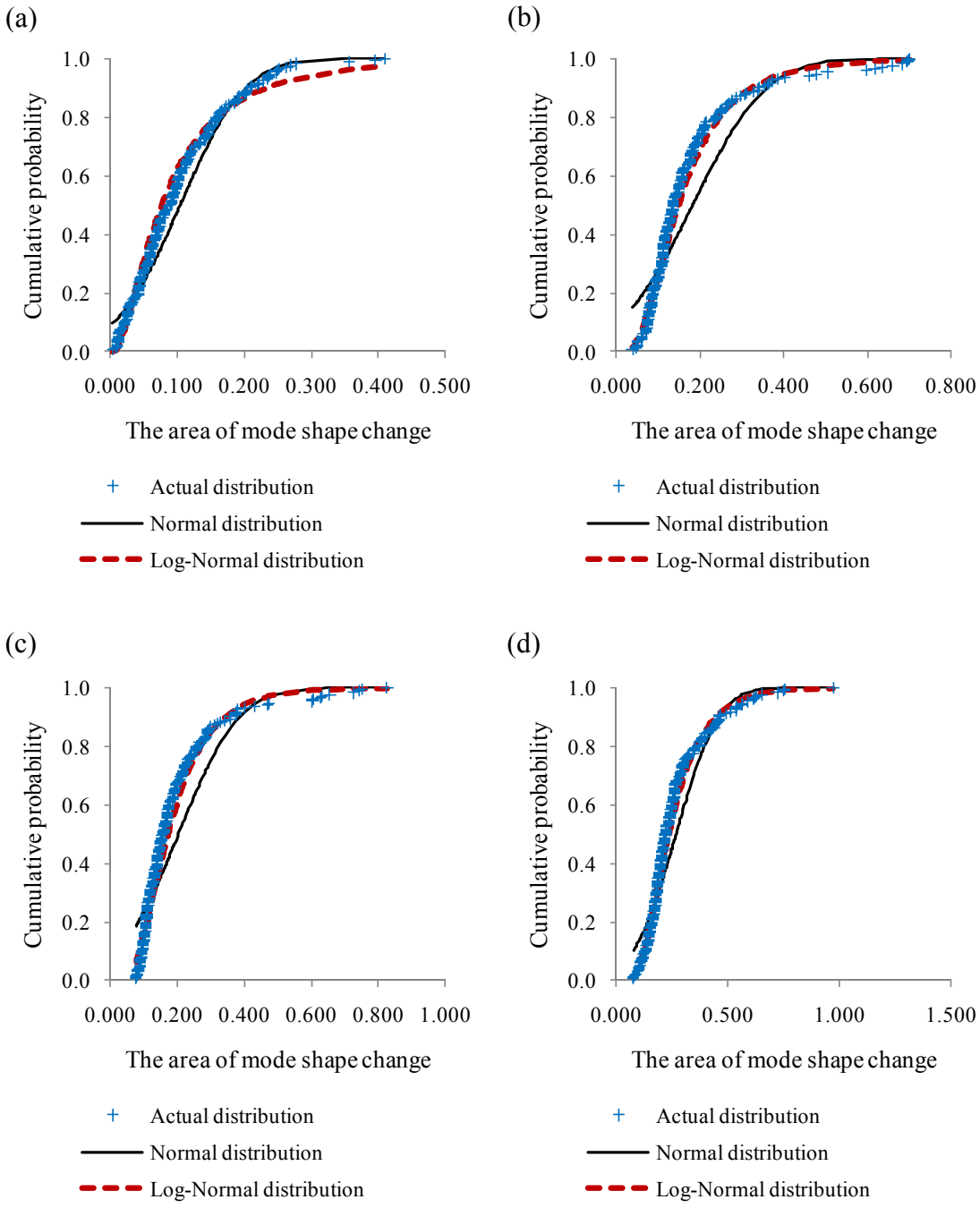

Figure G.4. Comparison of the actual cumulative probability distributions and the assumed Normal and Log-Normal distributions of ΔA, for Test Protocols: (a) 21, (b) 22, (c) 23, and (d) 24.

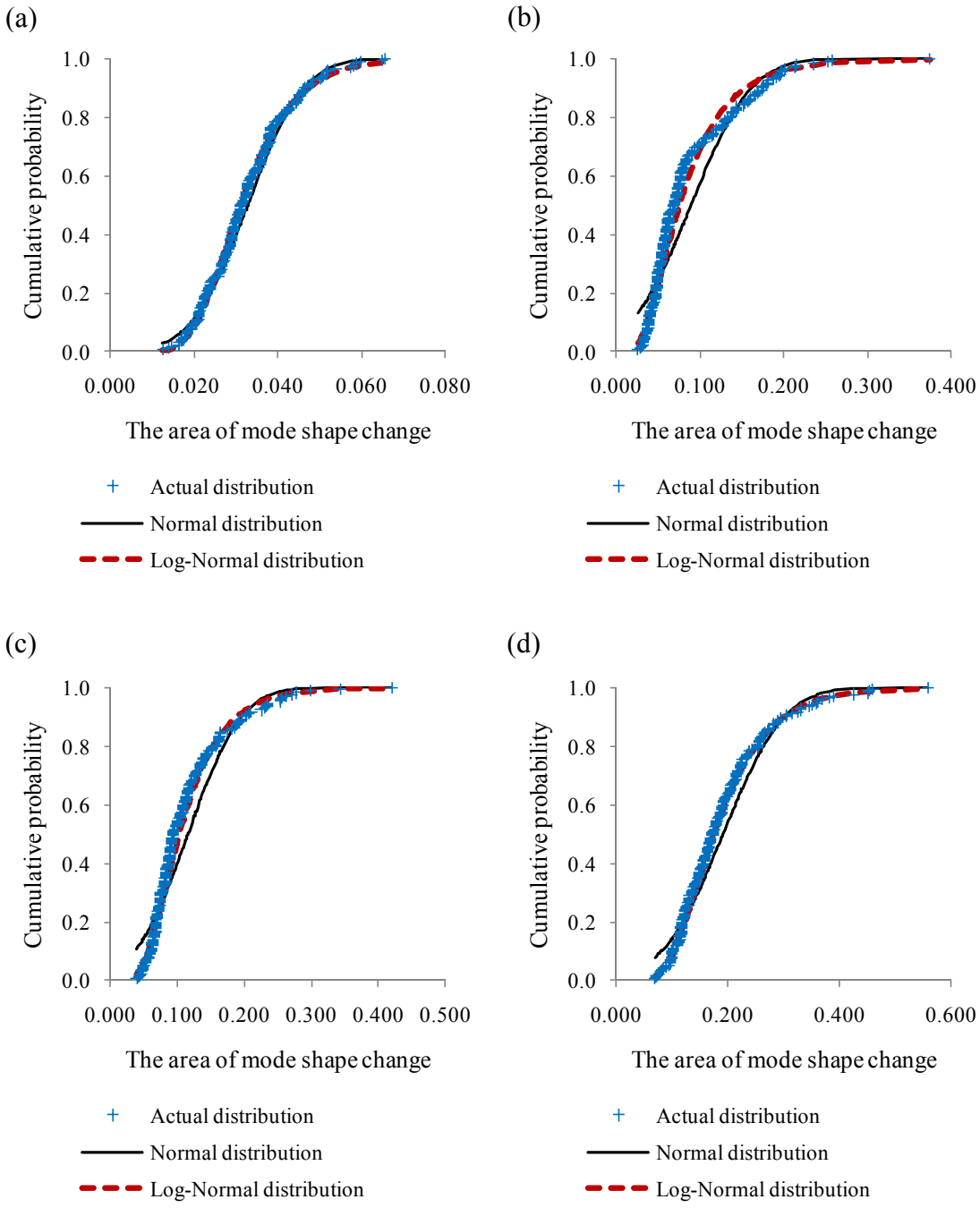

Figure G.5. Comparison of the actual cumulative probability distributions and the assumed Normal and Log-Normal distributions of ΔA, for Test Protocols: (a) 25, (b) 26, (c) 27, and (d) 28.

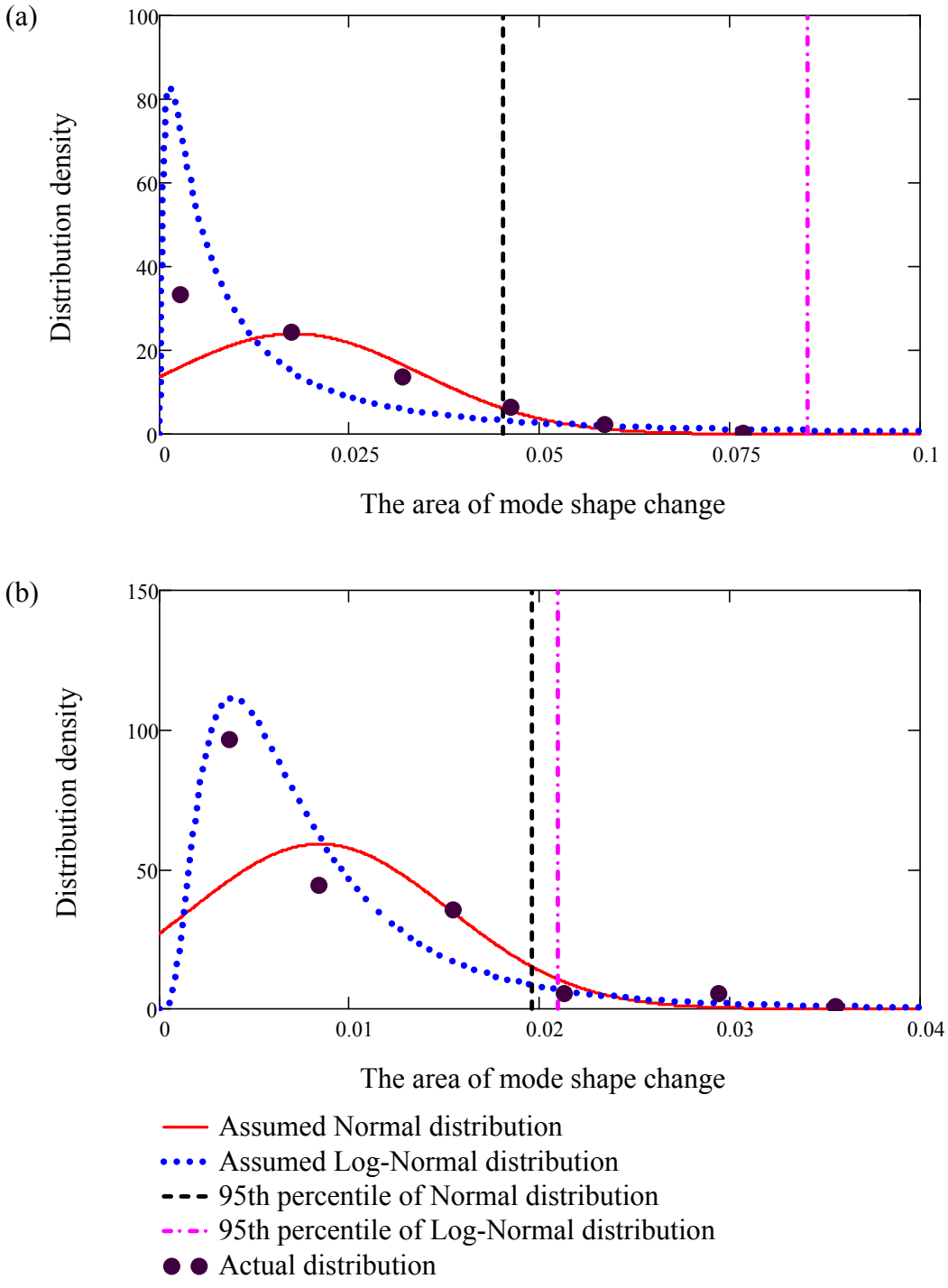

Figure G.6. Comparison of the probability density between the actual distribution and the assumed Normal and Log-Normal distributions of ΔA, for Test Protocols: (a) 9 and (b) 10.

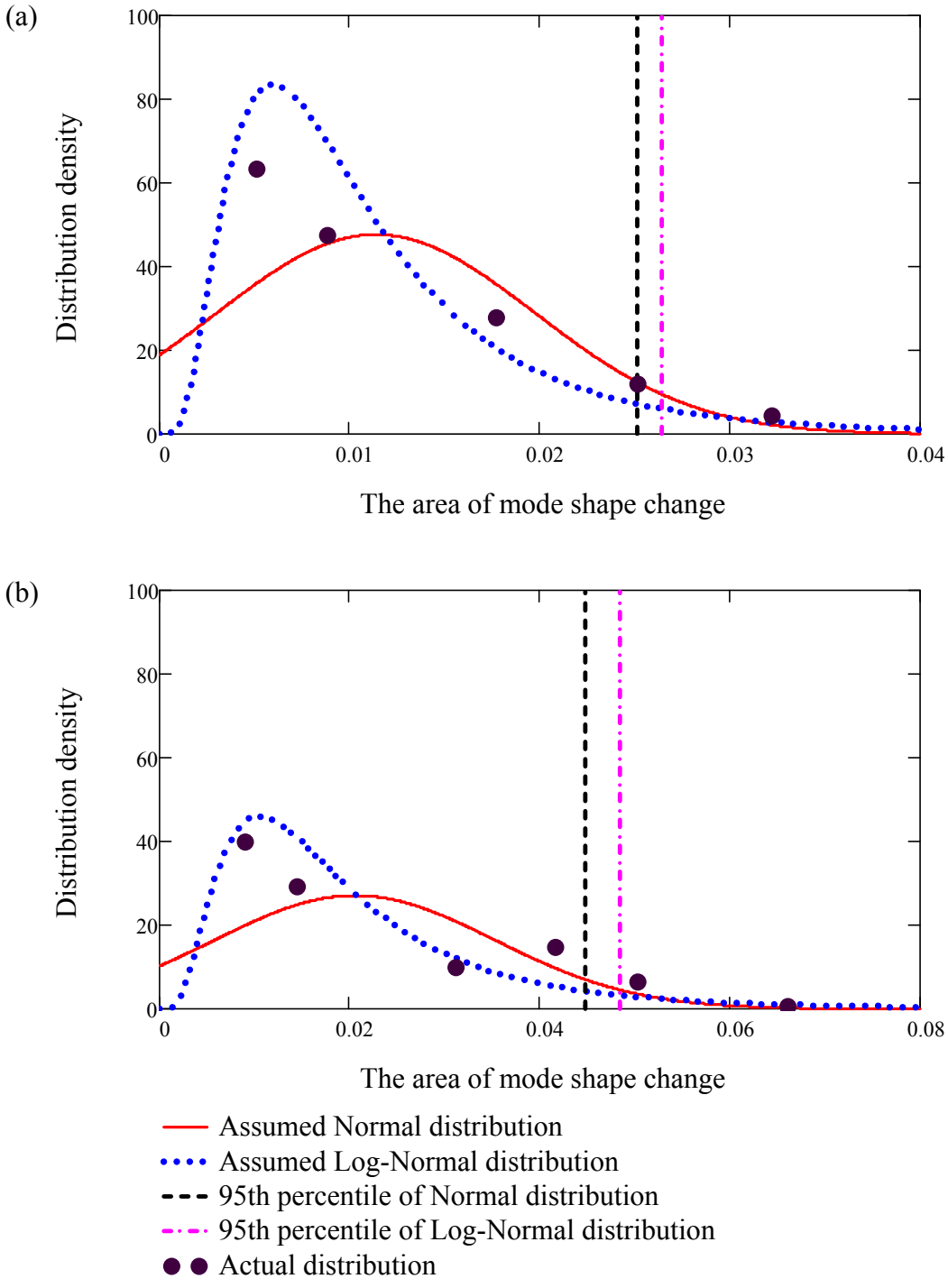

Figure G.7. Comparison of the probability density between the actual distribution and the assumed Normal and Log-Normal distributions of ΔA, for Test Protocols: (a) 11 and (b) 12.

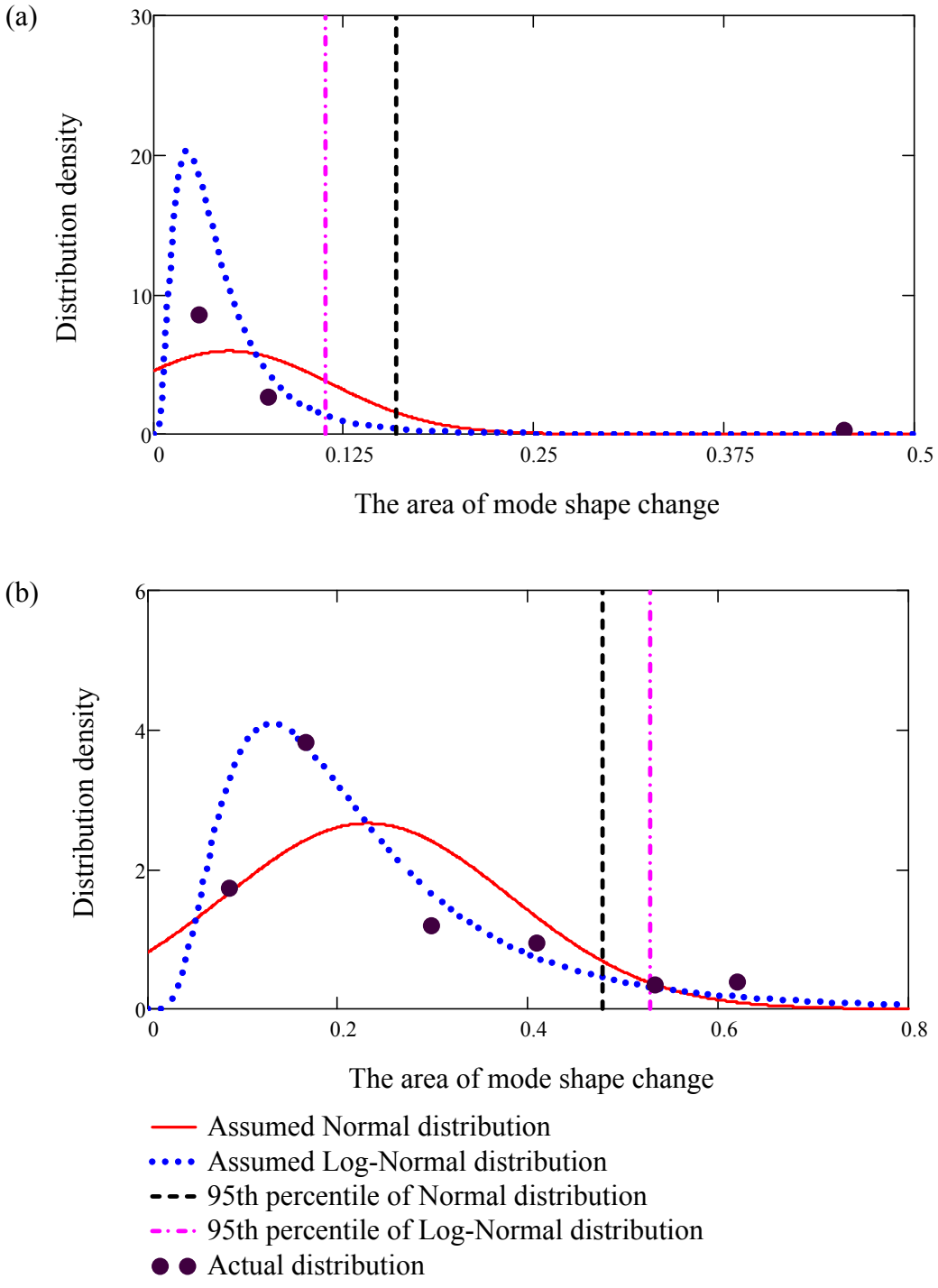

Figure G.8. Comparison of the probability density between the actual distribution and the assumed Normal and Log-Normal distributions of ΔA, for Test Protocols: (a) 13 and (b) 14.

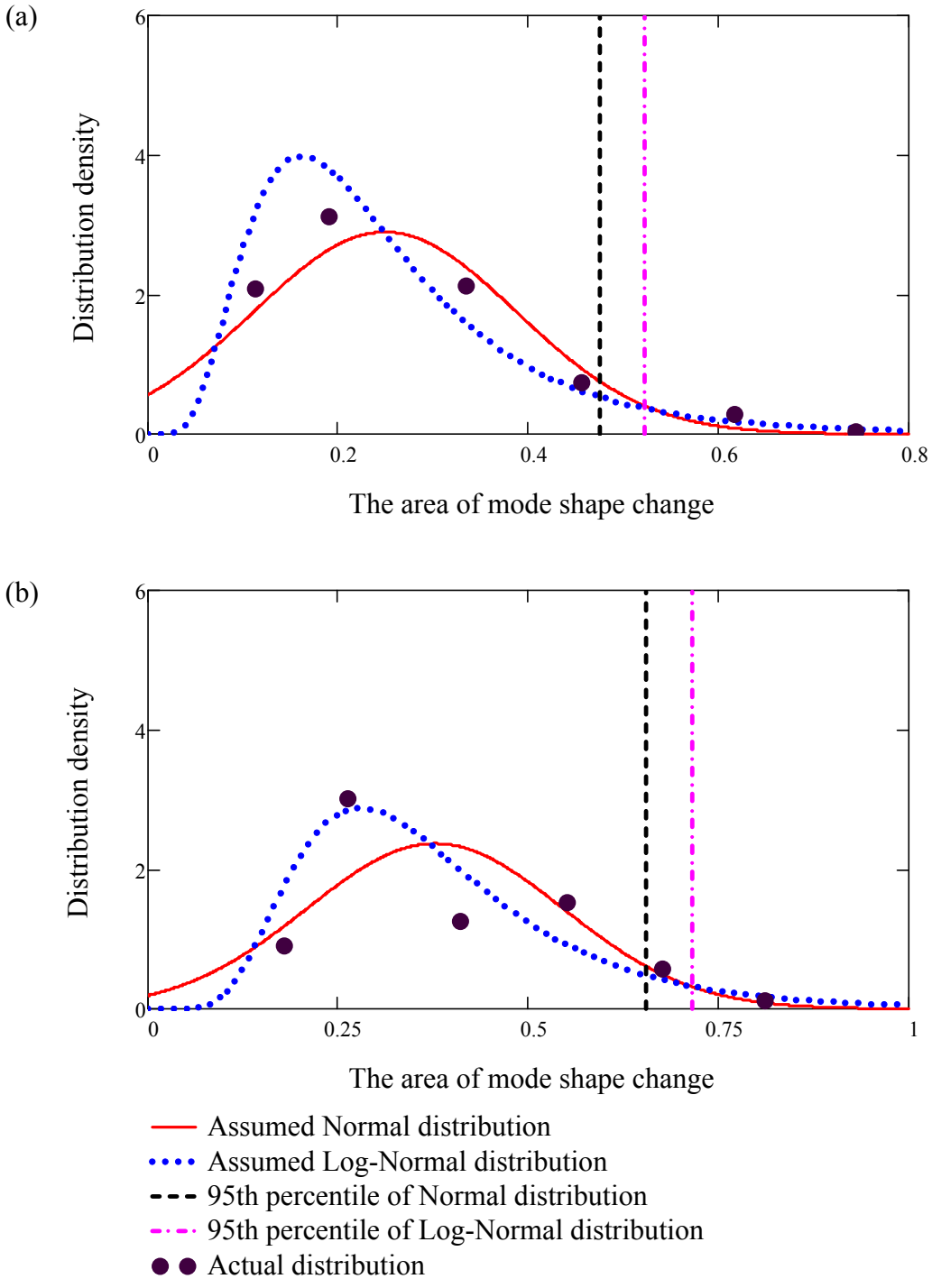

Figure G.9. Comparison of the probability density between the actual distribution and the assumed Normal and Log-Normal distributions of ΔA, for Test Protocols: (a) 15 and (b) 16.

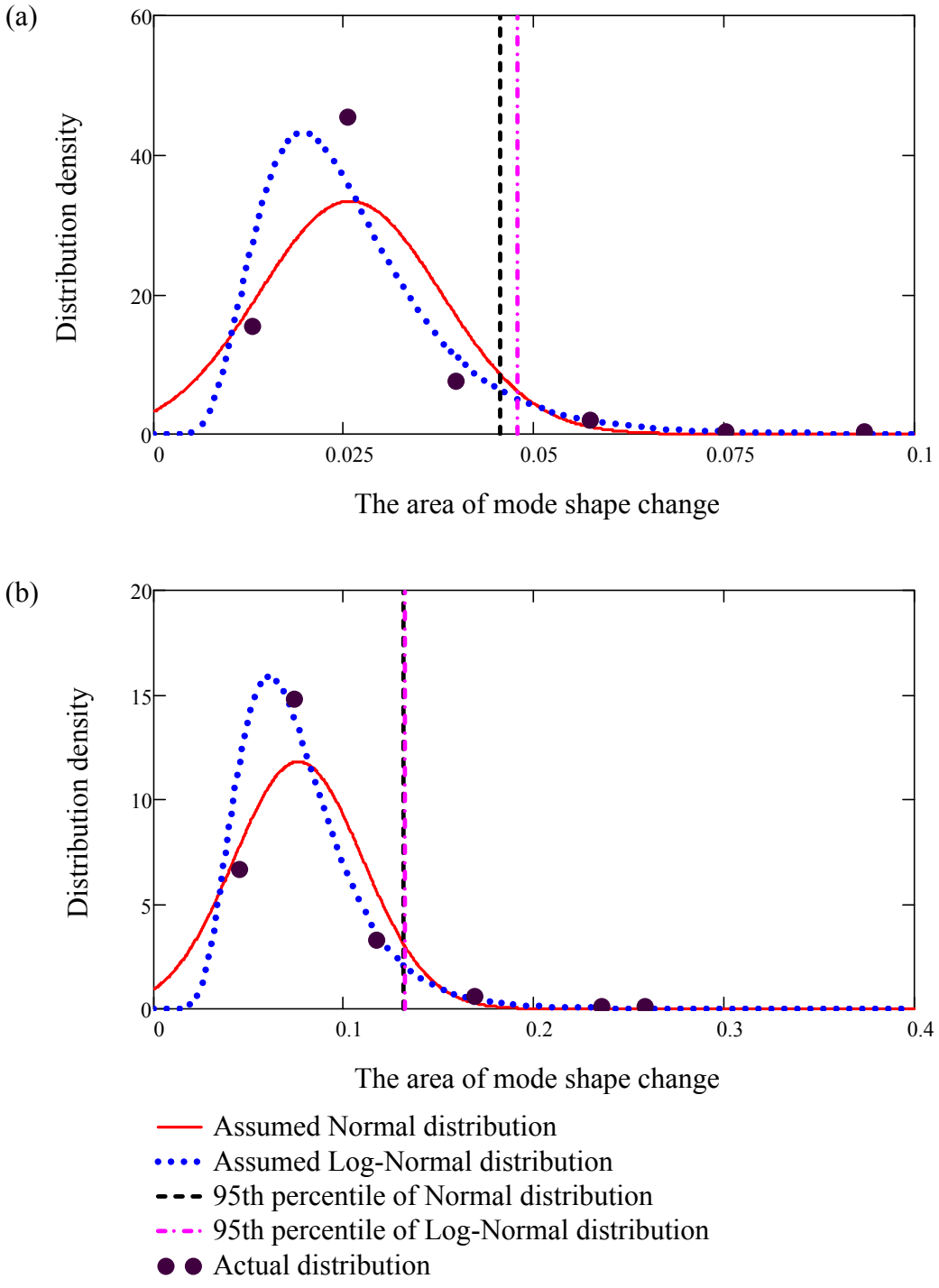

Figure G.10. Comparison of the probability density between the actual distribution and the assumed Normal and Log-Normal distributions of ΔA, for Test Protocols: (a) 17 and (b) 18.

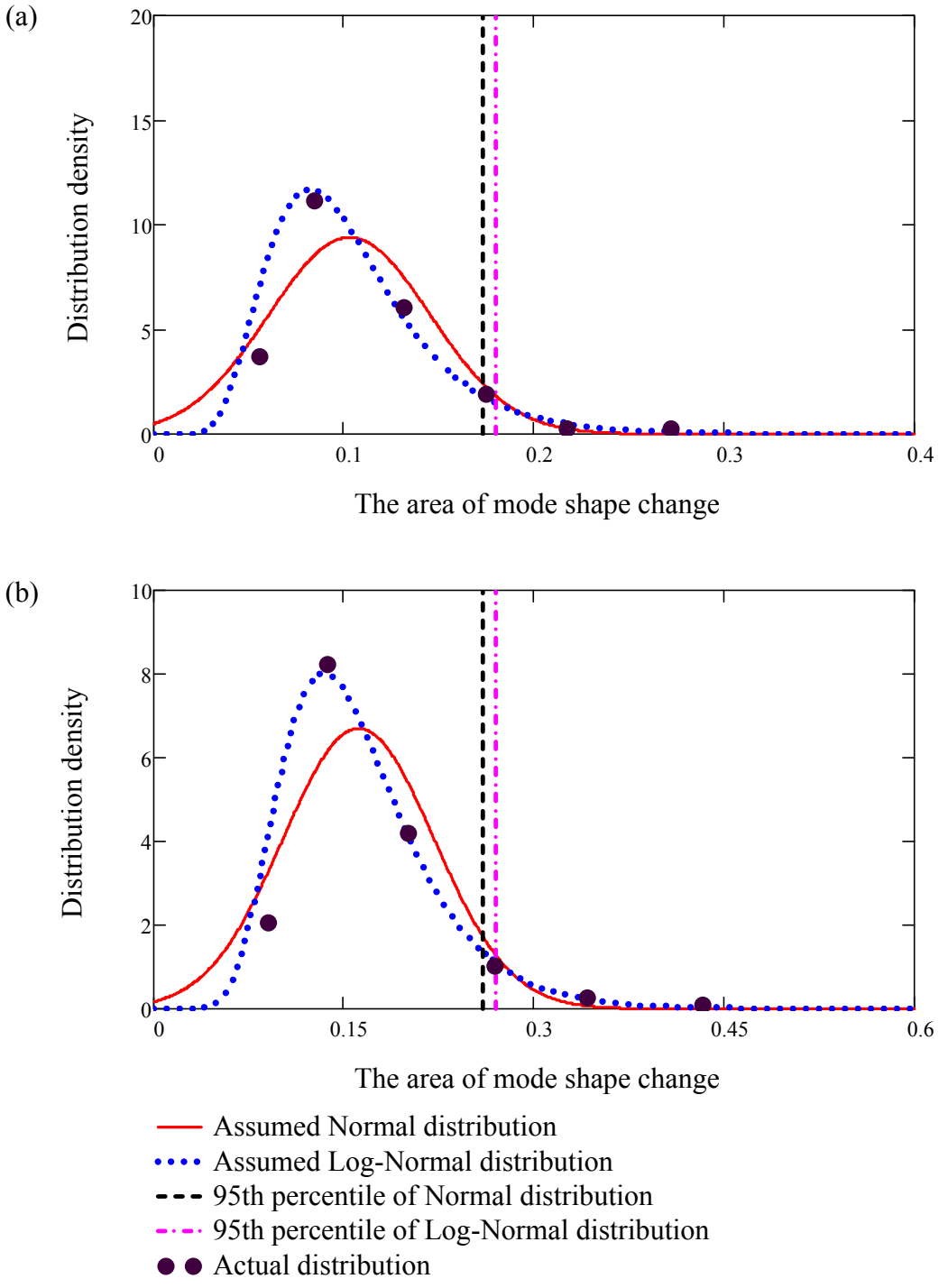

Figure G.11. Comparison of the probability density between the actual distribution and the assumed Normal and Log-Normal distributions of ΔA, for Test Protocols: (a) 19 and (b) 20.

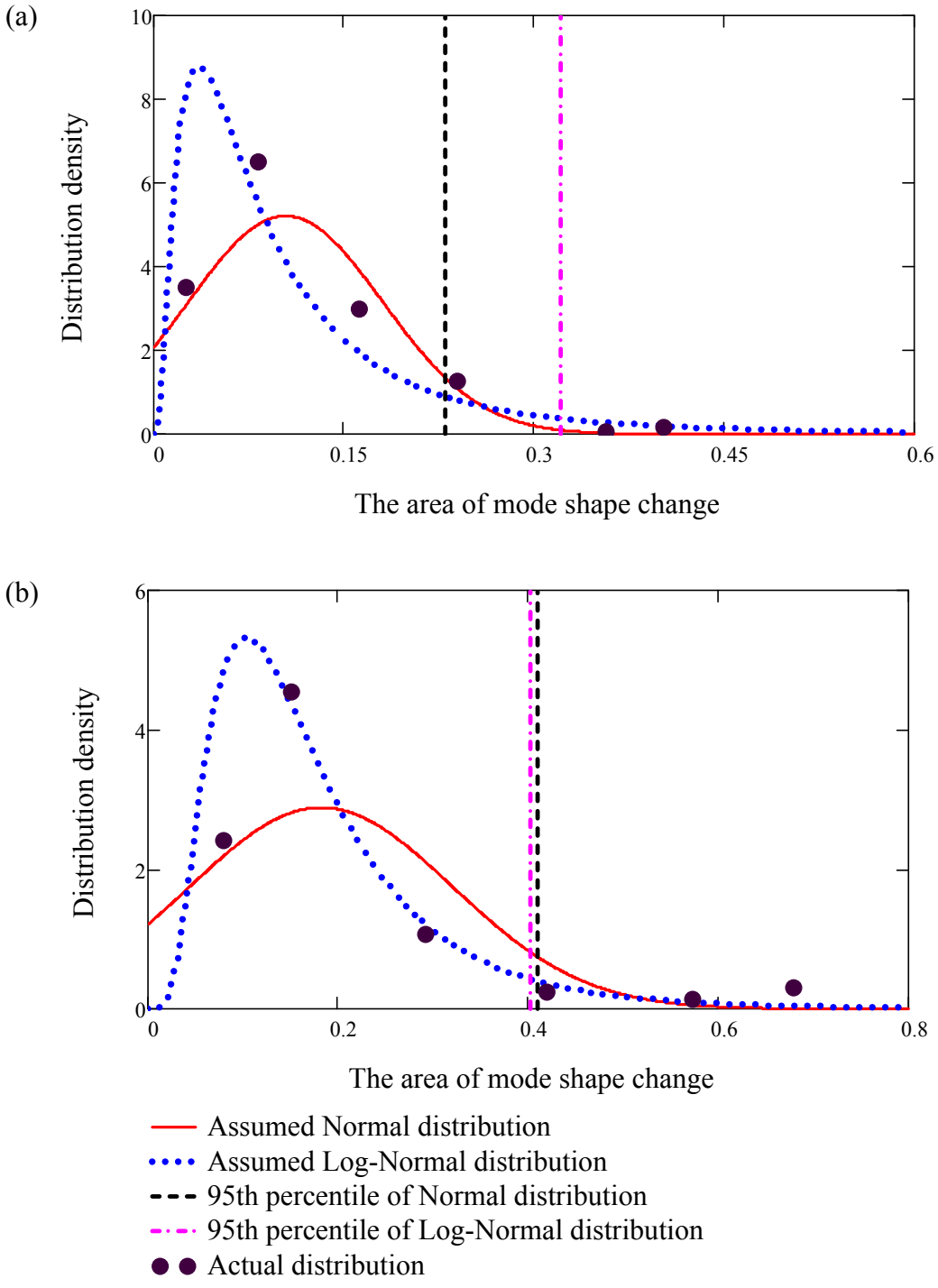

Figure G.12. Comparison of the probability density between the actual distribution and the assumed Normal and Log-Normal distributions of ΔA, for Test Protocols: (a) 21 and (b) 22.

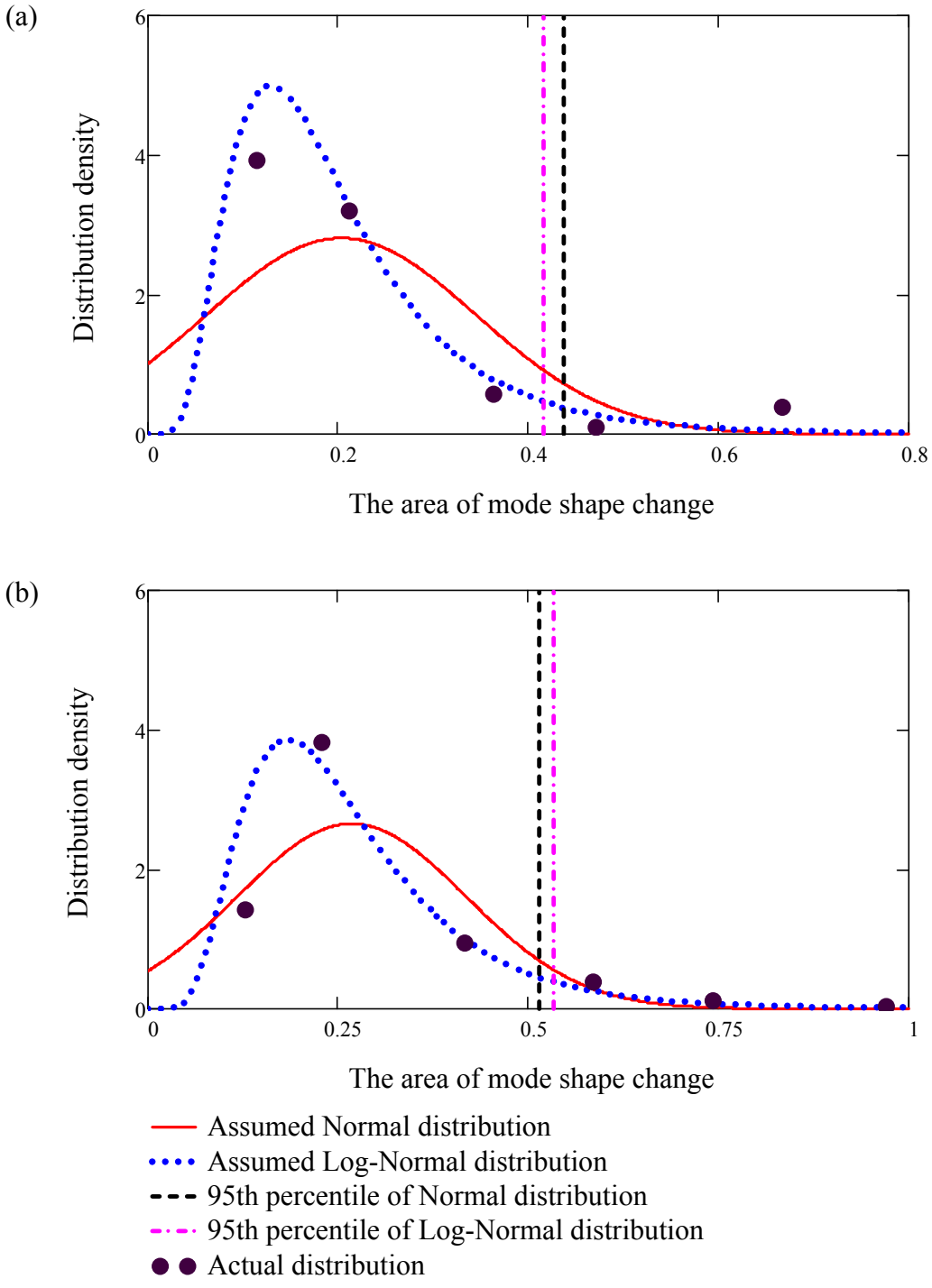

Figure G.13. Comparison of the probability density between the actual distribution and the assumed Normal and Log-Normal distributions of ΔA, for Test Protocols: (a) 23 and (b) 24.

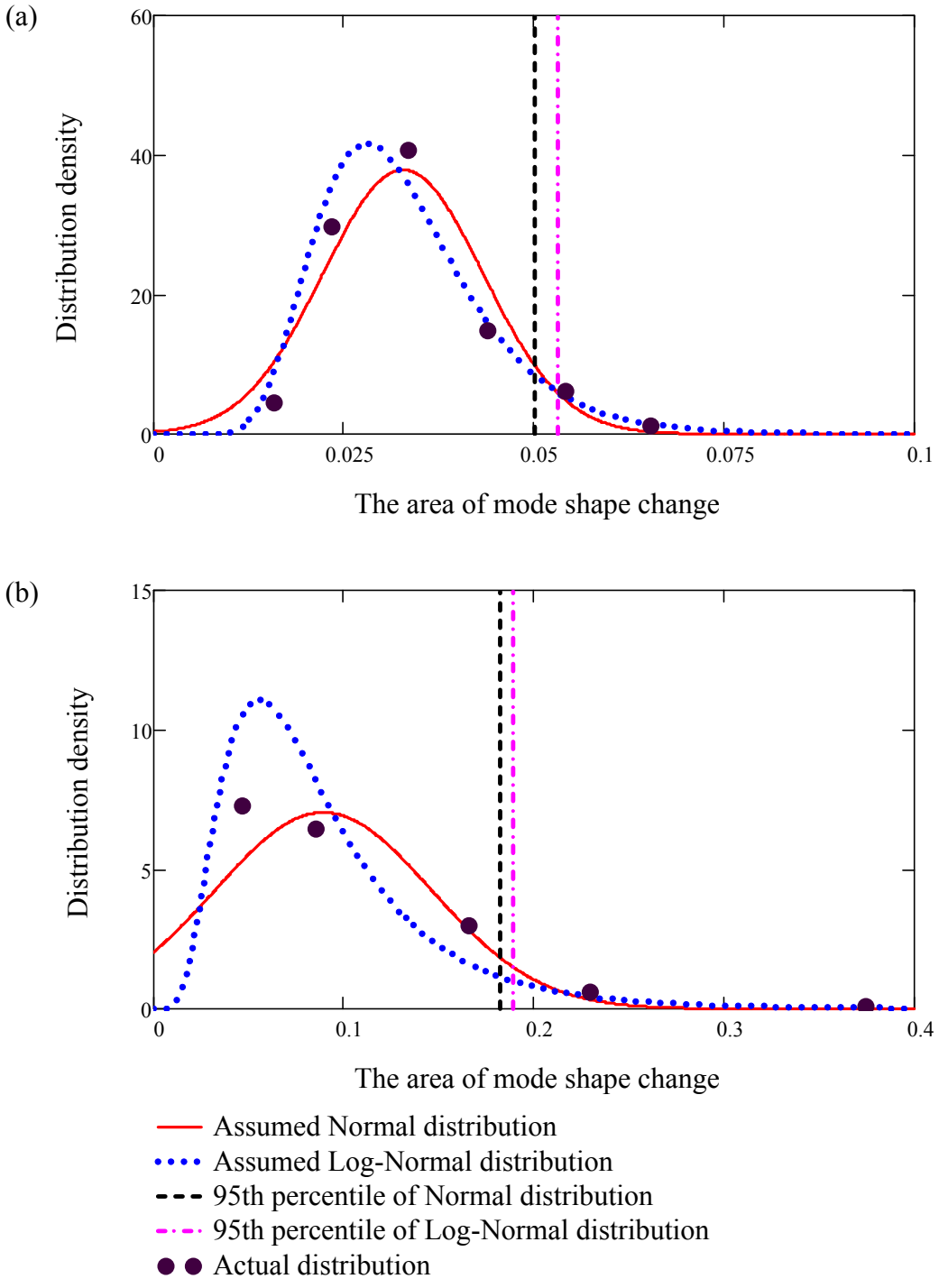

Figure G.14. Comparison of the probability density between the actual distribution and the assumed Normal and Log-Normal distributions of ΔA, for Test Protocols: (a) 25 and (b) 26.

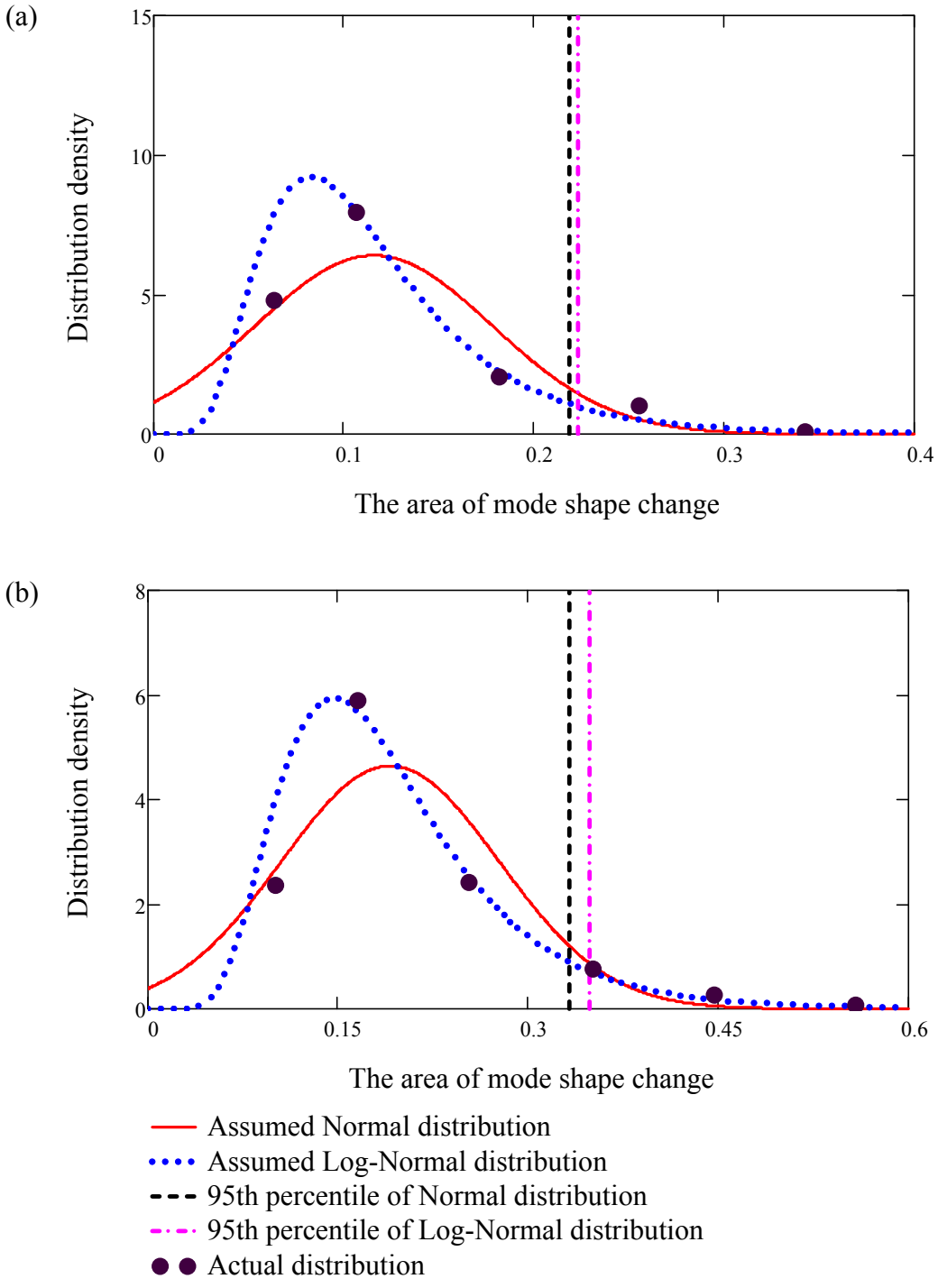

Figure G.15. Comparison of the probability density between the actual distribution and the assumed Normal and Log-Normal distributions of ΔA, for Test Protocols: (a) 27 and (b) 28.

APPENDIX H. **ADDITIONAL INFORMATION FOR DETECTION OF THE PRESENCE OF DAMAGE**

This appendix presents additional information for detection of the presence of damage, as described in Section 6.2.5, Section 6.2.6, and Section 6.2.7.

Tables H.1 to H.4 present the summary of area of change in the first mode shape due to Damage Cases 4 to 26 for different test trials when Test Protocol 1 was used, which are similar to the results listed in Table 6.7.

Tables H.5 to H.39 present the summary of area of change in the first mode shape due to Damage Cases 1 to 26 for different test trials when Test Protocols 2 to 8 were used.

Figures H.1 to H.8 present comparisons of the assumed Normal distributions of the area of mode shape change for the undamaged group of 170 pairs and the damaged group of 25 data pairs for Damage Cases 4 to 26, when Test Protocol 1 was used. The results in these figures are similar to those presented in Fig. 6.7.

Figures H.9 to H.35 present the distribution with the assumed Normal distribution for Damage Cases 1 to 26, when Test Protocols 2 to 4 were used.

Tables H.40 to H.43 present the probabilities that there was no change in condition using the assumed Normal distributions (i.e., the probability that the ΔA value obtained when there was a change in the condition did not exceed those that obtained when there was no change in condition), for Damage Cases 4 to 26 using all 28 Test Protocols, which are similar to results listed in Table 6.8.

Tables H.44 to H.47 present the probabilities that there was no change in condition using the assumed Log-Normal distributions (i.e., the probability that the ΔA value obtained when there was a change in the condition did not exceed those that obtained when there was no change in condition), for Damage Cases 4 to 26 using all 28 Test Protocols, which are similar to results listed in Table 6.9.

Tables H.48 to H.51 present the ratios of the area of the mode shape changes to the corresponding threshold values, defined as the 95^{th} percentile of assumed Log-Normal distributions, as listed in Table 6.6, due to Damage Cases 4 to 26 for all 28 Test Protocols, which supply additional information for Section 6.2.6.

Figures H.36 to H.42 present comparisons of mean ΔA values from 25 data pairs for all single damage cases to the 90% and 95% threshold values, when Test Protocols 2 to 8 were used, which are similar to the results presented in Fig. 6.9.

Figures H.43 to H.49 present ratios of area of mode shape change (the average of 25 values) to the 90% threshold values when Test Protocols 1 to 28 were used, which are similar to results presented in Figs. 6.10 to 6.16 where the ratios were calculated using 95% threshold values.

Table H.1. The summary of area of change in the first mode shape due to Damage Cases 4 to 9 for different test trials when Test Protocol 1 was used.

	Area of mode shape change					
Trials	Case 4	Case 5	Case 6	Case 7	Case 8	Case 9
set11	1.55%	2.64%	3.52%	2.35%	3.11%	2.79%
set12	1.56%	2.65%	3.38%	2.27%	3.04%	2.78%
set13	1.53%	2.61%	3.33%	2.34%	2.95%	2.78%
set14	1.53%	2.63%	3.32%	2.28%	2.93%	2.78%
set15	1.50%	2.61%	3.31%	2.36%	2.95%	2.70%
set21	1.81%	2.64%	3.52%	2.32%	3.11%	2.80%
set22	1.75%	2.63%	3.38%	2.24%	3.05%	2.79%
set23	1.76%	2.58%	3.34%	2.32%	2.95%	2.78%
set24	1.67%	2.63%	3.33%	2.26%	2.94%	2.78%
set25	1.75%	2.58%	3.32%	2.33%	2.96%	2.71%
set31	1.65%	2.66%	3.54%	2.36%	3.13%	2.82%
set32	1.66%	2.67%	3.41%	2.28%	3.07%	2.81%
set33	1.59%	2.62%	3.36%	2.36%	2.97%	2.80%
set34	1.60%	2.65%	3.35%	2.30%	2.96%	2.80%
set35	1.58%	2.62%	3.34%	2.37%	2.98%	2.73%
set41	1.79%	2.76%	3.63%	2.48%	3.22%	2.91%
set42	1.81%	2.79%	3.50%	2.40%	3.16%	2.90%
set43	1.75%	2.74%	3.45%	2.48%	3.06%	2.89%
set44	1.76%	2.75%	3.44%	2.42%	3.05%	2.89%
set45	1.73%	2.74%	3.43%	2.49%	3.07%	2.82%
set51	1.65%	2.72%	3.61%	2.44%	3.21%	2.89%
set52	1.66%	2.74%	3.48%	2.36%	3.14%	2.88%
set53	1.60%	2.70%	3.42%	2.44%	3.05%	2.88%
set54	1.60%	2.70%	3.41%	2.37%	3.03%	2.88%
set55	1.58%	2.70%	3.41%	2.45%	3.05%	2.80%
Min	1.50%	2.58%	3.31%	2.24%	2.93%	2.70%
Mean	1.66%	2.67%	3.42%	2.36%	3.05%	2.82%
STDEV	0.10%	0.06%	0.09%	0.07%	0.08%	0.06%
C.O.V	5.84%	2.20%	2.69%	3.06%	2.77%	2.11%

Min = Minimum value of the area of mode shape change in all trials;
Mean = The average value of the area of mode shape change in all trials;
STDEV = Standard deviation of the samples;
C.O.V = Coefficient of variation of the samples.

Table H.2. The summary of area of change in the first mode shape due to Damage Cases 10 to 15 for different test trials when Test Protocol 1 was used.

	Area of mode shape change					
Trials	Case 10	Case 11	Case 12	Case 13	Case 14	Case 15
set11	0.65%	0.47%	1.97%	0.58%	0.21%	0.49%
set12	0.67%	0.46%	1.93%	0.62%	0.22%	0.54%
set13	0.70%	0.51%	1.93%	0.67%	0.22%	0.50%
set14	0.81%	0.36%	1.89%	0.68%	0.29%	0.49%
set15	0.68%	0.36%	1.89%	0.59%	0.23%	0.49%
set21	0.64%	0.50%	1.98%	0.57%	0.27%	0.48%
set22	0.66%	0.48%	1.94%	0.59%	0.28%	0.53%
set23	0.69%	0.54%	1.94%	0.64%	0.28%	0.49%
set24	0.80%	0.38%	1.91%	0.65%	0.35%	0.48%
set25	0.67%	0.37%	1.90%	0.57%	0.29%	0.48%
set31	0.64%	0.48%	1.97%	0.56%	0.28%	0.48%
set32	0.65%	0.46%	1.94%	0.59%	0.28%	0.53%
set33	0.69%	0.52%	1.93%	0.65%	0.28%	0.50%
set34	0.79%	0.37%	1.90%	0.66%	0.35%	0.49%
set35	0.66%	0.42%	1.89%	0.56%	0.28%	0.49%
set41	0.64%	0.44%	1.97%	0.61%	0.28%	0.54%
set42	0.65%	0.42%	1.93%	0.65%	0.28%	0.57%
set43	0.69%	0.37%	1.92%	0.71%	0.28%	0.53%
set44	0.79%	0.46%	1.89%	0.72%	0.36%	0.52%
set45	0.66%	0.49%	1.89%	0.60%	0.28%	0.52%
set51	0.62%	0.46%	1.96%	0.61%	0.22%	0.49%
set52	0.65%	0.45%	1.92%	0.65%	0.22%	0.54%
set53	0.65%	0.50%	1.92%	0.71%	0.22%	0.50%
set54	0.75%	0.35%	1.88%	0.72%	0.29%	0.50%
set55	0.63%	0.39%	1.88%	0.61%	0.23%	0.49%
Min	0.62%	0.35%	1.88%	0.56%	0.21%	0.48%
Mean	0.68%	0.44%	1.92%	0.63%	0.27%	0.51%
STDEV	0.06%	0.06%	0.03%	0.05%	0.04%	0.02%
C.O.V	8.23%	13.06%	1.57%	8.15%	15.21%	4.74%

Min = Minimum value of the area of mode shape change in all trials;
Mean = The average value of the area of mode shape change in all trials;
STDEV = Standard deviation of the samples;
C.O.V = Coefficient of variation of the samples.

Table H.3. The summary of area of change in the first mode shape due to Damage Cases 16 to 21 for different test trials when Test Protocol 1 was used.

	Area of mode shape change					
Trials	Case 16	Case 17	Case 18	Case 19	Case 20	Case 21
set11	0.26%	6.98%	6.89%	5.45%	5.98%	6.60%
set12	0.13%	6.85%	7.22%	5.54%	5.99%	6.61%
set13	0.14%	7.07%	6.99%	5.54%	5.99%	6.66%
set14	0.21%	7.10%	7.07%	5.62%	5.99%	6.78%
set15	0.24%	6.96%	7.00%	5.51%	6.07%	6.63%
set21	0.21%	6.97%	6.88%	5.44%	5.97%	6.59%
set22	0.18%	6.83%	7.21%	5.53%	5.97%	6.60%
set23	0.19%	7.06%	6.98%	5.53%	5.98%	6.65%
set24	0.24%	7.09%	7.06%	5.61%	5.98%	6.77%
set25	0.26%	6.95%	6.99%	5.50%	6.05%	6.62%
set31	0.23%	6.97%	6.89%	5.44%	5.97%	6.60%
set32	0.14%	6.84%	7.21%	5.54%	5.98%	6.61%
set33	0.15%	7.06%	6.99%	5.54%	5.99%	6.66%
set34	0.19%	7.10%	7.06%	5.62%	5.99%	6.78%
set35	0.22%	6.96%	6.99%	5.50%	6.06%	6.63%
set41	0.21%	6.98%	6.89%	5.45%	5.98%	6.60%
set42	0.13%	6.85%	7.22%	5.55%	5.99%	6.62%
set43	0.14%	7.07%	6.99%	5.54%	5.99%	6.66%
set44	0.18%	7.11%	7.07%	5.63%	5.99%	6.78%
set45	0.20%	6.96%	7.00%	5.51%	6.07%	6.63%
set51	0.21%	6.99%	6.90%	5.46%	5.99%	6.61%
set52	0.13%	6.86%	7.23%	5.55%	6.00%	6.62%
set53	0.14%	7.08%	7.00%	5.55%	6.00%	6.67%
set54	0.18%	7.11%	7.08%	5.64%	6.00%	6.79%
set55	0.20%	6.97%	7.01%	5.52%	6.08%	6.64%
Min	0.13%	6.83%	6.88%	5.44%	5.97%	6.59%
Mean	0.19%	6.99%	7.03%	5.53%	6.00%	6.66%
STDEV	0.04%	0.09%	0.11%	0.06%	0.03%	0.07%
C.O.V	22.30%	1.32%	1.57%	1.08%	0.56%	1.00%

Min = Minimum value of the area of mode shape change in all trials;
Mean = The average value of the area of mode shape change in all trials;
STDEV = Standard deviation of the samples;
C.O.V = Coefficient of variation of the samples.

Table H.4. The summary of area of change in the first mode shape due to Damage Cases 22 to 26 for different test trials when Test Protocol 1 was used.

	Area of mode shape change				
Trials	Case 22	Case 23	Case 24	Case 25	Case 26
set11	6.50%	2.42%	2.42%	2.05%	2.13%
set12	6.52%	2.40%	2.40%	1.98%	2.15%
set13	6.58%	2.47%	2.47%	2.02%	2.17%
set14	6.45%	2.48%	2.48%	2.03%	2.20%
set15	6.29%	2.37%	2.37%	2.03%	2.23%
set21	6.49%	2.43%	2.43%	2.06%	2.14%
set22	6.51%	2.41%	2.41%	1.99%	2.17%
set23	6.57%	2.48%	2.48%	2.03%	2.18%
set24	6.44%	2.49%	2.49%	2.04%	2.21%
set25	6.27%	2.38%	2.38%	2.04%	2.24%
set31	6.50%	2.42%	2.42%	2.05%	2.13%
set32	6.52%	2.40%	2.40%	1.99%	2.16%
set33	6.58%	2.48%	2.48%	2.02%	2.17%
set34	6.45%	2.49%	2.49%	2.03%	2.20%
set35	6.28%	2.38%	2.38%	2.03%	2.23%
set41	6.51%	2.42%	2.42%	2.04%	2.13%
set42	6.53%	2.40%	2.40%	1.98%	2.15%
set43	6.58%	2.47%	2.47%	2.02%	2.17%
set44	6.45%	2.48%	2.48%	2.02%	2.20%
set45	6.29%	2.37%	2.37%	2.03%	2.22%
set51	6.52%	2.41%	2.41%	2.04%	2.12%
set52	6.53%	2.39%	2.39%	1.97%	2.14%
set53	6.59%	2.46%	2.46%	2.01%	2.16%
set54	6.46%	2.47%	2.47%	2.02%	2.19%
set55	6.30%	2.36%	2.36%	2.02%	2.22%
Min	6.27%	2.36%	2.36%	1.97%	2.12%
Mean	6.47%	2.43%	2.43%	2.02%	2.18%
STDEV	0.10%	0.04%	0.04%	0.02%	0.04%
C.O.V	1.59%	1.79%	1.79%	1.13%	1.64%

Min = Minimum value of the area of mode shape change in all trials;
Mean = The average value of the area of mode shape change in all trials;
STDEV = Standard deviation of the samples;
C.O.V = Coefficient of variation of the samples.

Table H.5. The summary of area of change in the first mode shape due to Damage Cases 1 to 3 for different test trials when Test Protocol 2 was used.

	Area of mode shape change		
Trials	Case 1	Case 2	Case 3
set11	7.96%	1.09%	0.62%
set12	7.98%	1.01%	0.62%
set13	7.79%	1.04%	0.62%
set14	8.09%	1.03%	0.64%
set15	8.12%	1.06%	0.66%
set21	8.02%	1.08%	0.69%
set22	8.04%	1.00%	0.72%
set23	7.85%	1.02%	0.71%
set24	8.15%	1.02%	0.74%
set25	8.19%	1.05%	0.76%
set31	7.96%	0.93%	0.66%
set32	7.98%	0.82%	0.70%
set33	7.79%	0.88%	0.68%
set34	8.08%	0.85%	0.72%
set35	8.12%	0.88%	0.74%
set41	7.92%	1.17%	0.63%
set42	7.94%	1.07%	0.66%
set43	7.75%	1.10%	0.65%
set44	8.05%	1.11%	0.68%
set45	8.09%	1.14%	0.70%
set51	7.93%	1.22%	0.64%
set52	7.95%	1.13%	0.67%
set53	7.76%	1.16%	0.65%
set54	8.05%	1.16%	0.69%
set55	8.09%	1.19%	0.70%
Min	7.75%	0.82%	0.62%
Mean	7.99%	1.05%	0.68%
STDEV	0.12%	0.11%	0.04%
C.O.V	1.56%	10.32%	5.82%

Min = Minimum value of the area of mode shape change in all trials;
Mean = The average value of the area of mode shape change in all trials;
STDEV = Standard deviation of the samples;
C.O.V = Coefficient of variation of the samples.

Table H.6. The summary of area of change in the first mode shape due to Damage Cases 4 to 9 for different test trials when Test Protocol 2 was used.

	Area of mode shape change					
Trials	Case 4	Case 5	Case 6	Case 7	Case 8	Case 9
set11	1.69%	1.43%	2.18%	0.88%	2.19%	2.01%
set12	1.73%	1.40%	2.15%	0.81%	2.14%	1.99%
set13	1.75%	1.79%	2.19%	0.82%	2.11%	2.00%
set14	1.74%	1.36%	2.17%	0.86%	1.94%	1.98%
set15	1.68%	1.37%	2.14%	0.76%	1.99%	1.95%
set21	1.71%	1.43%	2.17%	0.87%	2.21%	2.01%
set22	1.75%	1.41%	2.14%	0.80%	2.15%	1.98%
set23	1.77%	1.80%	2.19%	0.80%	2.10%	2.00%
set24	1.75%	1.36%	2.16%	0.85%	1.95%	1.98%
set25	1.70%	1.37%	2.13%	0.75%	1.99%	1.94%
set31	1.72%	1.27%	1.99%	0.73%	2.04%	1.82%
set32	1.76%	1.24%	1.95%	0.65%	1.98%	1.79%
set33	1.78%	1.63%	2.01%	0.66%	1.94%	1.81%
set34	1.76%	1.19%	1.98%	0.71%	1.77%	1.79%
set35	1.71%	1.20%	1.95%	0.62%	1.81%	1.74%
set41	1.77%	1.58%	2.29%	0.94%	2.33%	2.12%
set42	1.82%	1.55%	2.24%	0.89%	2.27%	2.10%
set43	1.84%	1.94%	2.29%	0.88%	2.24%	2.11%
set44	1.83%	1.50%	2.27%	0.92%	2.08%	2.09%
set45	1.76%	1.51%	2.24%	0.82%	2.11%	2.05%
set51	1.73%	1.58%	2.29%	1.00%	2.36%	2.15%
set52	1.77%	1.56%	2.24%	0.93%	2.29%	2.13%
set53	1.80%	1.95%	2.32%	0.93%	2.25%	2.14%
set54	1.78%	1.51%	2.27%	0.97%	2.10%	2.12%
set55	1.72%	1.52%	2.24%	0.88%	2.14%	2.08%
Min	1.68%	1.19%	1.95%	0.62%	1.77%	1.74%
Mean	1.75%	1.50%	2.17%	0.83%	2.10%	1.99%
STDEV	0.04%	0.21%	0.11%	0.10%	0.15%	0.12%
C.O.V	2.40%	13.74%	5.18%	12.09%	7.34%	6.11%

Min = Minimum value of the area of mode shape change in all trials;
Mean = The average value of the area of mode shape change in all trials;
STDEV = Standard deviation of the samples;
C.O.V = Coefficient of variation of the samples.

Table H.7. The summary of area of change in the first mode shape due to Damage Cases 10 to 15 for different test trials when Test Protocol 2 was used.

	Area of mode shape change					
Trials	Case 10	Case 11	Case 12	Case 13	Case 14	Case 15
set11	2.39%	0.23%	0.86%	0.81%	0.22%	0.51%
set12	2.28%	0.23%	0.89%	0.83%	0.23%	0.56%
set13	2.40%	0.20%	0.75%	0.70%	0.34%	0.58%
set14	2.35%	0.22%	0.75%	0.61%	0.41%	0.57%
set15	2.25%	0.20%	0.73%	0.70%	0.32%	0.50%
set21	2.34%	0.30%	0.92%	0.80%	0.20%	0.50%
set22	2.24%	0.32%	0.95%	0.83%	0.17%	0.54%
set23	2.36%	0.29%	0.81%	0.69%	0.28%	0.57%
set24	2.31%	0.29%	0.78%	0.60%	0.35%	0.57%
set25	2.21%	0.30%	0.79%	0.70%	0.31%	0.51%
set31	2.38%	0.22%	0.88%	0.93%	0.25%	0.34%
set32	2.28%	0.22%	0.91%	0.95%	0.24%	0.40%
set33	2.39%	0.20%	0.76%	0.80%	0.17%	0.41%
set34	2.35%	0.20%	0.77%	0.69%	0.19%	0.42%
set35	2.25%	0.20%	0.74%	0.81%	0.19%	0.36%
set41	2.36%	0.32%	0.83%	1.00%	0.34%	0.35%
set42	2.25%	0.31%	0.87%	1.03%	0.32%	0.38%
set43	2.37%	0.29%	0.71%	0.88%	0.16%	0.39%
set44	2.32%	0.31%	0.68%	0.77%	0.15%	0.40%
set45	2.22%	0.28%	0.70%	0.89%	0.22%	0.33%
set51	2.30%	0.32%	0.84%	0.93%	0.23%	0.41%
set52	2.20%	0.32%	0.87%	0.95%	0.21%	0.46%
set53	2.32%	0.27%	0.72%	0.80%	0.16%	0.47%
set54	2.27%	0.30%	0.72%	0.69%	0.23%	0.48%
set55	2.17%	0.30%	0.71%	0.81%	0.19%	0.42%
Min	2.17%	0.20%	0.68%	0.60%	0.15%	0.33%
Mean	2.30%	0.26%	0.80%	0.81%	0.24%	0.46%
STDEV	0.07%	0.05%	0.08%	0.12%	0.07%	0.08%
C.O.V	2.85%	17.81%	9.93%	14.54%	29.24%	17.47%

Min = Minimum value of the area of mode shape change in all trials;
Mean = The average value of the area of mode shape change in all trials;
STDEV = Standard deviation of the samples;
C.O.V = Coefficient of variation of the samples.

Table H.8. The summary of area of change in the first mode shape due to Damage Cases 16 to 21 for different test trials when Test Protocol 2 was used.

	Area of mode shape change					
Trials	Case 16	Case 17	Case 18	Case 19	Case 20	Case 21
set11	0.21%	7.12%	6.53%	6.54%	5.98%	7.88%
set12	0.19%	7.22%	6.50%	6.67%	6.02%	7.83%
set13	0.22%	7.19%	6.52%	6.64%	6.02%	7.90%
set14	0.18%	7.16%	6.48%	6.48%	6.02%	7.95%
set15	0.17%	7.17%	6.46%	6.61%	6.09%	7.80%
set21	0.25%	7.18%	6.60%	6.61%	6.05%	7.94%
set22	0.24%	7.28%	6.57%	6.73%	6.08%	7.89%
set23	0.21%	7.26%	6.59%	6.72%	6.08%	7.96%
set24	0.17%	7.22%	6.55%	6.55%	6.09%	8.01%
set25	0.16%	7.23%	6.53%	6.69%	6.15%	7.86%
set31	0.20%	7.12%	6.53%	6.54%	5.98%	7.88%
set32	0.18%	7.22%	6.50%	6.66%	6.02%	7.83%
set33	0.22%	7.19%	6.52%	6.64%	6.01%	7.89%
set34	0.18%	7.16%	6.48%	6.48%	6.02%	7.95%
set35	0.20%	7.17%	6.46%	6.61%	6.08%	7.80%
set41	0.23%	7.08%	6.49%	6.50%	5.95%	7.84%
set42	0.22%	7.18%	6.47%	6.63%	5.98%	7.79%
set43	0.25%	7.16%	6.48%	6.61%	5.98%	7.86%
set44	0.20%	7.12%	6.45%	6.45%	5.99%	7.91%
set45	0.21%	7.13%	6.43%	6.58%	6.05%	7.76%
set51	0.28%	7.09%	6.50%	6.51%	5.95%	7.85%
set52	0.24%	7.19%	6.47%	6.63%	5.99%	7.80%
set53	0.21%	7.16%	6.49%	6.61%	5.99%	7.86%
set54	0.20%	7.13%	6.45%	6.45%	5.99%	7.92%
set55	0.19%	7.14%	6.43%	6.58%	6.05%	7.77%
Min	0.16%	7.08%	6.43%	6.45%	5.95%	7.76%
Mean	0.21%	7.17%	6.50%	6.59%	6.02%	7.87%
STDEV	0.03%	0.05%	0.04%	0.08%	0.05%	0.06%
C.O.V	14.01%	0.70%	0.68%	1.21%	0.83%	0.82%

Min = Minimum value of the area of mode shape change in all trials;
Mean = The average value of the area of mode shape change in all trials;
STDEV = Standard deviation of the samples;
C.O.V = Coefficient of variation of the samples.

Table H.9. The summary of area of change in the first mode shape due to Damage Cases 22 to 26 for different test trials when Test Protocol 2 was used.

	Area of mode shape change				
Trials	Case 22	Case 23	Case 24	Case 25	Case 26
set11	7.77%	1.47%	1.40%	1.29%	1.17%
set12	7.78%	1.45%	1.37%	1.30%	1.19%
set13	7.78%	1.33%	1.25%	1.24%	1.17%
set14	7.81%	1.23%	1.21%	1.33%	1.19%
set15	7.81%	1.34%	1.23%	1.30%	1.27%
set21	7.84%	1.54%	1.47%	1.37%	1.24%
set22	7.84%	1.52%	1.44%	1.37%	1.26%
set23	7.84%	1.40%	1.32%	1.32%	1.24%
set24	7.87%	1.30%	1.28%	1.40%	1.26%
set25	7.88%	1.41%	1.30%	1.37%	1.34%
set31	7.77%	1.50%	1.43%	1.34%	1.21%
set32	7.78%	1.48%	1.39%	1.35%	1.23%
set33	7.78%	1.36%	1.28%	1.30%	1.22%
set34	7.80%	1.26%	1.23%	1.37%	1.23%
set35	7.81%	1.38%	1.25%	1.35%	1.31%
set41	7.74%	1.44%	1.38%	1.27%	1.14%
set42	7.74%	1.42%	1.34%	1.28%	1.17%
set43	7.74%	1.31%	1.23%	1.22%	1.16%
set44	7.77%	1.20%	1.19%	1.30%	1.16%
set45	7.78%	1.32%	1.21%	1.28%	1.24%
set51	7.74%	1.44%	1.37%	1.27%	1.15%
set52	7.75%	1.42%	1.33%	1.28%	1.16%
set53	7.75%	1.30%	1.22%	1.23%	1.15%
set54	7.78%	1.20%	1.18%	1.31%	1.16%
set55	7.78%	1.31%	1.20%	1.28%	1.24%
Min	7.74%	1.20%	1.18%	1.22%	1.14%
Mean	7.79%	1.37%	1.30%	1.31%	1.21%
STDEV	0.04%	0.10%	0.09%	0.05%	0.05%
C.O.V	0.52%	7.03%	6.83%	3.65%	4.35%

Min = Minimum value of the area of mode shape change in all trials;
Mean = The average value of the area of mode shape change in all trials;
STDEV = Standard deviation of the samples;
C.O.V = Coefficient of variation of the samples.

Table H.10. The summary of area of change in the first mode shape due to Damage Cases 1 to 3 for different test trials when Test Protocol 3 was used.

	Area of mode shape change		
Trials	Case 1	Case 2	Case 3
set11	7.72%	1.48%	0.85%
set12	7.52%	1.48%	0.80%
set13	7.27%	1.47%	0.79%
set14	7.31%	1.40%	0.80%
set15	7.42%	1.46%	0.57%
set21	7.74%	1.27%	0.76%
set22	7.55%	1.24%	0.70%
set23	7.28%	1.24%	0.69%
set24	7.32%	1.19%	0.70%
set25	7.44%	1.21%	0.52%
set31	7.66%	1.05%	0.80%
set32	7.47%	1.11%	0.75%
set33	7.22%	1.10%	0.75%
set34	7.26%	1.09%	0.74%
set35	7.37%	1.08%	0.53%
set41	7.76%	1.15%	0.78%
set42	7.57%	1.25%	0.75%
set43	7.32%	1.22%	0.75%
set44	7.36%	1.20%	0.75%
set45	7.47%	1.21%	0.52%
set51	7.74%	1.17%	0.81%
set52	7.54%	1.25%	0.77%
set53	7.29%	1.23%	0.74%
set54	7.33%	1.21%	0.76%
set55	7.44%	1.21%	0.56%
Min	7.22%	1.05%	0.52%
Mean	7.45%	1.24%	0.72%
STDEV	0.17%	0.13%	0.10%
C.O.V	2.25%	10.23%	13.56%

Min = Minimum value of the area of mode shape change in all trials;
Mean = The average value of the area of mode shape change in all trials;
STDEV = Standard deviation of the samples;
C.O.V = Coefficient of variation of the samples.

Table H.11. The summary of area of change in the first mode shape due to Damage Cases 4 to 9 for different test trials when Test Protocol 3 was used.

	Area of mode shape change					
Trials	Case 4	Case 5	Case 6	Case 7	Case 8	Case 9
set11	0.94%	1.58%	2.43%	1.08%	2.28%	2.28%
set12	0.95%	1.36%	2.56%	1.18%	2.27%	2.32%
set13	0.83%	1.64%	2.53%	1.08%	2.24%	2.28%
set14	1.00%	1.36%	2.58%	1.06%	2.25%	2.35%
set15	0.83%	1.31%	2.46%	1.02%	2.22%	2.33%
set21	0.99%	1.32%	2.23%	0.80%	2.11%	2.13%
set22	1.00%	1.15%	2.34%	0.92%	2.11%	2.17%
set23	0.89%	1.39%	2.30%	0.82%	2.06%	2.12%
set24	1.05%	1.09%	2.36%	0.81%	2.10%	2.20%
set25	0.89%	1.07%	2.28%	0.75%	2.06%	2.17%
set31	1.02%	1.03%	2.12%	0.63%	1.97%	1.90%
set32	1.02%	1.11%	2.21%	0.71%	1.92%	1.91%
set33	0.90%	1.46%	2.21%	0.69%	1.88%	1.94%
set34	1.07%	1.15%	2.19%	0.72%	1.94%	1.89%
set35	0.90%	1.00%	2.13%	0.70%	1.91%	1.93%
set41	0.92%	1.10%	2.15%	0.81%	2.05%	1.97%
set42	0.93%	1.19%	2.27%	0.91%	2.00%	1.98%
set43	0.86%	1.52%	2.25%	0.86%	1.95%	2.01%
set44	1.01%	1.24%	2.23%	0.89%	2.00%	1.96%
set45	0.86%	1.07%	2.17%	0.87%	1.96%	1.98%
set51	1.16%	1.24%	2.22%	0.80%	2.11%	2.04%
set52	1.17%	1.23%	2.33%	0.92%	2.07%	2.06%
set53	1.07%	1.55%	2.32%	0.85%	2.02%	2.08%
set54	1.24%	1.27%	2.30%	0.87%	2.06%	2.09%
set55	1.07%	1.11%	2.25%	0.87%	2.03%	2.07%
Min	0.83%	1.00%	2.12%	0.63%	1.88%	1.89%
Mean	0.98%	1.26%	2.30%	0.87%	2.06%	2.09%
STDEV	0.11%	0.18%	0.13%	0.14%	0.12%	0.14%
C.O.V	11.12%	14.50%	5.63%	15.85%	5.63%	6.92%

Min = Minimum value of the area of mode shape change in all trials;
Mean = The average value of the area of mode shape change in all trials;
STDEV = Standard deviation of the samples;
C.O.V = Coefficient of variation of the samples.

Table H.12. The summary of area of change in the first mode shape due to Damage Cases 10 to 15 for different test trials when Test Protocol 3 was used.

	Area of mode shape change					
Trials	Case 10	Case 11	Case 12	Case 13	Case 14	Case 15
set11	0.77%	0.33%	1.20%	1.08%	0.30%	0.92%
set12	0.88%	0.34%	1.11%	1.05%	0.38%	1.01%
set13	0.93%	0.28%	1.12%	1.11%	0.34%	1.02%
set14	0.90%	0.29%	1.09%	1.04%	0.40%	1.01%
set15	0.85%	0.26%	1.16%	1.09%	0.35%	1.10%
set21	0.80%	0.35%	1.19%	1.16%	0.30%	0.88%
set22	0.91%	0.39%	1.13%	1.13%	0.29%	0.96%
set23	0.97%	0.34%	1.15%	1.18%	0.30%	0.98%
set24	0.93%	0.30%	1.09%	1.11%	0.27%	0.97%
set25	0.88%	0.29%	1.17%	1.16%	0.27%	1.05%
set31	0.76%	0.31%	1.26%	1.14%	0.32%	0.88%
set32	0.87%	0.29%	1.17%	1.11%	0.37%	0.97%
set33	0.93%	0.30%	1.20%	1.16%	0.30%	0.99%
set34	0.89%	0.28%	1.16%	1.10%	0.34%	0.98%
set35	0.85%	0.28%	1.23%	1.12%	0.30%	1.05%
set41	0.83%	0.31%	1.19%	1.21%	0.35%	0.80%
set42	0.95%	0.29%	1.11%	1.16%	0.37%	0.90%
set43	1.00%	0.25%	1.13%	1.22%	0.33%	0.90%
set44	0.96%	0.25%	1.11%	1.15%	0.33%	0.89%
set45	0.91%	0.27%	1.16%	1.17%	0.35%	0.99%
set51	0.81%	0.35%	1.17%	1.08%	0.22%	0.94%
set52	0.93%	0.37%	1.09%	1.05%	0.34%	1.01%
set53	0.97%	0.29%	1.11%	1.11%	0.29%	1.04%
set54	0.94%	0.29%	1.08%	1.04%	0.29%	1.02%
set55	0.89%	0.30%	1.14%	1.07%	0.26%	1.10%
Min	0.76%	0.25%	1.08%	1.04%	0.22%	0.80%
Mean	0.89%	0.30%	1.15%	1.12%	0.32%	0.98%
STDEV	0.06%	0.04%	0.05%	0.05%	0.04%	0.07%
C.O.V	7.11%	11.81%	3.99%	4.66%	13.25%	7.47%

Min = Minimum value of the area of mode shape change in all trials;
Mean = The average value of the area of mode shape change in all trials;
STDEV = Standard deviation of the samples;
C.O.V = Coefficient of variation of the samples.

Table H.13. The summary of area of change in the first mode shape due to Damage Cases 16 to 21 for different test trials when Test Protocol 3 was used.

	Area of mode shape change					
Trials	Case 16	Case 17	Case 18	Case 19	Case 20	Case 21
set11	0.38%	6.51%	5.79%	4.99%	5.46%	6.19%
set12	0.45%	6.52%	5.86%	4.97%	5.42%	6.32%
set13	0.51%	6.53%	5.87%	5.01%	5.46%	6.34%
set14	0.43%	6.56%	5.83%	4.86%	5.41%	6.30%
set15	0.41%	6.57%	6.05%	5.06%	5.39%	6.28%
set21	0.30%	6.53%	5.82%	5.01%	5.48%	6.22%
set22	0.38%	6.55%	5.88%	4.99%	5.44%	6.34%
set23	0.46%	6.55%	5.90%	5.03%	5.48%	6.36%
set24	0.36%	6.59%	5.86%	4.88%	5.43%	6.33%
set25	0.38%	6.59%	6.07%	5.08%	5.41%	6.30%
set31	0.23%	6.46%	5.73%	4.94%	5.40%	6.14%
set32	0.35%	6.46%	5.80%	4.92%	5.37%	6.26%
set33	0.37%	6.47%	5.82%	4.96%	5.40%	6.28%
set34	0.25%	6.51%	5.77%	4.80%	5.36%	6.25%
set35	0.34%	6.51%	5.99%	5.01%	5.34%	6.22%
set41	0.30%	6.56%	5.83%	5.04%	5.50%	6.23%
set42	0.44%	6.56%	5.90%	5.02%	5.47%	6.36%
set43	0.35%	6.57%	5.91%	5.06%	5.50%	6.38%
set44	0.37%	6.60%	5.87%	4.90%	5.46%	6.35%
set45	0.36%	6.61%	6.09%	5.11%	5.43%	6.32%
set51	0.24%	6.53%	5.81%	5.01%	5.48%	6.21%
set52	0.34%	6.54%	5.88%	4.99%	5.44%	6.34%
set53	0.36%	6.55%	5.89%	5.03%	5.48%	6.36%
set54	0.26%	6.58%	5.85%	4.88%	5.43%	6.32%
set55	0.33%	6.59%	6.07%	5.08%	5.41%	6.29%
Min	0.23%	6.46%	5.73%	4.80%	5.34%	6.14%
Mean	0.36%	6.54%	5.89%	4.99%	5.43%	6.29%
STDEV	0.07%	0.04%	0.10%	0.08%	0.04%	0.06%
C.O.V	19.46%	0.63%	1.64%	1.53%	0.79%	0.99%

Min = Minimum value of the area of mode shape change in all trials;
Mean = The average value of the area of mode shape change in all trials;
STDEV = Standard deviation of the samples;
C.O.V = Coefficient of variation of the samples.

Table H.14. The summary of area of change in the first mode shape due to Damage Cases 22 to 26 for different test trials when Test Protocol 3 was used.

	Area of mode shape change				
Trials	Case 22	Case 23	Case 24	Case 25	Case 26
set11	6.07%	2.00%	2.12%	1.41%	1.38%
set12	6.13%	2.03%	2.08%	1.39%	1.47%
set13	6.13%	2.10%	2.08%	1.40%	1.39%
set14	6.12%	2.02%	2.03%	1.35%	1.42%
set15	6.18%	2.08%	2.13%	1.32%	1.39%
set21	6.09%	2.07%	2.15%	1.48%	1.38%
set22	6.16%	2.10%	2.10%	1.44%	1.45%
set23	6.15%	2.17%	2.09%	1.45%	1.37%
set24	6.15%	2.09%	2.07%	1.40%	1.41%
set25	6.20%	2.13%	2.14%	1.36%	1.38%
set31	6.01%	2.12%	2.22%	1.50%	1.43%
set32	6.08%	2.15%	2.17%	1.46%	1.49%
set33	6.07%	2.22%	2.17%	1.48%	1.42%
set34	6.07%	2.14%	2.13%	1.43%	1.47%
set35	6.12%	2.19%	2.22%	1.39%	1.43%
set41	6.11%	2.00%	2.11%	1.36%	1.32%
set42	6.18%	2.02%	2.06%	1.33%	1.43%
set43	6.17%	2.08%	2.07%	1.32%	1.33%
set44	6.16%	2.02%	2.01%	1.27%	1.36%
set45	6.22%	2.06%	2.11%	1.25%	1.33%
set51	6.09%	2.00%	2.12%	1.41%	1.37%
set52	6.15%	2.03%	2.07%	1.39%	1.46%
set53	6.15%	2.11%	2.08%	1.40%	1.38%
set54	6.14%	2.02%	2.02%	1.35%	1.41%
set55	6.20%	2.08%	2.12%	1.31%	1.38%
Min	6.01%	2.00%	2.01%	1.25%	1.32%
Mean	6.13%	2.08%	2.11%	1.39%	1.40%
STDEV	0.05%	0.06%	0.05%	0.06%	0.04%
C.O.V	0.81%	3.02%	2.59%	4.63%	3.17%

Min = Minimum value of the area of mode shape change in all trials;
Mean = The average value of the area of mode shape change in all trials;
STDEV = Standard deviation of the samples;
C.O.V = Coefficient of variation of the samples.

Table H.15. The summary of area of change in the first mode shape due to Damage Cases 1 to 3 for different test trials when Test Protocol 4 was used.

	Area of mode shape change		
Trials	Case 1	Case 2	Case 3
set11	7.23%	1.49%	0.70%
set12	9.10%	1.33%	0.75%
set13	7.72%	1.29%	0.84%
set14	7.13%	1.37%	0.70%
set15	8.28%	1.40%	0.85%
set21	7.13%	3.58%	0.73%
set22	9.02%	3.48%	0.76%
set23	7.63%	3.46%	0.82%
set24	7.03%	3.55%	0.74%
set25	8.20%	3.49%	0.82%
set31	7.18%	2.33%	0.74%
set32	9.21%	2.22%	0.81%
set33	7.82%	2.18%	0.89%
set34	7.08%	2.23%	0.78%
set35	8.39%	2.26%	0.86%
set41	7.32%	1.38%	0.69%
set42	9.34%	1.29%	0.73%
set43	7.95%	1.21%	0.75%
set44	7.22%	1.34%	0.66%
set45	8.53%	1.31%	0.77%
set51	7.19%	2.75%	0.81%
set52	9.13%	2.65%	0.86%
set53	7.78%	2.61%	0.96%
set54	7.07%	2.69%	0.85%
set55	8.33%	2.71%	0.90%
Min	7.03%	1.21%	0.66%
Mean	7.92%	2.22%	0.79%
STDEV	0.79%	0.85%	0.07%
C.O.V	9.91%	38.05%	9.28%

Min = Minimum value of the area of mode shape change in all trials;
Mean = The average value of the area of mode shape change in all trials;
STDEV = Standard deviation of the samples;
C.O.V = Coefficient of variation of the samples.

Table H.16. The summary of area of change in the first mode shape due to Damage Cases 4 to 9 for different test trials when Test Protocol 4 was used.

	Area of mode shape change					
Trials	Case 4	Case 5	Case 6	Case 7	Case 8	Case 9
set11	1.11%	1.74%	2.31%	1.44%	2.42%	2.30%
set12	1.12%	1.49%	2.37%	1.29%	2.42%	2.43%
set13	1.09%	2.02%	2.34%	1.48%	2.43%	2.47%
set14	1.10%	1.77%	2.53%	1.35%	2.40%	2.42%
set15	0.97%	1.60%	2.40%	1.44%	2.21%	2.33%
set21	1.19%	3.84%	4.30%	3.83%	4.49%	4.45%
set22	1.20%	3.62%	4.44%	3.72%	4.48%	4.48%
set23	1.22%	4.06%	4.27%	3.87%	4.33%	4.51%
set24	1.19%	3.84%	4.41%	3.77%	4.43%	4.52%
set25	1.06%	3.70%	4.34%	3.84%	4.28%	4.40%
set31	1.31%	2.48%	2.94%	2.57%	3.16%	3.11%
set32	1.31%	2.27%	3.03%	2.45%	3.15%	3.17%
set33	1.23%	2.69%	2.85%	2.60%	3.01%	3.20%
set34	1.26%	2.49%	3.04%	2.45%	3.13%	3.21%
set35	1.12%	2.35%	2.99%	2.56%	2.99%	3.11%
set41	1.21%	1.66%	2.35%	1.39%	2.40%	2.30%
set42	1.21%	1.43%	2.35%	1.29%	2.35%	2.36%
set43	1.11%	1.93%	2.34%	1.42%	2.31%	2.41%
set44	1.15%	1.70%	2.47%	1.37%	2.32%	2.41%
set45	1.04%	1.54%	2.44%	1.36%	2.17%	2.30%
set51	1.23%	3.09%	3.55%	3.11%	3.71%	3.66%
set52	1.25%	2.88%	3.68%	3.00%	3.65%	3.69%
set53	1.16%	3.29%	3.49%	3.15%	3.50%	3.70%
set54	1.16%	3.12%	3.66%	3.02%	3.59%	3.72%
set55	1.05%	2.97%	3.61%	3.13%	3.47%	3.56%
Min	0.97%	1.43%	2.31%	1.29%	2.17%	2.30%
Mean	1.16%	2.54%	3.14%	2.44%	3.15%	3.21%
STDEV	0.09%	0.85%	0.77%	0.97%	0.80%	0.82%
C.O.V	7.38%	33.55%	24.57%	39.97%	25.49%	25.52%

Min = Minimum value of the area of mode shape change in all trials;
Mean = The average value of the area of mode shape change in all trials;
STDEV = Standard deviation of the samples;
C.O.V = Coefficient of variation of the samples.

Table H.17. The summary of area of change in the first mode shape due to Damage Cases 10 to 15 for different test trials when Test Protocol 4 was used.

	Area of mode shape change					
Trials	Case 10	Case 11	Case 12	Case 13	Case 14	Case 15
set11	1.08%	0.56%	3.21%	1.98%	0.98%	1.19%
set12	0.97%	0.55%	2.36%	1.85%	0.81%	1.29%
set13	1.03%	0.52%	2.47%	1.96%	0.67%	1.01%
set14	0.90%	0.45%	2.41%	2.21%	1.01%	1.23%
set15	1.13%	0.64%	2.36%	1.97%	2.02%	1.39%
set21	1.08%	0.44%	3.12%	1.39%	1.09%	1.01%
set22	1.02%	0.55%	2.29%	1.44%	0.88%	1.05%
set23	1.02%	0.55%	2.34%	1.41%	0.75%	0.86%
set24	0.94%	0.43%	2.33%	1.41%	1.06%	0.96%
set25	1.16%	0.51%	2.30%	1.25%	2.14%	1.18%
set31	1.18%	0.41%	2.97%	1.80%	1.00%	0.91%
set32	1.06%	0.54%	2.29%	1.88%	0.84%	0.91%
set33	1.08%	0.51%	2.43%	1.85%	0.64%	0.74%
set34	1.00%	0.43%	2.37%	1.81%	0.98%	0.88%
set35	1.23%	0.61%	2.31%	1.67%	2.02%	1.07%
set41	1.07%	0.48%	2.94%	1.72%	0.90%	1.21%
set42	0.89%	0.64%	2.22%	1.82%	0.84%	1.27%
set43	0.95%	0.58%	2.44%	1.76%	0.71%	0.98%
set44	0.84%	0.53%	2.35%	1.70%	0.94%	1.22%
set45	1.05%	0.54%	2.23%	1.58%	1.89%	1.36%
set51	1.08%	0.54%	2.98%	1.53%	0.79%	2.25%
set52	0.94%	0.60%	2.30%	1.58%	0.63%	2.33%
set53	0.98%	0.57%	2.46%	1.55%	0.51%	2.02%
set54	0.87%	0.45%	2.40%	1.56%	0.83%	2.27%
set55	1.09%	0.62%	2.30%	1.40%	1.89%	2.41%
Min	0.84%	0.41%	2.22%	1.25%	0.51%	0.74%
Mean	1.03%	0.53%	2.49%	1.68%	1.07%	1.32%
STDEV	0.10%	0.07%	0.29%	0.23%	0.49%	0.51%
C.O.V	9.61%	12.59%	11.83%	13.96%	45.65%	38.49%

Min = Minimum value of the area of mode shape change in all trials;
Mean = The average value of the area of mode shape change in all trials;
STDEV = Standard deviation of the samples;
C.O.V = Coefficient of variation of the samples.

Table H.18. The summary of area of change in the first mode shape due to Damage Cases 16 to 21 for different test trials when Test Protocol 4 was used.

	Area of mode shape change					
Trials	Case 16	Case 17	Case 18	Case 19	Case 20	Case 21
set11	0.82%	6.23%	5.67%	4.70%	5.57%	5.85%
set12	0.71%	6.33%	5.74%	4.76%	5.35%	5.86%
set13	0.77%	6.33%	5.77%	4.63%	5.44%	5.69%
set14	0.77%	6.25%	5.68%	4.66%	5.33%	5.84%
set15	0.77%	6.32%	5.73%	4.76%	5.39%	5.91%
set21	0.79%	6.13%	5.57%	4.60%	5.47%	5.75%
set22	0.70%	6.23%	5.64%	4.67%	5.25%	5.77%
set23	0.76%	6.23%	5.67%	4.57%	5.34%	5.59%
set24	0.71%	6.15%	5.58%	4.56%	5.23%	5.74%
set25	0.73%	6.22%	5.63%	4.67%	5.29%	5.81%
set31	0.95%	6.20%	5.70%	4.69%	5.53%	5.80%
set32	0.82%	6.30%	5.77%	4.72%	5.31%	5.82%
set33	0.84%	6.28%	5.83%	4.67%	5.40%	5.66%
set34	0.84%	6.22%	5.71%	4.68%	5.29%	5.80%
set35	0.96%	6.28%	5.78%	4.81%	5.37%	5.86%
set41	0.80%	6.34%	5.85%	4.83%	5.66%	5.94%
set42	0.70%	6.44%	5.91%	4.86%	5.45%	5.96%
set43	0.71%	6.43%	5.96%	4.79%	5.52%	5.80%
set44	0.68%	6.35%	5.84%	4.82%	5.43%	5.94%
set45	0.74%	6.43%	5.91%	4.95%	5.51%	6.00%
set51	0.81%	6.15%	5.67%	4.64%	5.55%	5.77%
set52	0.63%	6.26%	5.74%	4.70%	5.32%	5.79%
set53	0.75%	6.27%	5.83%	4.65%	5.43%	5.62%
set54	0.70%	6.21%	5.71%	4.65%	5.31%	5.77%
set55	0.79%	6.25%	5.77%	4.78%	5.36%	5.83%
Min	0.63%	6.13%	5.57%	4.56%	5.23%	5.59%
Mean	0.77%	6.27%	5.75%	4.71%	5.40%	5.81%
STDEV	0.08%	0.08%	0.10%	0.10%	0.11%	0.10%
C.O.V	9.91%	1.33%	1.76%	2.03%	2.00%	1.75%

Min = Minimum value of the area of mode shape change in all trials;
Mean = The average value of the area of mode shape change in all trials;
STDEV = Standard deviation of the samples;
C.O.V = Coefficient of variation of the samples.

Table H.19. The summary of area of change in the first mode shape due to Damage Cases 22 to 26 for different test trials when Test Protocol 4 was used.

	Area of mode shape change				
Trials	Case 22	Case 23	Case 24	Case 25	Case 26
set11	5.77%	2.39%	2.19%	2.92%	3.03%
set12	5.60%	2.48%	2.31%	2.94%	2.84%
set13	5.67%	2.37%	2.42%	2.67%	2.81%
set14	5.63%	2.35%	2.11%	2.85%	2.84%
set15	5.68%	2.33%	2.47%	2.96%	3.05%
set21	5.67%	2.37%	2.11%	2.88%	2.98%
set22	5.50%	2.44%	2.24%	2.91%	2.80%
set23	5.57%	2.37%	2.38%	2.63%	2.76%
set24	5.53%	2.34%	2.03%	2.81%	2.80%
set25	5.58%	2.31%	2.36%	2.92%	3.01%
set31	5.72%	2.43%	2.23%	2.95%	2.99%
set32	5.55%	2.49%	2.32%	2.98%	2.84%
set33	5.62%	2.43%	2.45%	2.71%	2.80%
set34	5.59%	2.41%	2.11%	2.88%	2.85%
set35	5.63%	2.38%	2.52%	2.99%	3.02%
set41	5.87%	2.33%	2.21%	2.84%	2.86%
set42	5.69%	2.42%	2.28%	2.87%	2.74%
set43	5.76%	2.32%	2.38%	2.59%	2.69%
set44	5.73%	2.27%	2.08%	2.78%	2.74%
set45	5.77%	2.28%	2.57%	2.89%	2.91%
set51	5.69%	2.44%	2.28%	3.01%	3.06%
set52	5.52%	2.47%	2.38%	3.04%	2.83%
set53	5.59%	2.43%	2.50%	2.76%	2.85%
set54	5.56%	2.46%	2.17%	2.94%	2.87%
set55	5.61%	2.41%	2.59%	3.02%	3.09%
Min	5.50%	2.27%	2.03%	2.59%	2.69%
Mean	5.64%	2.39%	2.31%	2.87%	2.88%
STDEV	0.09%	0.06%	0.16%	0.12%	0.11%
C.O.V	1.62%	2.57%	6.88%	4.26%	3.94%

Min = Minimum value of the area of mode shape change in all trials;
Mean = The average value of the area of mode shape change in all trials;
STDEV = Standard deviation of the samples;
C.O.V = Coefficient of variation of the samples.

Table H.20. The summary of area of change in the first mode shape due to Damage Casess 1 to 3 for different test trials when Test Protocol 5 was used.

	Area of mode shape change		
Trials	Case 1	Case 2	Case 3
set11	6.59%	1.82%	1.80%
set12	6.43%	1.65%	2.32%
set13	6.81%	0.96%	1.74%
set14	6.35%	1.93%	1.68%
set15	6.85%	1.45%	1.38%
set21	6.64%	1.72%	1.92%
set22	6.49%	1.67%	2.34%
set23	6.86%	0.97%	1.79%
set24	6.40%	1.81%	1.82%
set25	6.91%	1.34%	1.44%
set31	6.61%	1.82%	1.43%
set32	6.46%	1.64%	1.84%
set33	6.83%	0.96%	1.31%
set34	6.37%	1.92%	1.34%
set35	6.88%	1.44%	1.07%
set41	6.50%	1.83%	1.73%
set42	6.34%	1.75%	2.38%
set43	6.71%	1.08%	1.77%
set44	6.25%	1.96%	1.58%
set45	6.76%	1.48%	1.39%
set51	6.58%	1.45%	1.56%
set52	6.43%	1.30%	2.04%
set53	6.80%	0.62%	1.45%
set54	6.34%	1.55%	1.45%
set55	6.85%	1.07%	1.14%
Min	6.25%	0.62%	1.07%
Mean	6.60%	1.49%	1.67%
STDEV	0.21%	0.37%	0.35%
C.O.V	3.18%	24.72%	20.95%

Min = Minimum value of the area of mode shape change in all trials;
Mean = The average value of the area of mode shape change in all trials;
STDEV = Standard deviation of the samples;
C.O.V = Coefficient of variation of the samples.

Table H.21. The summary of area of change in the first mode shape due to Damage Cases 4 to 9 for different test trials when Test Protocol 5 was used.

	Area of mode shape change					
Trials	Case 4	Case 5	Case 6	Case 7	Case 8	Case 9
set11	2.31%	1.16%	1.42%	0.60%	1.36%	1.31%
set12	2.32%	1.43%	1.44%	0.55%	1.33%	1.38%
set13	2.26%	1.21%	1.68%	0.50%	1.38%	1.11%
set14	2.13%	1.11%	1.52%	0.99%	1.49%	1.52%
set15	2.20%	1.34%	1.26%	0.85%	1.45%	1.23%
set21	1.92%	1.04%	1.29%	0.62%	1.23%	1.18%
set22	2.21%	1.37%	1.31%	0.45%	1.20%	1.24%
set23	2.10%	1.13%	1.55%	0.66%	1.44%	0.98%
set24	2.07%	1.03%	1.43%	0.95%	1.40%	1.44%
set25	2.19%	1.22%	1.16%	0.77%	1.32%	1.06%
set31	2.12%	1.38%	1.60%	0.89%	1.50%	1.39%
set32	2.31%	1.65%	1.60%	0.59%	1.53%	1.54%
set33	2.18%	1.43%	1.88%	0.52%	1.46%	1.24%
set34	2.07%	1.21%	1.67%	1.20%	1.64%	1.75%
set35	2.18%	1.53%	1.31%	0.77%	1.67%	1.30%
set41	2.43%	0.92%	1.08%	0.54%	1.05%	0.89%
set42	2.39%	1.22%	1.19%	0.56%	1.08%	0.96%
set43	2.36%	0.99%	1.40%	0.60%	1.09%	0.76%
set44	2.23%	0.84%	1.25%	0.73%	1.15%	1.19%
set45	2.27%	1.06%	0.91%	0.53%	1.21%	0.86%
set51	2.41%	1.42%	1.63%	0.86%	1.55%	1.43%
set52	2.59%	1.69%	1.64%	0.47%	1.58%	1.57%
set53	2.47%	1.48%	1.91%	0.68%	1.56%	1.28%
set54	2.34%	1.26%	1.71%	1.24%	1.68%	1.80%
set55	2.45%	1.57%	1.34%	0.76%	1.72%	1.34%
Min	1.92%	0.84%	0.91%	0.45%	1.05%	0.76%
Mean	2.26%	1.27%	1.45%	0.71%	1.40%	1.27%
STDEV	0.15%	0.23%	0.24%	0.21%	0.20%	0.26%
C.O.V	6.74%	17.88%	16.87%	29.96%	14.06%	20.70%

Min = Minimum value of the area of mode shape change in all trials;
Mean = The average value of the area of mode shape change in all trials;
STDEV = Standard deviation of the samples;
C.O.V = Coefficient of variation of the samples.

Table H.22. The summary of area of change in the first mode shape due to Damage Cases 10 to 15 for different test trials when Test Protocol 5 was used.

	Area of mode shape change					
Trials	Case 10	Case 11	Case 12	Case 13	Case 14	Case 15
set11	1.22%	0.90%	0.83%	0.90%	1.00%	0.68%
set12	0.70%	1.38%	0.55%	0.57%	0.65%	0.70%
set13	0.84%	1.36%	0.83%	0.37%	0.73%	0.60%
set14	0.75%	0.91%	0.99%	0.98%	1.08%	0.56%
set15	0.87%	1.67%	0.82%	0.56%	0.76%	0.72%
set21	1.37%	0.55%	0.68%	0.90%	0.67%	0.49%
set22	0.65%	1.06%	0.57%	0.59%	0.60%	0.74%
set23	0.99%	0.79%	0.76%	0.65%	1.03%	0.52%
set24	0.68%	0.47%	0.88%	1.04%	0.97%	0.54%
set25	0.82%	1.29%	0.77%	0.83%	0.60%	0.63%
set31	1.06%	0.44%	0.76%	0.72%	0.65%	0.68%
set32	0.53%	0.93%	0.53%	0.61%	0.59%	0.85%
set33	0.86%	0.84%	0.79%	0.49%	1.03%	0.72%
set34	0.57%	0.60%	0.92%	0.86%	0.80%	0.97%
set35	0.69%	1.13%	0.76%	0.61%	0.70%	0.67%
set41	1.58%	0.64%	0.98%	0.73%	0.99%	0.65%
set42	1.00%	1.18%	0.61%	0.58%	0.75%	0.91%
set43	1.13%	0.90%	0.90%	0.44%	0.75%	0.77%
set44	1.12%	0.44%	1.06%	0.78%	1.09%	0.60%
set45	1.34%	1.38%	0.88%	0.49%	0.78%	0.79%
set51	1.12%	0.82%	1.07%	0.68%	0.79%	0.61%
set52	0.65%	1.38%	0.64%	0.51%	0.51%	0.70%
set53	0.97%	1.15%	0.89%	0.62%	1.02%	0.49%
set54	0.67%	0.63%	1.10%	0.77%	0.85%	0.58%
set55	0.74%	1.64%	0.80%	0.68%	0.74%	0.70%
Min	0.53%	0.44%	0.53%	0.37%	0.51%	0.49%
Mean	0.92%	0.98%	0.81%	0.68%	0.81%	0.67%
STDEV	0.27%	0.37%	0.16%	0.17%	0.17%	0.12%
C.O.V	29.76%	37.55%	19.68%	25.39%	21.57%	18.04%

Min = Minimum value of the area of mode shape change in all trials;
Mean = The average value of the area of mode shape change in all trials;
STDEV = Standard deviation of the samples;
C.O.V = Coefficient of variation of the samples.

Table H.23. The summary of area of change in the first mode shape due to Damage Cases 16 to 21 for different test trials when Test Protocol 5 was used.

	Area of mode shape change					
Trials	Case 16	Case 17	Case 18	Case 19	Case 20	Case 21
set11	0.29%	7.87%	6.86%	5.03%	5.49%	6.63%
set12	0.36%	8.09%	6.54%	4.64%	5.42%	6.02%
set13	0.57%	7.39%	6.90%	4.80%	5.59%	6.29%
set14	0.78%	7.66%	6.89%	4.90%	5.17%	6.08%
set15	0.60%	7.55%	7.20%	4.79%	5.51%	6.20%
set21	0.58%	7.92%	6.91%	5.08%	5.54%	6.69%
set22	0.55%	8.14%	6.59%	4.70%	5.47%	6.07%
set23	0.48%	7.44%	6.96%	4.85%	5.64%	6.35%
set24	0.69%	7.72%	6.94%	4.96%	5.22%	6.14%
set25	0.41%	7.61%	7.26%	4.84%	5.57%	6.25%
set31	0.47%	7.89%	6.88%	5.05%	5.51%	6.65%
set32	0.45%	8.11%	6.56%	4.67%	5.44%	6.04%
set33	0.50%	7.41%	6.92%	4.82%	5.61%	6.32%
set34	0.71%	7.69%	6.91%	4.93%	5.19%	6.11%
set35	0.49%	7.58%	7.23%	4.81%	5.54%	6.22%
set41	0.45%	7.77%	6.76%	4.93%	5.39%	6.54%
set42	0.39%	8.00%	6.44%	4.55%	5.33%	5.92%
set43	0.27%	7.29%	6.81%	4.70%	5.49%	6.20%
set44	0.83%	7.57%	6.80%	4.81%	5.07%	5.99%
set45	0.50%	7.46%	7.11%	4.69%	5.42%	6.11%
set51	0.41%	7.86%	6.85%	5.02%	5.48%	6.62%
set52	0.44%	8.08%	6.53%	4.64%	5.41%	6.01%
set53	0.50%	7.38%	6.89%	4.79%	5.58%	6.29%
set54	0.64%	7.66%	6.88%	4.90%	5.16%	6.08%
set55	0.52%	7.55%	7.20%	4.78%	5.51%	6.19%
Min	0.27%	7.29%	6.44%	4.55%	5.07%	5.92%
Mean	0.51%	7.71%	6.87%	4.83%	5.43%	6.24%
STDEV	0.14%	0.25%	0.22%	0.14%	0.16%	0.23%
C.O.V	26.99%	3.31%	3.23%	2.89%	2.86%	3.61%

Min = Minimum value of the area of mode shape change in all trials;
Mean = The average value of the area of mode shape change in all trials;
STDEV = Standard deviation of the samples;
C.O.V = Coefficient of variation of the samples.

Table H.24. The summary of area of change in the first mode shape due to Damage Cases 22 to 26 for different test trials when Test Protocol 5 was used.

	Area of mode shape change				
Trials	Case 22	Case 23	Case 24	Case 25	Case 26
set11	5.87%	1.39%	1.20%	1.23%	1.36%
set12	5.37%	1.03%	1.35%	0.81%	1.14%
set13	5.47%	1.08%	1.60%	1.04%	0.89%
set14	6.11%	1.52%	1.43%	1.07%	1.21%
set15	5.19%	1.30%	1.26%	1.04%	0.78%
set21	5.92%	1.36%	1.09%	1.16%	1.27%
set22	5.42%	0.99%	1.25%	0.78%	1.04%
set23	5.52%	0.97%	1.53%	0.99%	0.78%
set24	6.17%	1.47%	1.32%	0.93%	1.14%
set25	5.24%	1.18%	1.16%	0.98%	0.73%
set31	5.89%	1.38%	1.08%	1.19%	1.31%
set32	5.38%	0.98%	1.30%	0.79%	1.08%
set33	5.49%	1.04%	1.57%	1.01%	0.82%
set34	6.13%	1.49%	1.33%	1.01%	1.10%
set35	5.21%	1.24%	1.20%	1.01%	0.70%
set41	5.77%	1.48%	1.22%	1.32%	1.45%
set42	5.27%	1.13%	1.46%	0.91%	1.24%
set43	5.37%	1.21%	1.69%	1.13%	1.04%
set44	6.02%	1.60%	1.47%	1.21%	1.11%
set45	5.09%	1.41%	1.35%	1.14%	0.80%
set51	5.86%	1.40%	1.19%	1.24%	1.39%
set52	5.36%	1.12%	1.44%	0.87%	1.22%
set53	5.46%	1.25%	1.63%	1.05%	1.10%
set54	6.10%	1.53%	1.48%	1.28%	0.94%
set55	5.18%	1.42%	1.33%	1.07%	0.80%
Min	5.09%	0.97%	1.08%	0.78%	0.70%
Mean	5.60%	1.28%	1.36%	1.05%	1.06%
STDEV	0.35%	0.20%	0.17%	0.15%	0.22%
C.O.V	6.25%	15.34%	12.32%	14.26%	21.09%

Min = Minimum value of the area of mode shape change in all trials;
Mean = The average value of the area of mode shape change in all trials;
STDEV = Standard deviation of the samples;
C.O.V = Coefficient of variation of the samples.

Table H.25. The summary of area of change in the first mode shape due to Damage Cases 1 to 3 for different test trials when Test Protocol 6 was used.

	Area of mode shape change		
Trials	Case 1	Case 2	Case 3
set11	7.13%	2.48%	3.74%
set12	6.69%	2.60%	2.98%
set13	8.21%	3.03%	2.78%
set14	8.85%	2.55%	2.76%
set15	7.25%	3.21%	3.74%
set21	6.90%	2.22%	4.08%
set22	6.69%	2.30%	3.12%
set23	7.54%	3.10%	3.08%
set24	8.34%	2.96%	3.39%
set25	6.96%	3.81%	4.49%
set31	5.32%	2.68%	1.80%
set32	4.88%	2.98%	2.04%
set33	6.56%	2.17%	2.04%
set34	7.01%	2.29%	1.92%
set35	5.56%	1.72%	2.69%
set41	6.25%	3.55%	2.13%
set42	5.88%	3.57%	1.75%
set43	7.19%	3.07%	2.42%
set44	7.95%	2.43%	2.45%
set45	6.39%	3.53%	2.63%
set51	6.28%	2.62%	2.35%
set52	6.08%	2.97%	1.96%
set53	6.81%	2.94%	2.02%
set54	7.59%	2.59%	1.80%
set55	6.27%	3.03%	2.07%
Min	4.88%	1.72%	1.75%
Mean	6.82%	2.82%	2.65%
STDEV	0.95%	0.50%	0.77%
C.O.V	13.85%	17.87%	28.92%

Min = Minimum value of the area of mode shape change in all trials;
Mean = The average value of the area of mode shape change in all trials;
STDEV = Standard deviation of the samples;
C.O.V = Coefficient of variation of the samples.

Table H.26. The summary of area of change in the first mode shape due to Damage Cases 4 to 9 for different test trials when Test Protocol 6 was used.

	Area of mode shape change					
Trials	Case 4	Case 5	Case 6	Case 7	Case 8	Case 9
set11	3.87%	2.27%	2.56%	1.71%	2.66%	2.19%
set12	4.28%	3.11%	2.21%	3.28%	3.68%	2.45%
set13	4.03%	2.07%	2.49%	2.71%	3.37%	2.06%
set14	3.11%	2.87%	3.02%	3.18%	2.92%	3.40%
set15	3.71%	2.22%	2.85%	3.25%	2.40%	2.16%
set21	3.57%	2.62%	1.67%	2.23%	3.17%	2.91%
set22	3.72%	3.03%	2.81%	3.25%	3.21%	2.80%
set23	3.61%	2.31%	1.78%	2.71%	3.03%	2.36%
set24	2.99%	2.51%	2.20%	2.74%	2.64%	3.08%
set25	3.58%	2.24%	2.17%	2.66%	2.10%	1.81%
set31	3.64%	3.13%	3.00%	2.63%	3.75%	2.43%
set32	3.52%	3.74%	2.40%	2.81%	3.09%	2.92%
set33	3.55%	3.10%	2.19%	1.52%	2.55%	2.56%
set34	3.43%	3.66%	3.34%	3.04%	2.96%	2.58%
set35	3.58%	2.79%	2.83%	2.99%	2.21%	2.24%
set41	4.42%	3.61%	3.14%	2.33%	2.27%	2.40%
set42	3.93%	4.61%	2.32%	3.05%	3.98%	3.02%
set43	4.24%	3.57%	3.02%	2.83%	2.82%	2.60%
set44	3.52%	4.40%	3.66%	3.72%	3.40%	3.84%
set45	3.55%	3.73%	3.20%	3.95%	3.16%	2.68%
set51	3.78%	2.25%	2.63%	1.70%	2.67%	2.33%
set52	4.16%	3.36%	2.21%	2.79%	3.37%	2.03%
set53	4.34%	2.26%	2.35%	2.44%	2.83%	1.70%
set54	3.51%	3.03%	2.81%	3.15%	2.76%	3.29%
set55	3.92%	2.23%	2.62%	3.21%	2.42%	2.19%
Min	2.99%	2.07%	1.67%	1.52%	2.10%	1.70%
Mean	3.74%	2.99%	2.62%	2.80%	2.94%	2.56%
STDEV	0.36%	0.71%	0.48%	0.58%	0.49%	0.51%
C.O.V	9.57%	23.80%	18.39%	20.89%	16.71%	19.80%

Min = Minimum value of the area of mode shape change in all trials;
Mean = The average value of the area of mode shape change in all trials;
STDEV = Standard deviation of the samples;
C.O.V = Coefficient of variation of the samples.

Table H.27. The summary of area of change in the first mode shape due to Damage Cases 10 to 15 for different test trials when Test Protocol 6 was used.

	Area of mode shape change					
Trials	Case 10	Case 11	Case 12	Case 13	Case 14	Case 15
set11	2.91%	2.53%	2.49%	2.30%	3.50%	3.31%
set12	2.47%	2.95%	2.73%	2.50%	3.32%	2.93%
set13	2.57%	2.61%	3.35%	3.41%	3.31%	4.12%
set14	2.89%	2.31%	2.58%	2.58%	3.02%	3.32%
set15	3.20%	2.85%	2.37%	2.55%	2.74%	2.95%
set21	3.57%	3.17%	2.31%	3.05%	2.96%	2.70%
set22	2.74%	1.97%	2.48%	2.67%	2.39%	3.48%
set23	3.99%	2.79%	2.89%	3.82%	2.99%	3.56%
set24	3.73%	4.19%	2.40%	3.52%	2.43%	3.64%
set25	3.70%	2.40%	1.96%	3.11%	2.42%	2.97%
set31	3.77%	4.14%	3.07%	4.13%	3.21%	2.50%
set32	2.32%	3.27%	2.80%	4.01%	2.61%	2.69%
set33	3.66%	3.74%	2.16%	3.84%	2.50%	3.40%
set34	4.30%	3.76%	1.71%	3.06%	2.88%	2.99%
set35	3.32%	3.15%	2.30%	3.11%	2.69%	2.22%
set41	4.59%	2.76%	2.62%	3.15%	3.07%	1.56%
set42	3.25%	3.44%	3.22%	2.61%	2.26%	2.35%
set43	3.67%	2.85%	2.12%	3.31%	1.86%	2.49%
set44	4.23%	2.08%	1.80%	2.43%	2.27%	2.68%
set45	4.65%	2.28%	1.88%	2.63%	2.55%	2.22%
set51	3.70%	3.15%	2.93%	3.13%	3.19%	2.17%
set52	2.73%	2.45%	3.31%	2.37%	2.34%	2.84%
set53	3.04%	3.15%	2.28%	2.54%	2.26%	3.04%
set54	3.97%	3.42%	2.18%	2.82%	2.19%	3.06%
set55	3.75%	2.51%	2.05%	2.15%	2.41%	2.97%
Min	2.32%	1.97%	1.71%	2.15%	1.86%	1.56%
Mean	3.47%	2.96%	2.48%	2.99%	2.69%	2.89%
STDEV	0.65%	0.60%	0.47%	0.56%	0.43%	0.56%
C.O.V	18.68%	20.31%	18.82%	18.68%	15.85%	19.34%

Min = Minimum value of the area of mode shape change in all trials;
Mean = The average value of the area of mode shape change in all trials;
STDEV = Standard deviation of the samples;
C.O.V = Coefficient of variation of the samples.

Table H.28. The summary of area of change in the first mode shape due to Damage Cases 16 to 21 for different test trials when Test Protocol 6 was used.

	Area of mode shape change					
Trials	Case 16	Case 17	Case 18	Case 19	Case 20	Case 21
set11	2.18%	6.38%	9.55%	8.06%	8.06%	9.68%
set12	3.11%	6.08%	8.57%	6.38%	7.06%	7.71%
set13	2.63%	8.54%	7.92%	6.37%	6.64%	9.85%
set14	1.65%	8.22%	8.54%	8.24%	7.60%	10.28%
set15	2.41%	8.75%	9.60%	6.60%	7.32%	8.77%
set21	2.06%	6.12%	8.87%	7.40%	7.69%	9.12%
set22	3.59%	5.82%	7.93%	5.98%	6.68%	6.95%
set23	3.12%	8.01%	6.94%	6.05%	6.20%	9.28%
set24	1.79%	7.93%	7.69%	7.83%	6.86%	9.76%
set25	2.50%	7.97%	8.79%	6.20%	6.90%	8.13%
set31	3.34%	4.60%	7.56%	6.18%	6.14%	7.84%
set32	2.40%	4.41%	6.62%	4.76%	5.39%	5.75%
set33	3.08%	6.64%	5.94%	4.44%	5.08%	7.96%
set34	2.81%	6.39%	6.68%	6.53%	5.69%	8.37%
set35	2.06%	6.97%	7.51%	4.72%	5.40%	7.07%
set41	1.80%	5.64%	8.53%	7.11%	7.38%	8.87%
set42	3.77%	5.39%	7.60%	5.17%	5.98%	6.88%
set43	3.66%	7.79%	6.84%	5.21%	5.80%	9.12%
set44	1.98%	7.36%	7.46%	7.50%	6.46%	9.35%
set45	2.43%	7.76%	8.50%	5.85%	6.62%	7.79%
set51	2.19%	5.44%	8.11%	6.73%	6.99%	8.40%
set52	3.92%	5.17%	7.26%	5.23%	5.68%	6.29%
set53	2.32%	7.22%	6.37%	5.41%	5.75%	8.58%
set54	2.37%	7.09%	6.98%	7.13%	6.14%	8.99%
set55	2.86%	7.28%	8.12%	5.51%	6.20%	7.48%
Min	1.65%	4.41%	5.94%	4.44%	5.08%	5.75%
Mean	2.64%	6.76%	7.78%	6.26%	6.47%	8.33%
STDEV	0.66%	1.23%	0.95%	1.07%	0.79%	1.16%
C.O.V	24.88%	18.21%	12.27%	17.01%	12.19%	13.93%

Min = Minimum value of the area of mode shape change in all trials;
Mean = The average value of the area of mode shape change in all trials;
STDEV = Standard deviation of the samples;
C.O.V = Coefficient of variation of the samples.

Table H.29. The summary of area of change in the first mode shape due to Damage Cases 22 to 26 for different test trials when Test Protocol 6 was used.

	Area of mode shape change				
Trials	Case 22	Case 23	Case 24	Case 25	Case 26
set11	9.53%	2.72%	2.19%	2.13%	2.77%
set12	7.48%	2.45%	1.93%	2.26%	4.00%
set13	9.44%	2.56%	1.88%	3.26%	2.78%
set14	10.70%	1.91%	1.66%	3.26%	2.79%
set15	8.79%	1.88%	2.47%	1.93%	3.39%
set21	9.03%	2.19%	3.17%	1.70%	2.54%
set22	7.20%	2.46%	2.47%	2.31%	3.45%
set23	8.97%	2.03%	2.61%	2.23%	2.08%
set24	10.15%	2.16%	1.89%	2.51%	2.04%
set25	8.38%	1.57%	2.14%	1.75%	2.49%
set31	7.53%	3.79%	3.67%	2.48%	3.23%
set32	5.44%	2.87%	3.64%	3.10%	3.03%
set33	7.68%	3.68%	3.46%	2.25%	3.23%
set34	8.66%	3.35%	2.46%	2.76%	3.06%
set35	6.91%	3.07%	2.27%	2.93%	2.82%
set41	8.43%	3.40%	3.56%	1.80%	2.55%
set42	6.74%	2.95%	2.77%	2.53%	3.04%
set43	8.49%	3.13%	2.80%	2.28%	2.98%
set44	9.60%	2.04%	1.60%	2.38%	2.45%
set45	7.79%	1.71%	2.52%	2.10%	2.49%
set51	8.26%	3.28%	3.65%	2.04%	2.30%
set52	6.37%	3.15%	3.01%	2.54%	2.77%
set53	8.34%	3.24%	3.23%	2.19%	2.75%
set54	9.39%	2.46%	2.09%	2.13%	2.29%
set55	7.54%	2.04%	2.77%	2.05%	2.24%
Min	5.44%	1.57%	1.60%	1.70%	2.04%
Mean	8.27%	2.64%	2.64%	2.36%	2.78%
STDEV	1.23%	0.64%	0.65%	0.43%	0.46%
C.O.V	14.85%	24.24%	24.61%	18.38%	16.64%

Min = Minimum value of the area of mode shape change in all trials;
Mean = The average value of the area of mode shape change in all trials;
STDEV = Standard deviation of the samples;
C.O.V = Coefficient of variation of the samples.

Table H.30. The summary of area of change in the first mode shape due to Damage Cases 1 to 3 for different test trials when Test Protocol 7 was used.

	Area of mode shape change		
Trials	Case 1	Case 2	Case 3
set11	6.28%	2.36%	3.46%
set12	7.96%	3.85%	4.74%
set13	7.35%	3.22%	2.78%
set14	7.69%	3.38%	3.91%
set15	6.94%	3.71%	3.26%
set21	6.20%	3.24%	4.84%
set22	7.55%	4.31%	5.95%
set23	7.39%	3.42%	4.46%
set24	8.00%	3.92%	4.50%
set25	6.63%	4.75%	5.32%
set31	3.93%	3.42%	3.43%
set32	4.38%	4.14%	4.12%
set33	5.67%	3.78%	2.46%
set34	6.45%	4.78%	3.85%
set35	5.01%	4.11%	2.47%
set41	4.02%	3.29%	2.80%
set42	5.13%	4.92%	2.72%
set43	6.56%	3.17%	3.57%
set44	7.12%	2.27%	4.34%
set45	5.53%	3.16%	2.64%
set51	5.01%	2.77%	3.33%
set52	5.57%	4.24%	4.62%
set53	5.96%	2.39%	4.17%
set54	6.88%	2.60%	4.28%
set55	6.18%	3.61%	3.52%
Min	3.93%	2.27%	2.46%
Mean	6.22%	3.55%	3.82%
STDEV	1.18%	0.75%	0.92%
C.O.V	19.06%	21.05%	24.05%

Min = Minimum value of the area of mode shape change in all trials;
Mean = The average value of the area of mode shape change in all trials;
STDEV = Standard deviation of the samples;
C.O.V = Coefficient of variation of the samples.

Table H.31. The summary of area of change in the first mode shape due to Damage Cases 4 to 9 for different test trials when Test Protocol 7 was used.

	Area of mode shape change					
Trials	Case 4	Case 5	Case 6	Case 7	Case 8	Case 9
set11	5.76%	3.47%	2.64%	3.40%	4.54%	4.58%
set12	4.15%	3.53%	3.87%	4.30%	4.26%	3.36%
set13	4.42%	2.87%	3.35%	2.93%	4.76%	4.67%
set14	3.28%	4.13%	3.42%	4.14%	4.24%	4.86%
set15	4.14%	2.68%	2.98%	4.35%	3.25%	3.21%
set21	6.06%	4.11%	3.00%	3.09%	3.61%	5.29%
set22	4.84%	4.31%	4.71%	3.93%	3.70%	3.26%
set23	5.12%	3.42%	4.51%	3.59%	5.14%	5.04%
set24	3.94%	4.24%	4.37%	4.65%	3.89%	5.45%
set25	5.28%	4.19%	4.00%	4.41%	3.55%	3.78%
set31	4.43%	3.90%	3.84%	4.24%	3.84%	4.88%
set32	3.53%	4.61%	3.49%	3.90%	2.69%	3.72%
set33	3.87%	3.45%	4.68%	4.61%	4.47%	4.50%
set34	3.36%	3.91%	4.78%	3.79%	3.71%	4.54%
set35	3.55%	3.96%	4.97%	4.00%	4.02%	3.25%
set41	4.87%	3.50%	3.18%	3.35%	3.45%	3.69%
set42	5.11%	3.54%	3.75%	2.76%	2.97%	3.67%
set43	4.42%	3.58%	3.37%	2.99%	3.83%	4.82%
set44	3.53%	3.87%	4.42%	2.57%	3.08%	5.54%
set45	4.25%	3.97%	3.10%	4.26%	2.05%	3.09%
set51	5.13%	3.34%	2.82%	3.53%	3.87%	3.89%
set52	3.49%	3.49%	3.78%	3.71%	3.13%	3.33%
set53	4.42%	3.44%	3.28%	2.82%	3.92%	5.28%
set54	2.47%	3.75%	3.89%	3.40%	4.14%	5.70%
set55	4.07%	2.72%	2.97%	4.47%	2.77%	3.07%
Min	2.47%	2.68%	2.64%	2.57%	2.05%	3.07%
Mean	4.30%	3.68%	3.73%	3.73%	3.71%	4.26%
STDEV	0.84%	0.48%	0.68%	0.62%	0.70%	0.87%
C.O.V	19.55%	13.08%	18.30%	16.74%	18.78%	20.47%

Min = Minimum value of the area of mode shape change in all trials;
Mean = The average value of the area of mode shape change in all trials;
STDEV = Standard deviation of the samples;
C.O.V = Coefficient of variation of the samples.

Table H.32. The summary of area of change in the first mode shape due to Damage Cases 10 to 15 for different test trials when Test Protocol 7 was used.

	Area of mode shape change					
Trials	Case 10	Case 11	Case 12	Case 13	Case 14	Case 15
set11	3.91%	4.25%	3.87%	3.87%	4.54%	3.95%
set12	4.40%	3.96%	2.83%	2.65%	3.16%	3.80%
set13	7.32%	3.45%	3.99%	3.95%	3.34%	5.23%
set14	4.05%	5.60%	3.73%	5.27%	4.59%	4.77%
set15	5.16%	2.93%	3.61%	3.63%	4.70%	3.69%
set21	4.91%	5.06%	4.46%	4.35%	4.02%	3.69%
set22	4.47%	3.66%	4.14%	2.92%	2.72%	5.41%
set23	5.47%	4.18%	4.96%	4.25%	2.38%	4.26%
set24	4.29%	5.35%	4.17%	5.54%	2.86%	4.05%
set25	4.13%	4.91%	4.61%	3.27%	3.06%	3.17%
set31	5.46%	5.53%	3.56%	5.42%	4.25%	2.16%
set32	4.66%	7.43%	4.28%	4.50%	4.25%	3.28%
set33	7.83%	5.75%	4.14%	4.58%	3.25%	4.01%
set34	5.76%	4.48%	3.52%	5.12%	4.48%	2.71%
set35	6.11%	4.67%	3.61%	3.96%	2.68%	2.68%
set41	5.70%	3.28%	4.83%	4.97%	4.34%	2.48%
set42	5.27%	4.39%	4.47%	4.66%	6.10%	3.65%
set43	8.06%	3.03%	4.24%	5.41%	4.21%	2.88%
set44	6.57%	4.44%	4.58%	4.18%	3.86%	3.17%
set45	6.59%	3.29%	4.02%	4.31%	4.20%	3.30%
set51	3.90%	4.64%	3.63%	5.11%	4.12%	2.25%
set52	3.93%	5.86%	3.53%	4.39%	4.37%	2.69%
set53	6.27%	4.28%	4.52%	4.75%	3.50%	4.31%
set54	3.90%	3.51%	4.39%	5.41%	3.69%	3.70%
set55	4.66%	4.03%	4.12%	3.13%	3.41%	3.33%
Min	3.90%	2.93%	2.83%	2.65%	2.38%	2.16%
Mean	5.31%	4.48%	4.07%	4.38%	3.84%	3.55%
STDEV	1.25%	1.05%	0.49%	0.82%	0.82%	0.85%
C.O.V	23.56%	23.53%	12.09%	18.73%	21.37%	24.08%

Min = Minimum value of the area of mode shape change in all trials;
Mean = The average value of the area of mode shape change in all trials;
STDEV = Standard deviation of the samples;
C.O.V = Coefficient of variation of the samples.

Table H.33. The summary of area of change in the first mode shape due to Damage Cases 16 to 21 for different test trials when Test Protocol 7 was used.

	Area of mode shape change					
Trials	Case 16	Case 17	Case 18	Case 19	Case 20	Case 21
set11	2.92%	5.71%	7.83%	6.37%	5.88%	7.52%
set12	3.04%	5.32%	8.99%	5.26%	7.41%	6.31%
set13	3.23%	6.42%	7.18%	5.23%	5.36%	11.60%
set14	1.91%	7.13%	7.74%	6.80%	5.01%	8.90%
set15	3.87%	6.76%	7.69%	5.25%	5.87%	8.35%
set21	4.01%	5.96%	7.65%	6.73%	5.79%	6.98%
set22	4.56%	4.50%	9.18%	5.77%	7.73%	6.45%
set23	4.82%	7.01%	6.98%	5.62%	5.79%	10.59%
set24	3.80%	7.75%	7.97%	6.96%	4.47%	8.63%
set25	4.48%	7.06%	8.22%	6.21%	6.02%	8.49%
set31	4.39%	3.71%	6.47%	3.88%	5.83%	6.35%
set32	4.14%	3.41%	7.39%	4.55%	4.66%	5.35%
set33	2.57%	5.05%	4.63%	3.46%	4.72%	8.25%
set34	3.10%	5.72%	5.76%	5.11%	4.54%	6.73%
set35	4.78%	5.75%	6.53%	3.80%	4.31%	6.43%
set41	4.01%	4.68%	6.75%	4.81%	6.85%	7.43%
set42	4.37%	4.35%	7.24%	5.93%	5.17%	5.54%
set43	3.60%	5.50%	5.02%	3.87%	5.83%	8.54%
set44	2.74%	6.26%	5.08%	5.64%	6.12%	7.26%
set45	4.92%	6.30%	6.93%	4.16%	5.15%	6.33%
set51	3.75%	4.70%	7.54%	4.18%	6.02%	6.89%
set52	3.75%	4.47%	8.39%	4.13%	5.10%	5.96%
set53	3.64%	5.62%	5.95%	4.09%	3.98%	9.62%
set54	3.42%	6.52%	7.50%	5.71%	4.12%	7.64%
set55	4.54%	6.50%	7.18%	4.60%	4.83%	7.77%
Min	1.91%	3.41%	4.63%	3.46%	3.98%	5.35%
Mean	3.77%	5.69%	7.11%	5.12%	5.46%	7.60%
STDEV	0.77%	1.12%	1.16%	1.03%	0.96%	1.53%
C.O.V	20.44%	19.68%	16.28%	20.18%	17.53%	20.09%

Min = Minimum value of the area of mode shape change in all trials;
Mean = The average value of the area of mode shape change in all trials;
STDEV = Standard deviation of the samples;
C.O.V = Coefficient of variation of the samples.

Table H.34. The summary of area of change in the first mode shape due to Damage Cases 22 to 26 for different test trials when Test Protocol 7 was used.

	Area of mode shape change				
Trials	Case 22	Case 23	Case 24	Case 25	Case 26
set11	8.36%	3.34%	3.99%	2.41%	3.45%
set12	5.65%	3.16%	3.26%	3.53%	4.05%
set13	6.85%	3.82%	3.01%	3.66%	2.60%
set14	8.15%	4.25%	3.09%	3.21%	1.88%
set15	7.86%	3.12%	3.26%	3.01%	4.03%
set21	8.54%	3.39%	5.31%	3.43%	3.61%
set22	5.44%	2.86%	4.18%	4.40%	5.45%
set23	7.45%	5.89%	3.74%	3.22%	3.61%
set24	8.18%	4.54%	3.41%	3.47%	3.04%
set25	6.83%	4.74%	4.82%	4.30%	4.74%
set31	6.37%	4.43%	4.12%	2.83%	3.11%
set32	3.74%	3.22%	5.38%	3.42%	3.23%
set33	5.09%	4.45%	2.71%	4.20%	4.57%
set34	5.17%	4.20%	3.32%	3.73%	3.02%
set35	5.52%	4.26%	3.58%	3.92%	2.65%
set41	6.44%	6.22%	5.43%	4.18%	4.44%
set42	5.15%	4.87%	5.59%	4.24%	3.34%
set43	5.57%	4.37%	3.88%	5.21%	4.66%
set44	5.02%	5.34%	4.16%	4.86%	3.71%
set45	6.22%	4.28%	4.18%	3.98%	2.30%
set51	6.77%	3.87%	4.21%	2.67%	3.89%
set52	4.17%	2.87%	4.49%	3.94%	3.50%
set53	5.87%	4.29%	2.68%	3.90%	4.34%
set54	6.29%	5.26%	3.22%	3.87%	3.50%
set55	6.62%	3.80%	3.06%	3.26%	4.54%
Min	3.74%	2.86%	2.68%	2.41%	1.88%
Mean	6.29%	4.19%	3.92%	3.71%	3.65%
STDEV	1.29%	0.89%	0.87%	0.66%	0.84%
C.O.V	20.55%	21.21%	22.06%	17.70%	23.08%

Min = Minimum value of the area of mode shape change in all trials;
Mean = The average value of the area of mode shape change in all trials;
STDEV = Standard deviation of the samples;
C.O.V = Coefficient of variation of the samples.

Table H.35. The summary of area of change in the first mode shape due to Damage Cases 1 to 3 for different test trials when Test Protocol 8 was used.

	Area of mode shape change		
Trials	Case 1	Case 2	Case 3
set11	8.14%	4.13%	5.49%
set12	7.80%	5.73%	3.96%
set13	8.75%	7.03%	5.08%
set14	10.98%	6.31%	5.98%
set15	6.31%	6.75%	4.76%
set21	10.39%	6.20%	6.39%
set22	8.78%	8.18%	6.93%
set23	10.05%	8.13%	6.87%
set24	12.54%	7.18%	7.07%
set25	7.31%	8.94%	8.81%
set31	7.16%	4.38%	7.49%
set32	7.58%	9.21%	5.26%
set33	7.80%	7.91%	6.44%
set34	9.86%	6.90%	5.97%
set35	5.56%	8.22%	7.21%
set41	9.16%	6.02%	5.86%
set42	8.42%	7.67%	6.24%
set43	9.30%	5.41%	6.16%
set44	10.08%	7.62%	6.14%
set45	6.53%	8.60%	5.45%
set51	8.33%	5.84%	5.27%
set52	8.79%	7.22%	7.31%
set53	8.70%	8.14%	7.08%
set54	10.74%	5.06%	8.58%
set55	6.90%	5.99%	6.58%
Min	5.56%	4.13%	3.96%
Mean	8.64%	6.91%	6.34%
STDEV	1.63%	1.38%	1.12%
C.O.V	18.88%	19.97%	17.67%

Min = Minimum value of the area of mode shape change in all trials;
Mean = The average value of the area of mode shape change in all trials;
STDEV = Standard deviation of the samples;
C.O.V = Coefficient of variation of the samples.

Table H.36. The summary of area of change in the first mode shape due to Damage Cases 4 to 9 for different test trials when Test Protocol 8 was used.

	Area of mode shape change					
Trials	Case 4	Case 5	Case 6	Case 7	Case 8	Case 9
set11	6.14%	5.64%	5.14%	7.04%	8.12%	6.72%
set12	5.74%	7.25%	6.78%	5.49%	4.45%	6.13%
set13	8.04%	4.89%	5.80%	5.24%	10.53%	5.85%
set14	4.51%	5.88%	4.15%	7.25%	5.81%	9.29%
set15	6.29%	5.37%	6.68%	5.77%	6.03%	6.36%
set21	5.65%	7.30%	5.30%	7.37%	8.58%	8.35%
set22	6.23%	7.01%	8.59%	7.21%	8.18%	6.46%
set23	8.13%	6.11%	7.03%	5.83%	11.98%	6.58%
set24	5.84%	6.80%	5.84%	7.86%	5.78%	10.33%
set25	5.47%	6.43%	6.68%	7.43%	6.20%	6.35%
set31	6.78%	6.37%	6.29%	9.26%	8.40%	8.86%
set32	5.92%	8.42%	7.77%	5.64%	5.83%	7.55%
set33	7.12%	6.17%	7.69%	6.92%	11.76%	7.04%
set34	5.91%	6.45%	5.29%	7.12%	7.46%	11.90%
set35	4.79%	6.16%	7.31%	8.12%	6.20%	7.33%
set41	6.13%	8.00%	6.49%	6.71%	8.74%	8.48%
set42	6.43%	6.75%	5.82%	7.01%	5.11%	4.68%
set43	8.47%	6.39%	5.49%	5.12%	10.65%	7.51%
set44	6.12%	8.55%	6.03%	8.27%	5.65%	11.36%
set45	6.61%	6.02%	6.69%	8.34%	7.08%	8.00%
set51	7.33%	5.37%	3.90%	6.42%	5.98%	7.11%
set52	6.83%	5.64%	7.94%	5.07%	7.27%	6.67%
set53	6.93%	5.23%	8.49%	6.52%	8.89%	5.57%
set54	5.87%	5.40%	4.63%	5.89%	6.53%	8.61%
set55	7.67%	4.60%	4.46%	6.02%	4.77%	3.98%
Min	4.51%	4.60%	3.90%	5.07%	4.45%	3.98%
Mean	6.44%	6.33%	6.25%	6.76%	7.44%	7.48%
STDEV	0.98%	1.02%	1.30%	1.11%	2.11%	1.89%
C.O.V	15.18%	16.17%	20.75%	16.47%	28.39%	25.21%

Min = Minimum value of the area of mode shape change in all trials;
Mean = The average value of the area of mode shape change in all trials;
STDEV = Standard deviation of the samples;
C.O.V = Coefficient of variation of the samples.

Table H.37. The summary of area of change in the first mode shape due to Damage Cases 10 to 15 for different test trials when Test Protocol 8 was used.

	Area of mode shape change					
Trials	Case 10	Case 11	Case 12	Case 13	Case 14	Case 15
set11	7.41%	8.77%	5.56%	6.58%	6.57%	7.83%
set12	6.94%	7.71%	6.38%	6.90%	7.71%	7.01%
set13	6.30%	8.96%	6.76%	7.30%	8.14%	5.03%
set14	7.55%	10.37%	8.80%	5.64%	9.33%	6.21%
set15	7.80%	5.78%	8.71%	7.79%	8.95%	4.59%
set21	9.41%	9.83%	5.29%	7.87%	6.19%	7.12%
set22	8.30%	6.93%	5.95%	5.92%	8.19%	8.97%
set23	7.06%	8.43%	6.44%	5.71%	7.19%	7.92%
set24	6.27%	9.74%	6.81%	7.01%	7.41%	7.76%
set25	7.81%	5.12%	7.52%	7.27%	8.01%	6.15%
set31	7.96%	9.21%	6.74%	6.14%	6.57%	6.98%
set32	6.80%	6.49%	5.08%	7.78%	7.02%	8.03%
set33	6.82%	6.34%	8.05%	6.75%	6.55%	5.93%
set34	8.75%	8.15%	7.81%	5.39%	7.07%	7.92%
set35	9.08%	6.76%	7.52%	10.31%	8.79%	3.27%
set41	10.04%	8.99%	6.17%	8.06%	5.91%	7.92%
set42	9.78%	7.78%	7.75%	8.19%	6.69%	9.25%
set43	10.00%	5.87%	8.01%	5.74%	6.53%	6.30%
set44	9.58%	7.13%	9.08%	8.13%	7.55%	8.24%
set45	10.88%	10.03%	6.97%	9.38%	8.94%	5.99%
set51	5.99%	8.62%	6.83%	6.35%	8.00%	7.86%
set52	5.14%	8.35%	7.36%	8.09%	8.59%	7.60%
set53	6.11%	7.52%	8.39%	6.34%	9.06%	6.91%
set54	8.73%	8.21%	8.32%	6.56%	8.41%	6.75%
set55	8.45%	9.79%	8.56%	9.90%	4.44%	5.67%
Min	5.14%	5.12%	5.08%	5.39%	4.44%	3.27%
Mean	7.96%	8.04%	7.23%	7.24%	7.51%	6.93%
STDEV	1.50%	1.45%	1.13%	1.32%	1.18%	1.38%
C.O.V	18.79%	18.07%	15.63%	18.17%	15.72%	19.92%

Min = Minimum value of the area of mode shape change in all trials;
Mean = The average value of the area of mode shape change in all trials;
STDEV = Standard deviation of the samples;
C.O.V = Coefficient of variation of the samples.

Table H.38. The summary of area of change in the first mode shape due to Damage Cases 16 to 21 for different test trials when Test Protocol 8 was used.

	Area of mode shape change					
Trials	Case 16	Case 17	Case 18	Case 19	Case 20	Case 21
set11	8.31%	7.81%	7.34%	7.86%	6.59%	7.13%
set12	6.74%	7.58%	9.12%	7.45%	9.62%	5.69%
set13	6.89%	10.71%	7.75%	5.08%	6.80%	8.12%
set14	6.06%	7.15%	10.43%	6.81%	6.64%	9.43%
set15	8.77%	7.68%	8.47%	6.09%	4.88%	9.96%
set21	8.10%	9.79%	9.60%	8.82%	8.84%	9.04%
set22	7.81%	9.59%	10.56%	10.13%	10.91%	7.46%
set23	6.52%	12.26%	9.40%	5.99%	7.56%	10.40%
set24	8.85%	9.44%	12.18%	9.38%	9.42%	11.87%
set25	8.29%	8.58%	9.85%	7.41%	6.27%	11.50%
set31	5.42%	7.78%	6.35%	7.24%	7.33%	6.00%
set32	6.91%	7.00%	8.42%	7.47%	8.40%	5.32%
set33	6.03%	10.65%	7.66%	5.15%	6.84%	7.66%
set34	7.31%	7.39%	9.34%	7.06%	8.59%	10.32%
set35	7.71%	6.47%	7.50%	6.09%	4.28%	9.08%
set41	9.08%	9.00%	7.95%	9.98%	10.03%	9.38%
set42	8.00%	9.67%	10.21%	9.80%	10.22%	8.40%
set43	7.77%	11.48%	7.78%	6.59%	8.56%	10.55%
set44	6.74%	9.37%	9.89%	9.24%	9.40%	10.59%
set45	8.39%	9.61%	9.15%	7.32%	6.41%	9.77%
set51	7.62%	7.07%	6.47%	7.31%	8.55%	7.45%
set52	7.04%	9.02%	8.84%	9.17%	10.20%	5.80%
set53	4.90%	9.88%	6.61%	5.51%	8.42%	9.02%
set54	6.19%	7.28%	9.91%	7.90%	8.97%	10.37%
set55	7.07%	7.11%	7.31%	7.64%	5.66%	9.92%
Min	4.90%	6.47%	6.35%	5.08%	4.28%	5.32%
Mean	7.30%	8.78%	8.72%	7.54%	7.98%	8.81%
STDEV	1.08%	1.55%	1.45%	1.48%	1.75%	1.85%
C.O.V	14.84%	17.62%	16.66%	19.69%	21.97%	20.95%

Min = Minimum value of the area of mode shape change in all trials;
Mean = The average value of the area of mode shape change in all trials;
STDEV = Standard deviation of the samples;
C.O.V = Coefficient of variation of the samples.

Table H.39. The summary of area of change in the first mode shape due to Damage Cases 22 to 26 for different test trials when Test Protocol 8 was used.

	Area of mode shape change				
Trials	Case 22	Case 23	Case 24	Case 25	Case 26
set11	9.49%	5.84%	6.72%	6.12%	6.65%
set12	7.84%	4.57%	7.82%	7.51%	6.18%
set13	9.94%	6.10%	6.40%	4.74%	6.12%
set14	9.81%	4.84%	7.39%	6.04%	5.36%
set15	6.64%	7.39%	7.71%	5.59%	7.28%
set21	11.85%	5.05%	7.26%	7.64%	6.33%
set22	9.61%	5.79%	8.18%	6.84%	7.83%
set23	10.22%	4.34%	6.69%	5.90%	6.66%
set24	11.99%	5.79%	8.17%	7.08%	6.83%
set25	8.86%	8.04%	8.69%	6.31%	7.64%
set31	9.05%	7.16%	6.78%	6.76%	8.46%
set32	7.40%	3.81%	7.17%	8.43%	7.01%
set33	8.97%	5.80%	6.61%	5.78%	6.42%
set34	10.16%	5.30%	7.66%	5.39%	6.08%
set35	5.88%	5.69%	7.14%	5.25%	7.67%
set41	9.78%	6.19%	6.00%	7.36%	8.76%
set42	8.20%	5.81%	7.23%	9.07%	6.05%
set43	8.88%	7.66%	7.23%	6.86%	6.33%
set44	10.24%	4.36%	8.06%	7.18%	5.85%
set45	8.15%	6.69%	8.00%	5.92%	9.09%
set51	10.19%	8.44%	5.96%	7.15%	7.69%
set52	8.35%	4.64%	8.66%	8.53%	8.29%
set53	9.94%	6.03%	7.26%	6.25%	6.57%
set54	10.07%	5.81%	7.36%	6.06%	5.16%
set55	7.32%	7.93%	7.39%	6.47%	7.22%
Min	5.88%	3.81%	5.96%	4.74%	5.16%
Mean	9.15%	5.96%	7.34%	6.65%	6.94%
STDEV	1.46%	1.25%	0.73%	1.06%	1.03%
C.O.V	15.91%	20.98%	9.92%	15.97%	14.88%

Min = Minimum value of the area of mode shape change in all trials;
Mean = The average value of the area of mode shape change in all trials;
STDEV = Standard deviation of the samples;
C.O.V = Coefficient of variation of the samples.

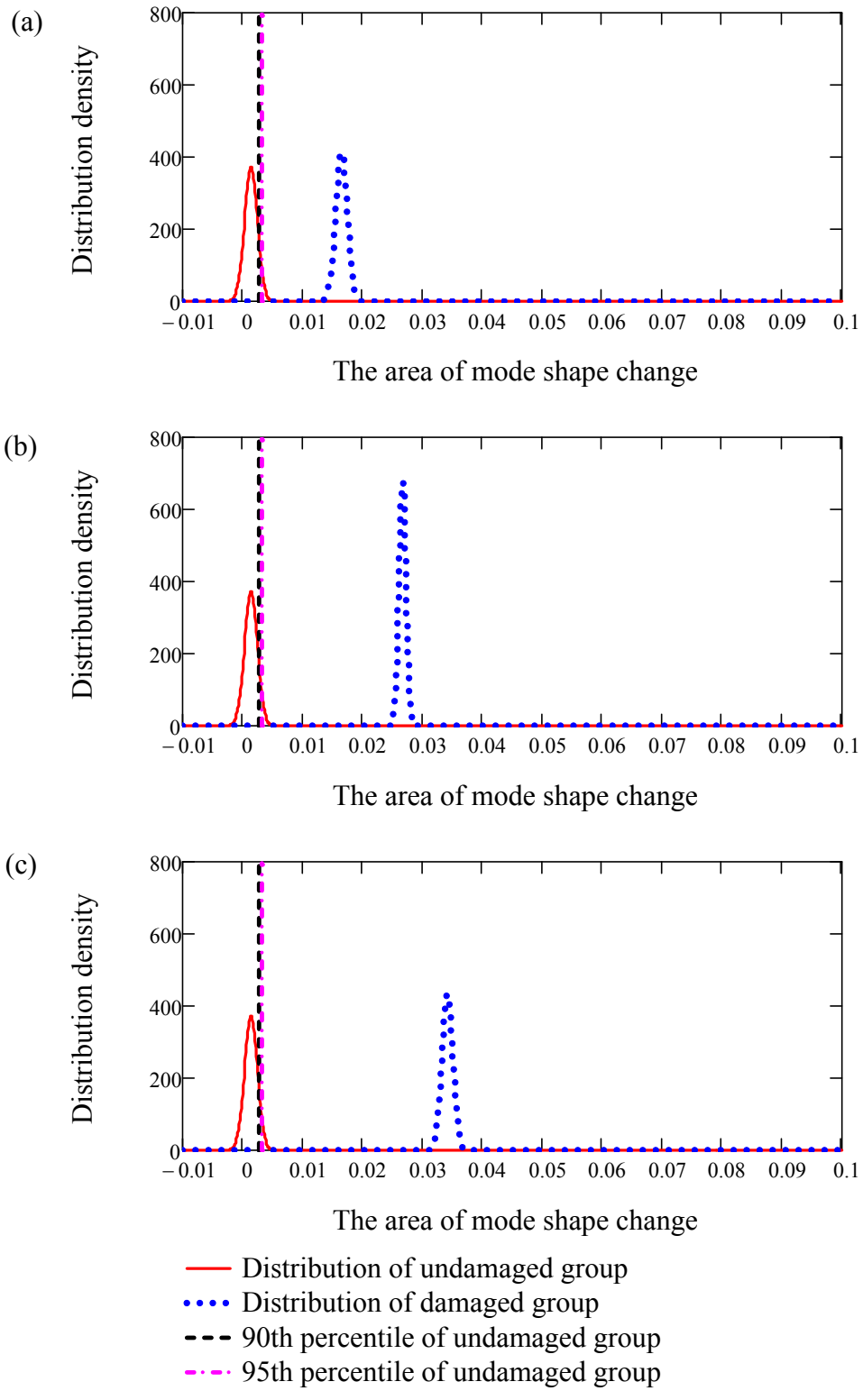

Figure H.1. Comparison of Normal distributions of the area of mode shape change for the undamaged group of 170 pairs and the damaged group of 25 data pairs for Damage Case: (a) 4, (b) 5, and (c) 6, when the Test Protocol 1 was used.

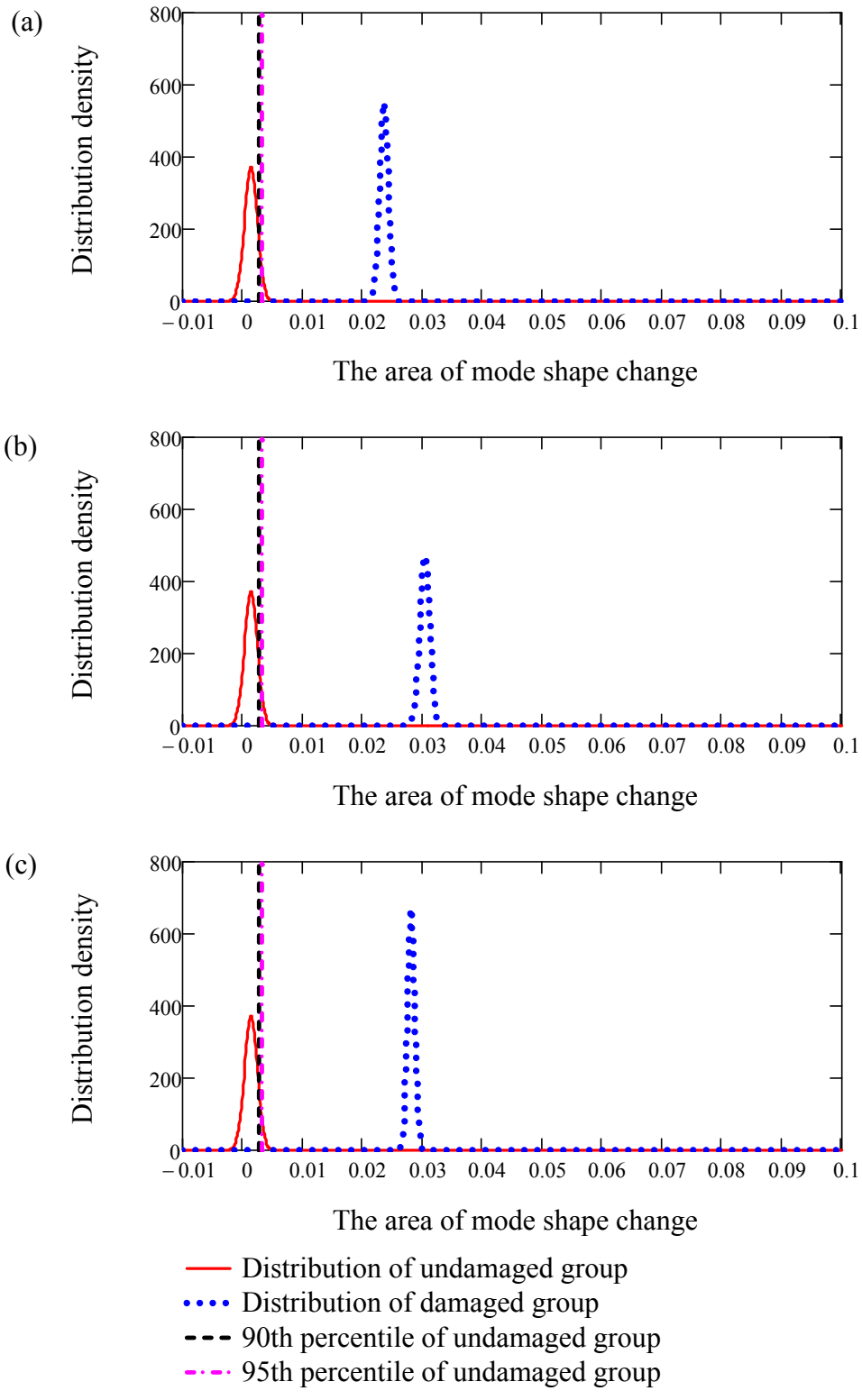

Figure H.2. Comparison of Normal distributions of the area of mode shape change for the undamaged group of 170 pairs and the damaged group of 25 data pairs for Damage Case: (a) 7, (b) 8, and (c) 9, when the Test Protocol 1 was used.

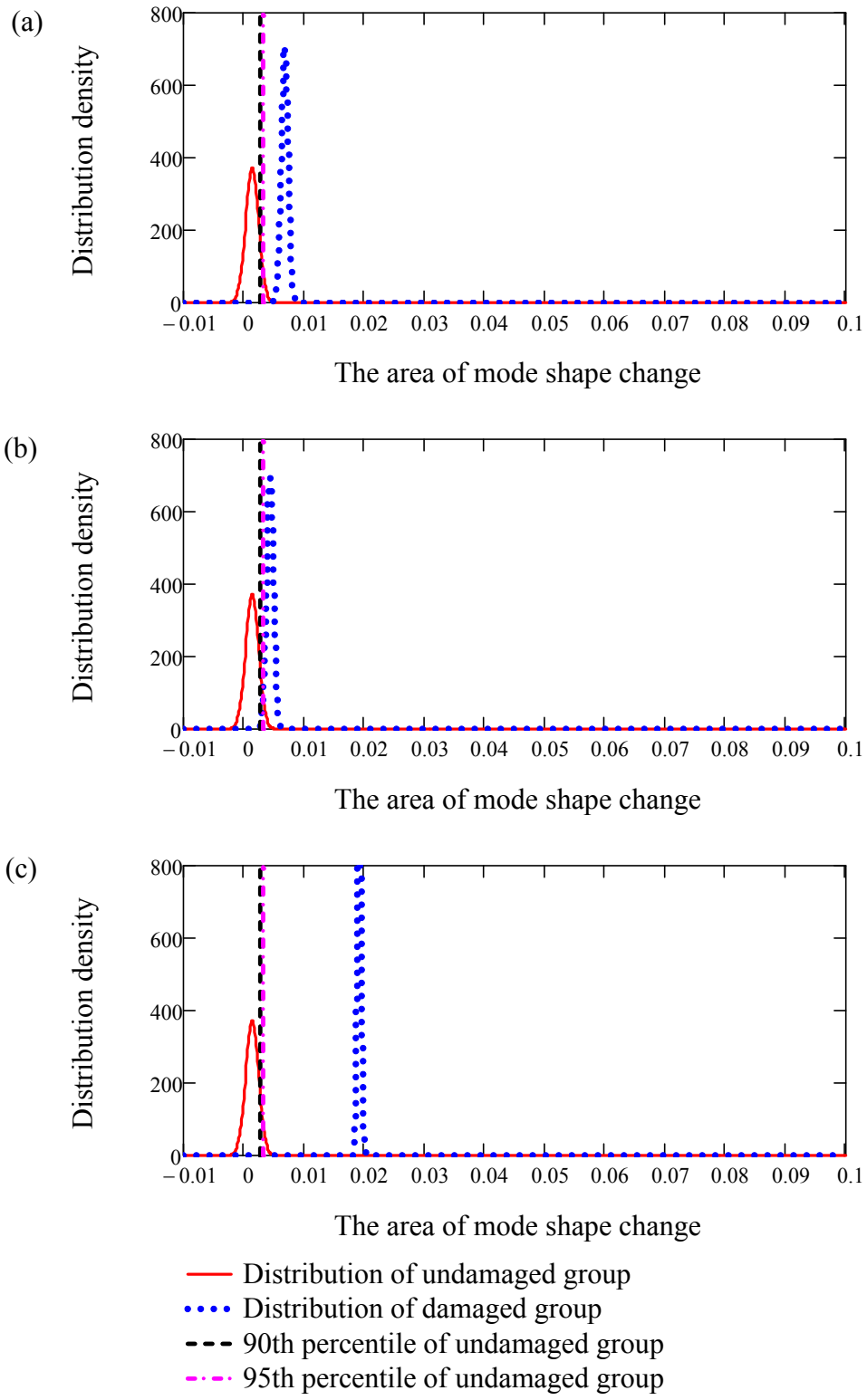

Figure H.3. Comparison of Normal distributions of the area of mode shape change for the undamaged group of 170 pairs and the damaged group of 25 data pairs for Damage Case: (a) 10, (b) 11, and (c) 12, when the Test Protocol 1 was used.

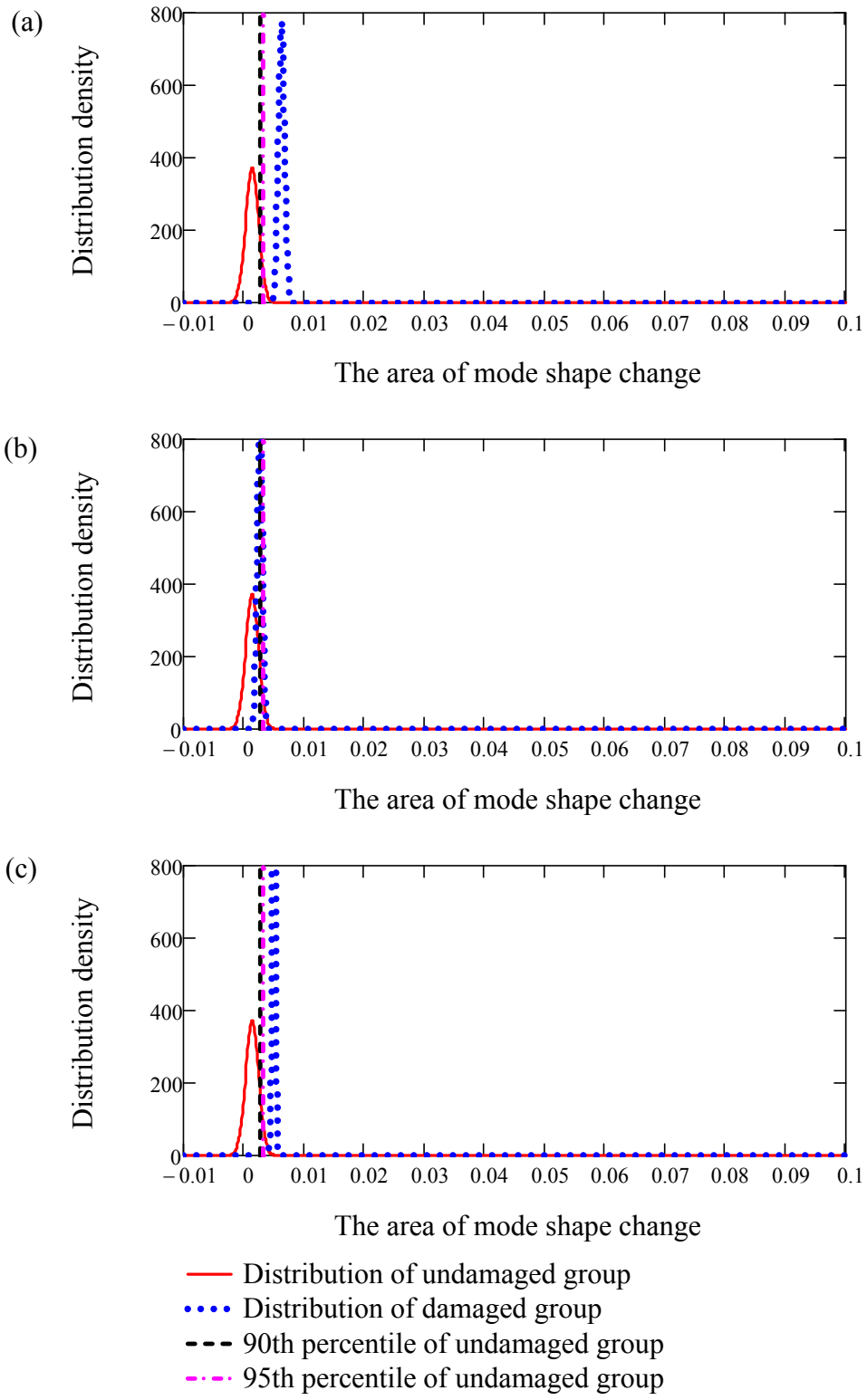

Figure H.4. Comparison of Normal distributions of the area of mode shape change for the undamaged group of 170 pairs and the damaged group of 25 data pairs for Damage Case: (a) 13, (b) 14, and (c) 15, when the Test Protocol 1 was used.

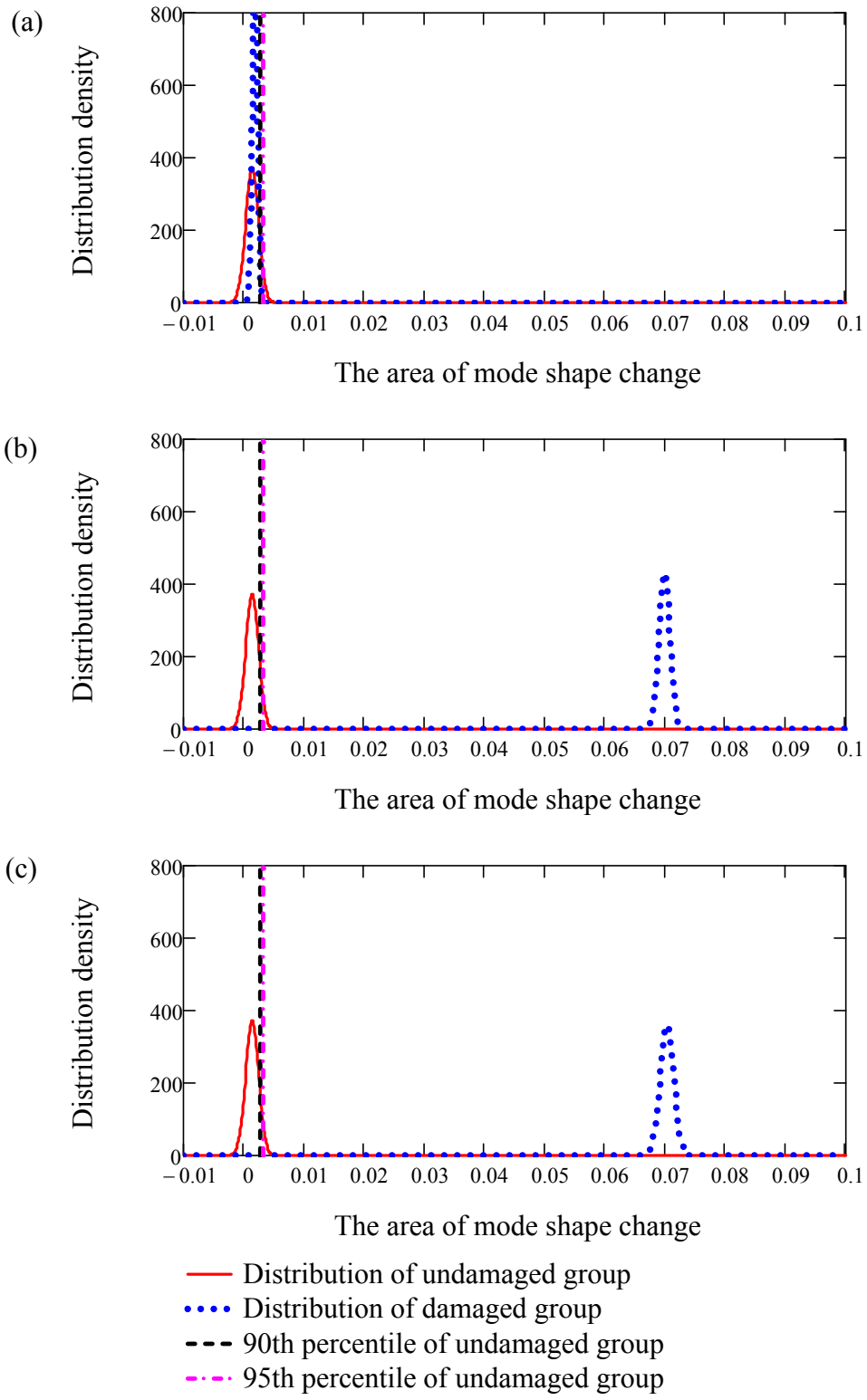

Figure H.5. Comparison of Normal distributions of the area of mode shape change for the undamaged group of 170 pairs and the damaged group of 25 data pairs for Damage Case: (a) 16, (b) 17, and (c) 18, when the Test Protocol 1 was used.

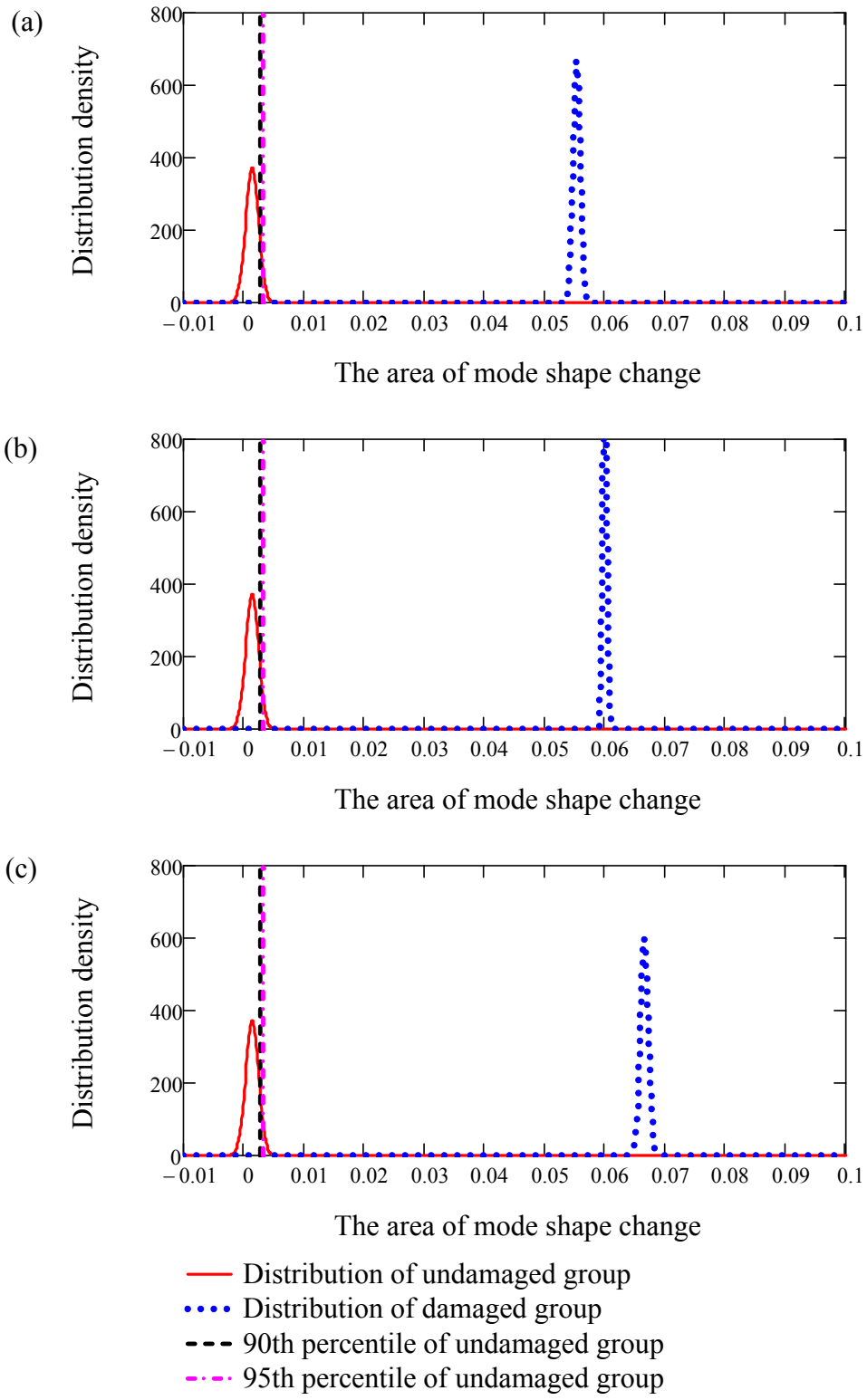

Figure H.6. Comparison of Normal distributions of the area of mode shape change for the undamaged group of 170 pairs and the damaged group of 25 data pairs for Damage Case: (a) 19, (b) 20, and (c) 21, when the Test Protocol 1 was used.

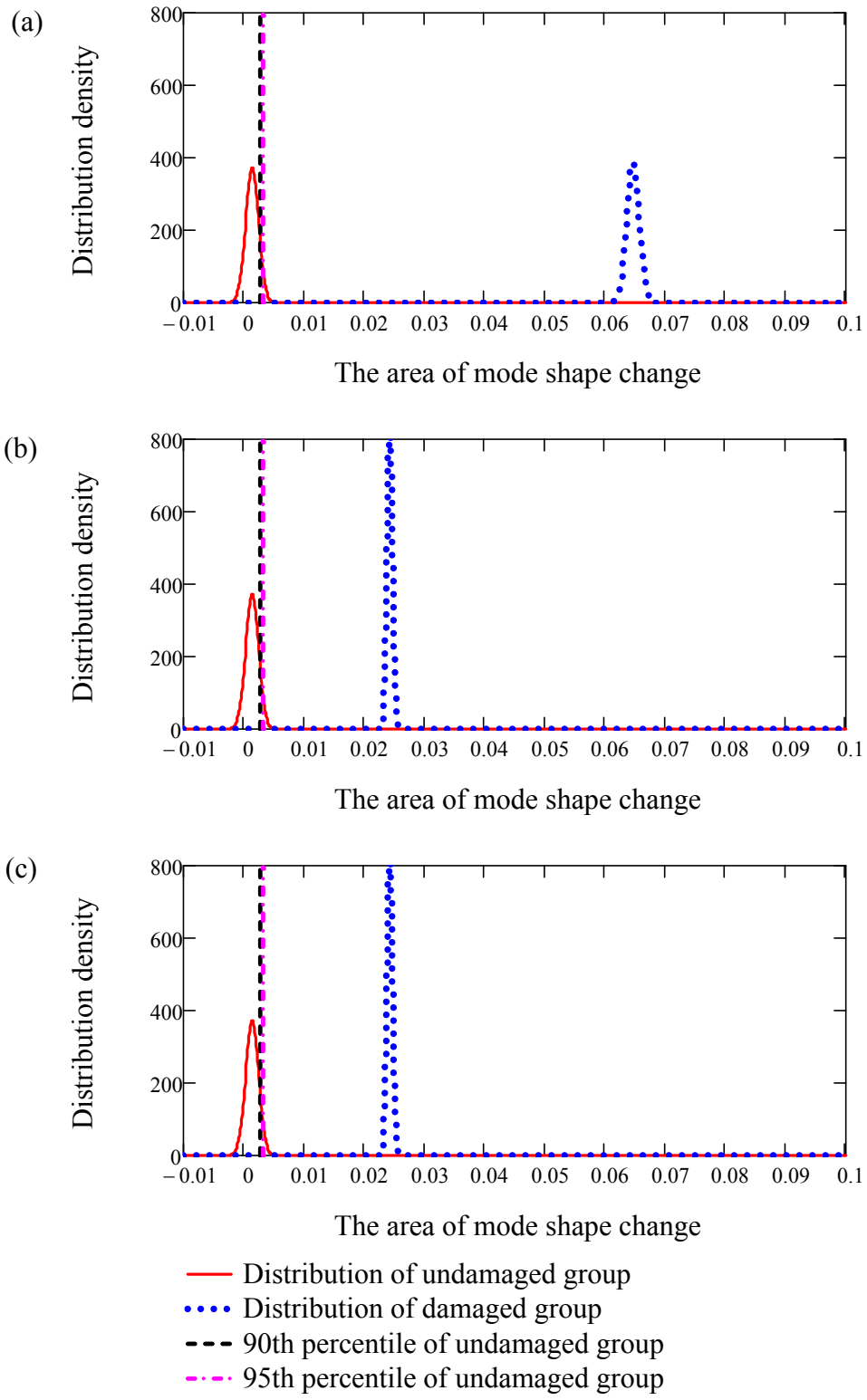

Figure H.7. Comparison of Normal distributions of the area of mode shape change for the undamaged group of 170 pairs and the damaged group of 25 data pairs for Damage Case: (a) 22, (b) 23, and (c) 24, when the Test Protocol 1 was used.

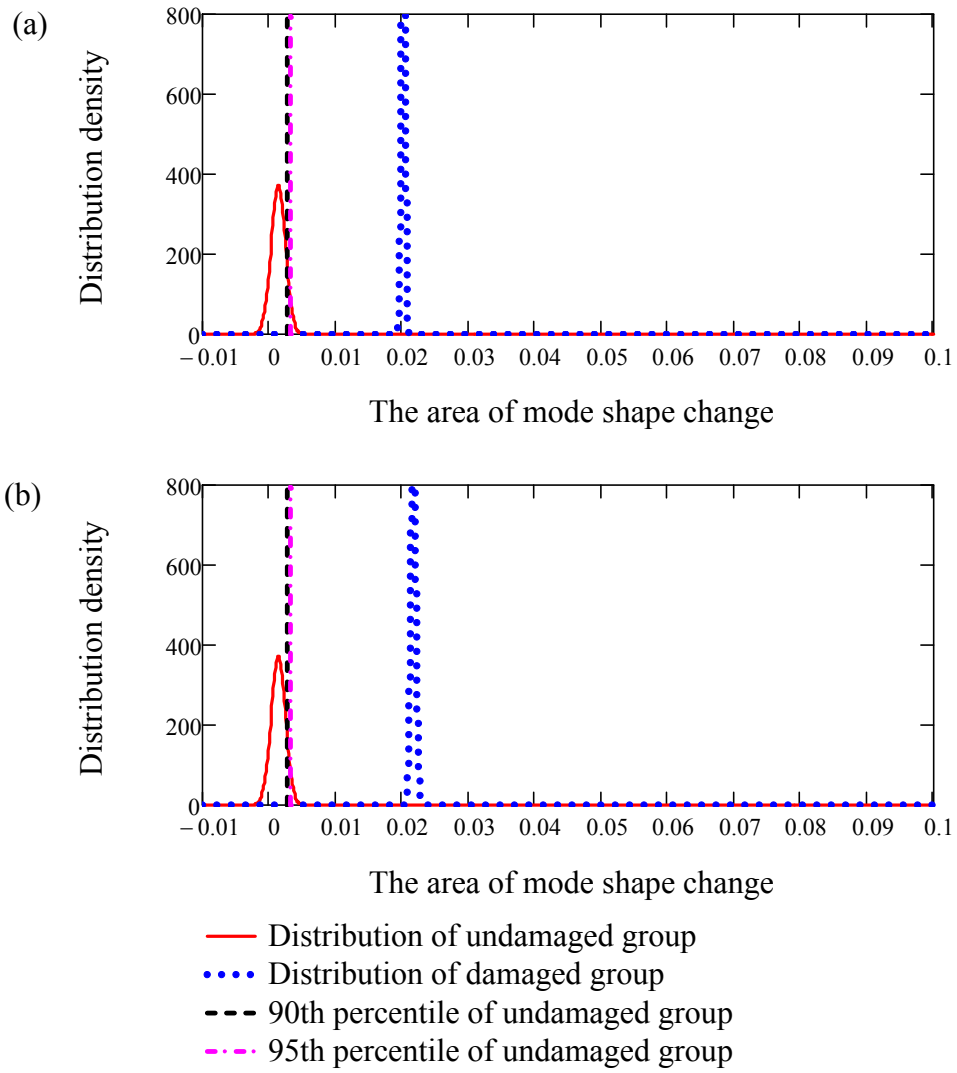

Figure H.8. Comparison of Normal distributions of the area of mode shape change for the undamaged group of 170 pairs and the damaged group of 25 data pairs for Damage Case: (a) 25 and (b) 26, when the Test Protocol 1 was used.

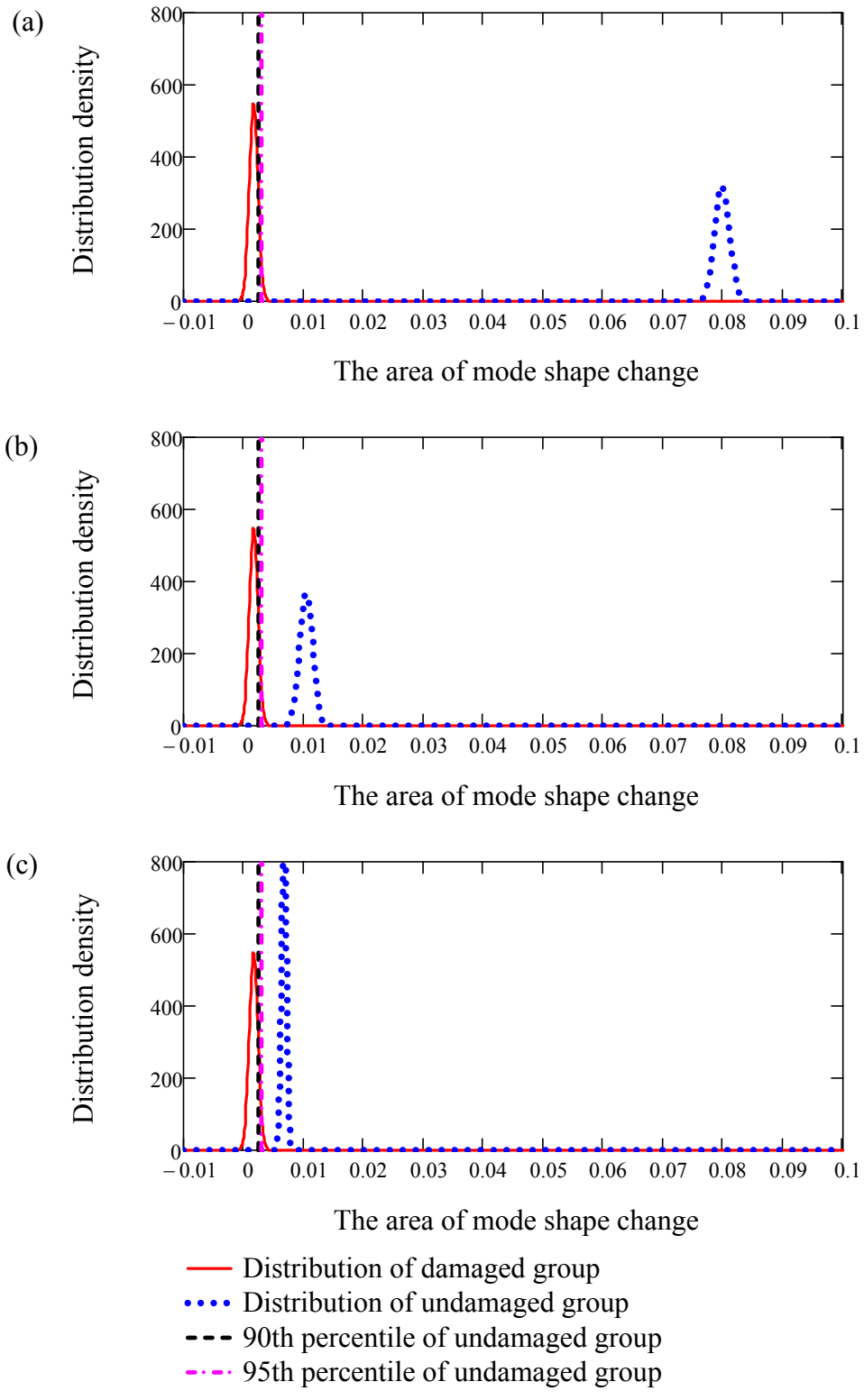

Figure H.9. Comparison of Normal distributions of the area of mode shape change for the undamaged group of 170 pairs and the damaged group of 25 data pairs for Damage Case: (a) 1, (b) 2, and (c) 3, when the Test Protocol 2 was used.

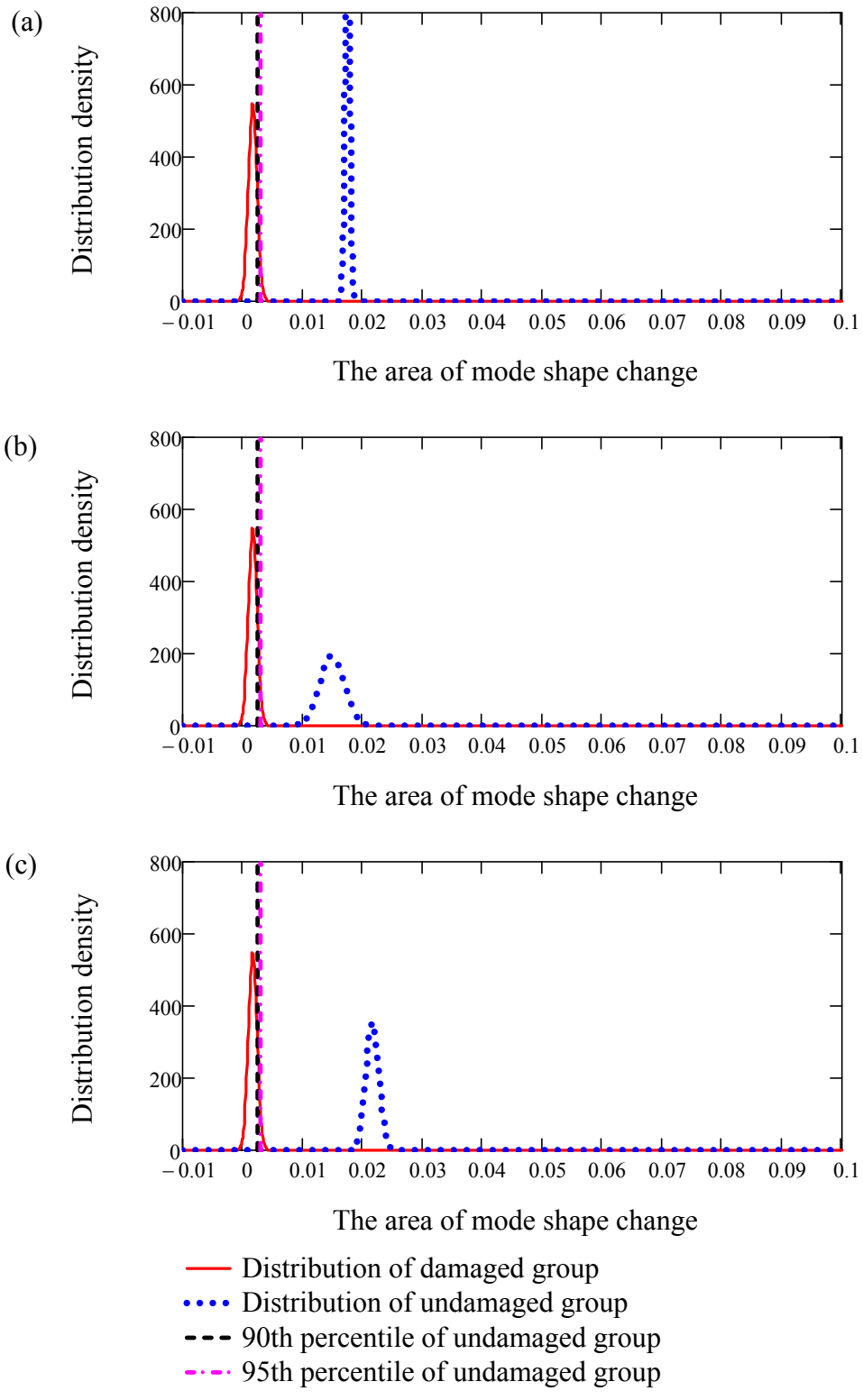

Figure H.10. Comparison of Normal distributions of the area of mode shape change for the undamaged group of 170 pairs and the damaged group of 25 data pairs for Damage Case: (a) 4, (b) 5, and (c) 6, when the Test Protocol 2 was used.

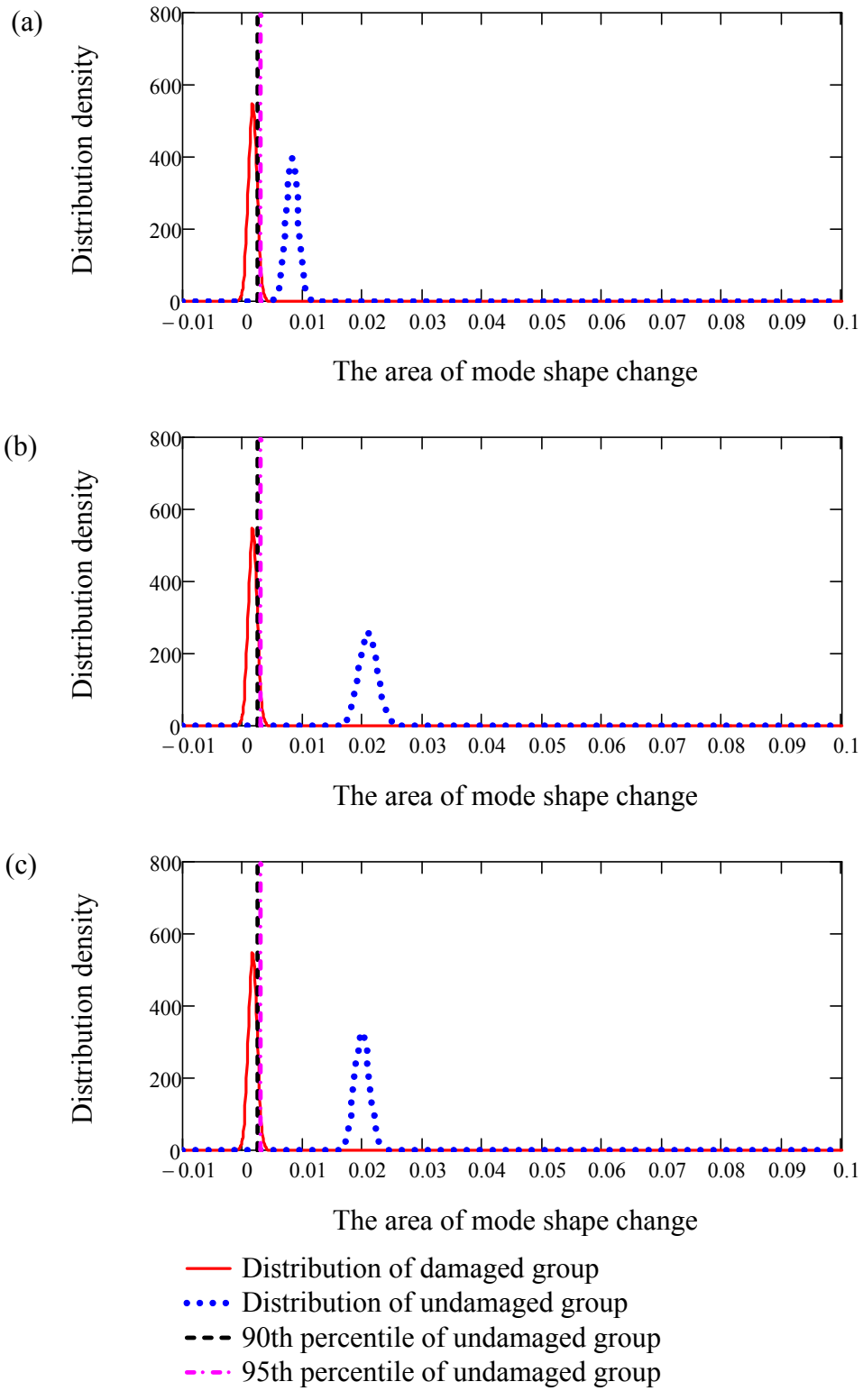

Figure H.11. Comparison of Normal distributions of the area of mode shape change for the undamaged group of 170 pairs and the damaged group of 25 data pairs for Damage Case: (a) 7, (b) 8, and (c) 9, when the Test Protocol 2 was used.

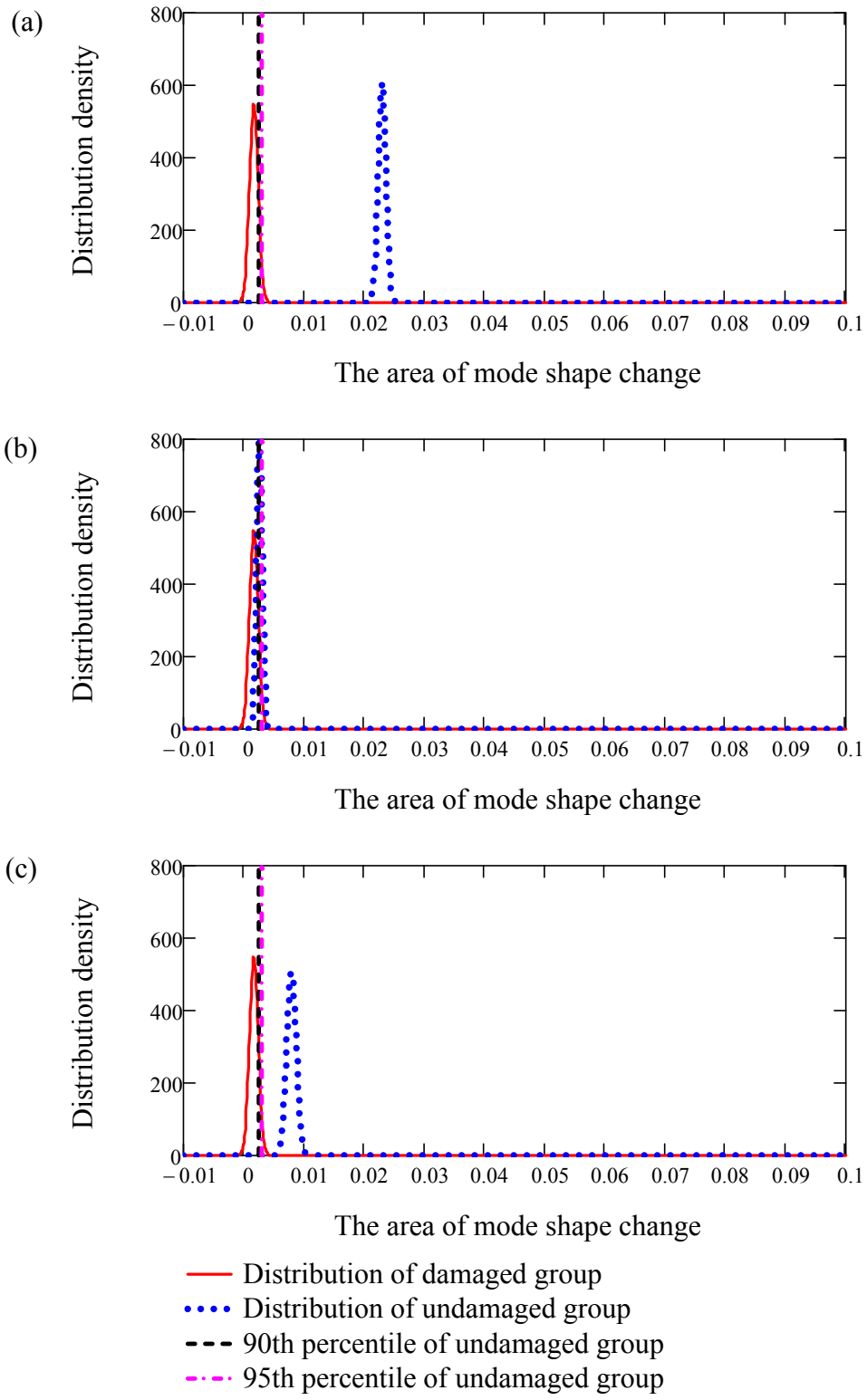

Figure H.12. Comparison of Normal distributions of the area of mode shape change for the undamaged group of 170 pairs and the damaged group of 25 data pairs for Damage Case: (a) 10, (b) 11, and (c) 12, when the Test Protocol 2 was used.

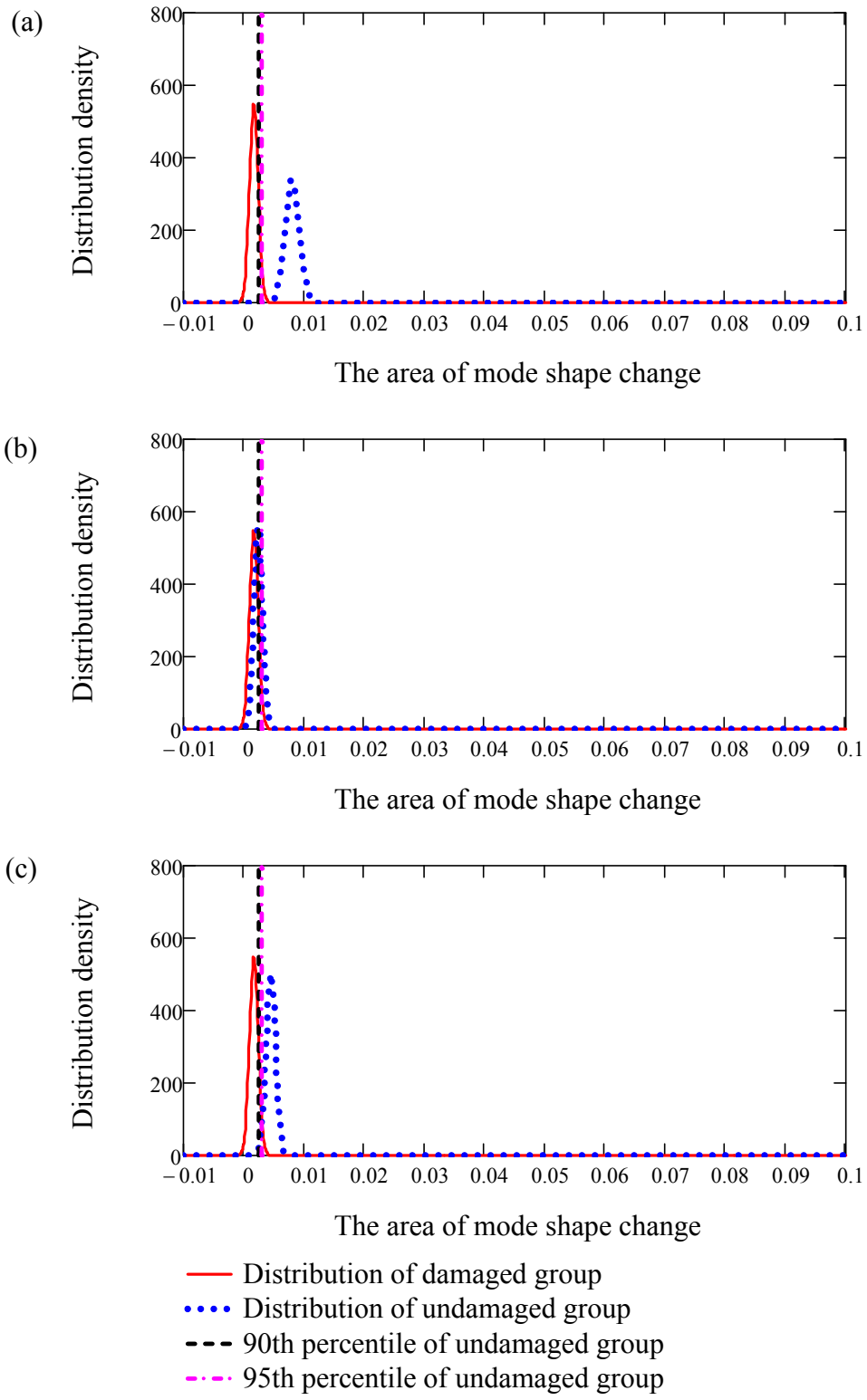

Figure H.13. Comparison of Normal distributions of the area of mode shape change for the undamaged group of 170 pairs and the damaged group of 25 data pairs for Damage Case: (a) 13, (b) 14, and (c) 15, when the Test Protocol 2 was used.

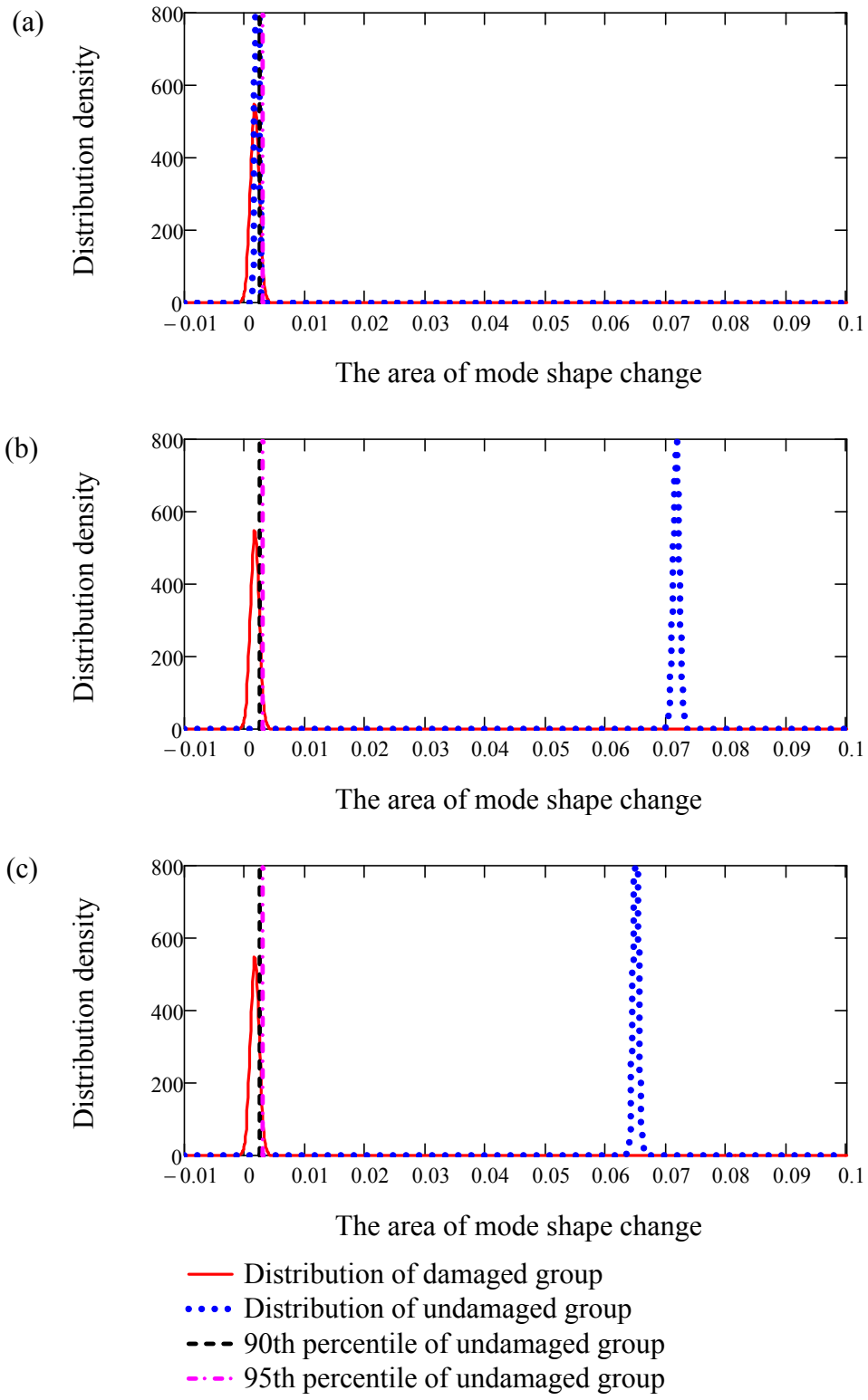

Figure H.14. Comparison of Normal distributions of the area of mode shape change for the undamaged group of 170 pairs and the damaged group of 25 data pairs for Damage Case: (a) 16, (b) 17, and (c) 18, when the Test Protocol 2 was used.

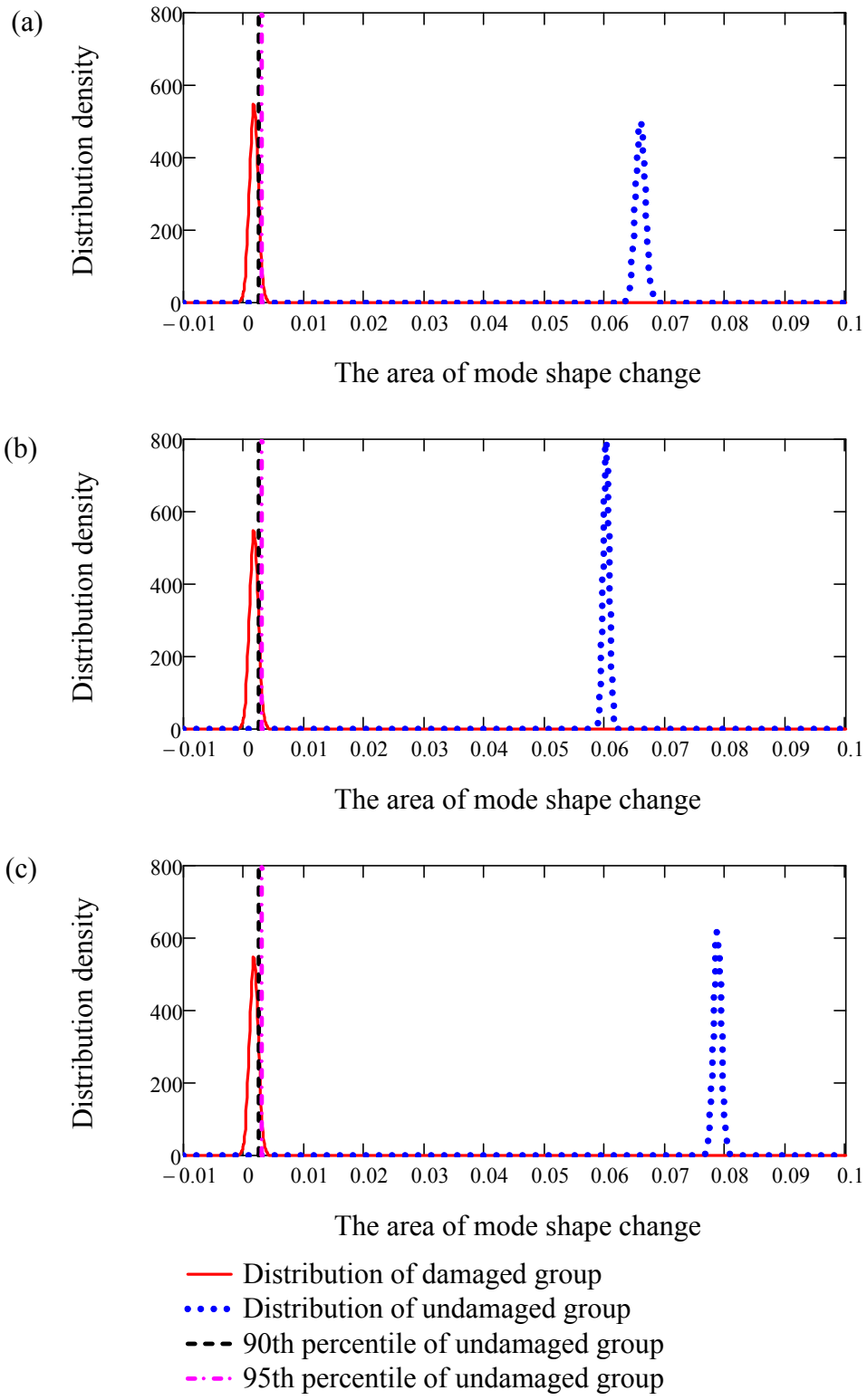

Figure H.15. Comparison of Normal distributions of the area of mode shape change for the undamaged group of 170 pairs and the damaged group of 25 data pairs for Damage Case: (a) 19, (b) 20, and (c) 21, when the Test Protocol 2 was used.

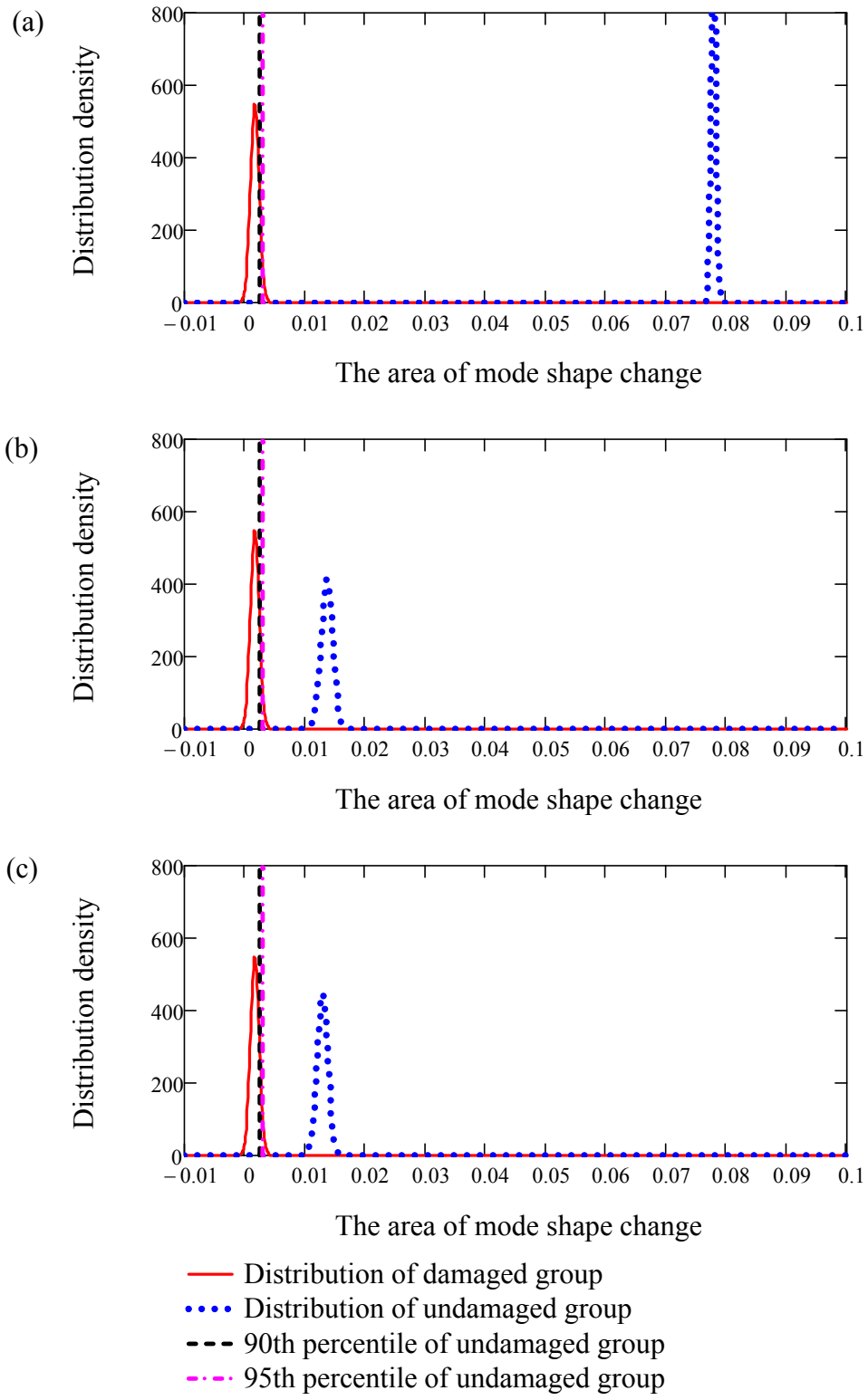

Figure H.16. Comparison of Normal distributions of the area of mode shape change for the undamaged group of 170 pairs and the damaged group of 25 data pairs for Damage Case: (a) 22, (b) 23, and (c) 24, when the Test Protocol 2 was used.

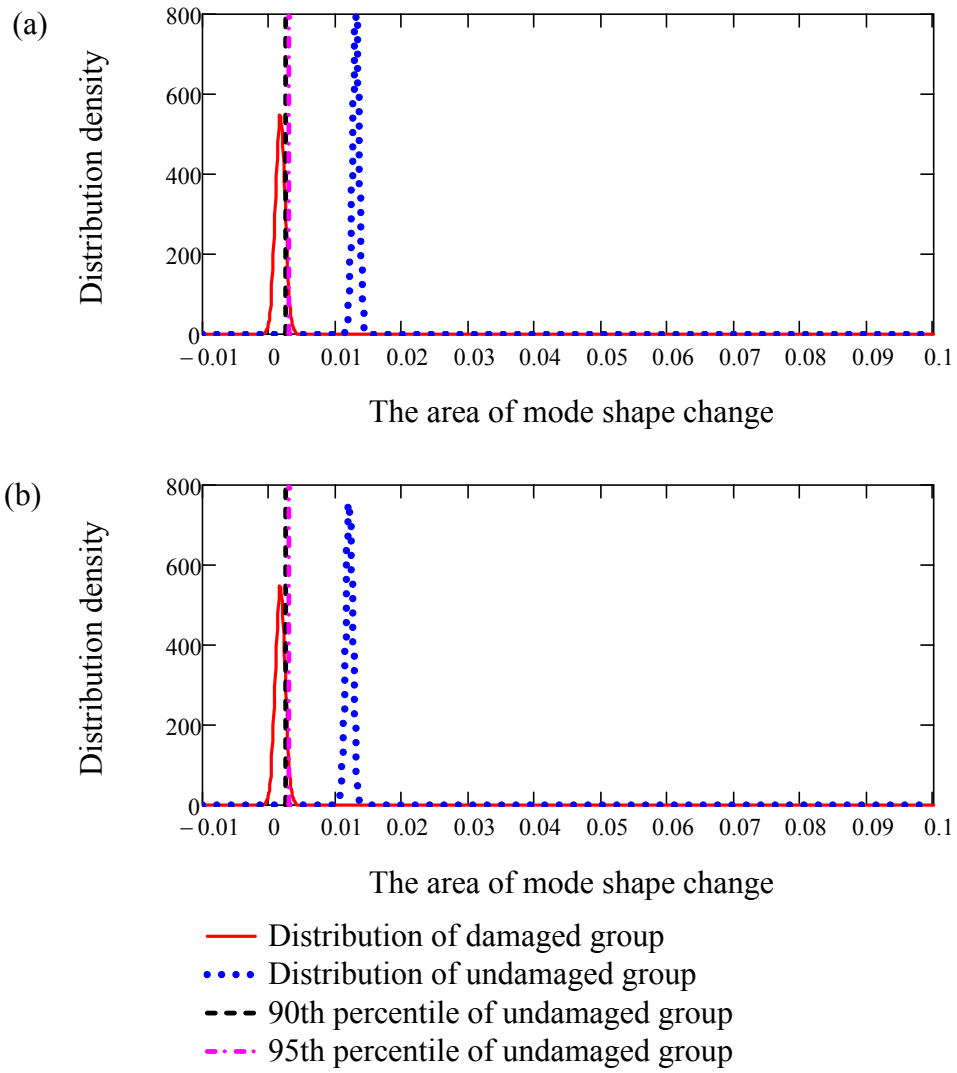

Figure H.17. Comparison of Normal distributions of the area of mode shape change for the undamaged group of 170 pairs and the damaged group of 25 data pairs for Damage Case: (a) 25 and (b) 26, when the Test Protocol 2 was used.

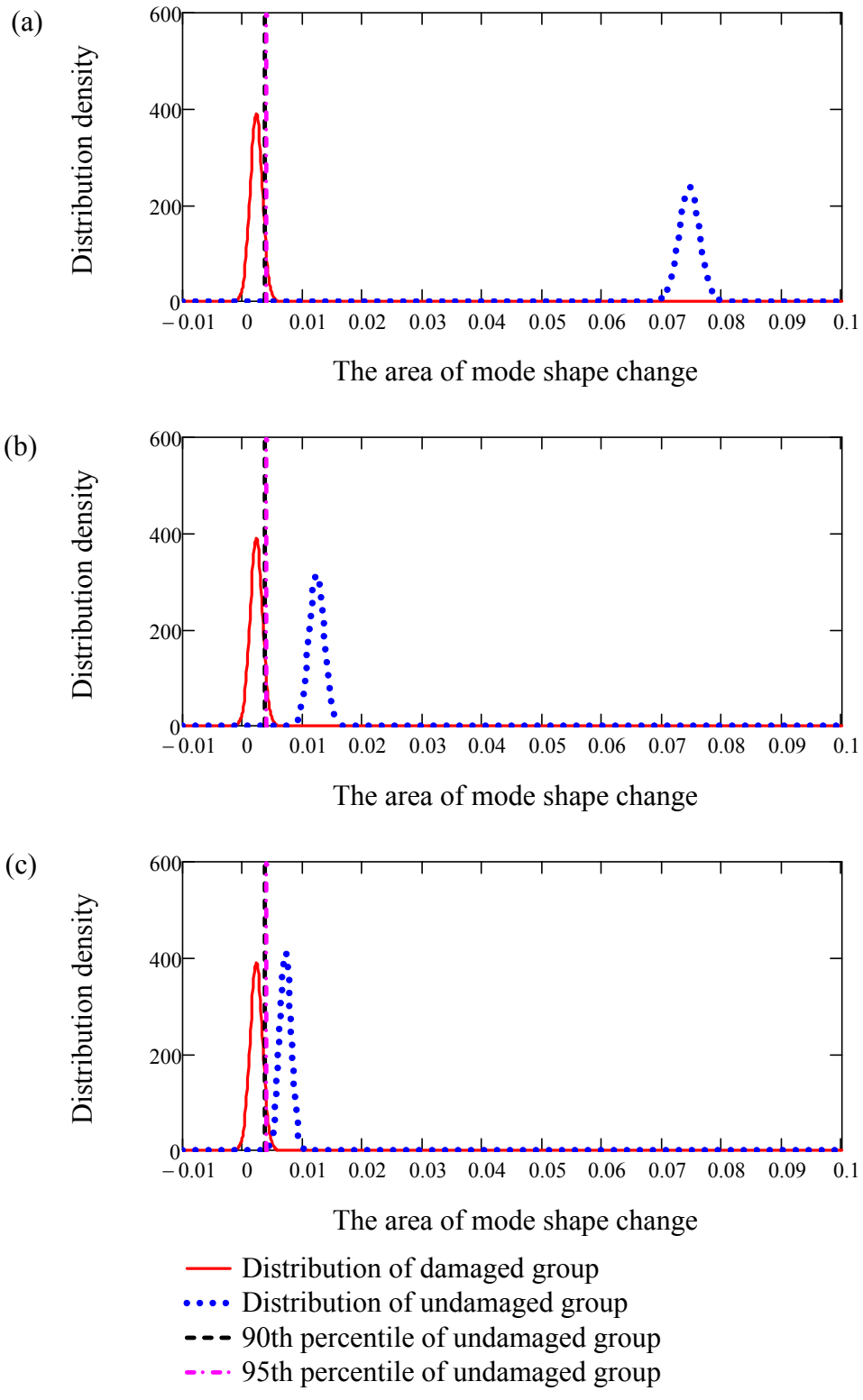

Figure H.18. Comparison of Normal distributions of the area of mode shape change for the undamaged group of 170 pairs and the damaged group of 25 data pairs for Damage Case: (a) 1, (b) 2, and (c) 3, when the Test Protocol 3 was used.

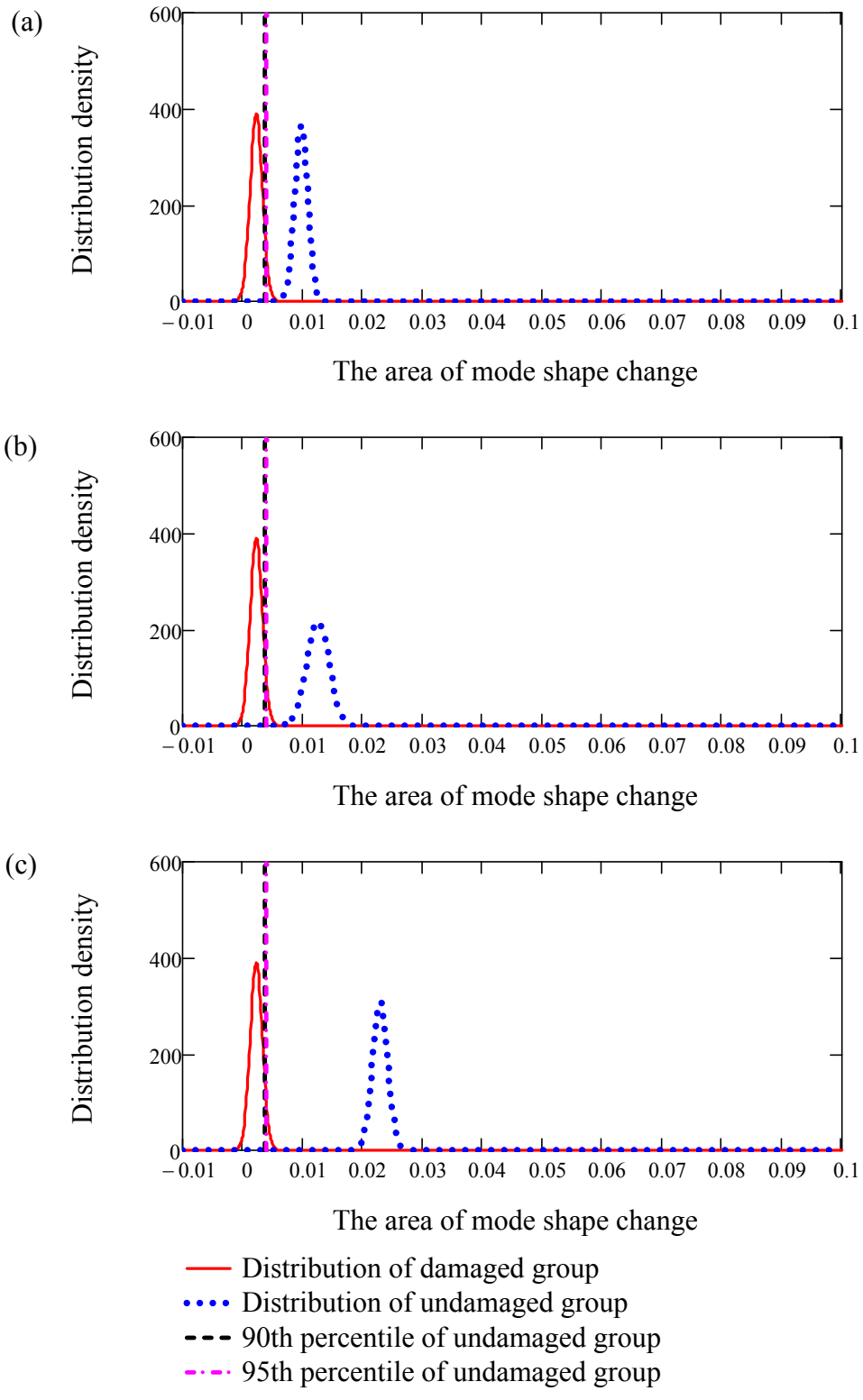

Figure H.19. Comparison of Normal distributions of the area of mode shape change for the undamaged group of 170 pairs and the damaged group of 25 data pairs for Damage Case: (a) 4, (b) 5, and (c) 6, when the Test Protocol 3 was used.

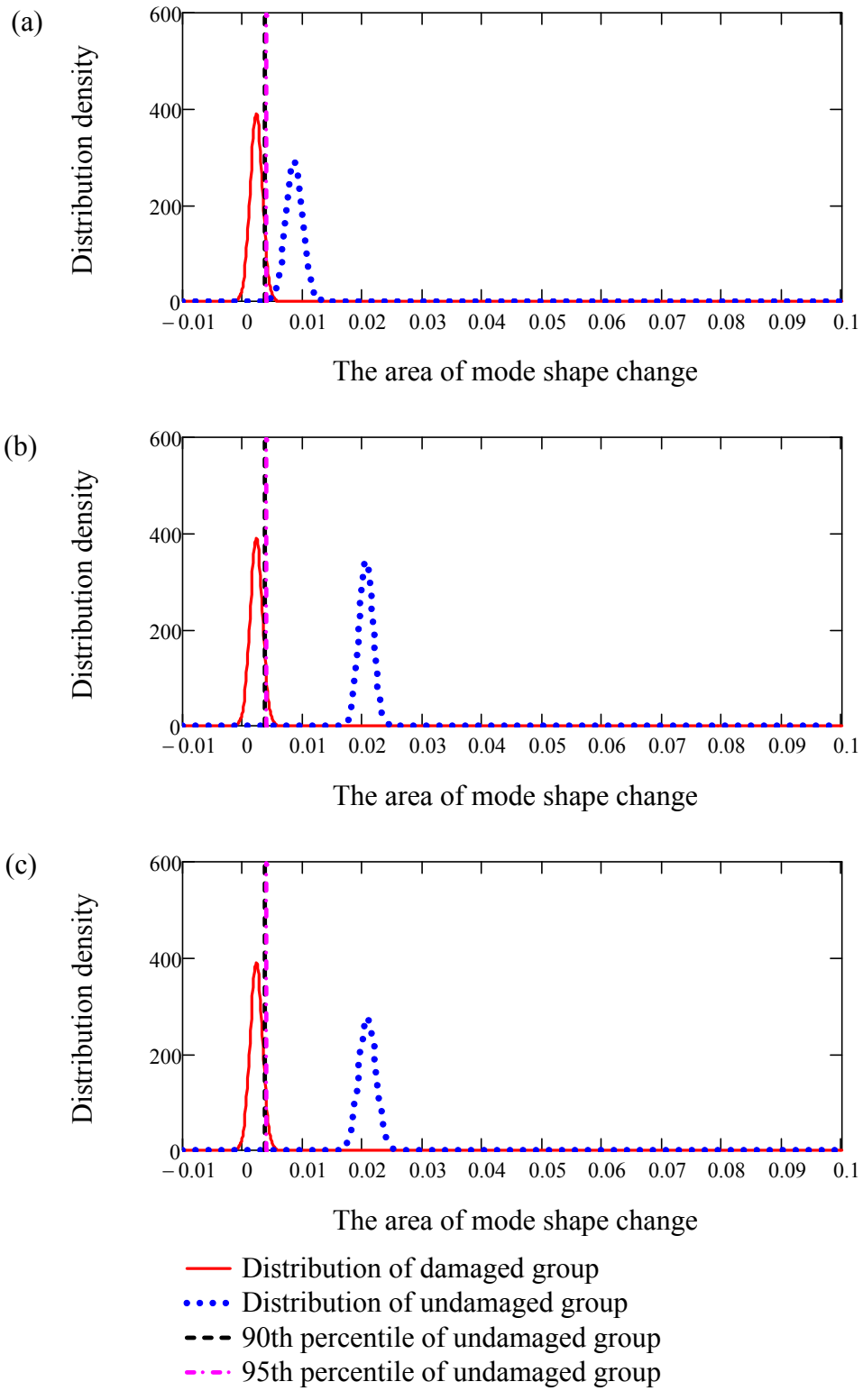

Figure H.20. Comparison of Normal distributions of the area of mode shape change for the undamaged group of 170 pairs and the damaged group of 25 data pairs for Damage Case: (a) 7, (b) 8, and (c) 9, when the Test Protocol 3 was used.

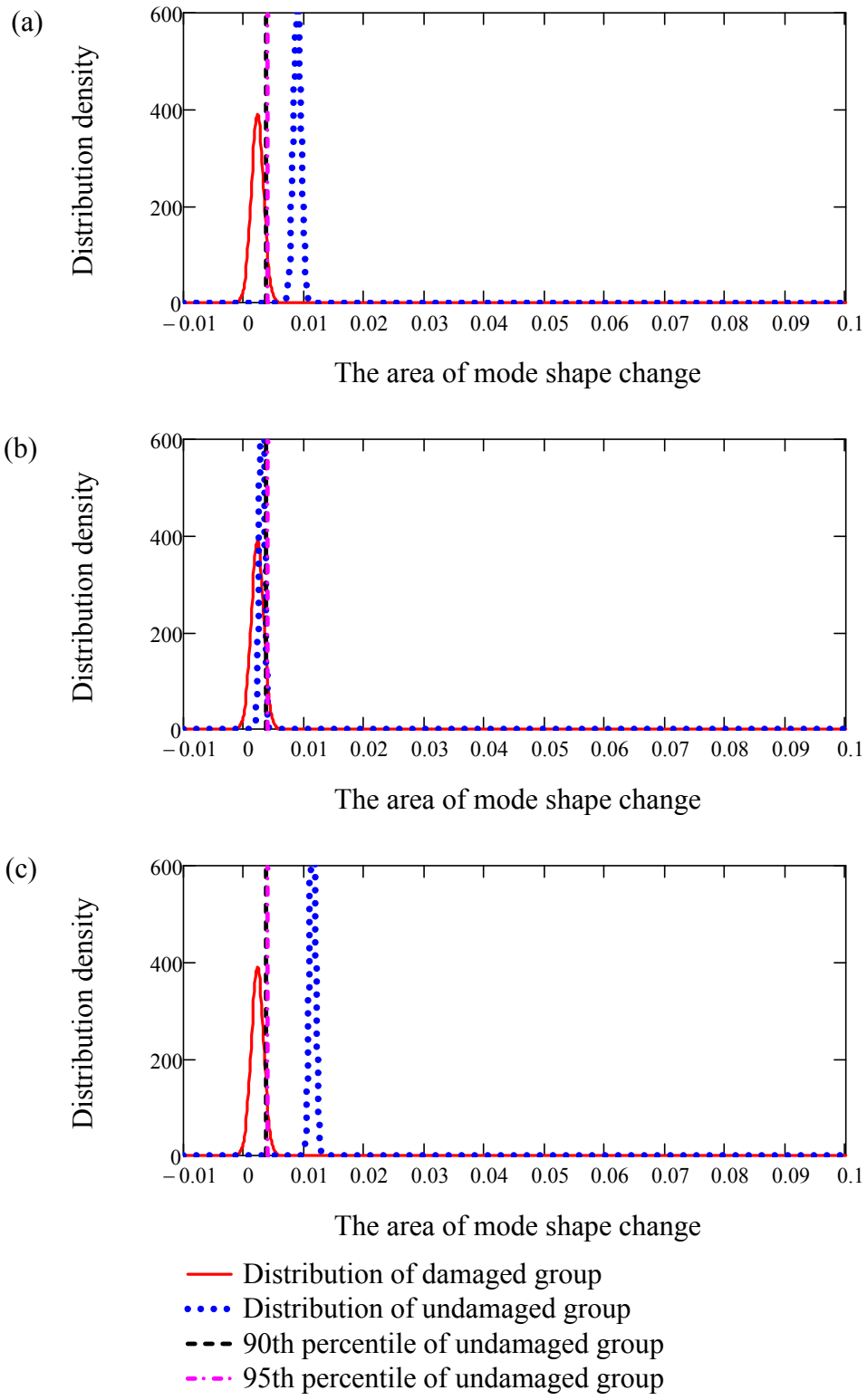

Figure H.21. Comparison of Normal distributions of the area of mode shape change for the undamaged group of 170 pairs and the damaged group of 25 data pairs for Damage Case: (a) 10, (b) 11, and (c) 12, when the Test Protocol 3 was used.

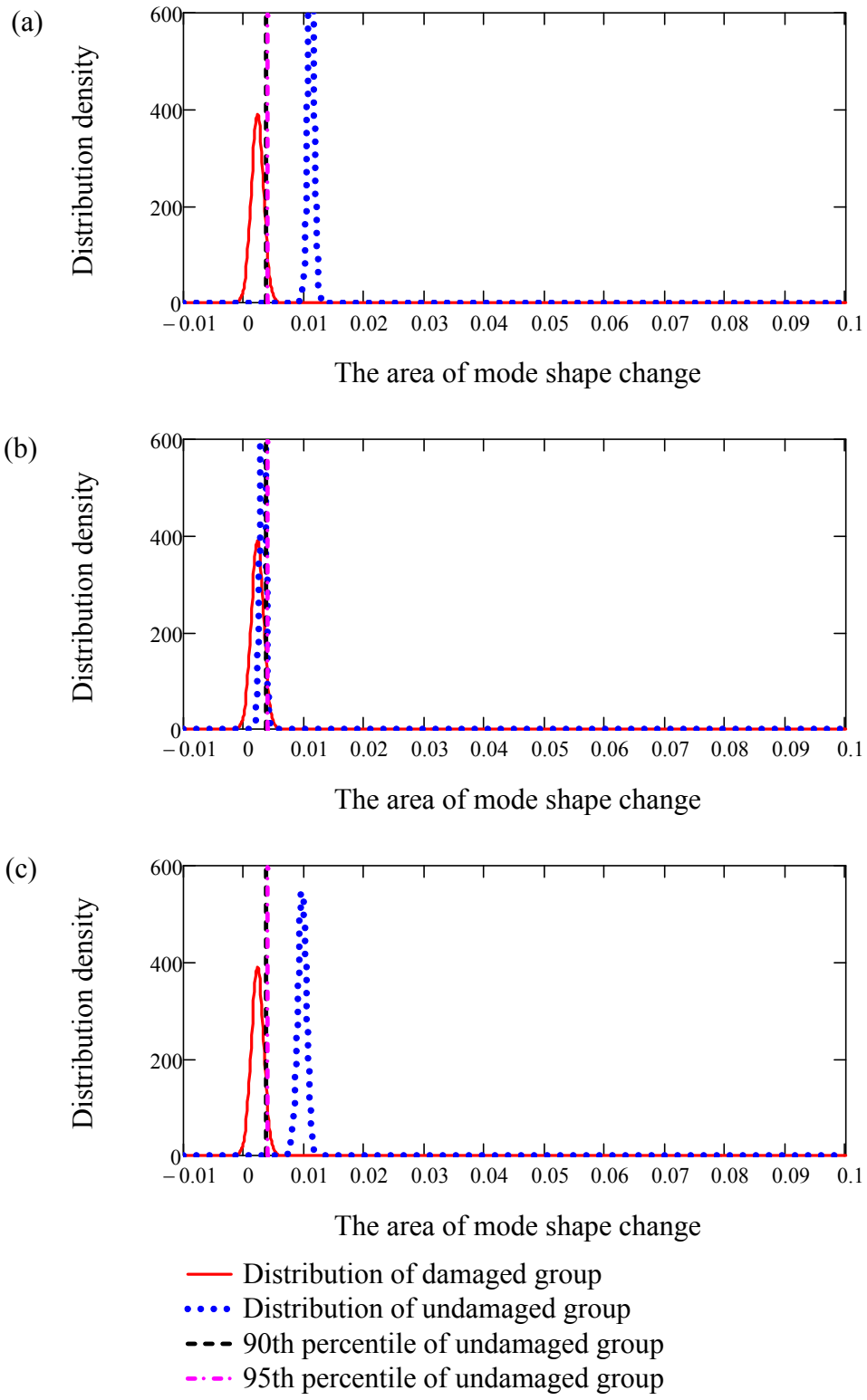

Figure H.22. Comparison of Normal distributions of the area of mode shape change for the undamaged group of 170 pairs and the damaged group of 25 data pairs for Damage Case: (a) 13, (b) 14, and (c) 15, when the Test Protocol 3 was used.

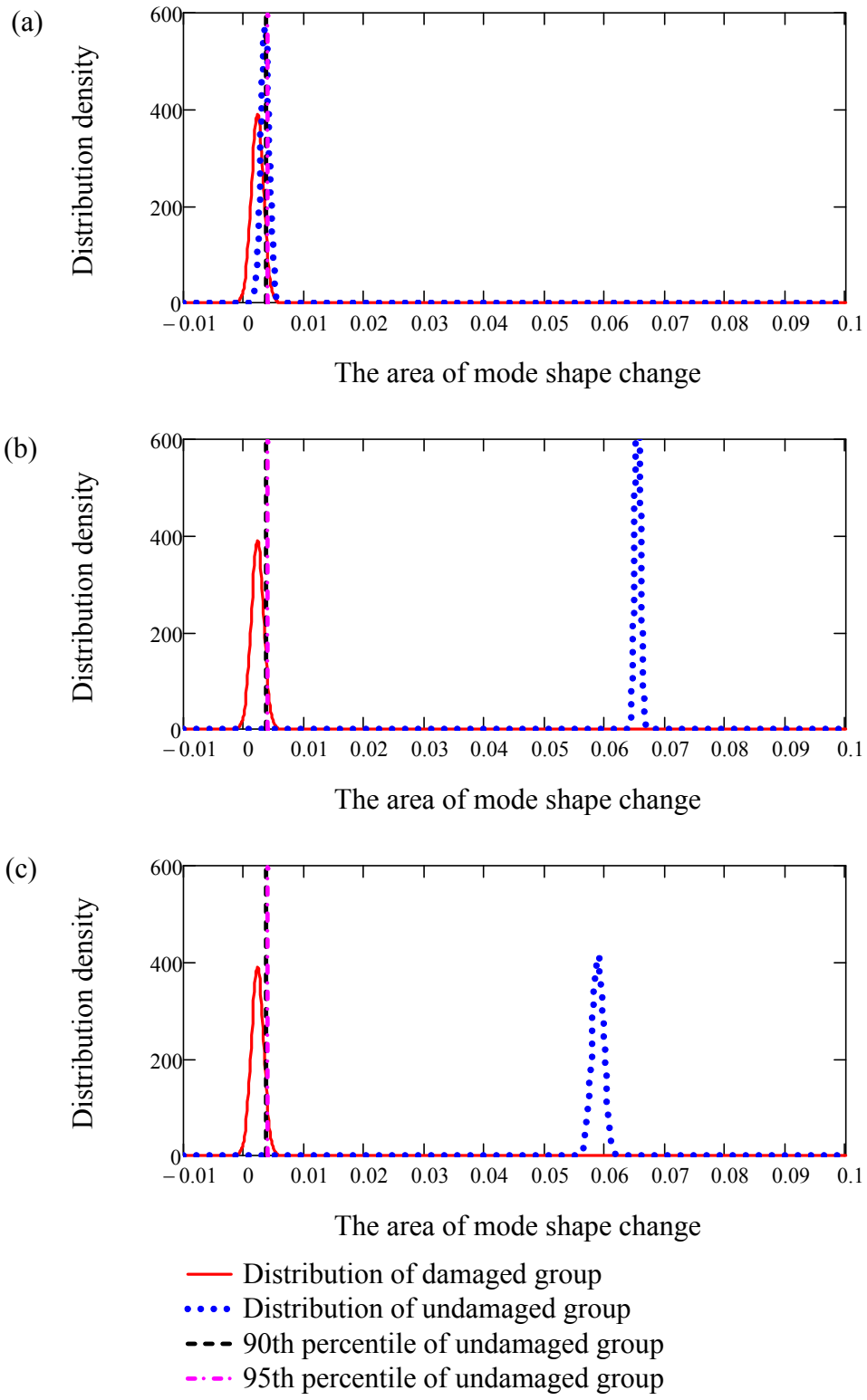

Figure H.23. Comparison of Normal distributions of the area of mode shape change for the undamaged group of 170 pairs and the damaged group of 25 data pairs for Damage Case: (a) 16, (b) 17, and (c) 18, when the Test Protocol 3 was used.

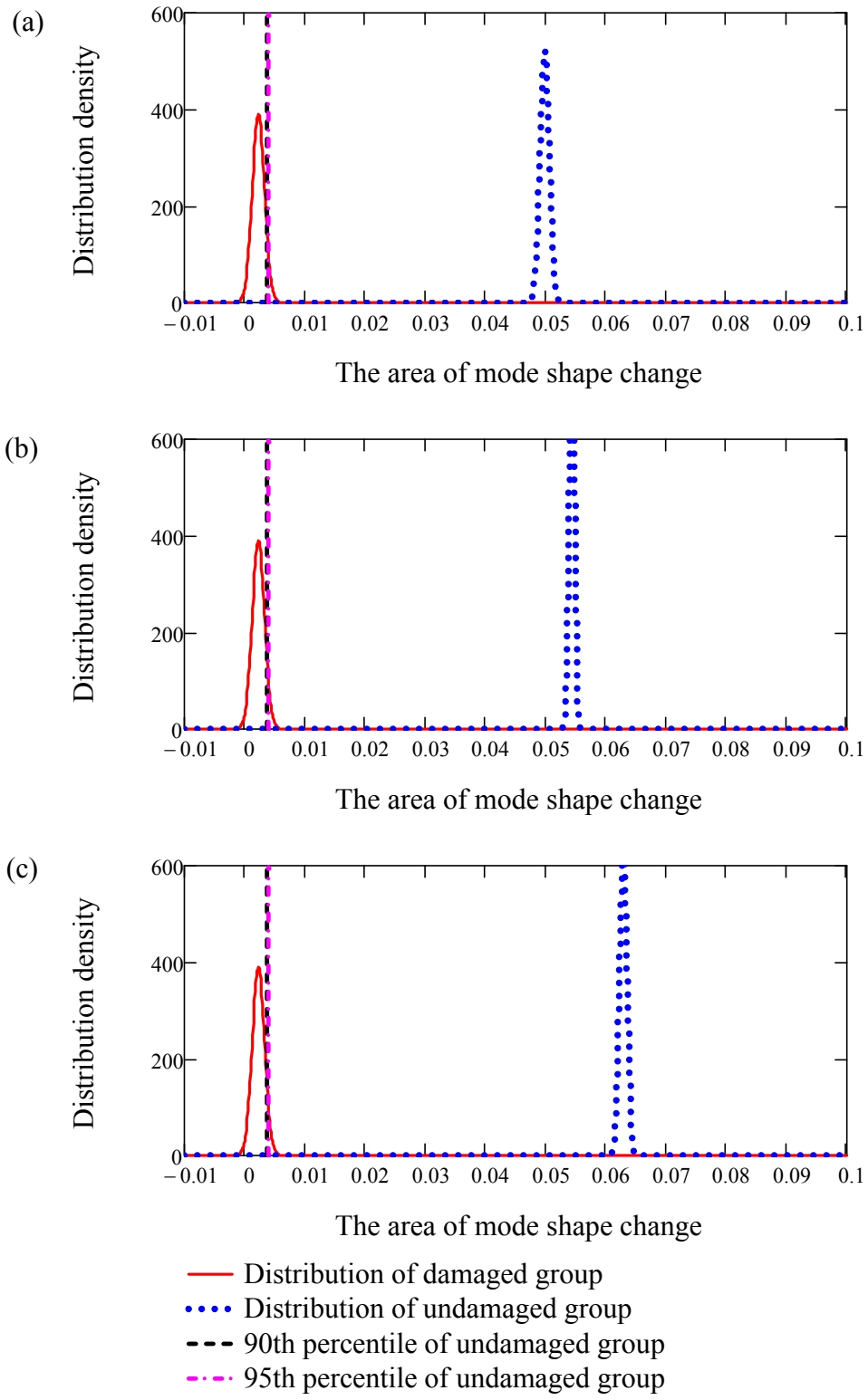

Figure H.24. Comparison of Normal distributions of the area of mode shape change for the undamaged group of 170 pairs and the damaged group of 25 data pairs for Damage Case: (a) 19, (b) 20, and (c) 21, when the Test Protocol 3 was used.

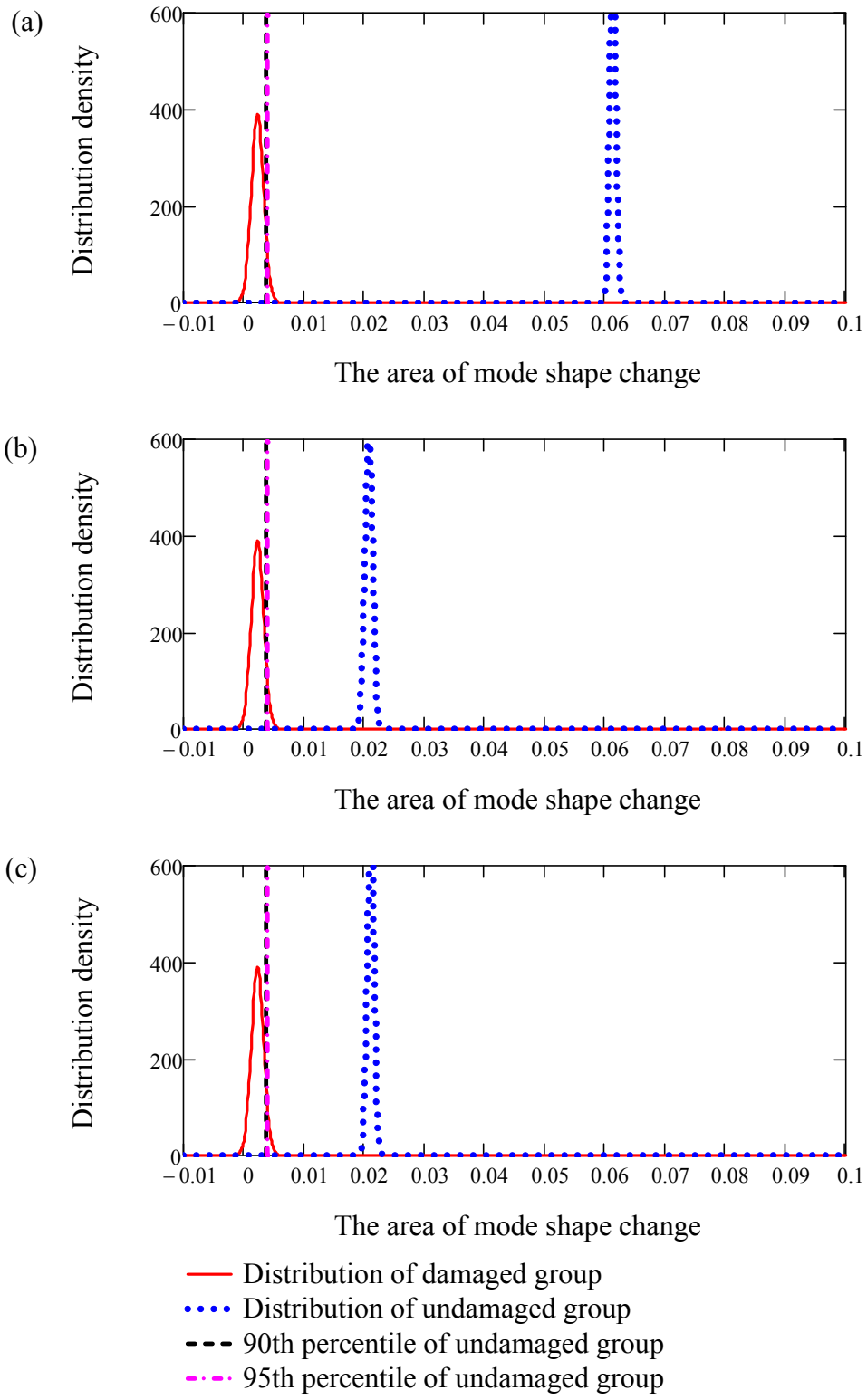

Figure H.25. Comparison of Normal distributions of the area of mode shape change for the undamaged group of 170 pairs and the damaged group of 25 data pairs for Damage Case: (a) 22, (b) 23, and (c) 24, when the Test Protocol 3 was used.

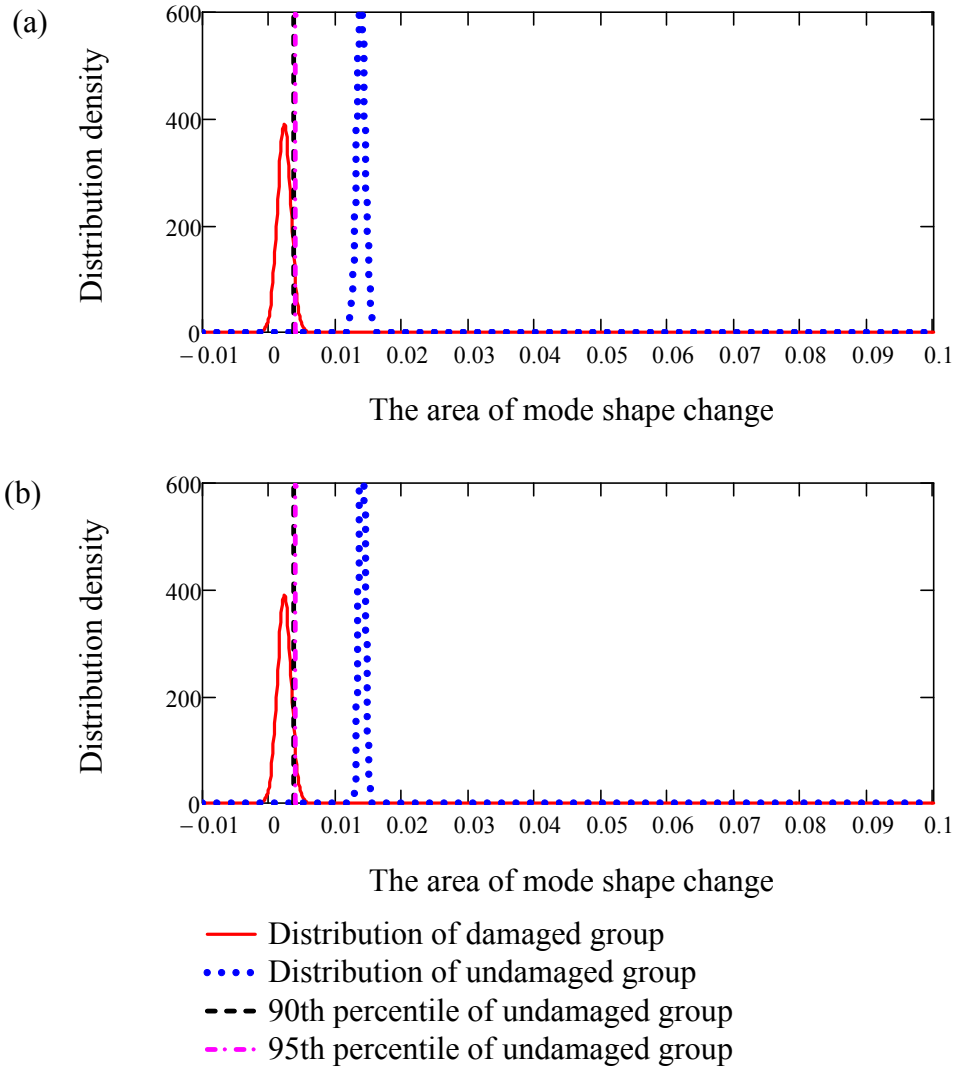

Figure H.26. Comparison of Normal distributions of the area of mode shape change for the undamaged group of 170 pairs and the damaged group of 25 data pairs for Damage Case: (a) 25 and (b) 26, when the Test Protocol 3 was used.

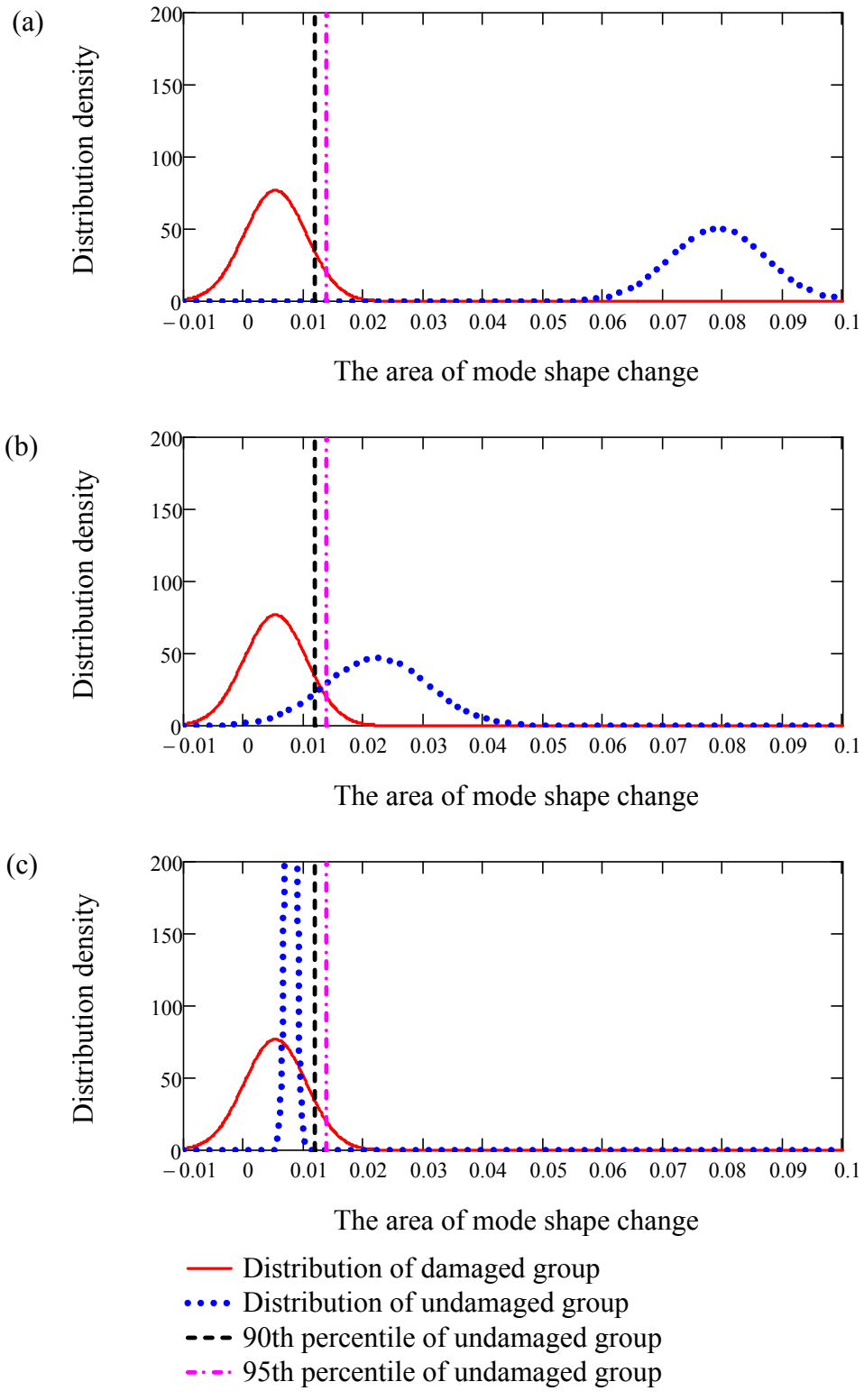

Figure H.27. Comparison of Normal distributions of the area of mode shape change for the undamaged group of 170 pairs and the damaged group of 25 data pairs for Damage Case: (a) 1, (b) 2, and (c) 3, when the Test Protocol 4 was used.

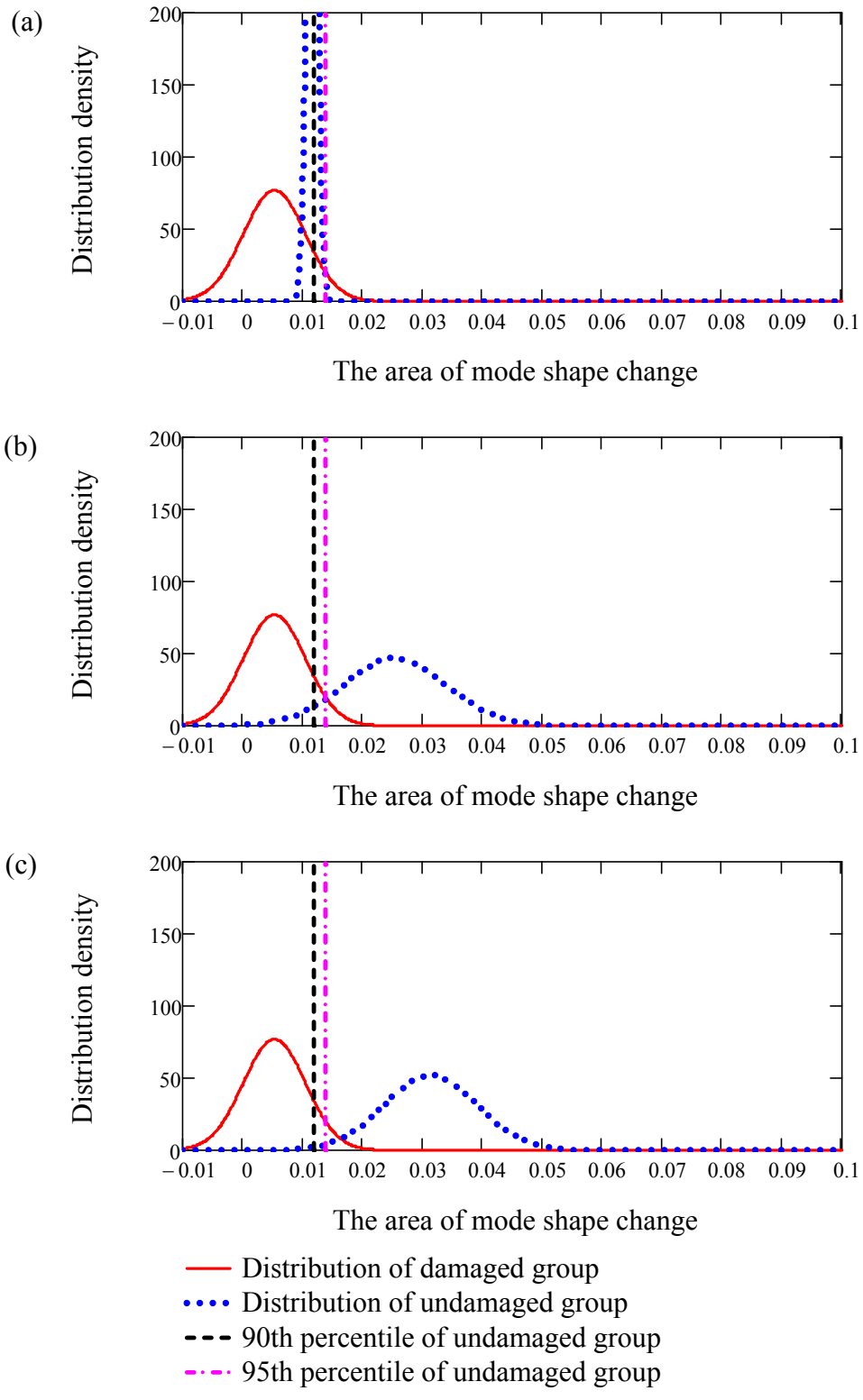

Figure H.28. Comparison of Normal distributions of the area of mode shape change for the undamaged group of 170 pairs and the damaged group of 25 data pairs for Damage Case: (a) 4, (b) 5, and (c) 6, when the Test Protocol 4 was used.

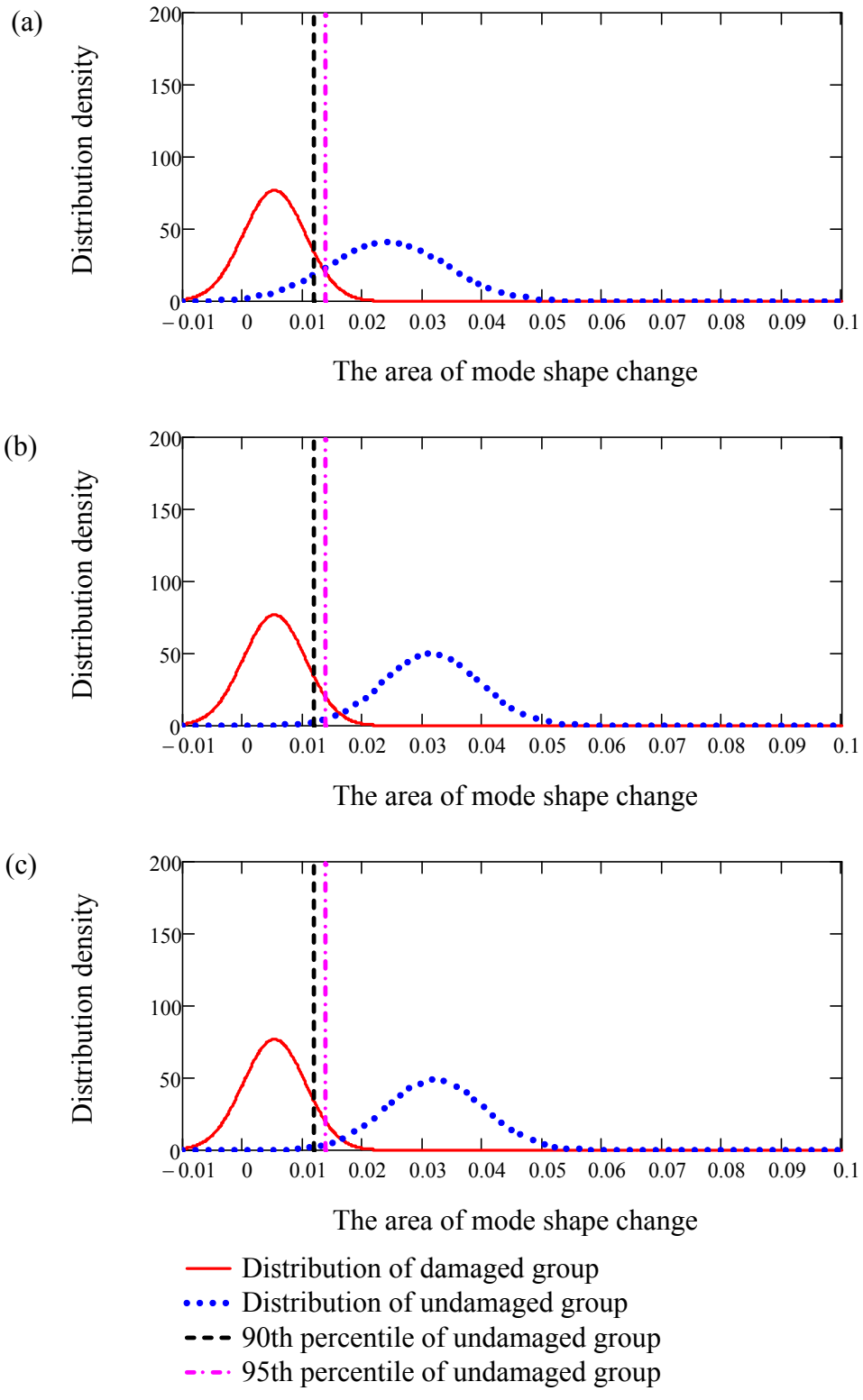

Figure H.29. Comparison of Normal distributions of the area of mode shape change for the undamaged group of 170 pairs and the damaged group of 25 data pairs for Damage Case: (a) 7, (b) 8, and (c) 9, when the Test Protocol 4 was used.

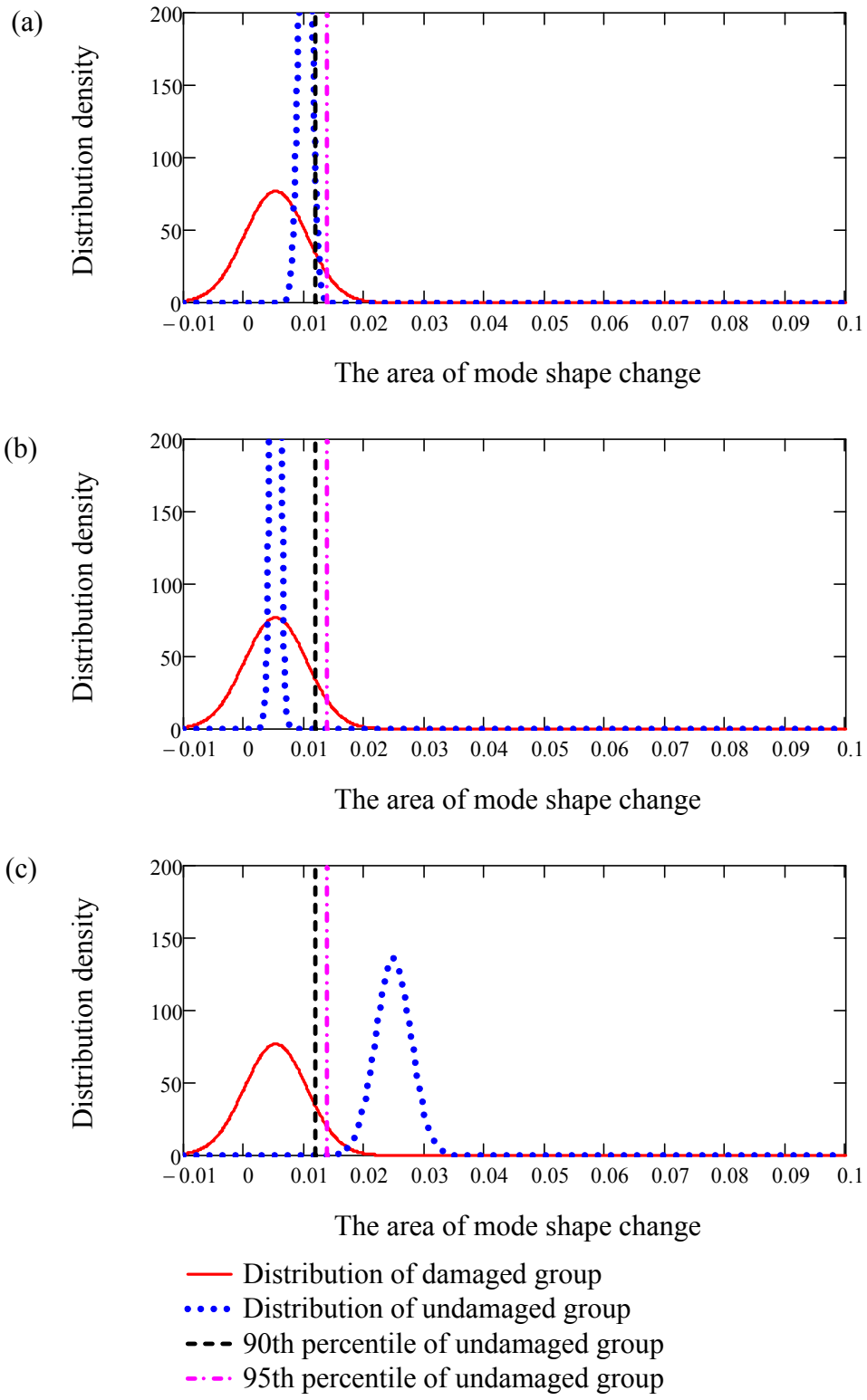

Figure H.30. Comparison of Normal distributions of the area of mode shape change for the undamaged group of 170 pairs and the damaged group of 25 data pairs for Damage Case: (a) 10, (b) 11, and (c) 12, when the Test Protocol 4 was used.

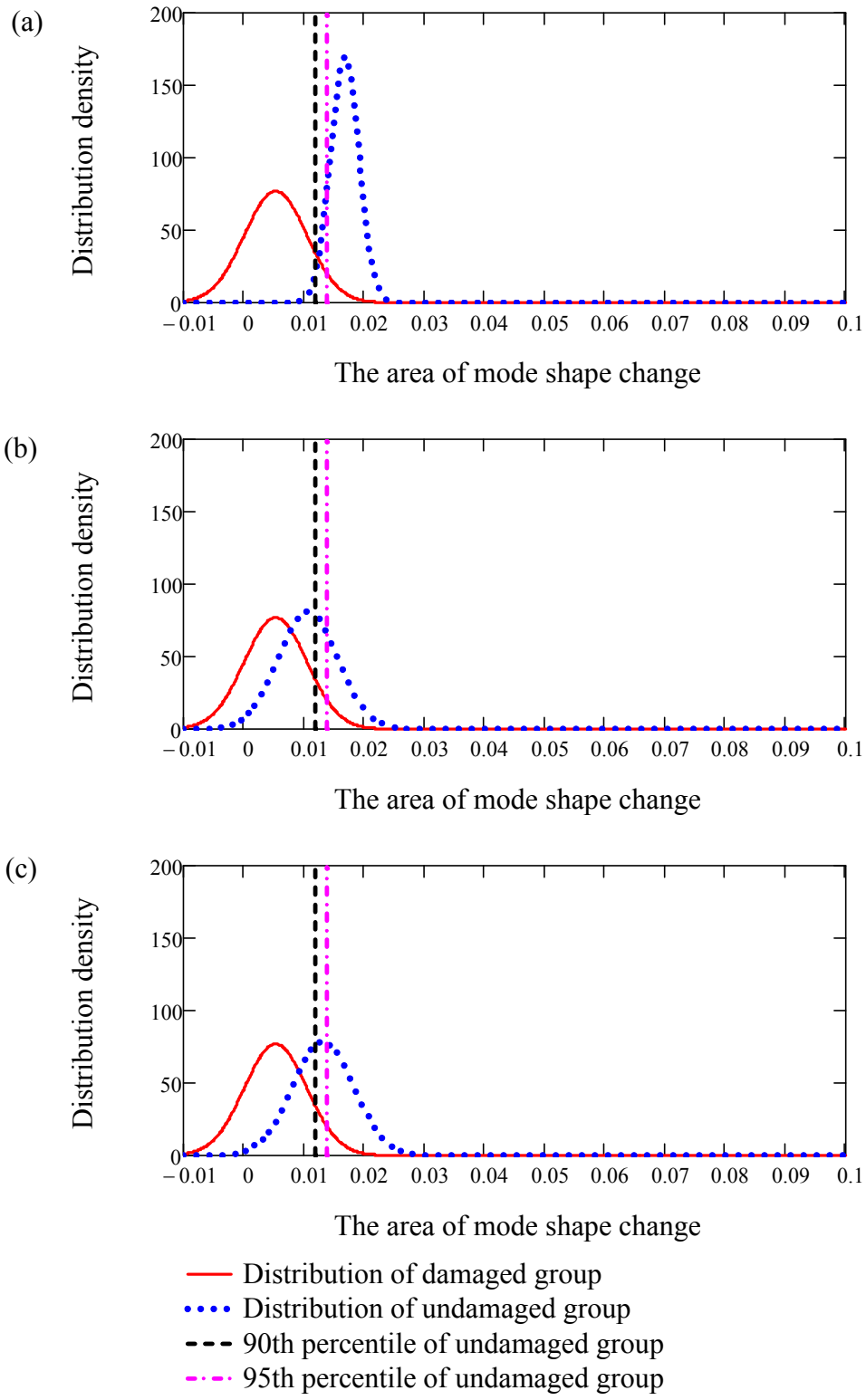

Figure H.31. Comparison of Normal distributions of the area of mode shape change for the undamaged group of 170 pairs and the damaged group of 25 data pairs for Damage Case: (a) 13, (b) 14, and (c) 15, when the Test Protocol 4 was used.

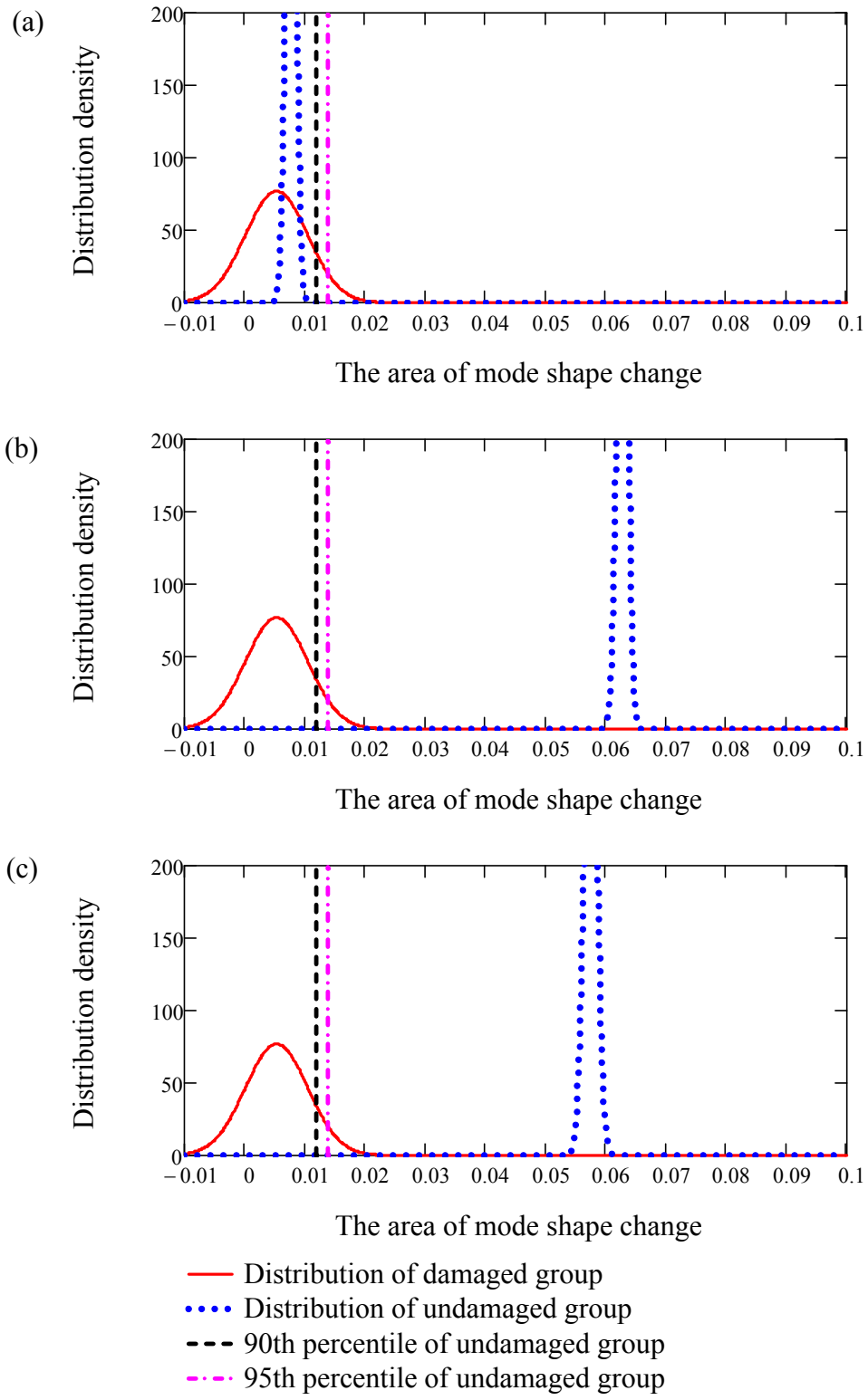

Figure H.32. Comparison of Normal distributions of the area of mode shape change for the undamaged group of 170 pairs and the damaged group of 25 data pairs for Damage Case: (a) 16, (b) 17, and (c) 18, when the Test Protocol 4 was used.

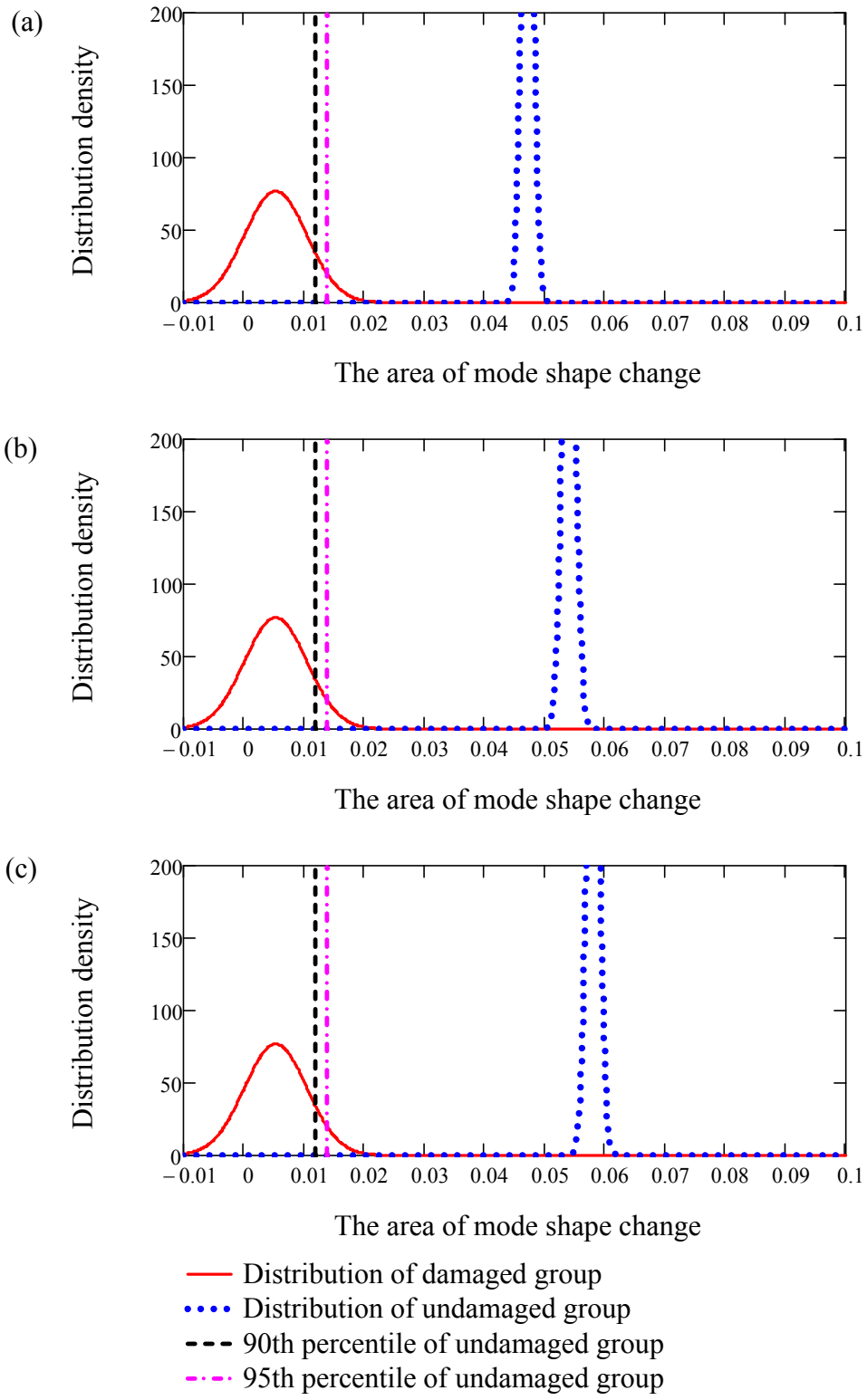

Figure H.33. Comparison of Normal distributions of the area of mode shape change for the undamaged group of 170 pairs and the damaged group of 25 data pairs for Damage Case: (a) 19, (b) 20, and (c) 21, when the Test Protocol 4 was used.

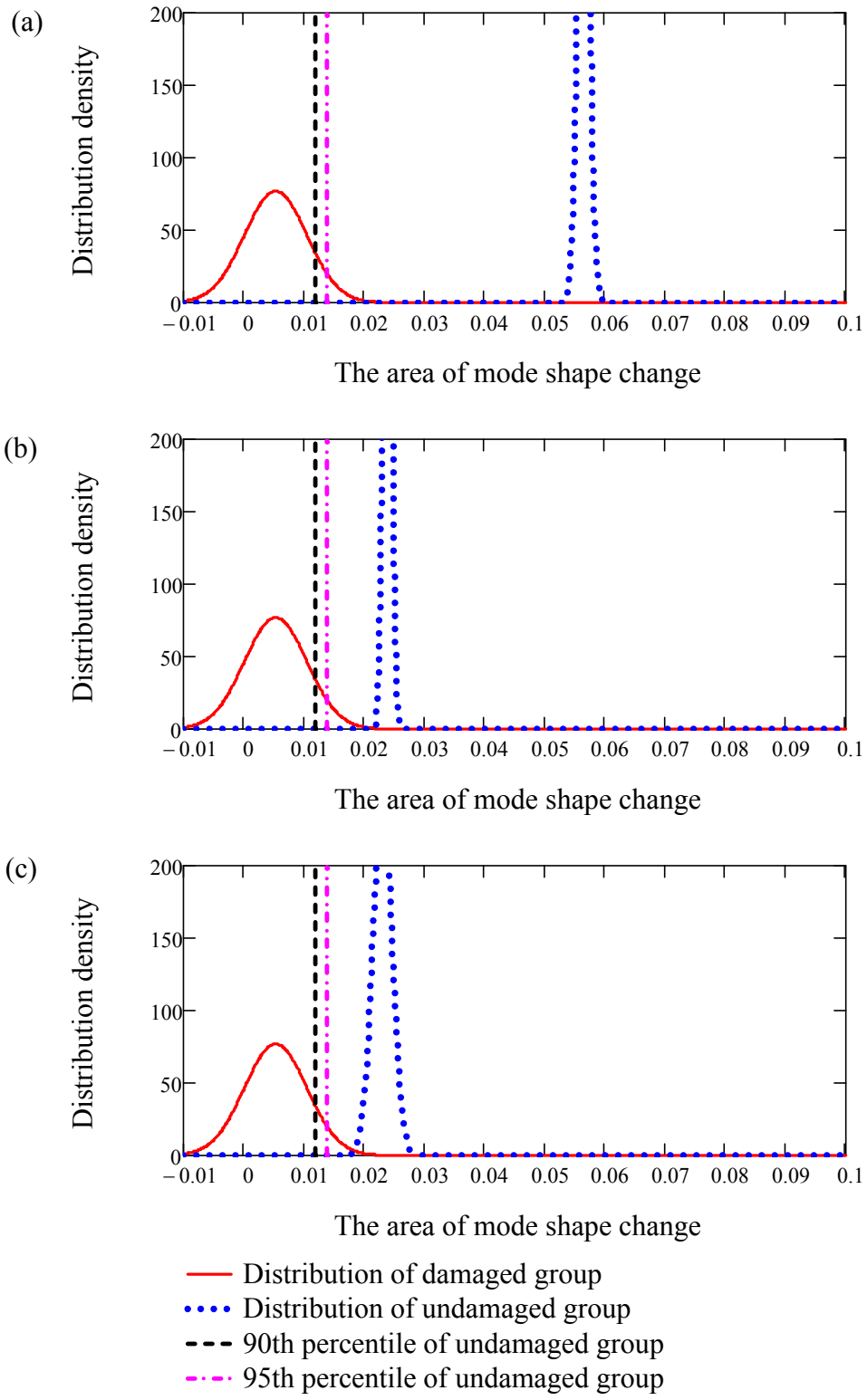

Figure H.34. Comparison of Normal distributions of the area of mode shape change for the undamaged group of 170 pairs and the damaged group of 25 data pairs for Damage Case: (a) 22, (b) 23, and (c) 24, when the Test Protocol 4 was used.

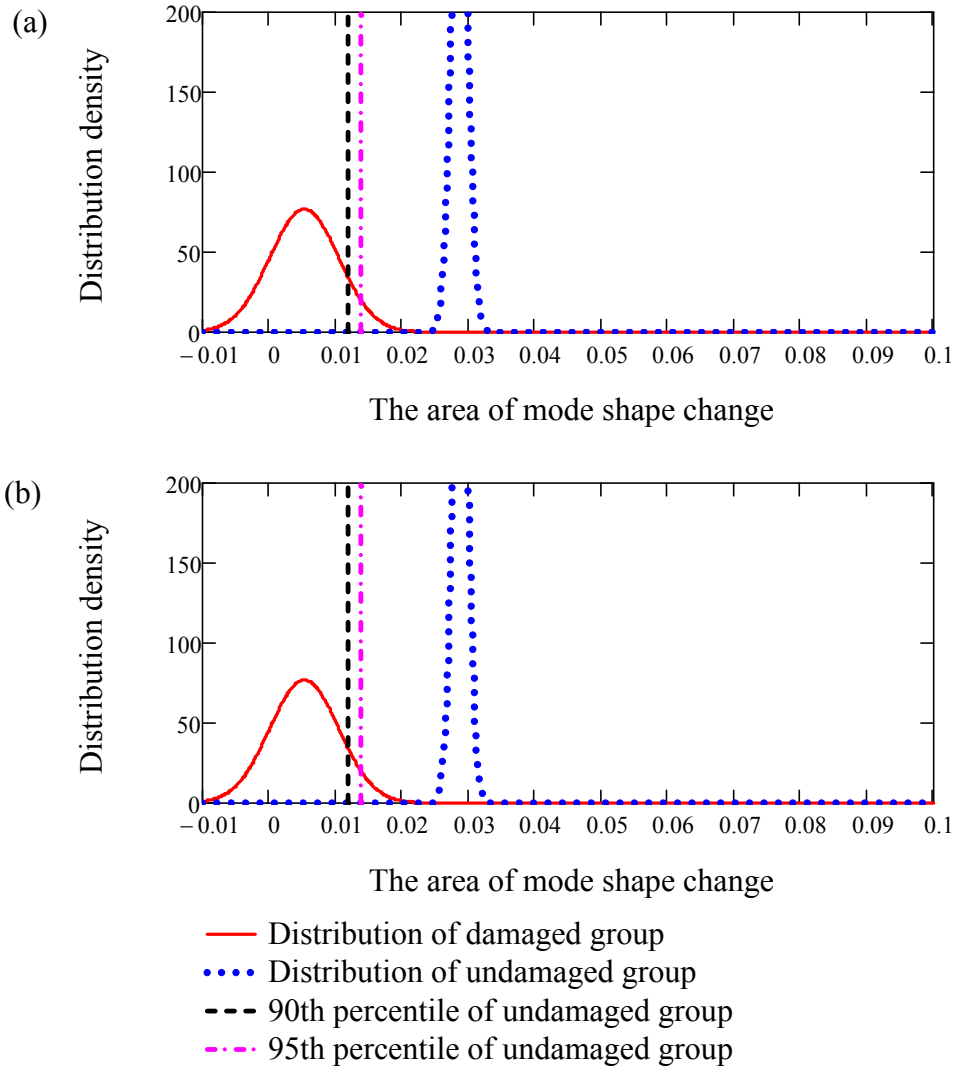

Figure H.35. Comparison of Normal distributions of the area of mode shape change for the undamaged group of 170 pairs and the damaged group of 25 data pairs for Damage Case: (a) 25 and (b) 26, when the Test Protocol 4 was used.

Table H.40. The probability that there was no change in condition using the assumed Normal distributions (i.e., the probability that the ΔA value obtained when there was a change in the condition did not exceed those that obtained when there was no change in condition), for Damage Cases 4 to 9 using all 28 Test Protocols.

Test Protocol	Damage Case					
	Case 4	Case 5	Case 6	Case 7	Case 8	Case 9
1	0.000%	0.000%	0.000%	0.000%	0.000%	0.000%
2	0.000%	0.000%	0.000%	0.000%	0.000%	0.000%
3	0.000%	0.000%	0.000%	0.000%	0.000%	0.000%
4	10.555%	2.201%	0.252%	4.221%	0.308%	0.287%
5	0.000%	0.942%	0.019%	27.568%	0.001%	1.526%
6	4.310%	31.300%	45.539%	37.756%	30.230%	48.516%
7	32.955%	54.013%	51.868%	51.848%	52.266%	34.480%
8	59.710%	61.961%	62.422%	52.400%	41.114%	39.749%
9	0.818%	0.000%	0.000%	0.000%	0.000%	0.000%
10	0.000%	0.000%	0.000%	0.000%	0.000%	0.000%
11	0.000%	0.000%	0.000%	0.000%	0.000%	0.000%
12	0.000%	0.000%	0.000%	0.000%	0.000%	0.000%
13	56.485%	60.995%	61.519%	60.864%	58.543%	59.378%
14	73.429%	80.325%	59.350%	57.806%	53.954%	62.641%
15	75.329%	82.474%	69.273%	53.833%	59.627%	71.192%
16	74.891%	81.983%	75.312%	54.866%	56.258%	78.444%
17	5.340%	0.000%	0.000%	0.000%	0.000%	0.000%
18	0.000%	0.018%	0.001%	0.000%	5.650%	1.735%
19	0.000%	0.185%	0.085%	0.000%	29.472%	14.048%
20	0.251%	4.872%	0.912%	0.000%	50.494%	36.017%
21	0.000%	3.044%	17.970%	0.000%	14.795%	6.068%
22	3.587%	1.399%	4.629%	8.370%	24.246%	18.136%
23	6.053%	2.565%	8.332%	8.682%	28.424%	18.405%
24	22.432%	7.766%	10.663%	8.019%	31.407%	18.704%
25	0.000%	5.329%	5.261%	0.368%	0.003%	0.036%
26	0.020%	26.180%	42.211%	49.644%	7.113%	32.228%
27	5.905%	18.622%	35.610%	49.974%	8.736%	33.403%
28	24.617%	12.234%	42.786%	58.350%	15.760%	41.053%

Table H.41. The probability that there was no change in condition using the assumed Normal distributions (i.e., the probability that the ΔA value obtained when there was a change in the condition did not exceed those that obtained when there was no change in condition), for Damage Cases 10 to 15 using all 28 Test Protocols.

Test Protocol	Damage Case					
	Case 10	Case 11	Case 12	Case 13	Case 14	Case 15
1	0.000%	0.000%	0.000%	0.000%	0.000%	0.000%
2	0.000%	0.000%	0.000%	0.000%	0.002%	0.000%
3	0.000%	0.000%	0.000%	0.000%	0.000%	0.000%
4	0.000%	0.000%	0.000%	2.161%	22.414%	13.883%
5	13.540%	14.797%	14.785%	30.002%	16.348%	28.483%
6	14.579%	30.965%	52.760%	28.864%	41.349%	33.375%
7	15.372%	30.068%	38.004%	30.191%	47.747%	57.679%
8	29.943%	28.377%	42.037%	42.331%	36.438%	48.751%
9	12.746%	35.969%	0.000%	0.000%	5.724%	20.601%
10	0.000%	49.879%	0.000%	0.000%	8.100%	0.000%
11	40.987%	63.141%	0.000%	0.000%	9.348%	0.000%
12	48.592%	60.374%	0.000%	0.000%	10.704%	0.000%
13	54.773%	48.966%	48.426%	42.874%	36.693%	32.919%
14	69.569%	40.072%	32.358%	22.042%	18.889%	13.446%
15	63.944%	37.367%	34.813%	24.886%	20.706%	9.490%
16	55.526%	36.739%	28.276%	29.766%	25.200%	17.713%
17	4.653%	37.327%	0.000%	0.000%	24.926%	23.250%
18	0.001%	52.695%	0.607%	9.178%	19.329%	5.078%
19	15.880%	44.056%	0.511%	17.926%	22.824%	7.842%
20	27.645%	55.553%	1.305%	14.540%	14.660%	16.706%
21	12.281%	35.385%	59.205%	60.827%	61.354%	57.318%
22	8.406%	58.772%	20.762%	59.852%	48.455%	56.504%
23	13.607%	60.925%	23.394%	64.536%	50.706%	54.233%
24	11.683%	60.885%	38.220%	67.579%	59.318%	54.679%
25	0.002%	21.562%	0.725%	4.527%	34.551%	5.019%
26	0.018%	68.693%	41.414%	34.264%	21.751%	4.911%
27	27.751%	52.118%	56.248%	52.431%	26.744%	5.964%
28	33.374%	44.587%	46.708%	39.905%	24.640%	13.131%

Table H.42. The probability that there was no change in condition using the assumed Normal distributions (i.e., the probability that the ΔA value obtained when there was a change in the condition did not exceed those that obtained when there was no change in condition), for Damage Cases 16 to 21 using all 28 Test Protocols.

Test Protocol	Damage Case					
	Case 16	Case 17	Case 18	Case 19	Case 20	Case 21
1	0.040%	0.000%	0.000%	0.000%	0.000%	0.000%
2	0.000%	0.000%	0.000%	0.000%	0.000%	0.000%
3	0.001%	0.000%	0.000%	0.000%	0.000%	0.000%
4	0.010%	0.000%	0.000%	0.000%	0.000%	0.000%
5	52.718%	0.000%	0.000%	0.000%	0.000%	0.000%
6	45.171%	0.104%	0.000%	0.118%	0.004%	0.001%
7	50.071%	8.570%	0.975%	15.538%	9.224%	1.404%
8	40.492%	18.317%	18.206%	37.238%	31.236%	20.330%
9	29.811%	0.002%	0.007%	5.933%	3.579%	0.920%
10	0.000%	0.002%	0.000%	0.000%	2.917%	0.000%
11	0.000%	0.012%	0.000%	0.569%	4.226%	1.744%
12	0.055%	0.661%	0.002%	8.902%	6.330%	2.966%
13	34.665%	26.414%	23.501%	37.027%	21.142%	23.018%
14	45.728%	55.765%	57.885%	56.368%	59.372%	57.774%
15	32.670%	51.588%	55.965%	51.694%	54.362%	46.169%
16	30.551%	63.446%	63.053%	55.004%	58.751%	46.126%
17	41.242%	0.000%	0.000%	0.000%	0.000%	0.000%
18	49.237%	0.000%	0.000%	0.000%	30.391%	0.004%
19	53.856%	0.000%	0.000%	0.000%	35.256%	25.532%
20	51.601%	0.000%	0.013%	0.000%	34.461%	42.198%
21	33.703%	0.000%	0.000%	4.661%	12.902%	36.611%
22	53.420%	0.193%	0.000%	0.000%	18.228%	40.352%
23	54.635%	0.110%	0.000%	0.010%	18.481%	54.396%
24	55.198%	0.382%	0.006%	0.062%	11.966%	55.263%
25	28.334%	1.435%	0.002%	0.000%	0.784%	2.201%
26	38.225%	36.741%	3.450%	0.000%	32.047%	0.005%
27	36.410%	44.104%	6.798%	0.049%	35.741%	30.676%
28	38.449%	64.496%	42.152%	5.194%	43.903%	38.736%

Table H.43. The probability that there was no change in condition using the assumed Normal distributions (i.e., the probability that the ΔA value obtained when there was a change in the condition did not exceed those that obtained when there was no change in condition), for Damage Cases 22 to 26 using all 28 Test Protocols.

Test Protocol	Damage Case				
	Case 22	Case 23	Case 24	Case 25	Case 26
1	0.000%	0.000%	0.000%	0.000%	0.000%
2	0.000%	0.000%	0.000%	0.000%	0.000%
3	0.000%	0.000%	0.000%	0.000%	0.000%
4	0.000%	0.000%	0.000%	0.000%	0.000%
5	0.000%	0.012%	0.000%	0.034%	4.581%
6	0.003%	44.999%	45.367%	59.333%	37.193%
7	5.109%	36.630%	45.149%	52.309%	54.234%
8	13.199%	68.211%	38.439%	54.818%	48.293%
9	2.574%	0.000%	0.000%	0.000%	0.000%
10	0.000%	0.000%	0.000%	0.000%	0.000%
11	0.631%	0.000%	0.000%	0.000%	0.000%
12	2.695%	0.000%	0.000%	0.000%	0.000%
13	32.868%	49.041%	35.670%	49.351%	33.460%
14	36.633%	27.345%	24.682%	38.790%	46.246%
15	28.596%	27.716%	23.855%	25.665%	38.843%
16	36.025%	24.724%	22.560%	34.356%	39.731%
17	0.000%	0.000%	0.000%	0.000%	0.000%
18	0.004%	0.376%	4.465%	18.125%	15.849%
19	52.276%	1.111%	5.081%	36.219%	34.607%
20	60.154%	13.779%	12.715%	54.225%	38.724%
21	51.176%	52.809%	55.358%	35.643%	39.684%
22	43.423%	38.037%	57.965%	61.428%	52.059%
23	55.663%	37.011%	53.975%	65.296%	51.257%
24	56.775%	45.455%	50.504%	59.702%	53.547%
25	0.019%	10.114%	6.947%	0.013%	0.044%
26	0.006%	31.221%	14.026%	46.406%	51.236%
27	56.586%	48.111%	15.909%	43.113%	47.797%
28	60.875%	53.932%	26.883%	40.530%	50.323%

Table H.44. The probability that there was no change in condition using the assumed Log-Normal distributions (i.e., the probability that the ΔA value obtained when there was a change in the condition did not exceed those that obtained when there was no change in condition), for Damage Cases 4 to 9 using all 28 Test Protocols.

Test Protocol	Damage Case					
	Case 4	Case 5	Case 6	Case 7	Case 8	Case 9
1	0.468%	0.120%	0.043%	0.175%	0.064%	0.064%
2	0.000%	0.000%	0.000%	0.000%	0.000%	0.000%
3	0.000%	0.000%	0.000%	0.000%	0.000%	0.000%
4	3.297%	0.312%	0.020%	0.745%	0.021%	0.020%
5	0.001%	1.829%	0.803%	24.769%	0.813%	2.174%
6	6.126%	30.897%	44.020%	37.888%	29.220%	47.043%
7	32.413%	51.741%	50.832%	50.505%	51.555%	33.934%
8	57.728%	60.266%	61.808%	50.837%	42.378%	40.578%
9	6.548%	0.310%	0.226%	0.272%	0.300%	0.311%
10	0.007%	0.000%	0.000%	0.000%	0.000%	0.000%
11	0.014%	0.000%	0.000%	0.000%	0.000%	0.000%
12	0.329%	0.000%	0.000%	0.000%	0.000%	0.000%
13	47.697%	61.242%	62.606%	61.812%	55.837%	58.263%
14	72.620%	84.009%	55.494%	54.771%	48.515%	57.291%
15	74.429%	86.051%	66.755%	50.835%	52.703%	67.763%
16	72.582%	82.878%	74.043%	51.669%	50.820%	77.457%
17	5.415%	0.000%	0.000%	0.000%	0.033%	0.021%
18	0.001%	0.078%	0.013%	0.000%	5.424%	2.108%
19	0.013%	0.548%	0.253%	0.000%	24.316%	12.612%
20	1.138%	5.213%	1.922%	0.005%	46.803%	32.432%
21	1.603%	8.254%	17.156%	0.357%	15.480%	10.047%
22	3.881%	2.167%	4.155%	6.375%	17.358%	13.328%
23	4.646%	2.589%	5.767%	6.035%	21.548%	12.392%
24	16.720%	7.248%	9.176%	7.612%	25.456%	14.601%
25	0.000%	6.316%	6.356%	0.458%	0.026%	0.246%
26	0.922%	21.016%	35.560%	42.846%	4.900%	29.557%
27	5.834%	14.632%	30.605%	42.207%	6.318%	30.437%
28	20.536%	11.358%	39.058%	54.099%	14.092%	38.523%

Table H.45. The probability that there was no change in condition using the assumed Log-Normal distributions (i.e., the probability that the ΔA value obtained when there was a change in the condition did not exceed those that obtained when there was no change in condition), for Damage Cases 10 to 15 using all 28 Test Protocols.

Test Protocol	Damage Case					
	Case 10	Case 11	Case 12	Case 13	Case 14	Case 15
1	3.567%	8.099%	0.309%	4.177%	16.863%	6.207%
2	0.000%	11.749%	0.000%	0.000%	20.026%	0.002%
3	0.000%	17.370%	0.000%	0.000%	15.022%	0.000%
4	5.550%	35.899%	0.026%	0.695%	10.521%	4.621%
5	12.050%	13.995%	14.250%	27.227%	15.263%	24.868%
6	14.943%	30.310%	51.007%	27.959%	39.363%	33.054%
7	13.695%	29.446%	35.684%	29.996%	47.529%	58.310%
8	29.854%	28.574%	40.825%	41.302%	35.860%	48.760%
9	14.899%	28.572%	0.898%	0.143%	11.894%	18.035%
10	9.074%	48.813%	0.000%	0.000%	7.042%	0.008%
11	28.974%	57.121%	0.000%	0.000%	7.897%	0.001%
12	36.973%	62.322%	0.000%	0.000%	9.420%	0.350%
13	48.990%	37.004%	34.103%	26.346%	20.591%	18.945%
14	66.257%	34.908%	27.637%	18.106%	16.078%	11.725%
15	59.567%	33.999%	28.296%	21.096%	18.054%	9.268%
16	54.467%	33.047%	25.065%	25.499%	23.012%	16.501%
17	5.170%	32.332%	0.000%	0.044%	21.314%	19.715%
18	0.056%	48.897%	0.429%	8.643%	14.423%	3.868%
19	14.628%	40.652%	0.858%	16.257%	19.839%	7.293%
20	24.757%	51.250%	2.462%	13.141%	12.118%	15.208%
21	12.544%	30.129%	46.130%	47.709%	49.796%	43.134%
22	6.308%	53.833%	13.384%	57.291%	37.841%	48.170%
23	9.586%	56.567%	14.848%	63.701%	42.130%	44.531%
24	10.000%	55.136%	29.630%	64.986%	53.011%	48.344%
25	0.011%	21.583%	1.536%	5.960%	33.537%	4.810%
26	0.464%	67.011%	32.026%	28.650%	16.613%	4.743%
27	24.332%	47.781%	50.480%	48.284%	21.770%	4.908%
28	31.057%	41.661%	43.750%	34.858%	21.477%	10.829%

Table H.46. The probability that there was no change in condition using the assumed Log-Normal distributions (i.e., the probability that the ΔA value obtained when there was a change in the condition did not exceed those that obtained when there was no change in condition), for Damage Cases 16 to 21 using all 28 Test Protocols.

Test Protocol	Damage Case					
	Case 16	Case 17	Case 18	Case 19	Case 20	Case 21
1	26.930%	0.004%	0.003%	0.013%	0.012%	0.013%
2	25.363%	0.000%	0.000%	0.000%	0.000%	0.000%
3	10.854%	0.000%	0.000%	0.000%	0.000%	0.000%
4	14.422%	0.000%	0.000%	0.000%	0.000%	0.000%
5	49.014%	0.000%	0.000%	0.000%	0.000%	0.000%
6	45.116%	0.027%	0.004%	0.034%	0.016%	0.002%
7	49.976%	8.346%	1.000%	14.779%	8.423%	0.721%
8	39.248%	18.165%	18.308%	37.029%	32.380%	21.385%
9	21.693%	3.493%	5.572%	10.900%	10.126%	8.786%
10	0.125%	0.337%	0.058%	0.408%	4.751%	5.744%
11	0.162%	0.434%	0.029%	2.321%	5.191%	3.273%
12	1.188%	2.714%	0.768%	8.505%	7.034%	4.834%
13	34.603%	10.719%	8.528%	20.543%	7.966%	9.419%
14	35.356%	48.927%	50.610%	48.181%	52.735%	51.211%
15	26.709%	45.936%	49.772%	44.987%	47.847%	39.715%
16	25.643%	59.520%	60.271%	50.000%	53.159%	44.090%
17	35.712%	0.000%	0.000%	0.000%	0.047%	0.047%
18	45.284%	0.000%	0.000%	0.000%	25.092%	0.114%
19	50.324%	0.000%	0.007%	0.000%	30.004%	22.367%
20	46.862%	0.007%	0.164%	0.002%	29.860%	37.563%
21	26.584%	1.316%	0.682%	9.736%	13.543%	29.720%
22	46.076%	0.648%	0.190%	0.226%	14.301%	29.315%
23	47.139%	0.506%	0.132%	0.337%	13.689%	49.468%
24	49.257%	1.425%	0.453%	0.883%	10.254%	47.929%
25	28.628%	0.952%	0.021%	0.000%	0.886%	1.830%
26	33.995%	27.882%	4.151%	0.183%	27.852%	0.513%
27	32.811%	37.260%	6.092%	0.421%	34.489%	24.695%
28	35.998%	62.903%	37.662%	5.617%	40.263%	37.398%

Table H.47. The probability that there was no change in condition using the assumed Log-Normal distributions (i.e., the probability that the ΔA value obtained when there was a change in the condition did not exceed those that obtained when there was no change in condition), for Damage Cases 22 to 26 using all 28 Test Protocols.

Test Protocol	Damage Case				
	Case 22	Case 23	Case 24	Case 25	Case 26
1	0.013%	0.158%	0.158%	0.266%	0.220%
2	0.000%	0.000%	0.000%	0.000%	0.000%
3	0.000%	0.000%	0.000%	0.000%	0.000%
4	0.000%	0.026%	0.026%	0.026%	0.026%
5	0.000%	1.530%	0.892%	4.152%	5.318%
6	0.003%	45.063%	45.432%	57.411%	35.510%
7	4.400%	36.093%	44.900%	51.174%	54.665%
8	13.985%	67.684%	36.233%	53.056%	46.407%
9	9.626%	0.070%	0.043%	0.062%	0.031%
10	4.338%	0.000%	0.000%	0.000%	0.000%
11	2.098%	0.000%	0.000%	0.000%	0.000%
12	4.735%	0.000%	0.000%	0.000%	0.000%
13	17.203%	35.984%	18.599%	37.049%	30.861%
14	34.673%	23.454%	21.187%	32.995%	39.666%
15	24.964%	24.060%	20.357%	21.449%	32.814%
16	33.705%	22.194%	20.613%	29.846%	34.837%
17	0.047%	0.032%	0.019%	0.009%	0.007%
18	0.195%	0.539%	2.796%	14.416%	12.529%
19	47.714%	2.070%	4.432%	31.963%	30.380%
20	56.205%	13.065%	11.454%	49.227%	34.416%
21	41.275%	41.643%	43.112%	28.124%	30.531%
22	32.228%	26.731%	49.959%	55.906%	42.933%
23	49.511%	26.614%	45.742%	62.947%	42.932%
24	49.946%	36.658%	42.028%	52.852%	46.651%
25	0.132%	9.944%	6.648%	0.091%	0.251%
26	0.801%	23.399%	10.838%	37.434%	47.353%
27	50.815%	43.315%	12.644%	37.085%	45.375%
28	55.979%	50.264%	24.968%	35.258%	46.180%

Table H.48. The ratios of the area of the mode shape changes to the corresponding threshold values, defined as the 95th percentile of assumed Log-Normal distributions, as listed in Table 6.6, due to Damage Cases 4 to 9 for all 28 Test Protocols.

Test Protocol	Damage Case					
	Case 4	Case 5	Case 6	Case 7	Case 8	Case 9
1	2.91	4.69	6.01	4.15	5.35	4.95
2	5.94	5.08	7.35	2.81	7.11	6.76
3	2.59	3.33	6.06	2.29	5.45	5.51
4	1.12	2.45	3.03	2.35	3.04	3.10
5	2.35	1.32	1.51	0.74	1.46	1.32
6	1.01	0.80	0.70	0.75	0.79	0.69
7	0.82	0.70	0.71	0.71	0.70	0.81
8	0.67	0.66	0.65	0.70	0.77	0.77
9	0.88	4.45	5.13	4.73	4.53	4.47
10	5.25	18.29	19.63	18.22	17.22	16.60
11	3.87	14.57	15.62	14.77	14.04	13.38
12	2.04	8.21	8.79	8.22	7.80	7.45
13	0.34	0.27	0.26	0.27	0.31	0.29
14	0.25	0.19	0.36	0.37	0.40	0.34
15	0.29	0.23	0.33	0.45	0.41	0.32
16	0.36	0.31	0.35	0.49	0.49	0.34
17	1.12	6.02	4.26	9.96	2.36	2.43
18	2.75	1.98	2.42	4.13	1.01	1.25
19	2.19	1.54	1.74	3.18	0.71	0.89
20	1.27	1.09	1.20	2.22	0.60	0.70
21	1.55	0.82	0.56	2.51	0.64	0.77
22	1.08	1.30	1.10	0.98	0.73	0.84
23	1.03	1.21	1.01	0.99	0.72	0.85
24	0.72	0.94	0.89	0.91	0.66	0.81
25	2.54	1.02	1.03	1.55	1.74	1.59
26	1.50	0.73	0.54	0.47	1.33	0.71
27	1.00	0.84	0.64	0.52	1.21	0.70
28	0.76	0.92	0.60	0.49	0.92	0.62

Table H.49. The ratios of the area of the mode shape changes to the corresponding threshold values, defined as the 95th percentile of assumed Log-Normal distributions, as listed in Table 6.6, due to Damage Cases 10 to 15 for all 28 Test Protocols.

	Damage Case					
Test Protocol	Case 10	Case 11	Case 12	Case 13	Case 14	Case 15
1	1.20	0.77	3.38	1.11	0.48	0.89
2	7.81	0.90	2.70	2.74	0.83	1.55
3	2.36	0.80	3.03	2.96	0.84	2.57
4	0.99	0.51	2.40	1.63	1.04	1.27
5	0.95	1.02	0.85	0.71	0.84	0.70
6	0.93	0.79	0.67	0.80	0.72	0.78
7	1.01	0.85	0.77	0.83	0.73	0.67
8	0.82	0.83	0.75	0.75	0.78	0.72
9	0.52	0.29	2.61	6.22	0.54	0.38
10	0.80	0.32	19.40	22.80	0.99	5.04
11	0.50	0.32	15.25	18.48	0.90	5.47
12	0.42	0.27	8.39	9.50	0.85	2.05
13	0.36	0.45	0.46	0.55	0.65	0.73
14	0.28	0.53	0.60	0.72	0.80	0.85
15	0.37	0.59	0.59	0.70	0.80	0.92
16	0.48	0.63	0.68	0.68	0.74	0.81
17	1.08	0.64	3.64	2.10	0.74	0.77
18	1.98	0.56	1.87	1.00	0.98	1.23
19	0.90	0.62	1.52	0.84	0.83	1.05
20	0.76	0.57	1.17	0.91	0.94	0.86
21	0.72	0.44	0.27	0.26	0.25	0.28
22	1.03	0.37	0.75	0.36	0.47	0.39
23	1.03	0.39	0.75	0.35	0.48	0.45
24	0.91	0.42	0.59	0.37	0.43	0.47
25	2.18	0.85	1.28	1.09	0.73	1.15
26	1.76	0.32	0.54	0.63	0.74	1.14
27	0.77	0.50	0.47	0.50	0.74	1.15
28	0.70	0.59	0.57	0.62	0.79	0.97

Table H.50. The ratios of the area of the mode shape changes to the corresponding threshold values, defined as the 95th percentile of assumed Log-Normal distributions, as listed in Table 6.6, due to Damage Cases 16 to 21 for all 28 Test Protocols.

	Damage Case					
Test Protocol	Case 16	Case 17	Case 18	Case 19	Case 20	Case 21
1	0.33	12.29	12.36	9.72	10.55	11.70
2	0.71	24.31	22.04	22.34	20.42	26.68
3	0.94	17.27	15.54	13.16	14.34	16.61
4	0.74	6.06	5.55	4.55	5.22	5.61
5	0.54	8.01	7.15	5.02	5.65	6.49
6	0.71	1.82	2.09	1.68	1.74	2.24
7	0.72	1.08	1.35	0.97	1.04	1.44
8	0.76	0.91	0.90	0.78	0.83	0.91
9	0.32	1.28	0.93	0.61	0.63	0.67
10	2.77	2.23	3.38	2.07	1.02	0.96
11	2.37	1.96	2.95	1.26	1.01	1.17
12	1.55	1.22	1.69	0.84	0.90	1.03
13	1.07	0.85	0.91	0.65	0.97	0.94
14	0.47	0.39	0.38	0.39	0.36	0.37
15	0.62	0.47	0.43	0.46	0.45	0.51
16	0.66	0.44	0.44	0.49	0.47	0.56
17	0.60	12.02	12.49	12.28	1.89	1.82
18	0.58	4.41	3.15	5.08	0.73	1.79
19	0.54	3.32	2.39	4.03	0.67	0.76
20	0.59	2.22	1.66	2.49	0.70	0.65
21	0.44	1.66	2.05	0.75	0.69	0.42
22	0.42	1.78	2.14	2.07	0.88	0.54
23	0.45	1.71	2.08	1.77	0.92	0.45
24	0.46	1.35	1.63	1.45	0.89	0.46
25	0.79	1.56	1.73	3.02	1.46	1.35
26	0.60	0.58	1.10	2.05	0.70	1.68
27	0.66	0.57	1.01	1.68	0.68	0.68
28	0.66	0.44	0.61	1.03	0.60	0.64

Table H.51. The ratios of the area of the mode shape changes to the corresponding threshold values, defined as the 95th percentile of assumed Log-Normal distributions, as listed in Table 6.6, due to Damage Cases 22 to 26 for all 28 Test Protocols.

	Damage Case				
Test Protocol	Case 22	Case 23	Case 24	Case 25	Case 26
1	11.37	4.27	4.43	3.55	3.82
2	26.41	4.66	4.41	4.44	4.11
3	16.19	5.49	5.56	3.66	3.70
4	5.45	2.31	2.23	2.77	2.78
5	5.82	1.33	1.41	1.09	1.10
6	2.22	0.71	0.71	0.63	0.75
7	1.19	0.80	0.74	0.70	0.69
8	0.95	0.62	0.76	0.69	0.72
9	0.64	7.81	8.27	8.08	8.38
10	1.05	35.53	35.34	37.02	36.13
11	1.33	27.13	26.98	29.15	28.39
12	1.03	15.37	15.43	15.74	15.82
13	0.73	0.45	0.67	0.45	1.12
14	0.57	0.69	0.72	0.54	0.47
15	0.67	0.70	0.73	0.69	0.57
16	0.64	0.72	0.78	0.64	0.60
17	2.14	2.34	2.45	2.52	2.55
18	1.64	1.59	1.44	0.85	0.87
19	0.56	1.25	1.18	0.67	0.68
20	0.54	0.92	0.95	0.57	0.67
21	0.32	0.31	0.29	0.42	0.39
22	0.51	0.56	0.38	0.35	0.43
23	0.44	0.61	0.45	0.35	0.48
24	0.45	0.54	0.50	0.43	0.47
25	1.74	1.00	1.09	1.78	1.60
26	1.54	0.64	0.87	0.50	0.46
27	0.47	0.53	0.89	0.57	0.54
28	0.48	0.52	0.76	0.62	0.55

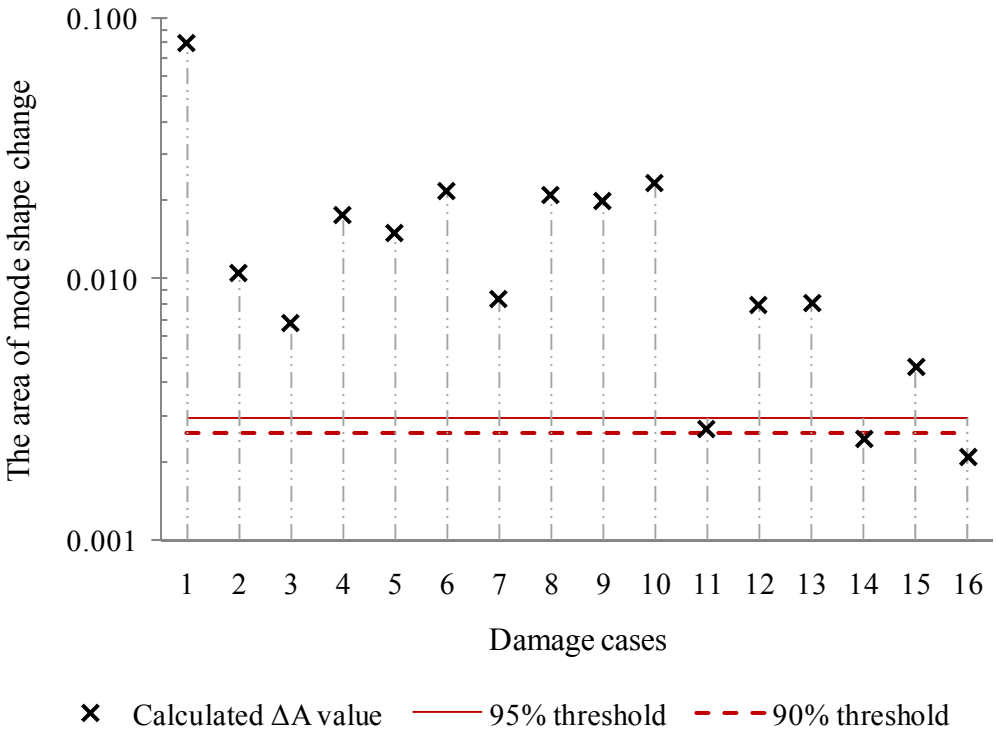

Figure H.36. Comparison of mean Δ*A* values from 25 data pairs for all single damage cases to the 90% and 95% threshold values, when the first mode, harmonic excitation, and bottom strain gauge data were used (Test Protocol 2).

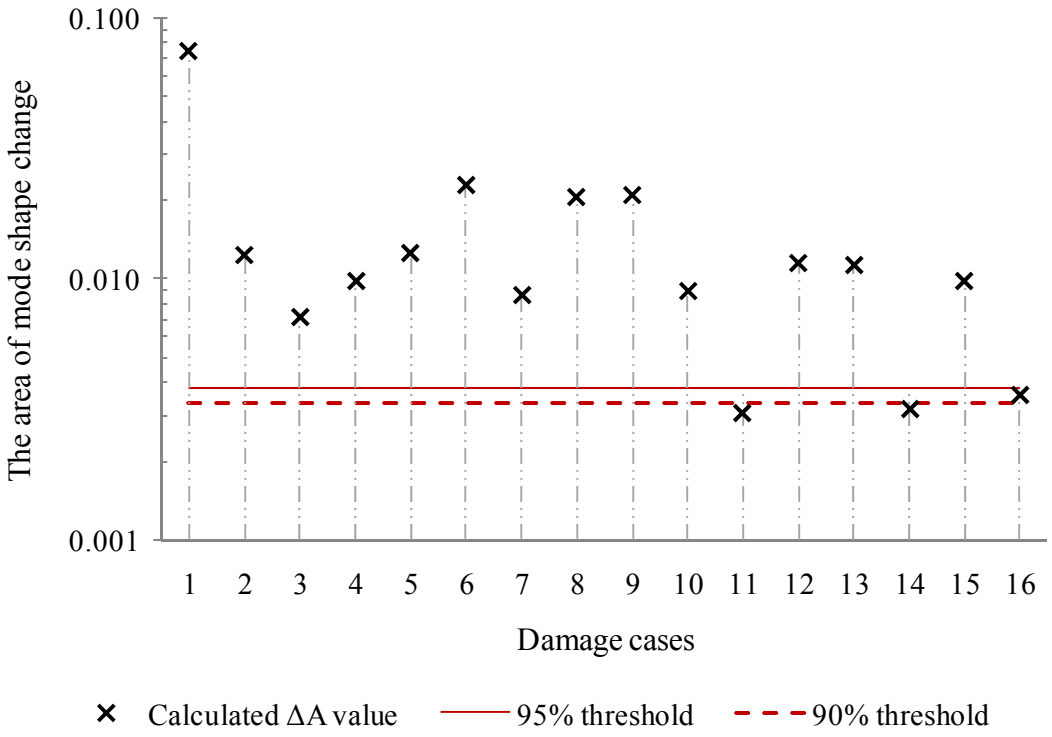

Figure H.37. Comparison of mean Δ*A* values from 25 data pairs for all single damage cases to the 90% and 95% threshold values, when the first mode, harmonic excitation, and middle strain gauge data were used (Test Protocol 3).

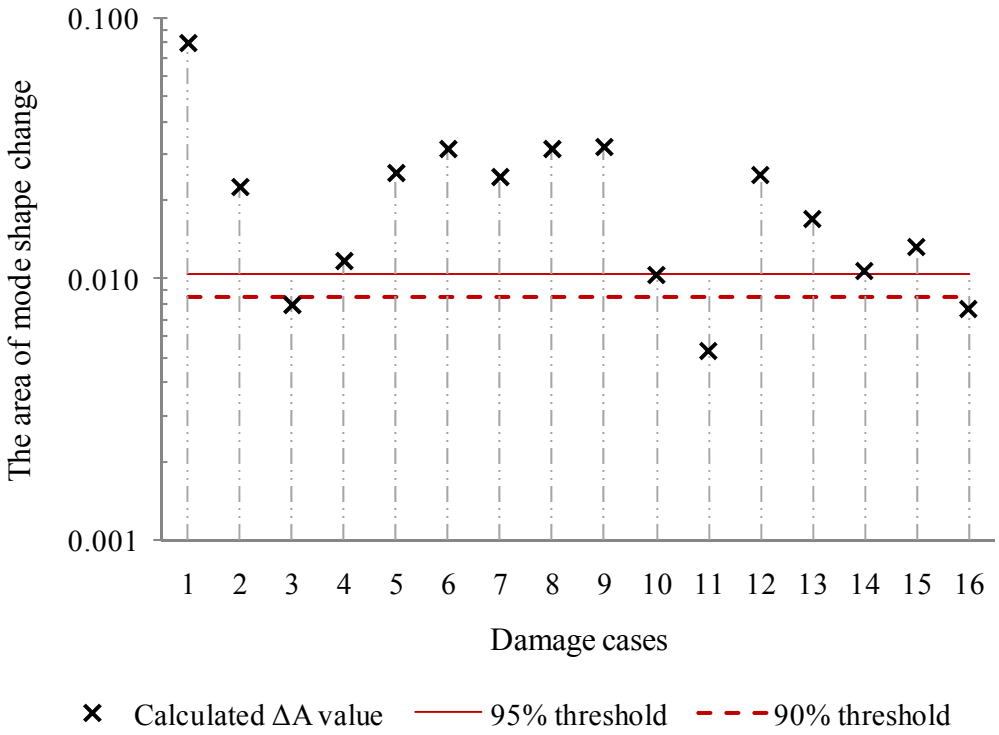

Figure H.38. Comparison of mean Δ*A* values from 25 data pairs for all single damage cases to the 90% and 95% threshold values, when the first mode, harmonic excitation, and top strain gauge data were used (Test Protocol 4).

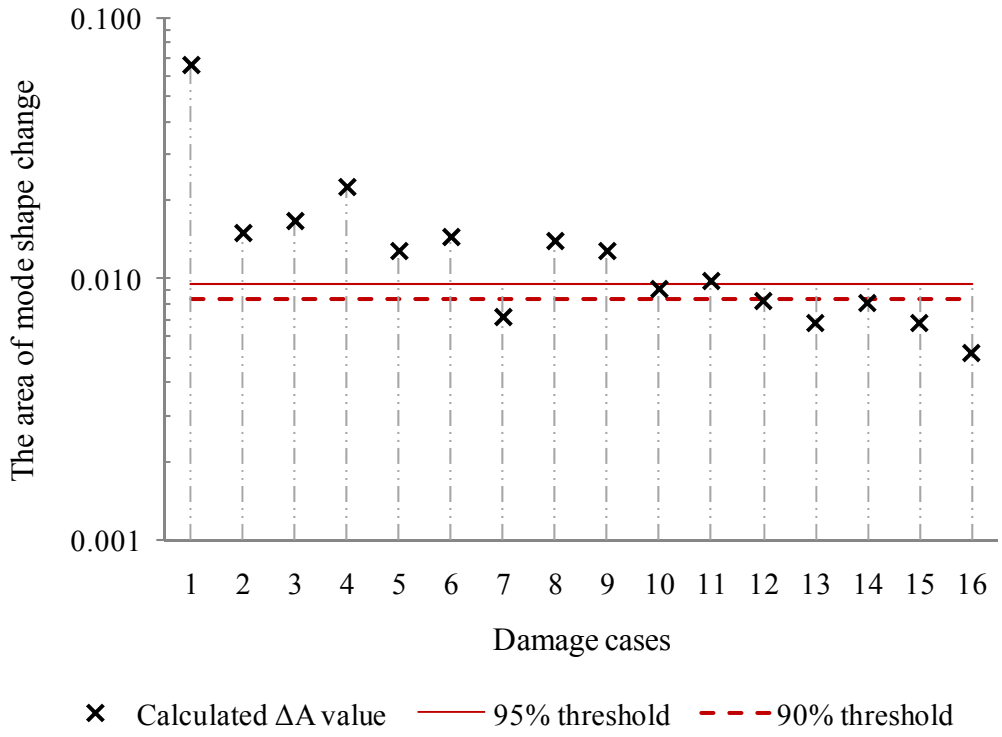

Figure H.39. Comparison of mean Δ*A* values from 25 data pairs for all single damage cases to the 90% and 95% threshold values, when the first mode, white noise random excitation, and acclerometer data were used (Test Protocol 5).

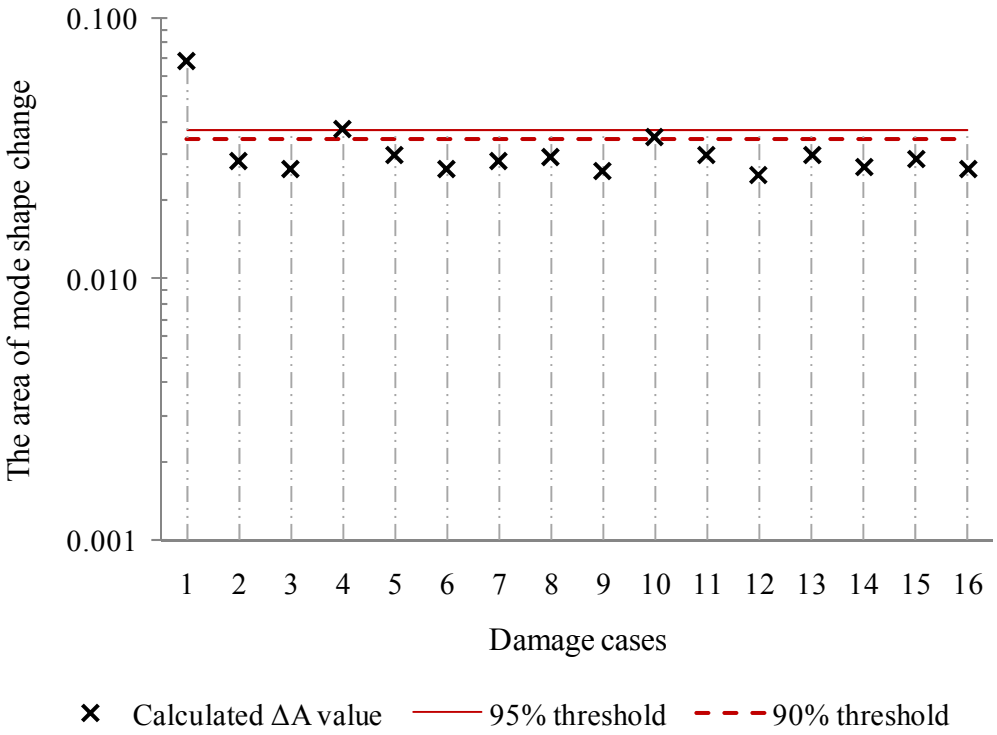

Figure H.40. Comparison of mean Δ*A* values from 25 data pairs for all single damage cases to the 90% and 95% threshold values, when the first mode, white noise random excitation, and bottom strain gauge data were used (Test Protocol 6).

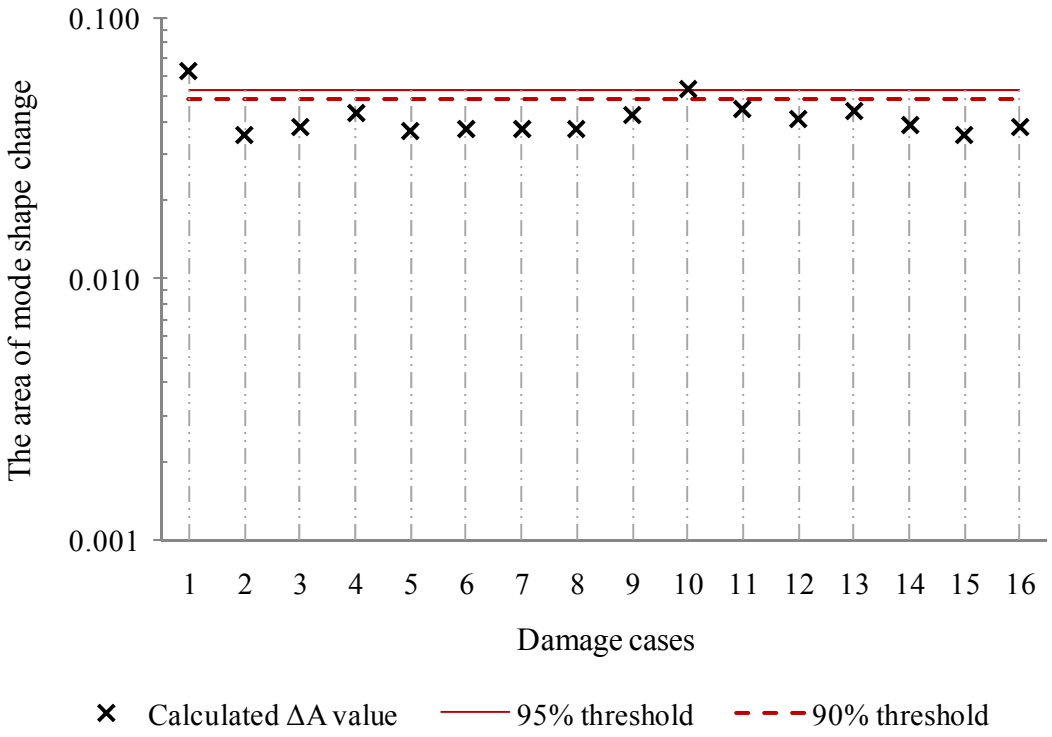

Figure H.41. Comparison of mean Δ*A* values from 25 data pairs for all single damage cases to the 90% and 95% threshold values, when the first mode, white noise random excitation, and middle strain gauge data were used (Test Protocol 7).

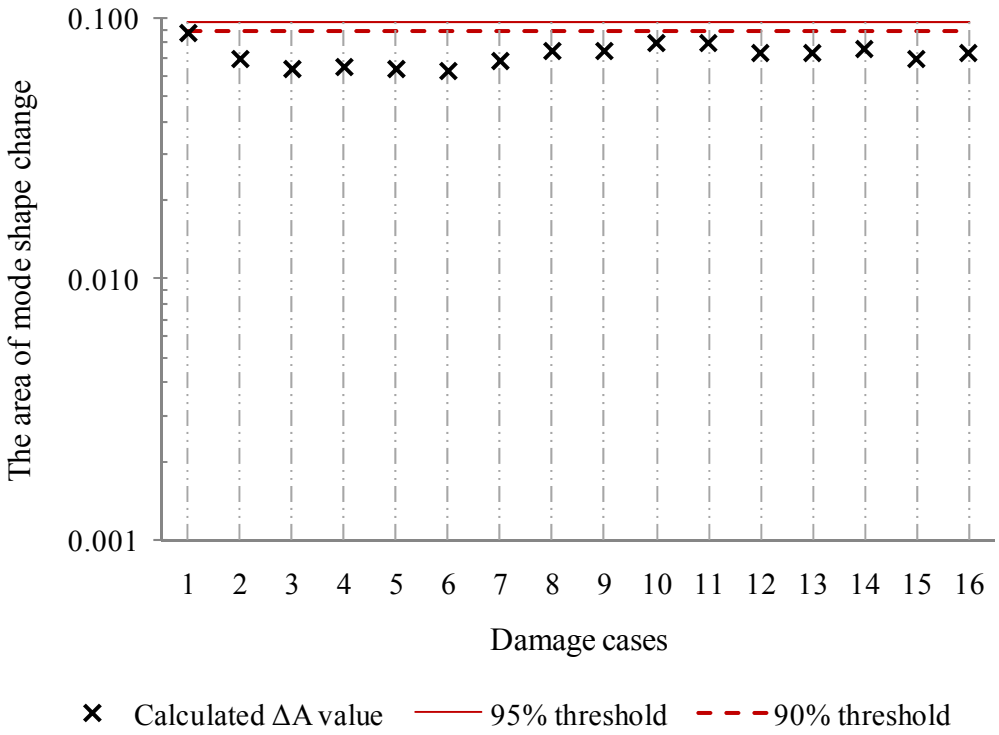

Figure H.42. Comparison of mean Δ*A* values from 25 data pairs for all single damage cases to the 90% and 95% threshold values, when the first mode, white noise random excitation, and top strain gauge data were used (Test Protocol 8).

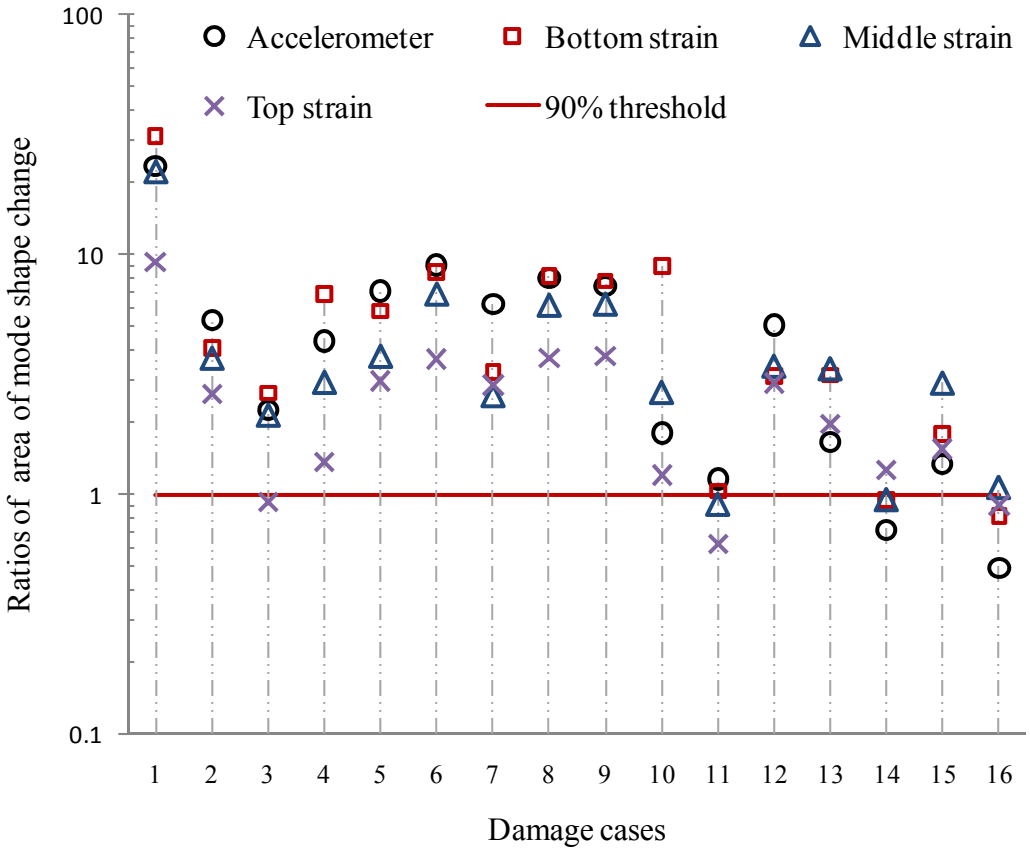

Figure H.43. Ratios of area of mode shape change (the average of 25 values) to the 90% threshold values for all sensor schemes and damage cases, when the first mode and harmonic excitation were used (Test Protocols 1 to 4).

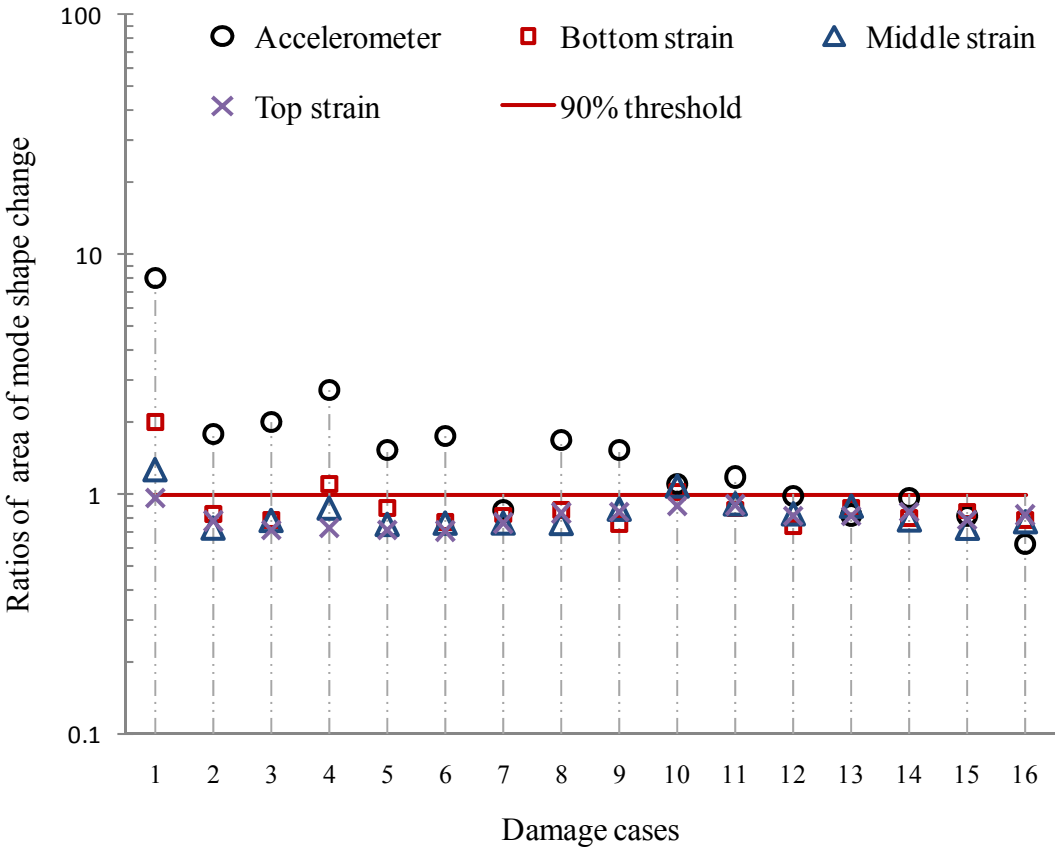

Figure H.44. Ratios of area of mode shape change (the average of 25 values) to the 90% threshold values for all sensor schemes and damage cases, when the first mode and white noise random excitation were used (Test Protocols 5 to 8).

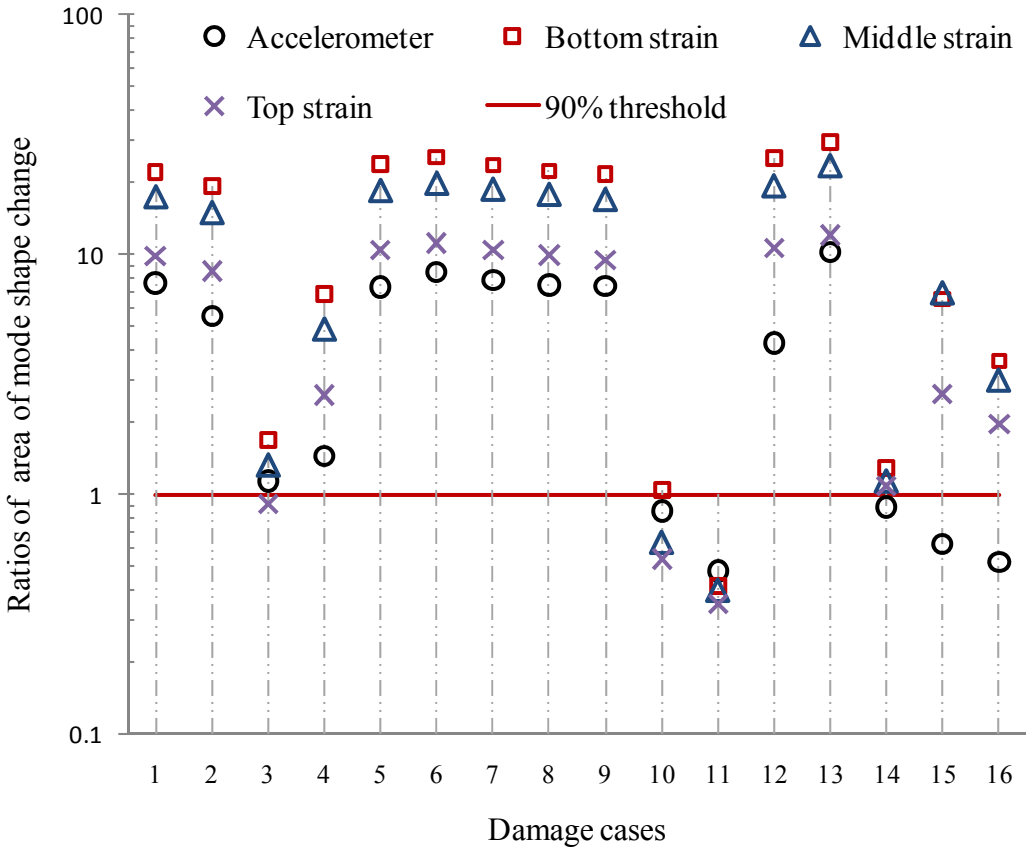

Figure H.45. Ratios of area of mode shape change (the average of 25 values) to the 90% threshold values for all sensor schemes and damage cases, when the second mode and harmonic excitation were used (Test Protocols 9 to 12).

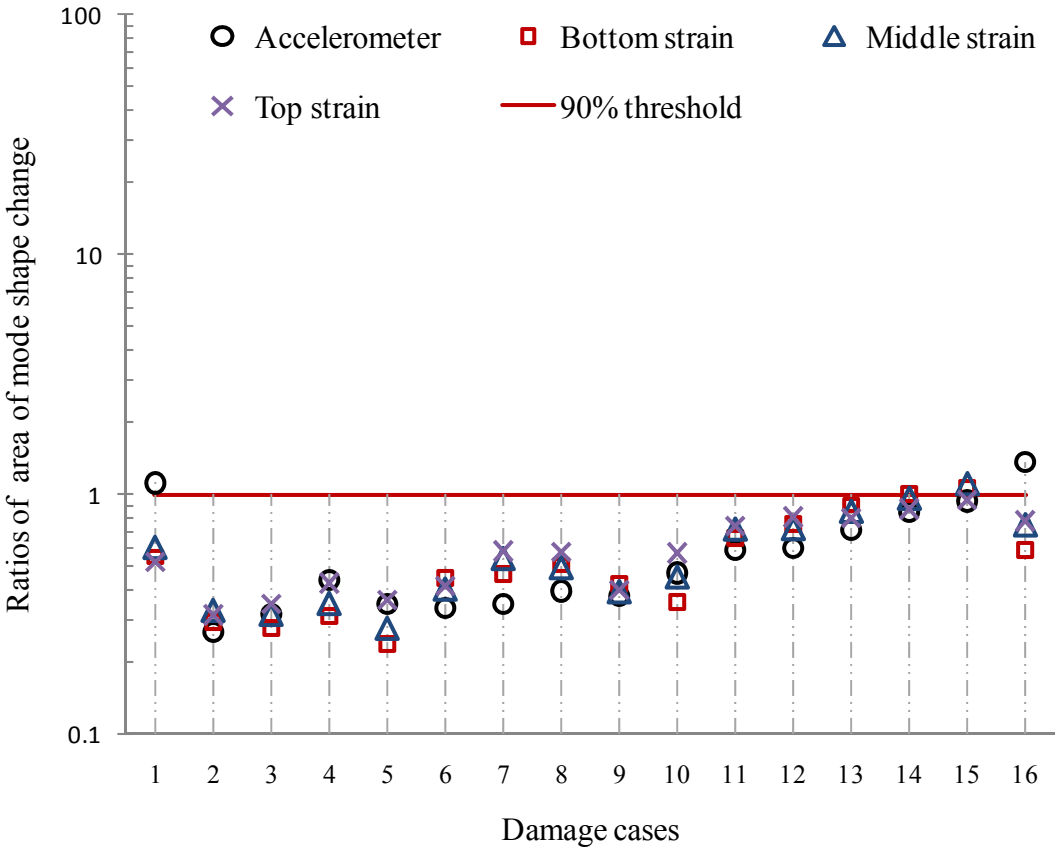

Figure H.46. Ratios of area of mode shape change (the average of 25 values) to the 90% threshold values for all sensor schemes and damage cases, when the second mode and white noise random excitation were used (Test Protocols 13 to 16).

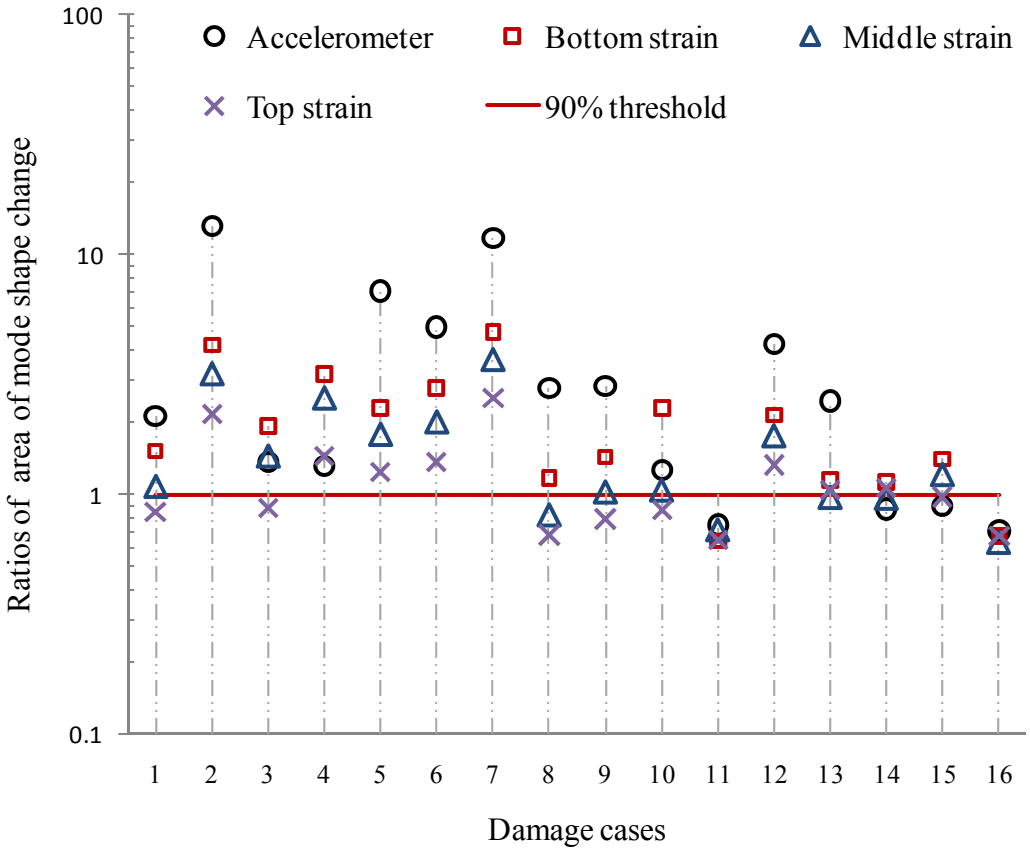

Figure H.47. Ratios of area of mode shape change (the average of 25 values) to the 90% threshold values for all sensor schemes and damage cases, when the third mode and white noise random excitation were used (Test Protocols 17 to 20).

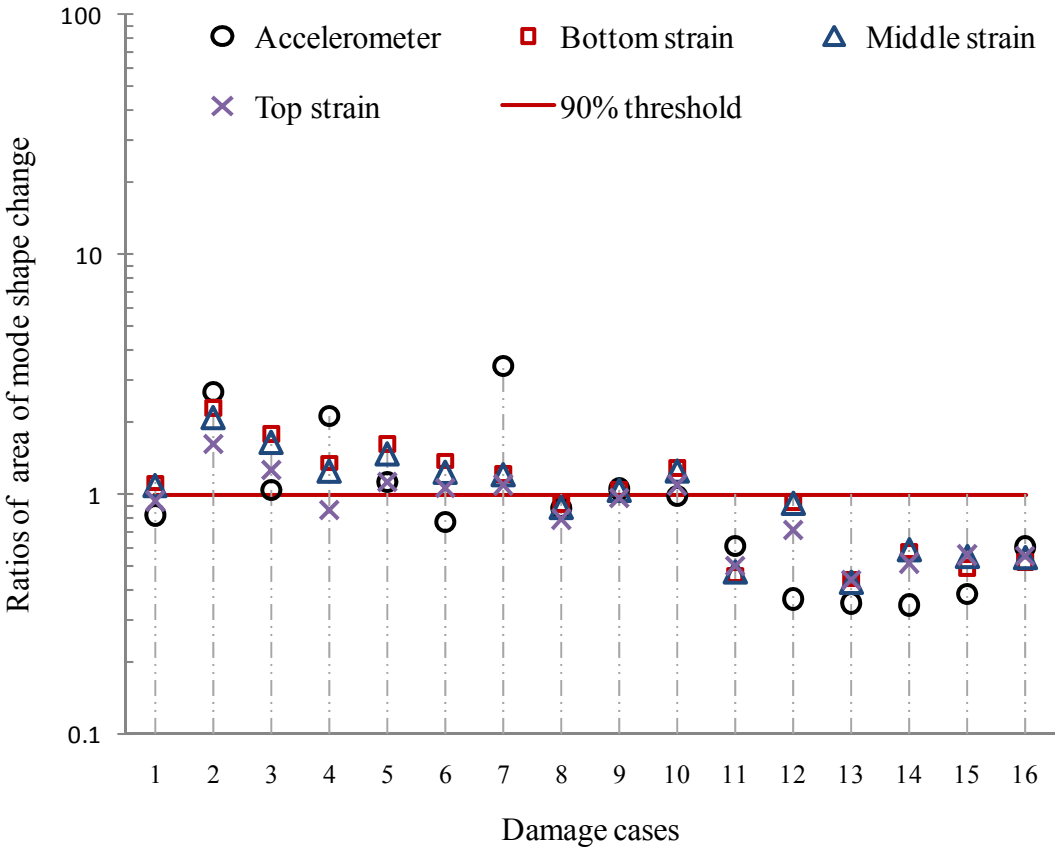

Figure H.48. Ratios of area of mode shape change (the average of 25 values) to the 90% threshold values for all sensor schemes and damage cases, when the fourth mode and white noise random excitation were used (Test Protocols 21 to 24).

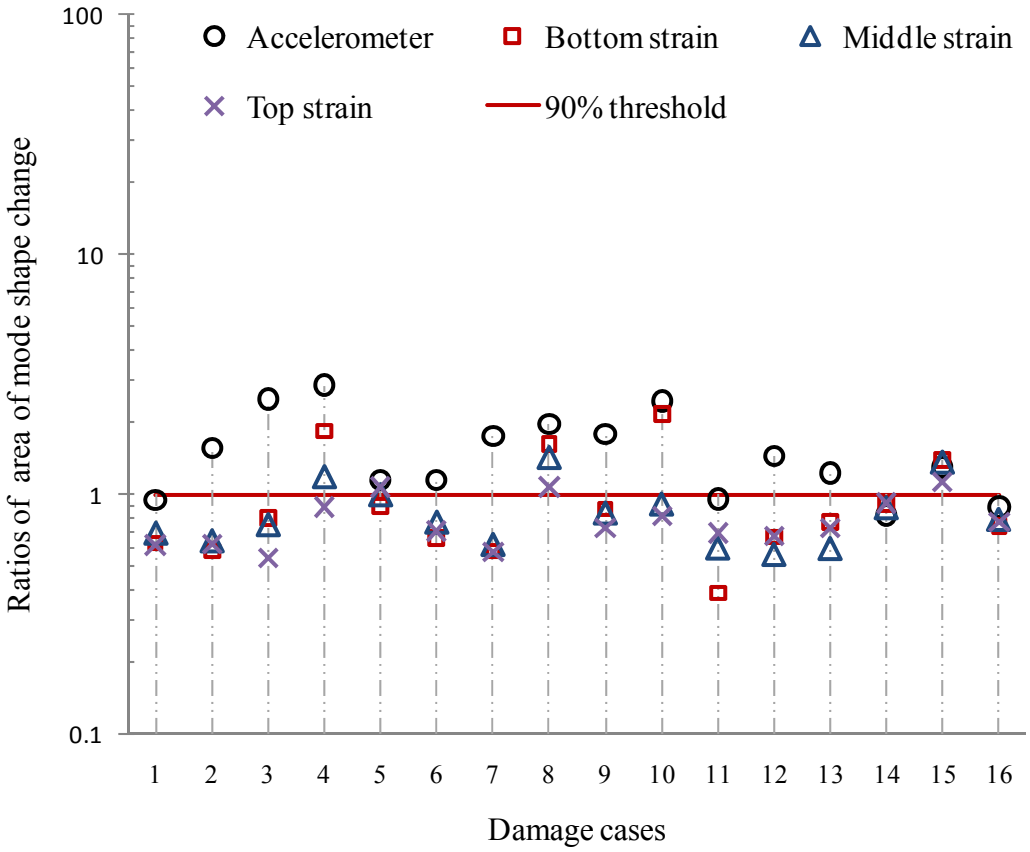

Figure H.49. Ratios of area of mode shape change (the average of 25 values) to the 90% threshold values for all sensor schemes and damage cases, when the fifth mode and white noise random excitation were used (Test Protocols 25 to 28).

APPENDIX I. **DETECTION OF DAMAGE CASE 1 USING COMMONLY AVAILABLE VBDD INDICATORS BASED ON THE FIRST MODE SHAPE**

This appendix present additional information for Section 6.3, providing damage localization of Damage Case 1 using commonly available VBDD indicators based on the first mode shape. The damage indicators used in this Appendix included change in mode shape method, damage index method, and change in mode shape curvature method.

Figures I.1 to I.3 present the results of damage localization using change in mode shape method, damage index method, and change in mode shape curvature method, respectively, when Test Protocol 2 was used.

Figures I.4 to I.6 present the results of damage localization using change in mode shape method, damage index method, and change in mode shape curvature method, respectively, when Test Protocol 3 was used.

Figures I.7 to I.9 present the results of damage localization using change in mode shape method, damage index method, and change in mode shape curvature method, respectively, when Test Protocol 4 was used.

Figures I.10 to I.12 present the results of damage localization using change in mode shape method, damage index method, and change in mode shape curvature method, respectively, when Test Protocol 5 was used.

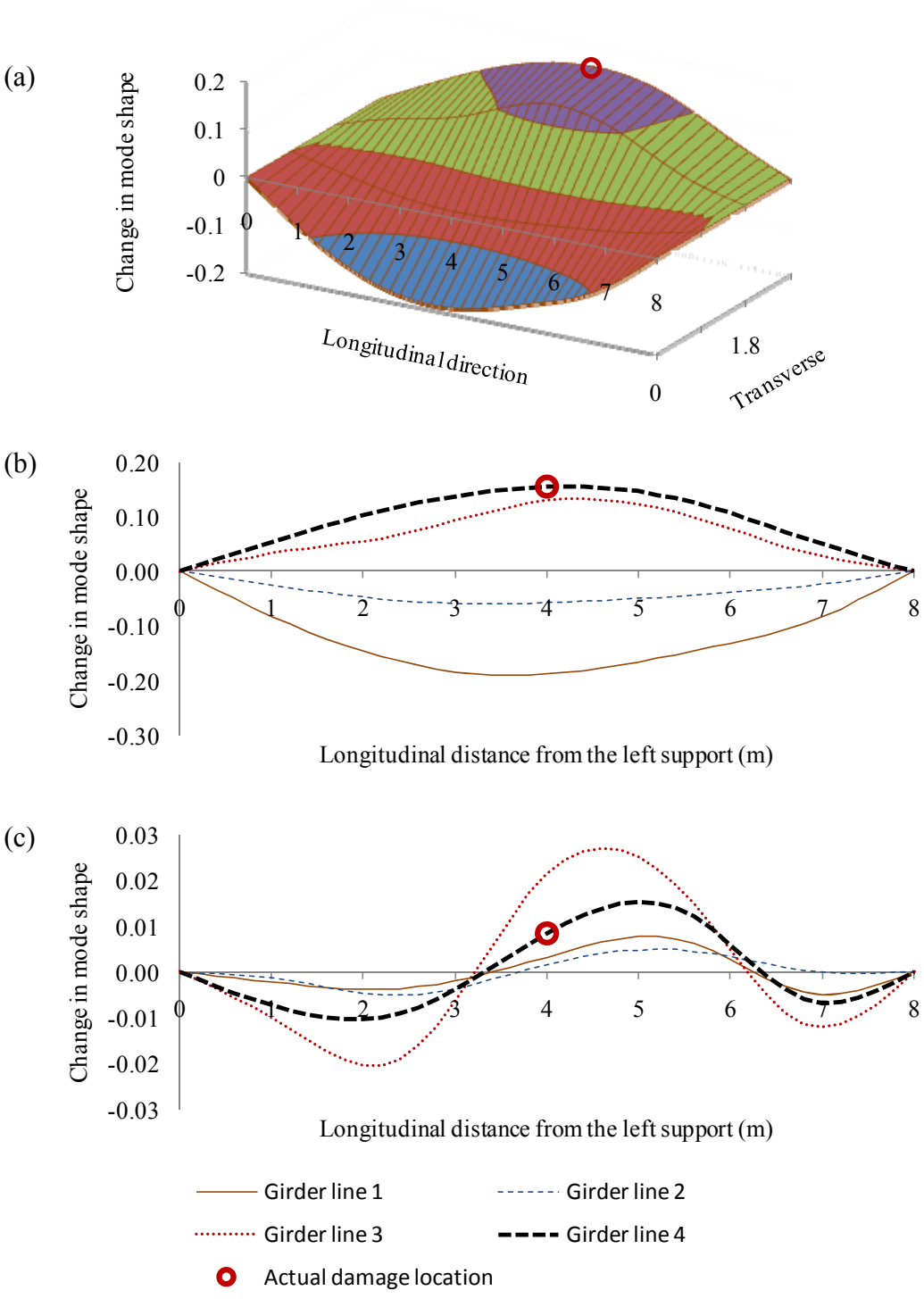

Figure I.1. Distribution of the change in the first mode shape due to Damage Case 1 using bottom strain gauge data with harmonic excitation: (a) 3D figure with unit area normalization over all measurement points; (b) 2D figure with unit area normalization over all measurement points; and (c) 2D figure with unit area normalization along individual girder lines.

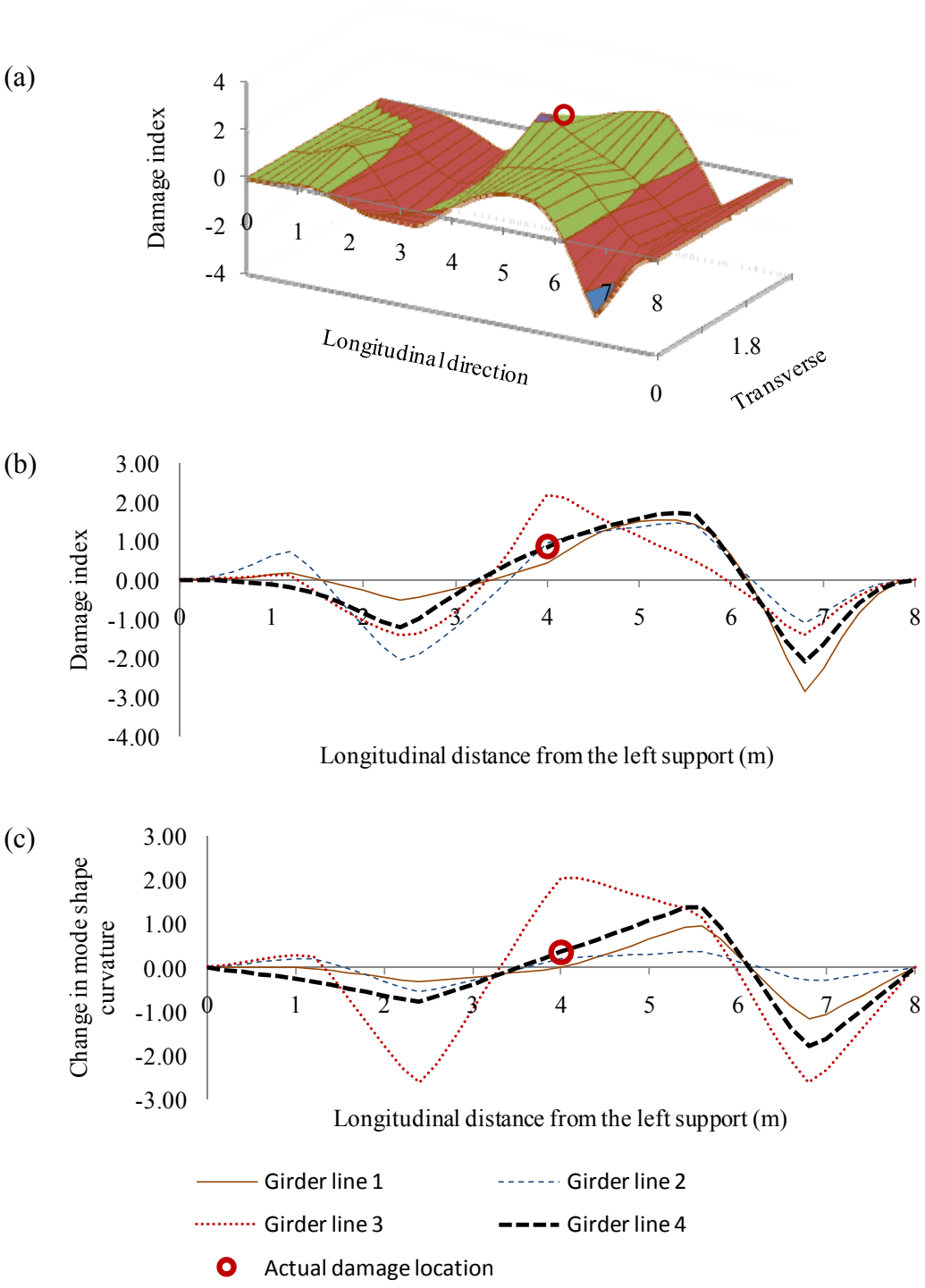

Figure I.2. Distribution of the damage index for the first mode due to Damage Case 1 using bottom strain gauge data with harmonic excitation: (a) 3D figure with unit area normalization over all measurement points; (b) 2D figure with unit area normalization over all measurement points; and (c) 2D figure with unit area normalization along individual girder lines.

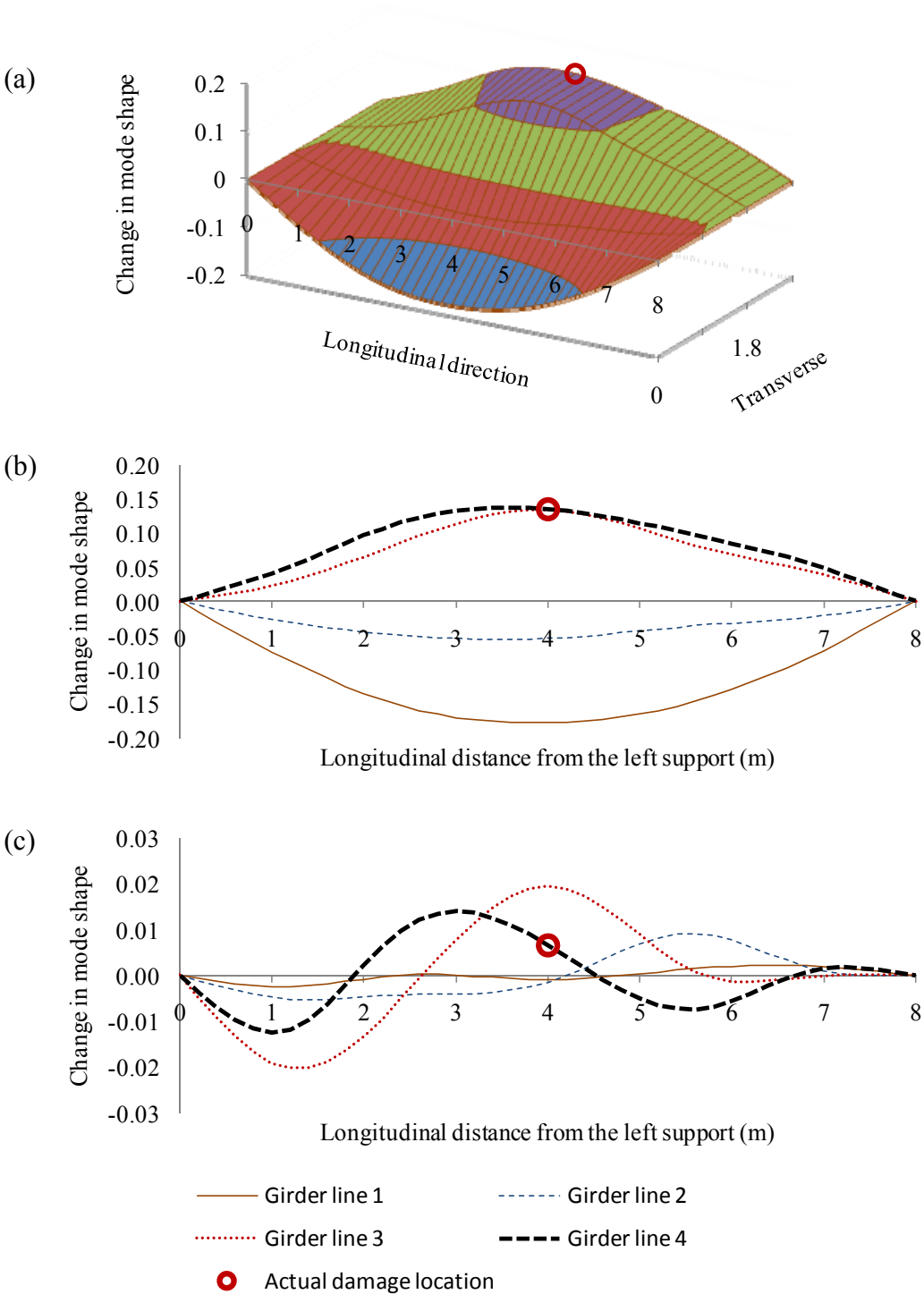

Figure I.3. Distribution of the change in the first mode shape due to Damage Case 1 using middle strain gauge data with harmonic excitation: (a) 3D figure with unit area normalization over all measurement points; (b) 2D figure with unit area normalization over all measurement points; and (c) 2D figure with unit area normalization along individual girder lines.

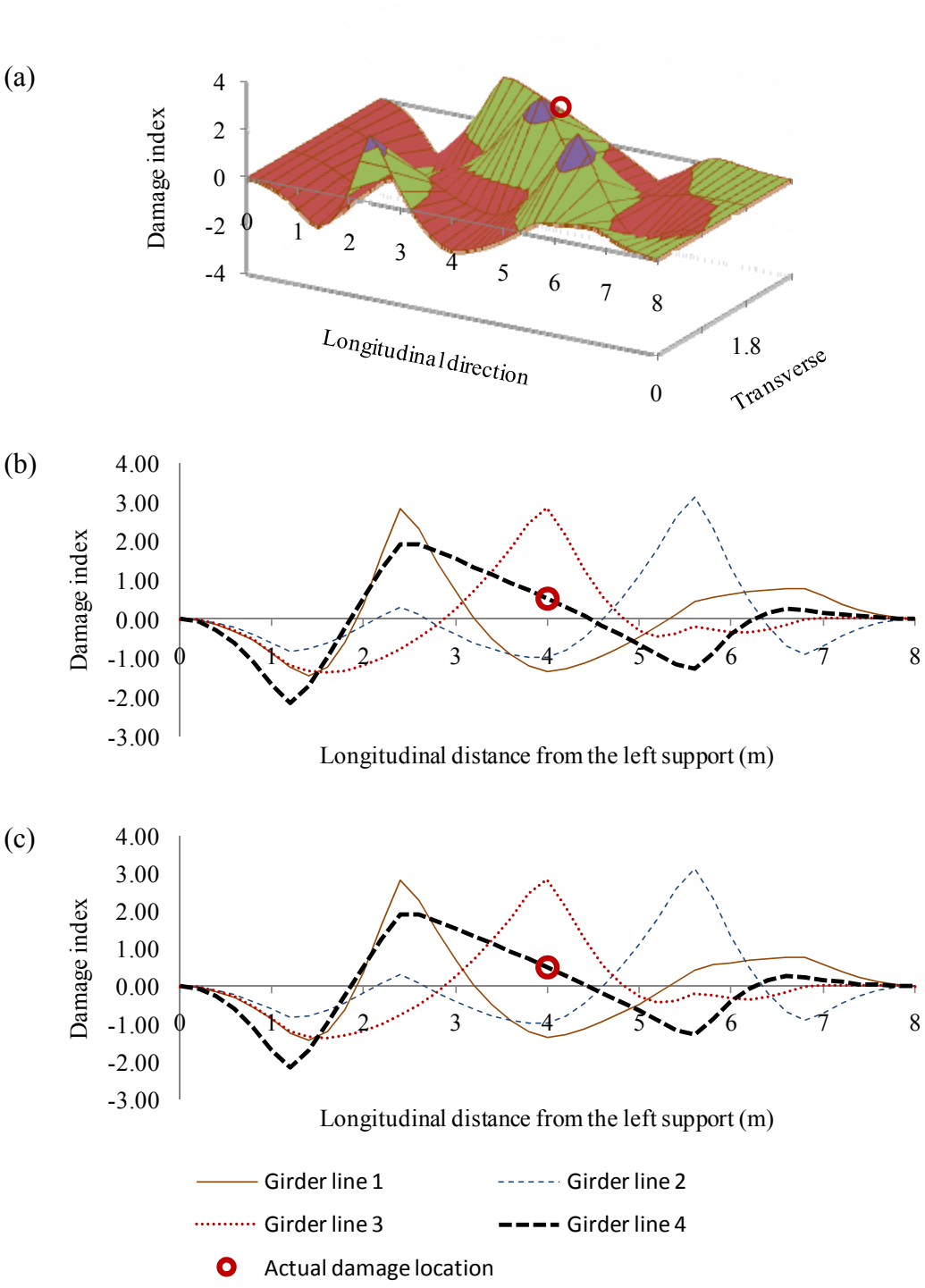

Figure I.4. Distribution of the damage index for the first mode due to Damage Case 1 using middle strain gauge data with harmonic excitation: (a) 3D figure with unit area normalization over all measurement points; (b) 2D figure with unit area normalization over all measurement points; and (c) 2D figure with unit area normalization along individual girder lines.

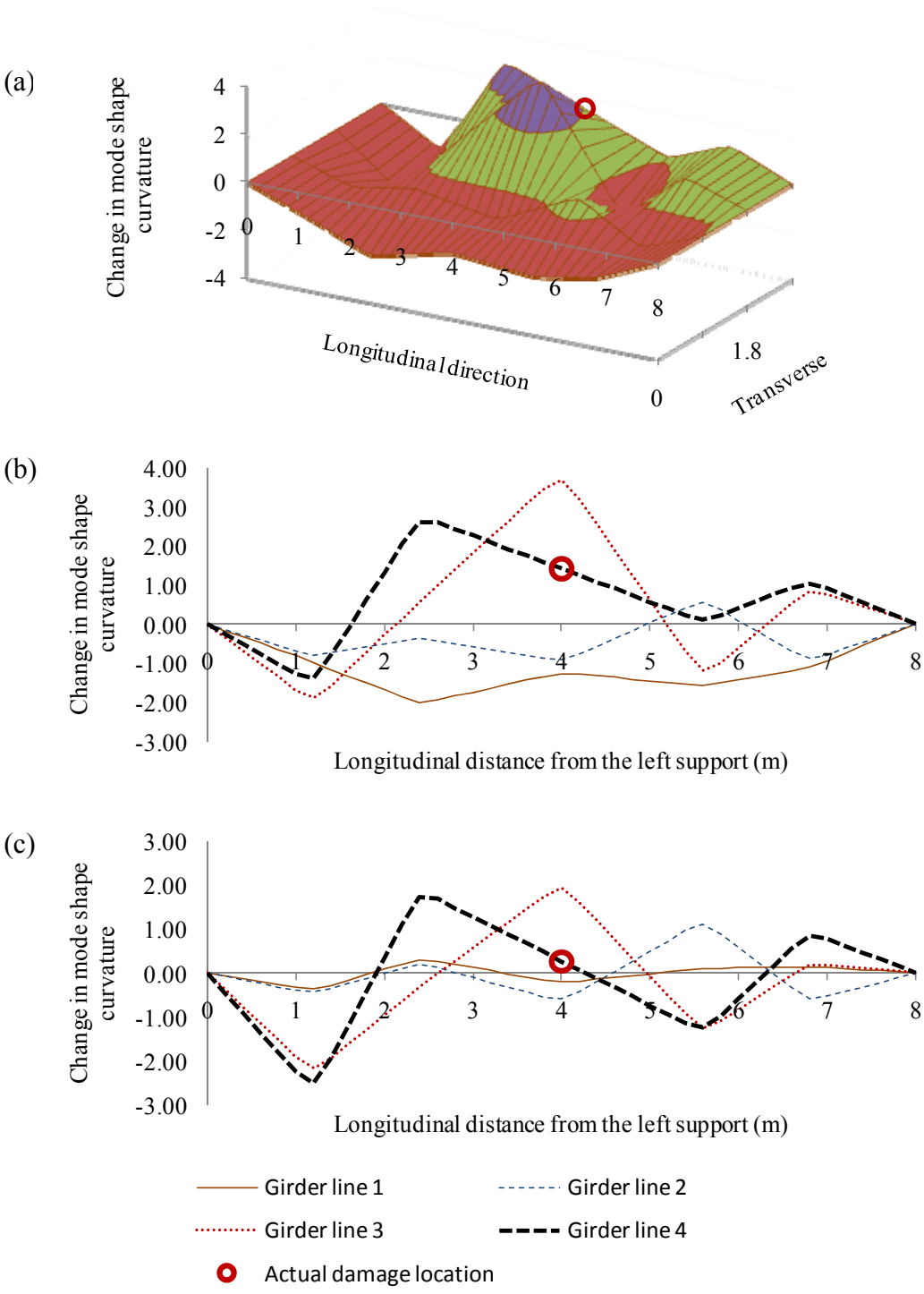

Figure I.5. Distribution of the change in mode shape curvature for the first mode due to Damage Case 1 using middle strain gauge data with harmonic excitation: (a) 3D figure with unit area normalization over all measurement points; (b) 2D figure with unit area normalization over all measurement points; and (c) 2D figure with unit area normalization along individual girder lines.

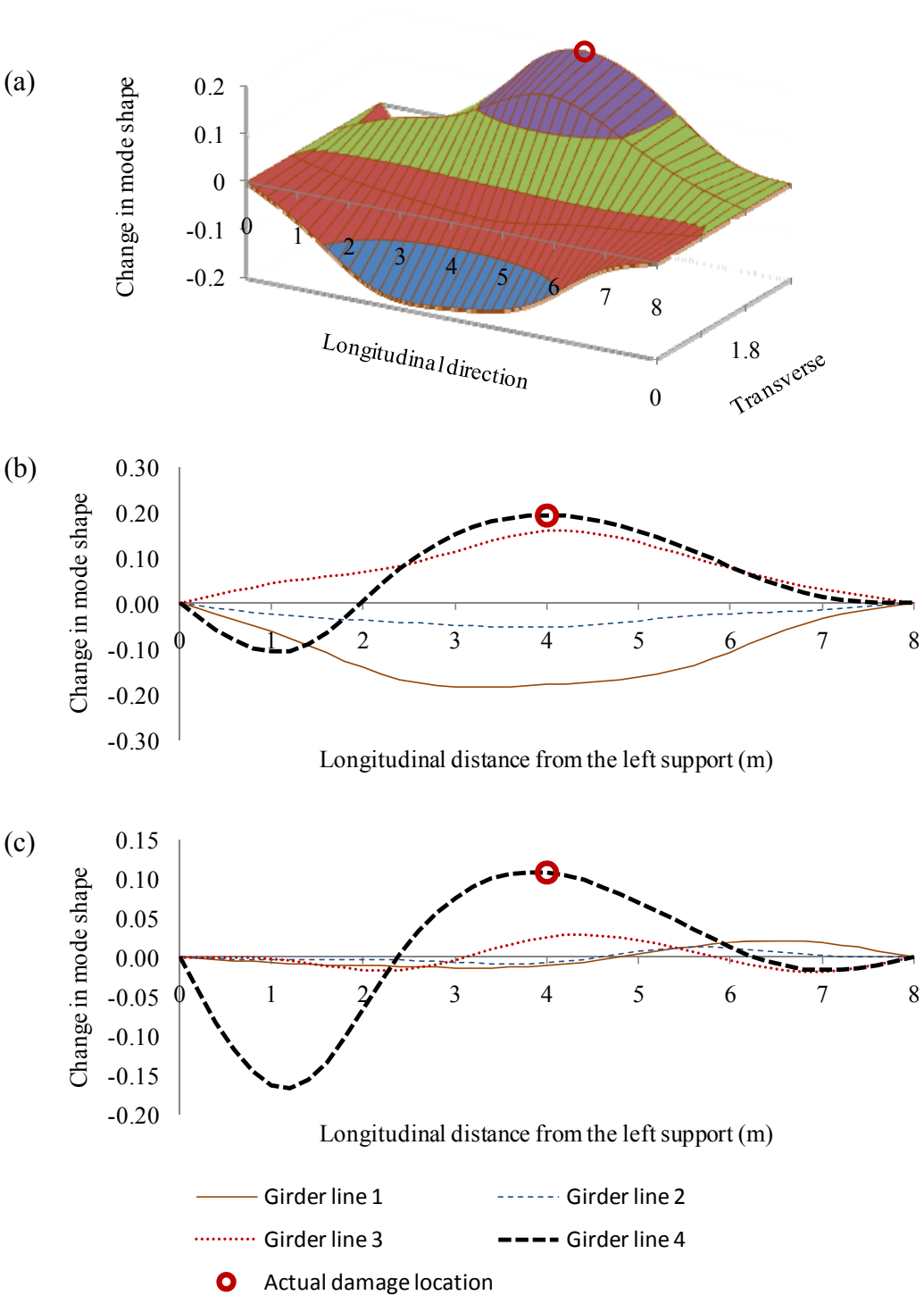

Figure I.6. Distribution of the change in the first mode shape due to Damage Case 1 using top strain gauge data with harmonic excitation: (a) 3D figure with unit area normalization over all measurement points; (b) 2D figure with unit area normalization over all measurement points; and (c) 2D figure with unit area normalization along individual girder lines.

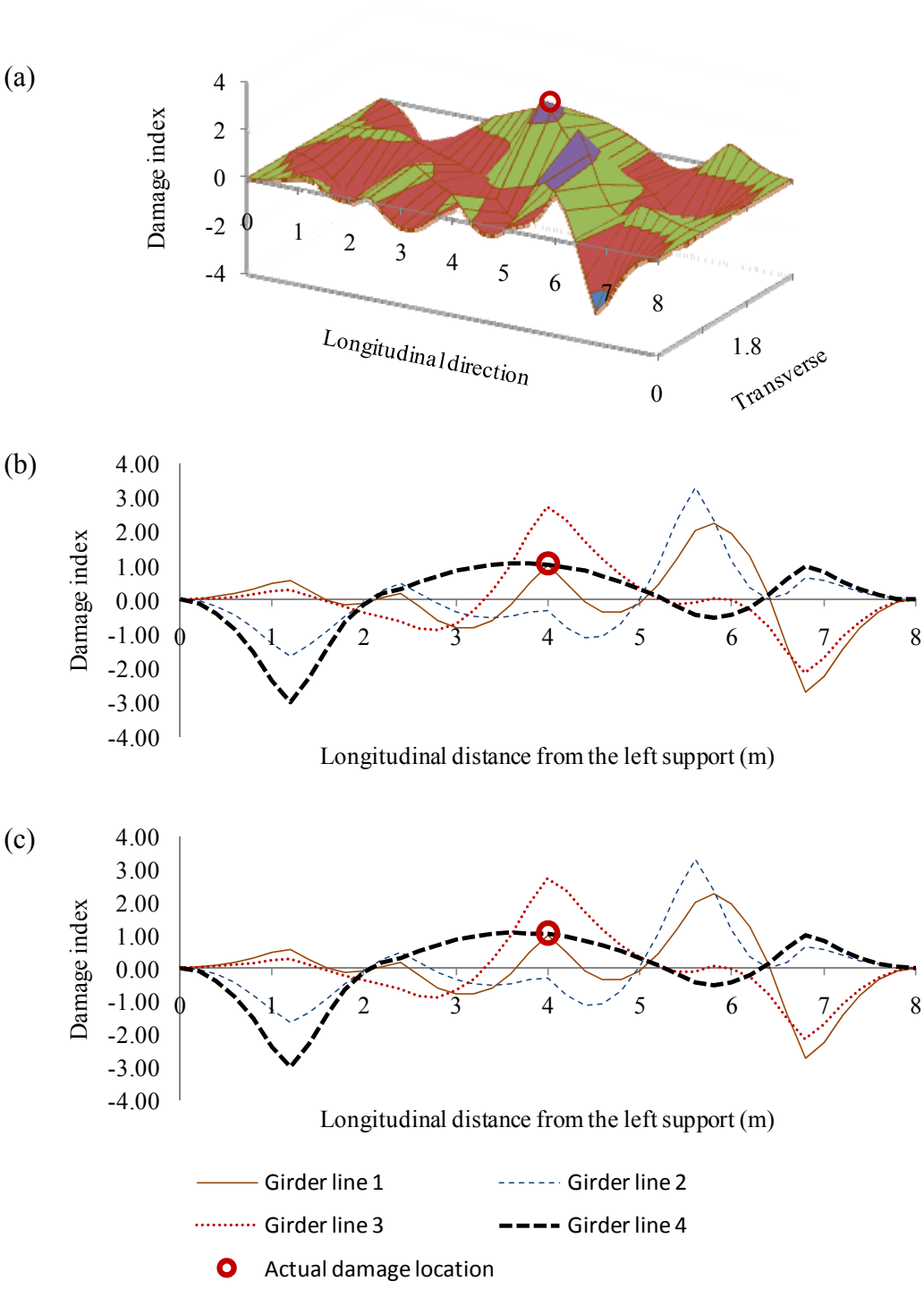

Figure I.7. Distribution of the damage index for the first mode due to Damage Case 1 using top strain gauge data with harmonic excitation: (a) 3D figure with unit area normalization over all measurement points; (b) 2D figure with unit area normalization over all measurement points; and (c) 2D figure with unit area normalization along individual girder lines.

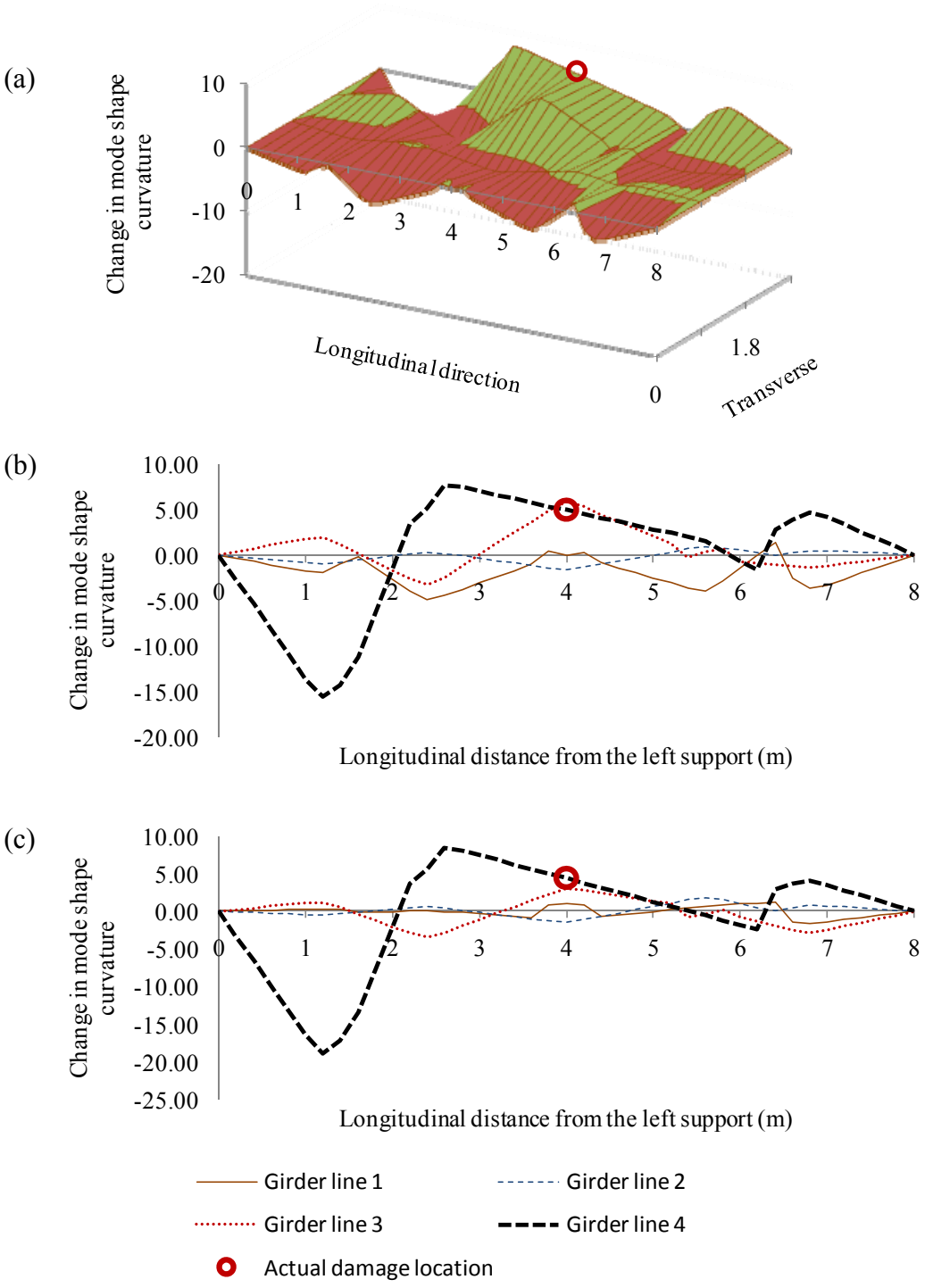

Figure I.8. Distribution of the change in mode shape curvature for the first mode due to Damage Case 1 using top strain gauge data with harmonic excitation: (a) 3D figure with unit area normalization over all measurement points; (b) 2D figure with unit area normalization over all measurement points; and (c) 2D figure with unit area normalization along individual girder lines.

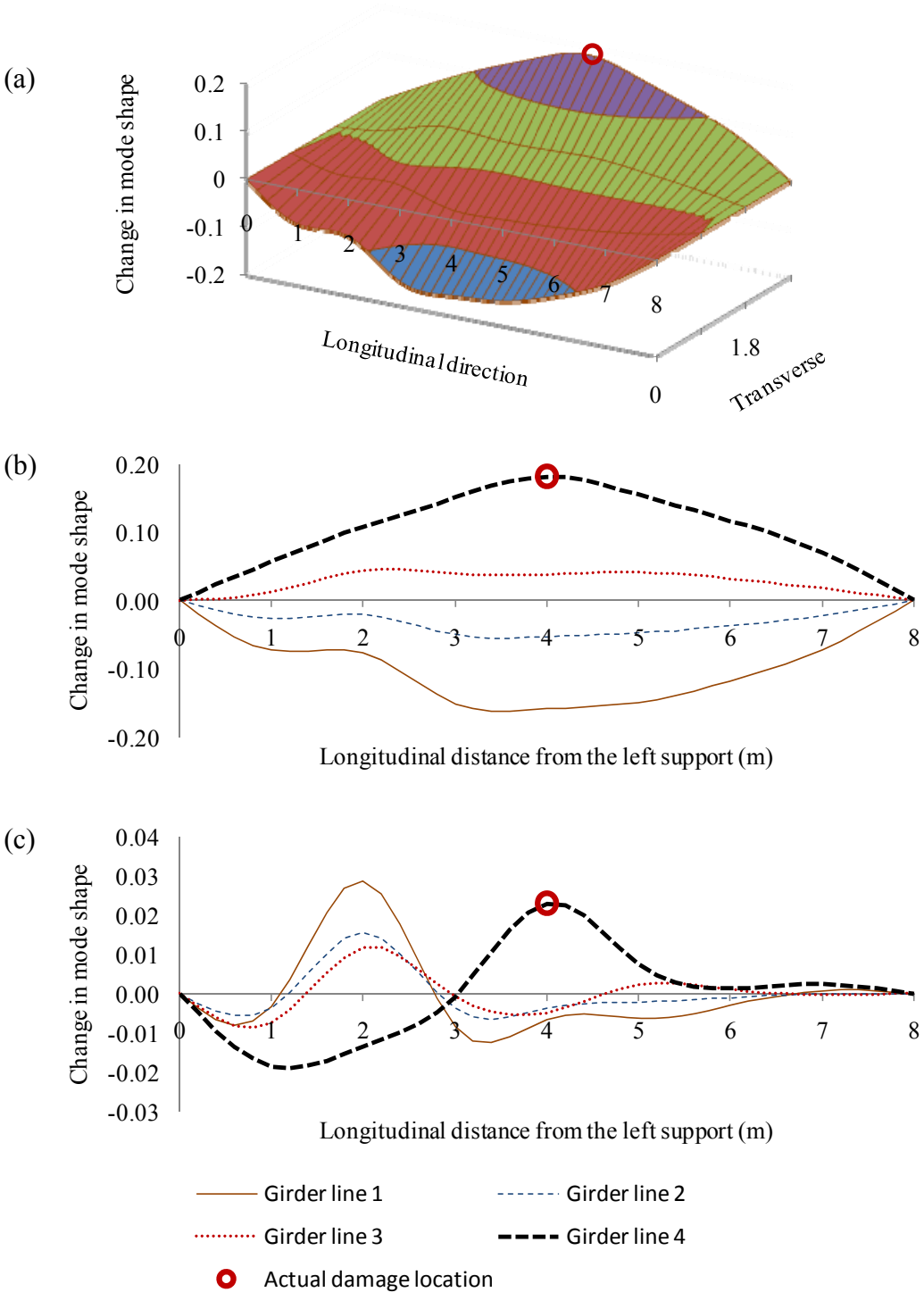

Figure I.9. Distribution of the change in the first mode shape due to Damage Case 1 using accelerometer data with white noise random excitation: (a) 3D figure with unit area normalization over all measurement points; (b) 2D figure with unit area normalization over all measurement points; and (c) 2D figure with unit area normalization along individual girder lines.

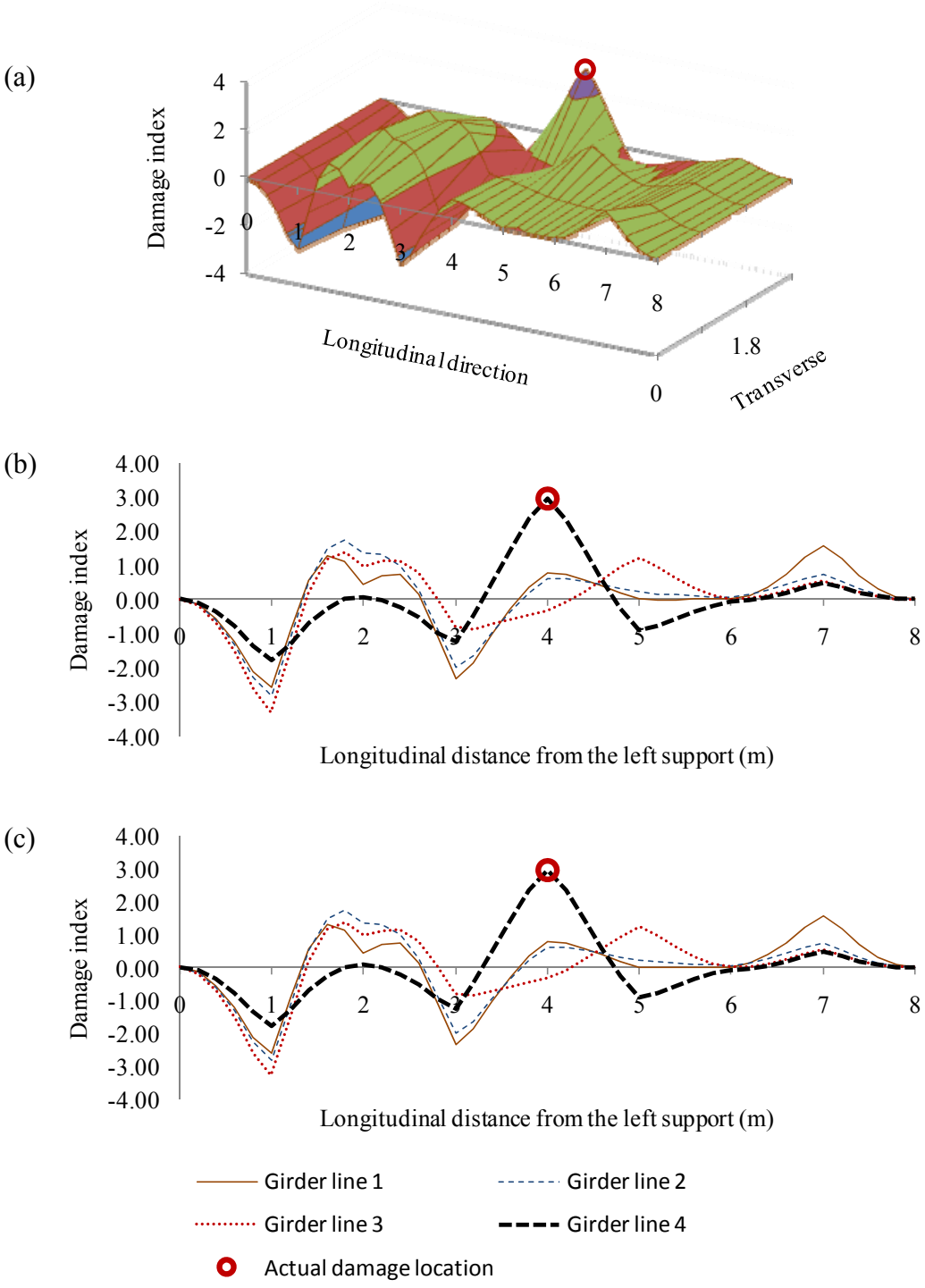

Figure I.10. Distribution of the damage index for the first mode due to Damage Case 1 using accelerometer data with white noise random excitation: (a) 3D figure with unit area normalization over all measurement points; (b) 2D figure with unit area normalization over all measurement points; and (c) 2D figure with unit area normalization along individual girder lines.

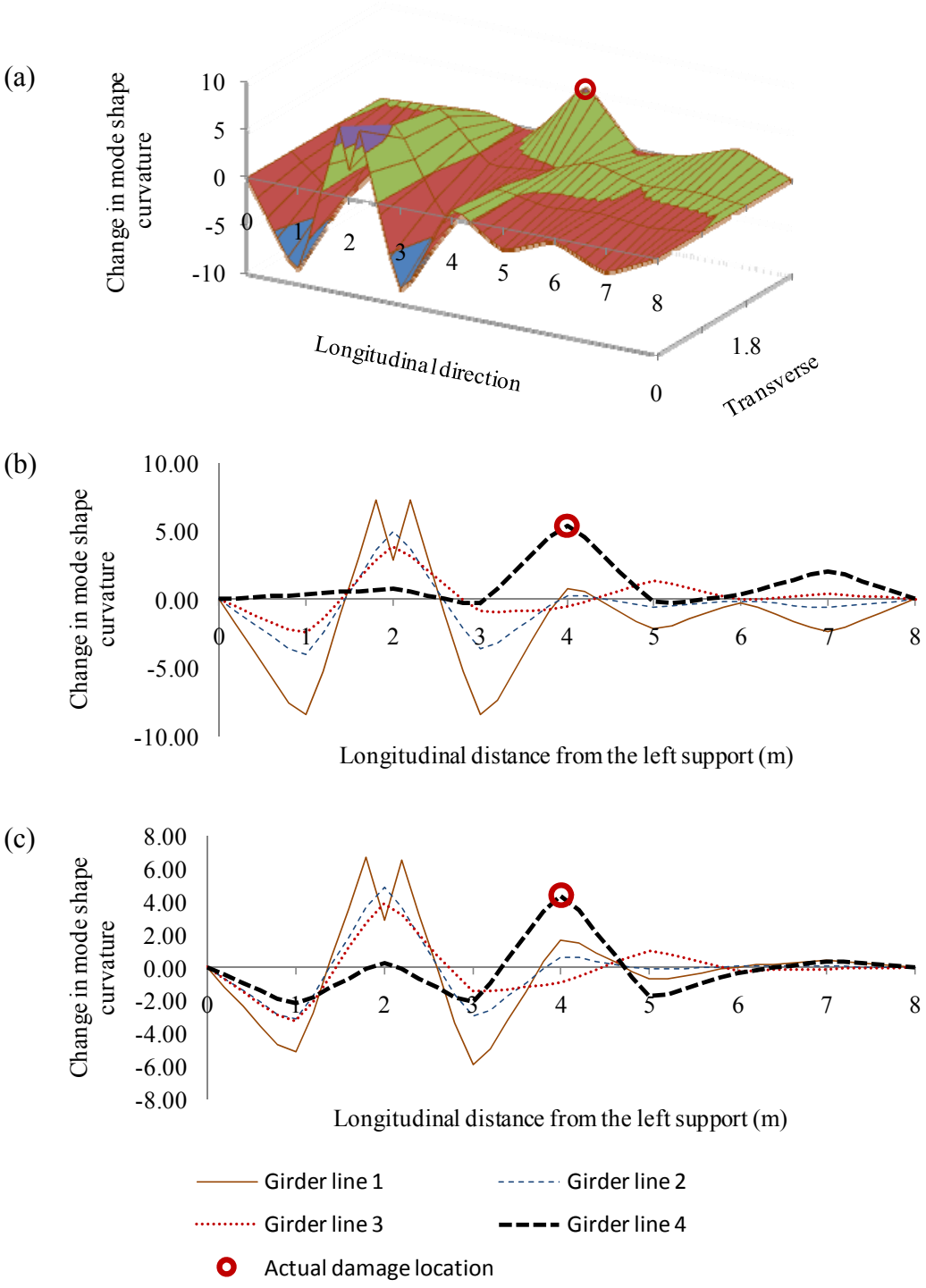

Figure I.11. Distribution of the change in mode shape curvature for the first mode due to Damage Case 1 using accelerometer data with white noise random excitation: (a) 3D figure with unit area normalization over all measurement points; (b) 2D figure with unit area normalization over all measurement points; and (c) 2D figure with unit area normalization along individual girder lines.

APPENDIX J. DETECTION OF DAMAGE CASE 1 USING HIGHER VIBRATION MODES WHEN ACCELEROMETER DATA AND WHITE NOISE RANDOM EXCITATION WERE USED

This appendix presents additional information for Section 6.3, providing damage localization of Damage Case 1 using commonly available VBDD indicators, based on the higher vibration modes extracted from accelerometer data (i.e., the 2^{nd}, 3^{rd}, 4^{th}, and 5^{th} modes), when white noise random excitation was used. The damage indicators used in this Appendix included change in mode shape method, damage index method, and change in mode shape curvature method.

Figures J.1 to J.4 present the results of damage localization using the change in mode shape method, when Test Protocols 13, 17, 21, and 25 were used, respectively.

Figures J.5 to J.8 present the results of damage localization using the damage index method, when Test Protocols 13, 17, 21, and 25 were used, respectively.

Figures J.9 to J.12 present the results of damage localization using the change in mode shape curvature method, when Test Protocols 13, 17, 21, and 25 were used, respectively.

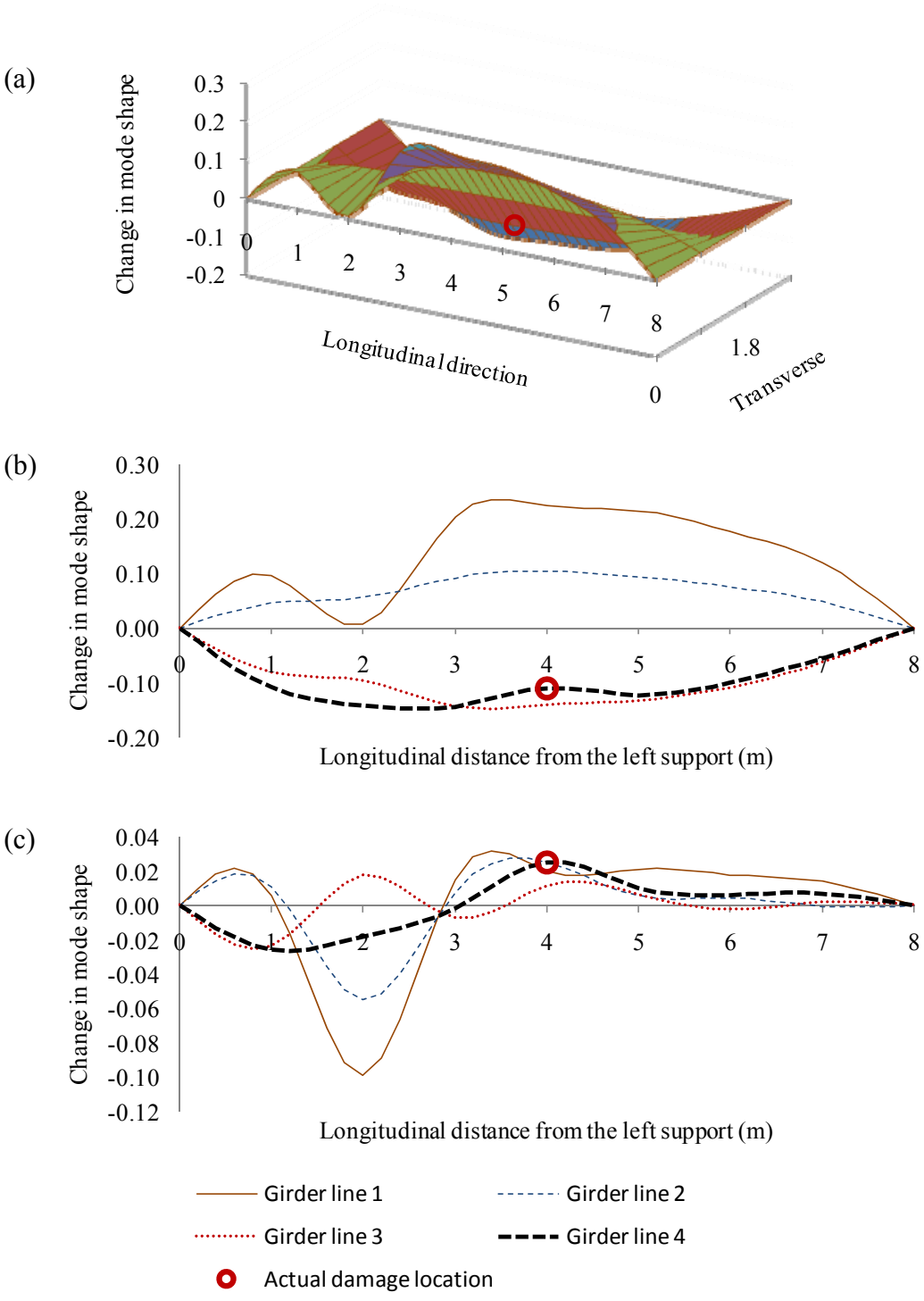

Figure J.1. Distribution of the change in the second mode shape due to Damage Case 1 using accelerometer data with white noise random excitation: (a) 3D figure with unit area normalization over all measurement points; (b) 2D figure with unit area normalization over all measurement points; and (c) 2D figure with unit area normalization along individual girder lines.

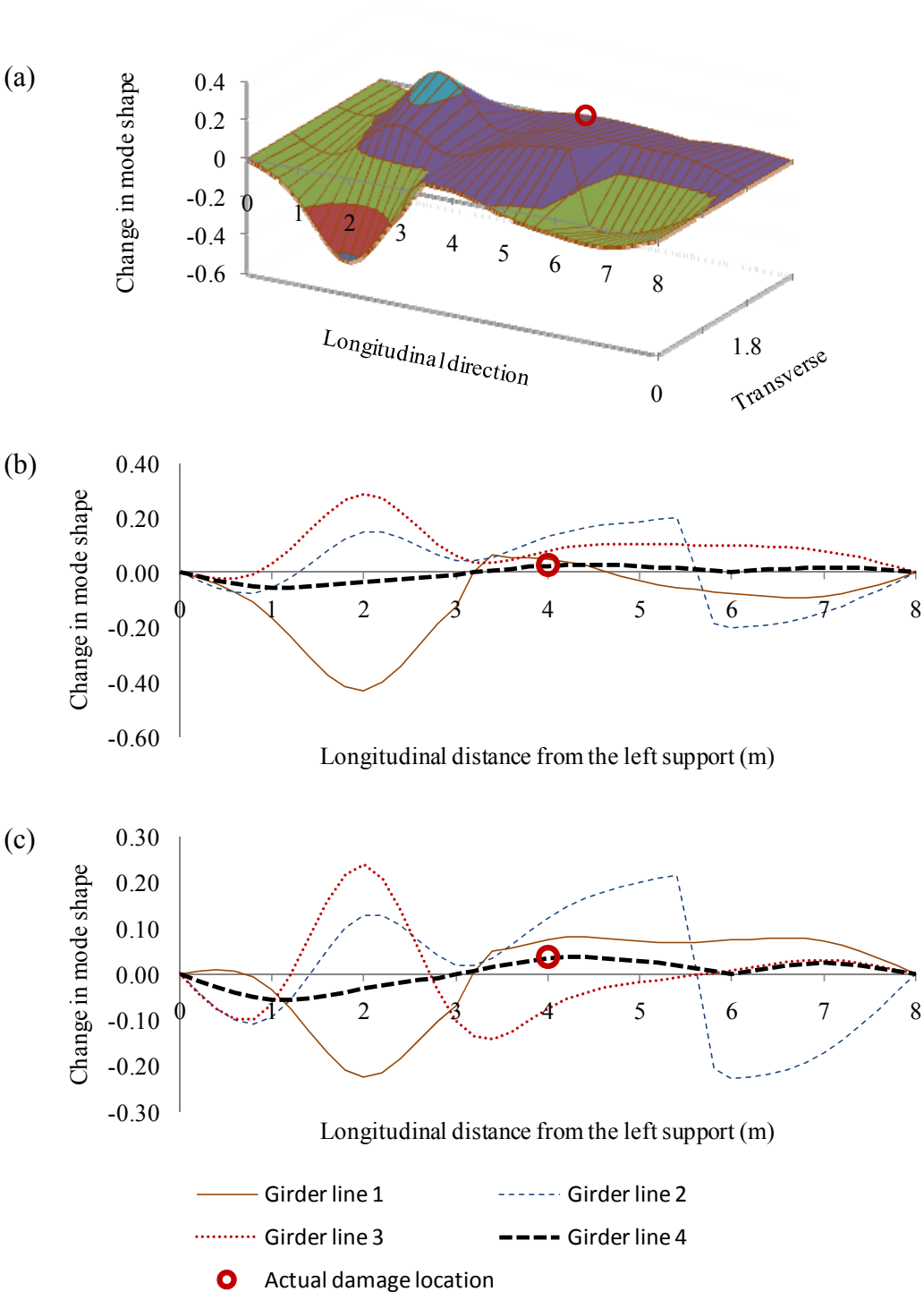

Figure J.2. Distribution of the change in the third mode shape due to Damage Case 1 using accelerometer data with white noise random excitation: (a) 3D figure with unit area normalization over all measurement points; (b) 2D figure with unit area normalization over all measurement points; and (c) 2D figure with unit area normalization along individual girder lines.

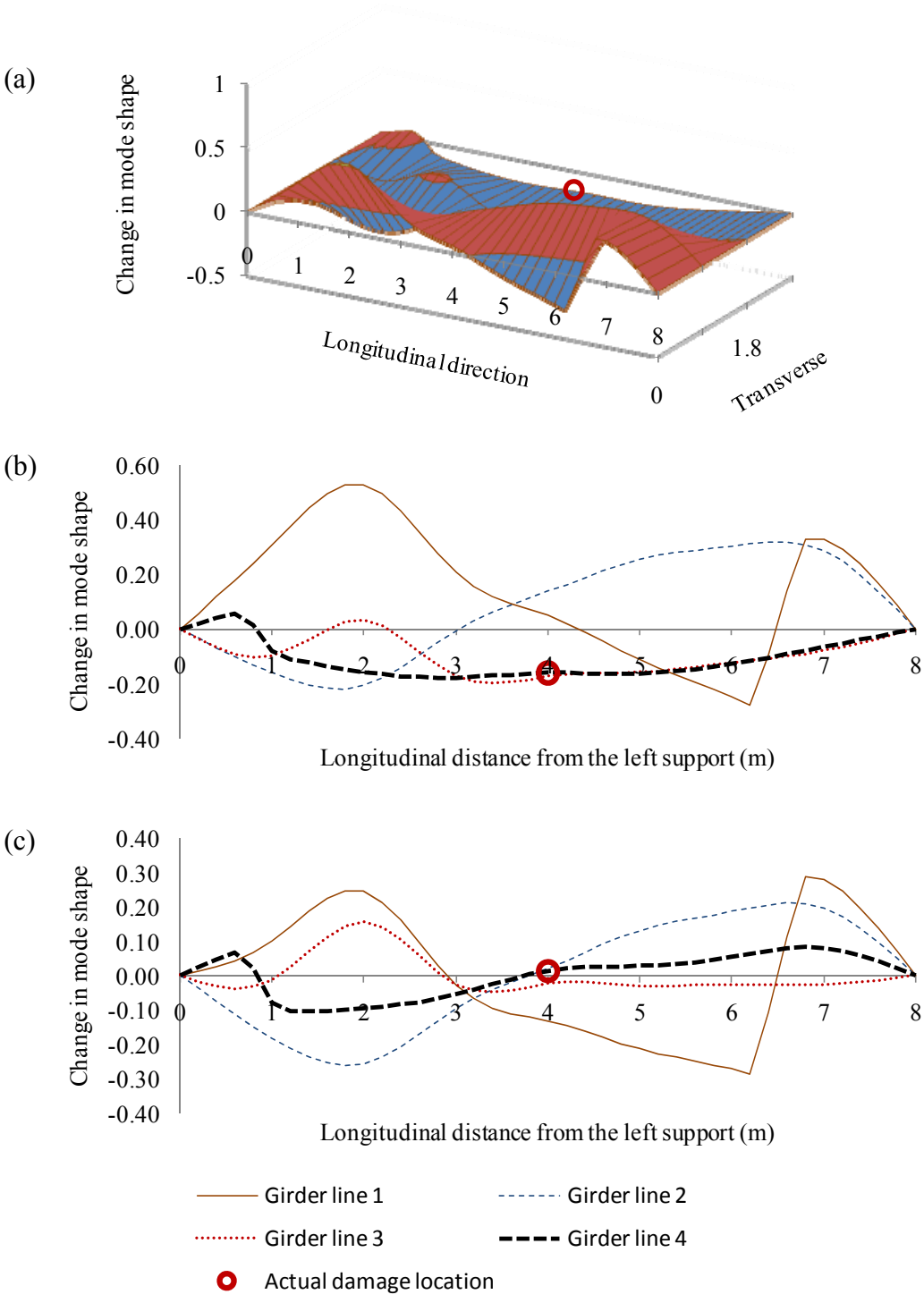

Figure J.3. Distribution of the change in the fourth mode shape due to Damage Case 1 using accelerometer data with white noise random excitation: (a) 3D figure with unit area normalization over all measurement points; (b) 2D figure with unit area normalization over all measurement points; and (c) 2D figure with unit area normalization along individual girder lines.

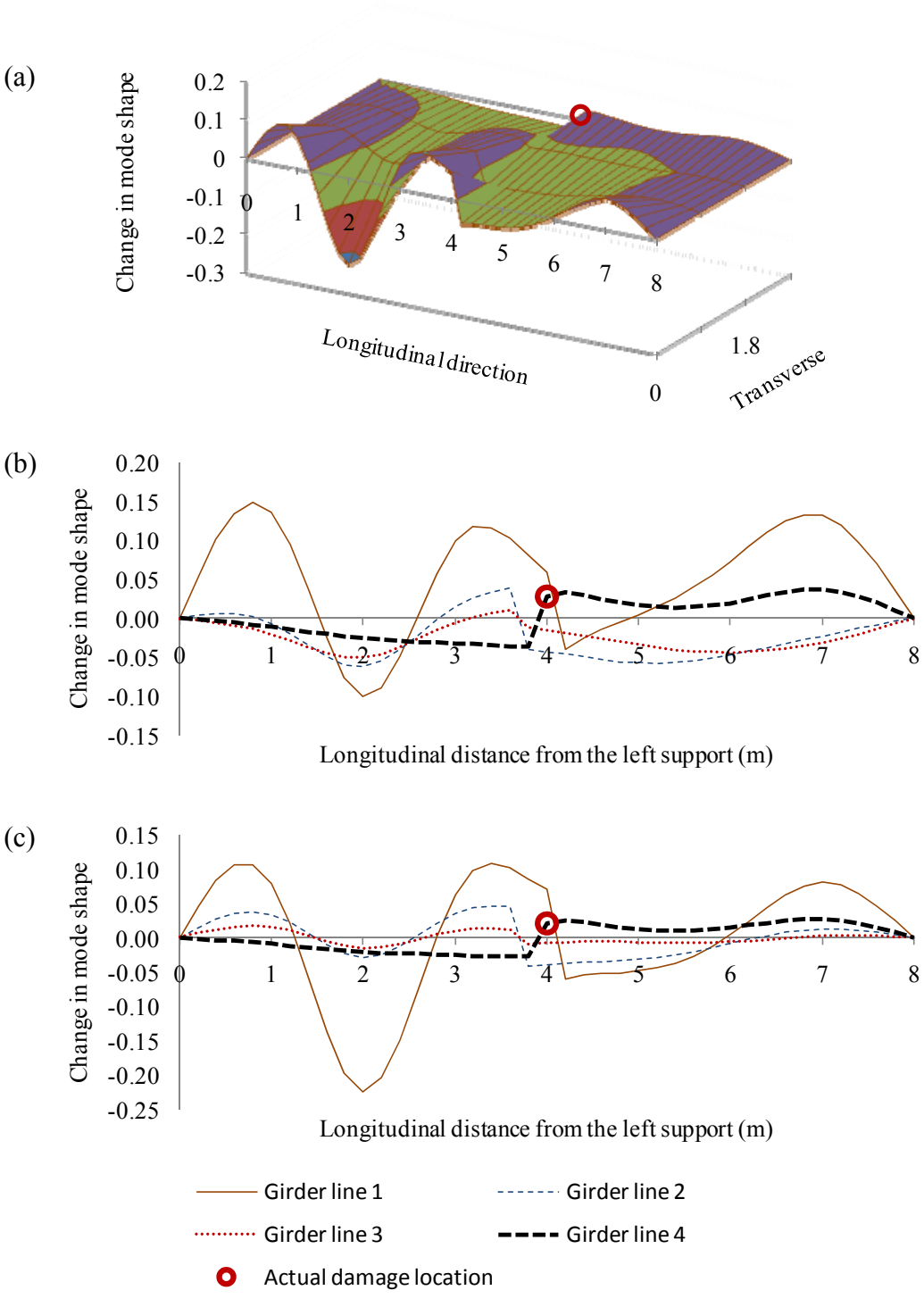

Figure J.4. Distribution of the change in the fifth mode shape due to Damage Case 1 using accelerometer data with white noise random excitation: (a) 3D figure with unit area normalization over all measurement points; (b) 2D figure with unit area normalization over all measurement points; and (c) 2D figure with unit area normalization along individual girder lines.

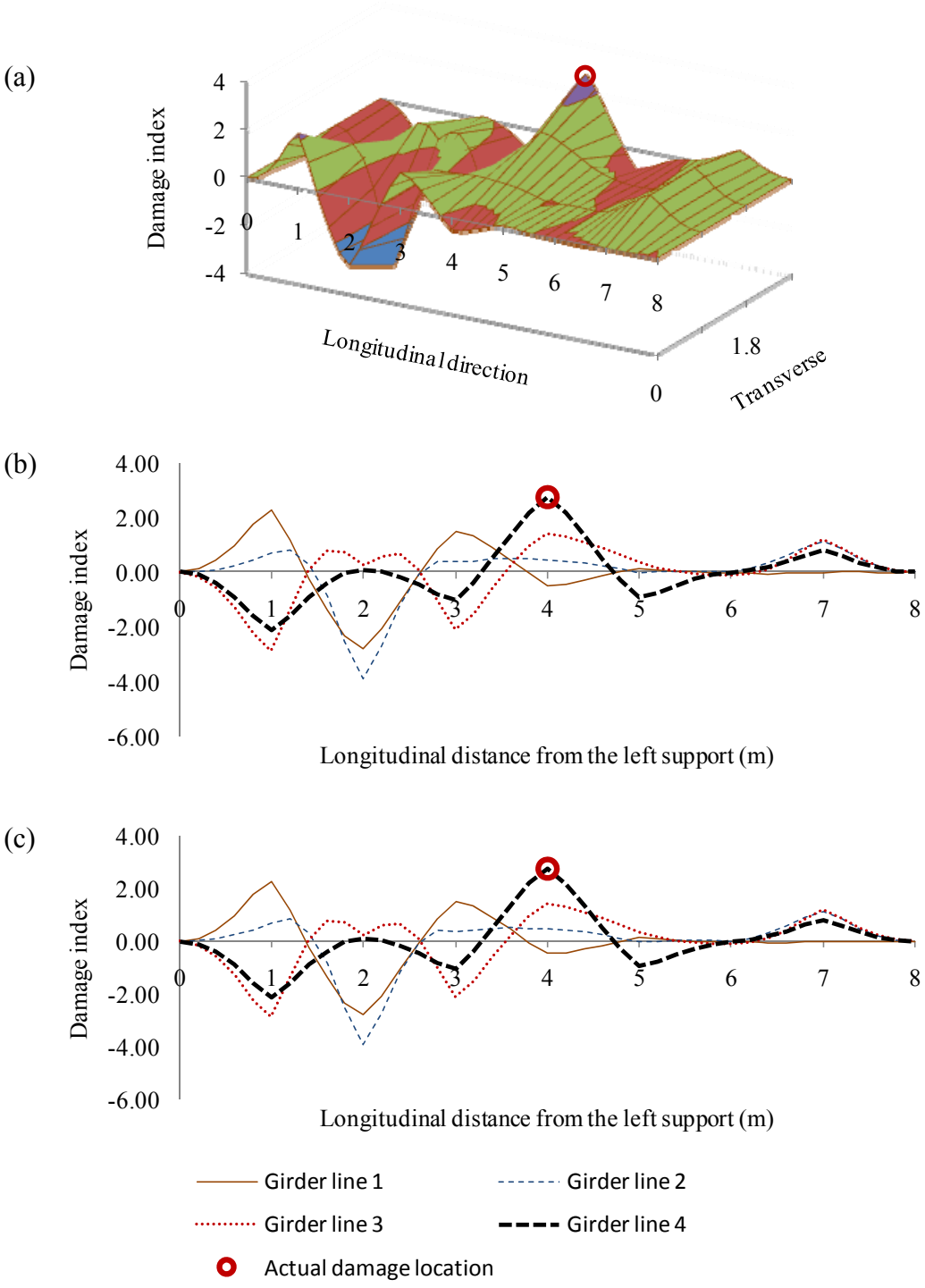

Figure J.5. Distribution of the damage index for the second mode due to Damage Case 1 using accelerometer data with white noise random excitation: (a) 3D figure with unit area normalization over all measurement points; (b) 2D figure with unit area normalization over all measurement points; and (c) 2D figure with unit area normalization along individual girder lines.

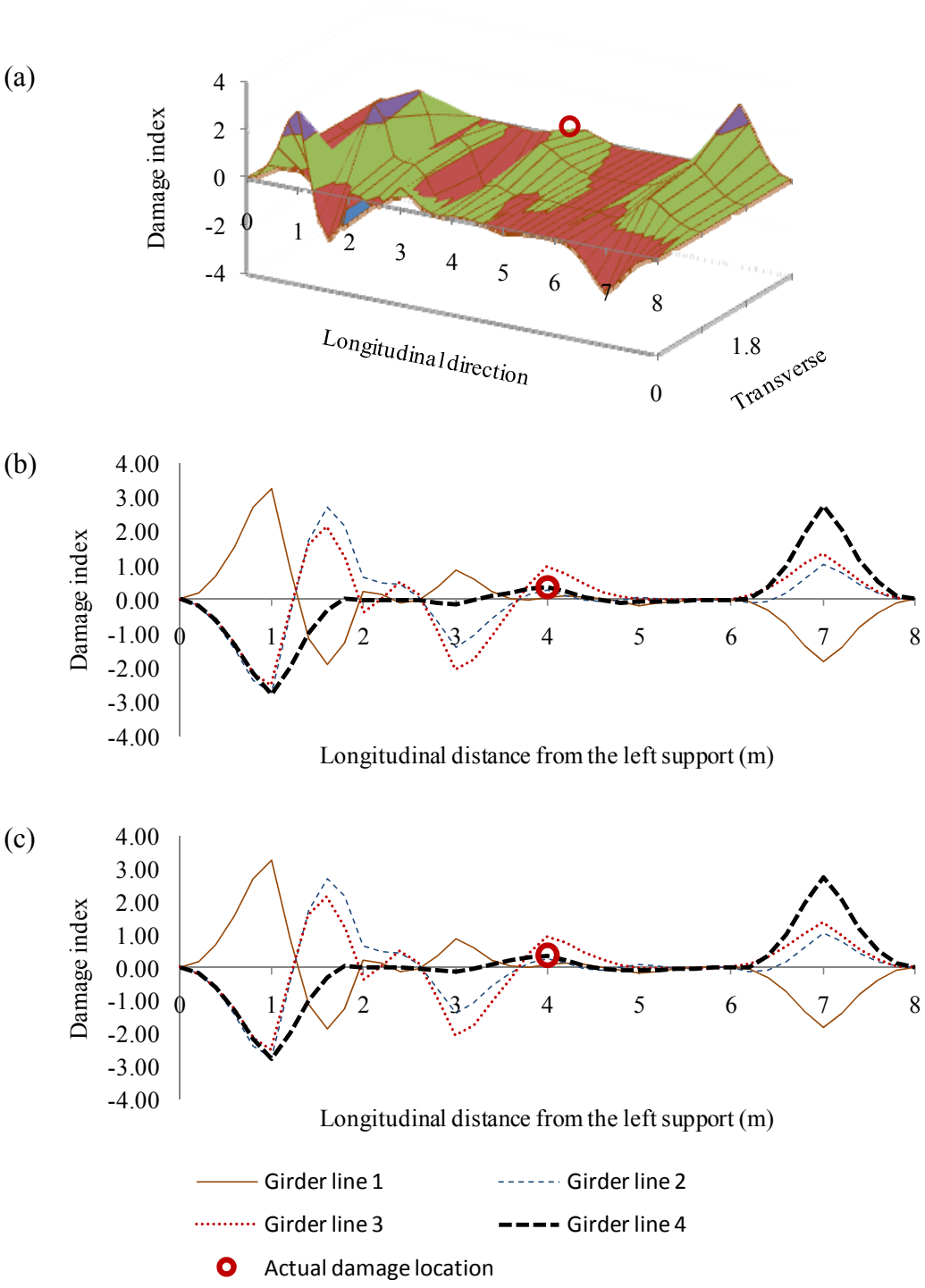

Figure J.6. Distribution of the damage index for the third mode due to Damage Case 1 using accelerometer data with white noise random excitation: (a) 3D figure with unit area normalization over all measurement points; (b) 2D figure with unit area normalization over all measurement points; and (c) 2D figure with unit area normalization along individual girder lines.

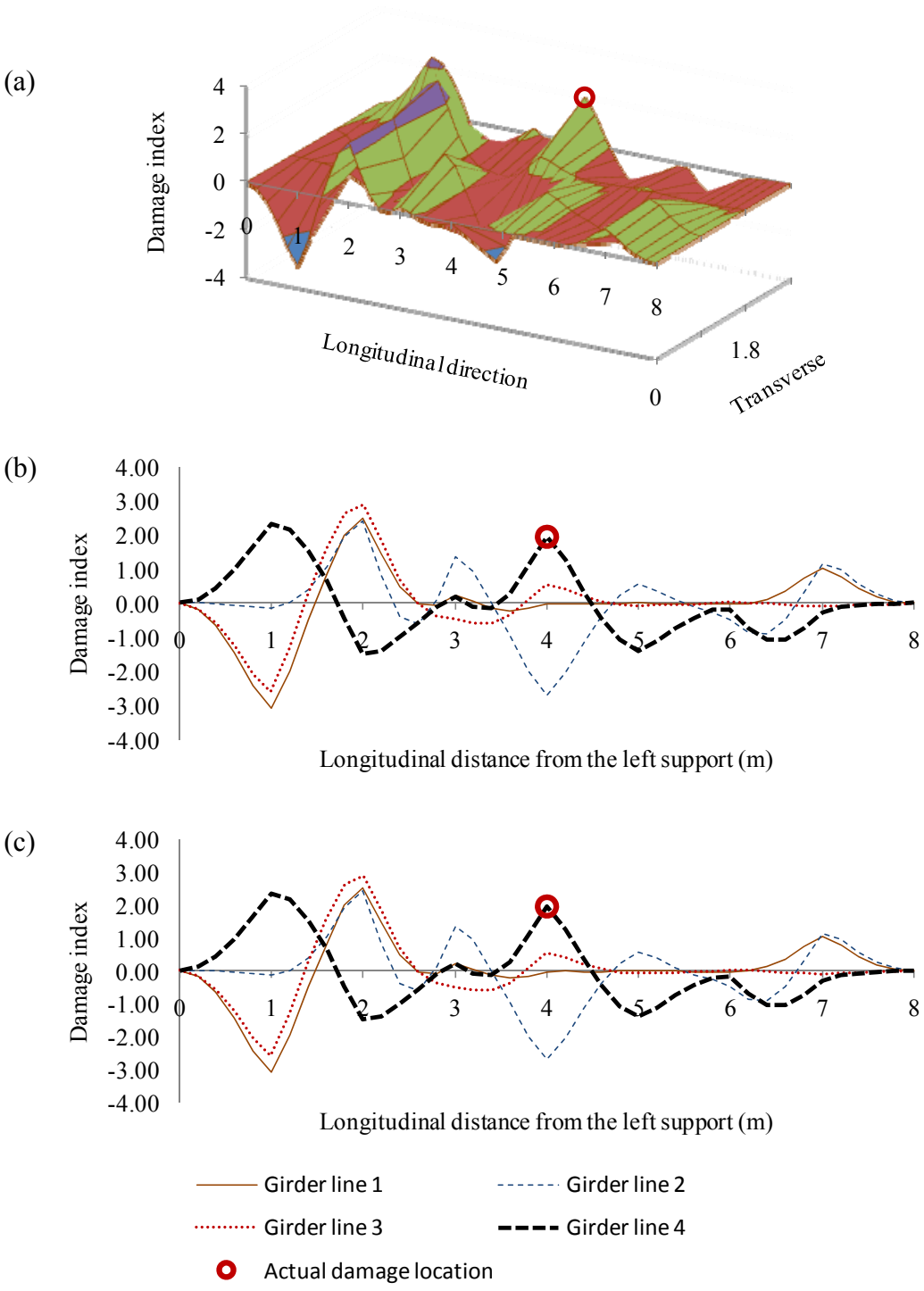

Figure J.7. Distribution of the damage index for the fourth mode due to Damage Case 1 using accelerometer data with white noise random excitation: (a) 3D figure with unit area normalization over all measurement points; (b) 2D figure with unit area normalization over all measurement points; and (c) 2D figure with unit area normalization along individual girder lines.

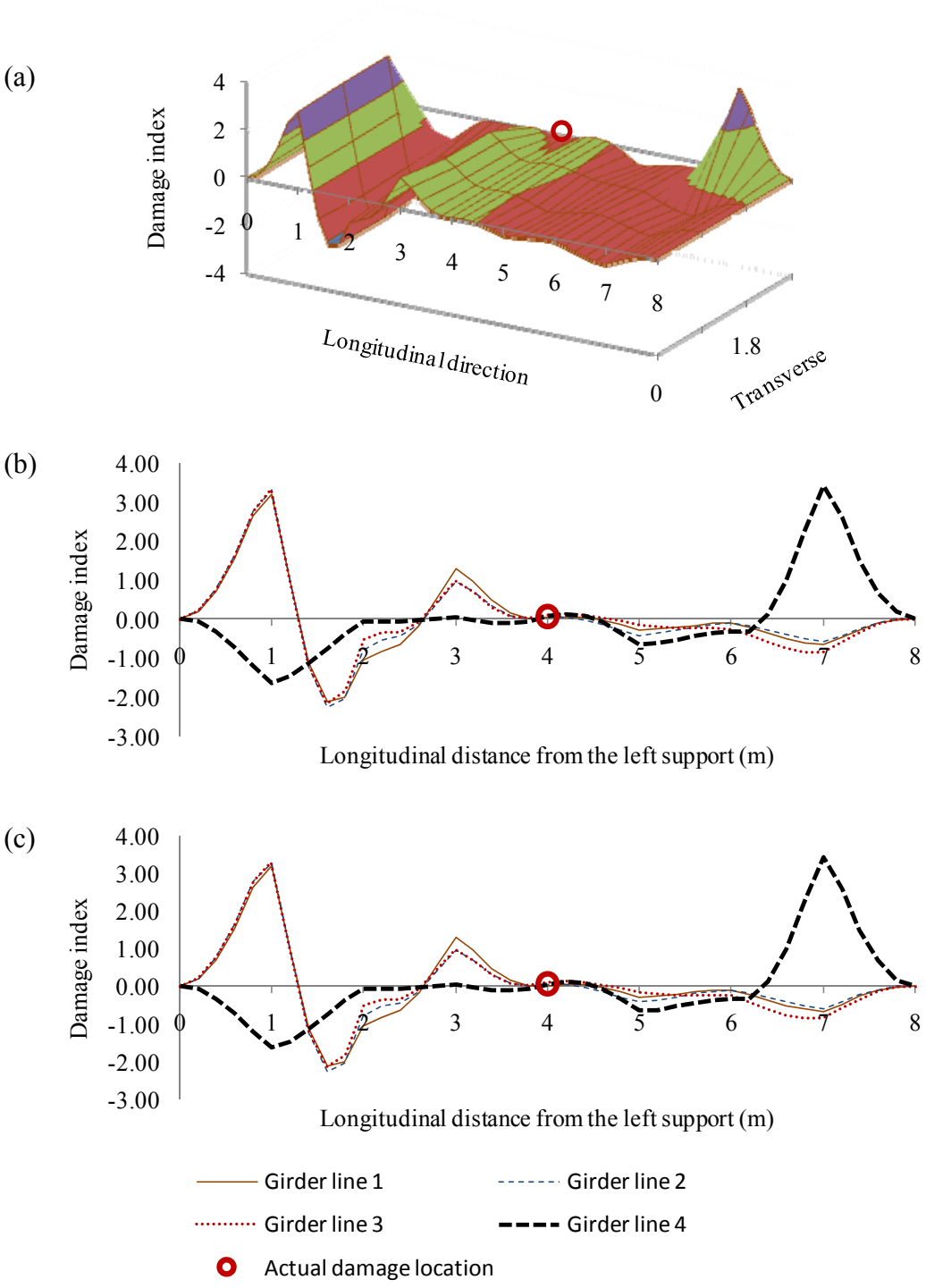

Figure J.8. Distribution of the damage index for the fifth mode due to Damage Case 1 using accelerometer data with white noise random excitation: (a) 3D figure with unit area normalization over all measurement points; (b) 2D figure with unit area normalization over all measurement points; and (c) 2D figure with unit area normalization along individual girder lines.

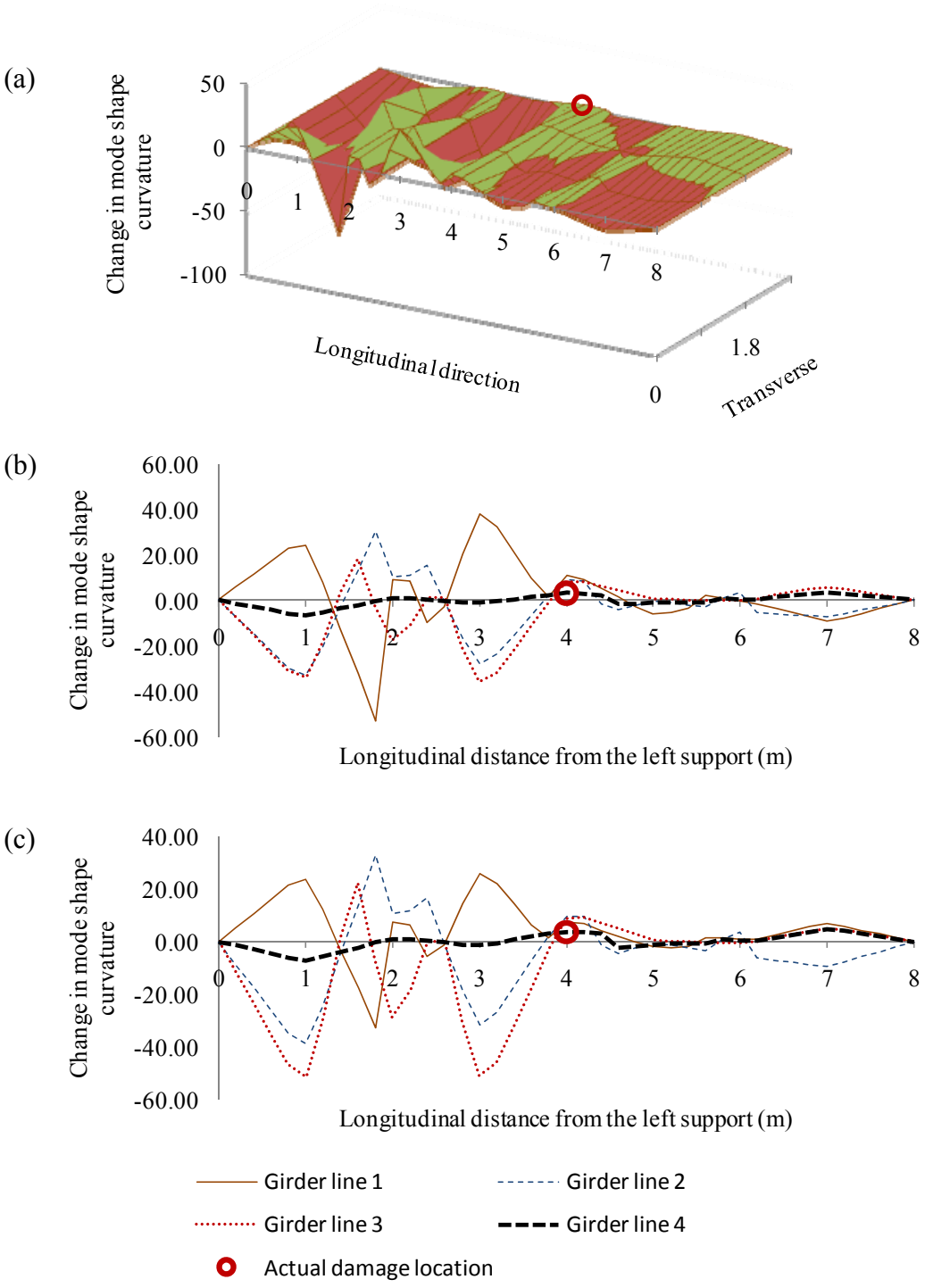

Figure J.9. Distribution of the change in mode shape curvature for the third mode due to Damage Case 1 using accelerometer data with white noise random excitation: (a) 3D figure with unit area normalization over all measurement points; (b) 2D figure with unit area normalization over all measurement points; and (c) 2D figure with unit area normalization along individual girder lines.

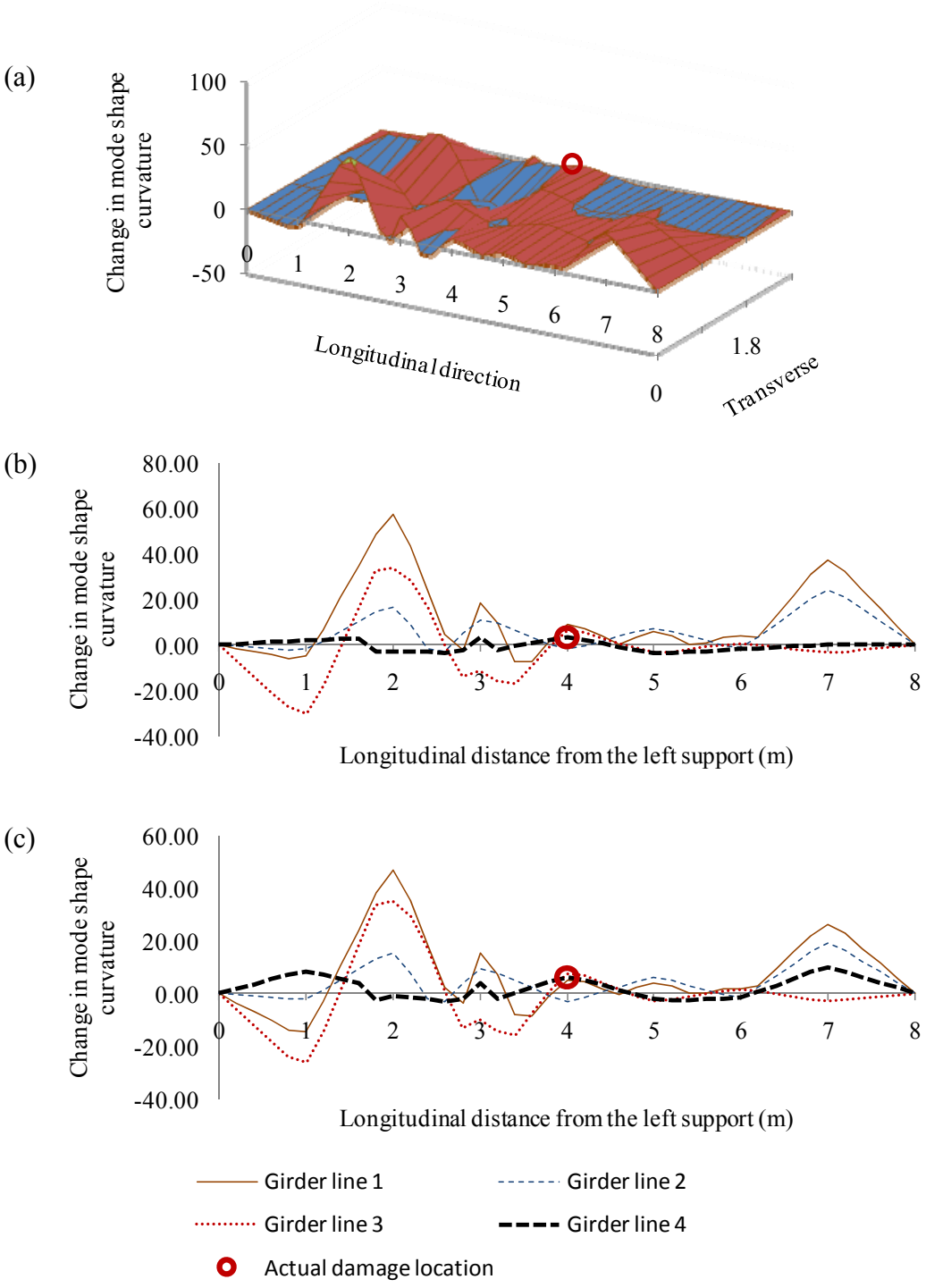

Figure J.10. Distribution of the change in mode shape curvature for the fourth mode due to Damage Case 1 using accelerometer data with white noise random excitation: (a) 3D figure with unit area normalization over all measurement points; (b) 2D figure with unit area normalization over all measurement points; and (c) 2D figure with unit area normalization along individual girder lines.

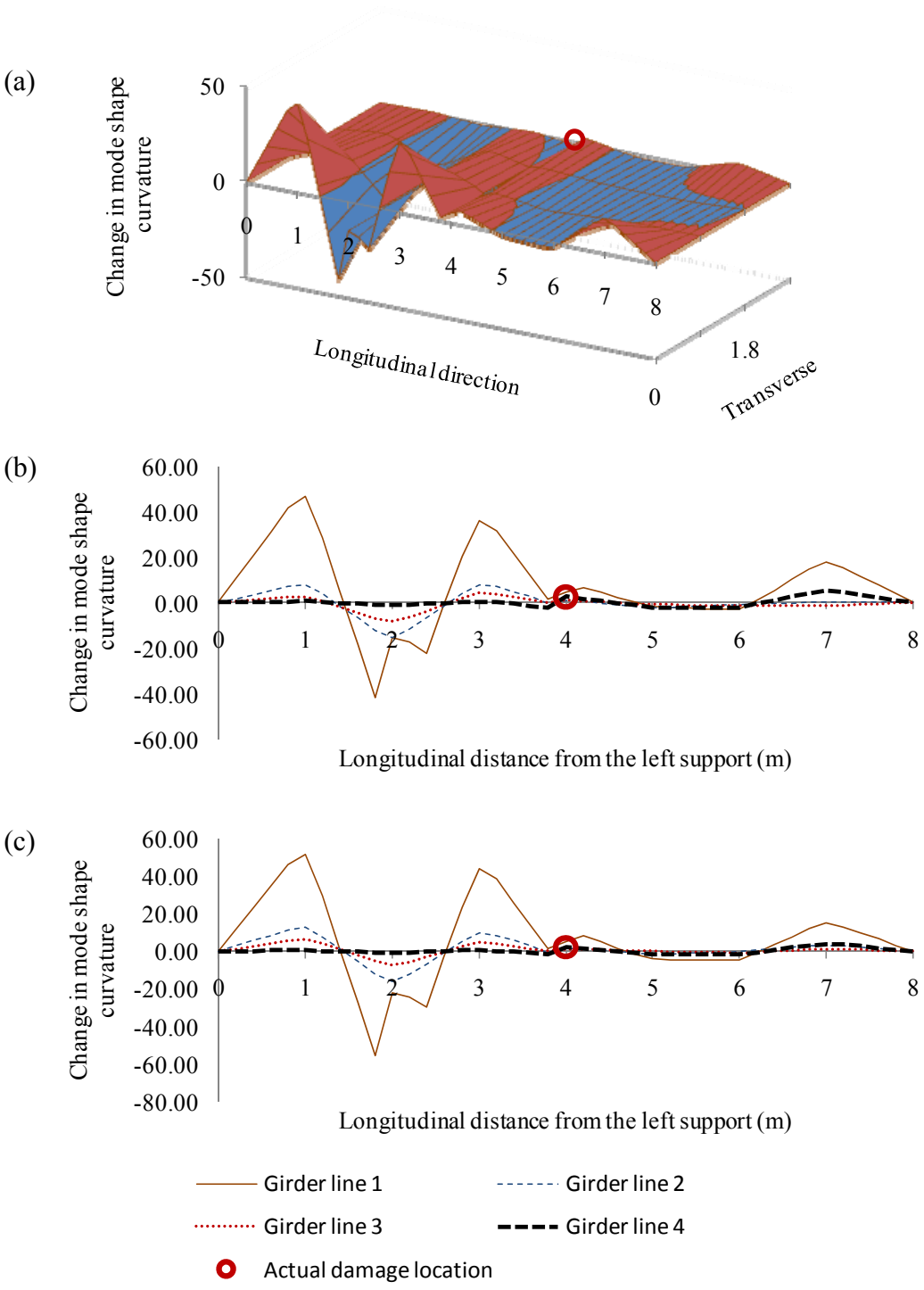

Figure J.11. Distribution of the change in mode shape curvature for the fifth mode due to Damage Case 1 using accelerometer data with white noise random excitation: (a) 3D figure with unit area normalization over all measurement points; (b) 2D figure with unit area normalization over all measurement points; and (c) 2D figure with unit area normalization along individual girder lines.

APPENDIX K. **DAMAGE DETECTION USING CHANGE IN THE FIRST MODE SHAPE FOR DAMAGE CASES 2 TO 16 WHEN ACCELEROMETER DATA AND HARMONIC EXCITATION WERE USED**

This appendix presents additional information for Section 6.3, providing damage localization of Damage Cases 2 to 16 using the change in mode shape method, when Test Protocol 1 was used, which are similar to results presented in Fig. 6.17.

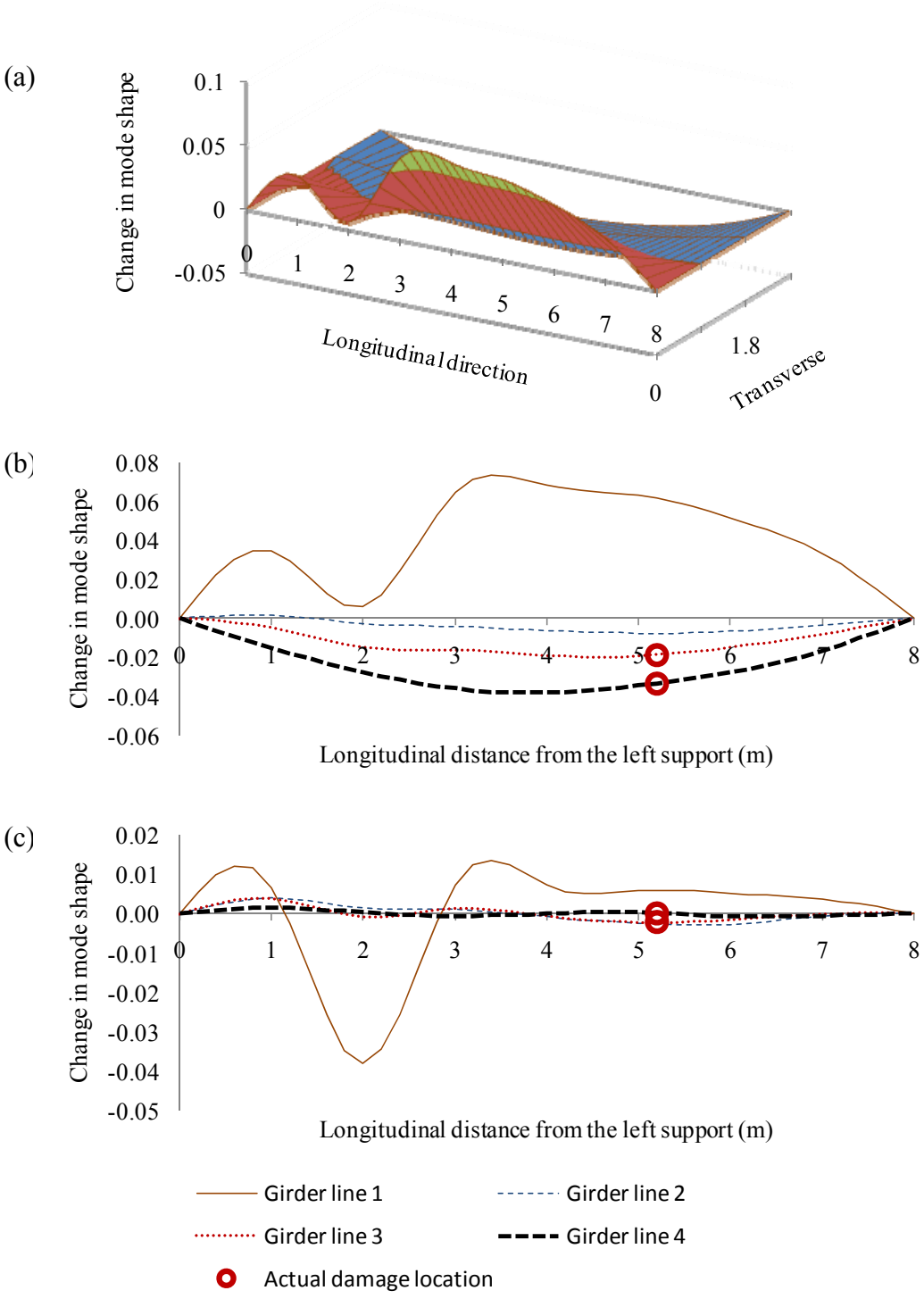

Figure K.1. Distribution of the change in the first mode shape due to Damage Case 2 using accelerometer data with harmonic excitation: (a) 3D figure with unit area normalization over all measurement points; (b) 2D figure with unit area normalization over all measurement points; and (c) 2D figure with unit area normalization along individual girder lines.

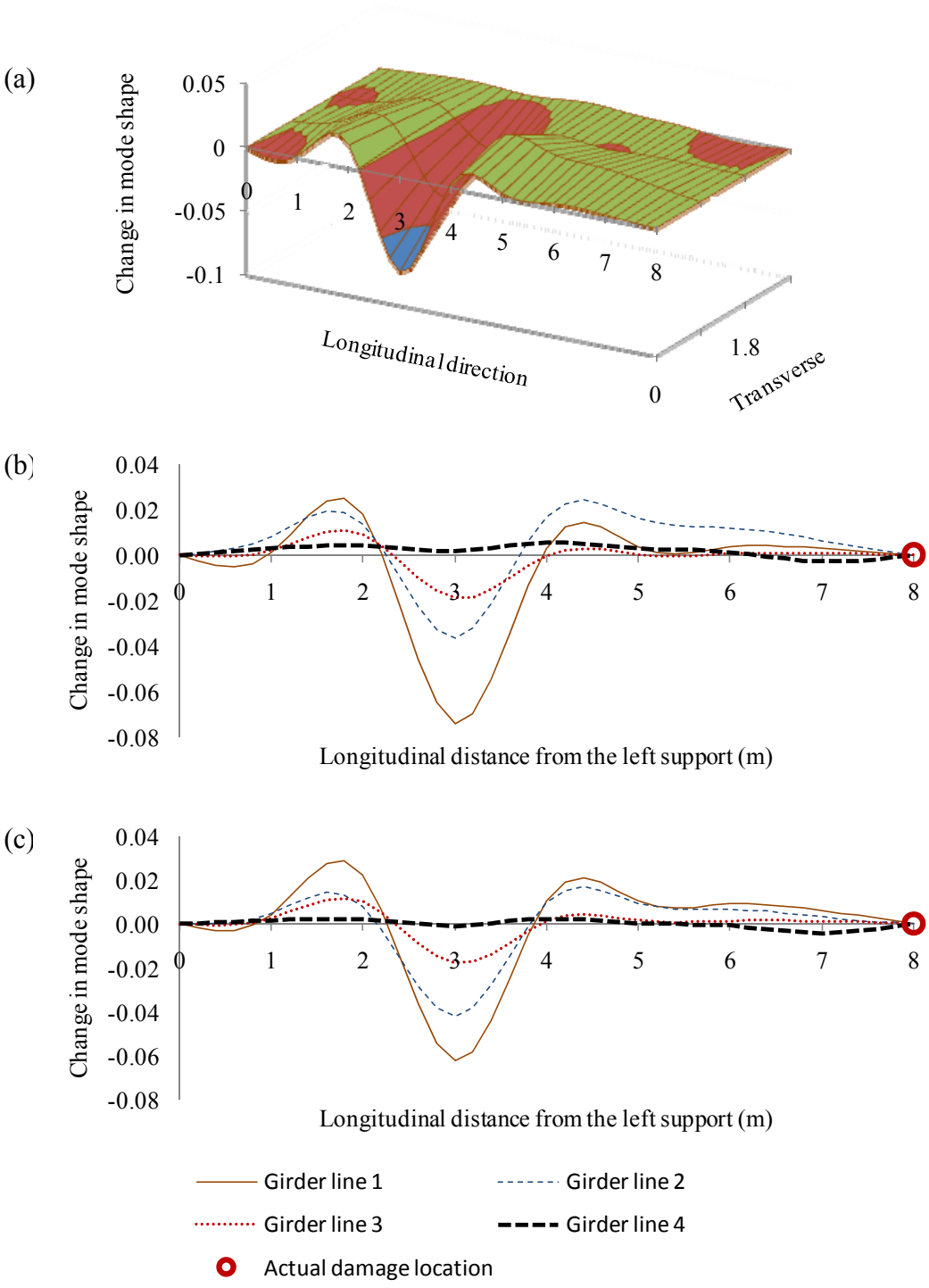

Figure K.2. Distribution of the change in the first mode shape due to Damage Case 3 using accelerometer data with harmonic excitation: (a) 3D figure with unit area normalization over all measurement points; (b) 2D figure with unit area normalization over all measurement points; and (c) 2D figure with unit area normalization along individual girder lines.

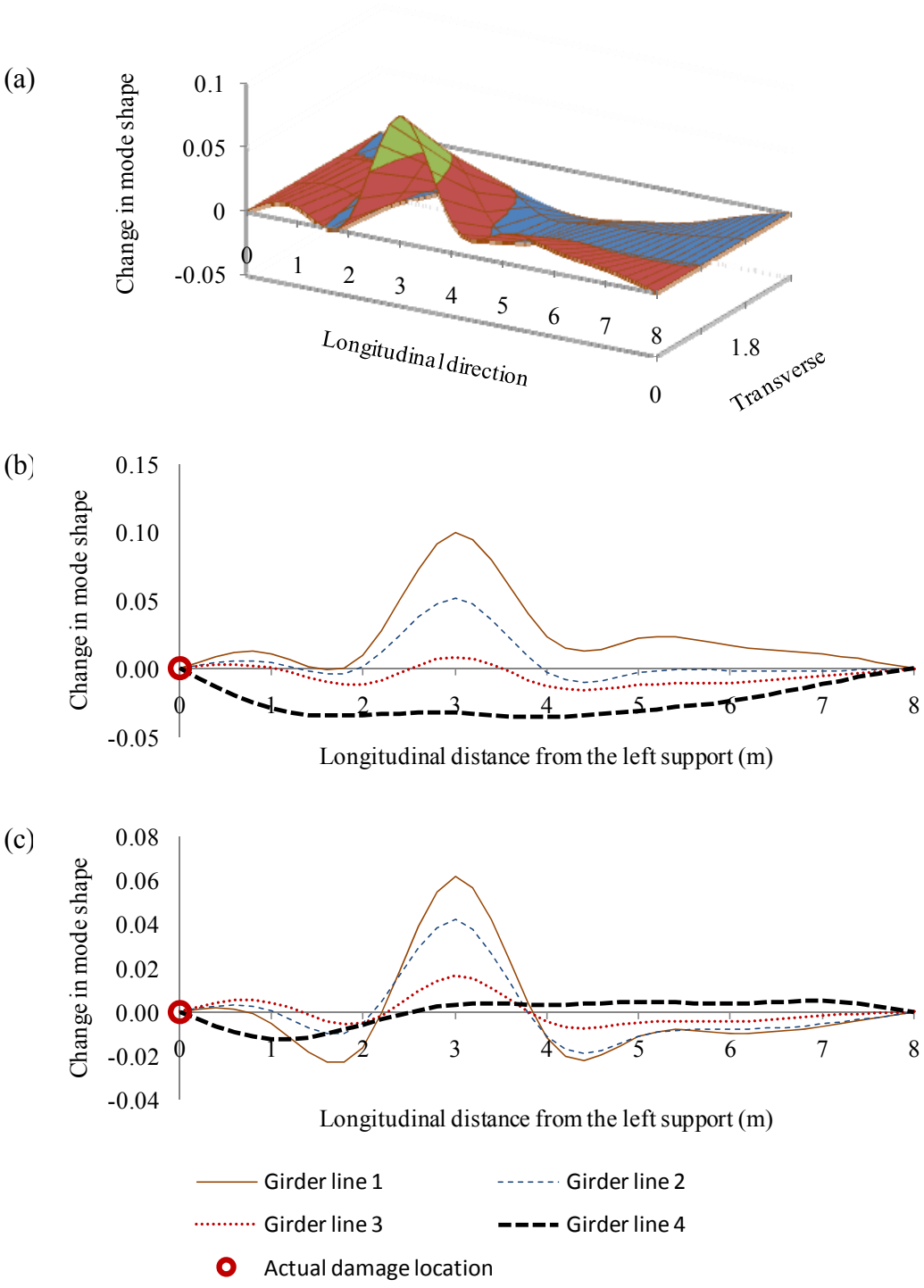

Figure K.3. Distribution of the change in the first mode shape due to Damage Case 4 using accelerometer data with harmonic excitation: (a) 3D figure with unit area normalization over all measurement points; (b) 2D figure with unit area normalization over all measurement points; and (c) 2D figure with unit area normalization along individual girder lines.

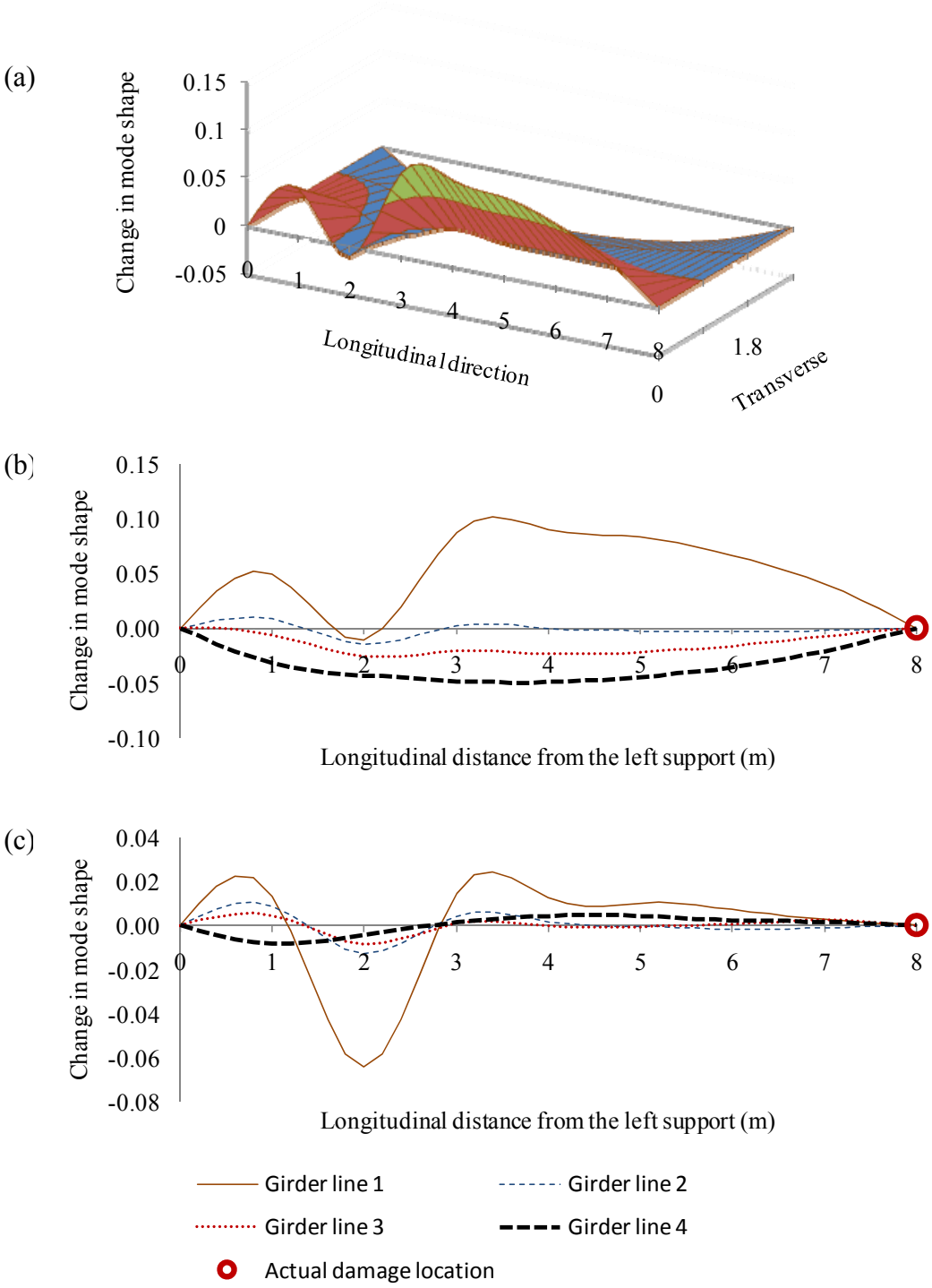

Figure K.4. Distribution of the change in the first mode shape due to Damage Case 5 using accelerometer data with harmonic excitation: (a) 3D figure with unit area normalization over all measurement points; (b) 2D figure with unit area normalization over all measurement points; and (c) 2D figure with unit area normalization along individual girder lines.

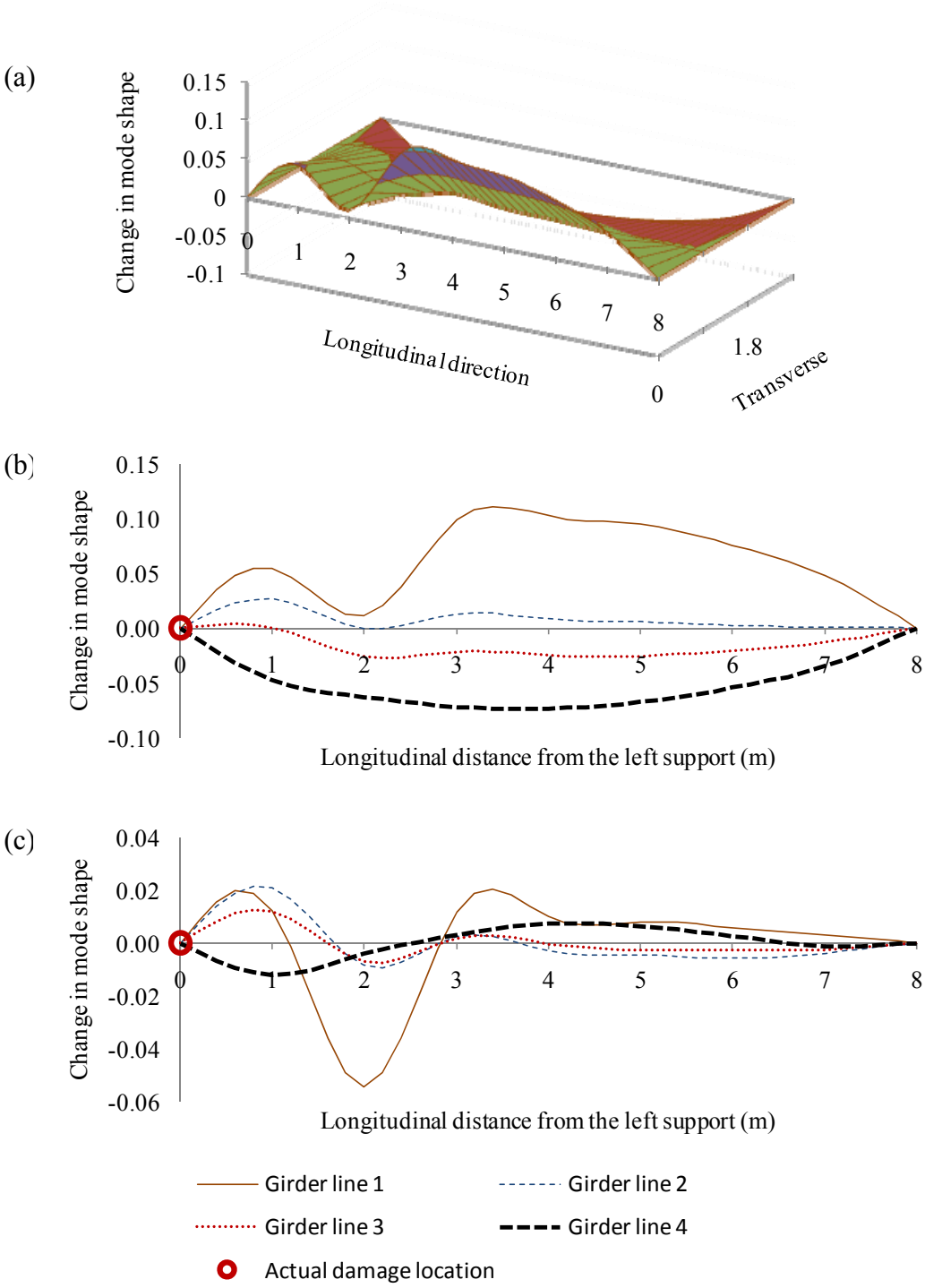

Figure K.5. Distribution of the change in the first mode shape due to Damage Case 6 using accelerometer data with harmonic excitation: (a) 3D figure with unit area normalization over all measurement points; (b) 2D figure with unit area normalization over all measurement points; and (c) 2D figure with unit area normalization along individual girder lines.

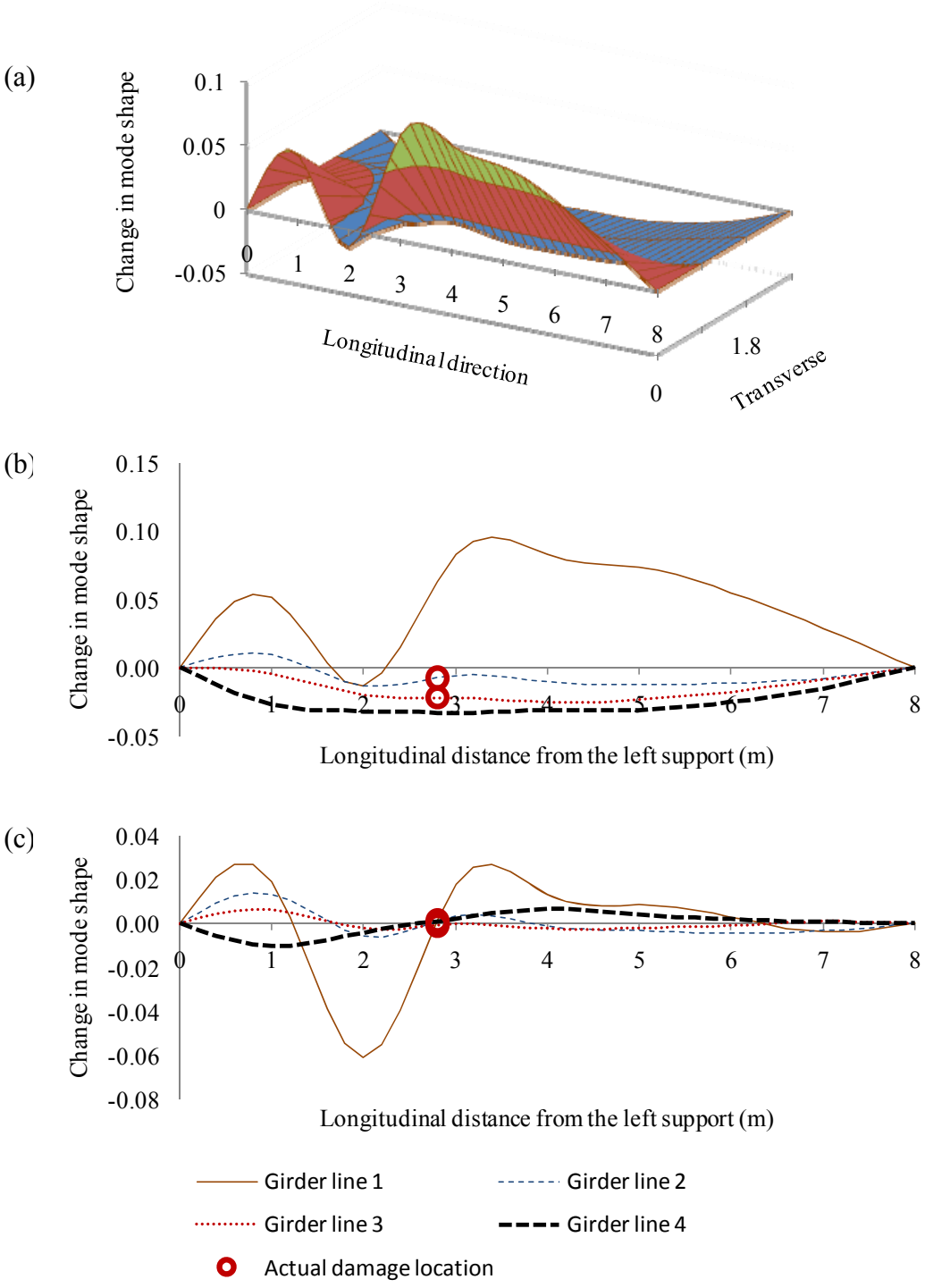

Figure K.6. Distribution of the change in the first mode shape due to Damage Case 7 using accelerometer data with harmonic excitation: (a) 3D figure with unit area normalization over all measurement points; (b) 2D figure with unit area normalization over all measurement points; and (c) 2D figure with unit area normalization along individual girder lines.

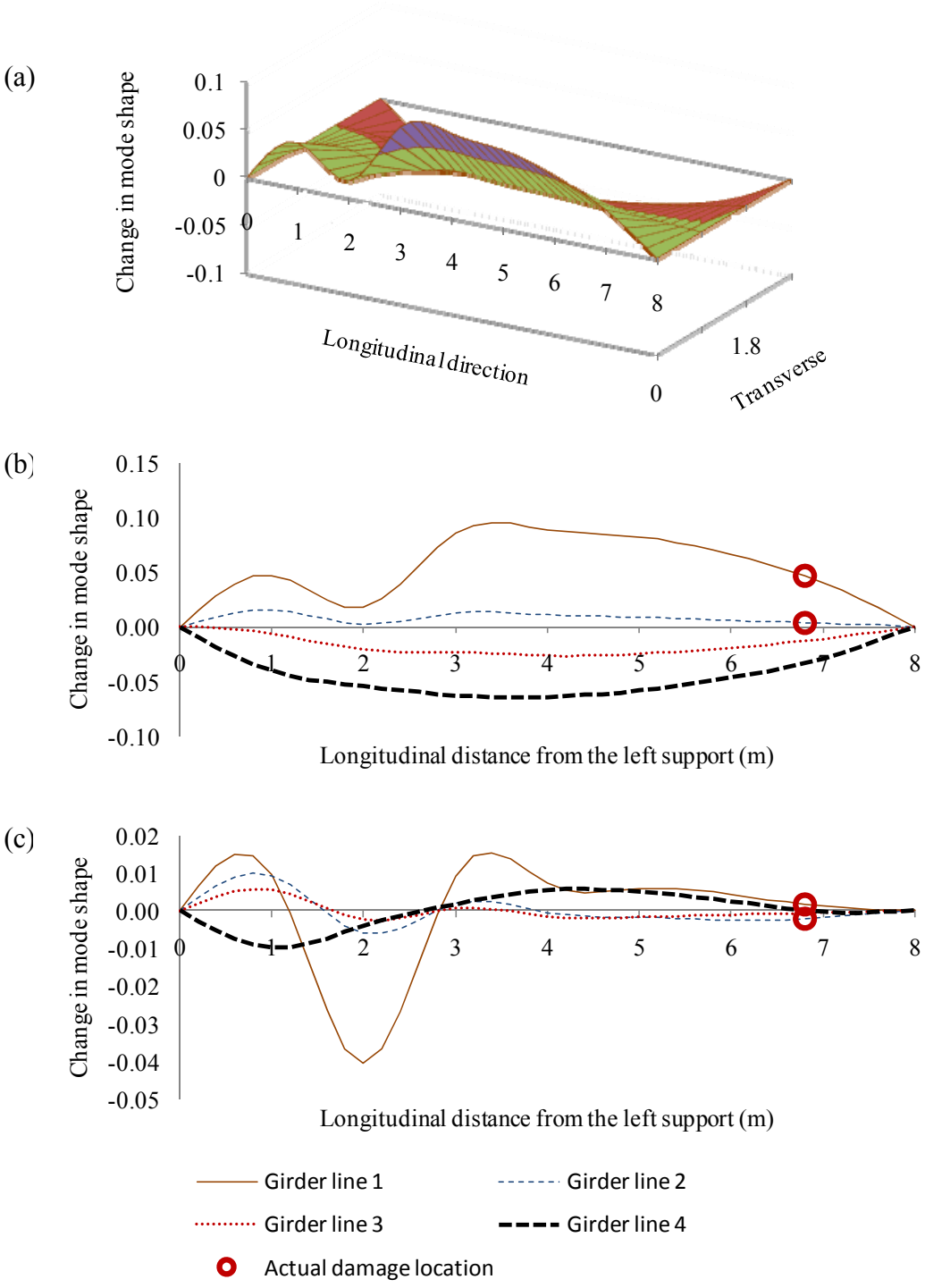

Figure K.7. Distribution of the change in the first mode shape due to Damage Case 8 using accelerometer data with harmonic excitation: (a) 3D figure with unit area normalization over all measurement points; (b) 2D figure with unit area normalization over all measurement points; and (c) 2D figure with unit area normalization along individual girder lines.

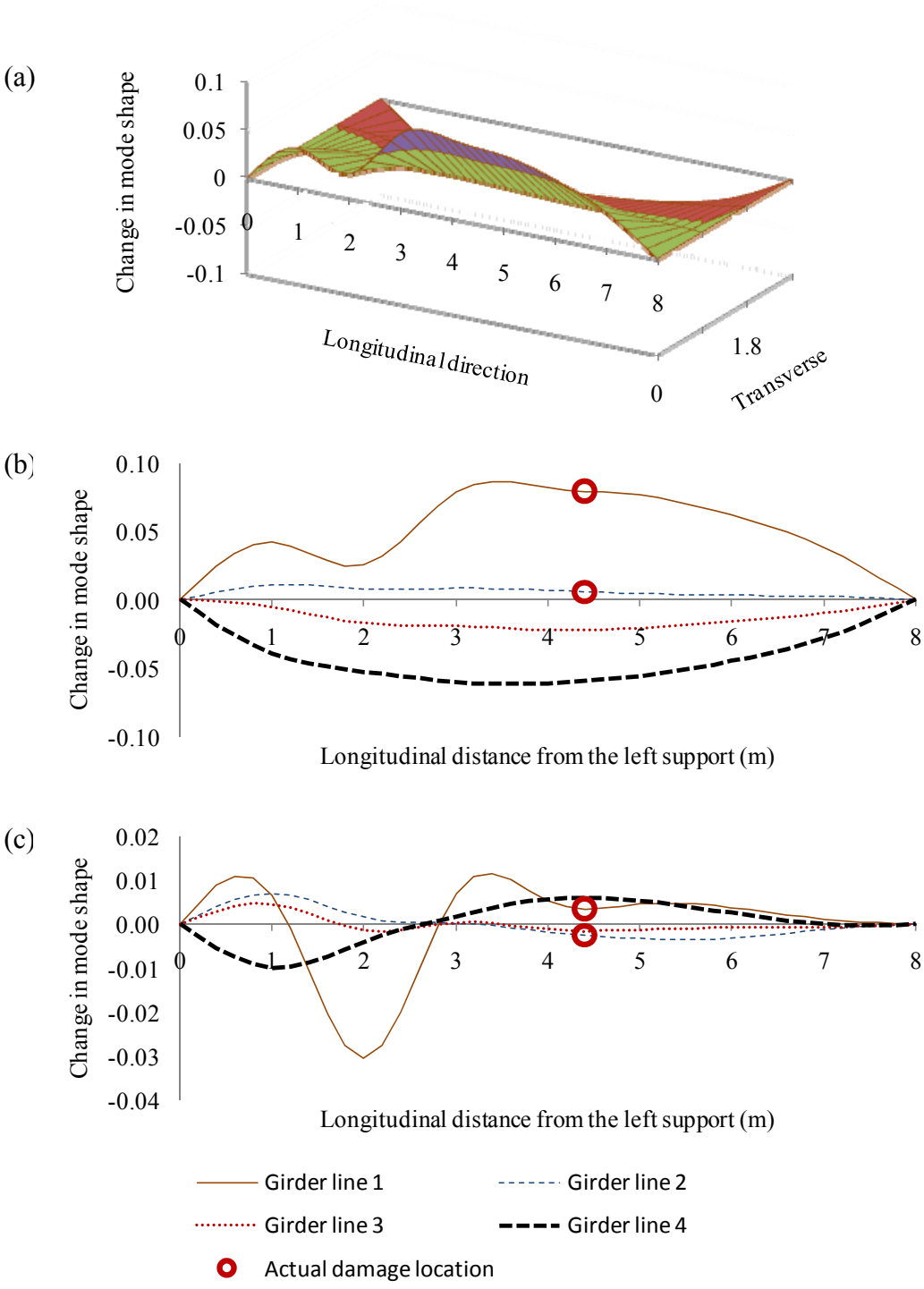

Figure K.8. Distribution of the change in the first mode shape due to Damage Case 9 using accelerometer data with harmonic excitation: (a) 3D figure with unit area normalization over all measurement points; (b) 2D figure with unit area normalization over all measurement points; and (c) 2D figure with unit area normalization along individual girder lines.

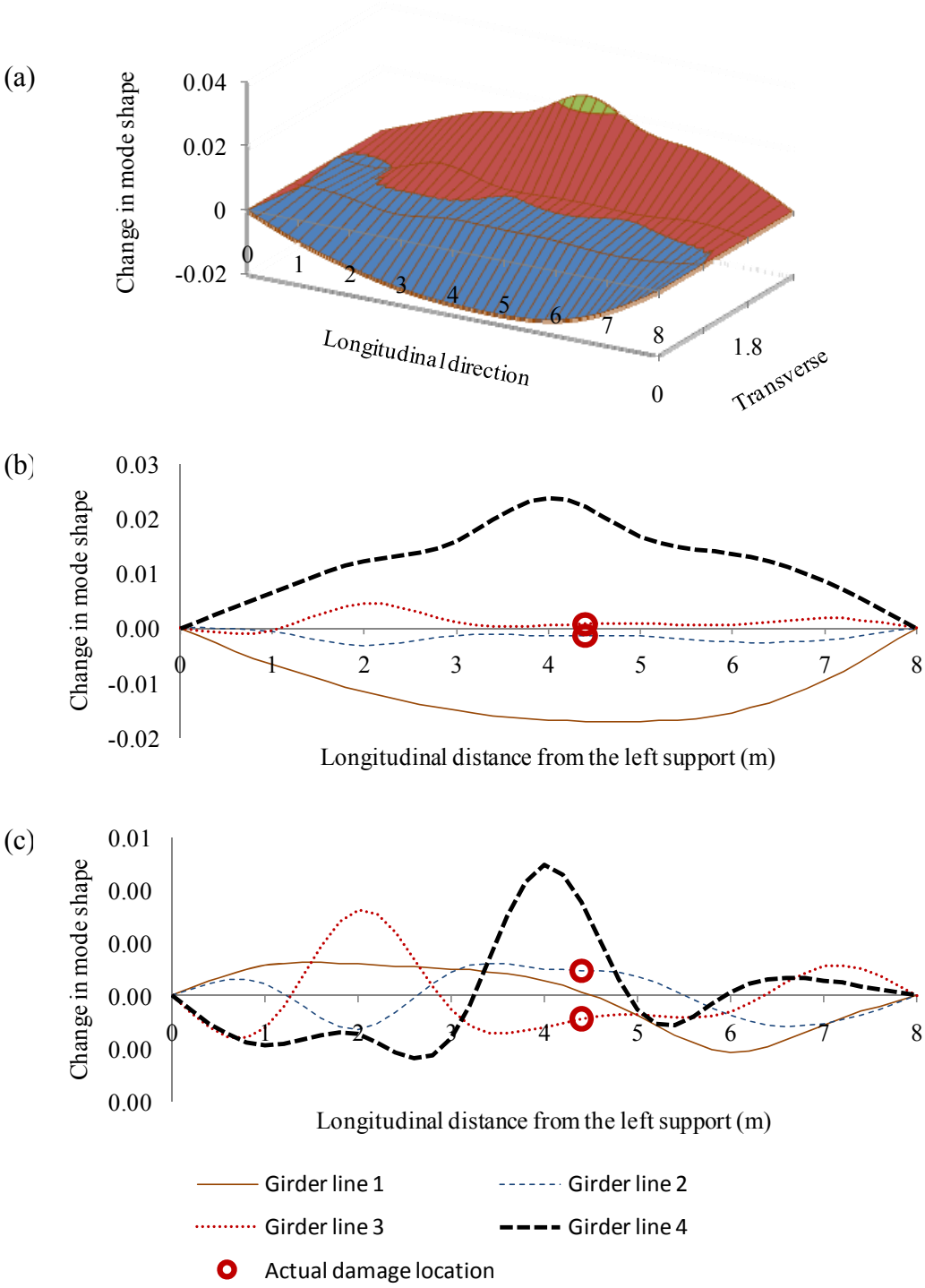

Figure K.9. Distribution of the change in the first mode shape due to Damage Case 10 using accelerometer data with harmonic excitation: (a) 3D figure with unit area normalization over all measurement points; (b) 2D figure with unit area normalization over all measurement points; and (c) 2D figure with unit area normalization along individual girder lines.

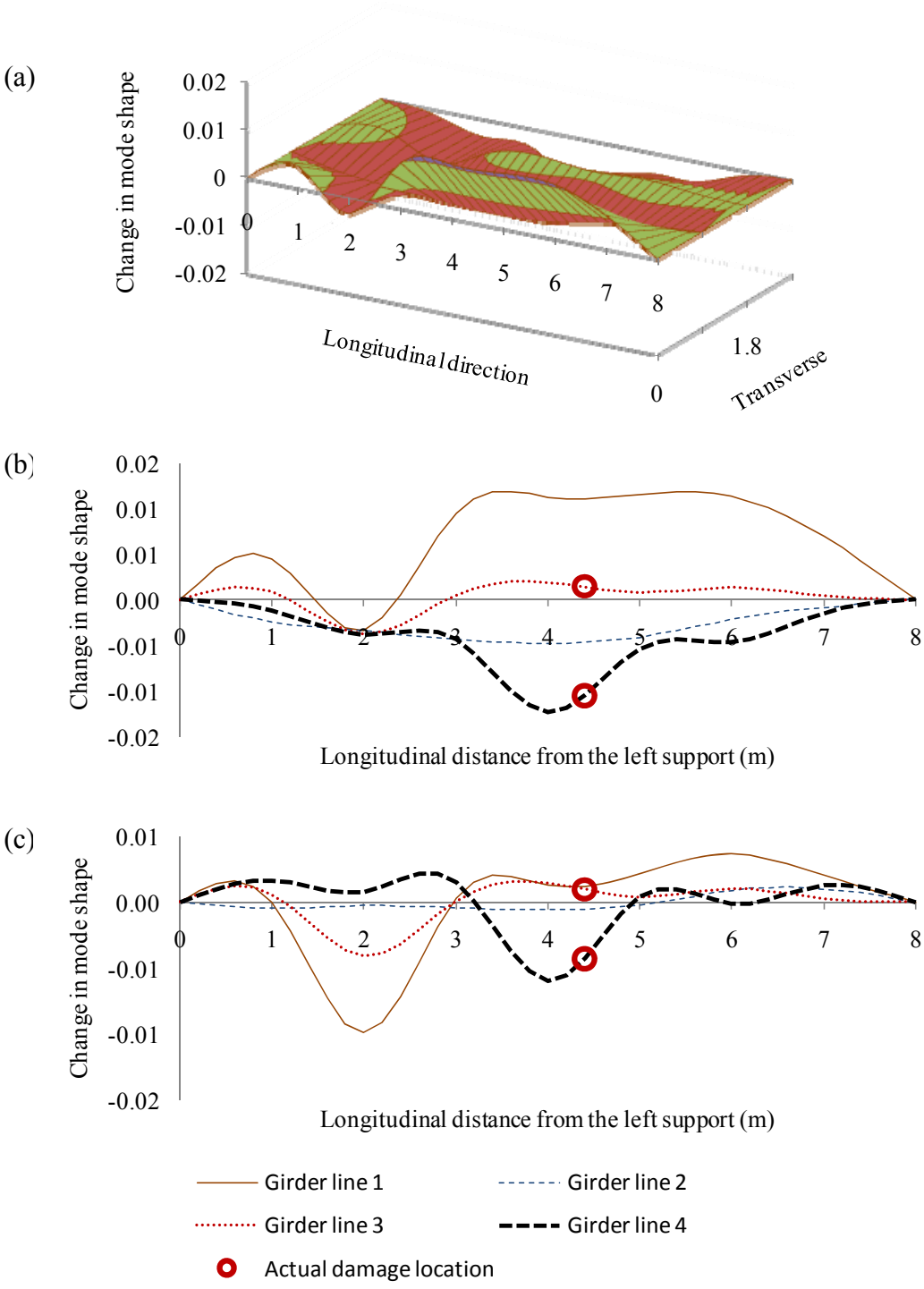

Figure K.10. Distribution of the change in the first mode shape due to Damage Case 11 using accelerometer data with harmonic excitation: (a) 3D figure with unit area normalization over all measurement points; (b) 2D figure with unit area normalization over all measurement points; and (c) 2D figure with unit area normalization along individual girder lines.

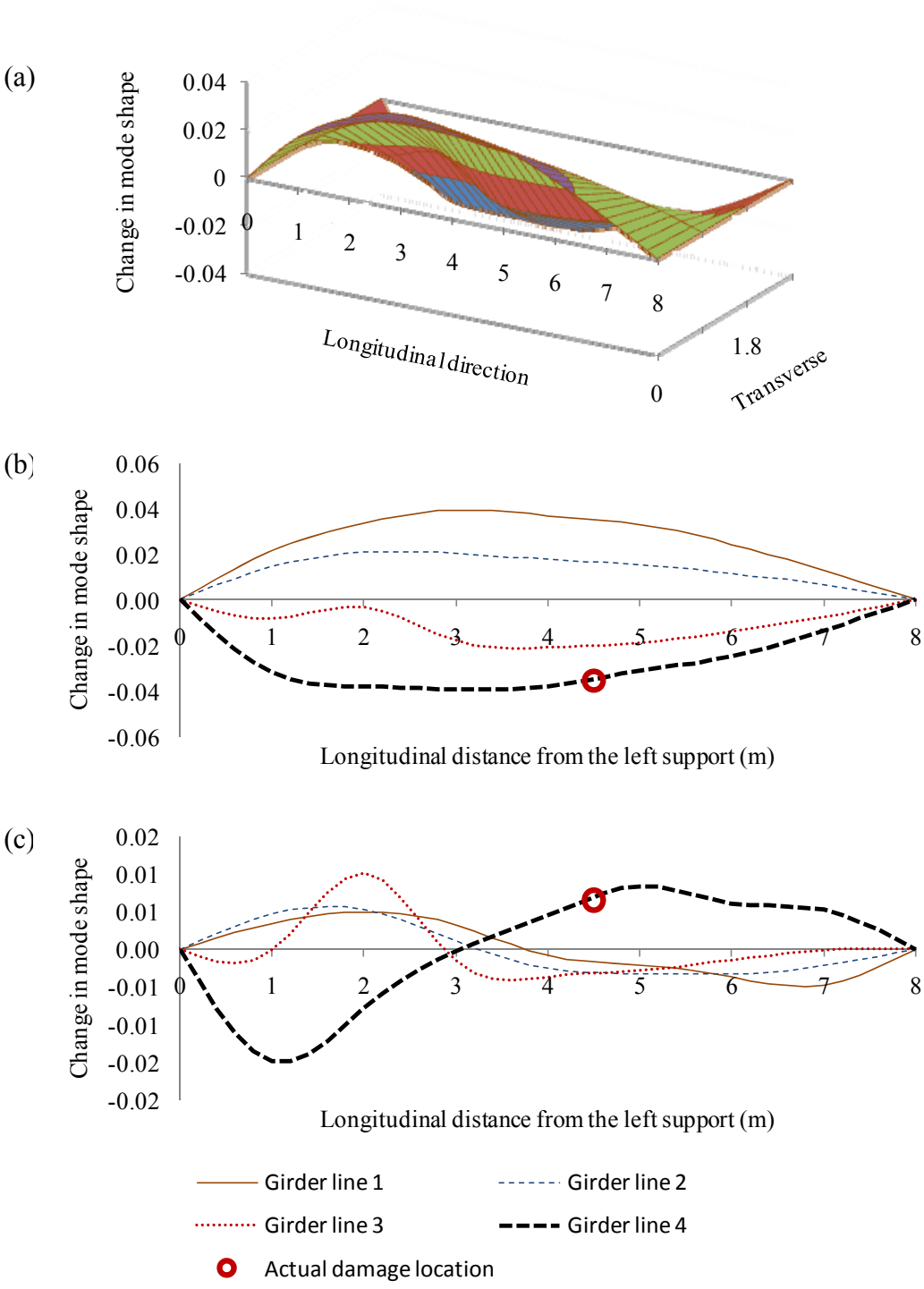

Figure K.11. Distribution of the change in the first mode shape due to Damage Case 12 using accelerometer data with harmonic excitation: (a) 3D figure with unit area normalization over all measurement points; (b) 2D figure with unit area normalization over all measurement points; and (c) 2D figure with unit area normalization along individual girder lines.

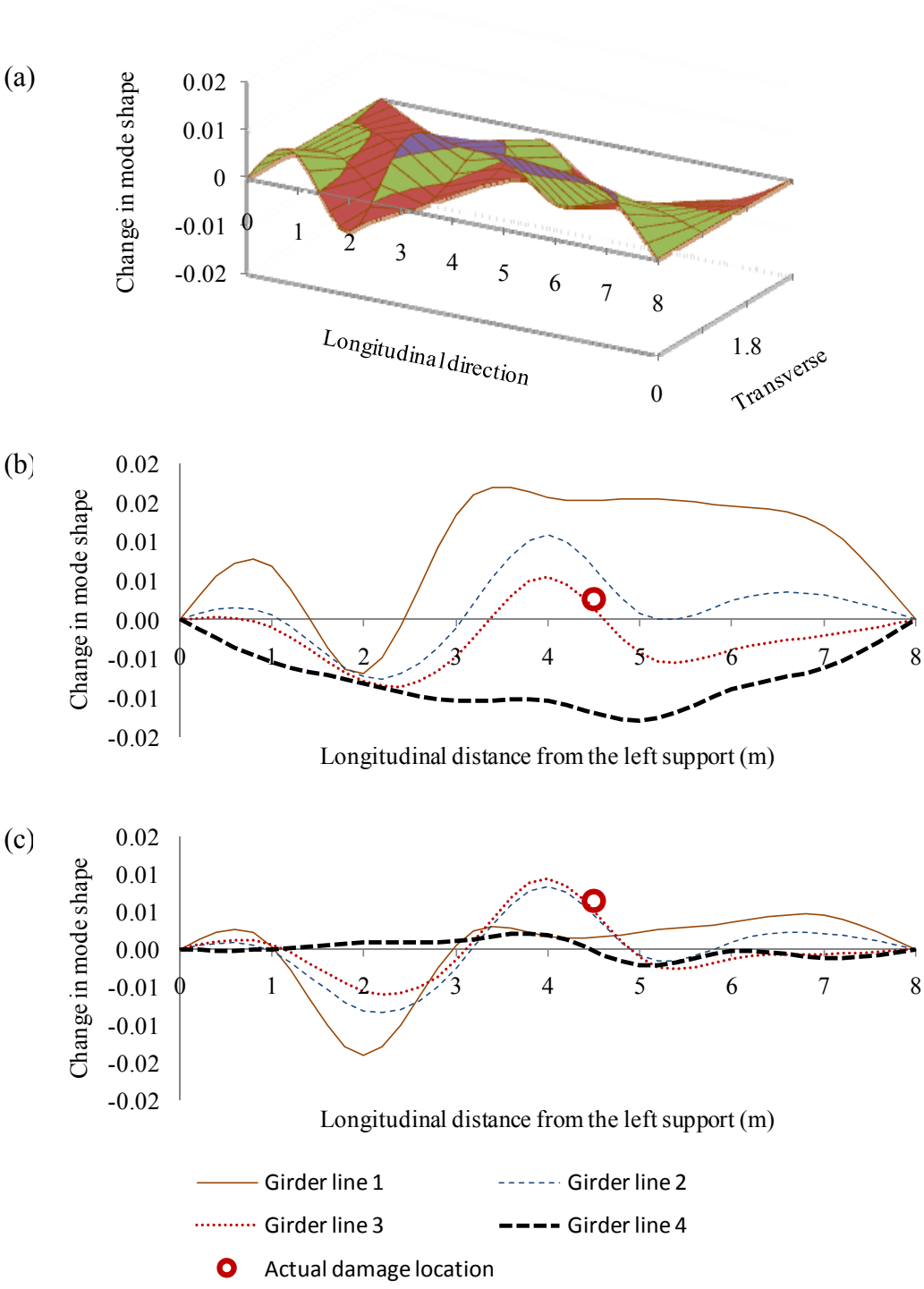

Figure K.12. Distribution of the change in the first mode shape due to Damage Case 13 using accelerometer data with harmonic excitation: (a) 3D figure with unit area normalization over all measurement points; (b) 2D figure with unit area normalization over all measurement points; and (c) 2D figure with unit area normalization along individual girder lines.

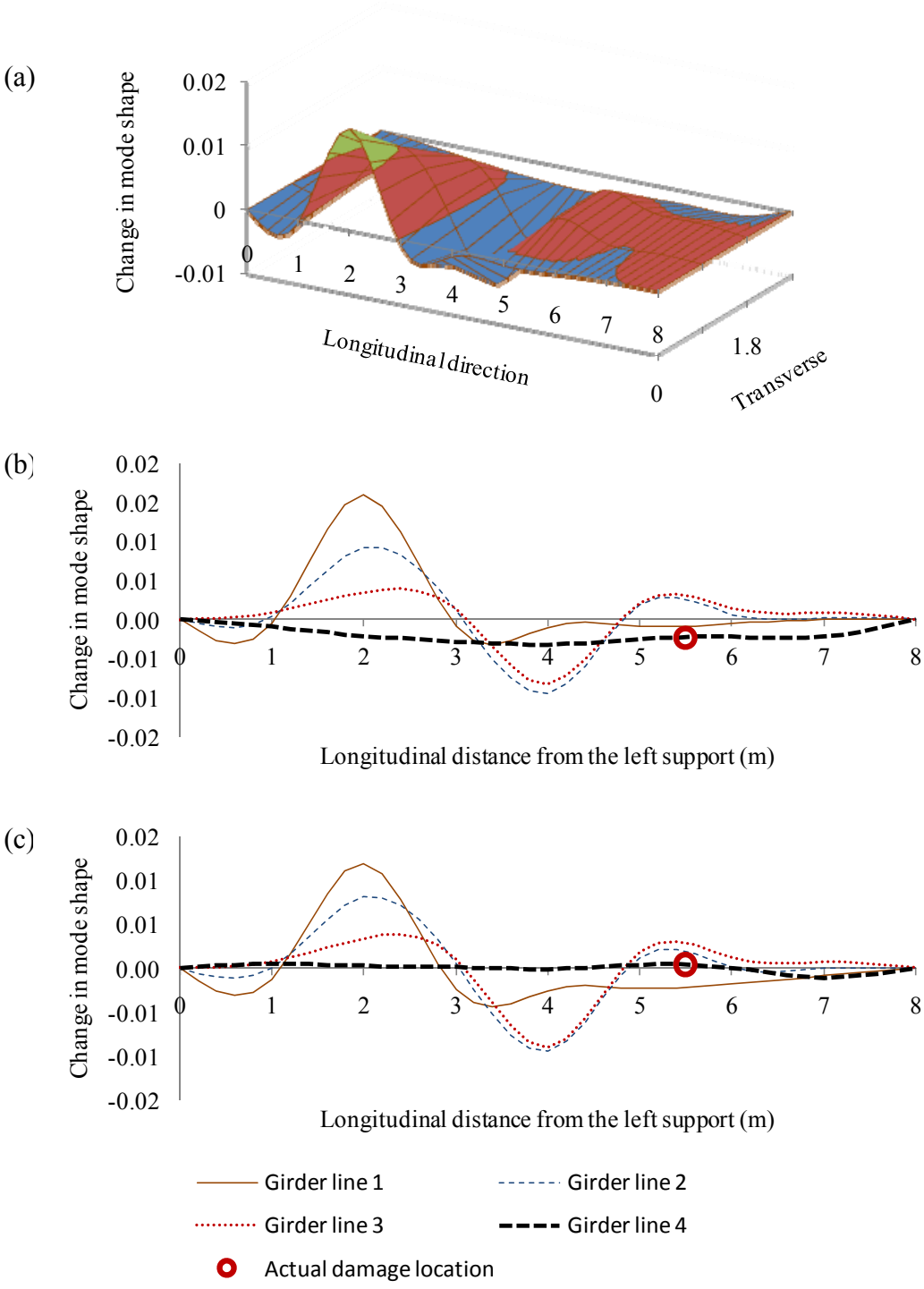

Figure K.13. Distribution of the change in the first mode shape due to Damage Case 14 using accelerometer data with harmonic excitation: (a) 3D figure with unit area normalization over all measurement points; (b) 2D figure with unit area normalization over all measurement points; and (c) 2D figure with unit area normalization along individual girder lines.

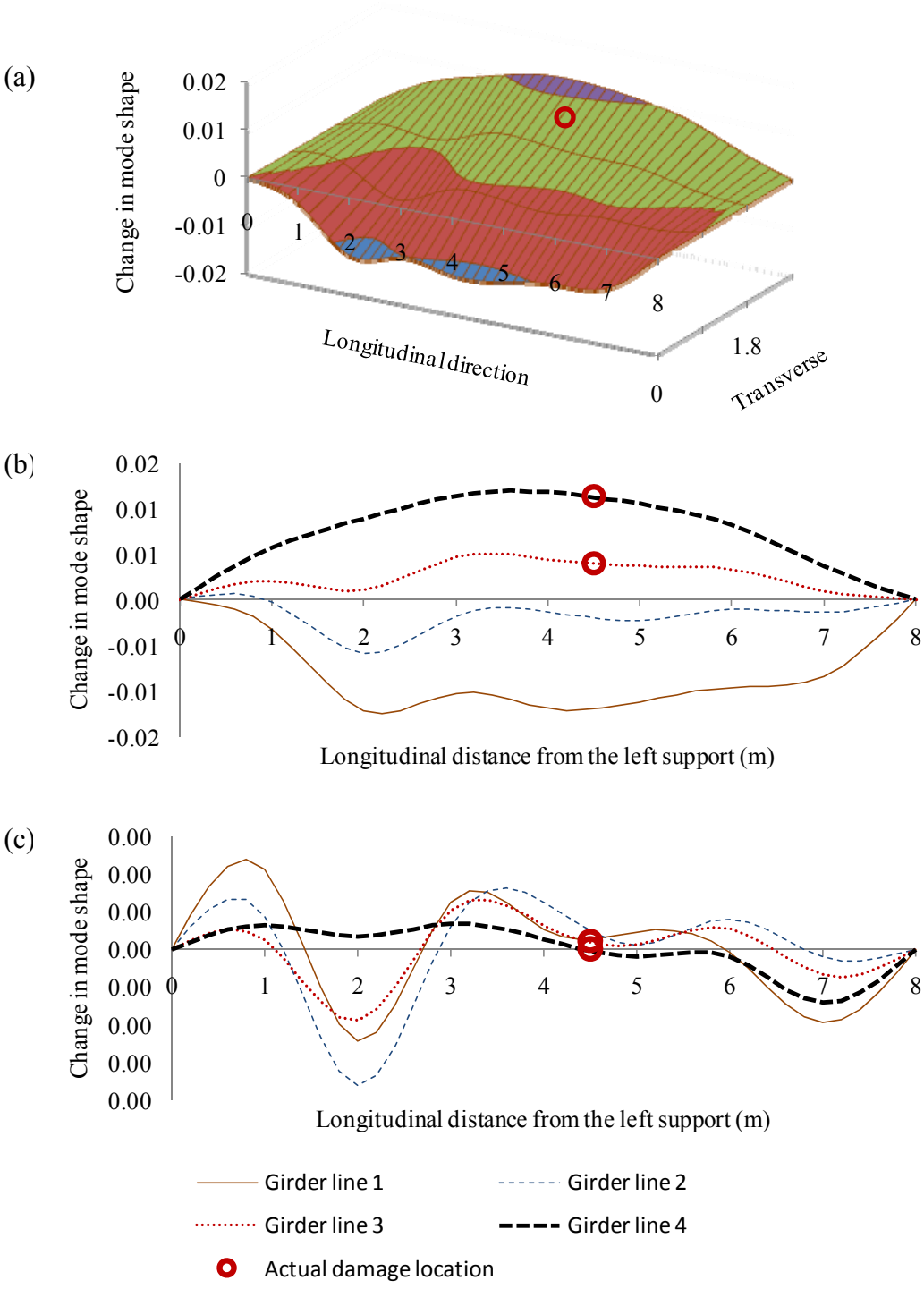

Figure K.14. Distribution of the change in the first mode shape due to Damage Case 15 using accelerometer data with harmonic excitation: (a) 3D figure with unit area normalization over all measurement points; (b) 2D figure with unit area normalization over all measurement points; and (c) 2D figure with unit area normalization along individual girder lines.

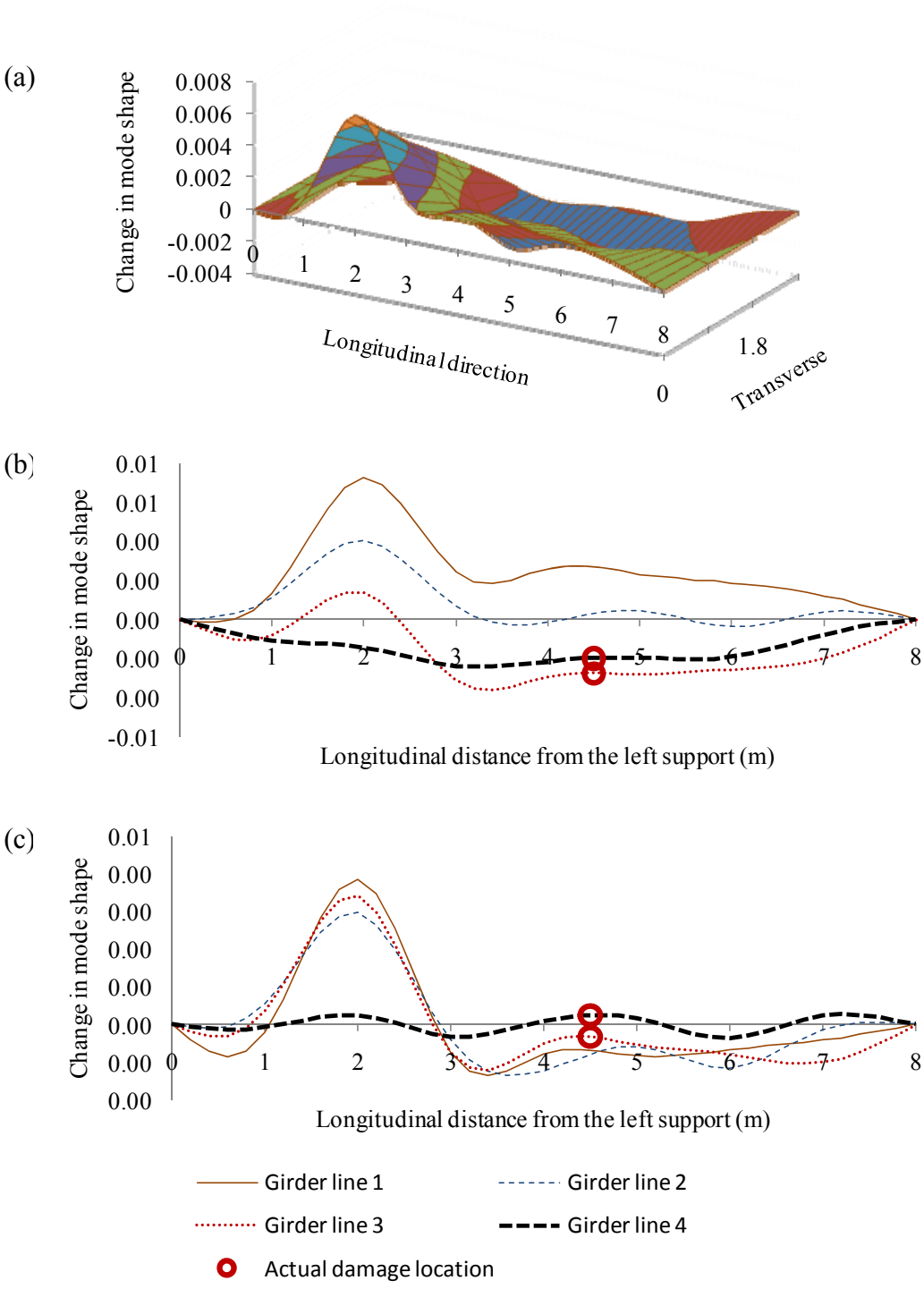

Figure K.15. Distribution of the change in the first mode shape due to Damage Case 16 using accelerometer data with harmonic excitation: (a) 3D figure with unit area normalization over all measurement points; (b) 2D figure with unit area normalization over all measurement points; and (c) 2D figure with unit area normalization along individual girder lines.

APPENDIX L. **USERS' MANUAL OF PROPORTIONAL CONTROLLER FOR HYDRAULIC VALVE**

TW002d

Travis Wiens
t.wiens@usask.ca

November 13, 2007

1 Introduction

When connected to a signal source, hydraulic proportional valve and actuator, and feedback LVDT, the controller applies a proportional control strategy to control the position of the actuator.

2 Warnings

This controller should be viewed as a prototype and is experimental in nature. Therefore, it should not be used in critical applications or situations where damage may result from malfunction.

The controller is not a sealed unit. It must not be exposed to moisture or hydraulic fluid, or be used in areas where explosion is a risk.

Be aware that the actuator is under automatic control and may behave unpredictably. Avoid placing body parts near the possible movement area of the actuator and load.

3 Maximum Values

- Input range: 0 - 5 V
- Feedback sensor range: 0 - 5V
- Control range: -10 - 10 V
- Power supply: 5 V DC, 1 A

4 Installation

1. Turn off hydraulic power source and power to LVDT and valve.
2. Connect the valve to the terminal strip. The positive valve terminal should be connected to the "O" (output) screw terminal and the negative valve connector should be connected to the "G" (Ground) screw terminal.
3. Connect the LVDT to the terminal strip. The positive LVDT signal should be connected to the "+" screw terminal and the negative signal to the "G" screw terminal.
4. Connect the desired signal source positive signal into the terminal marked "–" and the negative to "G".
5. The above connections are suitable for the shaker as tested, with the LVDT and valve connected such that applying a negative voltage to the valve leads to a positive velocity on the LVDT. If either signal is switched, the "+" and "–" connections may be switched. Note that the gain may have to be adjusted.
6. Apply power to the controller by plugging the AC adaptor into the barrel jack marked.
7. Begin generating the desired signal source.
8. Turn on LVDT and valve.
9. Turn on hydraulic power source.

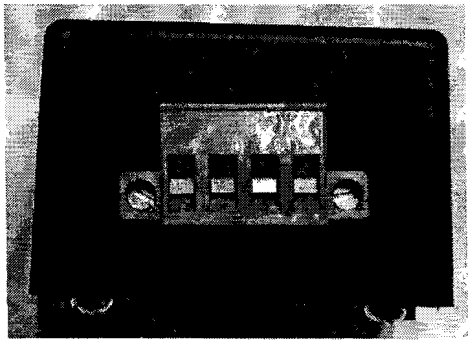

Figure 1: Terminal block. From left to right, the connections are "O" (Output), "+", "–", "G" (Ground).

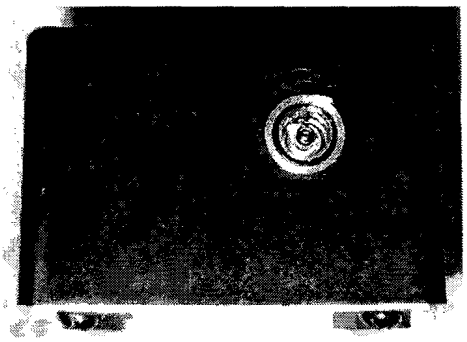

Figure 2: Power connection of controller.

5 Adjustment of Gain

The proportional gain has been set for proper operation. The gain may need to be adjusted due to changing components, changing operating conditions or wear on the system.

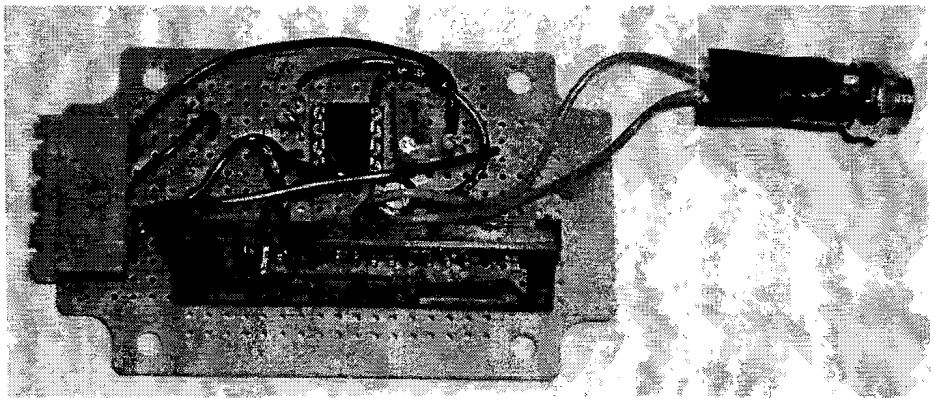

Figure 3: Controller circuit board. At the bottom is the DC-DC converter. Above this at left is the terminal block connection. The 8-pin DIP IC at the centre is the OP amp. To its right is the potentiometer used to set the gain. The power connector is at right.

1. Remove power from valve, pump, LVDT and controller.
2. Remove terminal block from valve by loosening the screws on either side of the block.
3. Remove the four screws on the bottom of the controller and remove the cover.

4. Remove the two screws securing the circuit board to the enclosure and gently remove the circuit board. Avoid static discharges near the board.
5. The gain may be adjusted by using a small screwdriver to rotate the trimmer pot, shown in Figure 3. Note that adjusting the gain may affect the "desired signal" required to achieve the same results.
6. Assembly is the reverse of disassembly.

6 Schematic

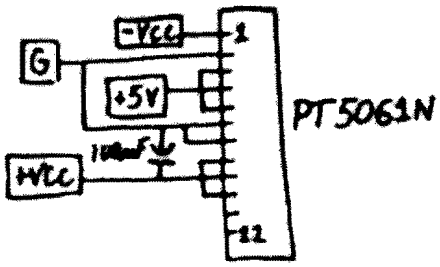

Figure 4: Schematic of DC-DC powersupply. The converter transforms 5 VDC into +/-12 V DC.

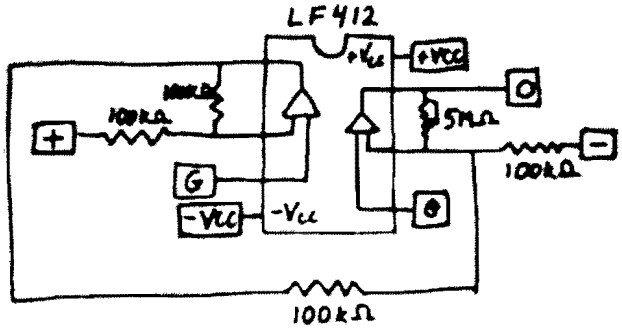

Figure 5: Schematic of op amp circuit.

An electrical schematic and bill of material can be found in Figures 4 and 5 and Table 1. Most components are common items and may be sourced from a variety of sources, such as Digikey. The LF412 chip is a dual operational amplifier which calculates the difference between "+" and "–" signals and applies a proportional gain to the difference. The large circuit board is a PT5061 DC-DC

Table 1: Bill of Materials

Ln	Description	Digikey Part No	Qty
1	PT5061N Regulator +/-12 V, +0.5 -0.25 A	PT5061N-ND	1
2	5.0 M Ohm Trim Pot	3296W-505LF-ND	1
3	5 V Wall Transformer 1.0 A	T977-P6P	1
4	100 k Ohm 1/4 W 5% Carbon Film Resistor	100KQBK	3
5	Terminal Block Plug 5.08 mm 4 pos	ED2411-ND	1
6	Terminal Block Header 5.08 mm 4 pos	ED1819	1
7	8 DIP socket	A32361	1
8	Dual JFET-IN OP amp LF412 8 DIP	296-7141-5-ND	1
9	100 uF 25 V Capacitor	P5152	1
10	2.5 mm Jack, Panel Mount	CP-6	1
11	Enclosure (Radioshack/Source)	2700283	1

converter required to provide the +/- 12 V rail voltaged required for a +/- 10 V output.

APPENDIX M. **MATHCAD ROUTINES FOR DATA PROCESSING**

M.1 Overview

This appendix lists the Mathcad routines used in this study. These routines included batch file operations for different trials in same health state, batch file operations for different health states, file operations for interpolation and normalization, routines for commonly available VBDD indicators, calculation of threshold values, distribution of the area of mode shape change, calculation of the probabilities of false indicator, and a sample calculation showing influence of different normalization schemes on the definition of change in mode shapes and change in mode shape curvatures.

M.2 Batch File Operation for Different Trials in Same Health State

Notes: Define the data files and paths by specifing the dir1, dir2, dir3, and dataname, where dir2 and dataname are vectors. r is rows and c is columns to read in.

```
batch_read(dir1, dir2, dir3, dataname, r, c) :=
    dir2_1 ← dir2  if rows(dir2) = 0
    dataname_1 ← dataname  if rows(dataname) = 0
    for i ∈ 1 .. last(dir2)
        for j ∈ 1 .. last(dataname)
            filename ← concat(dir1, dir2_i, dir3, dataname_j)
            M_i,j ← READFILE(filename, "delimited", r, c)
    M
```

Notes for summary function:

1. The purpose of this function is to summarize the results read from the batch_read function and batch write the summarized results to the output file which will be located in the same directory as the input files;
2. input files come from the batch_read function;
3. dir2 and dir3 are same as the values used in batch_read function;
4. output is a string value which give the filename of summarized results.

```
sets_summary(input, dir2, dir3, output) :=
    for i ∈ 1 .. rows(input)
        summary_i ← input_i,1
        for j ∈ 2 .. cols(input)
            summary_i ← augment(summary_i, input_i,j)
        filename ← concat(dir2_i, dir3, output)
        WRITEPRN(filename, summary_i)
    summary
```

Notes for dates_summary function:

1. input is the file read from batch_read including only mode shape information from all files;
2. file1 is the first file including all information of that file;
3. dir2 is testing dates.

```
dates_summary(input, file1, dir2) :=
    summary ← augment(file1^⟨2⟩, file1^⟨3⟩, file1^⟨4⟩)
    for i ∈ 1 .. rows(input)
        sum_i ← input_i,1
        for j ∈ 2 .. cols(input)  if cols(input) ≥ 2
            sum_i ← sum_i + input_i,j
        avg_i ← sum_i / cols(input)        Notes: average the results from different sets.
        summary ← augment(summary, avg_i)
    title ← augment("Note", "X", "Y", dir2^T)
    results ← stack(title, summary)
    results
```

```
N3_unit_norm(mode) :=
    N3 ← mode_3
    for i ∈ 1 .. last(mode)
        norm1_i ← mode_i / N3
    SumsqR ← norm1^T · norm1
    for i ∈ 1 .. last(mode)
        norm2_i ← norm1_i / √SumsqR
    norm2
```

The mode shapes were normalized to the 3rd node, this normalization will make sure that the mode shapes from different sets will keep consistant (i.e. to eliminate the effect of two reversed mode shape, which is actually identical). Then, the mode shape were normalized used unit norm normalization method.

```
sets_summary_xls(input, file1, dir2) :=
    summary ← augment(file1^⟨2⟩, file1^⟨3⟩, file1^⟨4⟩)
    summary_1,1 ← "--"
    summary_1,2 ← "--"
    summary_1,3 ← "Freq"
    summary_2,1 ← "--"
    summary_2,2 ← "--"
    summary_2,3 ← "Stdv"
    n ← rows(input_1)
    freq_stev ← submatrix(input_1, 1, 2, 1, 1)
    mode ← submatrix(input_1, 3, n, 1, 1)
    norm ← N3_unit_norm(mode)
    both ← stack(freq_stev, norm)
    sum ← both
    for j ∈ 2 .. rows(input)                    if rows(input) ≥ 2
        freq_stev ← submatrix(input_j, 1, 2, 1, 1)
        mode ← submatrix(input_j, 3, n, 1, 1)
        norm ← N3_unit_norm(mode)
        both ← stack(freq_stev, norm)
        sum ← augment(sum, both)
    summary ← augment(summary, sum)
    title ← augment("Note", "X", "Y", dir2^T)
    results ← stack(title, summary)
    results
```

Notes: This function is to combine different sets into one file. At the same time, the mode shapes were normalized to the 3rd node, this normalization will make sure that the mode shapes from different sets will keep consistant (i.e. to eliminate the effect of two reversed mode shape, which is actually identical). Then, the mode shape were normalized used unit norm normalization method.

Acceleration Mode 1 with Harmonic input:

Input informations (need ajustment according different types):

Testing dates, recorded sets and corresponding directories.

dir1 := CWD

	1
1	"Dec 03 07"
2	"Dec 11 07"
3	"Jan 18 08"
4	"Jan 21 08"
5	"Feb 25 08"
6	"Mar 03 08"
7	"Mar 07 08"
8	"Mar 08 08"
9	"Mar 10 08"
10	"Mar 11 08"
11	"Mar 14 08"
12	"Mar 15 08"
13	"May 26 08"
14	"July 04 08"
15	"July 05 08"
16	"July 18 08"
17	"July 19 08"

sets :=

	1
1	"Set 11111_Acceleration.shp"
2	"Set 22222_Acceleration.shp"
3	"Set 33333_Acceleration.shp"
4	"Set 44444_Acceleration.shp"
5	"Set 55555_Acceleration.shp"

setfile :=

	1
1	"set1"
2	"set2"
3	"set3"
4	"set4"
5	"set5"

Date of sets summary to wirit out in sequency:

d := 1

H_M1_Acc := "\r500n500\I2.5A0.4F12.61\Acceleration\"

dir2 := date dir3 := H_M1_Acc dataname := sets

Output information:

Batch read-in mode shape files including only mode information:

shps := batch_read[dir1, dir2, dir3, dataname, 1, $\binom{6}{6}$]

Need ajusting in some cases

Read-in the first mode shape file including all information:

file1 := batch_read(dir1, $dir2_1$, dir3, $dataname_1$, 1, 1)$_1$

Summarizing the mode shapes over different sets and writing the data into a file in the same directory:

set_summary_mode := sets_summary(shps, dir2, dir3, "mode 1_H_Acc.txt")

Summary of mode shape over different sets in one file. change the column number to control the different test date to consideration.

input := $(shps^T)^{\langle d \rangle}$

set_summary_model := sets_summary_xls(input, file1, setfile)

...\Mode 1_H_Acc.xls

Write the results into a Excel file.

set_summary_model

Part of sample output:

set_summary_model =

	1	2	3	4	5	6
1	"Note"	"X"	"Y"	"set1"	"set2"	"set3"
2	"--"	"--"	"Freq"	12.725	12.725	12.725
3	"--"	"--"	"Stdv"	0	0	0
4	1	0	0	0	0	0
5	2	1	0	0.125033	0.12498301	0.1249955
6	3	2	0	0.20060071	0.20055847	0.20055903
7	4	3	0	0.25634003	0.25629998	0.25633561
8	5	4	0	0.27461957	0.27458737	0.27461791
9	6	5	0	0.25762365	0.25759738	0.25762697
10	7	6	0	0.20789806	0.20786662	0.20790574
11	8	7	0	0.13295157	0.13292946	0.13296009
12	9	8	0	0	0	0
13	10	0	0.9	0	0	0
14	11	1	0.9	0.11619855	0.11619391	0.11618486
15	12	2	0.9	0.18539831	0.18538108	0.18535704
16	13	3	0.9	0.23464115	0.23462866	0.23463446
17	14	4	0.9	0.24968175	0.24968556	0.24969184
18	15	5	0.9	0.23191458	0.23192094	0.23192774
19	16	6	0.9	0.18365049	0.18364796	0.18366594
20	17	7	0.9	0.11165143	0.11166733	0.1116695
21	18	8	0.9	0	0	0
22	19	0	1.8	0	0	0
23	20	1	1.8	0.10826464	0.10823994	0.1082124
24	21	2	1.8	0.17191708	0.17192795	0.17192986
25	22	3	1.8	0.21679761	0.21679707	0.21672806
26	23	4	1.8	0.23001863	0.2300195	0.22995645
27	24	5	1.8	0.21237997	0.212401	0.21233503
28	25	6	1.8	0.16652914	0.16654707	0.16649775
29	26	7	1.8	0.09882467	0.09884379	0.0988194
30	27	8	1.8	0	0	0
31	28	0	2.7	0	0	0
32	29	1	2.7	0.09703627	0.09705452	0.09704683
33	30	2	2.7	0.15753141	0.15757022	0.15756825
34	31	3	2.7	0.19843522	0.19848383	0.1984921
35	32	4	2.7	0.21012026	0.21016565	0.21018592
36	33	5	2.7	0.19424537	0.1942969	0.19432026
37	34	6	2.7	0.15188324	0.15192196	0.15194437
38	35	7	2.7	0.09018471	0.09020037	0.09022695
39	36	8	2.7	0	0	...

Acceleration Mode 2 with Harmonic input:

Input informations (need ajustment according different types):
Testing dates, recorded sets and corresponding directories.

dir3 := "\r500n500\I2.5A0.4F13.74\Acceleration\" *Need to be ajusted*

Output information:

Batch read-in mode shape files including only mode information:

$$shps := batch\_read\left[dir1, dir2, dir3, dataname, 1, \begin{pmatrix} 6 \\ 6 \end{pmatrix}\right]$$

Need ajusting in some cases

Read-in the first mode shape file including all information:

$$file1 := batch\_read(dir1, dir2_1, dir3, dataname_1, 1, 1)_1$$

Summarizing the mode shapes over different sets and writing the data into a file in the same directory:

$$set\_summary\_mode := sets\_summary(shps, dir2, dir3, "mode 2\_H\_Acc.txt")$$

Summary of mode shape over different sets in one file. change the column number to control the different test date to consideration.

$$input := \left(shps^T\right)^{\langle d \rangle}$$

$$set\_summary\_model := sets\_summary\_xls(input, file1, setfile)$$

...\Mode 2_H_Acc.xls

set_summary_model

Acceleration Modes with White Noise input:

Input informations (need ajustment according different types):

Testing dates, recorded sets and corresponding directories.

dir3 := "\r1000n1000\I2.5S0.35\Acceleration\" *Need to be ajusted*

Output information:

Mode 1_WN

shps := batch_read[dir1, dir2, dir3, dataname, 1, (6 6)] **Need ajusting in some cases**

Read-in the first mode shape file including all information:

file1 := batch_read(dir1, dir2_1, dir3, dataname_1, 1, 1)_1

Summarizing the mode shapes over different sets and writing the data into a file in the same directory:

set_summary_mode := sets_summary(shps, dir2, dir3, "Mode 1_WN_Acc.txt") *Pay attention to file name*

Summary of mode shape over different sets in one file. change the column number to control the different test date to consideration.

input := (shps^T)^⟨d⟩

set_summary_model := sets_summary_xls(input, file1, setfile)

...\Mode 1_WN_Acc.xls

set_summary_model

Mode 2_WN

Mode 3_WN

Mode 4_WN

Mode 5_WN

Strain Mode 1 with Harmonic input:

Input informations (need ajustment according different types):
Testing dates, recorded sets and corresponding directories.

dir3 := "\r500n500\I2.5A0.4F12.61\Strain\\"

sets :=

	1
1	"set 1_1_strain.shp"
2	"set 1_2_strain.shp"
3	"set 1_3_strain.shp"
4	"set 1_4_strain.shp"
5	"set 1_5_strain.shp"

dataname := sets

Output information:

Batch read-in mode shape files including only mode information:

$$shps := batch\_read\left[dir1, dir2, dir3, dataname, 1, \begin{pmatrix} 6 \\ 6 \end{pmatrix}\right]$$ Need ajusting in some cases

Read-in the first mode shape file including all information:

$$file1 := batch\_read(dir1, dir2_1, dir3, dataname_1, 1, 1)_1$$

Summarizing the mode shapes over different sets and writing the data into a file in the same directory:

$$set\_summary\_mode := sets\_summary(shps, dir2, dir3, "mode\ 1\_H\_Str.txt")$$

Summary of mode shape over different sets in one file. change the column number to control the different test date to consideration.

$$input := \left(shps^T\right)^{\langle d \rangle}$$

$$set\_summary\_model := sets\_summary\_xls(input, file1, setfile)$$

...\Mode 1_H_Str.xls

set_summary_model

Strain Mode 2 with Harmonic input:

Strain Modes with White Noise input:

Input informations (need ajustment according different types):

Testing dates, recorded sets and corresponding directories.

dir3 := "\r1000n1000\I2.5S0.35\Strain\" *Need to be ajusted*

Output information:

Mode 1_WN

shps := batch_read[dir1, dir2, dir3, dataname, 1, (6 / 6)] **Need ajusting in some cases**

Read-in the first mode shape file including all information:

file1 := batch_read(dir1, dir2$_1$, dir3, dataname$_1$, 1, 1)$_1$

Summarizing the mode shapes over different sets and writing the data into a file in the same directory:

set_summary_mode := sets_summary(shps, dir2, dir3, "Mode 1_WN_Str.txt") *Pay attention to file name*

Summary of mode shape over different sets in one file. change the column number to control the different test date to consideration.

input := $(\text{shps}^{T})^{\langle d \rangle}$

set_summary_model := sets_summary_xls(input, file1, setfile)

...\Mode 1_WN_Str.xls

set_summary_model

Mode 2_WN

Mode 3_WN

Mode 4_WN

Mode 5_WN

M.3 Batch File Operation for Different Health States

Notes: Define the data files and paths by specifing the dir1, dir2, dir3, and dataname, where dir2 and dataname are vectors. r is rows and c is columns to read in.

```
batch_read(dir1, dir2, dir3, dataname, r, c) :=
    dir2_1 ← dir2  if rows(dir2) = 0
    dataname_1 ← dataname  if rows(dataname) = 0
    for i ∈ 1 .. last(dir2)
        for j ∈ 1 .. last(dataname)
            filename ← concat(dir1, dir2_i, dir3, dataname_j)
            M_i,j ← READFILE(filename, "delimited", r, c)
    M
```

Notes for summary function:

1. The purpose of this function is to summarize the results read from the batch_read function and batch write the summarized results to the output file which will be located in the same directory as the input files;
2. input files come from the batch_read function;
3. dir2 and dir3 are same as the values used in batch_read function;
4. output is a string value which give the filename of summarized results.

```
sets_summary(input, dir2, dir3, output) :=
    for i ∈ 1 .. rows(input)
        summary_i ← input_i,1
        for j ∈ 2 .. cols(input)
            summary_i ← augment(summary_i, input_i,j)
        filename ← concat(dir2_i, dir3, output)
        WRITEPRN(filename, summary_i)
    summary
```

Batch read-in Excel files:

```
batch_read_excel(dir1, dir2, dir3, dataname, r, c) :=
    dir2_1 ← dir2  if rows(dir2) = 0
    dataname_1 ← dataname  if rows(dataname) = 0
    for i ∈ 1 .. last(dir2)
        for j ∈ 1 .. last(dataname)
            filename ← concat(dir1, dir2_i, dir3, dataname_j)
            M_i,j ← READFILE(filename, "Excel", r, c)
    M
```

Notes for dates_summary function:

1. input is the file read from batch_read including only mode shape information from all files;
2. file1 is the first file including all information of that file;
3. dir2 is testing dates.

$$\text{dates\_summary}(\text{input}, \text{file1}, \text{dir2}) :=$$

```
title ← augment("Note", "X", "Y", dir2^T)
for j ∈ 1 .. cols(input)
    summary_j ← augment (file1_1,j)^⟨1⟩, (file1_1,j)^⟨2⟩, (file1_1,j)^⟨3⟩
    for i ∈ 1 .. rows(input)
        sum ← (input_i,j)^⟨1⟩
        n ← cols(input_i,j)
        for k ∈ 2 .. n
            sum ← sum + (input_i,j)^⟨k⟩
        avg ← sum / n
        summary_j ← augment(summary_j, avg)
    results_j ← stack(title, summary_j)
results
```

Acceleration Mode 1 with Harmonic input:

Input informations (need ajustment according different types):
Testing dates, recorded sets and corresponding directories.

dir1 := CWD

date :=

	1
1	"Dec 03 07"
2	"Dec 11 07"
3	"Jan 18 08"
4	"Jan 21 08"
5	"Feb 25 08"
6	"Mar 03 08"
7	"Mar 07 08"
8	"Mar 08 08"
9	"Mar 10 08"
10	"Mar 11 08"
11	"Mar 14 08"
12	"Mar 15 08"
13	"May 26 08"
14	"July 04 08"
15	"July 05 08"
16	"July 18 08"
17	"July 19 08"

dir2 := date dir3 := "\Summary\" dataname :=

	1
1	"Mode 1_H_Acc.xls"
2	"Mode 1_WN_Acc.xls"
3	"Mode 2_H_Acc.xls"
4	"Mode 2_WN_Acc.xls"
5	"Mode 3_WN_Acc.xls"
6	"Mode 4_WN_Acc.xls"
7	"Mode 5_WN_Acc.xls"
8	"Mode 1_H_Str.xls"
9	"Mode 1_WN_Str.xls"
10	"Mode 2_H_Str.xls"
11	"Mode 2_WN_Str.xls"
12	"Mode 3_WN_Str.xls"
13	"Mode 4_WN_Str.xls"
14	"Mode 5_WN_Str.xls"

Output information:

Batch read-in mode shape files:

$$shps := batch\_read\_excel(dir1, dir2, dir3, dataname, 4, 4)$$ Need ajusting in some cases

Read-in the first mode shape file including all information:

$$file1 := batch\_read\_excel\left[dir1, dir2_1, dir3, dataname, 4, \begin{pmatrix} 1 \\ 3 \end{pmatrix}\right]$$

Summary of the averaged mode shape over different testing dates:

$$date\_summary\_mode := dates\_summary(shps, file1, dir2)$$

...\Mode 1_H_Acc_Dec 03 - July 19.xls ...\Mode 1_WN_Acc_Dec 03 - July 19.xls ...\Mode 2_H_Acc_Dec 03 - July 19.xls ...\Mode 2_WN_Acc_Dec 03 - July 19.xls

$date\_summary\_mode_1$ $date\_summary\_mode_2$ $date\_summary\_mode_3$ $date\_summary\_mode_4$

...\Mode 3_WN_Acc_Dec 03 - July 19.xls ...\Mode 4_WN_Acc_Dec 03 - July 19.xls ...\Mode 5_WN_Acc_Dec 03 - July 19.xls

$date\_summary\_mode_5$ $date\_summary\_mode_6$ $date\_summary\_mode_7$

...\Mode 1_H_Str_Dec 03 - July 19.xls ...\Mode 1_WN_Str_Dec 03 - July 19.xls ...\Mode 2_H_Str_Dec 03 - July 19.xls ...\Mode 2_WN_Str_Dec 03 - July 19.xls

$date\_summary\_mode_8$ $date\_summary\_mode_9$ $date\_summary\_mode_{10}$ $date\_summary\_mode_{11}$

...\Mode 3_WN_Str_Dec 03 - July 19.xls ...\Mode 4_WN_Str_Dec 03 - July 19.xls ...\Mode 5_WN_Str_Dec 03 - July 19.xls

$date\_summary\_mode_{12}$ $date\_summary\_mode_{13}$ $date\_summary\_mode_{14}$

M.4 Batch File Operation for Interpolation and Normalization

2D cubic spline interpolation:

Coordinate of sensors:

X_Strain :=

	1
1	0
2	1.2
3	2.4
4	4
5	5.6
6	6.8
7	8

X_GL4 :=

	1
1	0
2	1.2
3	2.4
4	5.6
5	6.8
6	8

X_Accl :=

	1
1	0
2	1
3	2
4	3
5	4
6	5
7	6
8	7
9	8

Y :=

	1
1	0
2	0.9
3	1.8
4	2.7

Interpolated locations for Y direction to make the number of rows equal to the number of columns:

Y_Accl :=

	1
1	0
2	0.3
3	0.6
4	0.9
5	1.2
6	1.5
7	1.8
8	2.1
9	2.7

Y_Strain :=

	1
1	0
2	0.45
3	0.9
4	1.35
5	1.8
6	2.25
7	2.7

Note: Since 2D cubic spline interpolation function need a 2D array with equal rows and columns. As a results, this function converts 1D mode shapes to 2D arrays with equal rows and columns by 1D cubic spline interpolation fit first. Also, the strain mode over Girderline 4 was interpolated to 5 sensors from 4 ones by the cubic spline function.

$$
\begin{aligned}
&M\_2D(Data, Type) := \\
&\quad \text{if } Type = \text{"accl"} \\
&\quad\quad \text{for } j \in 1..4 \\
&\quad\quad\quad \text{for } i \in 1..9 \\
&\quad\quad\quad\quad M_{i,j} \leftarrow Data_{i+(j-1)\cdot 9} \\
&\quad\quad \text{for } i \in 1..9 \\
&\quad\quad\quad Mode^{\langle i \rangle} \leftarrow \text{interp}\left(\text{lspline}\left(Y, \left(M^{T}\right)^{\langle i \rangle}\right), Y, \left(M^{T}\right)^{\langle i \rangle}, Y\_Accl\right) \\
&\quad \text{if } Type = \text{"strain"} \\
&\quad\quad \text{for } j \in 1..3 \\
&\quad\quad\quad \text{for } i \in 1..7 \\
&\quad\quad\quad\quad M_{i,j} \leftarrow Data_{i+(j-1)\cdot 7} \\
&\quad\quad \text{for } k \in 1..6 \\
&\quad\quad\quad GL4_k \leftarrow Data_{21+k} \\
&\quad\quad GL4\_fit \leftarrow \text{interp}\left(\text{lspline}\left(X\_GL4, GL4\right), X\_GL4, GL4, X\_Strain\right) \\
&\quad\quad M^{\langle 4 \rangle} \leftarrow GL4\_fit \\
&\quad\quad \text{for } i \in 1..7 \\
&\quad\quad\quad Mode^{\langle i \rangle} \leftarrow \text{interp}\left(\text{lspline}\left(Y, \left(M^{T}\right)^{\langle i \rangle}\right), Y, \left(M^{T}\right)^{\langle i \rangle}, Y\_Strain\right) \\
&\quad Mode^{T}
\end{aligned}
$$

Specify X and Y n-vectors that determine the mesh for the matrix:

$$
Mxy(Type) := \begin{cases} \text{augment}(X\_Accl, Y\_Accl) & \text{if } Type = \text{"accl"} \\ \text{augment}(X\_Strain, Y\_Strain) & \text{if } Type = \text{"strain"} \end{cases}
$$

Computed spline coefficients:

$$
coef(Data, Type) := \text{lspline}(Mxy(Type), M\_2D(Data, Type))
$$

Fitting function for surface:

$$
fit(Data, Type, x, y) := \text{interp}\left[coef(Data, Type), Mxy(Type), M\_2D(Data, Type), \begin{pmatrix} x \\ y \end{pmatrix}\right]
$$

Final fit function by supply flowing parameters:

- mode: orginal input mode shape data recorded in one column
- sensor: "accl" or "strain"
- xgrid: expected number of gridlines in x direction for final interpolated mode shape (original input is 9 for "accl" and 7 for "strain");
- ygrid: expected number of gridlines in y direction for final interpolated mode shape (original input is 4 for "accl" and 4 for "strain");
- Fit_Mode_2D means the Fit mode shape was stored in a 2D array with xgrid rows and ygrid columns;
- Fit_Mode_1D means the Fit mode shape was stacked in a 1D array with xgrid time ygrid elements;

$$\text{Fit\_Mode\_2D}(\text{mode}, \text{sensor}, \text{xgrid}, \text{ygrid}) :=$$
$$\text{for } i \in 1 .. \text{xgrid}$$
$$\quad \text{X\_interp}_i \leftarrow 8 \cdot \frac{i - 1}{\text{xgrid} - 1}$$
$$\text{for } j \in 1 .. \text{ygrid}$$
$$\quad \text{Y\_interp}_j \leftarrow 2.7 \cdot \frac{j - 1}{\text{ygrid} - 1}$$
$$\text{for } t \in 1 .. \text{rows}(\text{X\_interp})$$
$$\quad \text{for } s \in 1 .. \text{rows}(\text{Y\_interp})$$
$$\quad\quad \text{Mode\_2D}_{t,s} \leftarrow \text{fit}(\text{mode}, \text{sensor}, \text{X\_interp}_t, \text{Y\_interp}_s)$$
$$\text{Mode\_2D}$$

$$\text{Fit\_Mode\_1D}(\text{mode}, \text{sensor}, \text{xgrid}, \text{ygrid}) :=$$
$$\text{for } i \in 1 .. \text{xgrid}$$
$$\quad \text{X\_interp}_i \leftarrow 8 \cdot \frac{i - 1}{\text{xgrid} - 1}$$
$$\text{for } j \in 1 .. \text{ygrid}$$
$$\quad \text{Y\_interp}_j \leftarrow 2.7 \cdot \frac{j - 1}{\text{ygrid} - 1}$$
$$\text{for } t \in 1 .. \text{rows}(\text{X\_interp})$$
$$\quad \text{for } s \in 1 .. \text{rows}(\text{Y\_interp})$$
$$\quad\quad \text{Mode\_2D}_{t,s} \leftarrow \text{fit}(\text{mode}, \text{sensor}, \text{X\_interp}_t, \text{Y\_interp}_s)$$
$$\text{for } j \in 1 .. \text{rows}(\text{Y\_interp})$$
$$\quad \text{for } i \in 1 .. \text{rows}(\text{X\_interp})$$
$$\quad\quad \text{Mode\_1D}_{i+(j-1)\cdot\text{rows}(\text{X\_interp})} \leftarrow \text{Mode\_2D}_{i,j}$$
$$\text{Mode\_1D}$$

Unit-area normalization over all points:

Numerical Quadrature based on revised Trapezoidal rule:

$$\begin{aligned}
&\text{trap_area}(\text{mode}) := \left|\begin{array}{l}
\text{xgrid} \leftarrow \text{rows}(\text{mode}) \\
\text{area} \leftarrow 0 \\
\text{for } i \in 1 .. (\text{xgrid} - 1) \\
\quad \left|\begin{array}{l}
\text{trap} \leftarrow \dfrac{\text{mode}_i + \text{mode}_{i+1}}{2\cdot(\text{xgrid} - 1)} \quad \text{if } \text{mode}_i \cdot \text{mode}_{i+1} \geq 0 \\
\text{trap} \leftarrow \dfrac{(\text{mode}_i)^2 + (\text{mode}_{i+1})^2}{2\cdot(\text{xgrid} - 1)\cdot(\text{mode}_i + \text{mode}_{i+1})} \quad \text{otherwise} \\
\text{area} \leftarrow \text{area} + \text{trap}
\end{array}\right. \\
\text{area}
\end{array}\right.
\end{aligned}$$

Numerical Quadrature based on cubic spline fit curve area, assume entire base equal to unit 1.

$$\begin{aligned}
&\text{area}(\text{input}, \text{ygrid}) := \left|\begin{array}{l}
r \leftarrow \text{rows}(\text{input}) \\
\text{xgrid} \leftarrow \dfrac{r}{\text{ygrid}} \\
\text{for } i \in 1 .. \text{xgrid} \\
\quad X_i \leftarrow \dfrac{i - 1}{(\text{xgrid} - 1)\cdot\text{ygrid}} \\
\text{sum} \leftarrow 0 \\
\text{for } j \in 1 .. \text{ygrid} \\
\quad \left|\begin{array}{l}
Y \leftarrow \text{submatrix}(\text{input}, (j - 1)\cdot\text{xgrid} + 1, j\cdot\text{xgrid}, 1, 1) \\
S \leftarrow \text{lspline}(X, Y) \\
\text{fit}(x) \leftarrow \text{interp}(S, X, Y, x) \\
\text{area} \leftarrow \displaystyle\int_0^{X_{\text{xgrid}}} \text{fit}(x)\ dx \\
\text{sum} \leftarrow \text{sum} + \text{area}
\end{array}\right. \\
\text{sum}
\end{array}\right.
\end{aligned}$$

Unit-area normalization function:

$$\begin{aligned}
&\text{unit_area_norm}(\text{mode}, \text{ygrid}) := \left|\begin{array}{l}
\text{area_sum} \leftarrow \text{area}(\text{mode}, \text{ygrid}) \\
\text{for } i \in 1 .. \text{rows}(\text{mode}) \\
\quad \text{norm}_i \leftarrow \dfrac{\text{mode}_i}{\text{area_sum}} \\
\text{norm}
\end{array}\right.
\end{aligned}$$

```
area_2d(modes, ygrid) :=
    r ← rows(modes)
    xgrid ← r / ygrid
    sub ← submatrix(modes, 1, xgrid, 1, 1)
    change ← area(sub, 1)
    for i ∈ 2 .. ygrid
        sub ← submatrix(modes, (i − 1)·xgrid + 1, i·xgrid, 1, 1)
        ch ← area(sub, 1)
        change ← stack(change, ch)
    change
```

Unit-area normalization over Gridline X:

```
unit_area_norm_x(mode, ygrid) :=
    n ← rows(mode)
    xgrid ← n / ygrid
    for j ∈ 1 .. xgrid
        mx_j ← mode_j
    normx ← unit_area_norm(mx, 1)
    for i ∈ 2 .. ygrid
        for j ∈ 1 .. xgrid
            mx_j ← mode_((i−1)·xgrid+j)
        modex ← unit_area_norm(mx, 1)
        normx ← stack(normx, modex)
    normx
```

Batch operation for Modes interpolation and normalization over all points:

Define normalization function [select either unit_norm(mode), or unit_norm_x(mode, ygrid)] :

```
norm_f(mode, xgrid, ygrid) := unit_norm(mode)
```

```
batch_normal_f(dir1, dir2, dir3, dataname, sensor, xgrid, ygrid, range) :=
  for i ∈ 1 .. xgrid
    X_interp_i ← 8 · (i − 1) / (xgrid − 1)
  for j ∈ 1 .. ygrid
    Y_interp_j ← 2.7 · (j − 1) / (ygrid − 1)
  for j ∈ 1 .. rows(Y_interp)
    for i ∈ 1 .. rows(X_interp)
      X_{i+(j−1)·rows(X_interp)} ← X_interp_i
      Y_{i+(j−1)·rows(X_interp)} ← Y_interp_j
  dates ← batch_read_excel[dir1, dir2, dir3, dataname, (1 1), 2]
  files ← batch_read_excel(dir1, dir2, dir3, dataname, range, 4)
  for i ∈ 1 .. cols(files)
    modes ← files_{1, i}
    for j ∈ 1 .. cols(modes)
      fit_modes^⟨j⟩ ← Fit_Mode_1D(modes^⟨j⟩, sensor, xgrid, ygrid)
      normal_modes^⟨j⟩ ← norm_f(fit_modes^⟨j⟩, xgrid, ygrid)
    combineXY ← augment(X, Y, normal_modes)
    combineTitle ← stack(dates_{1, i}, combineXY)
    batch_normal_i ← combineTitle
  batch_normal
```

Grid Points (Need ajusting according to requirements)

xgrid := 41

ygrid := 4

Acceleration Modes interpolation and normalization:

Input informations (need ajustment according different types):
Testing dates, recorded sets and corresponding directories.

dir1 := CWD

dir2 := "Summary"

dir3 := "\"

dataname :=

	1
1	"Mode 1_H_Acc_Dec 03 - July 19.xls"
2	"Mode 1_WN_Acc_Dec 03 - July 19.xls"
3	"Mode 2_H_Acc_Dec 03 - July 19.xls"
4	"Mode 2_WN_Acc_Dec 03 - July 19.xls"
5	"Mode 3_WN_Acc_Dec 03 - July 19.xls"
6	"Mode 4_WN_Acc_Dec 03 - July 19.xls"
7	"Mode 5_WN_Acc_Dec 03 - July 19.xls"

sensor := "accl"

range := 2

Notes: range equal to
- 2 for accl
- (2, 28) for bottom strain
- (29, 55) for middle strain
- (56, 82) for top strain

Calculation and writing

batch_normal := batch_normal_f(dir1, dir2, dir3, dataname, sensor, xgrid, ygrid, range)

Notes for writing:
Files have to be written one by one by changing file names and input matrix.

...\Mode 1_H.xls ...\Mode 1_WN.xls ...\Mode 2_H.xls

$batch\_normal_1$ $batch\_normal_2$ $batch\_normal_3$

...\Mode 2_WN.xls ...\Mode 3_WN.xls ...\Mode 4_WN.xls ...\Mode 5_WN.xls

$batch\_normal_4$ $batch\_normal_5$ $batch\_normal_6$ $batch\_normal_7$

Calculation and writing

M.5 Commonly Available VBDD Indicators

Change in Mode Shape

$$\text{change\_mode}(\text{undamage}, \text{damage}) := \text{damage} - \text{undamage}$$

$$\text{change\_mode\_2d}(\text{undamage}, \text{damage}) := \text{change\_mode}(\text{undamage}, \text{damage})$$

Change in Mode Shape Curvature

Notes: using relative beam length 1, as a result, h=1/(n-1);
using linear interpolation for end points at n=1 and n.

$$\text{curvature}(\text{modes}) := \left| \begin{array}{l} n \leftarrow \text{rows}(\text{modes}) \\ \text{for } i \in 2 .. (n-1) \\ \quad \text{curv}_i \leftarrow (\text{modes}_{i-1} - 2 \cdot \text{modes}_i + \text{modes}_{i+1}) \cdot (n-1)^2 \\ \text{curv}_1 \leftarrow 0 \\ \text{curv}_n \leftarrow 0 \\ \text{curv} \end{array} \right.$$

$$\text{change\_curvature}(\text{undamage}, \text{damage}) := \left| \begin{array}{l} \text{und} \leftarrow \text{curvature}(\text{undamage}) \\ d \leftarrow \text{curvature}(\text{damage}) \\ d - \text{und} \end{array} \right.$$

$$\text{change\_curvature\_2d}(\text{undamage}, \text{damage}) := \left| \begin{array}{l} r \leftarrow \text{rows}(\text{undamage}) \\ \text{xgrid} \leftarrow \frac{r}{\text{ygrid}} \\ \text{und} \leftarrow \text{submatrix}(\text{undamage}, 1, \text{xgrid}, 1, 1) \\ d \leftarrow \text{submatrix}(\text{damage}, 1, \text{xgrid}, 1, 1) \\ \text{change} \leftarrow \text{change\_curvature}(\text{und}, d) \\ \text{for } i \in 2 .. \text{ygrid} \\ \quad \left| \begin{array}{l} \text{und} \leftarrow \text{submatrix}\ \text{undamage}, (i-1) \cdot \text{xgrid} + 1, i \cdot \text{xgrid}, 1, 1 \\ d \leftarrow \text{submatrix}\ \text{damage}, (i-1) \cdot \text{xgrid} + 1, i \cdot \text{xgrid}, 1, 1 \\ \text{ch} \leftarrow \text{change\_curvature}(\text{und}, d) \\ \text{change} \leftarrow \text{stack}(\text{change}, \text{ch}) \end{array} \right. \\ \text{change} \end{array} \right.$$

Change in Flexibility

Notes: assume w1 and w1d equal to 1, it could be to have positive influence on the result.

$\omega_1 := 1 \quad \omega_{1d} := 1$

$$\text{change\_flexibility}(\text{undamage}, \text{damage}) := \left| \begin{array}{l} \text{und} \leftarrow \frac{1}{\omega_1^{\,2}} \cdot \text{undamage} \cdot \text{undamage}^{T} \\ \text{d} \leftarrow \frac{1}{\omega_{1d}^{\,2}} \cdot \text{damage} \cdot \text{damage}^{T} \\ \text{delta} \leftarrow \text{d} - \text{und} \\ \text{n} \leftarrow \text{rows}(\text{undamage}) \\ \text{for } i \in 1 .. \text{n} \\ \quad \text{del}_i \leftarrow \max\left(\text{delta}^{\langle i \rangle}\right) \\ \text{del} \end{array} \right.$$

$\text{ygrid} = 4$ change this value if necessary

$$\text{change\_flexibility\_2d}(\text{undamage}, \text{damage}) := \left| \begin{array}{l} \text{r} \leftarrow \text{rows}(\text{undamage}) \\ \text{xgrid} \leftarrow \frac{\text{r}}{\text{ygrid}} \\ \text{und} \leftarrow \text{submatrix}(\text{undamage}, 1, \text{xgrid}, 1, 1) \\ \text{d} \leftarrow \text{submatrix}(\text{damage}, 1, \text{xgrid}, 1, 1) \\ \text{change} \leftarrow \text{change\_flexibility}(\text{und}, \text{d}) \\ \text{for } i \in 2 .. \text{ygrid} \\ \quad \left| \begin{array}{l} \text{und} \leftarrow \text{submatrix}\left(\text{undamage}, (i-1)\cdot\text{xgrid}+1, i\cdot\text{xgrid}, 1, 1\right) \\ \text{d} \leftarrow \text{submatrix}\left(\text{damage}, (i-1)\cdot\text{xgrid}+1, i\cdot\text{xgrid}, 1, 1\right) \\ \text{ch} \leftarrow \text{change\_flexibility}(\text{und}, \text{d}) \\ \text{change} \leftarrow \text{stack}(\text{change}, \text{ch}) \end{array} \right. \\ \text{change} \end{array} \right.$$

Damage index mothod

Notes: assume the length of a segment from a to b equal to unit 1 for digital integration. This assumption has on influence on the results.

$$\text{damage\_index}(\text{und}, d) :=$$
$$n \leftarrow \text{rows}(\text{und})$$
$$\text{sum1} \leftarrow 0$$
$$\text{sum2} \leftarrow 0$$
$$\text{for } i \in 2 .. (n-1)$$
$$\quad \text{sum1} \leftarrow \text{sum1} + (\text{und}_{i-1} - 2\,\text{und}_i + \text{und}_{i+1})^2$$
$$\quad \text{sum2} \leftarrow \text{sum2} + (d_{i-1} - 2\,d_i + d_{i+1})^2$$
$$\quad \text{sub1}_i \leftarrow (\text{und}_{i-1} - 2\,\text{und}_i + \text{und}_{i+1})^2$$
$$\quad \text{sub2}_i \leftarrow (d_{i-1} - 2\,d_i + d_{i+1})^2$$
$$\text{for } i \in 2 .. (n-1)$$
$$\quad c_i \leftarrow \frac{(\text{sub2}_i + \text{sum2}) \cdot \text{sum1}}{(\text{sub1}_i + \text{sum1}) \cdot \text{sum2}}$$
$$c_1 \leftarrow 0$$
$$b \leftarrow \text{submatrix}(c, 2, n-1, 1, 1)$$
$$\mu \leftarrow \text{mean}(b)$$
$$\sigma \leftarrow \text{Stdev}(b)$$
$$\text{for } i \in 1 .. n-2$$
$$\quad z_i \leftarrow \frac{b_i - \mu}{\sigma}$$
$$z \leftarrow \text{stack}(0, z, 0)$$
$$z$$

$\text{ygrid} = 4$ change this value if necessary

$$\text{damage\_index\_2d}(\text{undamage}, \text{damage}) :=$$
$$r \leftarrow \text{rows}(\text{undamage})$$
$$\text{xgrid} \leftarrow \frac{r}{\text{ygrid}}$$
$$\text{und} \leftarrow \text{submatrix}(\text{undamage}, 1, \text{xgrid}, 1, 1)$$
$$d \leftarrow \text{submatrix}(\text{damage}, 1, \text{xgrid}, 1, 1)$$
$$\text{change} \leftarrow \text{damage\_index}(\text{und}, d)$$
$$\text{for } i \in 2 .. \text{ygrid}$$
$$\quad \text{und} \leftarrow \text{submatrix}\ \text{undamage}, (i-1) \cdot \text{xgrid} + 1, i \cdot \text{xgrid}, 1, 1$$
$$\quad d \leftarrow \text{submatrix}\ \text{damage}, (i-1) \cdot \text{xgrid} + 1, i \cdot \text{xgrid}, 1, 1$$
$$\quad \text{ch} \leftarrow \text{damage\_index}(\text{und}, d)$$
$$\quad \text{change} \leftarrow \text{stack}(\text{change}, \text{ch})$$
$$\text{change}$$

Change in uniform flexibility curvature method

$$\text{change\_uniform}(\text{undamage}, \text{damage}) := \left| \begin{array}{l} \text{und} \leftarrow \frac{1}{\omega_1^{\,2}} \cdot \text{undamage} \cdot \text{undamage}^{T} \\ \text{d} \leftarrow \frac{1}{\omega_{1d}^{\,2}} \cdot \text{damage} \cdot \text{damage}^{T} \\ \text{undf} \leftarrow \text{und}^{\langle 1 \rangle} \\ \text{df} \leftarrow \text{d}^{\langle 1 \rangle} \\ \text{n} \leftarrow \text{rows}(\text{undamage}) \\ \text{for } \ i \in 2 .. \text{n} \\ \quad \left| \begin{array}{l} \text{undf} \leftarrow \text{undf} + \text{und}^{\langle i \rangle} \\ \text{df} \leftarrow \text{df} + \text{d}^{\langle i \rangle} \end{array} \right. \\ \text{curv1} \leftarrow \text{curvature}(\text{undf}) \\ \text{curv2} \leftarrow \text{curvature}(\text{df}) \\ \text{uniform} \leftarrow \ \text{curv2} \ - \ \text{curv1} \\ \text{uniform} \end{array} \right.$$

$\text{ygrid} := 4$ change this value if necessary

$$\text{change\_uniform\_2d}(\text{undamage}, \text{damage}) := \left| \begin{array}{l} \text{r} \leftarrow \text{rows}(\text{undamage}) \\ \text{xgrid} \leftarrow \frac{\text{r}}{\text{ygrid}} \\ \text{und} \leftarrow \text{submatrix}(\text{undamage}, 1, \text{xgrid}, 1, 1) \\ \text{d} \leftarrow \text{submatrix}(\text{damage}, 1, \text{xgrid}, 1, 1) \\ \text{change} \leftarrow \text{change\_uniform}(\text{und}, \text{d}) \\ \text{for } \ i \in 2 .. \text{ygrid} \\ \quad \left| \begin{array}{l} \text{und} \leftarrow \text{submatrix}\ \text{undamage}, (i-1) \cdot \text{xgrid} + 1, i \cdot \text{xgrid}, 1, 1 \\ \text{d} \leftarrow \text{submatrix}\ \text{damage}, (i-1) \cdot \text{xgrid} + 1, i \cdot \text{xgrid}, 1, 1 \\ \text{ch} \leftarrow \text{change\_uniform}(\text{und}, \text{d}) \\ \text{change} \leftarrow \text{stack}(\text{change}, \text{ch}) \end{array} \right. \\ \text{change} \end{array} \right.$$

M.6 Threshold Values, Distribution of the Area of Mode Shape Change, and Probability of False Indicator

Batch read-in Excel files:

batch_read_excel(dir1, dir2, dir3, dataname, r, c) :=

$dir2_1 \leftarrow dir2 \quad \text{if} \quad rows(dir2) = 0$

$dataname_1 \leftarrow dataname \quad \text{if} \quad rows(dataname) = 0$

for $i \in 1 .. last(dir2)$

  for $j \in 1 .. last(dataname)$

    $filename \leftarrow concat(dir1, dir2_i, dir3, dataname_j)$

    $M_{i,j} \leftarrow READFILE(filename, "Excel", r, c)$

M

Input files:

Input informations (need ajustment according different types):

Testing dates, recorded sets and corresponding directories.

dir1 := CWD

dir2 :=

	1
1	"Dec 03 07"
2	"Dec 11 07"
3	"Jan 18 08"
4	"Jan 21 08"
5	"Feb 25 08"
6	"Mar 03 08"
7	"Mar 07 08"
8	"Mar 08 08"
9	"Mar 10 08"
10	"Mar 11 08"
11	"Mar 14 08"
12	"Mar 15 08"
13	"May 26 08"
14	"July 04 08"
15	"July 05 08"
16	"July 18 08"
17	"July 19 08"

sub_dir :=

	1
1	"\Summary\Damage detection\Change in mode shape\Unit area norm all 9by4\area summary\"
2	Summary\Damage detection\Change in mode shape\Unit area norm xgrid 9by4\area summary\"

$dir3 := sub\_dir_1$

dataname :=

	1
1	"Mode 1_H.xls"
2	"Mode 1_WN.xls"
3	"Mode 2_H.xls"
4	"Mode 2_WN.xls"
5	"Mode 3_WN.xls"
6	"Mode 4_WN.xls"
7	"Mode 5_WN.xls"

Summary of area change in mode shape:

Batch read-in mode shape files including only mode information:

$$file := batch\_read\_excel(dir1, dir2, dir3, dataname, 1, 1)$$

$$area\_sum := \left| \begin{array}{l} \text{for } j \in 1..cols(file) \\ \quad \left| \begin{array}{l} sum_j \leftarrow file_{1,j} \\ \text{for } i \in 2..rows(file) \\ \quad sum_j \leftarrow augment(sum_j, file_{i,j}) \end{array} \right. \\ total \leftarrow sum_1 \\ \text{for } j \in 2..cols(file) \\ \quad total \leftarrow stack(total, sum_j) \\ total \end{array} \right.$$

$cols(area\_sum) = 170$

$rows(area\_sum) = 42$

Assumed Normal Distribution:

Mean:

$$\mu\_n := \left| \begin{array}{l} \text{for } i \in 1..rows(area\_sum) \\ \quad D_i \leftarrow mean\left(area\_sum^T\right)^{\langle i \rangle} \\ D \end{array} \right.$$

Standard deviation:

$$\sigma\_n := \left| \begin{array}{l} \text{for } i \in 1..rows(area\_sum) \\ \quad D_i \leftarrow Stdev\left(area\_sum^T\right)^{\langle i \rangle} \\ D \end{array} \right.$$

Threshold at 90th and 95th percentile:

$$threshold\_n := \left| \begin{array}{l} th\_sum \leftarrow augment("Normal\_th\_90", "Normal\_th\_95") \\ \text{for } i \in 1..rows(area\_sum) \\ \quad \left| \begin{array}{l} threshold \leftarrow augment(qnorm(0.90, \mu\_n_i, \sigma\_n_i), qnorm(0.95, \mu\_n_i, \sigma\_n_i)) \\ th\_sum \leftarrow stack(th\_sum, threshold) \end{array} \right. \\ th\_sum \end{array} \right.$$

Assumed Log Normal Distribution:

Mean:

$$\mu\_Ln := \left| \begin{array}{l} \text{for } i \in 1 .. \text{rows}(area\_sum) \\ \quad D_i \leftarrow \text{mean } \ln\left(area\_sum^T\right)^{\langle i \rangle} \\ D \end{array} \right.$$

Standard deviation:

$$\sigma\_Ln := \left| \begin{array}{l} \text{for } i \in 1 .. \text{rows}(area\_sum) \\ \quad D_i \leftarrow \text{Stdev } \ln\left(area\_sum^T\right)^{\langle i \rangle} \\ D \end{array} \right.$$

Threshold at 90th and 95th percentile:

$$threshold\_Ln := \left| \begin{array}{l} th\_sum \leftarrow \text{augment}("Lognormal\_th\_90" , "Lognormal\_th\_95") \\ \text{for } i \in 1 .. \text{rows}(area\_sum) \\ \quad \left| \begin{array}{l} threshold \leftarrow \text{augment}(\text{qlnorm}(0.90 , \mu\_Ln_i , \sigma\_Ln_i) , \text{qlnorm}(0.95 , \mu\_Ln_i , \sigma\_Ln_i)) \\ th\_sum \leftarrow \text{stack}(th\_sum , threshold) \end{array} \right. \\ th\_sum \end{array} \right.$$

Actual distribution function:

cumulative distribution function:

$$\text{cpdf}(input) := \left| \begin{array}{l} n \leftarrow \text{rows}(input) \\ sorted \leftarrow \text{sort}(input) \\ a \leftarrow 1 \\ b \leftarrow 1 \\ \text{while } b \le n \\ \quad \left| \begin{array}{l} X_a \leftarrow sorted_b \\ \text{while } X_a = sorted_{b+1} \quad \text{if } b < n \\ \quad b \leftarrow b + 1 \\ Y_a \leftarrow \dfrac{b}{n} \\ b \leftarrow b + 1 \\ a \leftarrow a + 1 \end{array} \right. \\ output \leftarrow \text{augment}(X , Y) \\ output \end{array} \right.$$

Threshold at 90th and 95th percentile:

```
threshold_ac := | th_sum ← augment("Act_th_90" , "Act_th_95")
                | for i ∈ 1 .. rows(area_sum)
                |     distr ← cpdf (area_sum^T)^⟨i⟩
                |     threshold ← augment(distr_153,1 , distr_162,1)
                |     th_sum ← stack(th_sum , threshold)
                | th_sum
```

unnormalized distribution density function:

```
df(input, segment) := | mi ← min(input)
                      | ma ← max(input)
                      | interval ← (ma − mi / segment)
                      | r ← rows(input)
                      | input ← sort(input)
                      | ef ← 0
                      | output ← augment(0 , 0)
                      | for i ∈ 0 .. segment
                      |     count ← 0
                      |     sum ← 0
                      |     for j ∈ 1 .. r
                      |       if mi + i·interval − interval/2 < input_j ≤ mi + i·interval + interval/2
                      |           count ← count + 1
                      |           sum ← sum + input_j
                      |     if count > 0
                      |         tm ← augment(sum / count , count)
                      |         output ← stack(output , tm)
                      | output ← stack output , ( 2ma  0.1 )
                      | output
```

normalized distribution density function:

Area covered by the unnormalized density function:

$$\text{density\_area}(\text{input}) := \left| \begin{array}{l} X \leftarrow \text{input}^{\langle 1 \rangle} \\ Y \leftarrow \text{input}^{\langle 2 \rangle} \\ \text{fit}(x) \leftarrow \text{linterp}(X, Y, x) \\ \text{ar} \leftarrow \displaystyle\int_{\min(X)}^{\max(X)} \text{fit}(x)\, dx \\ \text{ar} \end{array} \right.$$

Normalized density function:

$$\text{normalized\_df}(\text{input}, \text{segment}) := \left| \begin{array}{l} \text{output} \leftarrow \text{df}(\text{input}, \text{segment}) \\ n \leftarrow \text{rows}(\text{output}) \\ \text{d\_area} \leftarrow \text{density\_area}(\text{output}) \\ \text{output}^{\langle 2 \rangle} \leftarrow \dfrac{\text{output}^{\langle 2 \rangle}}{\text{d\_area}} \\ \text{sub} \leftarrow \text{submatrix}(\text{output}, 2, n-1, 1, 2) \\ \text{sub} \end{array} \right.$$

Result summary:

$$\text{result\_sum}(\text{input}, \text{segment}) := \left| \begin{array}{l} \text{title1} \leftarrow \text{augment}(\text{"X"}, \text{"Freq"}) \\ \text{freq} \leftarrow \text{df}(\text{input}, \text{segment}) \\ \text{title2} \leftarrow \text{augment}(\text{"Min"}, \text{"Max"}) \\ \text{min\_max} \leftarrow \text{augment}(\min(\text{input}), \max(\text{input})) \\ \text{title3} \leftarrow \text{augment}(\text{"X"}, \text{"Density"}) \\ \text{normalized} \leftarrow \text{normalized\_df}(\text{input}, \text{segment}) \\ \text{temp1} \leftarrow \text{stack}(\text{title1}, \text{freq}) \\ \text{temp2} \leftarrow \text{stack}(\text{title2}, \text{min\_max}, \text{title3}, \text{normalized}) \\ \text{output} \leftarrow \text{augment}(\text{temp1}, \text{temp2}) \\ \text{output} \end{array} \right.$$

Result output:

$tp := 2 \qquad segment := 5$

...\tp_n5.xls

$$\text{result\_sum}\left(\text{area\_sum}^{T}\right)^{\langle tp \rangle}, \text{segment}$$

Testing procedures considered for plotting:

$r := 42$

Area change and the corresponding probability:

$th := cpdf\left(area\_sum^{T}\right)^{\langle r \rangle}$

90th Percentile: $p90 := 153$ $actual\_th95 := th_{p90,1} = 0.26702273$ $actual\_prob := th_{p90,2} = 90 \cdot \%$

95th Percentile: $p95 := 162$ $actual\_th95 := th_{p95,1} = 0.36631964$ $actual\_prob := th_{p95,2}$

x-axis of assumed distributions:

$x := th^{\langle 1 \rangle}$

Cumulative distribution function of Normal distribution:

$norm(t) := pnorm(t, \mu\_n_r, \sigma\_n_r)$

Cumulative distribution function of Lognormal distribution:

$lgnorm(t) := plnorm(t, \mu\_Ln_r, \sigma\_Ln_r)$

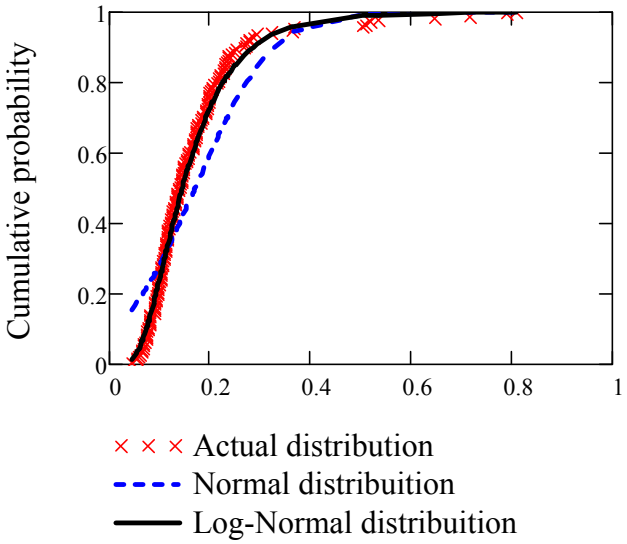

$title := augment("X", "Actual", "Normal", "Log-Norma$

$data := augment\left(x, th^{\langle 2 \rangle}, norm(x), lgnorm(x)\right)$

$plot\_data := stack(title, data)$

...\cdp.xls

plot_data

Coefficient of determination R-Square:

Total sum of squares:

$$SS_{tot}(y) := \sum_{i=1}^{rows(y)} (y_i - mean(y))^2$$

The sum of squares of residuals :

Ordinary and weighted least squares
The best-fit curve is often assumed to be that which minimizes the sum of squared . This is the (ordinary) (OLS) approach. However, in cases where the dependent variable does not have constant variance a sum of weighted squared residuals may be minimized; see . Each weight should ideally be equal to the reciprocal of the variance of the observation, but weights may be recomputed on each iteration, in an iteratively weighted least squares algorithm.

$$SS_{err}(y,f) := \sum_{i=1}^{rows(y)} (y_i - f_i)^2$$ for original least squares

$$SS_{err\_w}(y,f) := \sum_{i=1}^{rows(y)} \left(\frac{y_i - f_i}{y_i}\right)^2$$ (for weighted least squares)

Residual standard deviation:
the standard deviation of the residuals (residuals = differences between observed and predicted values). It is calculated as follows:

$$StdR(y,f) := \sqrt{\frac{\sum_{i=1}^{rows(y)} (y_i - f_i)^2}{rows(y) - 2}}$$ regular residual standard deviation (or Standard error of estimate)

$$StdR\_w(y,f) := \sqrt{\frac{\sum_{i=1}^{rows(y)} \left(\frac{y_i - f_i}{y_i}\right)^2}{rows(y) - 2}}$$ weighted residual standard deviation (or Standard error of estimate)

R-square:

$$R\_Square(y,f) := 1 - \frac{SS_{err}(y,f)}{SS_{tot}(y)}$$

R-Square and standard errors based on Cumulative Dsitribution functions:

```
R_square_sum := | r_sum1 ← augment("R2_n", "SSerr_n", "StdR_n", "W_StdR_n")
                | r_sum2 ← augment("R2_lgn", "SSerr_lgn", "StdR_lgn", "W_StdR_lgn")
                | r_sum ← augment(r_sum1, r_sum2)
                | for r ∈ 1 .. rows(area_sum)
                |     distr ← cpdf (area_sum^T)^⟨r⟩
                |     X ← distr^⟨1⟩
                |     Y ← distr^⟨2⟩
                |     f_norm ← norm(X)
                |     f_lgnorm ← lgnorm(X)
                |     err1 ← SS_err(Y, f_norm)
                |     err2 ← SS_err(Y, f_lgnorm)
                |     stdr1 ← StdR(Y, f_norm)
                |     stdr2 ← StdR(Y, f_lgnorm)
                |     stdr1w ← StdR_w(Y, f_norm)
                |     stdr2w ← StdR_w(Y, f_lgnorm)
                |     R_sq1 ← R_Square(Y, f_norm)
                |     R_sq2 ← R_Square(Y, f_lgnorm)
                |     R_sq ← augment(R_sq1, err1, stdr1, stdr1w, R_sq2, err2, stdr2, stdr2w)
                |     r_sum ← stack(r_sum, R_sq)
                | r_sum
```

Results summary and output

title_mean := stack("Normal Mean", μ_n)

title_std := stack("Normal STD", σ_n)

summary := augment(title_mean, title_std, threshold_ac, threshold_Ln, threshold_n, R_square_sum

...\Threshold and standard errors.xls

...\Area summary.xls

summary area_sum

Part of summary result:

summary =

	1	2	3	4	5
1	"Normal Mean"	"Normal STD"	"Act_th_90"	"Act_th_95"	gnormal_th_90"
2	0.00141697	0.00107138	0.0028835	0.0035926	0.00379488
3	0.00170129	0.0007275	0.00247491	0.00325764	0.0025683
4	0.00230243	0.00102508	0.00346954	0.00427984	0.00334363
5	0.00531793	0.00518958	0.00645764	0.01792083	0.00853913
6	0.00653018	0.00252703	0.00937213	0.01073326	0.00953098
7	0.00325612	0.00338555	0.00352712	0.01418534	0.00519156
8	0.00532558	0.00217632	0.00818653	0.00970211	0.00828951
9	0.02532351	0.00607721	0.0320982	0.0361508	0.03396546
10	0.03776464	0.0083548	0.04883533	0.0517702	0.04872723
11	0.06866162	0.01440428	0.0875684	0.09297759	0.08910203
12	0.09652527	0.02258459	0.12357489	0.13633643	0.12762836
13	0.04281005	0.01043486	0.05725089	0.06163811	0.05619855
14	0.01766498	0.01665966	0.03900192	0.05093513	0.05178742
15	0.00843858	0.00675301	0.01749179	0.02030148	0.0161647
16	0.01137913	0.00836968	0.02289542	0.02911297	0.0208864
17	0.02053768	0.01473792	0.04619171	0.04835126	0.0381196
18	0.02717711	0.0172801	0.05149765	0.05946237	0.04809481
19	0.02446662	0.03318087	0.05625041	0.0648315	0.04789721
20	0.04950986	0.0670098	0.07436397	0.10738581	0.08777878
21	0.2309657	0.14998371	0.45593362	0.58666981	0.42208666
22	0.24915725	0.13775665	0.43078865	0.51134156	0.42956772
23	0.377285	0.16838072	0.60196522	0.67746299	0.60732784
24	0.46083625	0.16860379	0.73404504	0.77510704	0.6983895
25	0.30174896	0.1297328	0.47399727	0.55040961	...

Summary of area change in mode shape due to damage:

Input informations (need ajustment according different types):
Testing dates, recorded sets and corresponding directories.

dir1 := concat(CWD, "Summary\Damage detection\Area of mode shape change\")

dir2 :=

	1
1	"Accl"
2	"B Strain"
3	"M Strain"
4	"T Strain"
5	"B_M curvature Strain"
6	"Best fit curvature Strain"

dir3 := "\"

dataname :=

	1
1	"Mode 1_H.xls"
2	"Mode 1_WN.xls"
3	"Mode 2_H.xls"
4	"Mode 2_WN.xls"
5	"Mode 3_WN.xls"
6	"Mode 4_WN.xls"
7	"Mode 5_WN.xls"

Batch read-in Mean and Standard Deviation of Normal distribution:

$$mean\_file := batch\_read\_excel\left[dir1, dir2, dir3, dataname, \begin{pmatrix} 28 \\ 28 \end{pmatrix}, 2\right]$$

$$stdev\_file := batch\_read\_excel\left[dir1, dir2, dir3, dataname, \begin{pmatrix} 29 \\ 29 \end{pmatrix}, 2\right]$$

$$stack\_column(file) := \left| \begin{array}{l} n \leftarrow cols(file) \\ output \leftarrow file^{\langle 1 \rangle} \\ \text{for } i \in 2..n \\ \quad output \leftarrow stack(output, file^{\langle i \rangle}) \\ output \end{array} \right.$$

Mean values for all damage cases and all test protocols

$$mean\_d := stack\_column(mean\_file)$$

Standard deviation values for all damage cases and all test protocols

$$stdev\_d := stack\_column(stdev\_file)$$

Batch read-in the area of mode shape change for Log-Normal distribution:

$$area\_file := batch\_read\_excel\left[dir1, dir2, dir3, dataname, \begin{pmatrix} 2 \\ 26 \end{pmatrix}, 2\right]$$

$$area\_file\_stack := stack\_column(area\_file)$$

$$\begin{array}{l} mean\_d\_lgn := \\ \quad \text{for } i \in 1..42 \\ \quad\quad temp \leftarrow mean\ ln\left(area\_file\_stack_i\right)^{\langle 1 \rangle} \\ \quad\quad \text{for } j \in 2..26 \\ \quad\quad\quad temp \leftarrow augment\ temp, mean\ ln\left(area\_file\_stack_i\right)^{\langle j \rangle} \\ \quad\quad output_i \leftarrow temp \\ \quad output \end{array}$$

$$\begin{array}{l} stdev\_d\_lgn := \\ \quad \text{for } i \in 1..42 \\ \quad\quad temp \leftarrow stdev\ ln\left(area\_file\_stack_i\right)^{\langle 1 \rangle} \\ \quad\quad \text{for } j \in 2..26 \\ \quad\quad\quad temp \leftarrow augment\ temp, stdev\ ln\left(area\_file\_stack_i\right)^{\langle j \rangle} \\ \quad\quad output_i \leftarrow temp \\ \quad output \end{array}$$

Define probability that there has been a change in condition by comparing two groups (undamaged and damaged groups):

Statistic values of undamaged group based on normal distribution:

mean_und := μ_n

stdev_und := σ_n

Plots of density function :

Original test protocols: tp := 1

Damage case: dc := 26

Segment of intervel for actual density function: segment := 5

Plot axias range:

$x_L := 0$ $x_U := 0.01$

$y_L := 0$ $y_U := 800$ $y := 0 .. y_U$

Plots of the actual, Normal and Log-Normal density function of undamaged groups:

Plots of normal density function of both undamaged and damaged sample groups:

Plot axias range:

$x_L := -0.01$ $x_U := 0.1$

$y_L := 0$ $y_U := 800$ $y := 0 .. y_U$

Normal distribution:

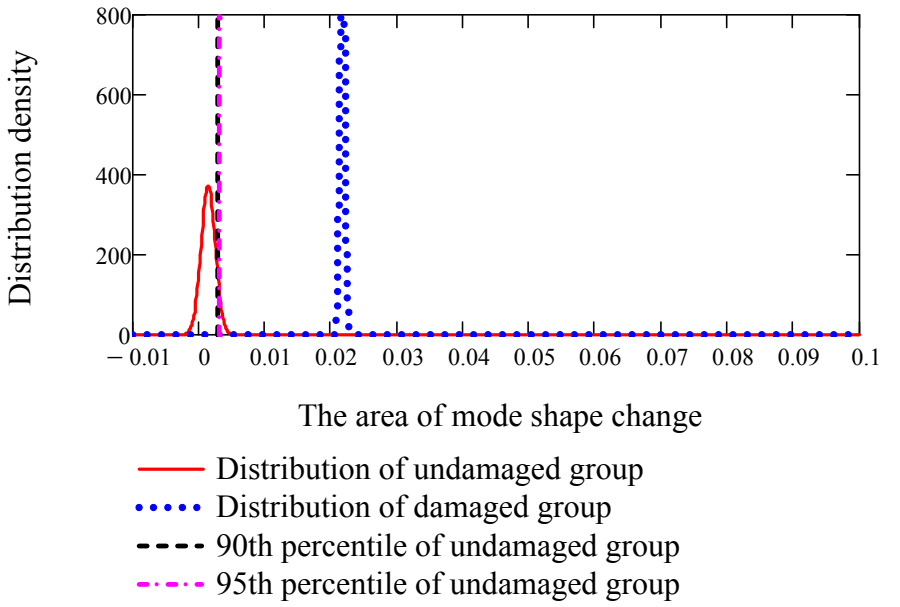

Log-Normal distribution:

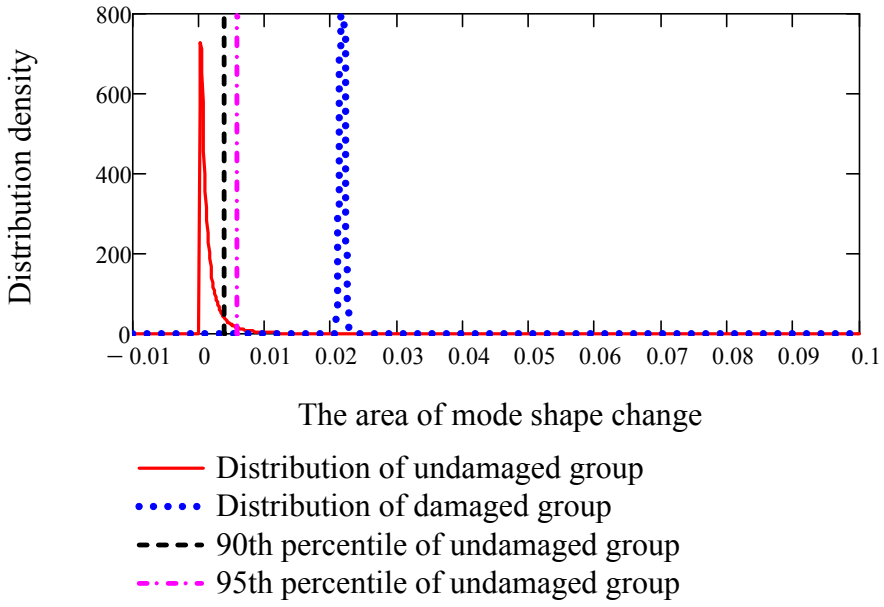

Probability that the value from the damaged group does not exceed that from undamaged group (i.e. the probability that there is no change in condition):

Normal distribution:

$$P_f(m1, std1, m2, std2) := \int_{-\infty}^{\infty} dnorm(x, m1, std1) \cdot \left(\int_{-\infty}^{x} dnorm(t, m2, std2)\, dt \right) dx$$

```
prob_sum := | prob ← "TP"
            | for j ∈ 1 .. 26
            |   prob ← augment(prob, j)
            | for i ∈ 1 .. 42
            |   | tp ← i
            |   | for j ∈ 1 .. 26
            |   |   tp ← augment(tp, P_f(mean_und_i, stdev_und_i, (mean_d_i)_1,j, (stdev_d_i)_1,j))
            |   | prob ← stack(prob, tp)
            | prob
```

Result output

...\Probability summary.xls

prob_sum

Log-Normal distribution:

$$P_{f\_lgn}(m1, std1, m2, std2) := \int_0^{\infty} dlnorm(x, m1, std1) \cdot \left(\int_0^{x} dlnorm(t, m2, std2)\, dt \right) dx$$

```
prob_sum_lgn := | prob ← "TP"
                | for j ∈ 1 .. 26
                |   prob ← augment(prob, j)
                | for i ∈ 1 .. 42
                |   tp ← i
                |   for j ∈ 1 .. 26
                |     tp ← augment(tp, P_f_lgn(μ_Ln_i, σ_Ln_i, (mean_d_lgn_i)_1,j, (stdev_d_lgn_i)_1,j))
                |   prob ← stack(prob, tp)
                | prob
```

Result output

...\Probability summary_LogNormal.xls

prob_sum_lgn

R-Square and standard errors based on Probability Density functions:

R_square_sum_df :=
r_sum1 ← augment("R2_n" , "SSerr_n" , "StdR_n" , "W_StdR_n")
r_sum2 ← augment("R2_lgn" , "SSerr_lgn" , "StdR_lgn" , "W_StdR_lgn")
r_sum ← augment(r_sum1 , r_sum2)
for r ∈ 1 .. rows(area_sum)
  distr ← normalized_df $\left(\text{area\_sum}^{T}\right)^{\langle r \rangle}$, 5
  X ← $\text{distr}^{\langle 1 \rangle}$
  Y ← $\text{distr}^{\langle 2 \rangle}$
  f_{norm} ← norm(X)
  f_{lgnorm} ← lgnorm(X)
  err1 ← $SS_{err}(Y , f_{norm})$
  err2 ← $SS_{err}(Y , f_{lgnorm})$
  stdr1 ← $StdR(Y , f_{norm})$
  stdr2 ← $StdR(Y , f_{lgnorm})$
  stdr1w ← $StdR\_w(Y , f_{norm})$
  stdr2w ← $StdR\_w(Y , f_{lgnorm})$
  R_sq1 ← $R\_Square(Y , f_{norm})$
  R_sq2 ← $R\_Square(Y , f_{lgnorm})$
  R_sq ← augment(R_sq1 , err1 , stdr1 , stdr1w , R_sq2 , err2 , stdr2 , stdr2w)
  r_sum ← stack(r_sum , R_sq)
r_sum

summary_df := augment(title_mean , title_std , threshold_ac , threshold_Ln , threshold_n , R_square_sum_df

summary_df

M.7 A Sample Calculation Showing the Relationship between Scaling Factors, when Different Normalization Schemes Used, and their Influence on the Definition of Change in Mode Shapes and Change in Mode Shape Curvatures

Using Acceleration Mode 1 for Harmonic excitation (Mode 1_H Accelerometer):

M.6.1. Mode shapes

M.6.1.1. Unit-norm normalization over all points:

Health State 1:

unitnorm_all_S1 :=

	1	2	3	4
1	0	0	0	0
2	0.125	0.116	0.108	0.097
3	0.201	0.185	0.172	0.158
4	0.256	0.235	0.217	0.198
5	0.275	0.25	0.23	0.21
6	0.258	0.232	0.212	0.194
7	0.208	0.184	0.167	0.152
8	0.133	0.112	0.099	0.09
9	0	0	0	0

X :=

	1
1	0
2	1
3	2
4	3
5	4
6	5
7	6
8	7
9	8

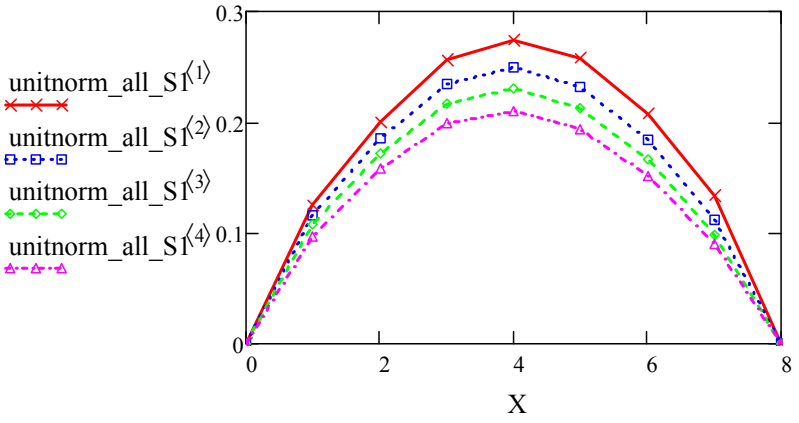

Health State 2:

unitnorm_all_S2 :=

	1	2	3	4
1	0	0	0	0
2	0.109	0.112	0.112	0.11
3	0.184	0.181	0.182	0.181
4	0.224	0.227	0.227	0.231
5	0.24	0.242	0.241	0.248
6	0.226	0.225	0.223	0.227
7	0.182	0.178	0.175	0.176
8	0.117	0.108	0.103	0.105
9	0	0	0	0

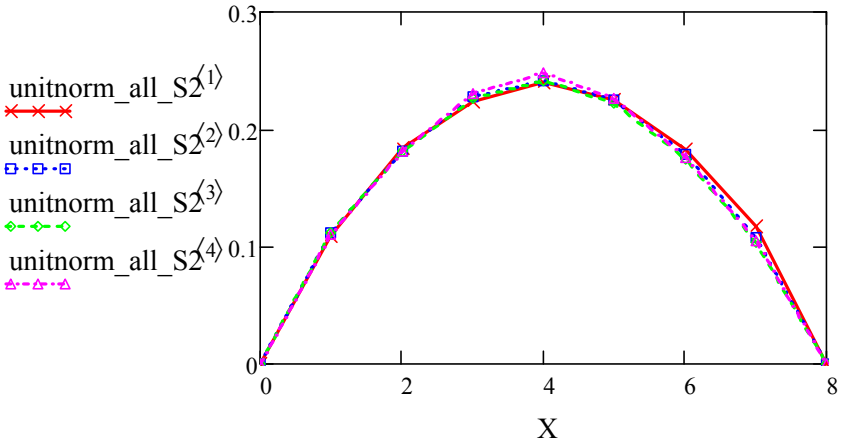

M.6.1.2. Unit-area normalization over all points:

Health State 1:

unitarea_all_S1 :=

	1	2	3	4
1	0	0	0	0
2	0.862	0.802	0.747	0.67
3	1.384	1.279	1.186	1.087
4	1.769	1.619	1.496	1.369
5	1.895	1.723	1.587	1.45
6	1.778	1.6	1.465	1.341
7	1.435	1.267	1.149	1.048
8	0.917	0.771	0.682	0.622
9	0	0	0	0

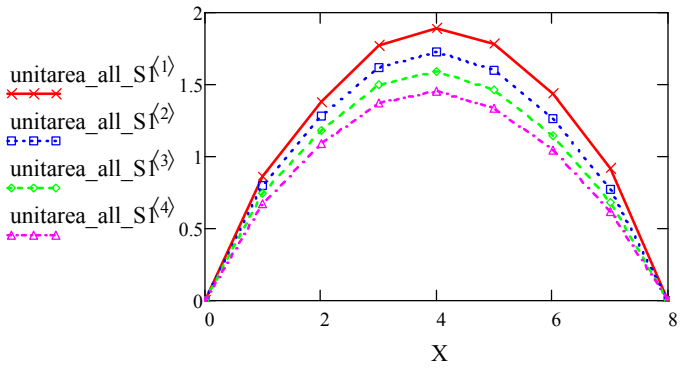

Scaling factor for all girder lines:

$$SF\_all\_S1 := \frac{unitarea\_all\_S1_{5,1}}{unitnorm\_all\_S1_{5,1}} \qquad SF\_all\_S1 = 6.90010548$$

$$unitnorm\_all\_S1 \cdot SF\_all\_S1 = \begin{pmatrix} 0 & 0 & 0 & 0 \\ 0.86248979 & 0.80172873 & 0.74669238 & 0.66962159 \\ 1.38410514 & 1.27919814 & 1.18631885 & 1.08714436 \\ 1.76870469 & 1.61903384 & 1.49555917 & 1.36947982 \\ 1.89484857 & 1.7229076 & 1.58679257 & 1.4501281 \\ 1.7776213 & 1.60035719 & 1.46523133 & 1.34062844 \\ 1.43455218 & 1.26732646 & 1.14894932 & 1.04828544 \\ 0.91741931 & 0.77057267 & 0.68187947 & 0.6224235 \\ 0 & 0 & 0 & 0 \end{pmatrix}$$

Which is Same as unitarea_all_S

Health State 2:

unitarea_all_S2 :=

	1	2	3	4
1	0	0	0	0
2	0.75	0.769	0.769	0.755
3	1.261	1.247	1.248	1.243
4	1.541	1.56	1.559	1.584
5	1.651	1.661	1.656	1.702
6	1.55	1.545	1.531	1.557
7	1.252	1.224	1.199	1.211
8	0.802	0.744	0.71	0.718
9	0	0	0	0

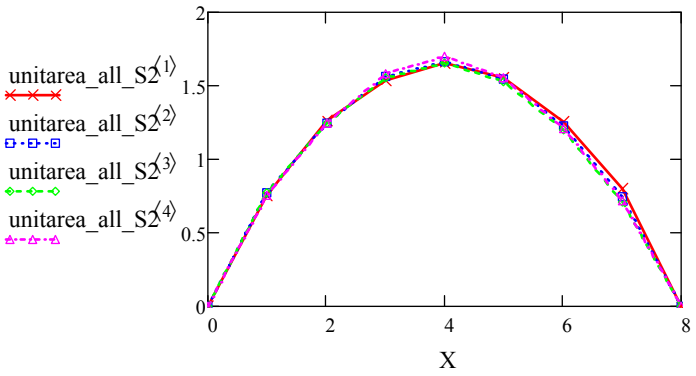

Scaling factor for all girder lines:

$$SF\_all\_S2 := \frac{unitarea\_all\_S2_{5,1}}{unitnorm\_all\_S2_{5,1}} \qquad SF\_all\_S2 = 6.86869647$$

$$unitnorm\_all\_S2 \cdot SF\_all\_S2 = \begin{pmatrix} 0 & 0 & 0 & 0 \\ 0.75042142 & 0.76887012 & 0.76868315 & 0.75536814 \\ 1.26112417 & 1.24650487 & 1.24752654 & 1.24330368 \\ 1.5407054 & 1.56017871 & 1.55866044 & 1.58356469 \\ 1.65112044 & 1.66089321 & 1.6564796 & 1.70229927 \\ 1.55013385 & 1.54464069 & 1.53073812 & 1.55706157 \\ 1.25181003 & 1.22446615 & 1.19881889 & 1.21111523 \\ 0.80246555 & 0.74431212 & 0.71043217 & 0.71830179 \\ 0 & 0 & 0 & 0 \end{pmatrix}$$

Which is same as unitarea_all_S2

Scaling factors are different for two damage cases:

$$\frac{SF\_all\_S1}{SF\_all\_S2} = 1.00457278$$

M.6.1.3. Unit-area normalization along each girder line:

Health State 1:

unitarea_xgrid_S1 :=

	1	2	3	4
1	0	0	0	0
2	0.687	0.708	0.719	0.706
3	1.103	1.129	1.142	1.146
4	1.409	1.429	1.44	1.444
5	1.51	1.521	1.527	1.529
6	1.416	1.413	1.41	1.413
7	1.143	1.119	1.106	1.105
8	0.731	0.68	0.656	0.656
9	0	0	0	0

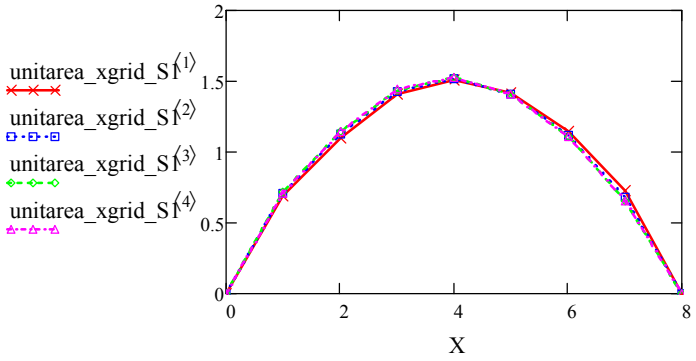

Scaling factors are different for each girder line:

Girder Line 1: $SF\_xgrid\_G1\_S1 := \frac{unitarea\_xgrid\_S1_{5,1}}{unitnorm\_all\_S1_{5,1}}$ $SF\_xgrid\_G1\_S1 = 5.49823387$

Girder Line 2: $SF\_xgrid\_G2\_S1 := \frac{unitarea\_xgrid\_S1_{5,2}}{unitnorm\_all\_S1_{5,2}}$ $SF\_xgrid\_G2\_S1 = 6.09205214$

Girder Line 3: $SF\_xgrid\_G3\_S1 := \frac{unitarea\_xgrid\_S1_{5,3}}{unitnorm\_all\_S1_{5,3}}$ $SF\_xgrid\_G3\_S1 = 6.64156345$

Girder Line 4: $SF\_xgrid\_G4\_S1 := \frac{unitarea\_xgrid\_S1_{5,4}}{unitnorm\_all\_S1_{5,4}}$ $SF\_xgrid\_G4\_S1 = 7.27503222$

Normalized mode shape:

$G1 := unitnorm\_all\_S1^{\langle 1 \rangle} \cdot SF\_xgrid\_G1\_S1 \quad G2 := unitnorm\_all\_S1^{\langle 2 \rangle} \cdot SF\_xgrid\_G2\_S1$

$G3 := unitnorm\_all\_S1^{\langle 3 \rangle} \cdot SF\_xgrid\_G3\_S1 \quad G4 := unitnorm\_all\_S1^{\langle 4 \rangle} \cdot SF\_xgrid\_G4\_S1$

$Normalized\_unitarea\_xgrid\_S1 := augment(G1, G2, G3, G4)$

$$Normalized\_unitarea\_xgrid\_S1 = \begin{pmatrix} 0 & 0 & 0 & 0 \\ 0.68726059 & 0.70784038 & 0.71871434 & 0.7060064 \\ 1.10290107 & 1.12939459 & 1.14186833 & 1.14621585 \\ 1.4093628 & 1.42943301 & 1.43952164 & 1.44389239 \\ 1.50987845 & 1.52114239 & 1.52733658 & 1.52892281 \\ 1.41646786 & 1.41294354 & 1.41033015 & 1.41347334 \\ 1.14309896 & 1.11891317 & 1.10589901 & 1.10524548 \\ 0.73103026 & 0.68033292 & 0.65632993 & 0.65624374 \\ 0 & 0 & 0 & 0 \end{pmatrix}$$

Same as unitarea_xgrid_S1

Health State 2:

unitarea_xgrid_S2 :=

	1	2	3	4
1	0	0	0	0
2	0.682	0.703	0.709	0.689
3	1.145	1.14	1.151	1.134
4	1.399	1.426	1.438	1.444
5	1.5	1.519	1.528	1.553
6	1.408	1.412	1.412	1.42
7	1.137	1.12	1.106	1.105
8	0.729	0.681	0.655	0.655
9	0	0	0	0

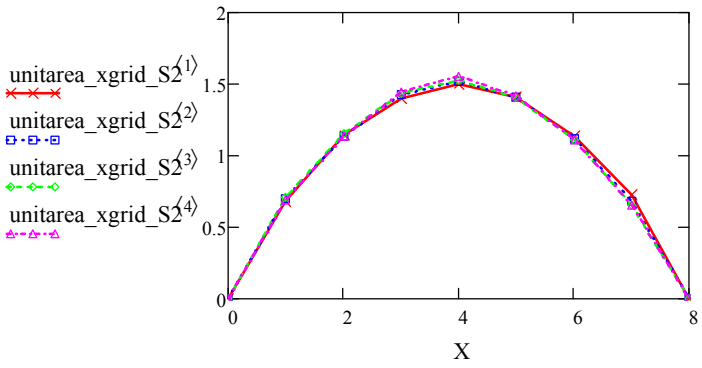

Scaling factors are different for each girder line:

Girder Line 1: $SF\_xgrid\_G1\_S2 := \frac{unitarea\_xgrid\_S2_{5,1}}{unitnorm\_all\_S2_{5,1}}$ $SF\_xgrid\_G1\_S2 = 6.23875327$

Girder Line 2: $SF\_xgrid\_G2\_S2 := \frac{unitarea\_xgrid\_S2_{5,2}}{unitnorm\_all\_S2_{5,2}}$ $SF\_xgrid\_G2\_S2 = 6.28004732$

Girder Line 3: $SF\_xgrid\_G3\_S2 := \frac{unitarea\_xgrid\_S2_{5,3}}{unitnorm\_all\_S2_{5,3}}$ $SF\_xgrid\_G3\_S2 = 6.33691894$

Girder Line 4: $SF\_xgrid\_G4\_S2 := \frac{unitarea\_xgrid\_S2_{5,4}}{unitnorm\_all\_S2_{5,4}}$ $SF\_xgrid\_G4\_S2 = 6.26490499$

Normalized mode shape:

$G1 := unitnorm\_all\_S2^{\langle 1 \rangle} \cdot SF\_xgrid\_G1\_S2 \quad G2 := unitnorm\_all\_S2^{\langle 2 \rangle} \cdot SF\_xgrid\_G2\_S2$

$G3 := unitnorm\_all\_S2^{\langle 3 \rangle} \cdot SF\_xgrid\_G3\_S2 \quad G4 := unitnorm\_all\_S2^{\langle 4 \rangle} \cdot SF\_xgrid\_G4\_S2$

$Normalized\_unitarea\_xgrid\_S1 := augment(G1, G2, G3, G4)$

$$Normalized\_unitarea\_xgrid\_S1 = \begin{pmatrix} 0 & 0 & 0 & 0 \\ 0.68159863 & 0.70297775 & 0.70917136 & 0.68896765 \\ 1.14546371 & 1.13967906 & 1.15094248 & 1.1340113 \\ 1.39940394 & 1.42647097 & 1.43798825 & 1.44436173 \\ 1.49969257 & 1.51855422 & 1.52823421 & 1.55265897 \\ 1.40796768 & 1.41226457 & 1.41222769 & 1.42018836 \\ 1.13700379 & 1.11952907 & 1.1060058 & 1.10465237 \\ 0.72886968 & 0.68052437 & 0.65543019 & 0.65515961 \\ 0 & 0 & 0 & 0 \end{pmatrix}$$

which is same as:

$$unitarea\_xgrid\_S2 = \begin{pmatrix} 0 & 0 & 0 & 0 \\ 0.68159863 & 0.70297775 & 0.70917136 & 0.68896765 \\ 1.14546371 & 1.13967906 & 1.15094248 & 1.1340113 \\ 1.39940394 & 1.42647097 & 1.43798825 & 1.44436173 \\ 1.49969257 & 1.51855422 & 1.52823421 & 1.55265897 \\ 1.40796768 & 1.41226456 & 1.41222769 & 1.42018837 \\ 1.1370038 & 1.11952907 & 1.1060058 & 1.10465238 \\ 0.72886968 & 0.68052437 & 0.6554302 & 0.65515961 \\ 0 & 0 & 0 & 0 \end{pmatrix}$$

Scaling factors are different for two health states for each girder line:

Girder Line 1: $\frac{SF\_xgrid\_G1\_S1}{SF\_xgrid\_G1\_S2} = 0.8813033$

Girder Line 2: $\frac{SF\_xgrid\_G2\_S1}{SF\_xgrid\_G2\_S2} = 0.97006469$

Girder Line 3: $\frac{SF\_xgrid\_G2\_S1}{SF\_xgrid\_G2\_S2} = 0.97006469$

Girder Line 4: $\frac{SF\_xgrid\_G2\_S1}{SF\_xgrid\_G2\_S2} = 0.97006469$

M.6.2 . Change in Mode Shape.

M.6.2.1. Unit-area normalization over all points:

ch_m_areanorm_all := unitarea_all_S2 − unitarea_all_S1

$$\text{ch\_m\_areanorm\_all} = \begin{pmatrix} 0 & 0 & 0 & 0 \\ -0.11206836 & -0.03285861 & 0.02199078 & 0.08574655 \\ -0.12298097 & -0.03269328 & 0.06120769 & 0.15615932 \\ -0.22799928 & -0.05885513 & 0.06310126 & 0.21408486 \\ -0.24372813 & -0.06201439 & 0.06968703 & 0.25217116 \\ -0.22748745 & -0.05571651 & 0.06550679 & 0.21643312 \\ -0.18274214 & -0.04286031 & 0.04986957 & 0.16282979 \\ -0.11495376 & -0.02626055 & 0.0285527 & 0.09587829 \\ 0 & 0 & 0 & 0 \end{pmatrix}$$

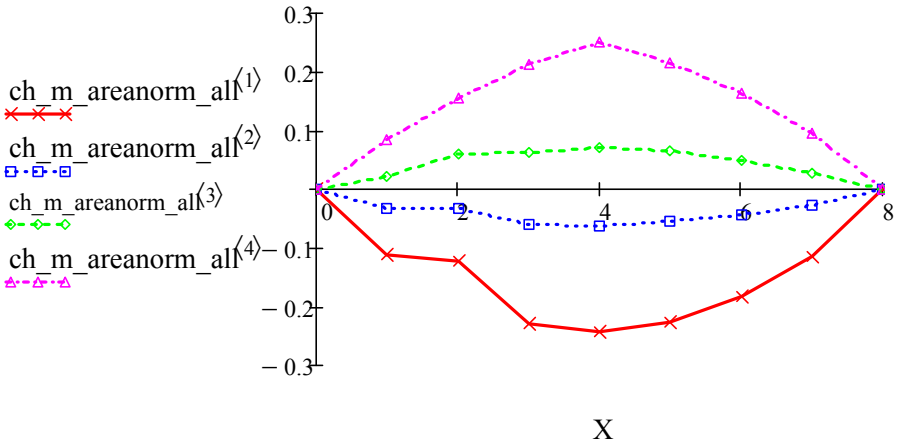

M.6.2.2. Unit-area normalization along each girder line:

ch_m_areanorm_xgrid:= unitarea_xgrid_S2 − unitarea_xgrid_S1

$$\text{ch\_m\_areanorm\_xgrid} = \begin{pmatrix} 0 & 0 & 0 & 0 \\ -0.00566196 & -0.00486263 & -0.00954298 & -0.01703875 \\ 0.04256263 & 0.01028447 & 0.00907415 & -0.01220454 \\ -0.00995887 & -0.00296204 & -0.00153339 & 0.00046934 \\ -0.01018589 & -0.00258818 & 0.00089763 & 0.02373616 \\ -0.00850018 & -0.00067898 & 0.00189753 & 0.00671503 \\ -0.00609516 & 0.0006159 & 0.00010679 & -0.0005931 \\ -0.00216059 & 0.00019145 & -0.00089973 & -0.00108413 \\ 0 & 0 & 0 & 0 \end{pmatrix}$$

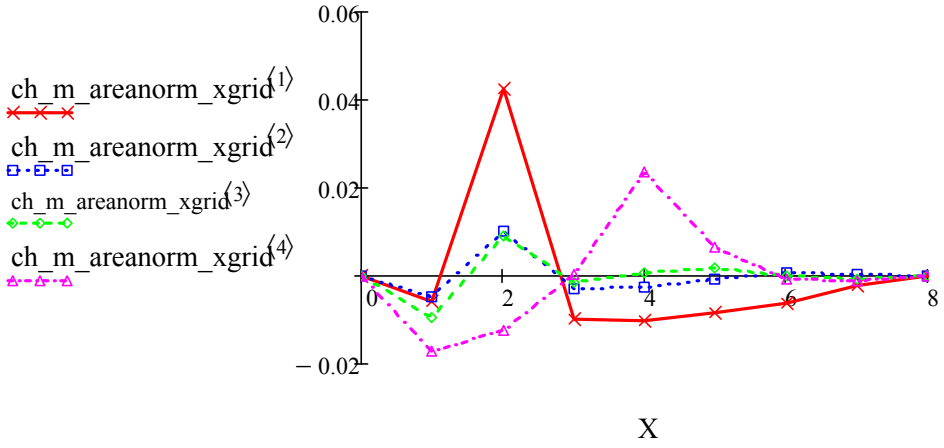

M.6.3. Mode Shape Curvature and Change in Mode Shape Curvature

M.6.3.1. Mode shape curvature

M.6.3.1.1. Unit-norm normalization over all points:

Health State 1:

modeshape := unitnorm_all_S1

curv1 := curvature(modeshape⟨1⟩) curv2 := curvature(modeshape⟨2⟩)

curv3 := curvature(modeshape⟨3⟩) curv4 := curvature(modeshape⟨4⟩)

curv := augment(curv1, curv2, curv3, curv4)

$$curv = \begin{pmatrix} 0 & 0 & 0 & 0 \\ -3.16168557 & -3.00757677 & -2.84810394 & -2.33827219 \\ -1.27085178 & -1.27658304 & -1.20936032 & -1.2538921 \\ -2.39723328 & -2.18859891 & -2.02206234 & -1.87069306 \\ -2.25732115 & -2.10013421 & -1.97371718 & -1.76366406 \\ -2.09473293 & -1.95225133 & -1.80607802 & -1.69591232 \\ -1.61447968 & -1.51856749 & -1.39859053 & -1.2384176 \\ -3.71274502 & -2.53973056 & -1.99240659 & -1.82315187 \\ 0 & 0 & 0 & 0 \end{pmatrix}$$

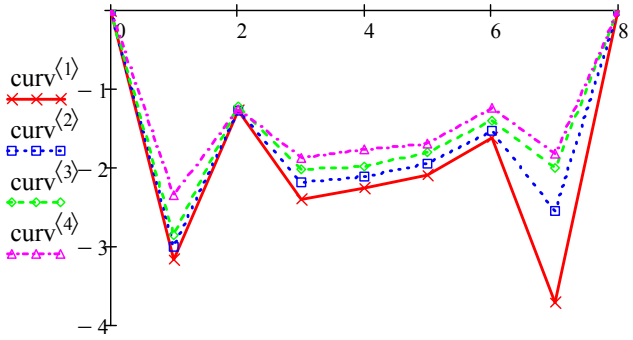

X

curv_unitnorm_all_S1 := curv

Health State 2:

modeshape := unitnorm_all_S2

curv1 := curvature(modeshape⟨1⟩) curv2 := curvature(modeshape⟨2⟩)

curv3 := curvature(modeshape⟨3⟩) curv4 := curvature(modeshape⟨4⟩)

curv := augment(curv1, curv2, curv3, curv4)

$$curv = \begin{pmatrix} 0 & 0 & 0 & 0 \\ -2.23361088 & -2.7136247 & -2.70062086 & -2.49183917 \\ -2.15350573 & -1.52772768 & -1.56265562 & -1.37597715 \\ -1.57622867 & -1.98427712 & -1.98758861 & -2.06410221 \\ -1.96976301 & -2.02161939 & -2.08305632 & -2.45959712 \\ -1.83871603 & -1.90007072 & -1.92108877 & -1.8701296 \\ -1.40715533 & -1.4906304 & -1.45790688 & -1.36845395 \\ -3.29025286 & -2.46132832 & -2.06893818 & -2.10101792 \\ 0 & 0 & 0 & 0 \end{pmatrix}$$

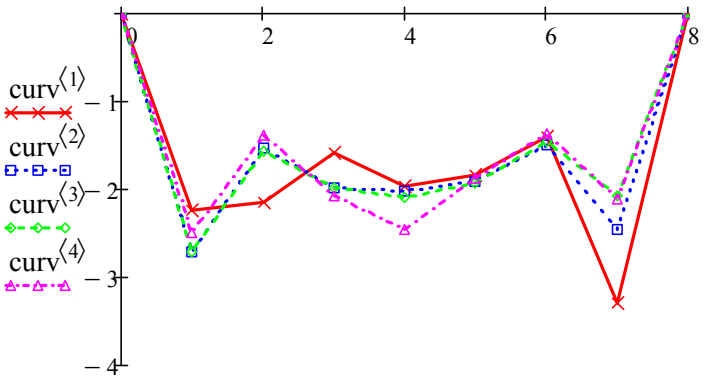

X

curv_unitnorm_all_S2:= curv

M.6.3.1.2. Unit-area normalization over all points:

Health State 1:

modeshape := unitarea_all_S1

curv1 := curvature(modeshape⟨1⟩) curv2 := curvature(modeshape⟨2⟩)

curv3 := curvature(modeshape⟨3⟩) curv4 := curvature(modeshape⟨4⟩)

curv := augment(curv1, curv2, curv3, curv4)

$$curv = \begin{pmatrix} 0 & 0 & 0 & 0 \\ -21.81596352 & -20.75259667 & -19.65221734 & -16.13432454 \\ -8.76901184 & -8.80855789 & -8.34471386 & -8.65198746 \\ -16.54116237 & -15.10156371 & -13.95244365 & -12.9079799 \\ -15.57575405 & -14.49114701 & -13.61885619 & -12.16946784 \\ -14.45387808 & -13.47074067 & -12.4621296 & -11.70197414 \\ -11.14008 & -10.47827546 & -9.65042182 & -8.54521222 \\ -25.61833248 & -17.52440877 & -13.74781549 & -12.57993978 \\ 0 & 0 & 0 & 0 \end{pmatrix}$$

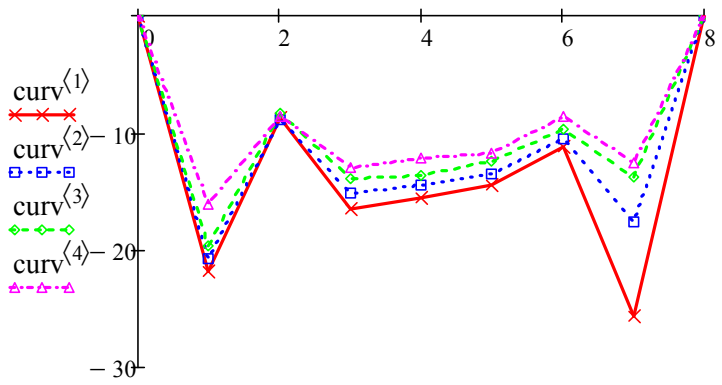

X

curv_unitarea_all_S1 := curv

Health State 2:

modeshape := unitarea_all_S2

curv1 := curvature(modeshape⟨1⟩) curv2 := curvature(modeshape⟨2⟩)

curv3 := curvature(modeshape⟨3⟩) curv4 := curvature(modeshape⟨4⟩)

curv := augment(curv1, curv2, curv3, curv4)

$$curv = \begin{pmatrix} 0 & 0 & 0 & 0 \\ -15.34199514 & -18.63906496 & -18.54974528 & -17.11568653 \\ -14.7917769 & -10.49349715 & -10.7334073 & -9.45117005 \\ -10.82663674 & -13.6293977 & -13.65214253 & -14.17769114 \\ -13.52970387 & -13.88588998 & -14.30788166 & -16.89422592 \\ -12.62958246 & -13.05100883 & -13.19537574 & -12.8453527 \\ -9.6653232 & -10.23868736 & -10.01391936 & -9.39949491 \\ -22.59974778 & -16.90611776 & -14.21090886 & -14.4312544 \\ 0 & 0 & 0 & 0 \end{pmatrix}$$

which is same as

$$SF\_all\_S2 \cdot curv\_unitnorm\_all\_S2 = \begin{pmatrix} 0 & 0 & 0 & 0 \\ -15.34199516 & -18.63906442 & -18.54974499 & -17.11568689 \\ -14.79177719 & -10.49349772 & -10.73340711 & -9.4511694 \\ -10.82663631 & -13.62939725 & -13.65214285 & -14.17769155 \\ -13.52970422 & -13.88588998 & -14.30788159 & -16.89422605 \\ -12.62958232 & -13.05100904 & -13.19537564 & -12.84535258 \\ -9.66532283 & -10.23868776 & -10.01391984 & -9.39949483 \\ -22.59974823 & -16.90611714 & -14.21090834 & -14.43125437 \\ 0 & 0 & 0 & 0 \end{pmatrix}$$

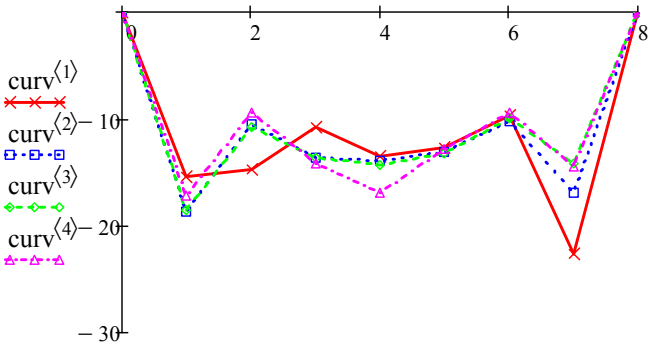

X

curv_unitarea_all_S2 := curv

M.6.3.1.3. Unit-area normalization along individual girder lines:

Health State 1:

modeshape := unitarea_xgrid_S1

curv1 := curvature(modeshape⟨1⟩) curv2 := curvature(modeshape⟨2⟩)

curv3 := curvature(modeshape⟨3⟩) curv4 := curvature(modeshape⟨4⟩)

curv := augment(curv1, curv2, curv3, curv4)

$$curv = \begin{pmatrix} 0 & 0 & 0 & 0 \\ -17.38368621 & -18.3223143 & -18.91586272 & -17.01100518 \\ -6.98744083 & -7.77701062 & -8.03204339 & -9.12210522 \\ -13.18054899 & -13.33305901 & -13.42965555 & -13.60935264 \\ -12.41127968 & -12.79412666 & -13.10856736 & -12.8307127 \\ -11.51733139 & -11.89321734 & -11.99518253 & -12.33781696 \\ -8.87678688 & -9.251192 & -9.28882739 & -9.00952813 \\ -20.41354048 & -15.47217094 & -13.23269466 & -13.26348806 \\ 0 & 0 & 0 & 0 \end{pmatrix}$$

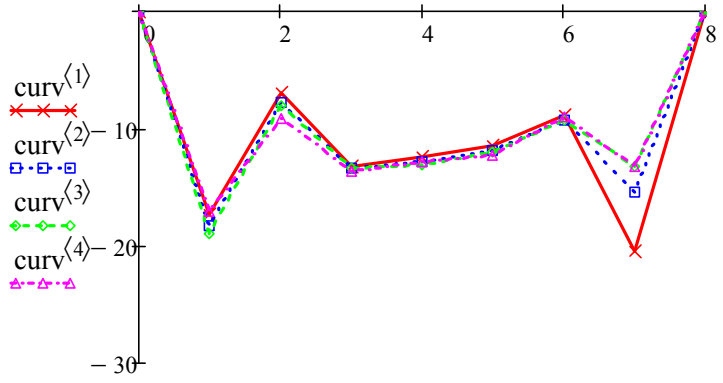

Verification:

$c1 := SF\_xgrid\_G1\_S1 \cdot curv\_unitnorm\_all\_S1^{\langle 1 \rangle}$

$c2 := SF\_xgrid\_G2\_S1 \cdot curv\_unitnorm\_all\_S1^{\langle 2 \rangle}$

$c3 := SF\_xgrid\_G3\_S1 \cdot curv\_unitnorm\_all\_S1^{\langle 3 \rangle}$

$c4 := SF\_xgrid\_G4\_S1 \cdot curv\_unitnorm\_all\_S1^{\langle 4 \rangle}$

$curv\_normalized := augment(c1, c2, c3, c4)$

$$curv\_normalized = \begin{pmatrix} 0 & 0 & 0 & 0 \\ -17.38368667 & -18.3223145 & -18.915863 & -17.01100554 \\ -6.98744027 & -7.77701044 & -8.0320433 & -9.1221054 \\ -13.18054921 & -13.33305869 & -13.4296553 & -13.60935226 \\ -12.41127961 & -12.7941271 & -13.10856791 & -12.8307129 \\ -11.51733153 & -11.89321689 & -11.99518174 & -12.33781678 \\ -8.87678685 & -9.25119232 & -9.28882773 & -9.00952795 \\ -20.41354043 & -15.472171 & -13.2326948 & -13.26348862 \\ 0 & 0 & 0 & 0 \end{pmatrix}$$

which is same as above matrix.

$curv\_unitarea\_xgrid\_S1 := curv$

Health State 2:

modeshape := unitarea_xgrid_S2

curv1 := curvature(modeshape⟨1⟩) curv2 := curvature(modeshape⟨2⟩)

curv3 := curvature(modeshape⟨3⟩) curv4 := curvature(modeshape⟨4⟩)

curv := augment(curv1, curv2, curv3, curv4)

$$curv = \begin{pmatrix} 0 & 0 & 0 & 0 \\ -13.93494714 & -17.04169197 & -17.11361574 & -15.6111353 \\ -13.43519072 & -9.59420166 & -9.90242214 & -8.62036678 \\ -9.83370208 & -12.46135469 & -12.59518765 & -12.93140384 \\ -12.28886515 & -12.69586534 & -13.20015904 & -15.40914214 \\ -11.47129581 & -11.93253395 & -12.17378394 & -11.71618445 \\ -8.77889517 & -9.36122912 & -9.23863725 & -8.57323411 \\ -20.52707552 & -15.45725882 & -13.11069408 & -13.16267763 \\ 0 & 0 & 0 & 0 \end{pmatrix}$$

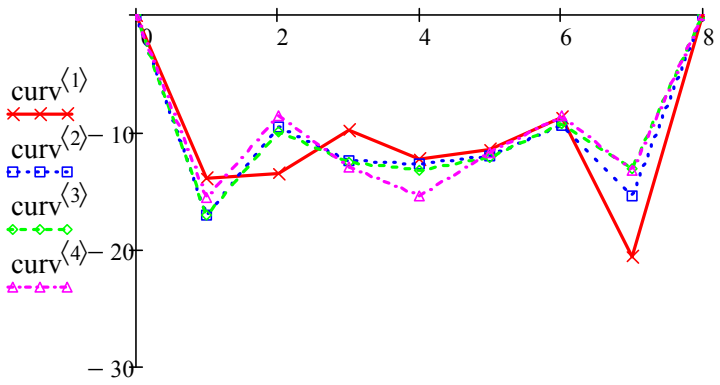

X

curv_unitarea_xgrid_S2 := curv

Verification:

$$c1 := SF\_xgrid\_G1\_S2 \cdot curv\_unitnorm\_all\_S2^{\langle 1 \rangle}$$

$$c2 := SF\_xgrid\_G2\_S2 \cdot curv\_unitnorm\_all\_S2^{\langle 2 \rangle}$$

$$c3 := SF\_xgrid\_G3\_S2 \cdot curv\_unitnorm\_all\_S2^{\langle 3 \rangle}$$

$$c4 := SF\_xgrid\_G4\_S2 \cdot curv\_unitnorm\_all\_S2^{\langle 4 \rangle}$$

$$curv\_normalized := augment(c1, c2, c3, c4)$$

$$curv\_normalized = \begin{pmatrix} 0 & 0 & 0 & 0 \\ -13.93494719 & -17.04169156 & -17.11361549 & -15.61113565 \\ -13.43519091 & -9.59420213 & -9.90242196 & -8.62036613 \\ -9.83370179 & -12.46135422 & -12.59518789 & -12.93140423 \\ -12.28886542 & -12.69586545 & -13.20015904 & -15.40914228 \\ -11.47129567 & -11.93253404 & -12.17378379 & -11.71618427 \\ -8.77889491 & -9.36122945 & -9.23863771 & -8.573234 \\ -20.52707583 & -15.45725833 & -13.1106935 & -13.16267766 \\ 0 & 0 & 0 & 0 \end{pmatrix}$$

which is same as above matrix.

M.6.3.1.4. Curvature of change in mode shape:

Unit-area normalization over all points:

modeshape := ch_m_areanorm_all

curv1 := curvature(modeshape⟨1⟩) curv2 := curvature(modeshape⟨2⟩)

curv3 := curvature(modeshape⟨3⟩) curv4 := curvature(modeshape⟨4⟩)

curv := augment(curv1, curv2, curv3, curv4)

$$curv = \begin{pmatrix} 0 & 0 & 0 & 0 \\ 6.47396838 & 2.11353171 & 1.10247206 & -0.98136198 \\ -6.02276506 & -1.68493926 & -2.38869344 & -0.79918259 \\ 5.71452563 & 1.47216602 & 0.30030112 & -1.26971123 \\ 2.04605018 & 0.60525702 & -0.68902547 & -4.72475808 \\ 1.82429562 & 0.41973184 & -0.73324614 & -1.14337856 \\ 1.4747568 & 0.2395881 & -0.36349754 & -0.85428269 \\ 3.0185847 & 0.61829101 & -0.46309338 & -1.85131462 \\ 0 & 0 & 0 & 0 \end{pmatrix}$$

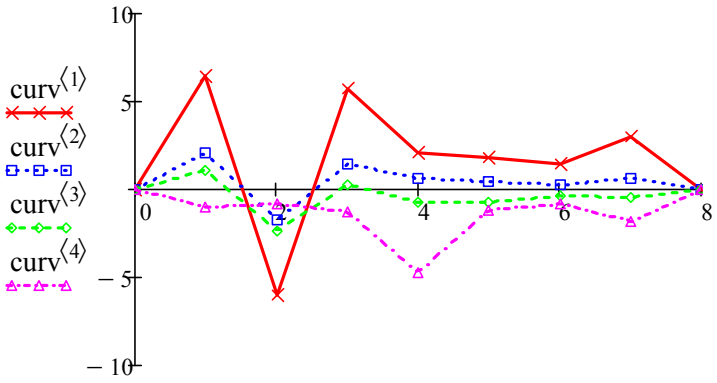

curv_ch_mode_unitarea_all := curv

Unit-area normalization along individual girder lines:

modeshape := ch_m_areanorm_xgrid

curv1 := curvature(modeshape⟨1⟩) curv2 := curvature(modeshape⟨2⟩)

curv3 := curvature(modeshape⟨3⟩) curv4 := curvature(modeshape⟨4⟩)

curv := augment(curv1, curv2, curv3, curv4)

$$curv = \begin{pmatrix} 0 & 0 & 0 & 0 \\ 3.44873907 & 1.28062234 & 1.80224698 & 1.39986989 \\ -6.44774989 & -1.81719104 & -1.87037875 & 0.50173843 \\ 3.34684691 & 0.87170432 & 0.8344679 & 0.6779488 \\ 0.12241453 & 0.09826131 & -0.09159168 & -2.57842944 \\ 0.04603558 & -0.03931661 & -0.17860141 & 0.62163251 \\ 0.09789171 & -0.11003712 & 0.05019014 & 0.43629402 \\ -0.11353504 & 0.01491213 & 0.12200058 & 0.10081043 \\ 0 & 0 & 0 & 0 \end{pmatrix}$$

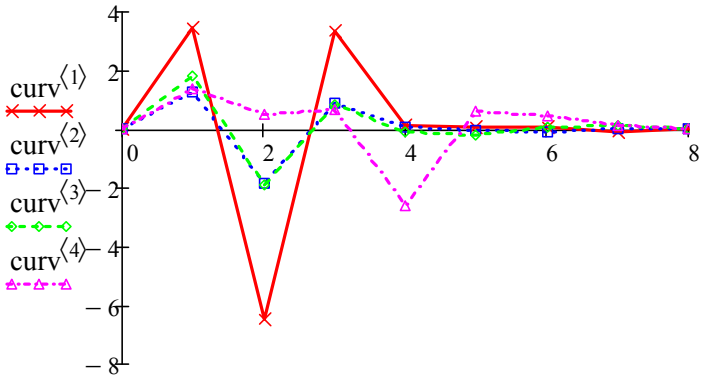

X

curv_ch_mode_unitarea_xgrid:= curv

M.6.3.2. Change in Mode shape curvature due to damage.

M.6.3.2.1. Unit-norm normalization over all points:

$$\text{ch\_mode\_curv} := \overrightarrow{|\text{curv\_unitnorm\_all\_S2}|} - \overrightarrow{|\text{curv\_unitnorm\_all\_S1}|}$$

$$\text{ch\_mode\_curv} = \begin{pmatrix} 0 & 0 & 0 & 0 \\ -0.92807469 & -0.29395206 & -0.14748307 & 0.15356698 \\ 0.88265395 & 0.25114464 & 0.3532953 & 0.12208506 \\ -0.82100461 & -0.20432179 & -0.03447373 & 0.19340915 \\ -0.28755814 & -0.07851482 & 0.10933914 & 0.69593306 \\ -0.2560169 & -0.05218061 & 0.11501075 & 0.17421728 \\ -0.20732435 & -0.02793709 & 0.05931635 & 0.13003635 \\ -0.42249216 & -0.07840224 & 0.07653158 & 0.27786605 \\ 0 & 0 & 0 & 0 \end{pmatrix}$$

$$\text{ch\_curv\_norm\_all} := \text{ch\_mode\_curv}$$

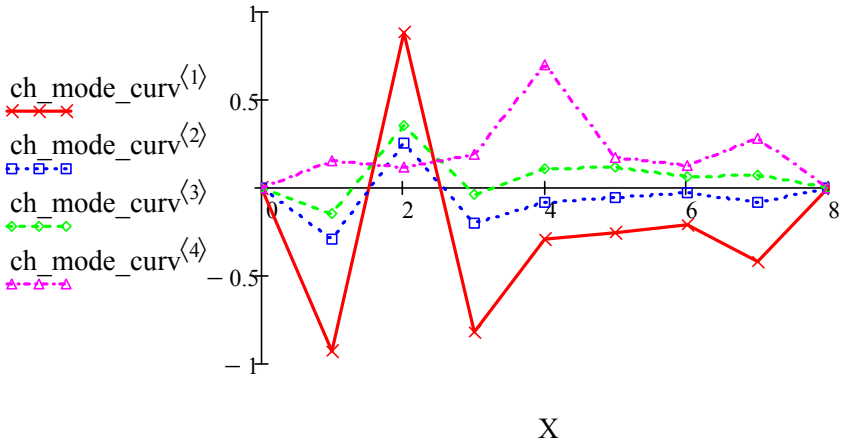

M.6.3.2.2. Unit-area normalization over all points:

$$\text{ch\_mode\_curv} := \overrightarrow{|\text{curv\_unitarea\_all\_S2}|} - \overrightarrow{|\text{curv\_unitarea\_all\_S1}|}$$

$$\text{ch\_mode\_curv} = \begin{pmatrix} 0 & 0 & 0 & 0 \\ -6.47396838 & -2.11353171 & -1.10247206 & 0.98136198 \\ 6.02276506 & 1.68493926 & 2.38869344 & 0.79918259 \\ -5.71452563 & -1.47216602 & -0.30030112 & 1.26971123 \\ -2.04605018 & -0.60525702 & 0.68902547 & 4.72475808 \\ -1.82429562 & -0.41973184 & 0.73324614 & 1.14337856 \\ -1.4747568 & -0.2395881 & 0.36349754 & 0.85428269 \\ -3.0185847 & -0.61829101 & 0.46309338 & 1.85131462 \\ 0 & 0 & 0 & 0 \end{pmatrix}$$

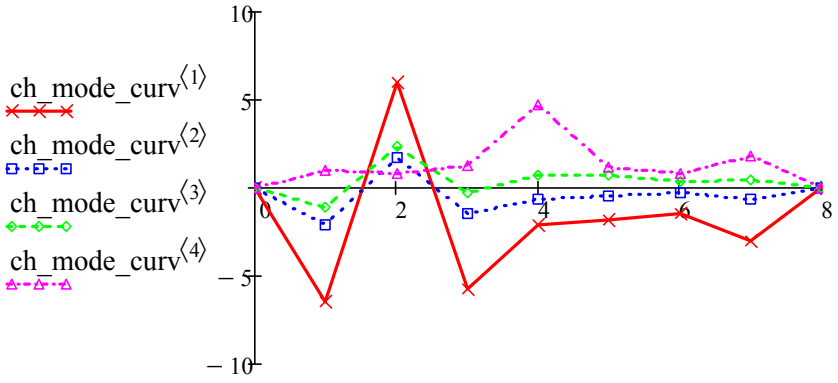

ch_curv_area_all := ch_mode_curv

M.6.3.2.3. Unit-area normalization along individual girder lines:

$$ch\_mode\_curv := \overrightarrow{|curv\_unitarea\_xgrid\_S2|} - \overrightarrow{|curv\_unitarea\_xgrid\_S1|}$$

$$ch\_mode\_curv = \begin{pmatrix} 0 & 0 & 0 & 0 \\ -3.44873907 & -1.28062234 & -1.80224698 & -1.39986989 \\ 6.44774989 & 1.81719104 & 1.87037875 & -0.50173843 \\ -3.34684691 & -0.87170432 & -0.8344679 & -0.6779488 \\ -0.12241453 & -0.09826131 & 0.09159168 & 2.57842944 \\ -0.04603558 & 0.03931661 & 0.17860141 & -0.62163251 \\ -0.09789171 & 0.11003712 & -0.05019014 & -0.43629402 \\ 0.11353504 & -0.01491213 & -0.12200058 & -0.10081043 \\ 0 & 0 & 0 & 0 \end{pmatrix}$$

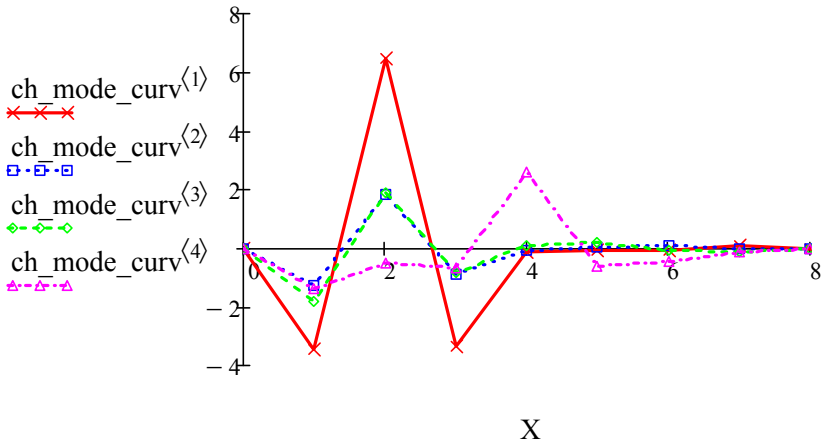

$$ch\_curv\_area\_xgrid := ch\_mode\_curv$$